Rôle des immunoglobulines sécrétoires dans les maladies inflammatoires chroniques de l'intestin

Eva Michaud

▶ **To cite this version:**

Eva Michaud. Rôle des immunoglobulines sécrétoires dans les maladies inflammatoires chroniques de l'intestin. Médecine humaine et pathologie. Université de Lyon, 2020. Français. NNT : 2020LYSES006 . tel-03173519

HAL Id: tel-03173519
https://theses.hal.science/tel-03173519

Submitted on 18 Mar 2021

HAL is a multi-disciplinary open access archive for the deposit and dissemination of scientific research documents, whether they are published or not. The documents may come from teaching and research institutions in France or abroad, or from public or private research centers.

L'archive ouverte pluridisciplinaire **HAL**, est destinée au dépôt et à la diffusion de documents scientifiques de niveau recherche, publiés ou non, émanant des établissements d'enseignement et de recherche français ou étrangers, des laboratoires publics ou privés.

N° d'ordre NNT : **2020LYSES006**

THESE de DOCTORAT DE L'UNIVERSITE DE LYON
opérée au sein de
Université Jean Monnet

Ecole Doctorale N° EDSIS488
Ecole Doctorale Science, Ingénierie, Santé

Spécialité de doctorat : Immunologie

Soutenue publiquement le 19/05/2020, par :
Eva Michaud

Rôles des immunoglobulines sécrétoires dans les Maladies Inflammatoires Chroniques de l'Intestin

---

Devant le jury composé de :

Pr. Xavier ROBLIN	Université Jean Monnet GIMAP – EA3064	Président
Dr. Nathalie VERGNOLLE	Université Toulouse Paul Sabatier IRSD – UMR 1220, INRA UMR 1416	Rapporteure
Pr. Philippe SEKSIK	Sorbonne Université CRSA – UMR S938	Rapporteur
Pr. Gilles BOSCHETTI	Université Claude Bernard Lyon 1 CIRI – U111/UMR5308	Examinateur
Pr. Stéphane PAUL	Université Jean Monnet GIMAP – EA3064	Directeur de thèse
Dr. Nicolas ROCHEREAU	Université Jean Monnet GIMAP – EA3064	Co-directeur de thèse

À Madeleine, même sans tout comprendre, tu aurais fêté ce manuscrit avec un broyé™

(Tu m'aurais dit d'en laisser pour les autres)

(J'aurais pas écouté)

« Il y a deux réponses à cette question, comme à toutes les questions : celle du poète et celle du savant. Laquelle veux-tu en premier ? »

- Pierre BOTTERO (1964 – 2009)

TABLE DES MATIÈRES

TABLE DES MATIÈRES....2
REMERCIEMENTS....5
TABLE DES ILLUSTRATIONS....8
ABBREVIATIONS....9
RÉSUMÉ....10
PARTIE I - INTRODUCTION....12
Chapitre 1 - Immunité muqueuse....13
A- Architecture de la muqueuse intestinale....13
1- Généralités....13
2- Différentiation cellulaire et fonction barrière....13
3- Particularités de l'épithélium colique....15
4- Sites immuns....16
B- Orientation de la réponse muqueuse....17
1- Maintien de la fonction barrière....17
2- Détection de signaux exogènes....18
3- Lymphocytes muqueux....20
4- Cellules M et immunosurveillance....21
C- Microbiote intestinal....23
1- Métabolisme commensal....23
2- Composition du microbiote....25
3- Induction de l'immunité....26
4- Régulation des espèces pathogènes....27
Chapitre 2 - Immunité sécrétoire....28
A- Caractéristiques des immunoglobulines sécrétoires....28
1- Structure générale des SIgs....28
2- Les glycosylations ont un rôle primordial dans les fonctions des SIg....30
B- Synthèse des SIg dans la muqueuse intestinale....31
1- Production T-indépendante des SIg : origines du répertoire naturel....32
2- Production T-dépendante : réponse à l'infection....34
C- Fonctions des Ig sécrétoires....34
1- Récepteurs....34
2- Transports des antigènes....36

3- Ajustement des processus inflammatoires....37
4- La cellule dendritique orchestre l'orientation de la réponse....39
5- Dualité de l'exclusion immune....39
D- Sélection du microbiote par les SIg et conséquences immunes....42
1- Qui sélectionne la flore ?....42
2- Stratégies microbiennes d'attraction des IgAs....42
3- Promotion de la sécrétion d'IgA par le microbiote :....43
4- La sélection du microbiote répond à des besoins évolutifs au cours du développement....44
5- Effets pathogéniques de la liaison IgA-microbiote....44
E- IgA1 versus IgA2 : impact sur l'homéostasie intestinale....45
1- Commutation isotypique....45
2- Spécificités fonctionnelles....45
3- Interactions avec le microbiote....45
Chapitre 3 – Maladies Inflammatoires Chroniques de l'Intestin....47
A- Des maladies des temps modernes....47
1- Une épidémiologie associée au mode de vie occidental....47
2- Des pathologies à l'étiologie complexe comprenant de nombreux facteurs de risques....50
B- Maladie de Crohn....53
1- Tableau général....53
2- Phase d'initiation....54
3- La dysbiose affecte l'immunité sécrétoire....57
4- Phase chronique....58
C- Rectocolite hémorragique....61
1- Tableau général....61
2- La rupture de la barrière est associée à un mucus défectueux....62
3- Les réponses Th_{17} et Th_9 alimentent l'inflammation médiée par les Th_2....65
D- Options thérapeutiques....67
OBJECTIFS DE LA THÈSE....71
PARTIE II – RÉSULTATS DE LA THÈSE....73
Chapitre 1 – Rôle physiologique des immunoglobulines sécrétoires....73
A- Article 1 : Impact de l'isoforme et de la classe d'IgA sur la réponse immunitaire....74
1- Article et résumé....74
2- Conclusions et perspectives....115
B- Article 2 : Dynamique de transport des SIgM et nouvelles stratégies d'immunisation....117
1- Article et résumé....117
2- Conclusions et perspectives....139

Chapitre 2 – Rôle pathogénique des IgA sécrétoires 141
A- Introduction 142
B- Article 3 : Rôle des polymorphismes NOD2 dans la régulation de la transcytose inverse des IgA dans la maladie de Crohn 144
C- Article 4 : Fonctions des sous-classes d'IgA et impact sur la dysbiose au cours de MICI 181
D- Conclusions et perspectives.....221
Chapitre 3 – Inhibition de la transcytose-inverse en conditions physiopathologiques 225
A- Résumé et article 5 : Compétition pour la transcytose inverse des IgA in vivo au cours de colite à Salmonelle 226
B- Conclusions et perspectives.....244
DISCUSSION GÉNÉRALE.....246
CONCLUSION GÉNÉRALE.....254
ANNEXES 255
Annexe 1 – Revue sur les IgM sécrétoires 255
Annexe 2 – Revue sur les MICI 272
Travaux annexes.....279
RÉFÉRENCES BIBLIOGRAPHIQUES.....334

REMERCIEMENTS

Je tiens à remercier le Professeur Philippe Seksik et le Docteur Nathalie Vergnolle pour avoir accepté d'évaluer ce travail de thèse. Merci également au Professeur Gilles Boschetti, pour avoir évalués mes travaux au cours de ces quatre dernières années avec tant de bienveillance, et pour avoir accepté d'examiner ce manuscrit. Merci au Professeur Xavier Roblin, pour sa disponibilité et sa collaboration à l'ensemble de ces travaux, et pour la présidence de ce jury.

Il en a fallu, du monde, pour venir à bout de ces quatre dernières années. J'aimerais en premier lieu remercier Stéphane et Nicolas. Merci d'avoir parié sur moi, d'avoir encouragé mes suggestions et démêlé mes interrogations. Merci de m'avoir poussé au mieux et de m'avoir respectée. On entend tout un tas d'histoires sordides sur la thèse ; merci d'avoir fait de la mienne un vrai moment d'apprentissage, un moment humain, avec ses hauts et ses bas, mais au cours duquel j'ai toujours progressé, j'ai grandi. Votre fierté est la mienne. Merci pour votre confiance.

Évidemment, ce travail est aussi celui d'un laboratoire. Cher tous, chers GIMAPiens, il n'y a pas eu un jour où je n'ai pas souri dans ce labo. Malgré les aléas de la vie, de la recherche, malgré les doutes et les échecs, il n'est pas un jour où je n'ai pas ri avec vous. C'est très rare, et très précieux, de travailler dans ces conditions. J'ai beaucoup appris à vos côté, des leçons de vie élémentaires (les murs porteurs dans une maison, la géographie, le capital choix des pneus de ma voiture, le dosage idéal du café de 9h,…). Merci également pour votre soutien technique, pour votre patience face à mon désordre organisé (si, si, promis), merci d'avoir toujours cherché à m'aider. Je suis tellement fière de faire partie de cette équipe (même si vous êtes une bande de ronchons café-théinés) (Surtout toi, Charles-Antoine). J'accepte bien sur toutes vos offrandes, sous forme de cookies au chocolat, pour célébrer mon inestimable présence dans vos rangs. Merci à Thomas Bourlet, directeur du GIMAP, pour avoir soutenu mes travaux et cherché des solutions, en ce contexte fin de thèse difficile. Merci à lui et à Marie-Ange, Charles-Antoine, Sofiane, Adrien, Caroline, Coraline, Sébastien, Béa, Melyssa, Grégoire, Cécilia, Benji, Estelle, Amélie, Fabienne, Blandine, Martin (même si t'es très occupé à sauver le monde), Hind et Fabrice pour avoir créé de beaux moments de convivialité, de partage, de rires, de petits-déjeuners. Merci d'avoir fait comme si vous ne saviez pas qui terminait les chocolats du GIMAP (!).

Plus individuellement, je remercie Blandine et Fabienne, qui en plus d'être une formidable équipe technique, occupent la position de coachs de vie, conseillères en relation, organisatrices d'évènements. Merci pour vos conseils avisés, pour votre bienveillance, pour les chasses aux œufs de paques, les arbres de Noëls, … les fêtes d'Halloween ?

Rémi, merci de m'avoir laissé te suivre pendant deux ans comme un petit caneton. Rémi, Martin et Alex, pour cette colloc' de bureau, pour les bons moments et les plus compliqués, merci. Notre amitié m'est précieuse. Merci à Estelle et Amélie, il était grand temps d'apporter un peu de Girl Power dans ces locaux. Merci pour le saucisson, la bière, les blagues de routiers, la danse, les perçages d'oreilles coordonnés et pour vos nombreux coups de main pendant mes manips. Je chéris ces moments. J'écris ces mots en plein confinement et vous me manquez.

Fabrice et Hind, un grand merci à vous. Merci d'avoir relu mes CV, d'avoir cru en moi, d'avoir promu mes candidatures, de m'avoir écoutée et soutenue. Je vous suis si reconnaissante, pour les opportunités que vous m'avez encouragées à saisir, pour nos discussions, pour vos personnalités entières et généreuses.

Plus encore, et pas des moindres, un immense merci à ma famille. Á mes parents, en premier lieu, qui ont soutenu mes projets et ma carrière depuis ce tout premier microscope pour enfant, un Noël il y a vingt ans. Il n'y pas de mot assez fort, il me semble, pour décrire l'amour et le soutien que vous m'avez offert. Merci d'avoir partagé mes joies et mes peines au cours de cette thèse, de vous être extasiés même quand vous ne compreniez pas ce que je disais, d'y croire parfois plus que moi, merci, merci, merci. Merci à mes frères et à ma soeur; Junior, merci d'avoir retapé un PC pour que je rédige dans de bonnes conditions, Lily, merci pour « *et … euuh … ta thèse … ca avance ?* ». Je vous aime (même si vous êtes deux têtes de nœuds). Je fais partie d'une grande (grande !) et belle famille : merci à mes cousins, et mes cousines, à mes oncles et mes tantes, pour avoir regardé mes progrès de loin et de les avoir soutenus à votre manière, d'avoir pris soin de moi à coups de mauvaises blagues et de bon vin. Merci à ma grand-mère, qui n'a pas eu le temps de voir cette page se tourner, j'espère t'avoir rendue fière. La famille c'est aussi les amis qu'on choisis. Merci à Gaétane (et Christophe !), Elise, Naomi, Aurore et Alexis, Anna, Elly et Eva. Here is to a full decade (*decade* guys !) of friendship. Merci d'avoir relu mes travaux, personnels et professionnels, merci pour les conseils, pour les chansons, pour les romans, pour les *pool parties*, les étés Toulousains et Parisiens, la philosophie des religions, les retraites à la mer et à la montagne, pour la douceur et la sécurité de votre amitié. Vous êtes des femmes formidables, et des amies irremplaçables.

Merci à Marc et Rachel, ma famille outre-Atlantique. Je vous aime tant, merci d'avoir prodigué conseils, amour et outrage justifié tout au long de mes travaux. Attendez-moi, j'arrive.

A mes amis Lyonnais (presque), ma petite famille locale. Emilien et Tifanie, pour ces soirées à refaire le monde à grands coups de Monbazillac, pour avoir célébré chaque étape franchie ces cinq dernières années ensemble, je vous souhaite tellement de bonheur. Anne-So et Corentin, compagnons doctorants, merci d'être mon foyer d'accueil, pour les late night memes, les photos de chats, les balades en forêt. Je vous aime d'amour. Sam et Léa, les gars, merci de me laisser voler votre adorable bébé de temps en temps, pour les cours du lundi soir et les burpees du mercredi, merci de vous être extasiés sur la science même quand c'était pas bien clair ce que je vous racontais. Merci d'être entiers, vous êtes parfaits.

Merci à tous ceux qui ont relu ce manuscrit, Stéphane et Nicolas, bien sûr, mais aussi Emilien, Gaétane, et Nathalie. Merci d'avoir pris sur votre temps, en pleine crise sanitaire et dans des délais restreints, pour moi.

Pour clôturer ces remerciements francophones, merci à toute l'équipe de l'ESTBB. Merci de m'avoir accueillie dans vos rangs pour ces derniers mois de thèse, ils en ont été grandement enrichis. Merci d'avoir accepté Gigi La Beaufétie. Nicolas (BFF), Mathieu, Monique, merci pour vos encouragements, pour « *Mais non c'est normal c'est la fin de thèse* », pour les titres et les inuendos, et les plateaux de fromage. J'ai tellement profité, tellement ri, à vos côtés, merci beaucoup.

Finally, few non-French-speaking people have also contributed immensely to the success of this PhD. Amongst them is the entire Fangasm community, thank you for the safe positive place, for making all weirdoes feel at home in this small corner of the Internet. Emily, Candis and Juli, thank you the joy you have sprinkled into my life over the past years. Kristin, you are honestly a gift to the world, I treasure our friendship and I missed you before I knew you (take that, Wes).

I would also like to thank Brandon Sanderson, whose stories I've listened to as I performed most of the experiments presented in this manuscript. The only reason no spren appears on the following diagrams and figures, is because all were unjustly edited out of the creative process. Your stories have made my heavier days so much lighter. Thank you for turning loss into Ideals.

And finally, Sooz, you get the last lines. You already know, by now, how much of a game-changer you have been. I hope I get to be half the woman you are. Here is to scholars and poets.

TABLE DES ILLUSTRATIONS

FIGURE 1 – ARCHITECTURE DE LA MUQUEUSE INTESTINALE. 14

FIGURE 2 – NATURE DES JONCTIONS ENTRE CELLULES EPITHELIALES INTESTINALES. 15

FIGURE 3 – RELATIONS HOTE-MICROBES DANS LE COLON. 16

FIGURE 4 – ROLE DE L'AUTOPHAGIE DANS L'IMMUNITE INNEE MUQUEUSE. 18

FIGURE 5 – VOIES IMPLIQUEES DANS L'INTEGRATION DE SIGNAUX INNES ENGAGES PAR LES PRR. 19

FIGURE 6 – RELATIONS ENTRE LES POPULATIONS LYMPHOCYTAIRES MUQUEUSES. 20

FIGURE 7 – RECONNAISSANCE DE L'ANTIGENE A LA SURFACE DES CELLULES M. 22

FIGURE 8 – EFFETS BENEFIQUES DES SCFA DANS L'HOMEOSTASIE INTESTINALE. 25

FIGURE 9 – ROLE DE LA PRODUCTION DE SCFA DANS LA PRODUCTION DE VITAMINE ET DU METABOLISME CELLULAIRE. 26

FIGURE 10 – STRUCTURE DES ISOFORMES D'IMMUNOGLOBULINE A HUMAINE. 29

FIGURE 11 – STRUCTURE DES ISOFORMES D'IMMUNOGLOBULINE M HUMAINE. 30

FIGURE 12 – PRODUCTION T-INDEPENDANTE ET T-DEPENDANTE DES IGA INTESTINALES 32

FIGURE 13 - INDUCTION DE LA COMMUTATION DE CLASSE (CSR) DANS LES LB MUQUEUX. 33

FIGURE 14 – RECEPTEUR AUX IGA ET IGM HUMAINES. 36

FIGURE 15 – TRANSCYTOSE ET TRANSCYTOSE INVERSE DES IGA. 37

FIGURE 16. FONCTIONS MUQUEUSES DES SIGA. 38

FIGURE 17 – MODELES D'EXCLUSION IMMUNE MEDIEES PAR LES SIGA. 41

FIGURE 18 – MODELE DES FONCTIONS SPECIFIQUES DES IGA1 ET DES IGA2. 46

FIGURE 19 – ÉPIDEMIOLOGIE DE LA MALADIE DE CROHN. 48

FIGURE 20 – ÉPIDEMIOLOGIE DE LA RECTOCOLITE HEMORRAGIQUE. 49

FIGURE 21 – PHENOTYPE DE LA MALADIE DE CROHN ET DIAGNOSTIC. 54

FIGURE 22 – PHYSIOPATHOLOGIE DE LA MALADIE DE CROHN. 55

FIGURE 23 – ROLE DES CYTOKINES PRO-INFLAMMATOIRES DANS LA MALADIE DE CROHN. 60

FIGURE 24 – DIAGNOSTIC ET PHENOTYPE DE LA RECTOCOLITE HEMORRAGIQUE. 61

FIGURE 25 – LESIONS DISTINCTES ASSOCIEES A LA MALADIE DE CROHN ET A LA RECTOCOLITE HEMORRAGIQUE. 62

FIGURE 26 – PHYSIOPATHOLOGIE DE LA RECTOCOLITE HEMORRAGIQUE. 63

FIGURE 27 – ROLE DES CYTOKINES PRO-INFLAMMATOIRES DANS LA RECTOCOLITE HEMORRAGIQUE. 66

FIGURE 28 – MODE D'ACTION DE TRAITEMENT ACTUELS DES MICI. 70

FIGURE 29 – MISE AU POINT DE LA PCR D'AMPLIFICATION DES REGION VARIABLES DES GENES DES CHAINES LOURDES DES IG. 222

TABLEAU 1 – BACTERIES PRODUISANT DES SCFA ET DES VITAMINES 24

TABLEAU 2 – BACTERIES IMPLIQUEES DANS DES MODELES DE MICI 52

TABLEAU 3 – TRAITEMENTS DES MICI ET EFFETS SECONDAIRES 69

TABLEAU 4 – NOMBRE DE CLONES IMMORTALISES PAR PIECE CHIRURGICALES (A, B, C). 222

ABBREVIATIONS

ADA	Anticorps anti-médicament
ADN	Acide désoxyribonucléique
ADCC	Cytotoxicité dépendante des anticorps
AMIS	Sélection immune médiée par les anticorps
AMP	Peptides antimicrobiens
Asn	Asparagine
Ca	Chaîne constante de l'immunoglobuline A
dIgA	IgA dimérique
CDR	Région déterminant la complémentarité
CLR	Récepteur aux lectines de type C
DC	Cellules dendritiques
FAE	Épithélium associé au follicule
FcαR, FcμR, Fcα/μR	Récepteurs au IgA, IgM et IgA/IgM
FMT	Greffe de microbiote fécal
GC	Centre germinatif
HFD	Régime riche en gras
IEC	Cellules Epithéliales Intestinales
IFN	Interféron
Ig	Immunoglobuline
IL	Interleukine
ILC	Lymphocytes innés
ILF	Follicule lymphoïde isolé
LB	Lymphocytes B
LT	Lymphocytes T
LPS	Lipopolysaccharide
MALT	Tissu lymphoïde associé à la muqueuse
MC	Maladie de Crohn
MICI	Maladies inflammatoires chronique de l'intestin

mIgA	IgA monomérique
MLN	Ganglion mésentérique
MoDC	Cellules dendritiques dérivées de monocytes circulants
MZB	lymphocytes de la zone marginale
NEC	Colite entérique nécrosante
NeuAc	Acide sialiques
NF-kB	*Nuclear factor kappa B*
NK	Cellule natural killer
NLR	Récepteur de type NOD
PAR	Récepteur activé par les protéases
PIgR	Récepteur aux immunoglobulines polymérique
PP	Plaque de Peyer
PRR	*Pathogen recognition receptors*
PUL	Locus d'utilisation des polysaccharides
RCH	Rectocolite hémorragique
ROS	Espèces réactives de l'oxygène
RT	Transcytose inverse
SC	Pièce sécrétoire
SCFA	Acides gras à chaîne courte
SFB	Bactéries segmentées filamenteuses
SIg, SIgA	Immunoglobuline (A) sécrétoire
TD	Voie T-dépendante
T_{fh}	Lymphocyte T follicular helper
Th	Lymphocyte T helper
TI	Voie T-indépendante
TLR	Récepteur de type toll
VH	Domaine variable de la chaîne lourde
VL	Domaine variable de la chaîne légère
WT	Phénotype sauvage

RÉSUMÉ

Les maladies inflammatoire chroniques de l'intestin sont des pathologies qui touchent les pays industrialisés ou en voie d'industrialisation. Elles sont particulièrement recensées en Amérique du Nord et en Europe de l'Ouest selon un gradient Nord-Sud, avec 3 à 20 nouveaux cas par an pour 100 000 habitants. L'augmentation constante de ces chiffres et des zones géographiques touchées en fait des enjeux majeurs de santé publique. Parmi les MICI, se distinguent principalement la maladie de Crohn (MC) et la rectocolite hémorragique (RCH). Toutes deux présentent une perte de la diversité microbienne intestinale, appelé dysbiose, et la mise en place de boucles inflammatoires recrutant des lymphocytes T, des phagocytes, et une importance sécrétion d'anticorps et cytokines pro-inflammatoires au niveau des sites lésés.

Les immunoglobulines sécrétoires (SIg) sont responsables de l'induction de la tolérance immune envers les membres de la flore commensale. Les SIgA en sont les principales actrices, bien qu'un rôle pour les SIgM dans le maintien du mutualisme commensal émerge progressivement des récents travaux sur le sujet. Chez l'homme, deux sous-classes d'IgA existent, les IgA1 et les IgA2. Seules les IgA2 ont la capacité, une fois sécrétée, d'être prises en charge par les cellule M des plaques de Peyer (PP) pour présenter l'antigène à une cellule dendritique (DC) DC-SIGN^{+}. Ce processus, appelé transcytose inverse (RT), requiert la liaison des récepteurs Dectin-1 et Siglec-5 à la membrane apicale des cellule M.

Le premier objectif de ma thèse est donc de démontrer que les IgM et les IgA, selon leur sous-classe et leur structure, peuvent avoir une fonction différentielle dans l'homéostasie intestinale. A cet effet, nous avons mis en place un modèle de DC dérivées de monocytes circulants, les moDC, co-cultivées avec différents isoformes et sous-classes d'IgA, pour comparer leur effet sur le phénotype et la transcription dans les DC. La RT est évaluée dans un modèle *in vitro* de follicule associé aux épithéliums (FAE), et dans un modèle *in vivo* de ligature intestinale, puis au cours d'immunisations orales et nasales chez la souris. Nous montrons (1) que les DC sont activées de manière différentielle selon qu'elles rencontrent une IgA1 ou une IgA2 monomérique, dimérique ou sécrétoire, (2) que l'affinité pour les différents récepteurs

aux IgA conditionne ces interactions, et (3) que les SIgM sont également capables d'effectuer la transcytose inverse pour promouvoir une immunité protectrice Th1-dépendante.

Le second objectif de ma thèse est d'élucider la composition du microbiote sélectionné par les deux sous-classes d'IgA dans la MC et dans la RCH, et l'impact des polymorphismes génétiques sur leur trafic intracellulaire. En purifiant ces IgA séparément, et le microbiote qui leur est associé, puis par l'étude de la RT *in vitro*, nous mettons en évidence une augmentation du taux de RT des IgA1 et de la sélection par celles-ci de bactéries bénéfiques pour l'intestin, dans la MC. De plus, les polymorphismes sur le gène NOD2 induisent une augmentation de la prise en charge des IgA chez les patients atteints de MC. Par contraste, la RCH présente une perte du transport des IgA toutes sous-classes confondues, ainsi qu'une diminution de la poly-réactivité. Ces constats inédits font le lien entre dysbiose microbienne et dérèglement humoral chez les patients atteints de MICI.

Enfin, le dernier objectif de ma thèse est la recherche de nouvelles voies thérapeutiques visant à limiter la transcytose inverse des IgA, pour diminuer l'apparition et la sévérité des symptômes associés à une colite sévère chez la souris. Nous avons donc induit une colite à Salmonelle chez la souris, après avoir prétraité les animaux avec deux glucans microbiens : le zymosan et le pullulan, promoteurs réponses Dectin-1 et Dectin-2 dépendantes, respectivement. Tous deux se révèlent protecteurs dans le modèle. Le zymosan est dépendant de sa fonction d'activation des TLR, et le pullulan, bien qu'il favorise la survie des animaux, ne semble pas affecter les paramètres inflammatoires. Ils sont tous deux limitants pour la translocation bactérienne dans la PP et empêchent la réabsorption des IgA par celles-ci.

Ce travail de thèse propose ainsi de nouvelles données quant à la mécanistique sous-jacente à l'établissement de la dysbiose intestinale. Il ouvre également la voie vers de nouvelles stratégies thérapeutiques visant à limiter la réactivité immunitaire face aux espèces bactériennes dysbiotiques. Ces stratégies peuvent s'appliquer non seulement au soin des MICI, mais aussi à celui de maladie métabolique dans lesquelles la dysbiose alimente la pathologie, telles que l'obésité ou le diabète de type 2.

PARTIE I - INTRODUCTION

Chapitre 1 - Immunité muqueuse

A- Architecture de la muqueuse intestinale

1- Généralités

L'intestin est tapissé d'un épithélium qui repose sur une couche de tissu conjonctif, la *lamina propria*. Cette couche monocellulaire, composé des différentes variétés d'entérocytes, s'organise en villosités couvrant une surface d'environ 250 m^2. La muqueuse intestinale contient également plus de 10^{18} bactéries, qui composent la flore commensale et dont la diversité varie selon le site du tube digestif. Certaines villosités débouchent sur une crypte intestinale, au fond de laquelle se trouvent les cellules souches intestinales, cellules au potentiel de différentiation multiple qui permet le remplacement des différents acteurs cellulaires de la barrière. L'intestin possède également son propre système nerveux autonome, qui stimule le passage du bol alimentaire et des matières fécales, mais aussi la sécrétion d'hormones, neurotransmetteurs et neuropeptides qui promeuvent l'homéostasie[1]. Les fonctions de l'intestin sont donc multiples, il doit permettre la dégradation des aliments ingérés par l'hôte, l'absorption des nutriments liés à cette dernière, ainsi que le développement d'une réponse adaptée aux différents microorganismes rencontrés.

2- Différentiation cellulaire et fonction barrière

Quatre types d'entérocytes sont retrouvés dans la muqueuse : les cellules épithéliales intestinales (IEC), les cellules de Paneth, les cellules caliciformes, et les cellules *microfold* (M) (**Fig. 1**). Les IEC sont des cellules ciliées polarisées qui constituent une barrière naturelle contre l'invasion des tissus par des microorganismes ou des protéines étrangères[2]. Elles permettent également le transport d'anticorps vers la lumière intestinale (transcytose). Elles représentent la majorité des cellules de l'épithélium intestinal. Au fond des cryptes intestinales, se trouvent les cellules de Paneth, dont le rôle principal est la production de peptides antimicrobiens (AMP)[3]. Ces derniers s'accumulent sous forme de granules dans le cytosol et sont secrétés en réponse à l'interleukine(IL)-22 et l'IL-18[4]. Les AMP permettent la ségrégation du microbiote et éliminent les espèces opportunistes. Deux grandes familles d'AMP sont produites par les cellules de Paneth : les défensines (α-, β-, et θ-défensines) et les cathélicidines, qui ont toutes deux pour but de former un pore dans la membrane bactérienne [5]. Les α-

défensines ont un rôle privilégié dans la prévention de l'invasion des tissus par des bactéries pathogènes [6], en particulier *Salmonella typhimurium* [7].

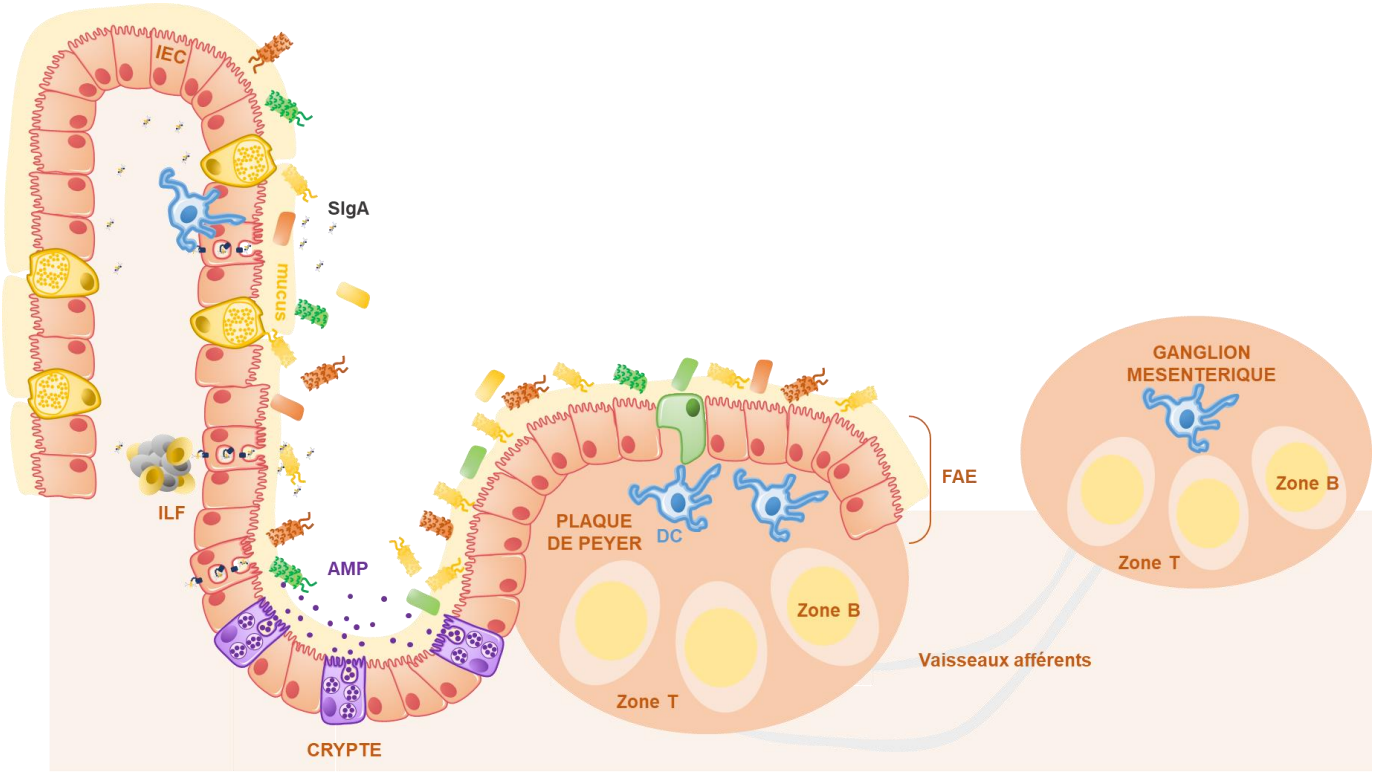

Figure 1 – Architecture de la muqueuse intestinale.
Les cellules caliciformes (jaune) qui jonchent l'épithélium sécrètent le mucus, les cellules de Paneth (violet) synthétisent des peptides antimicrobiens au fond des cryptes intestinales et entretiennent les cellules souches intestinales, et les cellules épithéliales intestinales tapissent l'épithélium et assurent la détection de signaux innés. Les signaux immuns sont intégrés au niveau de la plaque de Peyer (PP) localement, grâce à l'échantillonnage des antigènes par les cellules M (vert) et les DC de la PP, et du ganglion mésentérique en distal.

L'épithélium intestinal est également recouvert d'une ou plusieurs couches de mucus, qui est produit par les cellules caliciformes[8]. Ces dernières, des cellules polarisées à forte capacités de sécrétion, produisent différentes mucines qui s'organisent en réseaux plus ou moins lâches et retiennent à la fois les bactéries de la flore intestinale, mais aussi les différents peptides synthétisés par les cellules de Paneth, les cellules épithéliales et les bactéries de la flore[8,9]. Tous ces entérocytes sont soudés les uns aux autres par des jonctions serrées et des jonctions adhérentes (**Fig. 2**) conférant à la muqueuse sa propriété barrière.

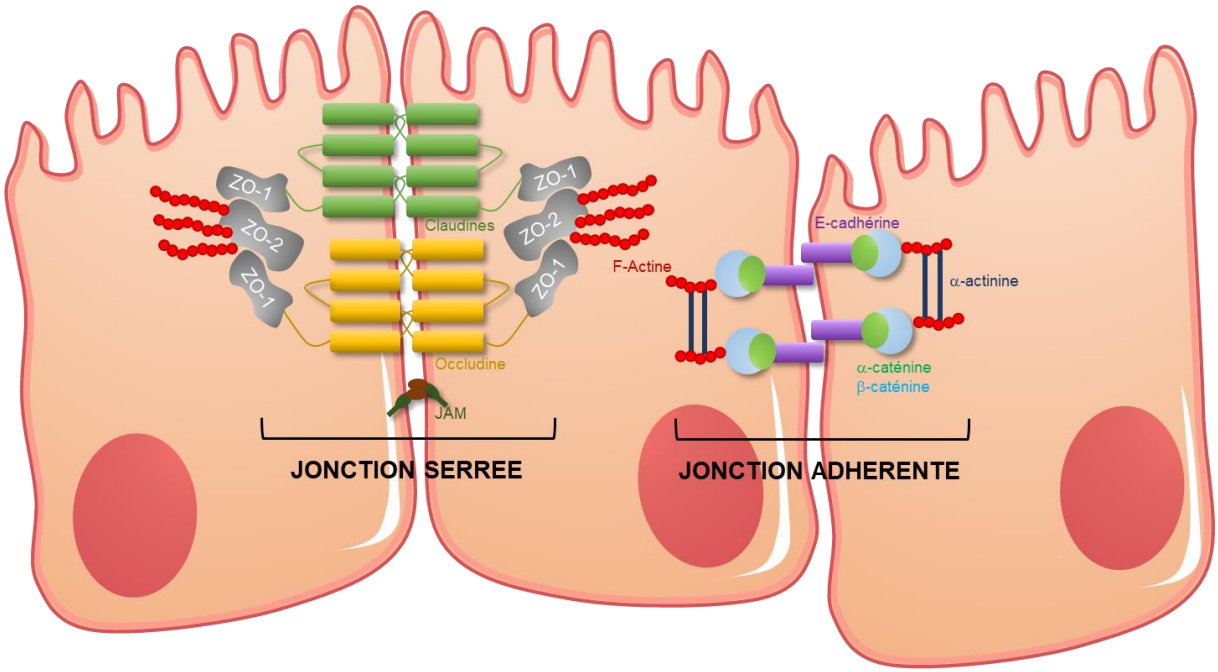

Figure 2 – Nature des jonctions entre cellules épithéliales intestinales.
Chaque cellule est reliée à la suivante via des jonctions serrées et des jonctions adhérentes. Les jonctions serrées sont localisées à la membrane apicale latérale, et sont constituées de trois protéines transmembranaires : les claudines, les occludines, et les complexes JAM (Junctional Adhesional Molecules). Celles-ci interagissent directement avec le cytosquelette d'actine grâce aux zonulines (ZO-1). Les jonctions adhérentes reposent essentiellement sur l'association entre E-cadhérines et α- et β-caténines, également connectées au cytosquelette d'actine. D'après Collins, et al. *Physiol Rep (2017).*

3- Particularités de l'épithélium colique

Le maintien des IEC coliques dépend des récepteurs activés par les protéases intestinales (PAR), ceux-ci régulant la prolifération et de la survie des cellules souches intestinales [10]. La distinction entre l'intestin grêle et le colon se traduit par un gradient d'expression génique qui évolue le long du tissu [11]. Le colon, où se trouvent beaucoup plus de bactérie par rapport à l'intestin grêle, contient en effet une plus forte concentration de cellules caliciformes [11,12]. La distribution et le phénotype de ces cellules varient également selon qu'elles se trouvent près des cryptes ou non [11]. L'intestin grêle présente plutôt des cellules de Paneth [11,12]. Ce nombre accru de cellules caliciformes permet la sécrétion d'une double couche de mucus qui régule les interactions hôte-bactéries (**Fig. 3**). Cette couche supplémentaire établit une zone tampon entre l'hôte et la flore, et limite l'adhérence bactérienne à l'épithélium. Composée de mucines particulièrement glycosylées, la couche la plus éloignée de ce mucus promeut l'ancrage des bactéries de la flore *via* les O-glycans des mucines [13]. Le colon contient également des cellules

sensibles au pH intestinal encore méconnues et dont le profile transcriptomique indique un rôle dans la régulation de la satiété et de la survie cellulaire[11].

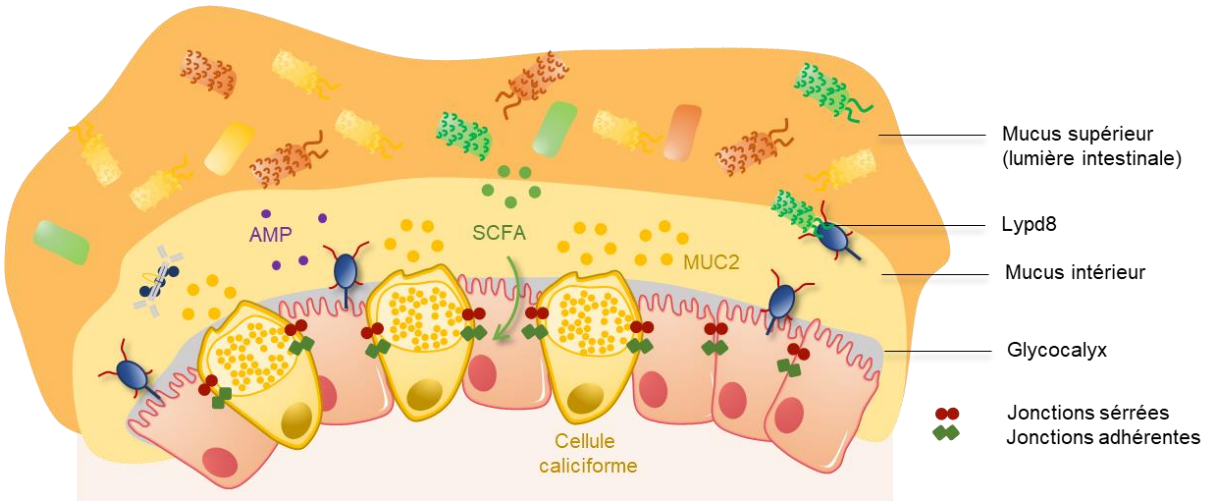

Figure 3 – Relations hôte-microbes dans le colon.
Dans le colon, l'abondante flore commensale est séparée de l'épithélium par une couche de mucus intérieur contenant des mucines polymérisées (MUC2 en est la principale). Cette couche retient également les SIgA, les AMP 9 moins abondants dans le colon) et les métabolites bactériens (SCFA). Lypd8, protéine ancrée des les glycosylphosphatidylinositol (GPI) de la membrane des IEC, promeut la ségrégation entre les deux zones en liant les bactéries intestinale limitrophes, en particulier les bactéries flagellées.

4- Sites immuns

Le système immunitaire muqueux, interaction directe et étroite avec l'épithélium qui lui est associé (MALT), est un bras à part entière de l'immunité possédant plusieurs sites inducteurs. Le premier est la plaque de Peyer (PP)[14] (**Fig. 1**), dont le nombre et la localisation varient entre individus, et au cours de la vie de ceux-ci[15]. Située entre deux cryptes intestinales, la PP forme un dôme sous la muqueuse qui comprend trois grandes structures : (i) une zone folliculaire, (ii) une zone inter-folliculaire, et (iii) l'épithélium associé au follicule (FAE) (**Fig. 1**). Dans le FAE, les cellules M permettent le transport d'antigènes, de protéines, et de microorganismes depuis la lumière intestinale vers la zone folliculaire (cf chapitre B-4). Les centres germinatifs (GC) des follicules de la PP comprennent des lymphocytes B (LB), des cellules dendritiques (DC) et des macrophages[14]. Cet organe lymphoïde secondaire permet ainsi une réponse rapide et locale qui est associée à une forte prolifération immunitaire. Les cellules naïves et activées circulent entre la PP et le ganglion mésentérique (MLN) le plus proche.

La muqueuse peut également comprendre des follicules lymphoïdes isolés (ILF)[16], retrouvés essentiellement dans le colon et dont la fonction est encore peu comprise. Ils sont induits en réponse à des signaux de la flore commensale[17]. Contrairement à la PP, un ILF est un agrégat éphémère d'environ un millier de cellules qui tend à disparaître lorsque le signal

diminue. Bien que sa localisation au sein du tissus muqueux soit assez variable, il possède néanmoins lui aussi un FAE, qui comprend également des cellules M[18].

B- Orientation de la réponse muqueuse

La protection de la muqueuse intestinale repose sur plusieurs mécanismes de l'immunité, dont l'induction de voies innés de transduction des signaux muqueux endo- et exogènes.

1- Maintien de la fonction barrière

La sécrétion constitutive de protéase par les cellules épithéliales préserve la muqueuse de l'adhérences bactérienne à l'épithélium et régule les interactions hôte-microbes, notamment en limitant la formation de biofilms [19]. La structure en brosse de la membrane apicale des IEC permet ensuite l'immobilisation et l'invagination rapide de molécules et de microorganismes. Dans les IEC et les cellules de Paneth murines, l'autophagie prend en charge l'élimination de ces bactéries intracellulaires[3] (**Fig. 4**). Les IEC initient alors l'inflammation par la transduction des signaux exogènes, issus de pathogènes[20], et endogènes tels l'IL-1 produite par les cellules M de la PP et le TNF-α[21]. L'ensemble converge vers la voie NF-κB, facteur de transcription clé de l'inflammation. La réponse des IEC inclut, entre autres, la sécrétion d'IL-18 [4] et l'expression de signaux de domiciliation, tels que l'IL-8, GRO-α, GRO-β, MCP-1 ou MIP-3α [22–25] pour le recrutement de neutrophiles et de macrophages. L'inflammation impacte néanmoins la stabilité des jonctions serrées et adhérentes : l'interféron(IFN)-γ module la synthèse des protéines nécessaires à la mise en place de ces jonctions[26]. En parallèle donc, les IEC répondent à l'IL-36 pour promouvoir la réparation de la muqueuse au cours de l'inflammation[27]. L'IL-15, l'IL-13[28,29], et les métabolites commensaux[30], également recrutés lors de l'inflammation, favorisent la sécrétion de mucus par l'hôte, et donc le maintien de l'intégrité épithéliale.

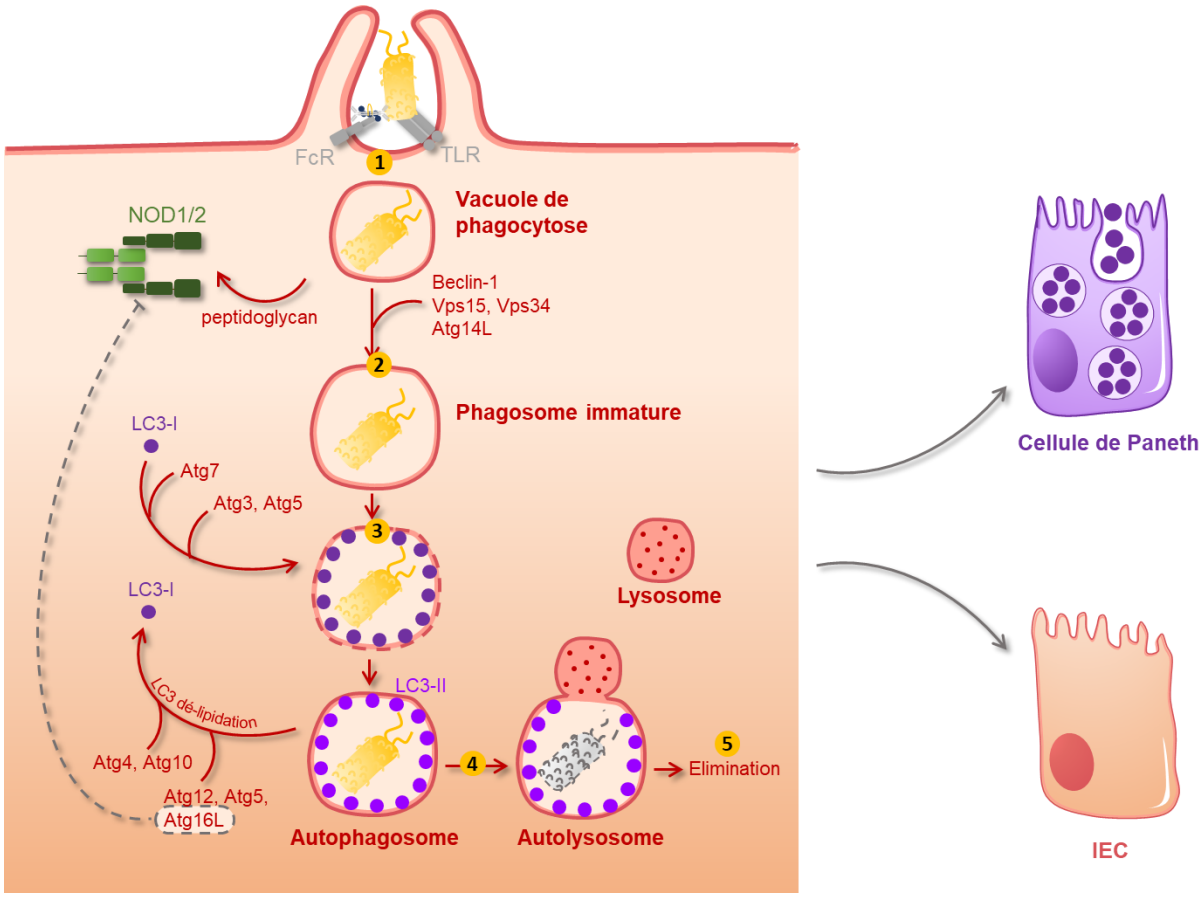

Figure 4 – Rôle de l'autophagie dans l'immunité innée muqueuse.
L'internalisation de pathogènes par les IEC ou les cellules de Paneth à lieu selon un mode de reconnaissance qui est encore débattu. Le cargo antigénique est dégradé en cinq étapes : (1) initiation, (2) formation de phagosome et nucléation de la membrane, (3) expansion du phagosome, (4) fusion avec un lysosome et (5) dégradation du contenu, régulées par les protéines Atg. L'initiation requiert l'assemblage du complexe Vps34-Beclin1. Atg12 et LC3 (light chain 3), sont ensuite nécessaires à la formation de l'autophagosome. LC3 s'associe aux microtubules pour séquestrer le cargo. Atg12 est ensuite conjuguée à Atg5 par Atg7 dans complexe protéique avec Atg16L1. Grâce à Atg7 et Atg3, il permet de conjuguer LC3 avec des phosphatidylethanolamine (PE), pour former la forme LC3-II qui s'insère dans la membrane de l'autophagosome. La maturation de l'autophagosome se termine par la fusion avec un lysosome en un autolysosome. Les hydrolases lysosomales dégradent ensuite le contenu puis le complexe Atg5-Atg12-Atg16L1 dé-lipide LC3-II en LC3-1. Les peptidoglycans bactériens internalisés activent NOD2, régulé par la protéine Atg16L1 selon un mode autophagie-indépendant.

2- Détection de signaux exogènes

L'homéostasie muqueuse repose sur des senseurs innés, les *pathogen recognition receptors* (PRR), afin d'ajuster la tendance naturelle de la muqueuse à l'inflammation (**Fig. 5**). Pour cela, les cellules épithéliales expriment de nombreux *Toll-like receptors* (TLR), *NOD-like receptors* (NLR), et récepteurs aux lectines de type C (CLR), répondant à des signatures antigéniques microbiennes conservées. Ainsi, l'activation des TLR2[31], 4[32], et 7[33] par les métabolites bactériens limitent l'induction de l'inflammation envers la flore commensale et

favorise la sécrétion d'AMP[33] pour contrer l'expansion de bactéries opportunistes [34]. Cette activation soutient la production d'anticorps dans la muqueuse[35–37]. Comme elle tend naturellement à augmenter la perméabilité intestinale[38], la transcription des gènes *tlr* est finement régulée par l'IL-4 et l'IL-13[39].

A l'opposée, l'inflammation est promue par les NLR cytosoliques NOD1 et NOD2, ainsi que les récepteurs aux lectines de type C (CLR) membranaires Dectine-1, -2, et -3. L'activation de NOD1 et NOD2 par divers peptidoglycane bactériens converge vers l'activation de la voie NF-κB[40], et est régulée par la protéine de l'autophagie Atg16[41]. L'engagement de Dectin-1 par les N-glycosylations portées par les β-glucans fongiques[42] et par les anticorps sécrétoires muqueux [43] conduit à l'activation de voies lymphocytaires Th_1/Th_{17} [4244,45]. Dectin-2 recrute l'inflammasome NLRP3 lors d'infections fongiques[46,47] et parasitaires[48], notamment par la reconnaissance de motifs mannose [49].

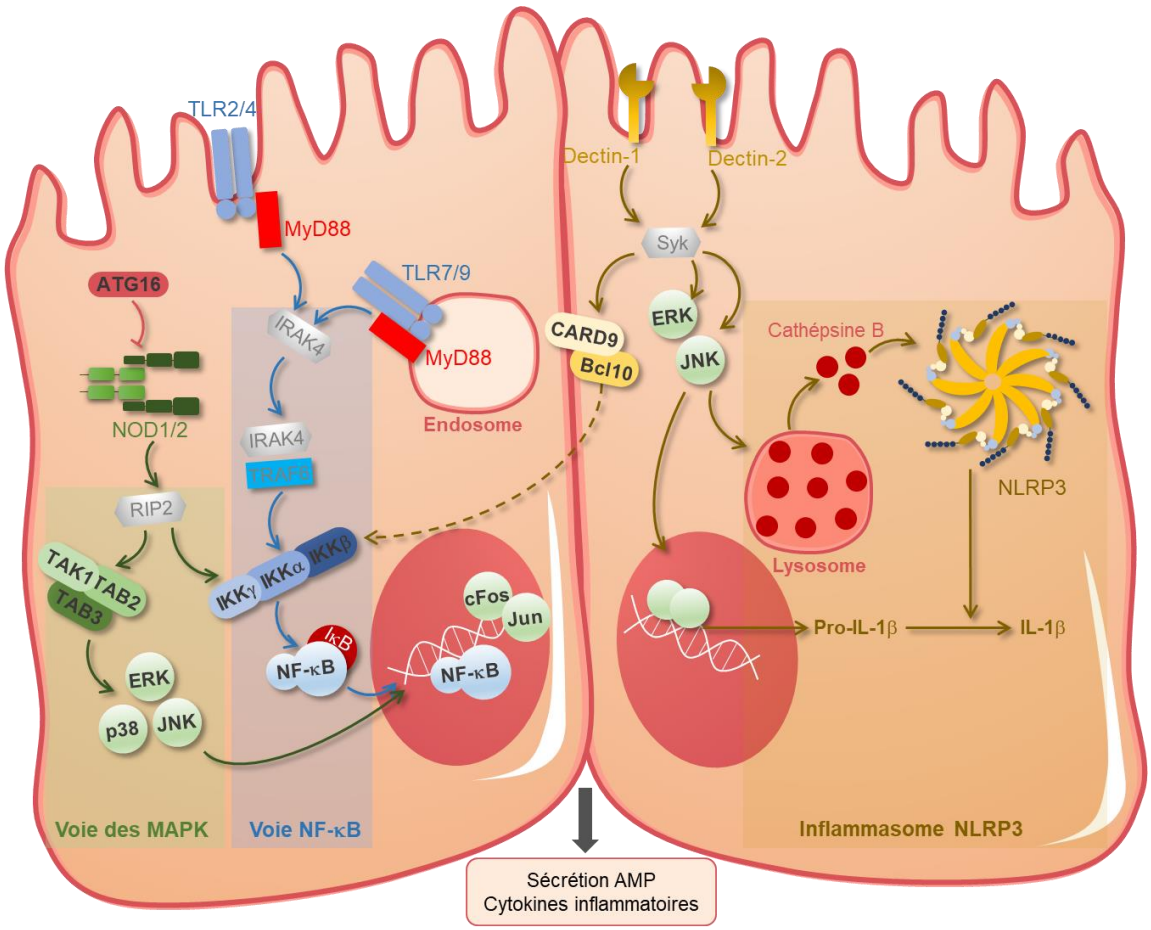

Figure 5 – Voies impliquées dans l'intégration de signaux innés engagés par les PRR.
L'activation des recepteurs Toll, NOD et Dectin converge vers la voie de signalisation NF-κB, maintenu inactif par l'inhibiteur IκB, libéré par le complexe IKKγ–α–β. L'activation par les TLR requiert la phosphorylation de MyD88 puis d'IRAK4. Les recepteurs NOD recrutent eux l'adapteteur RIP2 par interaction avec des domaine CARD. Celui-ci peut ensuit interagir avec la voie NF-κB via l'interaction avec des proteines TRAF, ou bien avec la voie des MAPK (Mitogen Activated Protein Kinase). Se forme ainsi un Nodosome, une plateforme de signalisation. Les facteurs de transcriptions ERK et JNK recruté par l'activation des TLR ou de Dectin-1 et – 2 permet d'induire la rupture du lysosome et stimule la formation de l'inflammasome NLPR3.

3- Lymphocytes muqueux

Le long de la *lamina propria*, plusieurs familles de lymphocyte atypiques, les ILC, assurent la réponse à un stress environnemental par un premier niveau de cytotoxicité et/ou la sécrétion de cytokine. Les ILC1 sécrètent de l'IFN-γ et des médiateurs cytotoxiques[50], les ILC2 de l'IL-4 et de l'IL13[50] et les ILC3 de l'IL-17 [51]. Les cytokines des ILC sont complémentaires à celles des LT CD4$^+$ *helper* (Th) pro-inflammatoires (**Fig. 6**) comprenant les Th_1, Th_2, Th_9, Th_{17}, et Th_{22}.

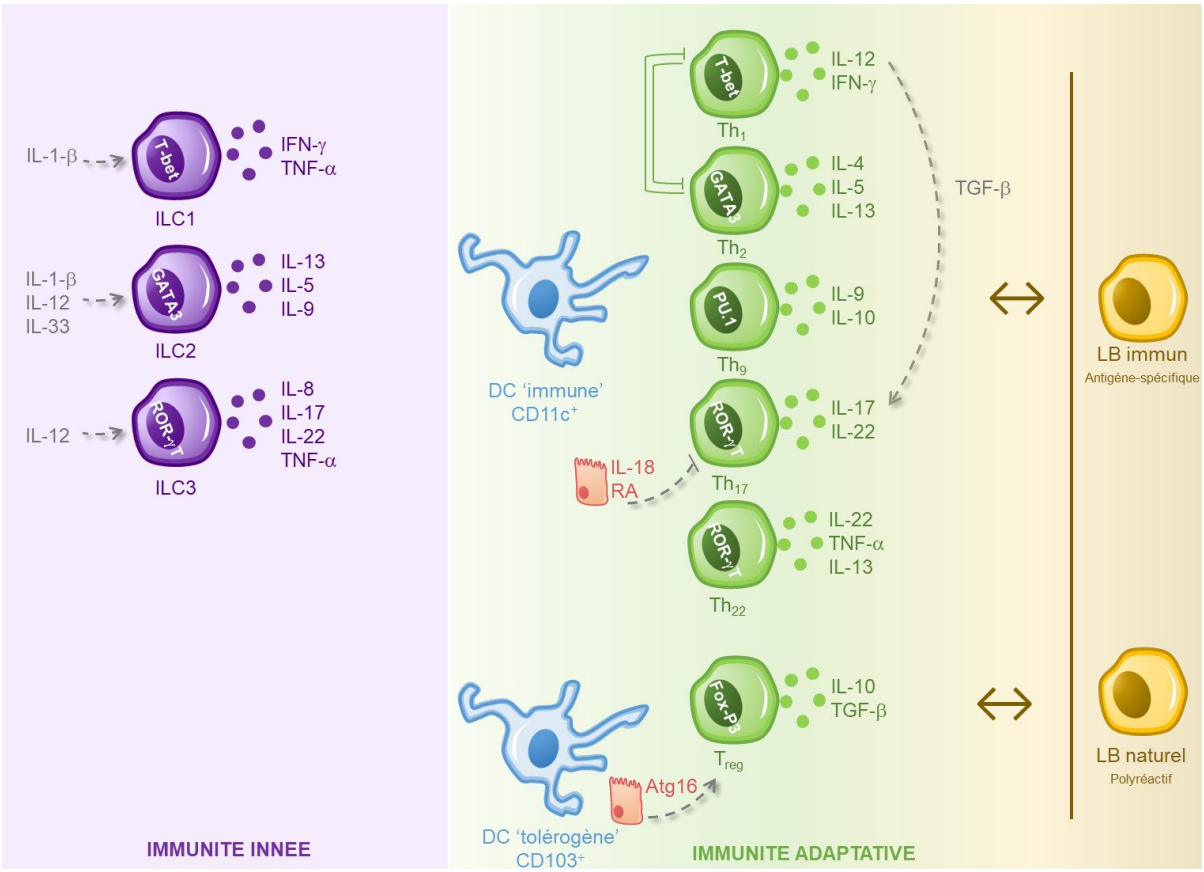

Figure 6 – Relations entre les populations lymphocytaires muqueuses.
Les LT helper et les ILC expriment un panel de cytokine et de facteur de transcriptions identiques. Les signaux tissulaires activent les ILC instantanément. Les LT helper doivent d'abord être sélectionnés puis s'expandre selon la spécificité de leur récepteur (TCR). Les ILC1 et Th_1, par la sécrétion d'interféron, protègent des virus, protozoaires et des bactéries intracellulaires. Les ILC2, les Th_2 et les Th_9 répondent aux helminthes. Les ILC3, les Th_{22} et les Th_{17} répondent aux champignons et aux bactéries extracellulaires. Il est accepté que les LB produisant des IgA de haute affinité (LB « Immuns ») stimulent l'immunité Th_1, Th_2, et Th_{17}, tandis que les LB naturels, produisant des Ig poly-réactives, tendent à stimuler l'expansion de T_{reg}, ce qui favorise le mutualisme commensal.

Les Th_1, caractérisés par la sécrétion d'IL-12 et d'IFN-γ, induisent principalement des réponses cytotoxiques et une forte phagocytose par les phagocytes résidents des tissus, tandis

que les Th_2, caractérisés par la sécrétion d'IL-4, d'IL-5 et d'IL-13[52], soutiennent l'immunité humorale [53]. La transition d'un phénotype Th_1 vers un phénotype Th_{17} est induite par le TGF-β et d'IL-6 au cours de l'inflammation [54]. Elle favorise l'élimination de bactéries extracellulaires par la sécrétion d'IL-17 et d'IL-22 [55]. Le rôle des Th_9 est encore méconnu, mais il existe un axe régulateur entre ILC2 et Th_9, caractérisé par la sécrétion d'IL-9, qui apparaît très impliqué dans l'induction de MICI, d'allergies alimentaires, et de l'asthme [56].

Ces phénomènes inflammatoires sont tempérés par les LT régulateurs (T_{reg}) : ils induisent la tolérance immune envers les antigènes luminaux alimentaires ou commensaux. Les T_{reg} sont induits au niveau de la PP par les DC $CD103^+$ [57] et se distinguent par un phénotype $CD4^+$ $FoxP3^+$ et la sécrétion d'IL-10. Chez le nouveau-né humain, la maturation de T_{reg} est associée à la colonisation de la muqueuse [58].

Tous ces LT peuvent, en collaboration avec les DC muqueuses, activer des LB qui sécrètent majoritairement de l'IgA indispensable à la protection des muqueuses et dont nous discuterons ultérieurement.

4- Cellules M et immunosurveillance

La polarisation des réponses T est étroitement associée aux cellules M du FAE. La cellule M est spécialisée dans l'échantillonnage des antigènes luminaux (**Fig. 7**) [59–62] grâce à : (i) l'importante glycosylation de la membrane apicale favorisant les interactions avec les lectines microbiennes [59,63]; (ii) l'expression membranaire de TLR [64,65] et des CLR [43] et (iii) les protéines membranaires spécialisées comme la GP-2, qui reconnaît les protéines FimH bactériennes [59], ou les Siglecs (liant les acides sialiques)[43,66]. L'endocytose de ces antigènes par transcytose inverse, complexés ou non, est en partie promue par la flore commensale[62].
Les DC et macrophage muqueux s'insèrent dans la poche intra-épithéliale de la cellule M (**Fig. 7**) : les antigènes leurs sont transmis *via* des prolongements TNT (*Tunneling nanotubes*), après quoi ils sont présentés aux populations T effectrices et stimulent la production d'IgA sécrétoire [62,67]. L'établissement de réponses antigènes-spécifiques Th_1, Th_{17}, et Th_{22} [68] requiert l'axe TLR-Myd88 [64] au niveau des cellules M. Cette proximité immédiate limite la dissémination des microorganismes dans la muqueuse [59,62,67]. Cependant, la cellule M constitue justement une voie d'entrée pour les pathogènes, dont *L. monocytogenes*, *Mycobacterium tuberculosis, S. Typhimurium*, HIV-1, les virus de la grippe, de la polio et les réovirus [59,62]. L'absence de cellule M diminue la virulence de certains d'entre eux [59,60,65], mais entraîne aussi la perte des réponses protectrices contre le pathogène *Salmonella Typhi* [59]. À noter que les LB eux-mêmes peuvent

échantillonner les antigènes de la lumière intestinale au niveau des cellules M indépendamment des DC (**Fig. 7**)[69]. Les cellules M sont donc l'interface entre l'hôte et la flore commensale, interactions qui ne reposent pas seulement sur l'immunité de l'hôte mais aussi sur la diversité de ce microbiote.

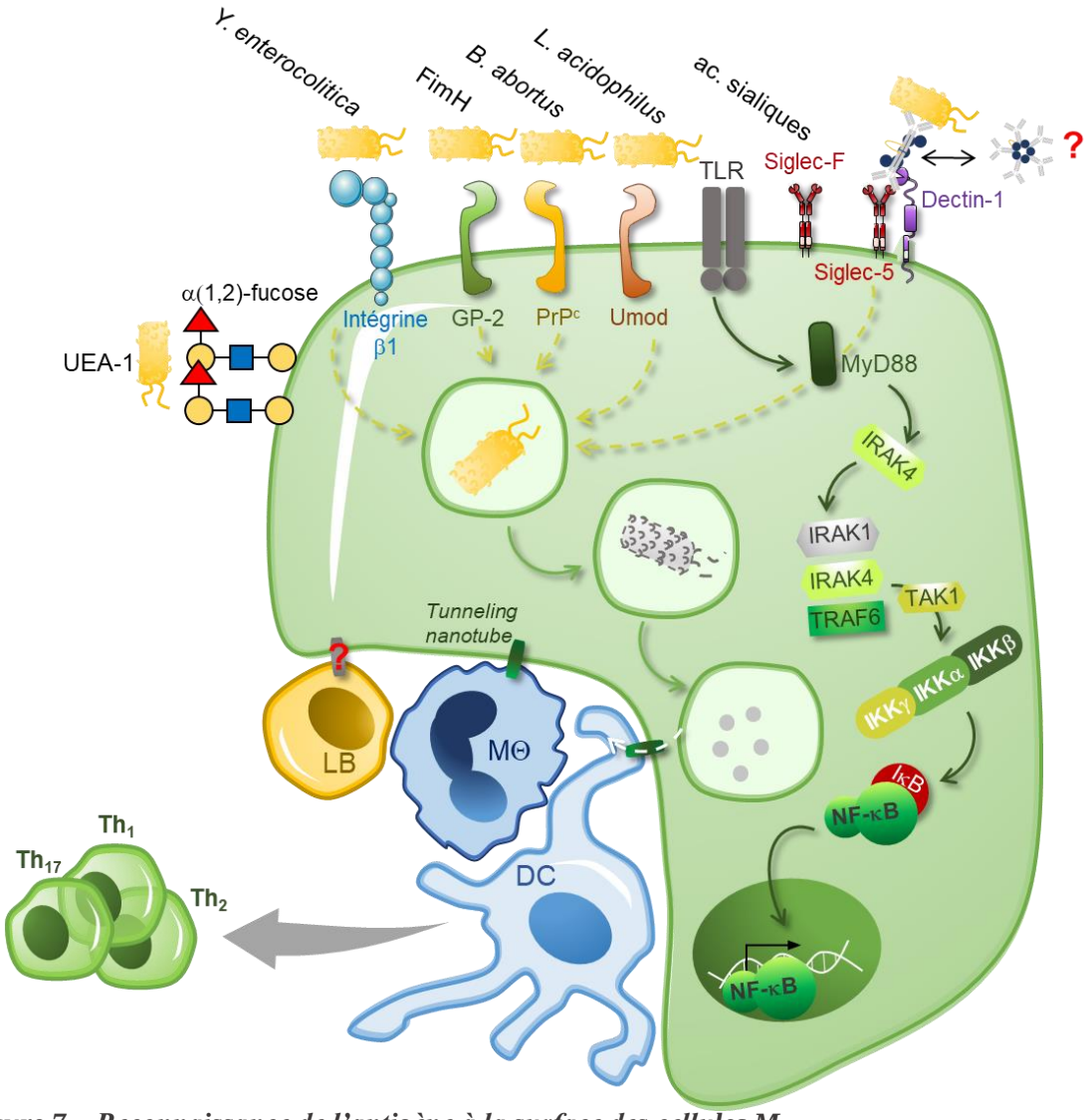

Figure 7 – Reconnaissance de l'antigène à la surface des cellules M.
La lectine de plantes UEA-1 s'agglutine sur les résidus glycosylés de type α(1,2)-fucose. Les invasines de Yersinia *lient les intégrines β-1 des cellules M après activation préalable de l'activateur intracellulaire Aif1. La protéine GP-2 (glycoprotein-2) reconnait les bactéries à pili de type 1 (FimH$^+$). Les bactéries* Brucella abortus *et* Lactobacillus acidophilus *sont internalisées par la protéine prion PrP^c et Umod (Uromodulin) respectivement. Les protéines Siglecs (dont Siglec-F (ref) et Siglec-5(ref)) permettent la reconnaissance d'acide sialiques commensaux et de l'hôte. Les antigènes internalisés subissent la transcytose inverse puis sont acheminés le long des TNT (tunneling nanotubes) vers les cellules présentatrices d'antigènes et les effecteurs de la poche de la cellule M. Les LB peuvent échantillonner ces antigènes indépendamment des DC, selon un mode non-caractérisé. Les SIgA muqueuses complexées ou non à des antigènes, effectuent cette transcytose inverse selon un mécanisme Dectin-1-dépendant. Les SIgM, sont soupçonnées de capacités similaires.*

C- Microbiote intestinal

Il est difficile d'établir une carte précise des réseaux bactériens qui caractérisent une muqueuse intestinale en bonne santé, puisque ceux-ci varient entre individus en fonctions de leurs habitudes alimentaires, et de leurs modes de vies. Cependant, la flore régule les mêmes fonctions clés chez tous les individus dont la tolérogénisation de la muqueuse, la dégradation du bol alimentaire, et la régulation des espèces opportunistes.

1- Métabolisme commensal

La flore commensale a recours à plusieurs métabolismes pour assurer la dégradation des carbohydrates non digestibles par l'hôte et du mucus[70]. Par exemple, deux souches d'*Escherichia coli*, l'une commensale et l'une pathogène, métabolisent les mêmes sources carbonées mais selon un ordre métabolique différent[70]. La flore se distingue des bactéries opportunistes par son utilisation unique du carbone environnant, notamment *via* la production d'acides gras à chaîne courte (SCFA), qui favorisent la néoglucogenèse et le catabolisme du glucose (**Fig. 8**) [71]. La synthèse d'acétate, de propionate et de n-butyrate[72] représente ainsi jusqu'à 10% du besoin calorique quotidien d'un adulte [73]. Le groupe des *Firmicutes,* dont les espèces *Ruminococcus* et *Faecalibacterium,* en est un producteur majeur (**Tableau 1**). *Faecalibacterium prausnitzii* est ainsi directement associée à un environnement anti-inflammatoire [74–76]. L'utilisation des O-glycans de la mucine stimule la croissance des producteurs de n-butyrate, et l'expansion de T_{reg} [13]. La croissance de la bactérie mucolytique *Akkermansia muciniphila* est donc corrélée à celle d'*Anaerostipes caccae* [77], productrice de SCFA, au contrôle de l'inflammation et au métabolisme du glucose dans des modèles murins d'obésité et de de diabète de type 2 [78,79].

Les SCFA, en particulier le n-butyrate, sont reconnus *via* les récepteurs GPR41[80] et GPR43[81] des IEC pour la régulation des besoins énergétiques de l'hôte [82]. Ce faisant, la synthèse de SCFA est concomitante à celle des vitamines B et K[71,83] et régule le cycle de Krebs[71,83] (**Fig. 9**). La sécrétion de SCFA par les espèces *Prevotella* et *Atopobium* active la transcription de PARRα dans les cellules intestinales [84] et facilite la β-oxydation des lipides et leur stockage notamment *via* les espèces *Bacteroides aerofasciens* et *Lactobaillus paracasei* [8586].
Il est également à noter que certaines bactéries commensales participent au métabolisme des acides biliaires [87]. Synthétisés par le foie, ils ont principalement des effets antimicrobiens et

sont dégradés par oxydation par les espèces *Bifidobacterium*, *Lactobacillus*, *Bacteroides* et *Clostridium*[87].

Tableau 1 – Bactéries produisant des SCFA et des vitamines
LGG : souche commerciale de Lactobacillus rhamnosus *; LAB : Lactobacilles commerciales*
D'après Leblanc, et al. *Microbial cell factories (2017).*

Microorganisme(s)	Type	Métabolite(s)
Ruminococcus, Faecalibacterium	Commensale	Butyrate
Bifidobactérie	Probiotique	Acétate/lactate
L. salivarius spp *salcinius* JCM 1230 *L. agilis* JCM 1048	Probiotique	Propionate/butyrate
L. acidophilus CRL 1014	Probiotique	Acétate/butyrate/propionate
LGG	Probiotique	Propionate
B. longum SP 07/3	Probiotique	Propionate/acétate
B. bifidum MF 20/5	Probiotique	Propionate/acétate
L. gasseri PA 16/8	Probiotique	Propionate
L. plantarum WCSF1	Commensale	Folate
Bifidobactérie	Alimentaire	Thiamine
Lactococcus, Leuconostoc	Alimentaire	Thiamine
L. sanfranciscencis	Alimentaire	Thiamine
L. lactis	Alimentaire	Riboflavine
L. fermentum	Alimentaire	Riboflavine
Leuconostoc mesenteroides et *Propionibacterium freudenreichii*	Alimentaire	Riboflavine
L. plantarum	Alimentaire	Riboflavine
Souche 151 LAB	Alimentaire	Folate
Souche 40 LAB	Alimentaire	Folate
Souche 36 LAB	Alimentaire	Folate
L. fermentum CECT 5716	Probiotique	Vit. B2 et B9
LGG	Probiotique	Vit. B1, B2 et B9
B. adolescentis DSM 18350	Probiotique	Folate

Chez l'homme, le microbiote d'individus sains peut être classifié selon trois entérotypes (*clusters*) dont les bactéries dominantes sont respectivement de la famille des *Bacteroides*, des *Prevotella*, et des *Ruminococcaceae* [88]. Quatre espèces dominent le microbiote adulte : *C. leptum*, *C. coccoides*, *Bacteroides* and *Bifidobacterium* [89]. *Bifidobacterium* est associé à la colonisation précoce des muqueuses et à l'établissement du commensalisme [89]. La dominance de ces espèces limite l'expansion de bactéries mucolytiques et des bactéries segmentées filamenteuses (SFB), groupes qui incluent des espèces à tendances opportunistes[90].

Une mesure communément utilisée pour évaluer l'état du microbiote est le *ratio* fécal *Firmicute/Bacteroides* [89,91]. Celui-ci, lorsqu'il augmente, a été associé à l'obésité, et lorsqu'il diminue à la perte de poids[91]. Il est particulièrement bas chez le nourrisson et la personne âgée, mais significativement plus élevé chez l'adulte [89].

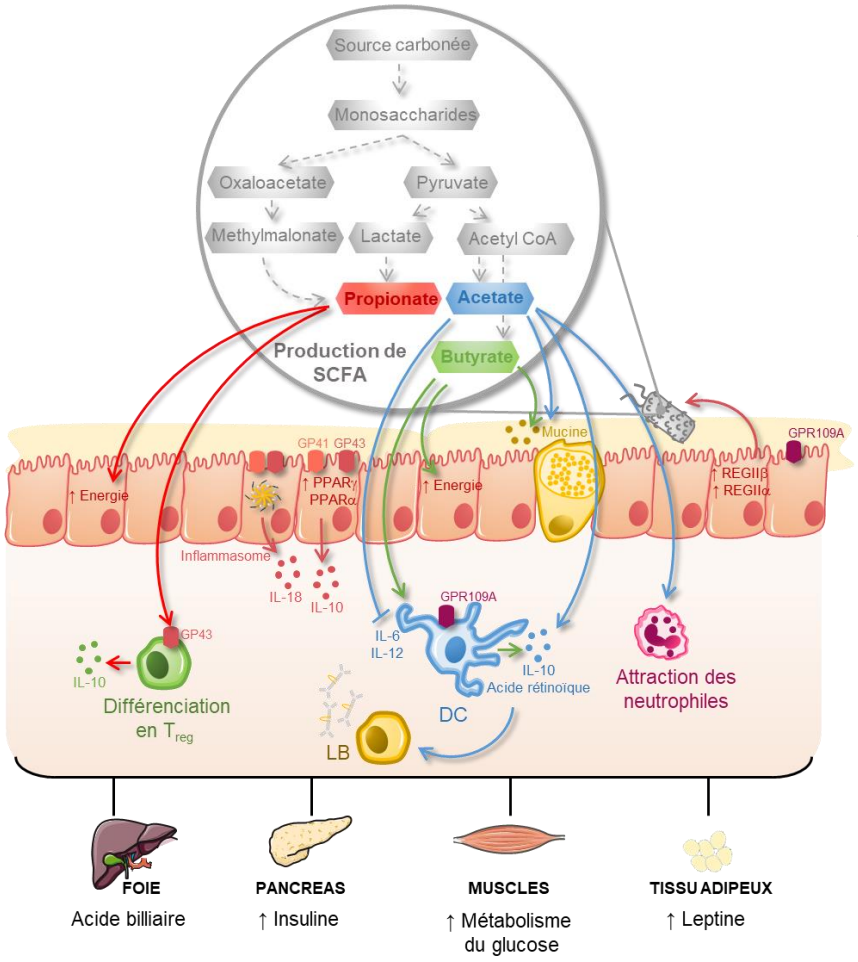

Figure 8 – Effets bénéfiques des SCFA dans l'homéostasie intestinale.
Le butyrate, l'acétate, et le propionate sont les plus abondants. Akkermansia municiphilla *est un producteur majeur de propionate. La synthèse de butyrate est dépendante de la fermentation de l'amidon, dominée par* Ruminococcus bromii. Faecalibacterium prausnitzii, Eubacterium rectale, Eubacterium hallii, *et* Ruminococcus bromii, *produisent la majorité de la production de butyrate. Ces SCFAs sont utilisés comme source d'énergie. et retrouvés dans la circulation sanguines où ils modulent la glycémie et le cholesterol. Les SCFA sont détectées par des récepteurs couplés aux proteins G régulant le métabolisme des lipides et du glucose (GPR109A, GP43 et les GP41), exprimés par les cellules épithéliales et immunitaires. Ils stimulent la production d'IL-10, d'IL-18, d'acide rétinoïque et des PPAR (peroxisome proliferator-activated receptor) impliqués dans l'adipogenèse et limitent ainsi l'engagement de signaux inflammatoires.*

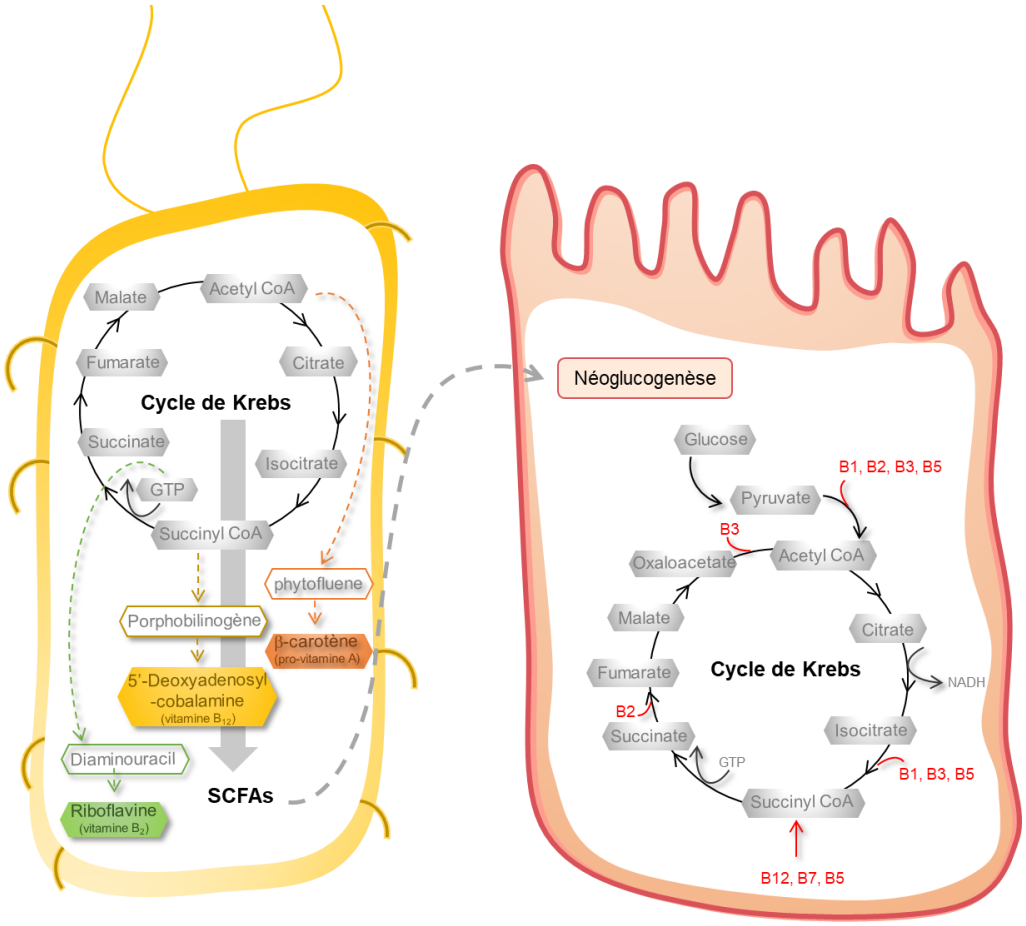

Figure 9 – Rôle de la production de SCFA dans la production de vitamine et du métabolisme cellulaire.
La voie de symthèse des SCFAs requiert le cycle de Krebs et permet la synthèse des vitamines du groupe B (B1 thiamine, B2 riboflavine, B3 niacine, B5 acide panthothenique, B7 biotine, et B12 cobalamine), A et K. Elles participent au métabolisme des bactéries luminales et des cellules épithéliales par la stimulation de la néoglucogénèse et du catabolisme du glucose (droite).

3- Induction de l'immunité

La composition de la flore influence l'équilibre entre populations lymphocytaires $CD4^+$, et l'entérotype d'un individu conditionne son profil immunitaire [88]. Chez le nourrisson, l'induction de l'équilibre T_{reg}/Th_{17} est associée à *Propionibacterium* [92]. Chez l'adulte, les espèces *Bacteroides* et les *Prevotella* sont associées respectivement à l'immunité Th_1 [93] et Th_{17} [94]. Par ailleurs, les lactobacilles et les bactéries du groupe *Clostridia* favorisent l'induction des T_{reg} [93]. Dans la muqueuse oro-pharyngée, *Streptoccoccus salivarus* génère une légère immunosuppression locale et régule ainsi la transcription de plus de 500 gènes de l'hôte impliqués dans l'immunité[95].

Les métabolites bactériens aussi promeuvent un environnement tolérogène. : la production de SCFA limite la sécrétion d'IL-8 par les IEC, une cytokine connue pour son rôle chimio-attractant pour les neutrophiles muqueux [96]. Le n-butyrate, par l'induction de TGF-

β dans les IEC, est un inducteur indirect de T_{reg} [97]. La sécrétion d'acétate par *Bifidobacterium dentum* régule la sécrétion de la mucine MUC2 [98], et favorise la glycosylation de celle-ci [99].

L'axe immunité-flore commensale au niveau intestinal a également des effets sur d'autres sites muqueux : la rupture ou l'altération de la colonisation intestinale par la flore commensale chez le souriceau affecte la migration d'ILC2 vers le poumon et augmente la sensibilité aux infections respiratoires [100].

4- Régulation des espèces pathogènes

La simple présence de ces communautés bactériennes bénéfiques génère une compétition pour le milieu qui réprime la prolifération de bactéries pathogènes. Les bactéries commensales sont plus efficaces dans l'absorption de nutriments et métabolites muqueux, et sécrètent des composés antimicrobiens limitant la croissance de bactéries pathogènes [101].
Ainsi, des espèces de la famille *Bacteroides* limitent la prolifération du pathogène *Salmonella enterica* serovar Typhimurium chez la souris [102]. La production de propionate par des *Bacteroides* propionate génère un stress acide dans le cytosol de *S.* Typhimurium qui ralentit la croissance bactérienne et augmente la résistance de la muqueuse à l'infection [102]. De même, l'exposition du pathogène nosocomial *S. aureus* à une bactérie commensale de la peau, *Corynobacterium striatum,* diminue la transcription des gènes impliqués dans la virulence de *S. aureus*[103]. Dans des modèles murins, la colonisation intestinale par le pathogène *Citrobacter rodentium* est limitée par le microbiote, notamment grâce à la consommation de fucose au cours de l'infection [104,105]. Par ailleurs, les métabolites commensaux favorisent l'activation de NOD2 en réponse aux peptidoglycanes bactériens [106], régulant ainsi la prolifération de bactéries exogènes.

La ségrégation des espèces luminales selon qu'elles sont commensales ou pathogènes, et les réponses immunes, dépendent de la sécrétion d'immunoglobulines sécrétoires (SIg), dont les immunoglobulines A sécrétoires (SIgA) font partie. Pour comprendre les dynamiques d'interaction entre réseaux bactériens intestinaux et immunité muqueuse, il est donc nécessaire de caractériser cette composante humorale de l'immunité muqueuse.

Chapitre 2 - Immunité sécrétoire

A- Caractéristiques des immunoglobulines sécrétoires

Les immunoglobulines sécrétoires (SIg) constituent la première ligne de défense immunitaire contre l'invasion des tissus muqueux par des microbes exogènes mais participent également à la colonisation par la flore commensale. Cette fonction sécrétoire est assurée par la multimérisation des immunoglobulines A (IgA) et des immunoglobulines (M) grâce à la liaison à la chaîne J, et à l'acquisition de la pièce sécrétoire au cours de leur transcytose vers la lumière intestinale (**Fig. 10, Fig. 11**).

1- Structure générale des SIgs

Les IgA, chez l'homme, sont divisées en deux sous-classes, les IgA1 et les IgA2, dont les chaînes lourdes (Cα) sont codées par deux gènes distincts. Dans le tube digestif, les SIgA1 sont majoritaires, sauf dans le colon où la sécrétion d'IgA2 domine [107–109]. Le monomère d'IgA et d'IgM (**Fig. 10, Fig. 11**) respecte une structure conservée chez tous les anticorps humains, à savoir : l'assemblage de deux chaînes lourdes et de deux chaînes légères structurées en domaines globulaires. Quatre de ces domaines forment la chaîne lourde, dont un domaine variable (VH) à l'extrémité N-terminale, et deux forment la chaîne légère dont un variable (VL). VH et VL sont associées par ponts disulfures. Ces deux sous-types d'IgA diffèrent au niveau de la région charnière, plus longue pour l'IgA1 que pour l'IgA2 (**Fig. 10**). La liaison à la chaîne J *via* des ponts disulfures permet la formation de multimères : les SIgA sont dimériques et les SIgM pentamériques [110]. La protéine MZB-1, lie l'IgA dans sa partie Cα terminale et stabilise les liaisons entre chaîne lourdes et chaîne légères pour l'insertion optimale de la chaîne J [111]. Cette multimérisation des SIg augmente ainsi leur valence et donc leur avidité. La chaîne J inhibe également la dégradation intracellulaire de l'IgA au cours du transport à travers les cellules épithéliales muqueuse [111]. C'est au cours de celle-ci que s'effectue l'ajout de la pièce sécrétoire sur l'Ig [112]. La liaison à la SC est plus stable avec l'IgA qu'avec l'IgM [113], protège la SIg des clivages protéolytiques [114], et requiert la présence de la chaîne J [115].

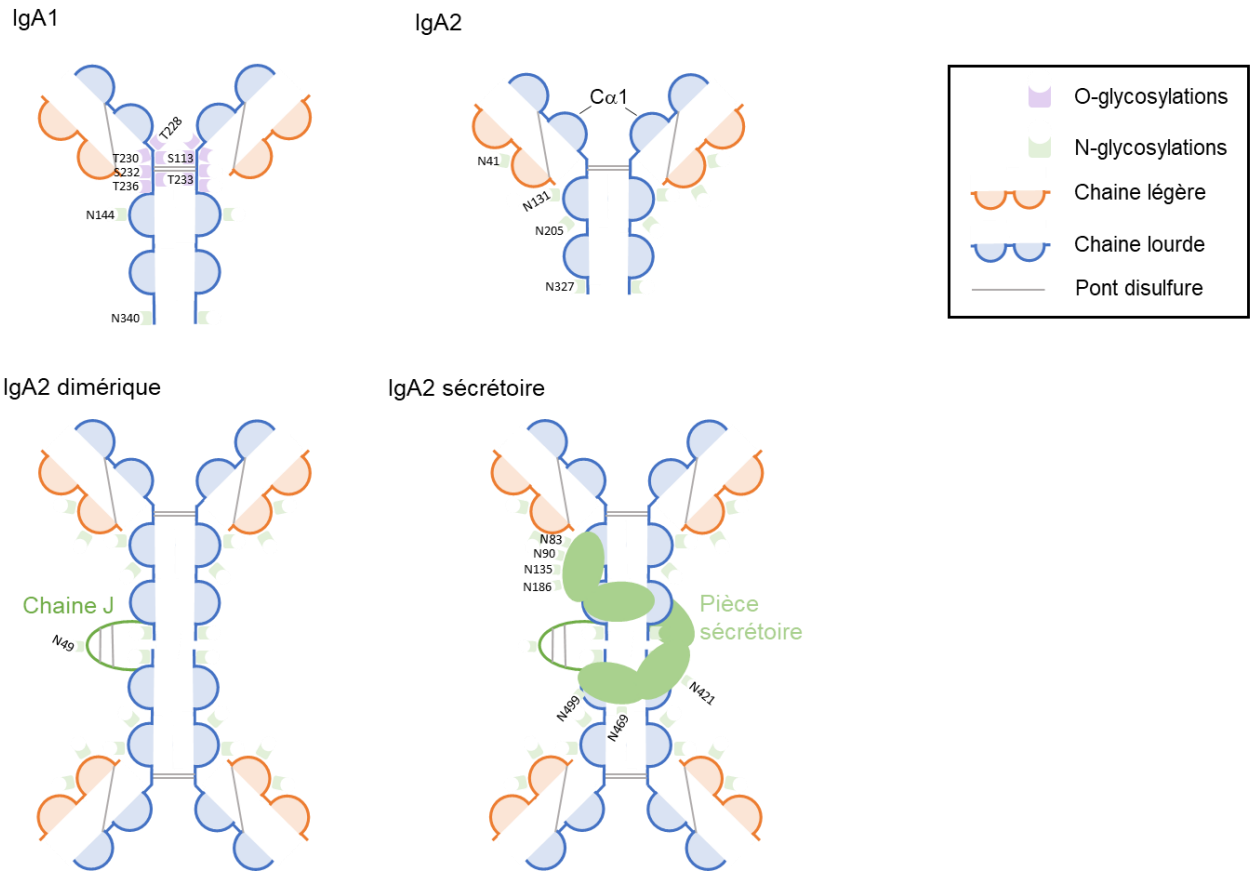

Figure 10 – Structure des isoformes d'immunoglobuline A humaine.
Les IgA1 humaines possèdent une région charnière plus longue que les IgA2 sur laquelle trois à six sites de glycosylation ont été caractérisés : T225, T228, S230, S232, T233, T236. Sur ces sites les motifs GalNac (N-galactosamine) et Gal (galactose) rendent l'IgA1 théoriquement plus hydrophile. L'IgA1 possèdent deux sites des N-glycosylation (N144 et N340), et l'IgA2 quatre (N41, N131, N206, N327). Le domaine Cα1 permet la transcytose inverse. La chaîne J lie la partie C-terminale des chaînes lourdes (IgA1 ou IgA2). La SC, N-glycosylée sur sept sites, s'associe à la partie constante des dimères d'IgA (ici, IgA2).

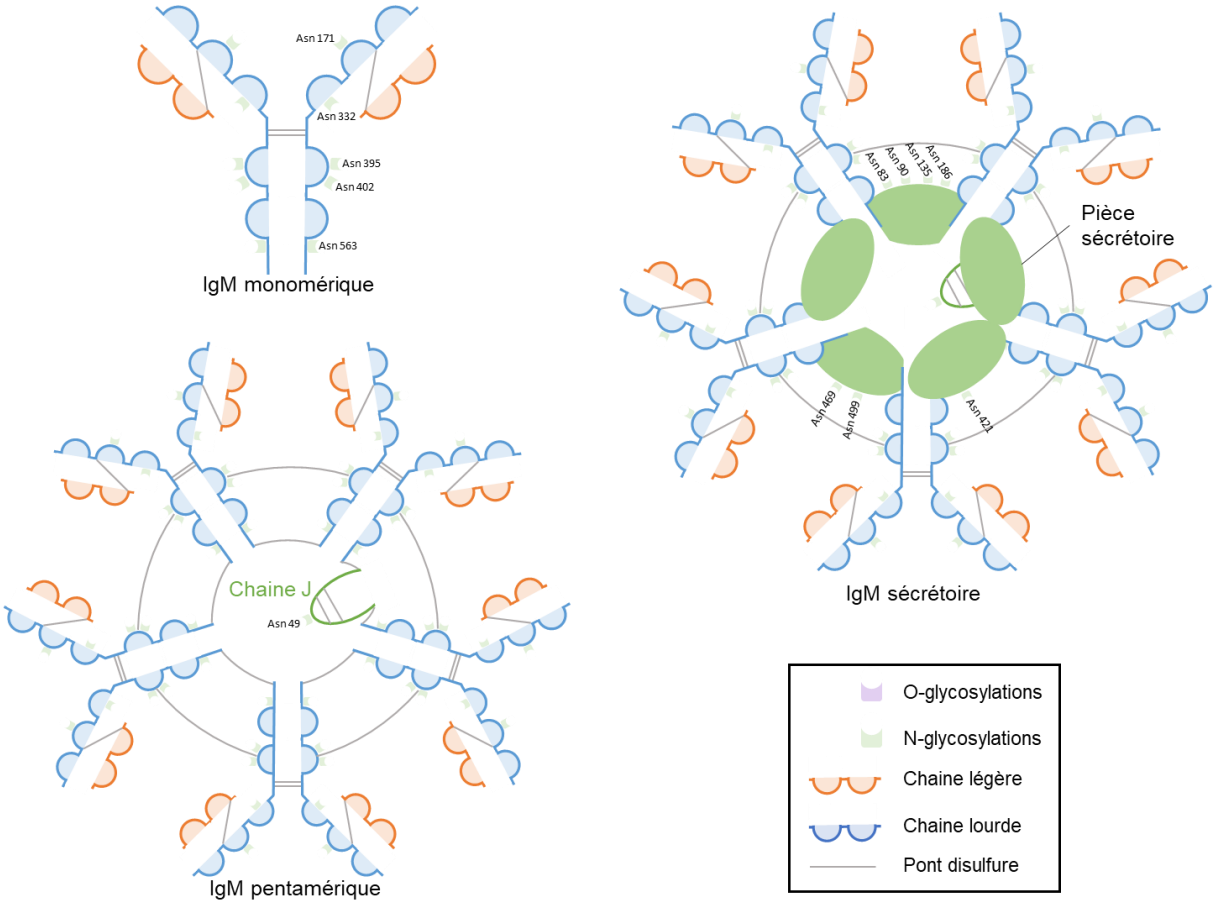

Figure 11 – Structure des isoformes d'immunoglobuline M humaine.
Les IgM humaines possèdent cinq sites des N-glycosylation : N171, N332, et N395 sont occupés par des glycans complexes, tandis que N402 et N563 le sont par des oligomannose. L'absence de sialylations sur l'IgM affecte les capacités d'inhibitrices des IgM sur l'expansion des LT. La chaîne J lie deux monomères au niveau de la partie C-terminale des chaînes lourde pour fermer le pentamère. La SC s'associe à la partie constante des monomère d'IgM une fois le pentamère formé et au cours du transport à travers les cellules épithéliales.

2- Les glycosylations ont un rôle primordial dans les fonctions des SIg

Les IgA[116,117118], les IgM[119], la chaîne J et la SC[120,121] sont largement glycosylées. Ce sont soit des O-glycosylations, soit des N-glycosylations. Les IgA1 sont ainsi majoritairement O-glycosylées [116,117], en particulier au niveau de la région charnière, riche en Sérine (S) et Thréonine (T). Des glycosylations sont ainsi retrouvées sur trois à six sites de O-glycosylation potentiels : T225, T228, S230, S232, T233, T236 [116,122–126]. Les motifs N-galactosamine (GalNac) sont les premiers glycans ajoutés, auxquels sont ajoutées des galactosylations (Gal) ou des sialylations (NeuAc) [126]. Chez l'homme des déficiences en galactose sur ces sites O-glycosylés affectent vraisemblablement la pathogenèse de la

néphropathie à IgA[122,127]. La présence des GalNAc, selon leur nombre, modifie les propriétés hydrophobes de la région charnière[126]. L'IgA1 porte également deux sites de N-glycosylation, N144 et N340, qu'elle partage avec l'IgA2 (N131 et N327) et qui contiennent une forte concentration de glycans complexes[128]. Le niveau de sialylation de l'IgA1 en limite les propriétés effectrices : la désialylation de l'IgA1 entraîne une hausse de l'activation macrophagique et des neutrophiles [128]. En conséquence, l'IgA2 est moins sialylée que l'IgA1 (ce qui correspond à ses fonctions effectrices, Chapitre C), en particulier sur les sites N131 et N327, partagés avec l'IgA1 [128]. L'IgA2 est d'ailleurs principalement N-glycosylée[118] sur quatre sites : N41, N131, N206, N327[123,125,128]. De plus, l'absence de N-glycosylations, en particulier portées par le domaine Cα1, empêche le transport des IgA2 dans la PP[43].(cf Chapitre C-2) De la même manière, l'IgM est N-glycosylée sur cinq sites, la position N563 étant critique pour la formation de la SIgM fonctionnelle[129] (**Fig. 11**). L'absence de N-glycosylation empêche la sécrétion de l'IgM, qui s'agrège dans le cytosol[129]. Ici aussi, un faible taux de sialylation est associé à l'inflammation[130]. Cela dit, le rôle des glycosylations des SIgM n'est pas décrit dans le transport et/ou la qualité des réponses associées aux SIgM.

B- Synthèse des SIg dans la muqueuse intestinale

La détection d'antigènes luminaux par les cellules M est l'un des facteurs principaux déclenchant l'initiation de la production d'IgA intestinale [61]. Chez l'homme comme chez la souris, on distingue alors deux populations d'Ig sécrétoires : les SIg naturelles, et les SIg « immunes », de haute affinité. Il est admis que la sécrétion d'IgA naturelles est induite par signaux thymo-independants (TI) et celle d'IgA spécifiques par des signaux thymo-dépendants (TD)[131] (**Fig. 12**).

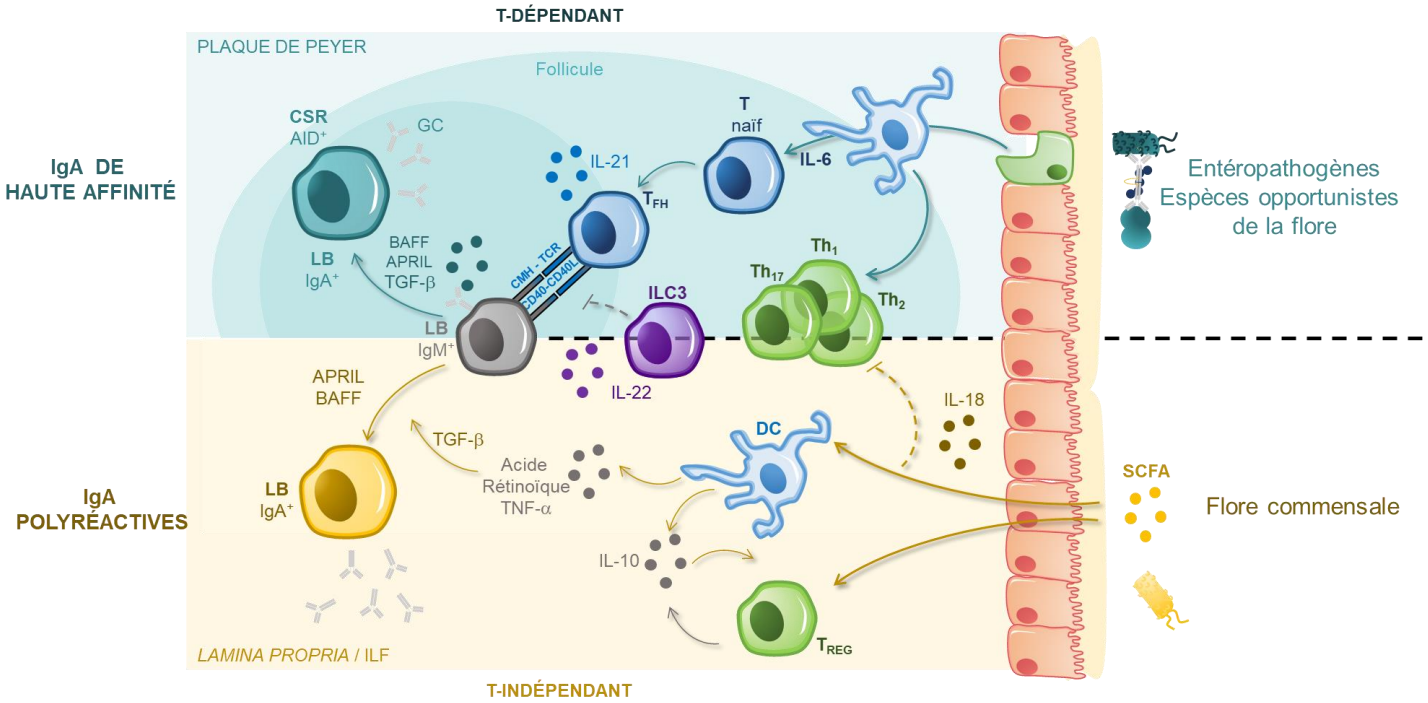

Figure 12 – Production T-indépendante et T-dépendante des IgA intestinales

Dans la PP les DC échantillonnent les antigènes et bactéries muqueux, produisent de l'IL-6 et migrant vers la zone inter-folliculaire des PP où ells engagent des LT CD4$^+$ qui se différencient en T_{fh}. Ces T_{fh} migrant à leur tour vers le follicule, engagent les LB IgM$^+$ via les interactions conventionnelles CMH-II/TCR et CD40-CD40L. Les DC induisent l'expression du récepteur au TGF-β (Tip-DC) par la production d'oxide nitrique (NO). Les LB se différentient ensuite en LB IgA$^+$ par l'expression d'AID (activation-induced deaminase) en réponse au TGF-β et à l'IL-21 produits par les T_{fh} . C'est le TGF-β qui dirige la CSR vers l'isotype IgA. Dans les ILF, la production d'IgA est T-indépendante : le TNF-a produit en abondance par les DC en réponse aux SCFA active l'ensemble des DC de l'ILF qui sécrètent le TGF-β et l'acide rétinoique . En réponse, les la secretion de BAFF et APRIL, toujours par les DC, facilite la CSR des LB préalablement active par les TLR.

1- Production T-indépendante des SIg : origines du répertoire naturel

Chez la souris, les lymphocytes B-1 (comprenant les populations B-1a et B-1b) et ceux de la zone marginale (MZB), secrètent les Ig naturelles [132–134]. Les précurseurs des plasmocytes à IgA intestinaux sont les B-1b[135,136] de la cavité péritonéale, tandis que les B-1a de ce compartiment sont à l'origine des IgM naturelles circulantes [137]. Chez l'homme, les populations homologues sont controversées, bien que le phénotype CD20$^+$ CD27$^+$ CD43$^+$ corresponde à une population de LB secrétant constitutivement des Ig et pouvant engager des LT selon un mode semblable aux B-1 murins[138,139]. Le phénotype CD19$^+$ CD27$^+$ IgD$^+$ IgM^{high} correspond aux lymphocytes MZB, et alimente les populations spléniques de lymphocytes naturels chez l'homme. Ces différents LB sont inclus dans le répertoire au moment de leur recirculation dans la PP grâce à l'expression du marqueur CCR6, et indépendamment des centres germinatifs [137]. La sécrétion d'IgA est ensuite déclenchée sous l'égide de stimulations au TGF-β ou à l'acide

rétinoïque [134,140], et repose sur les signaux TLR et les cytokines BAFF et APRIL [131,141] (**Fig. 13**). Cet axe TLR-APRIL est induit par les signaux microbiens de la flore commensale, *via* la production d'IL-10 [142] [141].

Le répertoire des Ig naturelles est préexistant à toute infection, et est établit en partie par les Ig maternelles transmises au cours de la grossesse, puis de l'allaitement [143]. Il est, au niveau des muqueuses, essentiellement composé d'IgA et d'IgM polyréactives, réactives pour de nombreux motifs glycosylés, l'ADN exogène, le LPS, et la flagelline [137,143]. Ces SIg ont un large spectre et une faible affinité [137]. Elles sélectionnent les membres de la flore commensale grâce à cette forte poly-réactivité : ce sont souvent des IgA liant de nombreux glycans microbiens, quelle que soit leur provenance [137].

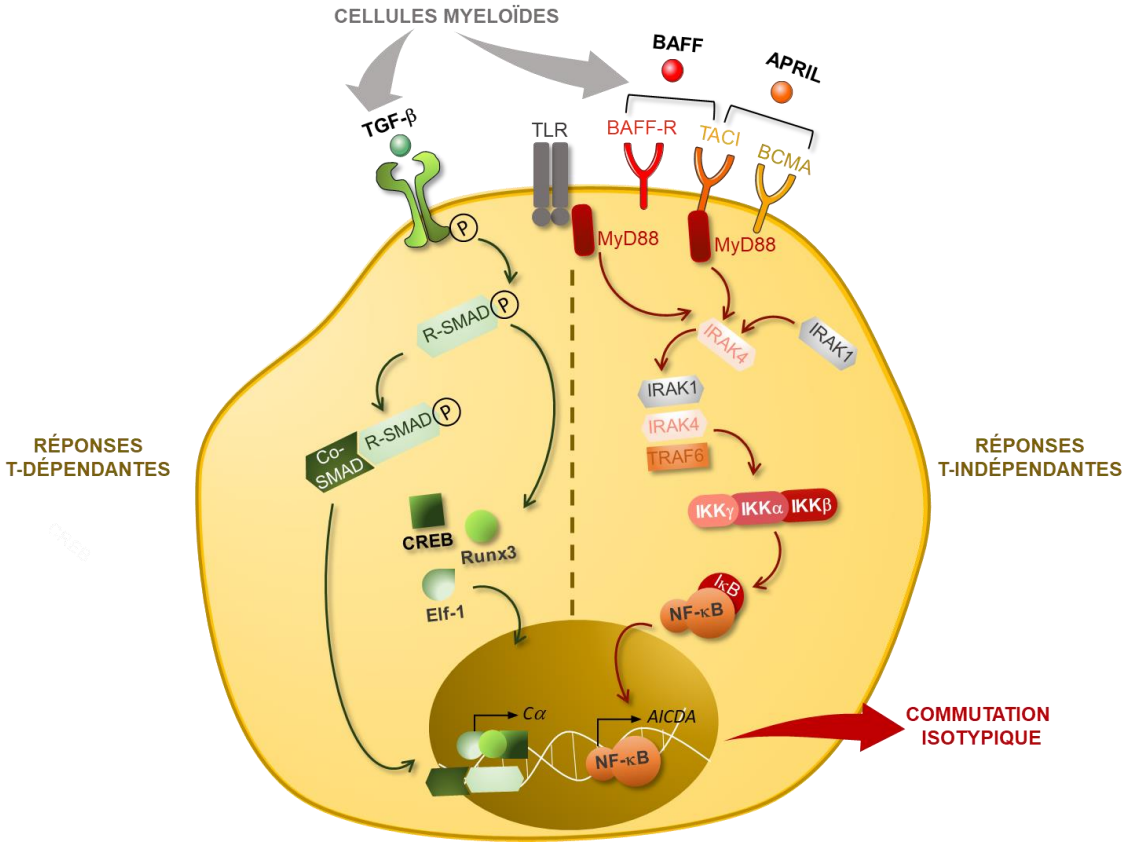

Figure 13 - Induction de la commutation de classe (CSR) dans les LB muqueux.
La liaison de BAFF promeut aussi la survie, la maturation et la prolifération des LB. Toutes deux lient TACI; BAFF lie BAFF-R (BAFF receptor) et APRIL lie BCMA (B cell maturation antigen). L'engagement de TACI l'adaptateur MyD88 et l'activattion de NF-κB via *IRAK-1 (IL-1 receptor–associated kinase 1), IRAK-4, TAK1 (TGF-β activated kinase-1), et la dégradation de l'inhibiteur IκB par le complexe IKK (IκB kinase). NF-κB lie des motifs κB sur le promoteur du gène codant pour l'enzyme AID. L'engagement des TLRs favorise la CSR vers l'isotype IgA* via *une cascade liée au domaine TIR (Toll–IL-1 receptor) du TLR. Le TGF-β active la phosphorylation de son récepteur, puis celle de protéines R-SMAD (receptor-regulated SMAD). Complexées avec les co-SMAD (common-partner SMAD), elles sont transloquées vers le noyau où elles lient les SBE (SMAD-binding elements) du gène Cα.. Ces complexes peuvent également s'associer avec des co-facteurs induits par le TGF-β : Runx3 (Runt-related transcription factor 3), liant les RBE (RUNX binding elements); CREB (cyclic adenosine monophosphate response element–binding protein), liant les CRE (cyclic adenosine monophosphate response element), et ELF-1 (Ets-like factor-1), liant un site de liaison aux Ets du gène Cα..*

2- Production T-dépendante : réponse à l'infection

La réponse aux pathogènes ou bien le contrôle de phyla atypiques de la flore commensale tels que les bactéries segmentées filamenteuses (SFB), est médiée des IgA de haute affinité. Dans la PP, les LT *follicular helper* (T_{fh}) des centres germinatifs induisent la maturation des LB les produisant [144,145], avec une préférence vers le CDR2 lors des mutations hypersomatiques [146] [147]. Ces interactions sont enclenchées par la sécrétion des chimiokines comme RANKL, ou de cytokines comme l'IL-21 [148–150], entraînant l'expansion des LB dans les centres germinatifs, et le développement de l'immunité Th_{17} [150] (**Fig. 12**). Afin de promouvoir le mutualisme commensal, l'expansion des T_{fh} est limitée par l'ATP exogène et les ILC3 des niches inter-folliculaires [144,145]. À cet effet, la présentation d'antigènes commensaux par les ILC3 interfère physiquement avec l'interaction T_{fh}-LB *via* la production d'IL-22 [145] (**Fig. 12**). Le microbiote limite la production d'IgA de haute affinité par l'induction de T_{reg} $ROR\gamma T^{+}$ $Helios^{-}$ $CD4^{+}$ [151]. Ceux-ci expriment alors le facteur c-maf, limitant l'induction de cytokine Th_{17}, et favorisant celle de l'IL-10[151].

C- Fonctions des Ig sécrétoires

Dans la muqueuse, les Ig effectuent la sélection immune médiée par les anticorps (AMIS) : elles limitent les phénomènes de dysbiose, c'est à dire la dérégulation de la diversité microbienne au profit d'espèces opportunistes promotrices de l'inflammation. Elles doivent cependant identifier spécifiquement tout pathogène entérique.

1- Récepteurs

Le FcαRI (CD89), le récepteur Fcα/μR, le récepteur à la transferine (CD71), DC-SIGN, Dectin -1 et le pIgR contribuent à la fonction des SIgA dans l'intestin (**Fig. 14**). FcαRI est présent à la surface des neutrophiles, éosinophiles, monocytes, cellules dendritiques ou encore certains macrophages[152–156]. L'ARN du gène *FCAR* subit un épissage alternatif qui permet l'ajustement d'une réponse inflammatoire[157]. Il permet notamment l'échantillonnage des antigènes luminaux par les DC interstitielles de la muqueuse [155], et entraîne la phagocytose, le relargage de molécules cytotoxiques et d'espèces réactives de l'oxygène (ROS), et la cytotoxicité médiée par les anticorps (ADCC). Structurellement proche du FcαR, le Fcα/μR peut lier à la fois les IgM et les IgA. Il est exprimé uniquement dans la *lamina propria* et les centres germinatifs de certains follicules [158]. À la surface des MZB murins [159,160], il participe à

l'endocytose de complexes Ig-antigènes, permet l'activation des TLR, et la production de cytokines [159,160].

CD71, le récepteur à la transferrine 1, est exprimé par les IEC du colon et l'intestin, les LB muqueux, et la plupart des cellules de lignée érythroïde[161]. C'est un récepteur d'endocytose qui engage les IgA sécrétoires tissulaires [162] *via* les glycosylations portées par les SIgA [162]. Il permet ainsi le transport spécifique de complexes SIgA1-antigènes vers la *lamina propria* [163,164].

DC-SIGN et Dectin-1, lient tous les deux les SIgA et sont notamment exprimés par les DC tissulaires, et par les cellules M de la PP respectivement [43,165]. Leurs rôles dans ce processus seront discutés plus en avant de ce manuscrit, et correspondent à l'établissement de réponses aux antigènes du soi et aux antigènes commensaux [166–168]. Pour ces deux récepteurs, une glycosylation optimale des IgA est nécessaire à leur prise en charge [43,169].

Le récepteur lymphocytaire FCRL3 polarise également les réponses muqueuses : porté par les T_{reg}, son activation spécifique par les SIgA lève la fonction répressive des T_{reg} sur l'inflammation[170]. En effet, l'engagement de FCRL3 induit la co-expression de RORγT et FoxP3 et le basculement vers la sécrétion d'IL-17 et d'IFN-γ[170].

Le récepteur aux immunoglobulines polymériques, pIgR, reconnaît les Ig polymériques de manière générale. Il est exprimé à la membrane basale des IEC et induit leur transport vers la membrane apicale. Les infections muqueuses tendent à augmenter son expression, ce qui accroît la sécrétion locale d'IgA [171172].

Il est plus difficile de caractériser les récepteurs mis en jeu pour la reconnaissance spécifique de l'IgM. Le FcμR (TOSO/FAIM3), caractérisé cette dernière décennie, est peu étudié en contexte muqueux (**Fig. 14**). Des souris déficientes pour ce récepteur présentent une faible réponse antimicrobienne, une altération de la formation des centres germinatifs et une augmentation de la production d'autoanticorps[173,174]. Il joue ainsi un rôle dans la tolérance au soi, et aux microbes commensaux, le phénotype ressemblant fortement à celui de souris SIgM$^{-/-}$[175,176].

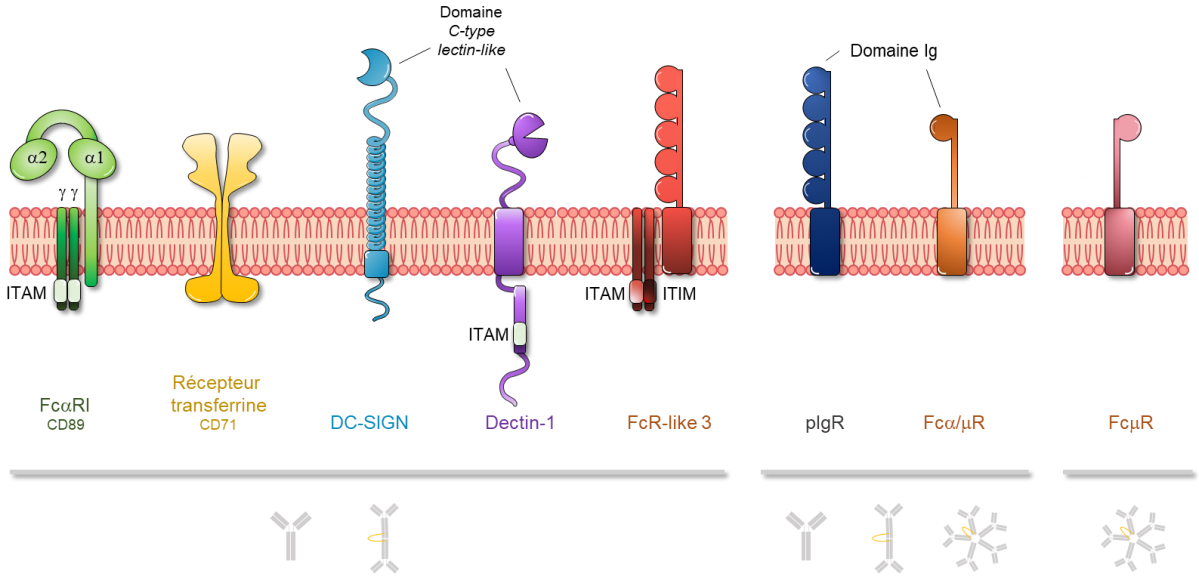

Figure 14 – Récepteur aux IgA et IgM humaines.
Le FcαR est associé à deux chaines g transmembranaires possédants des motifs ITAM (immunoreceptor tyrosine-based activation motif) qui transduisent les signaux pro- et anti-inflammatoires. Le récepteur à la transferrine fixe le fer et les IgA. DC-SIGN et Dectin-1 sont des récepteurs aux lectines de type C qui fixent les glycosylations des IgA. Dectin-1 lie également les β-glucans fongiques. Le récepteur FcR-like 3 (FcRL3) lie les IgA sécrétoires pour médier la transition des T_{reg} en Th_{17}; la présence de motifs activateurs ITAM et inhibiteurs ITIM lui confèrent une grande adaptabilité de réponse. pIgR est le réceptuer de la transcytose des IgA et des IgM et permet leur transport depuis le pole basal des IEC vers la lumière intestinale. Les structures exactes du Fcα/μR et du FcμR restent peu décrite à ce jour, bien q'ils possèdent tous les deux un domaine de type immunoglobuline extracellulaire. Le Fcα/μR est exprimé par les LB matures, les macrophages, et les cellules mésangiales du rein. Le FcμR par les LB immatures et matures chez lesquels il régule l'engagement du BCR.

2- Transports des antigènes

Les IgA1, les IgA2, et les IgM polymériques sont prises en charge à la membrane basale des IEC par le pIgR pour être sécrétées dans la lumière intestinale selon un mécanisme appelé **transcytose**. Elles peuvent effectuer ce trajet sous forme de complexe immuns, et neutraliser un antigène présent dans la *lamina propria* (**Fig. 15**). Il s'agit d'un transport vésiculaire, au cours duquel le pIgR est clivé pour que la partie SC du récepteur reste liée aux IgA (**Fig.15**). La liaison à la chaîne J est cruciale pour ce transport : une susceptibilité accrue à la dysbiose, et une augmentation significative des phyla promoteurs de dysbiose tels qu'*Akkermansia*, (phylum *Verrucomicrobia)* ou les protéobactéries sont observées en son absence[111].

Le trajet retour, appelé **transcytose inverse** (RT), a lieu au niveau des cellules M, grâce au récepteur Dectin-1 et à son co-récepteur Siglec-5 [43]. Après reconnaissance des N-glycosylations et d'acides sialiques des IgA par ces derniers[43], les complexes immuns sont transportés vers le dôme sous-épithélial de la PP (**Fig. 15**). La RT n'a lieu qu'avec des SIgA2

humaines, et les SIgA murines, en raison de leurs abondantes N-glycosylations. Les complexes immuns interagissent ensuite directement avec le récepteur DC-SIGN des DC enchâssées dans la poche de la cellule M. C'est ici que se polarise la réponse cellulaire muqueuse vers un profil tolérogène ou bien inflammatoire. Les β-glucans, ligands naturels de Dectin-1, promeuvent ainsi les réponses Th_{17} [177]. Ces phénomènes de sécrétion et de réabsorption dynamiques sont essentiels à la bonne fonction des IgA muqueuses et promeuvent une forte responsivité immune.

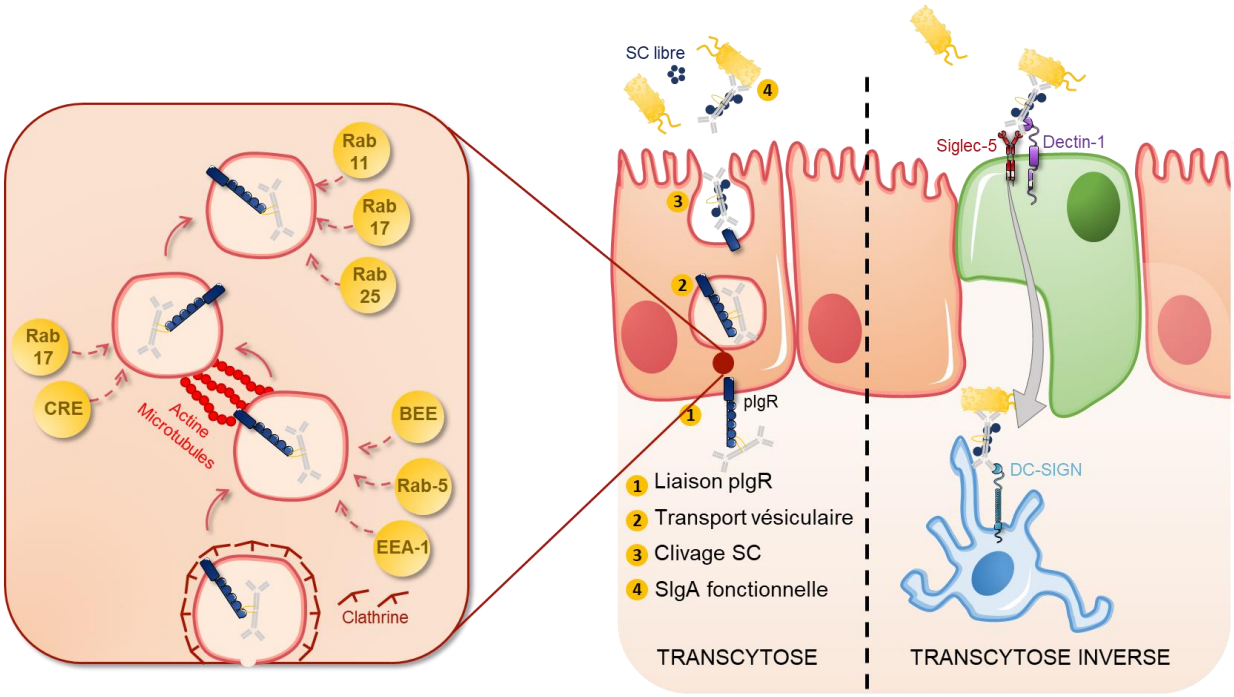

Figure 15 – Transcytose et transcytose inverse des IgA.
Le transport baso-apical des IgA est médié par le pIgR et repose sur un trafic vésiculaire permettant la formation de vésicules de clathrine. Les protéine Rab-5 et EEA-1 sont recrutées par la vésicules alors formée qui remonte le long du cytosquelette d'actine et des microtubules vers la membrane apicale. Les protéines Rab-17, Rab-25 et Rab-11 promeuvent la fusion avec la membrane apicale, au cours de laquelle la partie SC du pIgR est clivée et reste fixée aux IgA. Ce même mécanisme prend en charge les IgM, qui acquièrent la SC de la même manière. La SC peut également être clivée puis sécrétée sous forme libre dans la lumière intestinale où elle participe également à la sélection de microorganismes. La transcytose-inverse (RT) est médiée par la reconnaissance des N-glycans des IgA par Dectin-1 et des des sialylations des IgA par Siglec-5 à la membrane apicale des cellules M. A l'issue de ce processus, les IgA présentent l'antigène aux DC de la poche des cellules M en engageant le récepteur DC-SIGN. Chez l'homme, seules les IgA2 effectue la RT.

3- Ajustement des processus inflammatoires

Les réponses aux pathogènes peuvent être induites par la RT : les complexes immuns entraînent la sécrétion de cytokines pro-inflammatoires, et l'activation de LT $CD4^+$, de monocytes et de macrophages [178]. Ainsi, un complexe IgA-pathogène pénètre la PP plus aisément qu'un complexe IgA-commensale chez la souris[179]. L'invasion des tissus et la sur-

activation des voies de l'inflammation[180,181,182] par les entéro-pathogènes *Shigella flexneri* [183,184], *Salmonella* Typhimurium[179] [181,185], et *Vibrio cholerae* [186] est donc abrogée. Plusieurs modes d'action des SIgA existent [187](**Fig. 16**) : elles peuvent interagir avec les pathogènes intracellulaires directement dans les endosomes des cellules épithéliales, ou avec les pathogènes de la lumière intestinale. De manière similaire, les SIgA régulent l'expansion de bactéries atypiques telles que les SFB ou les espèces *Akkermansia*, lorsqu'elles sont induites par le TGF-β et IL-33 [188].

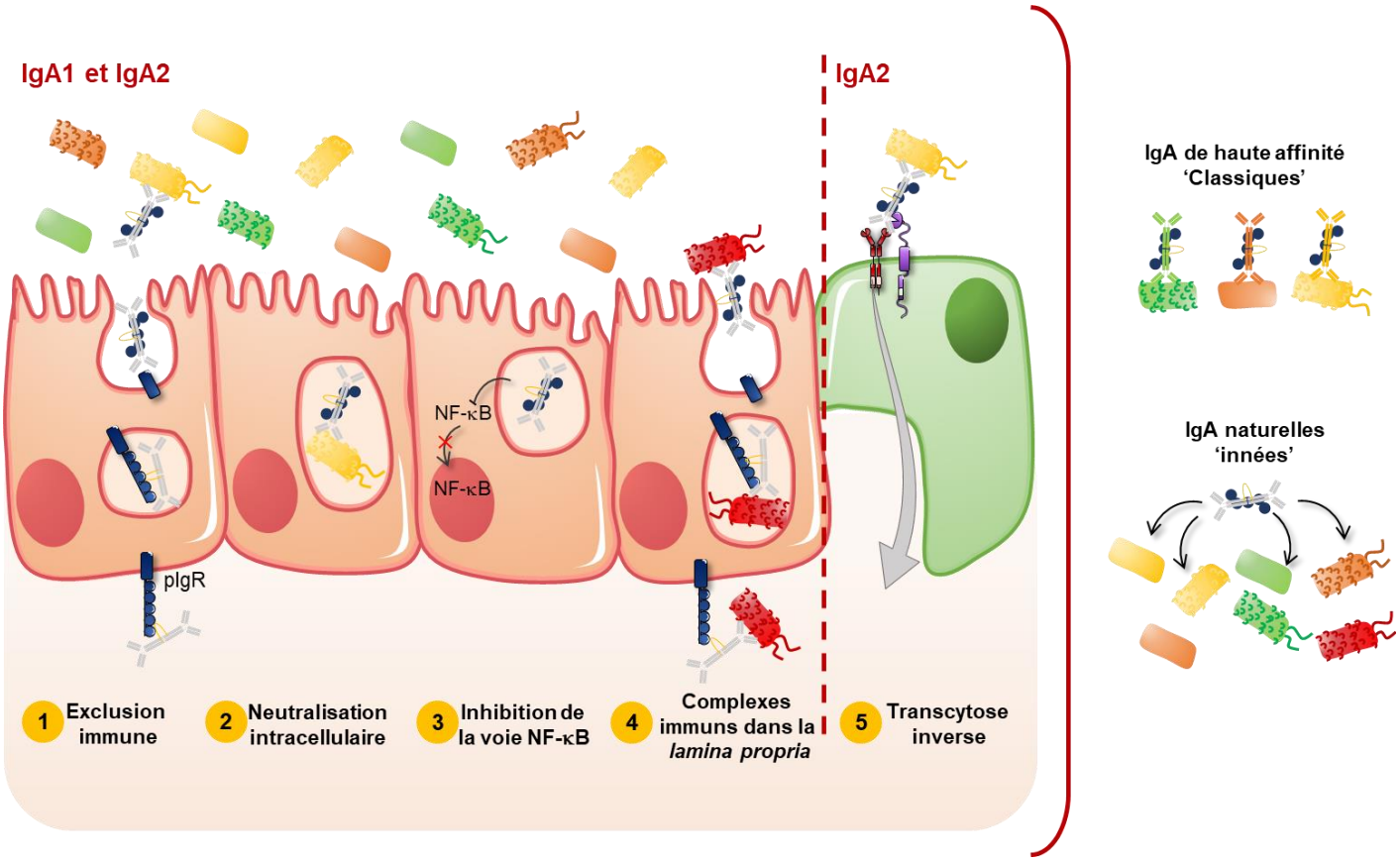

Figure 16. Fonctions muqueuses des SIgA.
(1) Les IgA polymériques de la lamina propria *sont transportées* via *la transcytose à travers les IEC où elles ségrégent les bactéries commensales des bactéries pathogènes. (2) Au cours de la transcytose, les IgA peuvent intercepter les virus et bactéries intracellulaires et les excréter sous forme de complexes non-virulents. (3) La neutralisation des LPS de bactérie Gram- dans les endosomes apicaux par les IgA en cours de transcytose abroge la signalisation NF-κB et l'activation de l'inflammation. (4) Les IgA neutralisent les agents infectieux ayant envahi la* lamina propria *au cours de l'inflammation, le transport par le pIgR permet leur retour dans la lumière intestinale. (5) La RT permet l'adressage ciblé des antigènes aux DC du dôme sous-épithélial de la PP. Ces antigènes sont ensuite présentés aux LT naïfs de la PP permet l'activation des circuits inflammatoires Th-dépendants. Ce transport peut avoir lieu avec des bactérie commensales, et conduit cette fois à la tolérogénisation de la muqueuse par l'induction de T_{reg}. Cette fonction de sélection des bactéries commensales est attribuée aux IgA polymérique naturelles.*

En parallèle, les SIgA réduisent l'inflammation envers les futurs membres de la flore commensale. Transmises lors de l'allaitement, elles limitent ainsi les réponses adaptatives du nouveau-né [189] et le protège d'éventuelles inflammations liées à la mise en place de ce microbiote dans des cas de colite nécrosantes (NEC) [190]. Les SIgA régulent l'inflammation directement par l'induction de T_{reg} et d'IL-10 [191], dans un modèle de DC dérivées de la moelle osseuse. Par ailleurs, la glycosylation des SIgA elle-même est un compétiteur discret de l'adhésion de certaines bactéries pathogènes à leurs cibles [192] : *E. coli* lie naturellement les N-glycans portés par l'IgA au lieu d'adhérer à des cellules de colon humain [193].

4- La cellule dendritique orchestre l'orientation de la réponse

Les DC muqueuses, caractérisées par le phénotype $CD11c^+$ $CX3CR1^+$, échantillonnent les antigènes luminaux *via* des prolongements de dendrites directement insérés dans l'épithélium [194,195]. Les DC captent également les échantillons via le récepteurs DC-SIGN après transcytose-inverse des IgA [43]. Les DC $CD103^+$ migrent jusqu'au MLN pour y présenter l'antigène [194,195], et secrètent du TGF-β qui stimule la commutation de classe vers l'isotype IgA [196]. En réponse à des complexes IgA-bactérie commensale, l'expression des molécules de co-stimulation par ces DC diminue, au profit d'une forte expression de gènes régulateurs de TLR et de l'induction de T_{reg} [197,198]. Cette programmation de la DC dépend de l'engagement du FcαRI : la liaison de complexes immuns à IgA1 ou IgA2 à ce récepteur sur la DC induit des ILC3 et des Th_{17}, tous deux promoteurs de l'inflammation[145,199]. Ce changement fonctionnel est lié à un changement métabolique augmentant la glycolyse intracellulaire et favorisant la transcription de gènes de l'inflammation [199]. Quand le FcαRI n'est pas engagé, la production d'IFN-γ, IL-5, et IL-13 par ces DC diminue, au profit de celle de TGF-β et d'acide rétinoïque[198], et la DC évolue vers un phénotype immunosuppresseur [200].

5- Dualité de l'exclusion immune

L'exclusion immune, par l'agglutination classique de complexes immuns a lieu entre des IgA de hautes affinités et des bactéries dont la densité est déjà forte ($>10^8$) au niveau de la lumière intestinale[201]. Ce mécanisme repose sur une collision aléatoire entre l'anticorps et son antigène : à faible densité de croissance, la rareté de cet événement limite l'utilisation de ce mécanisme comme processus de sélection principal [201]. Reste donc une seconde option, la « croissance enchainée » (*enchained growth*) : l'IgA lie la bactérie au moment de sa division, au niveau du septum, et force la bactérie à se répliquer en amas clonal[202]. Cela favorise

l'extinction clonale d'une souche pathogène, limite le transfert de gène horizontal, et privilégie l'élimination de bactéries à fort taux de réplication mais dont la densité est encore faible [202,203]. À forte densité bactérienne, les deux modes d'actions sont retrouvés, puisque l'agglutination comme la croissance enchaînée y ont lieu. Un taux de réplication élevé est donc considéré comme un comportement pathogène par l'exclusion immune. Ainsi, une IgA monoclonale isolée chez une femme saine inhibe *in vitro* la croissance d'*E. coli* invasives (AIEC) mais pas celle de la souche commensale *Lactobacillus paracasei* [182204].

Les bactéries commensales, généralement à faible taux de réplication, ne sont ainsi pas impactées. Leur sélection se fait sur la base d'interactions non-conventionnelles, où la bactérie lie les O- et des N-glycan portés par les IgA, dont ceux de la pièce sécrétoire[43,186,201]. De fait, les *Bacteroides* possèdent la machinerie complète permettant d'utiliser les N-glycans de l'hôte comme source carbonée[205]. La liaison à *B. thetaiotaomicron* selon ce modèle promeut l'expression d'un *locus* d'utilisation des polysaccharides qui favorise l'installation de réseaux microbiens bénéfiques[206]. La liaison aux IgA, simplifie transitoirement l'ancrage de bactéries dans le mucus pour favoriser l'établissement de niches microbiennes [207201]. Il existe ainsi un axe mucine-SCFA qui favorise l'expansion des T_{reg}, et des LB IgA^+ dans le colon [13].

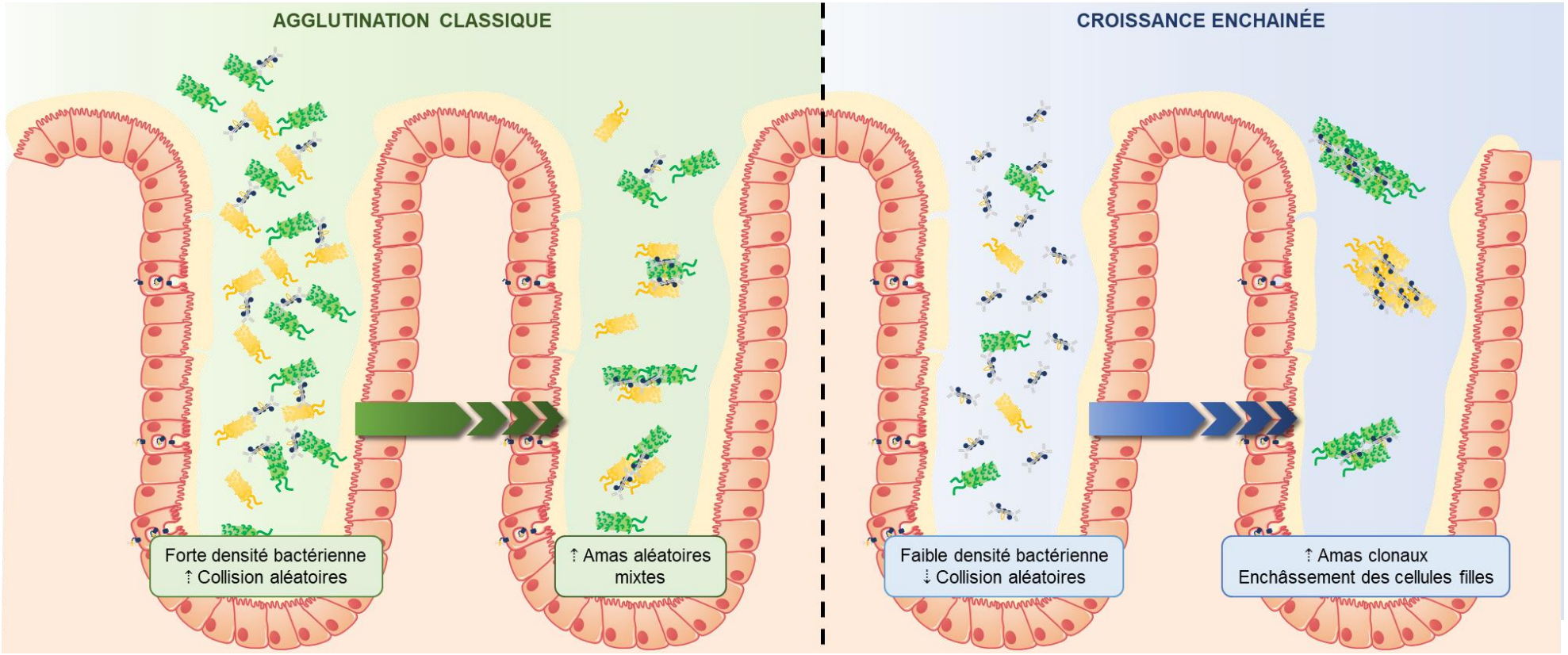

Figure 17 – Modèles d'exclusion immune médiées par les SIgA.
L'agglutination classique par les SIgA (gauche) est efficace à forte densite bactérienne, où les amas formés peuvent impliquer différentes espèces et seront drainés par les fluides intestinaux. Une forte densité microbienne favorise la probabilité de la rencontre IgA-bactérie, quelle que soit l'espèce. A faible densité bactérienne, la liaison des IgA piège les bactéries aux moment de leur division : elles poussent donc en amas clonaux autour des SIgA et sont elles-aussi drainées par le transit intestinal.

D- Sélection du microbiote par les SIg et conséquences immunes

1- Qui sélectionne la flore ?

Bien que minoritaires, les SIgM favorisent les interactions bénéfiques entre l'hôte et les microorganismes intestinaux (**Revue 1, Annexe 1**). La sécrétion d'IgM muqueuse est innée, constitutive[133] et compense les déficits en IgA (SIgAd) [208,209]. Chez l'individu sain, la fraction IgA^+ IgM^+, présente une meilleure diversité microbienne que la fraction IgA^+ IgM^- [133]. Les patients SIgAd présentent une dysbiose modérée mais asymptomatique [209] [133,208,209], qui suggèrent que, bien que l'IgM ne récapitule pas toutes les fonctions muqueuses de l'IgA, elle tempère au moins les phénomènes inflammatoires. Les réponses IgM préservent principalement la diversité des actinobactéries (comprenant les espèces *Bifidobacterium*) [209,210], notamment par l'expansion accrue de LB $CD19^+$ $CD27^+$ IgM^+ IgD^- [209]. Cependant, l'IgM ne contrôle pas l'abondance des Protéobacteries, fonction assurée par les IgA et non compensée chez les patients SIgAd [208,209].

En conditions saines, la translocation au niveau de la *lamina propria* de LB $IgG2^+$ et $IgG3^+$ sélectionne une partie du microbiote [211]. Chez la souris, ils sont issus de la PP et du MLN [189]. Ces IgG sériques convergent vers les mêmes cibles bactériennes que les IgA ce qui inclut les espèces bénéfiques comme *Faecalibacterium praustzinii* et *Bifidobacterium longum,* mais aussi des espèces pathogènes d'*E. coli* [211]. Chez les patients SIgAd, l'augmentation des réponses IgG anti-commensales muqueuses et systémiques corrèle avec une diminution générale des paramètres inflammatoires, et converge également vers des cibles normalement associées aux IgA[211].

2- Stratégies microbiennes d'attraction des IgAs

Les mécanismes mis en place par la flore commensale pour rester attractive auprès des IgA témoignent d'une singulière coévolution. *Bacteroides fragilis* possède ainsi un *locus ccf* codant pour les protéines de capsules dont elle active la transcription lorsque des résidus glycosylées de l'hôte dans les mucus sont détectés [212]. Ce signal de remodelage promeut l'opsonisation de la bactérie par les SIgA *via* des interactions glycans-glycans, et son enchâssement dans les cryptes intestinales [212,213]. Il limite également l'invasion par des compétiteurs exogènes [213]. L'activation du *locus Polysaccharide Utilisation Locus* (PUL) chez *B. thetaiotaomicron* en réponse à la liaison IgA lui permet de métaboliser le fructan alimentaire [206] : l'IgA favorise à la fois la colonisation bactérienne mais aussi le métabolisme. La

dégradation du fructan en divers SCFA permet la croissance d'autres espèces bénéfiques alors que sa perte induit la ré-émergence d'espèces à potentiel opportuniste telles que *Blautia* ou les SFB [212,214]. La liaison IgA-lactobacilles protège du dérèglement du *ratio Firmicutes/Bacteroidetes* au cours d'une dysbiose chez la souris [215]. Enfin, la synthèse de super-antigènes par les *Lachnospiraceae* sélectionne l'activation non-spécifique des LB VH3+ [216]. Seules les espèces commensales de ce taxon ont jusqu'à là été capables de produire de tels composés [216], ce qui suggère que la flore commensale sélectionne l'IgA qui promeut sa colonisation.

3- Promotion de la sécrétion d'IgA par le microbiote :

Localement, la présence même transitoire de bactéries opportunistes au niveau de l'intestin permet de re-programmer toute la séquence immune de l'intestin par la transcription durable des gènes des SIg[217]. Les métabolites de ces bactéries, en particulier l'acide heptodecanoique, pentadécanoïque, la scopolamine, et l'acide N-acetylaspartaglutamique, induisent la synthèse d'IgA qui facilitent le transit des bactéries et limitent leur motilité [217]. La résurgence d'espèces pharyngées chez le patient SIgAd suggère que ni l'IgM ni l'IgG muqueuse ne peut compenser cette fonction des IgA [211]. À l'inverse, les bactéries commensales comme les lactobacilles tolérogénisent l'environnement muqueux en conditionnant les DC, puis la production d'IgA, *via* l'induction d'IL12, d'IL-10[218,219] et de TGF-β [197]. De même, l'IL-33 induite par les commensales soutient la synthèse d'IgA et réprime la synthèse précoce d'IL-1α : le microbiote limite l'engagement vers les voies inflammatoires [188]. En l'absence de cette signalisation, la dysbiose lié à l'expansion des espèces *Akkermansia* et SFB se met en place [188]. La dysbiose engendre un profil immunitaire inflammatoire, associée à la production d'IL-17 et d'IL-22 [151] .

La plupart des IgA ont une propension à lier les glycans microbiens. Les glycosylations de la SC sont à l'origine d'interactions entre anticorps et bactéries du microbiote : parmi elle, 27 motifs sont spécifiquement engagés pour la reconnaissance de bactérie de la flore [220]. Il est ainsi supposé que la distinction entre microbe pathogène ou commensal soit médiée par la pièce sécrétoire qui, seule, peut également identifier et agglutiner des bactéries muqueuses[121]. De plus, les SIgA monoclonales de plasmocytes intestinaux ont une spécificité croisée pour les O-glycans bactériens, et neutralisent le LPS d'espèces opportunistes dont le pathogène nosocomial *Klebsiella pneumoniae* [221]. Selon ce même principe, les Ig humaines circulantes ciblant certains glycans réagissent également par spécificité croisée sur les glycans bactériens de la flore commensale [137,220]. Chez la souris, les

ordres des *clostridiales,* des *bacteriodales,* des *lactobacillales,* et des *deferribacterales* sont associés au développement du répertoire Ig anti-glycans [222]. Ce répertoire est, de plus, intrinsèquement lié à l'haplotype du MHC porté par les souris[223].

4- La sélection du microbiote répond à des besoins évolutifs au cours du développement

La mise en place du mutualisme a lieu dans les premières semaines de vie du nourrisson. Les IgA maternelles limitent les réponses adaptatives chez le nourrisson [189] par la mise en place d'un répertoire anti-glycan étendu [143] [222]. L'absence de ces IgA limitant la diversification du microbiote du nouveau-né, l'allaitement protège de la survenue d'une entérocolite nécrosante (NEC) [190]. Une augmentation de la signalisation TLR-dépendante, la sécrétion élevée TI d'IgM [189,224] et l'inhibition de la CSR[224] rendent alors la muqueuse particulièrement tolérogène.

Les taux fécaux d'IgA corrèlent avec l'abondance des *Bifidobacteria* et des *Enterobacteriaceae* et cette tendance se déplace vers un enrichissement des *Firmicutes* après la première année de vie [225]. À ce stade, les SIgM et les SIgA co-sélectionnent les même espèces, alors que les IgG semblent identifier une part distincte du microbiote [225]. Cette réponse IgG, principalement IgG2b et IgG3, également transmise par la mère, conditionne l'activation des T_{fh} et limite les réponses envers les membres nouvellement acquis du microbiote [189].

5- Effets pathogéniques de la liaison IgA-microbiote

Les antigènes alimentaires influent sur l'orientation des interactions IgA-microbiote. Un modèle murin d'allergie alimentaire montre une augmentation du taux salivaire d'IgA et de la liaison de ces IgA au microbiote buccal [226]. L'induction de cette dysbiose facilite l'expansion de la bactérie opportuniste *Citrobacter sp* qui promeut l'intensification des réponses Th_2 *via* la sécrétion d'IL-33 [226]. Ainsi, ces derniers ont une tendance naturelle à promouvoir le recrutement de T_{fh}, la maturation des PP et la formation d'ILF [227]. Un régime riche en gras (*High Fat Diet*, HFD) augmente l'abondance de bactéries IgA^+, et une diminution de l'activation de DC $CD103^+$ $CD11b^+$, cellules promotrices de réponses IgA dans le colon [228]. L'élévation de la glycémie est corrélée à un enrichissement des *Lactobacillus* IgA^+ et plus généralement à une forte proportion de *Firmicutes* IgA^+, espèces corrélées à la prise de poids et à l'augmentation de la glycémie chez l'individu sain [147,215]. Ces *Lactobacillus,* lorsqu'ils ne sont pas liés à l'IgA, protègent les souris des conséquences du régime HFD, et de l'enrichissement en *Firmicutes* [215], suggérant que la liaison à l'IgA est pathogénique. La

génération d'Ig anti-commensales augmente donc avec la délétion du gène *p2rx7*, nécessaire à la captation de l'ATP exogène par les T_{fh}[147].

E- IgA1 versus IgA2 : impact sur l'homéostasie intestinale

1- Commutation isotypique

L'orientation vers la sous-classe IgA1 ou IgA2 chez l'homme est peu caractérisée, les facteurs sous-tendant ce choix également peu définis. La chimiokine APRIL et le facteur TSLP peuvent influencer la commutation depuis un LB $IgA1^+$ vers un phénotype $IgA2^+$ [229]. Les deux sous-type sont également inductibles depuis un LB IgM^+ [131].

2- Spécificités fonctionnelles

Il existe quelques différences fonctionnelles entre les deux sous-classes d'IgA humaines [230] : les SIgA1 auront plutôt tendances à reconnaître des antigènes protéiques alors que les SIgA2 ont plutôt des propriétés anti-LPS [231]. Par ailleurs, les SIgA2 se trouvent plutôt dans les sécrétions, en particulier le colon, particulièrement à cause des N-glycosylations qui leur permettent une interaction privilégiée avec le mucus [232]. Les SIgA1 sont, elles, incapables d'effectuer la transcytose-inverse. Elles ont une fonction plutôt anti-inflammatoire, là où les SIgA2 ont plutôt tendance à stimuler l'inflammation, notamment par l'activation des neutrophiles et des macrophages[128]. *In vitro,* les IgA2 promeuvent ainsi la formation de NET (*Neutrophil Extracellular Traps*) par les neutrophiles, la libération d'IL-8 et de TNF-α *in vitro via* la liaison du FcαR et l'activation des voies intracellulaire dépendantes des protéines Syk et Erk[128].

3- Interactions avec le microbiote

Enfin, une donnée peu connue est l'importance du sous-type d'IgA dans l'interaction avec le microbiote (**Fig. 18**). Les récents travaux de Sterlin, *et al.* [220] constituent l'un des tous premiers éléments de réponse. Ainsi, si les IgA1 et les IgA2 humaines tendent à reconnaître un spectre similaire de glycans, les IgA2 sont associées à la reconnaissance préférentielle de motifs terminaux Galα et Neu5Ac. La co-fixation de bactéries par IgA1 et IgA2 favorise la sélection d'espèces d'actinobactéries, alors que l'IgA2 se lie préférentiellement aux *Bacteroidetes.* Il est intéressant de noter, de fait, que l'IgA1 favorise la sécrétion d'IL-10. La distribution de ces schémas de sélection varie également : dans l'intestin

grêle, IgA1 et IgA2 co-identifient et contribuent à la sélection des mêmes espèces, alors que dans le colon, cette sélection semble essentiellement associée aux IgA2 [220], un schéma qui suit le *ratio* IgA1/IgA2 retrouvé au niveau de ces deux sites. De manière générale, les IgA monoclonales lient les espèces *Roseburia*, *Ruminococcus*, *Clostridium* et *Blautia*, avec 2 glycans reconnus par toutes les Ig de l'étude : $(Gal\beta1\text{-}1GlcNac\beta\text{-}OCH_2CH_2)_2$ et $(GlcA\beta1\text{-}3GlcNac\beta1\text{-}4)_{20}$. Les IgA ont donc des fonctions différentes selon leur nature, leur mode d'induction, leur sous-type, et le lieu où elles sont sécrétées.

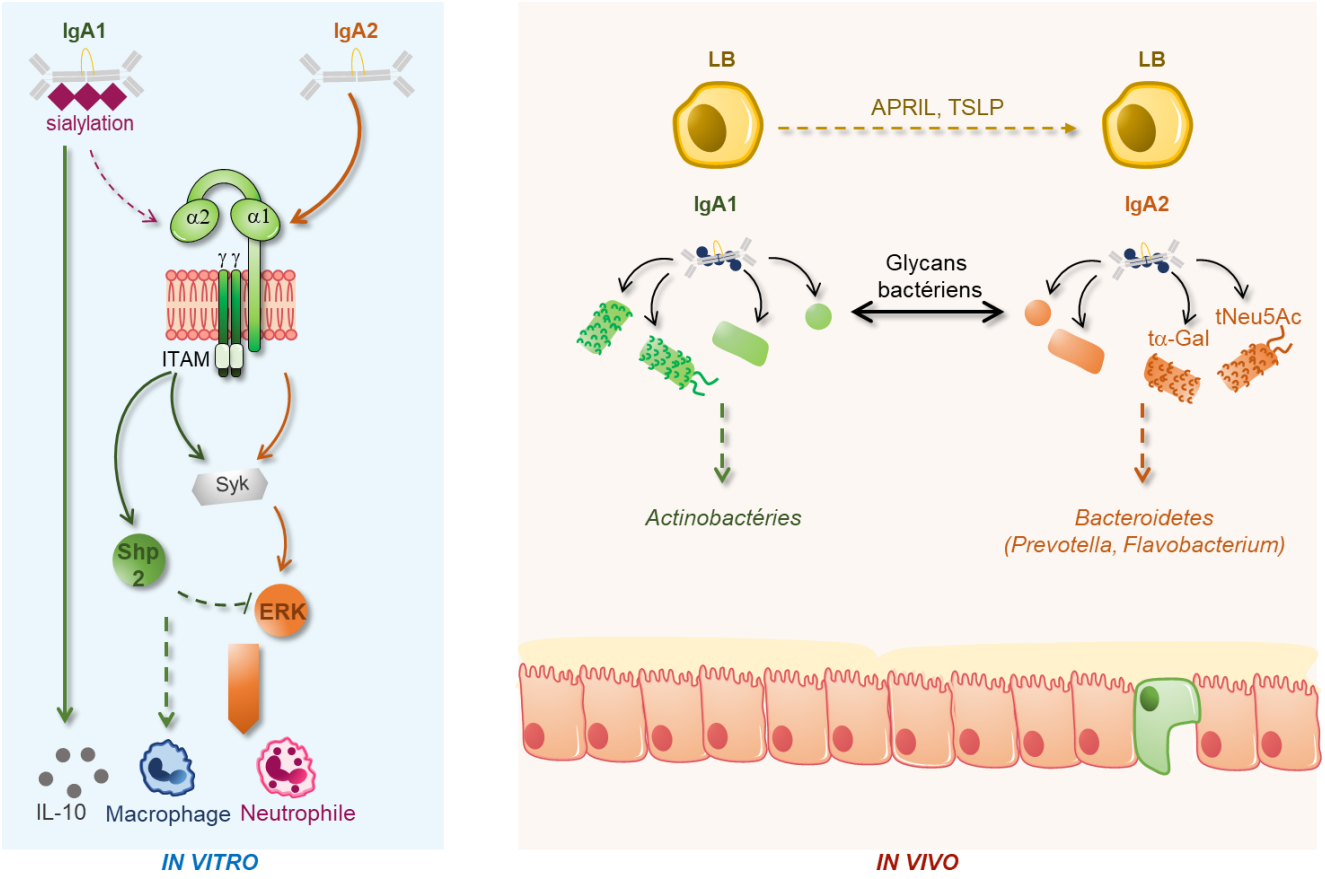

Figure 18 – Modèle des fonctions spécifiques des IgA1 et des IgA2.
Les sialylation des IgA1 limitent la signalisation sur le FcαRI in vitro et les fonctions activatrices des IgA1. Les IgA2 ont une activité FcαRI-médiée pro-inflammatoire et déclenchent notamment la NETose et la sécrétion d'IL-8 in vitro. *La reconnaissance des glycans bactériens dans la muqueuse colique favorise un large spectre de reconnaissance de la flore commensale par les IgA1 et IgA2, avec une préférance vers les motifs terminaux α-Gal (t α-Gal) et acides sialiques (t Neu5Ac) pour l'IgA2. Le basculent d'un LB IgA1$^+$ à un LB IgA2$^+$ est possible en réponse à la production des cytokines APRIL et TSLP (lymphopoïétine stromale thymique). La liaison d'IgA1 sur des bactéries déjà IgA2$^+$ favorise la sélection des Actinobactérie, tandis que les IgA2 seules identifient préférentiellement les* Bacteroidetes.

Chapitre 3 – Maladies Inflammatoires Chroniques de l'Intestin

A- Des maladies des temps modernes

1- Une épidémiologie associée au mode de vie occidental

Les MICI sont des pathologies qui se manifestent selon un rythme de poussées et de rémission, pour lesquelles aucun traitement curatif n'existe à ce jour. Parmi elles, on distingue principalement la maladie de Crohn (MC) et la rectocolite hémorragique (RCH). La MC touche les parois profondes de l'intestin, tandis que la RCH touche uniquement le colon et se caractérise par une ulcération superficielle des tissus muqueux [233].

Elles sont essentiellement recensées en Amérique du Nord et en Europe de l'Ouest selon un gradient Nord-Sud, avec 3 à 20 nouveaux cas par an pour 100 000 habitants[234,235]. (**Fig. 19, Fig. 20**). Ce sont des maladies du jeune adulte, avec deux pics d'incidence pour la MC (25-30 ans, puis plus faiblement 50-60 ans) [234] et un seul pic de diagnostic entre 30 et 40 ans pour la RCH[236]. Bien que les MICI ne soient pas associées à une forte mortalité, elle sont associées à de nombreux facteurs de morbidité[233], et un coût médical direct estimé entre 4,5 et 5,6 milliards d'euros annuels en Europe[236]. Il s'agit clairement de maladies liées à l'industrialisation et à la production alimentaire de masse, généralement pauvre en fibres [237].

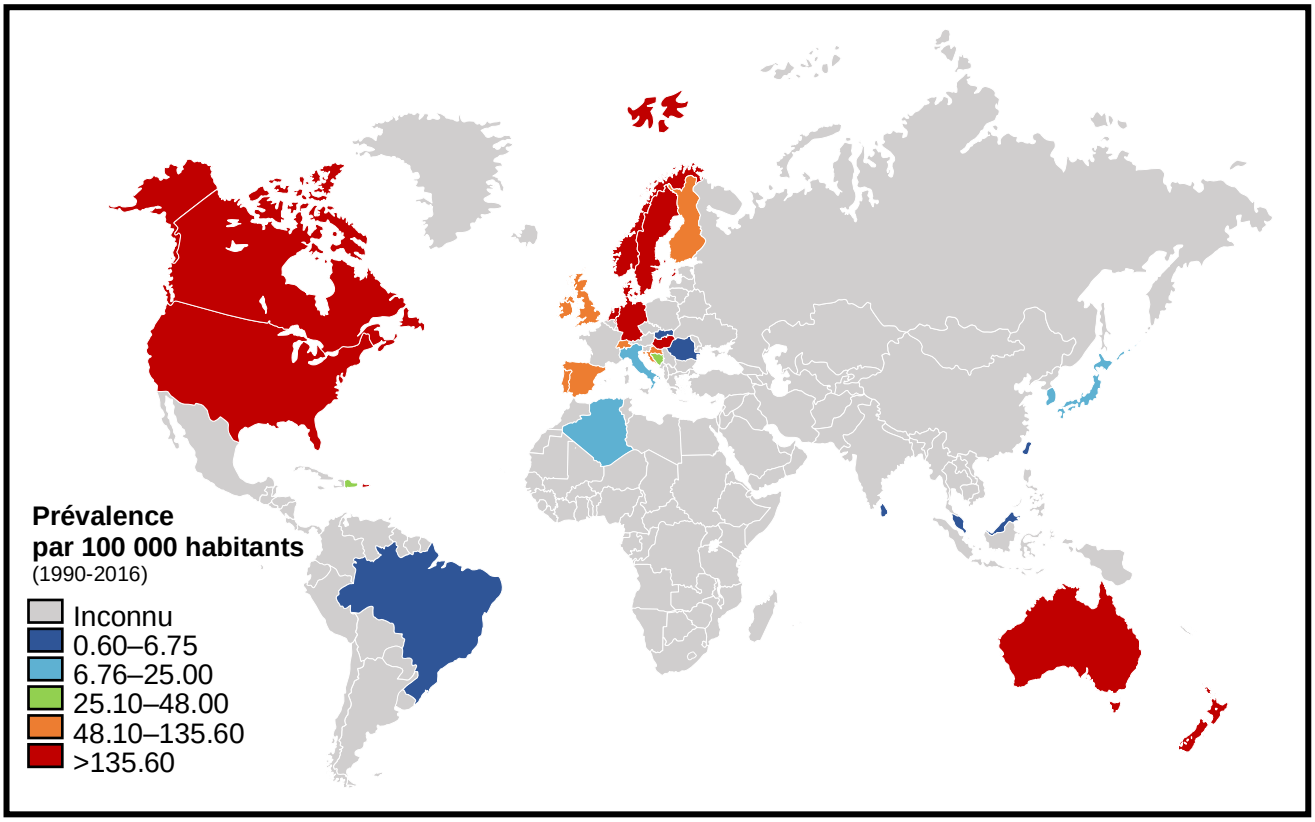

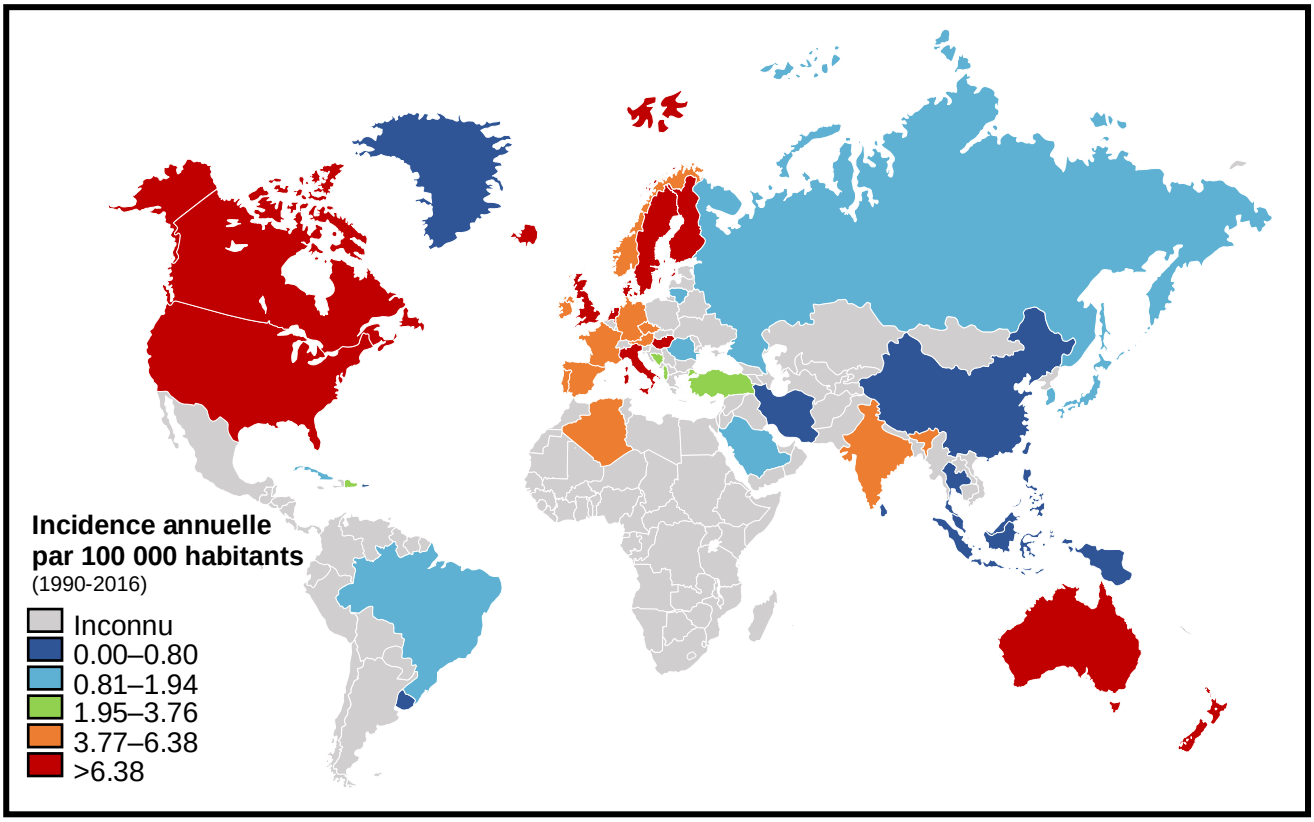

Figure 19 – Épidémiologie de la maladie de Crohn.
Carte de la prévalence en quintiles (haut) et de l'incidence annuelles (bas) de la maladie de Crohn. D'après Ng, et al. *Lancet (2018)*

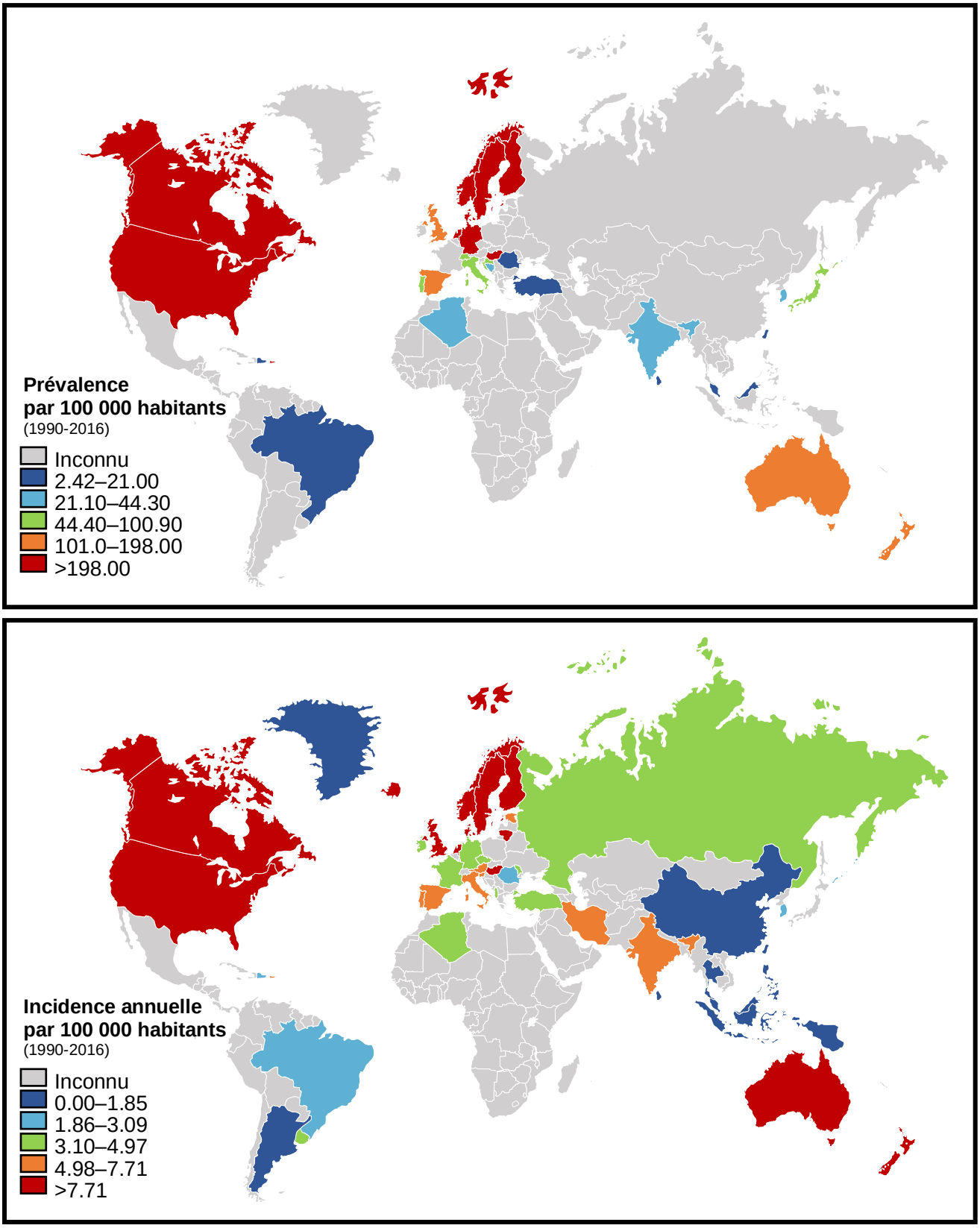

Figure 20 – Épidémiologie de la rectocolite hémorragique.
Carte de la prévalence en quintiles (haut) et de l'incidence annuelle (bas) de la rectocolite hémorragique. D'après Ng, et al. *Lancet (2018)*

2- Des pathologies à l'étiologie complexe comprenant de nombreux facteurs de risques

a. Influence de l'hérédité

Les polymorphismes génétiques impactent la localisation de l'inflammation : une atteinte colique est associée aux allèles de gène codant pour le CMH (*HLA*) [238–241] en particulier le CMH de classe II [242]. L'hétérozygotie pour le variant allélique HLA-DRB1*01:03 confère un avantage sélectif dans la RCH [242] : le faible taux d'hétérozygotie observée chez ces patients indique donc une affinité moindre pour des antigènes coliques. En revanche, une atteinte de l'intestin grêle (MC) est plutôt associée à des mutations sur le gène *CARD15* (codant pour NOD2) [243,244], qui sont les plus fréquentes[245,246]. NOD2 collabore notamment avec le produit du gène *ATG16L1* dont il permet le recrutement à la membrane plasmique [247], et qui est également un gène de susceptibilité à la MC [248]. Ce dernier implique donc l'autophagie comme modulateur clé des MICI. Plusieurs autres gènes mutés dans les MICI sont, de manière générale, impliqués dans la composition – et l'interaction avec – le microbiote, dont les gènes *VDR, FUT2, LCT, NOD2, TLR2* et *TLR4* [249,250]. Des mutations sur le gène *MUC2*, mucine principale du glycocalyx muqueux, sont associées à la mise en place précoce de la dysbiose [251,252]. Des polymorphismes variés sur des gènes impliqués dans l'activation et de maintien de l'immunité lymphocytaire (*TNFSF11, PTPN22, IL2RA, IL27*) [248], de la fonction barrière de l'épithélium (*HNF4A, CDH1*) [253,254], ou encore de la voie des macrophages (locus 3p21 codant pour MST1) [255] sont également corrélés aux MICI et à la dysbiose. Des modifications épigénétique dont la méthylation de l'ADN[256] et l'acétylation des histones H4[257] sur de nombreux gènes de la voie Th_{17} et de la réponse aux bactéries[256], augmentent également la susceptibilité à la MC [258]. Les associations génétiques n'expliquent cependant qu'un faible pourcentage de la variance associée aux MICI.

b. Une succession de paramètres environnementaux conditionne l'apparition des MICI

Toute perturbation de l'écologie microbienne est susceptible d'induire l'inflammation (**Tableau 2**) : les MICI, particulièrement la MC, sont corrélées à la prise régulière d'antibiotique, d'anti-inflammatoires non-stéroïdiens[259–261], et a un historique de gastroentérites récurrentes, dont les infections à *Salmonella* et *Campylobacter* [261,262]. La composition en fibre [237] et en acide gras saturés [214] de l'alimentation, et la présence d'additifs et de conservateurs, affectent aussi la diversité microbienne.

Les habitudes de vie telles que le tabagisme[263–266], l'utilisation d'hormones contraceptives, les thérapies de conversion hormonales, et la mise au monde des nourrissons (allaitement[267,268], césarienne, médicalisation de l'accouchement [269,270]) sont corrélés à la survenue des MICI[271,272]. À noter que le tabagisme actif restreint l'incidence de la RCH[273] bien qu'il n'améliore pas la progression de la maladie[274]. De manière générale, l'exposition dans l'enfance à un différentiel de pathogènes bactériens et parasitaires semble limiter l'incidence des MICI [275]. Ces évènements de la petite enfance ont plutôt des effets sur le développement de MC, la RCH serait en revanche influencée par l'environnement à l'instant *t* et à l'âge adulte [268,276].

Tableau 2 – Bactéries impliquées dans des modèles de MICI
Casp1 : caspase 1; DSS : sodium de dextran sulfate; MICI : maladies inflammatoires chroniques de l'intestin; MyD88 : myeloid differentiation primary-response protein 88*; NA : non applicable; Nlrp6 :* NOD- LRR- and pyrin domain-containing 6*; Rag2 :* recombination-activating gene*; Tbx21 : T-box21 (code pour T-bet); Tgfr2 :* transforming growth factor-β receptor 2*; TLR :* toll-like receptor*; TNBS : Acide sulphonique 2,4,6-trinitrobenzene; TRUC : souris Tbx21$^{-/-}$ Rag2$^{-/-}$. WT : sauvage; * : transmissible à des hôtes mutants; ° : transmissible à des hôtes WT.*

Bactérie commensale	Hôte	Génotype	Maladie	Récepteur	Mécanisme inducteur potentiel
Espèces commensales associées à la protection contre le développement de MICI					
Clostridium spp. Cluster IV et XIVa	Souris	WT	Colite au DSS	Inconnu	Induction des T_{reg}
Flore altérée de Shaedler	Souris	WT	Colite au DSS	MyD88 et TRIF	Induction des T_{reg}
Bacteroides fragilis	Souris	WT	Colite au TNBS	TLR2, MyD88	Induction des T_{reg} via le polysaccharide A
Bacteroides vulgatus	Souris	*Il2*$^{-/-}$	Colite spontanée	Inconnu	Suppression de la colite médiée par E. coli dans les souris *Il2*$^{-/-}$
Faecalibacterium prausnitzii	Humain	NA	MICI	Inconnu	Induction d'IL-10 par les monocytes circulants
Espèces commensales associées au développement de MICI					
E. coli	Souris	*Il10*$^{-/-}$	Colite spontanée	Inconnu	Mono-colonisation de souris axéniques
E. coli	Souris	*Il2*$^{-/-}$	Colite spontanée	Inconnu	Mono-colonisation de souris axéniques
Enterococcus faecalis	Souris	*Il10*$^{-/-}$	Colite spontanée	Inconnu	Mono-colonisation de souris axéniques
B. vulgatus	Rat	transgénique *HLA-B27-B2m*	Colite spontanée	Inconnu	Mono-colonisation de rat axéniques
B. vulgatus	Souris	*Il10r2*$^{-/-}$ *Tgfbr2*$^{-/-}$	Colite spontanée	Inconnu	Colonisation de souris traitées aux antibiotiques
Bacteroides thetaiotaomicron	Souris	*Il10r2*$^{-/-}$ *Tgfbr2*$^{-/-}$	Colite spontanée	Inconnu	Colonisation de souris traitées aux antibiotiques
B. thetaiotaomicron	Souris	Transgénique *HLA-B27-B2m*	Colite spontanée	Inconnu	Mono-colonisation de souris axéniques
Bacteroides unifirmatis	Rat	*Il10r2*$^{-/-}$ *Tgfbr2*$^{-/-}$	Colite spontanée	Inconnu	Colonisation de souris traitées aux antibiotiques
Klebsiella pneumonia *°	Souris	*Tbx21*$^{-/-}$ *Rag2*$^{-/-}$	Colite spontanée	Inconnu	D'autres bactéries commensales sont requises pour l'induction de la colite
Proteus mirabilis *°	Souris	*Tbx21*$^{-/-}$ *Rag2*$^{-/-}$	Colite spontanée	Inconnu	D'autres bactéries commensales sont requises pour l'induction de la colite
Helicobacter tiphlonius *	Souris	*Tbx21*$^{-/-}$ *Rag2*$^{-/-}$	Colite spontanée	Inconnu	Transmissible à des souris TRUC non-colitogéniques
Prevotellaceae *°	Souris	*Nlrp6*$^{-/-}$*Asc*$^{-/-}$ *ou Casp1*$^{-/-}$	Colite au DSS	Inconnu	Altération de la signalisation de l'IL-18
TM7	Souris	*Nlrp6*$^{-/-}$*Asc*$^{-/-}$ *ou Casp1*$^{-/-}$	Colite au DSS	Inconnu	Altération de la signalisation de l'IL-18
Bilophila wadsworthia	Souris	*Il10*$^{-/-}$	Colite spontanée	Inconnu	Consommation d'un régime comprenant des acides gras dérivés de lait

B- Maladie de Crohn

1- Tableau général

La MC est une maladie hétérogène dans ses manifestations et ses complications ; elle peut toucher n'importe quelle partie du tube digestif, de la bouche à l'anus. Environ 50% des patients doivent avoir recours à une chirurgie entre 2 à 10 ans après le diagnostic [277], et 50% de ceux-ci font une rechute. Les symptômes incluent des douleurs abdominales, diarrhées parfois hémorragiques, perte de poids, nausées, vomissements, et dans certains cas de la fièvre. Plusieurs phénotypes, qui incluent l'état de la muqueuse (phénotype inflammatoire, sténosés, et perforant) et la localisation de l'inflammation (iléale, colique, ou iléocolique) sont décrit par la classification de Montréal (**Fig. 21**) [278]. La pathologie touche les tissus profonds du tube digestif [279], ce qui se traduit par l'observation d'ilots inflammatoires alternant zones lésées et zones d'apparence saine. L'architecture des cryptes intestinales est déstabilisée : elles présentent un raccourcissement ou une atrophie, des abcès, ou des granulomes [234]. L'ulcération profonde de l'épithélium conduit à l'érosion de la couche musculaire et à des détachements de la muqueuse qui rompent la barrière intestinale [279]. Ces phénomènes s'accompagnent d'une réorientation des réponses LT vers un profil Th_1/Th_{17} qui soutient cette inflammation[277], et une réduction de la diversité commensale[280] entraînant une baisse de l'absorption de nutriments et de la synthèse de vitamines [281].

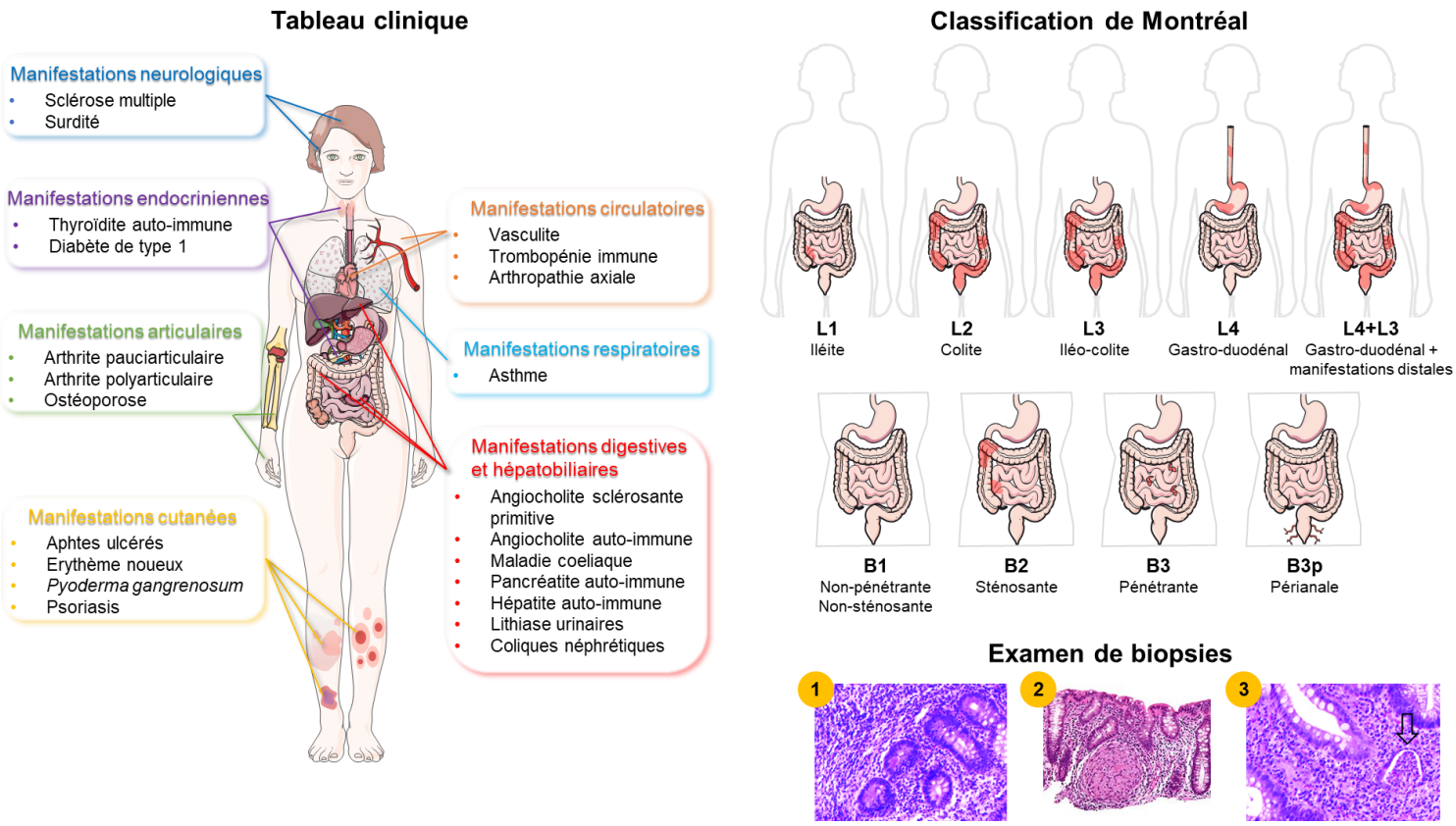

Figure 21 – Phénotype de la maladie de Crohn et diagnostic.
Tableau clinique des manifestations intra- et extra-intestinales associées à la maladie de Crohn (gauche). La classification de Montréal identifie cinq phénotypes selon la localisation de la maladie (L1 à L4+L3). D'autres lésions associées à la sévérité du phénotype complètent cette description (B1-B3p). Une partie du diagnostic se fait également sur biopsies, dans lesquelles on recherche des infiltrats lymphocytaires et de neutrophiles (1), des granulomes (2), ou des abcès des cryptes intestinales (3, fl1èche). Coloration hématoxyline-éosine (H-E), 50x (1), 200x (2, 3), Stanton, et al. *ACG Case Rep J (2017).*

2- Phase d'initiation

a. Augmentation de la perméabilité intestinale

Les MICI sont caractérisées par la rupture de la barrière intestinale (**Fig. 21**). Dans la MC, cela se traduit par une rupture des jonctions serrées *via* la redistribution spatiale des claudines[282], les polymorphismes génétiques [282], ou la consommation importante d'additifs alimentaires[283]. En parallèle, la synthèse de métabolites promouvant l'expression de protéines des jonctions est défectueuse chez les patients [284]. L'induction locale de TNF-α et l'IFN-γ augmente la perméabilité des jonctions et favorisent l'apoptose des IEC[285–287]. Ces mécanismes favorisent les phénomènes de dysbiose. Une baisse simultanée de la sécrétion de mucus[251] et d'AMP[288] dérégule la zone tampon entre l'hôte et le microbiote, et favorise l'expansion de

bactéries opportunistes. En conséquence, les patients atteint de CD ont des taux d'ADN bactérien circulants significativement plus élevés qu'un individu sain, témoin d'une importante translocation bactérienne depuis le compartiment muqueux[289]. Ces réponses attirent un important infiltrat de neutrophiles et de macrophages, et favorisent le stress oxydatif, la protéolyse, la libération de cytokine pro-inflammatoires [290]. Les dommages infligés aux tissus par ces différentes cascades entraînent la libération de produits cytosoliques et nucléaires, aux propriétés intrinsèquement inflammatoires, les DAMP [290].

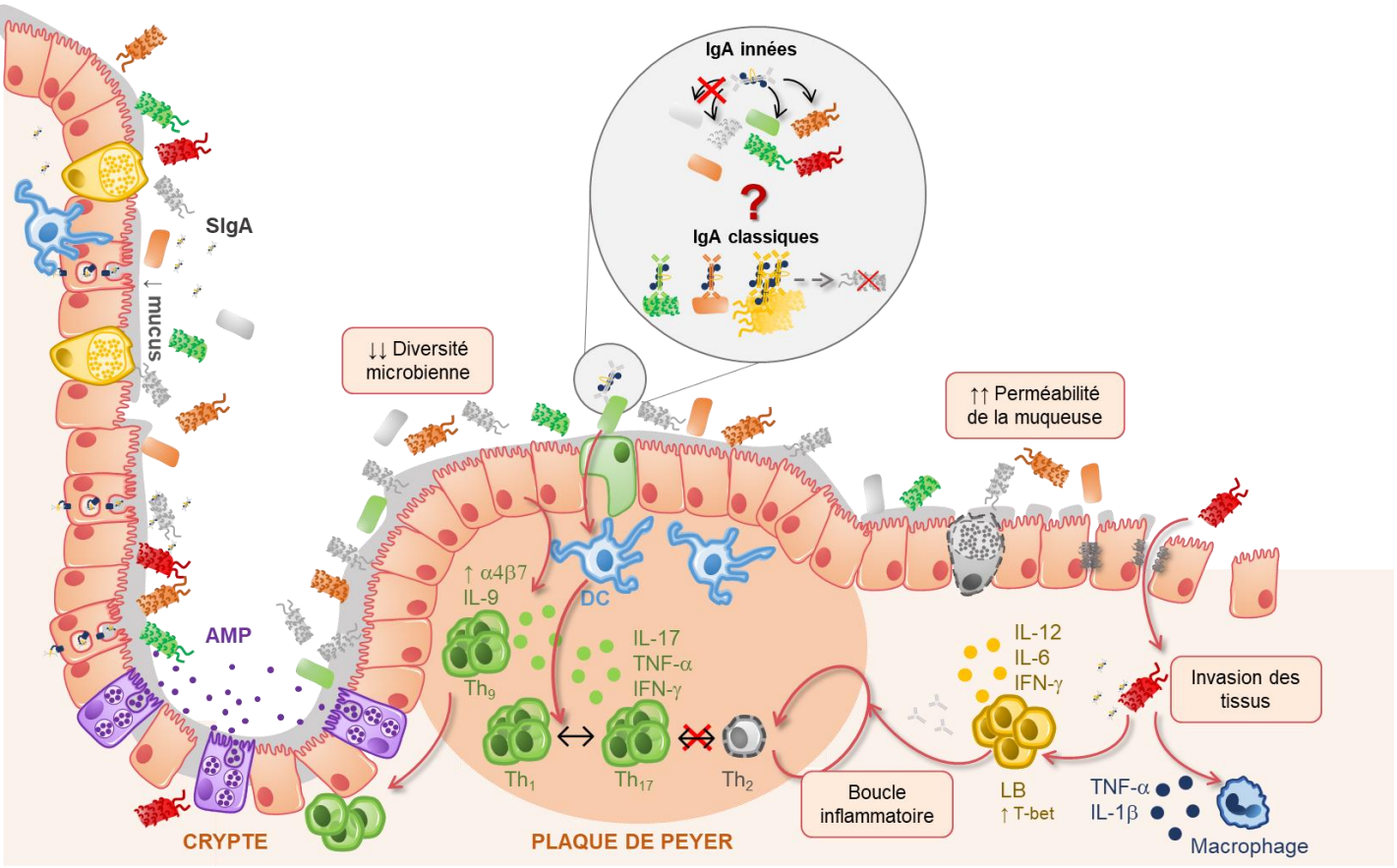

Figure 22 – Physiopathologie de la maladie de Crohn.
La maladie de Crohn est caractérisée par une perte de diversité microbienne concomitante à une augmentation de la perméabilité intestinale liée à une diminution de la sécrétion de mucus et une rupture des jonction serrées. L'invasion de la muqueuse par les bactéries luminales entraîne le recrutement et l'activation de macrophages et de plasmocytes a IgA et à IgG qui stimule l'immunité Th_1 et Th_{17}. La sécrétion intense de TNF-α soutient la mise en place d'une boucle inflammatoire qui recrute continuellement de nouveaux effecteur grâce à l'expression des intégrines α4β7. Le rôle et la nature des IgA dans l'établissement de cette boucle n'est pas décrit.

b. L'autophagie contribue à la mise en place de la dysbiose

Les voies de l'autophagie conduisant à l'élimination de pathogènes intracellulaires sont dérégulées soit par des polymorphismes génétiques [291], soit par l'augmentation de l'expression d'effecteurs clés de la voie comme ATG2 ou LC3 dans la MC[292,293]. Ces défauts impactent la biologie des cellules de Paneth, dont le nombre diminue chez les patients présentant des polymorphismes sur le gène *ATG16L* [294]. NOD2 est justement régulé par ce gène, et de fréquents polymorphismes de perte d'activité de NOD2 sont retrouvés chez les patients atteints de MC. Ils corrèlent avec une perte de l'abondance des espèces bénéfique *Roseburia sp.* et *Faecalibacterium prausnitzii*[295]. Également, la baisse de la sécrétion d'AMP coïncide avec une moindre responsivité des monocytes circulants chez les patients[296]. Les microbes opportunistes pourraient donc exploiter la sur-activation de l'autophagie pour envahir les tissus sous-muqueux, les pressions de sélection ayant alors diminué.

c. La dysbiose microbienne entraîne un changement métabolique favorable à l'inflammation

La caractéristique microbienne phare de la MC est la diminution du ratio *Firmicutes/Bacteroidetes* au sein de la flore commensale[297–299], celui-ci est affecté par l'augmentation de l'abondance des Proteobactéries (particulièrement les Enterobacteriaceae) et la diminution de celle des *Firmicutes* et des *Verrucomicrobia* [13,300,301]. Les SFB sont, elles, plus abondantes[301]. L'expansion des espèces oro-pharyngées telles que *Gemella, Peptostreptococcus,* et *Streptococcus* dans le microbiote fécal de patients atteints de MC mais pas de l'individu sain [302] suggère une perte de la compartimentation des muqueuses.

Ces changements témoignent d'un basculement depuis un métabolisme carboné vers celui des lipides [298], et de la perte de métabolites bactériens nécessaires à l'homéostasie[13]. Ainsi, la MC est largement associée à la perte des espèces *Eubacterium rectale*[13] et *Faecalibacterium prautzinii* [76,303], producteurs privilégiés de butyrate et promoteurs de la croissance d'autres espèces bénéfiques telles que *Roseburia sp* [304]. L'intégralité des réseaux bactériens en est affectée, en témoigne la baisse significative simultanée des espèces productrices de n-butyrate *Blautia faecis, Roseburia inulinovorans* et *Ruminococcus torque*[305]. Celles-ci appartiennent à un cluster d'espèces bactériennes, comprenant majoritairement des Lachnospiraceae et des Ruminococcaceae, dont la composition est prédictive de rechutes post-chirurgicales, d'échecs thérapeutiques, ou bien de phénotypes sévères[306]. Leur disparition est significativement associée à l'atrophie et au dysfonctionnement des cellules de Paneth[307]. D'autres travaux modélisent la signature microbienne de la MC par l'algorithme « ne contient pas de

Faecalibacterium, ou de Peptostreptococcaceae, ni encore d'*Anaerostipes* ou de Christensenellaceae ; ou bien, ceux-ci contient Fusobacterium et *Escherichia* mais pas *Collinsella* et *Methanobrevibacter* » [308]. Ainsi, il apparaît que le métabolisme des SCFA gouverne non seulement la composition des niches microbiennes, mais promeut également un retour à l'homéostasie, un phénotype modéré, ou le succès d'une stratégie thérapeutique dans la MC.

3- La dysbiose affecte l'immunité sécrétoire

Au cours de la MC, les SIg perdent leur rôle anti-inflammatoire: un basculement depuis la sécrétion d'IgA dimériques, vers celle d'IgG et d'IgA monomériques s'opère[309]. Ces phénomènes ne sont pas seulement locaux : la présence d'anticorps circulants contre les antigènes commensaux [309,310] corrèle avec une maladie plus longue et plus sévère [310]. La liaison IgA-microbiote devient pathogénique : l'augmentation des fractions de la flore commensales liées aux IgA et aux IgG corrèle avec l'activité de la maladie [302,311]. De fait, y a globalement plus de bactéries Ig^+ dans le microbiote fécal des patients[302]. Ces fractions sont notamment enrichies par des espèces de la flore pharyngée comme *Peptostreptococcus*, et *Streptococcus* [302]. D'autre part, la liaison à *E. coli* coïncide avec le développement de maladies articulaires associées à la MC, et l'exacerbation de l'immunité Th_{17}[312,313]. Deux phénomènes semblent donc avoir lieu : (i) la liaison à l'IgA permet à la bactérie opportuniste de se maintenir dans l'intestin avant d'être drainée par le flux intestinal ; (ii) la liaison aux IgA élimine les membres de la flore commensale.

La fonction des IgG et des IgM de ce contexte semble compensatoire : la sécrétion d'IgM caractérise l'entrée en rémission, elle-même associé à une diminution du taux fécal d'IgA[314]. Le taux fécal d'IgG augmente aussi dans la MC [302]. Chez la souris, les bactéries associées au développement de l'inflammation sont justement celles qui n'étaient pas identifiées par les IgA [315]. Les fractions IgG^+ du microbiote contiennent notamment les espèces *Ruminococcus sp* et *Flavonifractor plautii*, toutes deux capables d'envahir les cellules épithéliales *in vitro* [316]. L'IgG identifie donc des pathobiontes muqueux dans la MC.

4- Phase chronique

a. *Initiation de la réponse*

Les cellules dendritiques, normalement tolérogènes en conditions homéostatiques, deviennent extrêmement inductibles au cours de la MC, en particulier *via* l'expression accrue des récepteurs TLR2 et 4 [317]. Elles sécrètent des cytokines pro-inflammatoires, dont l'IL-12 et l'IL-6 [290], qui activent les ILC muqueux. Ces derniers, répondent par la sécrétion de TNF-α, IL-17, IL-22 et IFN-γ qui ont un fort pouvoir remodelant sur les réponses cellulaires adaptatives. Ils entraînent l'accumulation d'ILC3 et d'ILC1 muqueux chez les patients atteints de MC [318,319]. L'IFN-γ induit également l'apparition de LT $CD4^+$ porteurs de marqueur NK et produisant l'IL-17 et l'IL-22 (Nat rev gastro 2016). De la même manière, les macrophages intestinaux ($CD14^-$), au lieu de promouvoir les interactions hôte-microbiote par une faible responsivité, changent de phénotype ($CD14^+$ $CD33^+$ $CD68^+$) chez les patients atteints de MC[290,320] : une partie exprime en effet des marqueurs de DC ($CD205^+$ $CD209^+$), qui les rends fortement inductibles et ils sécrètent de nombreux facteurs pro-inflammatoires dont l'IL-6, l'IL-23 et le TNFα [321].

b. *Activation de l'immunité cellulaire par les signaux commensaux*

La MC est caractérisée par une inflammation dominée par les cytokines Th_1 et Th_{17}, induits en réponse à l'IL-12, l'IL-18, l'IL-23 et au TGF-β [322]. Le transfert de microbiotes d'individus sains dans des souris axéniques (*germ-free*) induit l'expansion de T_{reg} $ROR\gamma T^+$ dans l'intestin, celui de patients MICI entraîne une forte augmentation des $CD4^+$ $IL17A^+$[323]. D'autre part, l'inflammation de type Th_{17} est soutenue par certains membres de la flore commensale, dont les espèces *Prevotella* [94,313] et les SFB[313]. En effet, leur adhésion à la muqueuse corrèle avec l'activation des Th_{17} et à la sécrétion d'IgA[313]. Cet effet est attribué aux IgA dimériques, les formes monomérique induisant plutôt l'expansion de T_{reg} $Foxp3^+$ [324]. Le basculement vers la sécrétion d'IgA monomérique observée chez les patients pourrait donc être un mécanisme de défense en réponse à l'inflammation.

Cette polarisation de la réponse est systémique, les patients présentent ainsi des LT $CD4^+$ circulants réagissant à des antigènes commensaux *via* la production de cytokines IL-17, TNF-α, et IFN-γ [310], qui leur confère un phénotype mixte Th_1/Th_{17}. Ils sont phénotypiquement différents des Th_1, qui eux acquièrent des propriétés cytotoxiques similaires aux LT $CD8^+$ [325]. Les plasmocytes à IgG retrouvés chez les patients dont la maladie est active sécrètent également

de l'IFN-γ, de l'IL-12 et de l'IL-6 qui stimulent la production autologue d'IFN-γ par les Th_1 et leur prolifération [326]. Tous ces lymphocytes suractivés sont, de plus, résistant à l'apoptose qui régule leur expansion en condition saines [290]. À cet effet, ils présentent une augmentation de l'expression de l'IL-2R et de la production d'IL-2, cytokine responsable du maintien des LT, pourrait en être l'origine [290].

Une hypothèse encore peu évoquée par la littérature actuelle est la possibilité que ces réactions exagérées ne trouvent pas leur source dans le microbiote intestinal, mais dans le microbiote d'autres sites muqueux. Par exemple, des souches buccales de *Klebsiella*, lorsqu'elles sont inoculées dans l'intestin de souris gnotobiotiques, sont de fortes inductrices de Th_1 et colonisent facilement l'intestin dysbiotique [327]. Une translocation bactérienne d'un site muqueux à l'autre, ou bien celle de cellules amorcées par des antigènes d'un autre site muqueux, pourraient donc être à l'origine de l'inflammation dans la MC. Moins ambitieusement, ce phénomène pourrait également être à l'origine de poussées inflammatoires qui caractérisent la pathologie.

c. Remodelage de la sécrétion cytokinique

En conditions homéostatiques, l'IL-33 et le TGF-β induits par la flore commensale participent à la cicatrisation et la tolérance immune. Dans la MC, leurs expressions est particulièrement accrue dans les phases aiguës de la maladie, sans que des effets bénéfiques ne soient observés. L'IL-33, recrute sur les phases ultérieures de l'inflammation les T_{reg} $FoxP3^+$, [328]. Le facteur c-maf, induit par les signaux commensaux dans les LT $CD4^+$, est un élément clé dans leur induction, et son absence fournit un terrain favorable au développement de la colite [151]. En parallèle, les voies de l'IL-10 soutenant l'activation et l'expansion des T_{reg} sont abrogées [329,330] (**Fig. 23**).

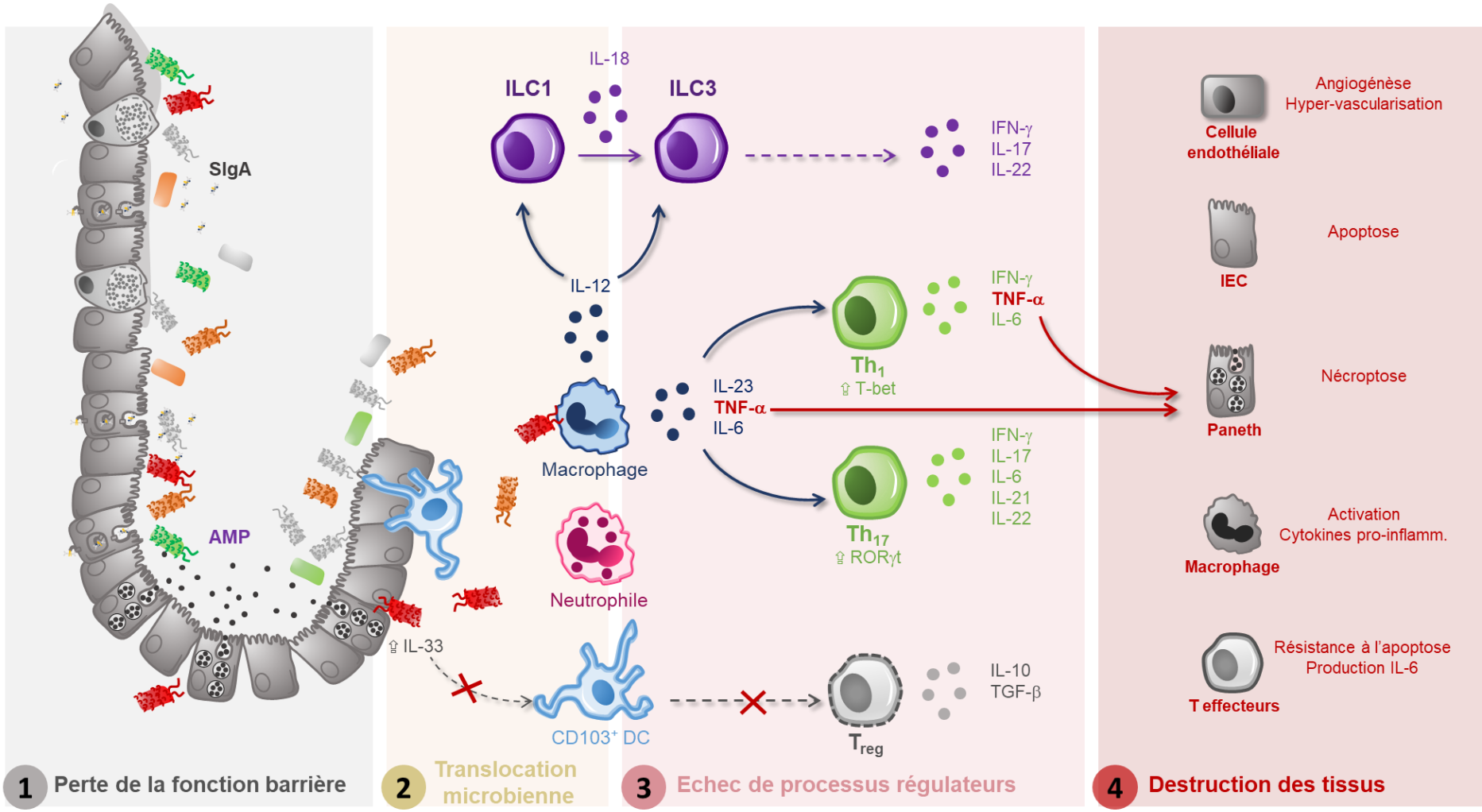

Figure 23 – Rôle des cytokines pro-inflammatoires dans la maladie de Crohn.
L'ouverture de la barrière intestinale (1) facilite l'invasion des tissus par les bactéries luminales (2) et le recrutement d'effecteurs innés (macrophages, neutrophiles). Dans le même temps, l'immunité perds le contrôle des processus régulateurs dépendants de l'IL-10 (3) et favorise l'expansion de population Th_1 et Th_{17}. La sécrétion concomitante de TNF-α entraîne la mise en place d'une boucle inflammatoire permettant une vascularisation anarchique, l'apoptose des IEC et l'activation continue d'effecteurs pro-inflammatoires.

C- Rectocolite hémorragique

1- Tableau général

La RCH fonctionne également sur un mode poussées-rémissions qui peuvent être très prolongées, de plusieurs mois à plusieurs années parfois, contrairement à la MC. Les symptômes couramment évalués sont la diarrhée et la présence de sang et de mucus dans les selles. Les douleurs abdominales indiquant principalement une MC, la RCH se diagnostique par une augmentation de la fréquence des mouvements péristaltiques, ou d'éventuelles crampes abdominales, une incontinence, des défécations nocturnes, et une fatigue accrue [233]. La classification de Montréal définit plusieurs phénotypes dépendant de l'étendue de la maladie (**Fig. 24**). Le suivi biologique surveille principalement les infiltrats de neutrophiles, de lymphocytes, et la concentration d'anticorps anti-neutrophiles circulants [331] (**Fig. 24**).

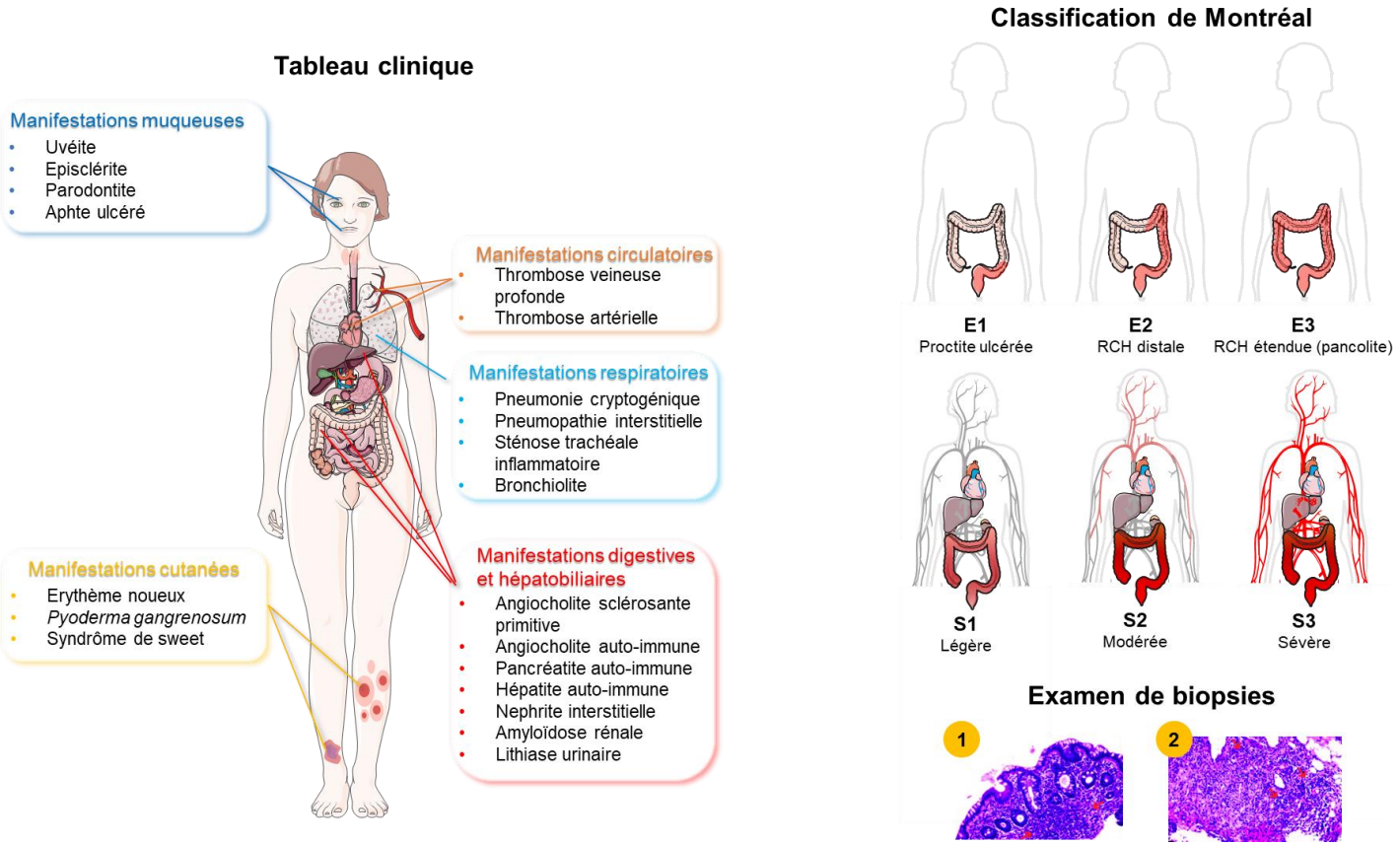

Figure 24 – Diagnostic et phénotype de la rectocolite hémorragique.
Tableau clinique des manifestations intra- et extra-intestinales associées à la rectocolite hémorragique (gauche). La classification de Montréal identifie trois phénotypes selon la localisation de la maladie (E1 à E3). La détection de marqueur inflammatoire dans la circulation sanguine est associée à la sévérité du phénotype et complète cette description (S1 à S3). Une partie du diagnostic se fait également sur biopsies, dans lesquelles on recherche des infiltrats de neutrophiles (1,2, flèches rouges), et/ou des lésion ulcérées (2), Coloration (H-E), 200x, Zhu, et al. *Medicine (Baltimore) (2018).*

À la différence de la MC, le patients atteints de RCH présentent une muqueuse extrêmement friable et granuleuse, dans laquelle on observe une ulcération étendue du tissu et une irrigation sanguine anarchique [332] (**Fig. 25**). Alors que dans la MC on observe une alternance de zones lésées et de zones saines, les ulcères au cours de la RCH s'accompagnent d'une forte inflammation des tissus muqueux environnants [333]. Le consensus actuel est que cette inflammation est principalement alimentée par une réponse Th_2, et s'accompagne également d'une dysbiose microbienne.

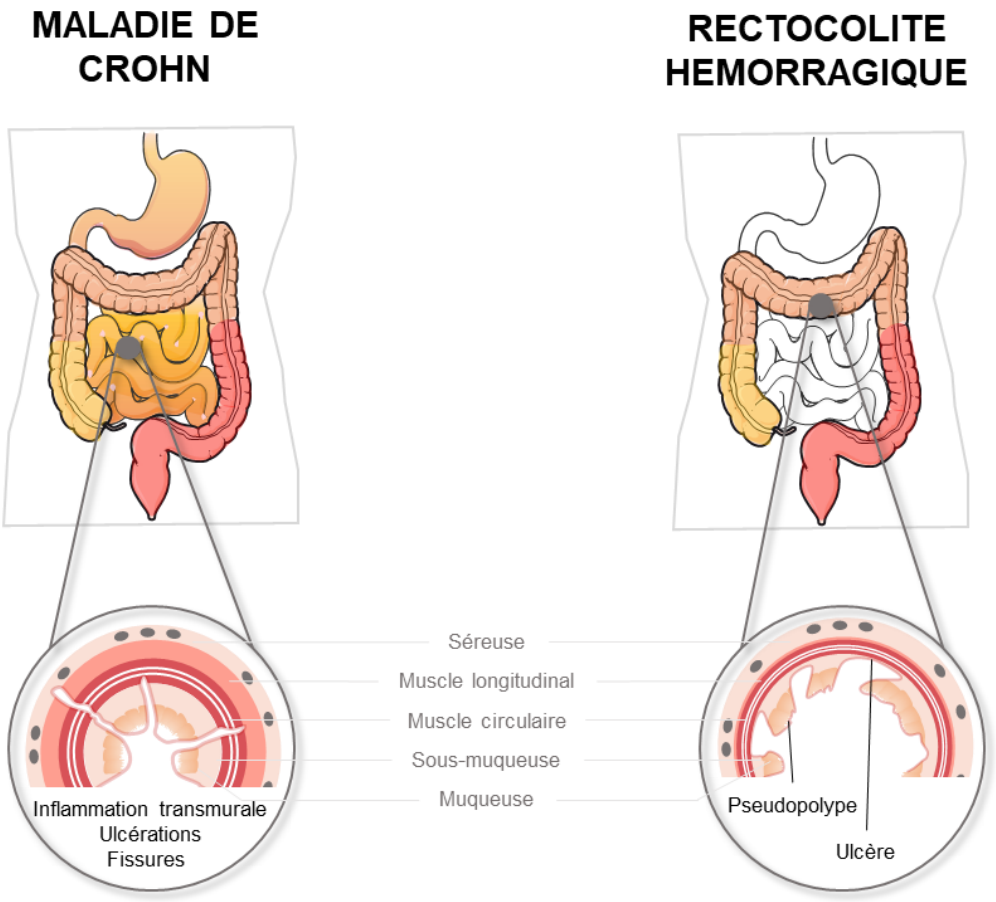

Figure 25 – Lésions distinctes associées à la maladie de Crohn et à la rectocolite hémorragique.
La MC entraîne une ulcération profonde des tissus qui peut affecter l'intestin jusqu'à la couche séreuse. Elle se manifeste par ilots inflammatoires, entrecoupés de zones d'apparence saine. La RCH présente un phénotype plus étendu qui ne touche pas les couches profondes du colon et rend la muqueuse extrêmement friable. L'ulcération étendue entraîne la formation de pseudopolypes qui augmentent le risque de développer un cancer colorectal.

2- La rupture de la barrière est associée à un mucus défectueux

a. Le mucus est perméable à l'invasion bactérienne

L'intégrité de la double-couche de mucus du colon est altérée dans la RCH : les cellules caliciformes y sont déplétées spécifiquement [334] (**Fig. 26**). Cela affecte la qualité et les propriétés restauratrices de ce mucus. Ainsi, la sécrétion de peptides en trèfle (TFF),

promoteurs de cicatrisation muqueuse, par les cellules caliciformes diminue dans la RCH chez l'homme et la souris [335,336]. En conséquence, le mucus de patients RCH est particulièrement perméable aux bactéries environnantes [334] alors que celui de patients en rémission reste imperméable. Des constats similaires sont fait chez des souris déficientes pour le gène *MUC2, Tlr5, IL-10,* et pour les O-glycan de la mucine [334], qui suggèrent que la qualité du mucus, son mode de sécrétion et le métabolisme des cellules caliciformes sont impliqués dans la rupture de la barrière intestinale.

Les cytokines pro-inflammatoires, en particulier l'IL-13 produites par les Th_2 entraînent l'apoptose des IEC et la rupture des jonctions serrées[337,338]. La sécrétion du récepteur nucléaire PPAR-γ, limitante pour la production de cytokines et de chimiokines pro-inflammatoires, est réduite dans les colonocytes de patients atteints de RCH [339]. Cette sécrétion dépend de la voie TLR4, et suggère que la réponse sollicitée par la flore microbienne est défectueuse.

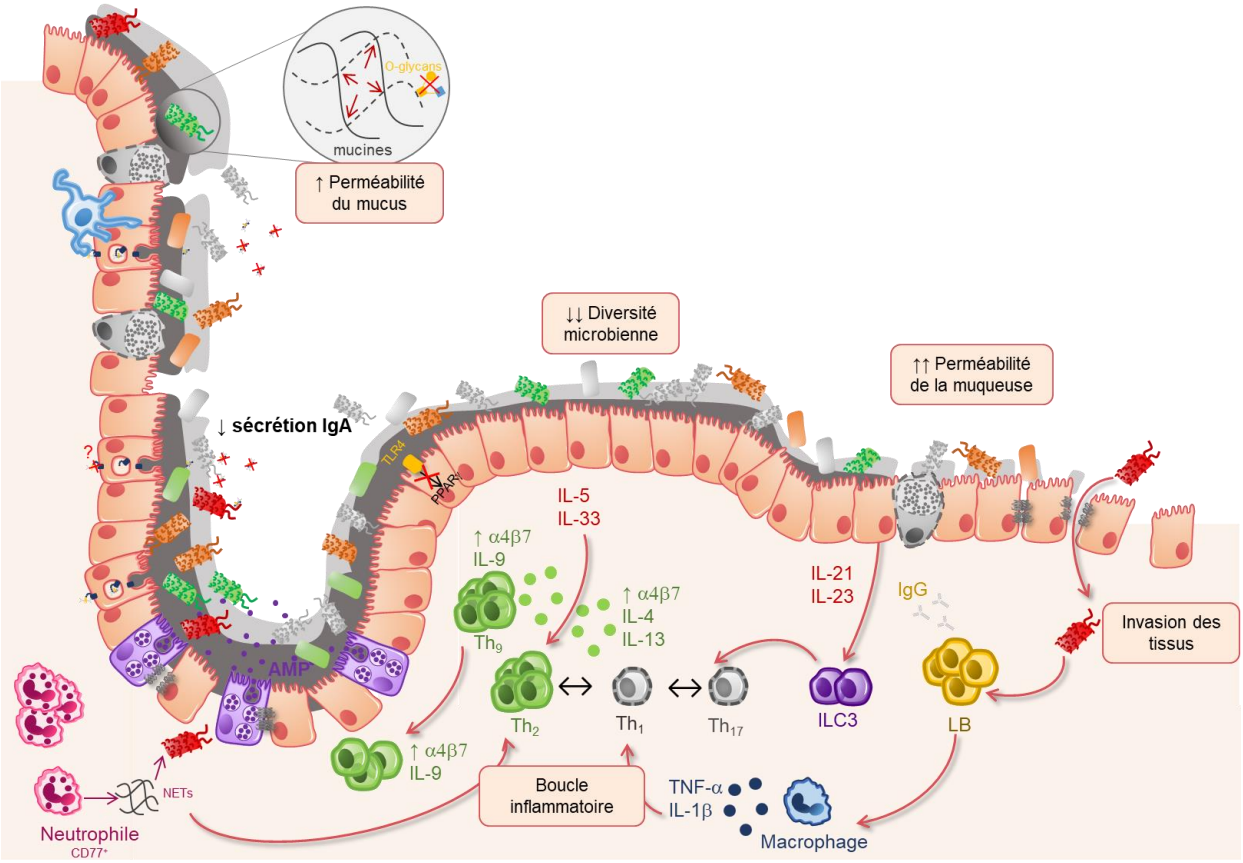

Figure 26 – Physiopathologie de la rectocolite hémorragique.
La RCH est caractérisée par une perte de diversité microbienne et à l'augmentation de la perméabilité intestinale liée à une augmentation de la perméabilité du mucus. Les bactéries de la flore adhèrent directement à l'épithélium. L'invasion de la muqueuse par les bactéries entraîne l'activation de neutrophiles qui effectuent la NETose, et de Th_9 produisant de l'IL-9 au niveau des cryptes intestinales. L'immunité Th_2 et suractivées et l'inflammation est soutenue par les Th_1, les Th_{17} et la production d'IgG anti-commensales. La sécrétion intense de TNF-α soutient la mise en place d'une boucle inflammatoire qui recrute continuellement de nouveaux effecteur grâce à l'expression des intégrines α4β7.

b. L'altération du mucus favorise l'adhérence à la muqueuse et entretien la dysbiose

Il y a généralement une meilleure diversité bactérienne dans la RCH que dans la MC [306,340,341], mais les bactéries utilisant le métabolisme des SCFA restent désavantagées. L'abondance des espèces *Roseburia* et *Faecalibacterium* [341,342], et plus généralement des *Firmicutes* [343], diminue. Ici cependant, le ratio *Firmicutes/Bacteroidetes* diminue parce que l'abondance de ces deux ordres est réduite[344,345]. Cette déplétion paraît en réalité être une translocation vers les ganglions mésentériques[346].

Des espèces impliquées dans le cycle de vie du mucus comme les *Akkermansia*[342] sont sous-représentées tandis que des espèces invasives comme *Escherichia sp., Helicobacter sp.,* et *Campylobacter* sp, sont particulièrement sur-représentées[343]. L'utilisation des O-glycan de la mucine est fortement réduite[13], indiquant un changement de métabolisme : la restauration de la production de butyrate dans la muqueuse soutient en général une période de rémission[347]. Cette réorientation métabolique pourrait expliquer l'augmentation de l'adhérence bactérienne à la muqueuse [343]. En effet, l'infection de souris susceptible à la colite par un pathobionte *E. coli* adhérent isolé chez les patients atteints de RCH, induit une colite plus sévère [348].

Peu étudié, il semble également que le microbiote fongique ait un rôle à jouer dans la RCH : ainsi, les patients porteurs de polymorphismes sur le gène codant pour Dectin-1 présentent une forme sévère de la RCH [349]. La dysbiose fongique chez les patients atteints de RCH, mais pas ceux atteints de MC, suggère que le ratio *Basidiomycota/Ascomycota* pourrait être un bon biomarqueur de distinction entre les deux maladies [350].

c. La réponse IgA est inefficace contre la dysbiose

Parmi les espèces retrouvées dans la fraction Ig+ du microbiote fécal, les *Actinomyces* et *Gemella* sont particulièrement enrichies [302]. Des analyses sur biopsies de patients indiquent que, s'il y a bien une augmentation de la synthèse d'IgA par les plasmocytes dans la RCH, celle-ci n'est pas sécrétée en conséquence [351]. Les IgA produites chez les patients RCH sont, de plus, majoritairement auto-réactives[352]. Par ailleurs, la sécrétion d'IgG tissulaire augmente, et celle d'IgG anti-commensales est associée à la sévérité de l'inflammation[351]. Il s'agit principalement d'IgG1[353,354], des autoanticorps issus d'infiltrats de plasmocytes circulants dans la muqueuse. Ces plasmocytes à IgG sont clonalement proche de plasmocytes à IgA1 qui se relocalisent principalement au niveau des zone lésées[355]. Ils expriment notamment le récepteur de domiciliation CXCR4 [356]. L'engagement du récepteur aux IgG (FcRγ) porté par les macrophages par ces clones à IgG entraîne un phénotype macrophagique pathogénique caractérisé par la production de TNF-α et d'IL-1β [356]. Ces macrophages orientent

la réponse vers un profil Th_{17} [357]. L'absence d'IgA fonctionnelle laisse donc le champ libre à l'exacerbation de l'inflammation selon des mécanismes dépendants de l'axe IgG-microbiote.

3- Les réponses Th_{17} et Th_9 alimentent l'inflammation médiée par les Th_2

a. Initiation de la réponse

Les cryptes intestinales de patients atteints de RCH présentent une accumulation d'ILC3 [358] et de neutrophiles $CD77^+$ [359,360]. Les premiers sont mobilisés par la sécrétion de GM-GSF [358], d'IL21, et d'IL-23[361,362] issue du microbiote[362]. Les seconds sont induit par le TNF-α produit par les NKT (*Natural Killer T cells*) [363]. Ces ILC3 ont une propension accrue à la transcription des gènes *IL17A* et *IL22* [318], et promeuvent un environnement fortement inflammatoire. Les neutrophiles contribuent à cet environnement par une forte activité bactéricide [360] soutenue par le relargage massif de NET [360,364].

L'élimination des espèces bénéfiques peut donc être la résultante d'un cercle vicieux : le microbiote induit les ILC3, qui préparent à l'inflammation, au cours de laquelle les neutrophiles éliminent les bactéries. Comme dans la MC, les réponse NK sont également défectueuses : ceux-ci s'accumulent dans la muqueuse, et répondent à un glycolipide du soi par la production d'IL-13[290]. Leur activation empire donc les dommages tissulaires infligés à la barrière.

b. Orientation de l'inflammation

Les DC $CD103^+$, normalement promotrices des populations T_{reg}, présentent une baisse généralisée de l'expression des TLR [365]. Elles gagnent au cours d'une RCH la capacité d'induire des phénotypes colitogéniques de LT [365]. Les lymphocytes impliqués sont préférentiellement des Th_1 ou Th_{17} [366,367]. En parallèle, l'IL-5 [368] et de l'IL-33 [369] induisent une augmentation locale de Th_2 $IL\text{-}13^+$ $GATA3^+$[367]. Les Th_2 produisent de l'IL-4[370] suite à l'activation de PAR-2 [371] ou une stimulation à l'IL-33 [369] chez les patients et dans des modèles murins expérimentaux [369,371]. Ils sont également responsables de la sécrétion d'IL-13, impliquée dans la rupture des jonctions serrées[337].

Chez l'homme et la souris, l'expansion de Th_9 corrèle avec la promotion des dommages muqueux au cours de la RCH : ils s'accumulent *via* les intégrines αEβ7 [372] au niveau des sites lésés pendant l'inflammation [373]. Ces Th_9 ont la capacité, à eux seuls, d'induire une colite inflammatoire via la sécrétion d'IL-9 [374]. L'inhibition de leur expansion, ou de la sécrétion d'IL-9, suffit à rétablir un phénotype sain chez la souris[374]. Leur accumulation dans les tissus inflammés dépend également du ligand TL1A de la famille des TNF [375], et de l'IL-36 [376,377].

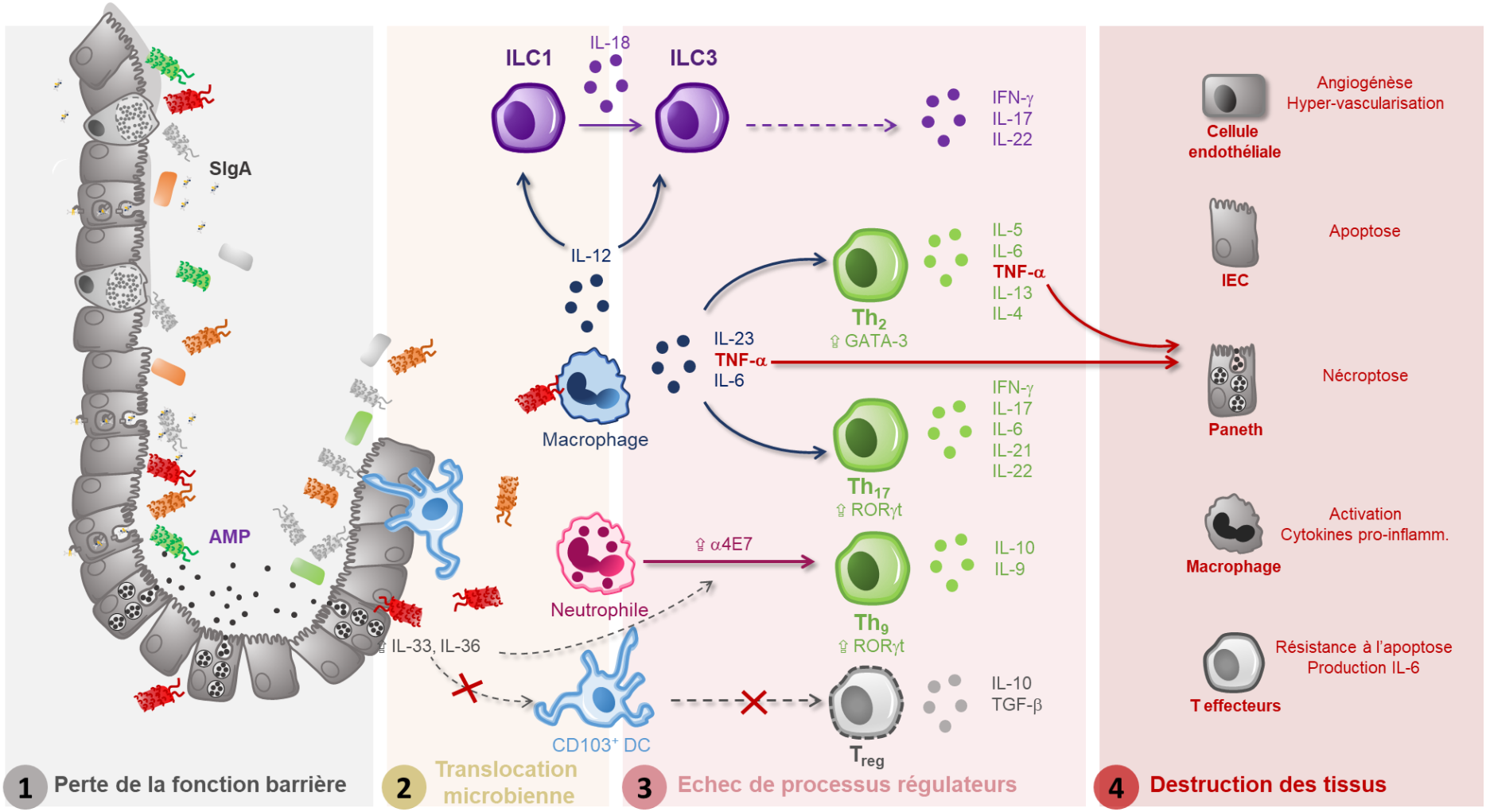

Figure 27 – Rôle des cytokines pro-inflammatoires dans la rectocolite hémorragique.

L'ouverture de la barrière intestinale (1) facilite l'invasion des tissus par les bactéries luminales (2) et le recrutement d'effecteurs innés (neutrophiles CD77$^+$, NK, macrophage). Dans le même temps, l'immunité perds le contrôle des processus régulateurs dépendants de l'IL-10 et de l'IL-36 (3) et favorise l'expansion de population Th_2, Th_{17} et Th_9. La sécrétion concomitante de TNF-α entraîne la mise en place d'une boucle inflammatoire permettant une vascularisation anarchique, la perméabilisation du mucus, l'apoptose des IEC et l'activation continue d'effecteurs pro-inflammatoires.

D- Options thérapeutiques

Les stratégies thérapeutiques pour la prise en charge des MICI dépendent de la sévérité de la maladie et de son phénotype. (**Tableau 3** [234], **Fig.27**). Il est de plus en plus envisagé d'utiliser des traitements antibiotiques pour contrecarrer la dysbiose intestinale, sans résultats avérés [378]. Ils sont plutôt indiqués comme agents combinés avec une thérapie anti-TNF. Plusieurs anticorps anti-TNF déjà commercialisés sont prescrits en routine (infliximab, adalimumab, et certolizumab pegol). Leur utilisation précoce retarde le moment de la première chirurgie [379]. Cependant, le développement d'anticorps anti-médicaments (ADA) est la cause des nombreux échecs thérapeutiques de ces thérapies [234]. La composition du microbiote en *Bifidobacterium, Collinsella, Lachnospira, Roseburia,* et *Eggerthella* influence le succès de ces stratégies [306]. A noter que nombre de ces taxa participent au métabolisme des SCFA.

L'inhibition sélective de récepteurs clé de domiciliation des cellules immunitaire comme les intégrines $\alpha 4\beta 7$ par des anticorps monoclonaux (Vedolizumab, natalizumab) constitue une voie de traitement alternative. De même, les inhibiteurs de calcineurines ayant montré d'excellents résultats dans l'induction de la rémission chez les patients RCH [380], les anti-TNF seront plutôt utilisés en thérapie de sauvetage, avec des résultats variables [380].

Néanmoins, de nombreux patients dans les cinq premières années de traitement, quel qu'il soit, font face à des échecs thérapeutiques tels que le dernier recours est la résection chirurgicale de la zone lésée. C'est le cas d'hémorragie incontrôlée, de perforation du colon, ou de développement de carcinomes muqueux [233]. Environ 50% des patients feront une rechute à la suite de la chirurgie [277]. La composition du microbiote de part et d'autre de l'anastomose – la zone réséquée – influence cette rémission, notamment l'abondance la production de n-butyrate[381]. Les espèces *Bacteroides, Dorea,* et *Dialister* sont particulièrement contingentes à cette rémission[381]. Environ 14% des malades les plus sévère recevront de multiples chirurgies sur les 10 à 15 ans après le diagnostic de la maladie, et devront recourir à la poste d'une stomie permanente [382].

Enfin, l'option thérapeutique de la greffe de microbiote fécal (FMT) est très prometteuse. Si celle-ci donne peu de résultats dans la MC [383], elle apparaît bien plus efficace dans la RCH. Elle peut être administrée par voie rectale, au cours d'une endoscopie, ou sous forme de comprimés, avec jusqu'ici peu d'effets secondaires [383,384]. L'élimination d'espèces dysbiotiques au préalable, en particulier parmi les *Bacteroides*, permet d'améliorer son efficacité et la persistance de la flore greffée [347]. Chez les patients pour qui elle fonctionne, la FMT induit une amélioration de la diversité bactérienne et de la richesse de leur microbiote,

ainsi que des changements d'écologie microbienne chez le patient [385]. Elle permet ainsi la ré-induction des *Clostridium, Blautia sp., Ruminococcus sp., Parabacteroides spp., et Barnesiella sp.* [385,386], et une diminution des *Bacteroidetes* [385]. Si la FMT permet d'atteindre la rémission, le suivi de long terme (rare, dans la plupart des études) montre une perte du greffon avec le temps. L'administration d'antibiotiques avant la greffe facilite la prise de celle-ci, en éliminant les communautés préexistantes chez le receveur [387].

Tableau 3 – Traitements des MICI et effets secondaires

HBV : Virus de l'hépatite B; i. m : intra-musculaire; i. v : intra-veineuse; s. c : sous-cutanée; SLE : Lupus systémique érythémateux; Tb : tuberculose. D'après Feuerstein, Cheifetz. Mayo Clinic Proc.(2017).

Classe	Molécule	Route	Efficacité rémission	Effets secondaires
5-Aminosalycilates	Mesalamine Balsalazide Sulfasalazine	Orale Rectale	Induction et maintenance	Maux de tete Nausée Diarrhée Exacerbation de symptômes Nephrite intersticielle Anémie hémolytique Hépatite
Corticosteroides	Prednisone Budesonide Methylprednisolone	Orale Rectale i.v	Induction seule	Ostéopénie/porose Nécrose avasculaire Infection Prise de poids Insomnie Sautes d'humeur Délire Cataracte Glaucome Changements dermatologiques Retard de cicatrisation Insuffisance adrénale
Thiopurines	Azathioprine Mercaptopurine	Orale	Maintenance	Nausée Vomissement Transaminases élevées Suppression de la moelle osseuse Pancréatite Infection Lymphome non-Hodgkinien Cancers de la peau (non-mélanomes) Dysplasie cervicale
Methotrexate	Methotrexate	s. c ou i. m	Induction et maintenance	Infection Cytopénies Transaminases élevées Nausées/ vomissements Symptomes grippaux Ulcères oraux Toxicité pulmonaire Contre-indiqué pendant la grossesse
Anti-TNF	Infliximab Adalimumab Certolizumab pegol	i. v s. c	Induction et maintenance	Réaction au site d'injection Lymphome non-Hodgkinien Lymphome hépatosplénique Melanome Réactivation d'infection Tb / HBV latente SLE médicamenteux Maladies démyélinisantes Psoriasis - Eczema
Molécules d'adhésion	Natalizumab Vedolizumab	i.v	Induction et maintenance	Réaction à l'injection Infection Polypes naso-pharyngés Leucoencephalopathies progressive multifocale
Inhibiteurs IL-12/IL-23	Ustekinumab	i.v ou s.c	Induction et maintenance	Réaction à l'injection Cancers de la peau Leucoencephalopathies postérieure réversible Tb

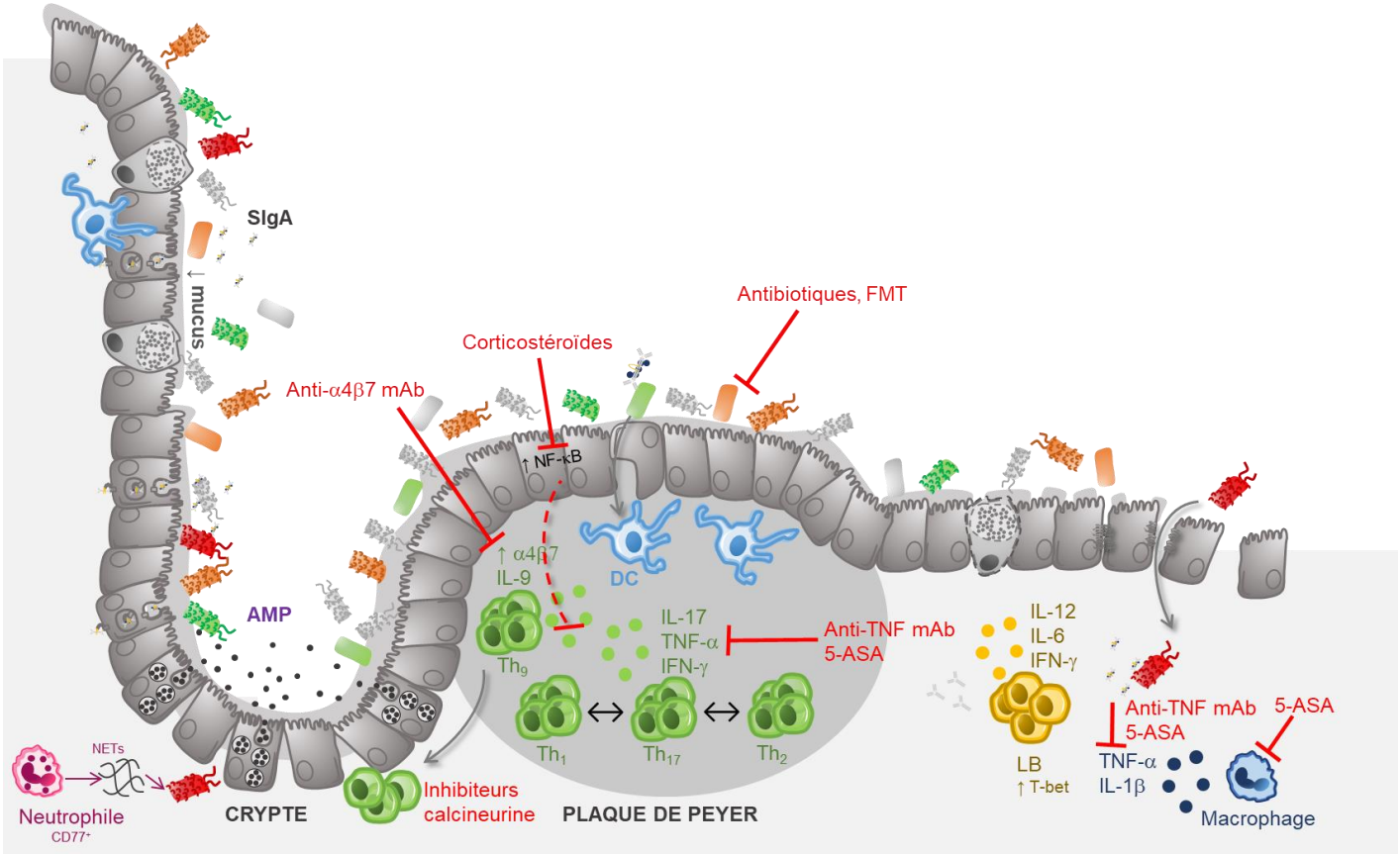

Figure 28 – Mode d'action de traitement actuels des MICI.
Les antibiotiques ralentissent l'expansion de bactéries opportunistes, les anticorps monoclonaux anti-α4β7 et anti-TNF limitent respectivement la migration des effecteurs immuns et l'activité du TNF-α sur le site de l'inflammation. Les corticostéroïdes ont un effet général immunosuppresseur et limitent l'engagement de la voie NF-κB. Les 5-aminosalycilates (5-ASA) inhibent la production de cyclo-oxygenase, de prostaglandines et d'IL-1 par les macrophages. Les inhibiteurs de calcineurines empêche l'activation lymphocytaire en inhibant la transcription de gène des cytokines pro-inflammatoires. La FMT pourrait réinduire l'expansion d'espèces bactérienne disparues chez le patient.

OBJECTIFS DE LA THÈSE

Les MICI sont caractérisées par une dysbiose persistante et une sur-activation des voies de l'inflammation, dont l'origine est souvent multiple : régime alimentaire, mode de vie, traitements antibiotiques et infections récurrentes. Elles sont également corrélées à plusieurs défauts génétiques, comme par exemple certains polymorphismes sur le gène NOD. Les SIgA, en condition saines, participent à la régulation et la sélection du microbiote et des espèces pathogènes intestinales. Les SIgM, bien que minoritaires, sont également sécrétées dans les muqueuses et semblent complémenter les SIgA pour la sélection du microbiote et l'induction de la tolérance. Leurs rôles exacts et leurs modalités de transport à travers les muqueuses ne sont que partiellement connus. Chez l'homme, les fonctions spécifiques correspondant aux isotypes IgA1 et aux IgA2 mais aussi aux isoformes monomériques, dimériques ou sécrétoires restent peu décrites en condition saines. Elles le sont d'autant moins en conditions inflammatoires, et les profils de sélection microbienne associés à ces sous-classes dans les MICI n'ont pas été étudiés.

Dans un premier temps, nous avons investigué le rôle des IgA et des IgM sur la réponse muqueuse en conditions physiologiques **(Revue 1, Annexe 1)**. Nous supposons que la sous-classe et la multimérisation des IgA conditionnent l'orientation de la réponse en polarisant l'activation les DC et de la réponse adaptative. Dans un modèle de DC dérivées de monocytes circulants (moDC), nous avons montré (1) que les IgA1 induisent un phénotype de DC tolérogène tandis que les IgA2 induisent un phénotype pro-inflammatoire, (2) que la dimérisation des IgA amplifie ces réponses, et (3) que l'affinité de l'IgA1 et de l'IgA2 pour FcαRI et DC-SIGN respectivement conditionne ces interactions (**Article 1 ;** *Eur. J. Immunol***.** Sous presse). Nous avons ensuite évalué les capacités de RT des IgM *in vitro* et avons démontré qu'au même titre que les IgA, elles effectuent la RT selon un mode récepteur-dépendant et peuvent être prises en charge par DC-SIGN à l'issue de ce transport (**Article 2,** soumis). Ce transport met en jeu le FcμR (TOSO), dont nous avons démontré l'expression à la surface des cellules M.

Dans un second temps, nous avons étudié les dynamiques de transport, la fonction, et les interactions avec le microbiote des IgA au cours de MICI **(Revue 2, Annexe 2)**. Nous

démontrons que les patients atteints de MC et porteurs de polymorphismes du gène *NOD2* présentent une augmentation de la RT **(Article 3 ;** *Nature Communications***,** sous presse). Ceci s'explique, d'après nos résultats, par le fait que NOD2 régule négativement les récepteurs de la RT, Dectin-1 et Siglec-5 ; son abrogation entraîne donc une hausse de leur expression et, probablement, de la prise en charge des IgA à la membrane apicale des cellules M. Nous avons souhaité analyser les mécanismes et les conséquences liés à cette prise en charge accrue. Grâce à la mise en place d'un protocole reproductible de purification distinguant les IgA1 des IgA2 à partir de selles, nous avons analysé séparément les IgA1 et les IgA2 en fonction du microbiote qu'elles sélectionnent, de leur réactivité, et leur capacité à effectuer la RT dans la MC et dans la RCH **(Article 4,** en préparation**)**. Nous avons ainsi mis en évidence que (1) dans la MC, les IgA1 lient significativement plus d'espèces bénéfiques et qu'elles acquièrent la capacité d'effectuer la RT ; (2) dans la RCH, les IgA perdent leur réactivité aux glycans et ni l'IgA1 ni l'IgA2 ne peuvent effectuer la RT. Ces phénomènes qui n'ont jamais été décrit jusque-là, pourraient contribuer à l'établissement et/ou au maintien de la dysbiose dans les MICI.

Enfin, ayant montré que la RT des IgA est affectée dans les MICI, nous avons exploré de nouvelles voies thérapeutiques visant à limiter la RT des complexes IgA/bactéries dans des modèles murins de colite à Salmonelle. Nous supposions que l'administration de glycans bactériens aurait un effet compétiteur pour l'interaction Dectin-1-IgA et limiterait l'apparition et la sévérité des symptômes. Un crible *in vitro* nous a permis d'isoler un β-glucan agoniste de Dectin-1 limitant la RT des IgA, le zymosan (**Article 5**, en préparation). En parallèle nous avions choisi un α-glucan n'inhibant pas la RT, mais activant l'immunité Dectin-2-dépendante comme témoin. Contrairement à nos attentes, ces deux composés se sont révélés protecteurs lorsqu'ils étaient administrés oralement en prétraitement avant l'infection par *Salmonella* Typhimurium. Tous deux limitent la translocation de complexes IgA-Salmonelle dans la PP. Cela dit, seul le zymosan a entraîné une diminution significative du score d'activité de la maladie, et des concentrations en marqueurs inflammatoires. Le pullulan permet une meilleure survie, mais pas une amélioration de symptômes, contraste qu'il nous faudra investiguer plus amplement.

Chapitre 1 – Rôle physiologique des immunoglobulines sécrétoires

A- Article 1 : Impact de l'isoforme et de la classe d'IgA sur la réponse immunitaire

1- Article et résumé

Les IgA co-existent sous forme monomérique et dimérique dans la circulation, et sous forme sécrétoire au niveau des muqueuses. Chez l'homme, elles comprennent deux sous-classes, les IgA1 et les IgA2, qui ont des propriétés distinctes et dont l'abondance varie selon la localisation. Ces IgA sont produites selon deux modes : d'une part des IgA naturelles et polyréactives induites selon un mode T-indépendant et ciblant un large spectre de motifs du soi ou de la flore commensale. D'autre part des IgA de haute affinité, issues de mécanismes T-dépendants, particulièrement recrutées par la réponse aux pathogènes. Peu de travaux documentent l'impact de l'isoforme et de l'isotype d'IgA sur l'orientation des réponses immunes. Nous avons donc testé l'effet de ces paramètres sur la polarisation des cellules dendritiques et les profils de liaison aux différents récepteurs des IgA.

Nous montrons ainsi que les IgA1 ont un rôle plutôt anti-inflammatoire, qui s'accompagne d'une meilleure affinité pour le FcαRI (CD71). À l'opposé, nous confirmons le rôle pro-inflammatoire des IgA2, qui est associé à une affinité accrue pour DC-SIGN. L'ensemble des IgA testées, quel que soit l'isoforme, conserve des capacités d'induction des LT $CD8^+$ et notamment de leurs capacités cytotoxiques. Ce profil de réponse est amplifié par la dimérisation des IgA, bien que les IgA2 dimériques soient plus enclines à la stimulation des DC, dans un modèle de DC dérivées des monocytes sanguins (moDC) ainsi que sur des DCs intestinales, que les IgA1 dimériques.

(Article sous presse, *European Journal of Immunology*)

Impact of IgA isoforms on their ability to activate dendritic cells and to prime T cells

Short: IgA is a mediator of adaptive immunity

Rémi GAYET[1*], Eva MICHAUD[1*], Francesco NICOLI[2], Blandine CHANUT[1], Mireille PAUL[3], Nicolas ROCHEREAU[1], Christophe GUILLON[4], Zhiguo HE[5], Laura PAPAGNO[2], Gilles BIOLEY[5], Blaise CORTHESY[6], Stéphane PAUL[1**].

Affiliations:

[1] GIMAP/EA3064, Université de Lyon, CIC 1408 Vaccinology, F42023 Saint-Etienne, France.
[2] Sorbonne Universités, UPMC Univ Paris 06, DHU FAST, CR7, Centre d'Immunologie et des Maladies Infectieuses (CIMI-Paris), Paris, France; ¶INSERM U1135, CIMI-Paris, Paris, France.
[3] SAINBIOSE, INSERM U1059, University of Lyon, Saint-Etienne, F-42023, France.
[4] Retroviruses and Structural Biochemistry, Univ Lyon, CNRS, UMR5086, Institut de Biologie et Chimie des Protéines, Lyon, France.
[5] BiiGC/EA2521, Université de Lyon, F42023 Saint-Etienne, France.
[6] R&D Laboratory of the Division of Immunology and Allergy, CHUV, Centre des Laboratoires d'Epalinges, 1066 Epalinges, Switzerland.

* The two authors contribute equally to the work
** Corresponding author: Stéphane PAUL; stephane.paul@chu-st-etienne.fr
Faculté de médecine de St-Etienne, Laboratoire GIMAP
10 rue de la Marandière, 42270 St Priest-en-Jarez
Tel: +33 (0) 4 77 42 14 84; Fax: +33 (0) 4 77 42 14 86

Abstract

Human IgA could be from different isotypes (IgA1/IgA2) and/or isoforms (monomeric, dimeric or secretory). Monomeric IgA mainly IgA1 are considered as an anti-inflammatory isotype whereas dimeric/secretory IgA have clearly dual pro- and anti-inflammatory effects. Here, we show that IgA isotypes and isoforms display different binding abilities to FcαRI, Dectin-1, DC-SIGN and CD71 on monocytes-derived dendritic cells (moDC). We describe that IgA regulate the expression of their own receptors and trigger modulation of moDC maturation. We also demonstrate that dimeric IgA2 and IgA1 induce different inflammatory responses leading to cytotoxic $CD8^+$ T cells activation. moDC stimulation by dimeric IgA2 was followed by a strong pro-inflammatory effect. Our study highlights differences regarding IgA isotypes and isoforms in the context of DC conditioning. Further investigations are needed on the activation of adaptive immunity by IgA in the context of microbiota/IgA complexes during Antibody-Mediated Immune Selection (AMIS).

Keywords : IgA, isoform, secretory, dendritic cells

Introduction

With a production of around 75 mg/kg/day, human immunoglobulin A (IgA) are the most produced antibodies in the body by comparison with IgG (~22 mg/kg/day) or with IgM (~7 mg/kg/day). In particular, IgA are the main isotypes found in mucosal fluids, such as vaginal and gastric secretions, saliva and colostrum [1]. IgA can be produced as monomeric (mIgA) or dimeric (dIgA) forms after binding with J-chain. The secretory forms (SIgA) are generated by recovering the secretory component (SC) from the polymeric immunoglobulin receptor (pIgR) during epithelial transcytosis [2]. IgA are mainly monomeric in the serum (80% to 99% depending on the individual) [3] whereas mucosal IgA are predominantly dimeric. Human IgA1 and IgA2 differ by the size of their hinge region between the Cα1 and Cα2 regions, their shape, their amino acid sequence and especially their glycosylation profiles [4] [5]. IgA1 contain two N-linked glycosylation and five O-glycosylation sites whereas IgA2 are devoid of O-glycosylation but contain two additional N-glycosylation sites [5]. The proportion of IgA1 is globally higher (~85%) as compared to IgA2, especially in the blood, the spleen (~95%), the nasal mucosa (~96%), the proximal small intestinal mucosa (till 84%) or the colostrum (~65%) [5, 6]. IgA2 are preferentially found in colonic fluids (~65%) and the female reproductive system [5]. Human IgA were described to bind several receptors such as the Fcα receptor I (FcαRI) [7], the transferrin receptor (CD71) [8], Dectin-1 (Dectin-1) [9] or Dendritic Cell-Specific Intercellular adhesion molecule-3-Grabbing Non-integrin (DC-SIGN) [10]. Serum IgA are derived from plasma cells in the bone marrow whereas dIgA are produced by plasma cells from the *lamina propria* beneath the mucosa epithelium [11]. They have been extensively studied since their function, called immune exclusion, is one of the first lines of protection in mucosal surfaces. This consists of commensal or pathogen bacteria coating by respectively low- or high-affinity IgA, controlling their entrance across the intestinal epithelium. Nevertheless, in addition to this anti-inflammatory function, dIgA and SIgA were recently described as pro-inflammatory actors in mucosa by recruiting neutrophils [12, 13] or by transporting mucosal

antigens (Ag) to Ag presenting cells (APC) such as macrophages and dendritic cells (DC) in the *lamina propria* or Peyer's patches. In such case, inflammation can be induced after IgA recognition by receptors such as the transferrin receptor (transferrinRCD71) [1]. Given the role of IgA in the microbiota selection during the first years of life, it is suggested that the functions of IgA are tightly regulated between defense mechanisms against pathogens and the antibody-mediated immunoselection (AMIS) [14-16]. mIgA are mainly described for their anti-inflammatory effect in the serum [17] even if a study recently described a pro-inflammatory effect mediated through FcαRI [18]. Roles of IgA are highly diverse depending on the environment and would deserve to be investigated in details. Differential interactions of IgA isotypes and isoforms with their cognate receptors, such as C-type lectin receptors, may explain the diversity of related immune responses. In addition, location of dIgA in the mucosa areas compared to serum monomeric IgA could result in different immune functions. Finally, both IgA1 and IgA2 are found in mucosal secretion, raising the question of their respective local functions. Here, we aimed to clarify the difference between IgA1 and IgA2 in their ability to bind to DC and to induce pro- or anti-inflammatory response. The immunostimulatory effects of polymeric IgA *vs* monomeric IgA were also compared.

Results

IgA1 and IgA2 bind to different receptors on moDC populations.

To determine whether the binding capacity of IgA isotypes and isoforms on APCs was different, the interaction of monoclonal monomeric, dimeric and secretory IgA1 and IgA2 with IgA receptors on human monocyte-derived dendritic cells (moDC) was compared. Interestingly, we observed the high expression of FcαRI, CD71, DC-SIGN but also for the first time of Dectin-1 on moDC surface (Fig. 1A). mIgA1 bound specifically to FcαRI and CD71 and mIgA2 bound specifically to FcαRI, Dectin-1 and DC-SIGN (Fig. 1A and B). mIgA2/FcαRI, mIgA2/DC-

SIGN, mIgA1/CD71 co-localization present the highest staining intensity (Fig. 1A and B). Dimeric IgA bind with the same restricted specificity but with less avidity. Secretory IgA weakly binds to the different tested receptors (Fig. 1A and B). Specificity of IgA1 for CD71 and FcαRI and IgA2 for FcαRI, Dectin-1 and DC-SIGN were also confirmed using monomeric and different dimeric IgA1 and IgA2 purified from hybridomas using HELA-transfected cells with FcαRI, CD71, Dectin-1 and DC-SIGN (Sup. Fig. 1). We then wondered whether mIgA uptake was affected by the profile of IgA receptors expressed on moDC (Fig. 1C). Interestingly, almost no IgA^+ moDC were observed when the cells expressed only one of the IgA receptors, suggesting the requirement for at least two different receptors to significantly increase the IgA internalization by moDC (Fig. 1C, Supplementary Fig. 3A). In contrast, the frequency of IgA^+ cells increase 2, 3 and 4 times for moDC expressing respectively two, three and four receptors, indicating a proportional correlation between the expression of IgA receptors on DC and their ability to internalize IgA (Fig. 1C, Supplementary Fig. 3A). A predominant role of DC-SIGN and Dectin-1 for IgA2 isoforms uptake was suggested since 90% of IgA^+ cells expressed at least these two receptors (Supplementary Fig. 3A).

The binding affinities of IgA isotypes on different receptors were then compared by thermopheresis with increasing ligand/receptors molar *ratio*. We observed a higher affinity of mIgA2/dIgA2 than dIgA1 and mIgA1 to DC-SIGN **(Fig. 1D)** which is also confirmed by affinity-based ELISA assay (**Suppl. Fig. 2D**) and immunofluorescence. dIgA2 and dIgA1 bound also Dectin-1 with the same affinity **(Fig. 1G and Supplementary Fig. 2C)** which is not confirmed by immunofluorescence and ELISA assay due probably to the inherent conformation of the recombinant receptor **(Suppl. Fig. 2D).** dIgA1 and to a less extent mIgA1 were able to bind to CD71 **(Fig. 1E).** Affinity for FcαRI was higher for dIgA1 but almost the same for mIgA1 and mIgA2 **(Fig. 1F and Supplementary Fig. 2B)**. Thus, we emphasized a

different binding capacity of IgA isotypes to FcαRI, Dectin-1, DC-SIGN and CD71 expressed on moDC.

Dimeric IgA induce an over-expression of their cognate receptors on DC surface.

moDC had been described as comprising two subsets discriminated by the expression of the surface marker CD1a (**Supplementary Figure 3B and 3C**) and displaying different functions [19, 20]. We hypothesized that IgA binding could induce the up-regulation of their receptors. Without any stimulation, moDC constitutively express DC-SIGN, Dectin-1 and a low level of FcαRI but did not express CD71 (**Supplementary Figure 3C**). Only a 2-fold CD71 over-expression on moDC after a treatment with TNF-α, IL-1β and IL-6 was observed (**Fig. 2A-D**), as previously described [21]. Likewise, treatment of moDC with dimeric or secretory IgA1 and IgA2 significantly increased CD71 and FcαRI expressions by around 1.3-fold (**Fig. 2A and B**). In addition, incubation of moDC with all the IgA isotypes and isoforms except mIgA2 led to a 1.5-fold increase of DC-SIGN and Dectin-1 expression (**Fig. 2C and D**). Thus, we pointed out the capacity of dimeric IgA1 and IgA2 to increase the expression of their receptors, especially DC-SIGN and Dectin-1. This effect was more pronounced on CD1a- moDCs (mDC2) with the IgA2 (Supplementary Fig. 3B).

Dimeric IgA efficiently mature moDC .

Since both IgA isotypes and isoforms differently interact with receptors on moDC, we wondered whether they also differently stimulated moDC. To avoid a potential effect of endotoxins that could be present in our IgA preparations, experiments were performed in the presence of polymyxin B. In this case, a conserved ability of moDC to be activated with a cytokine cocktail was observed (**Fig. 3A-D**). Expression of CD80 was not affected by incubation with any IgA isotype or isoform (**Fig. 3A**). mIgA had a limited effect on the expression of co-stimulatory molecules on moDC. In contrast, expression of CD40 was

increased by 1.2-folds by dIgA1 and SIgA1 and by 1.5-folds with dIgA2 and SIgA2 (**Fig. 3B**). In addition, dIgA1 induced a 1.3-folds increase of CD86 and HLA-DR up to 2.1-fold with dIgA2 (**Fig. 3C and D**).Thus, moDC seem to be more efficiently activated by dimeric IgA isoforms, especially dIgA2. The same ability of dimeric IgA2 to upregulate CD86 and HLA-DR were also observed on the activation of human mucosal $CD1a^+$ or $CD1a^-$ DCs purified from Crohn's patient gut biopsies **(Supplementary Fig. 4A-C).**

dIgA2 and dIgA1 induce different inflammatory profiles in moDC

In order to characterize the immune profile triggered by monomeric, dimeric or secretory IgA1 and IgA2, we performed a transcriptomic analysis of IgA-treated moDC **(Fig. 4A-C)**. mIgA1 increased the expression of genes involved both in innate immune cells attraction such as chemokine (C-C motif) ligand 16 (CCL16), chemokine (C-X-C motif) ligand 1 CXCL1, CXCL10 and in immune cell maturation/activation such as tumor necrosis factor ligand superfamily (TNF_{SF11}) (**Fig. 4A**). In contrast, mIgA2 decreased expression of CXCL1, CXCL10 and TNF_{SF11}. In addition, 14 other genes involved in cell attraction such as CCL19, CXCL8, CXCL2 or CCL5 or in immune cell activation such as CSF2, RELB, IL-12A/B were down-regulated more than 2-folds (**Fig. 4A**). Gene expression profiles after dIgA and SIgA activation were quite similar, suggesting a low impact of the secretory component (**Fig. 4B-C**). 16 genes over-expressed by mIgA1 were down-regulated by dIgA1 as CCL16, IFNγ, CD40L and TNF_{SF11} but also genes involved in pathogens recognition (TLR9 or TLR7), in angiogenesis (CXCL12) and in monocytes and T cell recruitment (CCL11, CCL8 and CCL13) (**Fig. 4A-B**). dIgA1 also decreased expression of genes involved in immune cell maturation and activation (CLEC4C, IL-2, IL-12 A/B and CSF2) (**Fig. 4A-B**). The most mIgA2 down-regulated genes were significantly up-regulated by dIgA2 (TNF□, CD40L, IFN-γ and IL-12A/B) (**Fig. 4A-B**). In particular, neutrophils, macrophages and T cell chemoattractant and maturating coding genes

such as CCL19, CXCL8, CXCL1 and CXCL2 and CSF2 were over-expressed (**Fig. 4A-B**). All together, these results indicate that IgA isotypes but also isoforms induce different inflammatory profiles of gene expression in moDC. No or low influence of SC in DC activation has been observed (**Fig. 4C**). In order to get further insights into the effect of IgA interaction with moDC, cytokine production was measured in the moDC culture supernatants after IgA stimulation **(Fig. 4D-F)**. Similar effects on cytokine secretion were observed between dimeric and secretory IgA **(Fig. 4D-E)**. In contrast, the dimeric isoforms were much more potent than the monomers to stimulate cytokine production by moDC. TNF-α and IL-6 levels were increased 5-fold and 10-fold by dIgA1 (**Fig. 4D**) and 33-fold and 700-fold by dIgA2, respectively (**Fig. 4E**). In addition, an increase of around 1.5-fold of IL-16 was observed with dIgA1 and IL-23 secretion was increased by 4-fold after stimulation with dIgA2 (**Fig. 4D-E**). Dimeric IgA also induced a concomitant production of the anti-inflammatory cytokine IL-10, which was increased by 1.6-folds with dIgA1 (**Fig. 4D**) or 7-folds with dIgA2 (**Fig. 4E**). Although a similar secretion of the T cell chemoattractant IL-16 was observed between dIgA1 and dIgA2 stimulation (**Fig. 4F**), dIgA2 induced a higher secretion of pro-inflammatory cytokines such as TNF-α (~80-fold), IL-6 (~2-fold) and IL-12p40 (~20-fold) combined with IL-23 (~5-fold) than dIgA1 (**Fig. 4F**). Our results indicate a stronger effect of dIgA on gene transcription and cytokine secretion by DC compared to mIgA. In addition, the effect of dIgA2 was stronger than dIgA1 and skewed towards a pro-inflammatory profile.

IgA2 induce a strong activation of cytotoxic CD8 T lymphocytes

To assess the quality of DC conditioning with IgA, we first compared the ability of mIgA1 and mIgA2 to induce T cell proliferation in a mixed lymphocyte reaction (MLR). No increase in the proportion of activated $CD25^+$ $CD4^+$ T cell was observed in the presence of moDC after mIgA1 or mIgA2 stimulation (**Fig. 5A**). Interestingly, whereas only a limited effect was

induced by mIgA1, a significant 1.4-fold increase of activated $CD25^{+}CD8^{+}$ T cell proportion was observed after mIgA2 stimulation (**Fig. 5B**). We then used a human model of *in vitro* T cell priming to test the influence of mIgA1 and mIgA2 on the activation of specific effector CD8 T cells from naïve T cells [22]. Melan-A-specific CD8 T cells were primed in the presence of both mIgA1 and mIgA2 (**Fig. 5C, Supplementary Fig. 5**). Interestingly, the presence of mIgA2, but not mIgA1, yielded a higher expression of the transcription factor T-bet (**Fig. 5D, Supplementary Figure 5)** within primed T cells, which was not the case for Eomes (**Fig. 5E**). Increase expression of granzyme B and perforin in Melan-A-specific T cells was observed only with mIgA2 (**Fig. 5F-G, Supplementary Fig. 5**). Preliminary datas suggest that the effect of IgA2 was enhanced with its dimeric form (**Supplementary Fig. 5)**. Taken together, these findings show that both monomeric IgA1 and IgA2 can promote the induction of antigen-specific CD8 T cell responses, but with a highest potential and a Th1 *bias* for IgA2.

Discussion

In this study, we aimed to clarify the ability of different IgA isotypes and isoforms to interact with their putative receptors expressed on moDC and their related immune effector functions. We have found that IgA1 preferentially bind to FcαRI whereas the affinity of IgA2 is higher for DC-SIGN and that their respective affinities are increased with the dimerization. We also highlighted that dimeric IgA, modulate the expression of their own receptors on moDC. In addition, we demonstrated that dIgA stimulate DC, either by down regulated inflammatory genes with dIgA1 or by increasing expression and secretion of pro-inflammatory molecules with dIgA2. Such immune profiles may engage various pathways leading to the observed priming of functional cytotoxic $CD8^{+}$ T cells. “Classical” moDC called mDC1 were described as CD1a expressing cells, secreting a high amount of IL-12p70 and inducing a Th1 differentiation [23]. However, a study described the presence of a functionally distinct cell

subset, called mDC2 cells, which did not express the CD1a marker [19]. Our study further describes differences between mDC1 and mDC2 [19, 20] such as diverse expression profiles of IgA receptors at steady state and differential responses to interaction with IgA isotypes and isoforms. Indeed, expression of surface activation markers was modulated only on mDC2 after a mIgA stimulus. Interestingly, stimulation of mDC2 with LPS led to an opposite effect, suggesting that this subset uses different pathways to respond to mIgA or LPS. Functional studies of individual mDC1 or mDC2 subsets would specify more precisely their role in the modulation of immunity in response to interaction with IgA. In addition, the FcαRI, the transferrin receptor (CD71) and the DC-specific ICAM-3 grabbing nonintegrin (DC-SIGN) were found to be expressed on blood myeloid cells and on moDC [24] [21] [25]. We similarly demonstrate that Dectin-1 is expressed on these cells. FcαRI is a transmembrane receptor which interacts with the Fc domain of both IgA1 and IgA2, with a higher avidity for immune complexes than monomeric or dimeric IgA. The presence of alternative IgA receptors was suggested by addition of anti-FcαRI antibody on moDC which did not abrogate IgA binding [26]. CD71 was described as an IgA1 specific receptor, with a higher avidity for monomeric IgA on Daudi cells [8]. Alternatively, since incubation with mannose decreased SIgA binding on moDC, competition for C-type lectin receptors which bind glycans was suspected. Thus, both DC-SIGN on Chinese hamster ovary (CHO-S) or THP-1 cells and Dectin-1 on intestinal epithelial cells were shown to specifically bind SIgA [9, 10]. Our study demonstrates a higher affinity of IgA1, especially the dimeric form for CD71. We also show here the ability of DC-SIGN and Dectin-1 to interact with mIgA2/dIgA2. Thus, our results suggest a potential regulatory function of IgA that depends more particularly on the expression of DC-SIGN and Dectin-1 on DC. Since DC-SIGN (i) is highly expressed on moDC (ii) preferentially binds IgA2, especially dIgA2 and (iii) its expression is increased by dIgA2, one could hypothesize that these processes contribute to the stronger DC activation and the subsequent CD8 T cell

induction observed with dIgA2. As DC-SIGN is involved in DC interaction with T cells *via* ICAM3 [25], it's up-regulation by dIgA2 could play a role in CD8 T cell activation. Based on our observations, it would be interesting to study the pro- or anti-inflammatory effect of IgA molecules in relationship to receptor expression in various cells and tissues as for example in mucosa. Except their role in IgA nephropathy [27], serum monomeric IgA1 were thought to play a minor role in immunity whereas both the proportion and the function of monomeric IgA2 remain to be clarified. Monomeric IgA induce anti-inflammatory response in absence of antigen *via* the FcαRI [28], for example by inducing death of activated neutrophils [29]. A role for other receptors has been suspected since inhibition of Th17 cell response by mIgA occurred independently of FcαRI and DC-SIGN [30]. Our results demonstrate a slight induction of chemoattracting and maturing molecules response induced by mIgA1 with (i) down-regulation of the CD86 co-stimulatory molecule and (ii) absence of pro-inflammatory genes up-regulation and limited production of cytokine. Interestingly, we also demonstrate a mIgA1/CTL pathway with induction of (i) CCL8 and IL-16 expression, two T cell chemo-attractants [31], (ii) proteins involved in T cell activation such as CD40 or TAPBP, a molecule involved in MHC-I processing [32], and (iii) a mIgA1-dependent cytotoxic CD8 T cell activation. In this context, further investigations focusing on a potent regulatory role of this cell population, *e.g.* involving killing pro-inflammatory cells, are worth to pursue.

One important function of dIgA is to impede inflammation. This process is mediated either by immune exclusion or by direct effects such as induction of tolerogenic DC *via* SIgA binding on DC-SIGN [33]. Interestingly, we demonstrate that dIgA1 amplify the anti-inflammatory effect of mIgA1 on moDC. Indeed, dIgA1 downregulate pro-inflammatory genes in moDC and trigger a low diversity of cytokines secreted in limited quantity compared to dIgA2 except for IL-16 and IL-21. Besides, some studies showed anti-inflammatory properties of TNF-α and IL-6 depending on their quantities and timing of expression [34, 35] [36]. In addition, the high

secretion of IL-12p40 in absence of IL-12p35 or p19 counterparts to form respectively IL-12p70 or IL-23 [37] could indicate the formation of the IL-12p80 homodimer, considered as a CD8 T cell or DC chemoattractant [38]. Since IgA1 may also induce T cell recruitment *via* CCL5 and IL-16 chemoattractant and promote CD8 T cell response, investigating the involvement of T cell in anti-inflammatory response could be relevant. DIgA are also involved in pro-inflammatory mechanisms, for example through the recruitment and activation of neutrophils in mucosa [12, 13]. Besides, immune complexes could modulate the inflammatory effect described above. Binding of antigens to mIgA1 forms immune complexes which are internalized by mature and immature DC *via* FcαRI to induce a pro-inflammatory response [18, 21]. It would be interesting to investigate the type and amplitude of immune response induced by dIgA1 bound to their specific Ag to observe whether the same pro-inflammatory response as mIgA1 takes place. This concept would be in adequacy with the dual function described for mucosal dIgA. Indeed, interaction of IgA with commensal bacteria induce tolerance whereas interaction with pathogens induce either immune exclusion or pro-inflammatory response with recruitment of immune cells such as neutrophils [39] [12]. In addition, an alternative observation related to the dual role of IgA in the intestine is linked to the T cell-dependent (TD) or independent (TI) induction of IgA production. Indeed, it is suggested that TD response induce high affinity IgA responsible for the pro-inflammatory response to pathogens whereas low affinity IgA induced by a TI pathway bind microbiota or inoffensive elements to trigger immune tolerance [39]. In this context, our results would require more investigation to determine whether the TI-induced IgA are mostly IgA1 and TD-induced IgA mostly IgA2. A second explanation of the dual role of dIgA could be that dIgA1 would be in charge of anti-inflammatory responses whereas dIgA2 would induce a pro-inflammatory response. Indeed, dIgA2 induce a clear pro-inflammatory response regarding the gene expression and the cytokine secretion profiles of moDC. Proteins involved in the inflammatory NF-κB pathway such as

RELB or NFKB1 are over-expressed and TNF-α and IL-6 are highly produced by DC. In parallel, IL-12p40, which is a subunit of IL-23, is highly secreted together with IL-23, indicating a potential role of in inducing a Th17 response after moDC activation by dIgA2 [40]. This result is in accordance with the Th17/IgA axis recently highlighted [41]. Moreover, recruitment of neutrophils by IgA in the intestine is well documented [12, 13]. In accordance with this finding, we have observed that dIgA2 induce over-expression of neutrophil chemoattractants by moDC such as CXCL8, CXCL1, CXCL2 and CCL3. Here, we pointed out a limited role played by secretory component (SC) in the interaction of SIgA with moDC and their activation. We may hypothesize that SC does not interfere with the effects triggered by dIgA, but could be required for immune exclusion [42] and to stabilize dIgA in the intestinal environment [43]. Our preliminary data demonstrate that when mIgA1 and mIgA2 were used to stimulate human mucosal $CD11c^+$ DC extracted from human biopsies, similar results than with moDC were observed (**Supplementary Figure S3**). We need to determine which mucosal DC subsets are implicated in the interaction with IgA and how dimeric or secretory IgA act on such cells. Several DC populations have been described in intestinal mucosa such as the $CD103^+$ DC, thought to be involved in Ag presentation in mesenteric lymph node [44], or the $CX3CR1^+$ DC, thought to be involved in Ag capture in the *lamina propria* [45]. The expression of IgA receptors on these populations, together with their inflammatory profile in response to IgA stimulation should be explored. The functionality of CTLs such as the intraepithelial CD8 αα [46], as well as the non-conventional intestinal T cells such as the Mucosal-Associated Invariant T cells (MAIT) in the gut should also be considered to understand the impact of IgA isotypes and isoforms. Indeed, supernatant of activated MAIT cells induces the production of IgA by B cells [47].

We observed significant DCs activation by dimeric IgA2 isoforms compared to monomeric IgA1/2 or dimeric IgA1. This mechanism could be explained by a different ability (affinity or

avidity) of binding to different receptors but also to the same receptors. Indeed, affinities of mIgA isoforms with their receptors are quite weak and similar, suggesting a low activation signaling in downstream. The ability of the different IgAs to bind to multiple receptors at the same time is also an important issue. The activation process may require a threshold of linked receptors as demonstrated for example for the TCR cross-linking. The transcriptomic signature is clearly different between different isotypes and isoforms so the activation/inhibition process is also different. Another important issue/possibility could be the different glycosylation pattern of IgAs which could first explain the different affinities/avidities observed to the different receptors but could be also implicated in the binding to other sugar-specific receptors. Finally, dIgA2 activation is closely related to DC-SIGN, Dectin-1 and to a lesser extent to FcR□, since they are the main IgA2-binding receptors. The simultaneous cross-linking of these three receptors in moDC could lead to high $CD8^+$ T cell activation. Our hypothesis would require investigating the relationship between IgA isoforms/isotypes and their receptors, the cross-binding and the downstream pathways.

We have demonstrated that while IgA can bind to different receptors displayed on moDC, dIgA1 present a better affinity for FcαRI and dIgA2 for DC-SIGN. Our data also highlight that dIgA1 induce an exacerbation of the anti-inflammatory response induced by mIgA1 in the absence of antigen. In contrast, we showed a strong pro-inflammatory response induced by moDC activated with dIgA2. Interestingly, both processes lead to activation of CD8 T cells. We have also emphasized a modulatory role of IgA which induced the overexpression of their own receptors on DC. Here we show the relationship between IgA isotypes and isoforms and their functionality in the control of immune responses. The ability of the different IgA to stimulate/regulate mucosal immunity should be considered in physiopathological conditions such as Inflammatory Bowel Diseases, IgA nephropathy or coeliac disease [27, 48]. Our results are also of importance for the use of IgA to serve as mucosal vaccine vector [49, 50].

Materials and methods (see also Supplemental methods)

Flow cytometry

Cell staining was performed in a buffer containing PBS, FBS (2%) and EDTA (1mM). Dead cell exclusion was performed with 7AAD (BD Biosciences, Le Pont de Claix, France) or with a LIVE/DEAD™-488nm staining (Invitrogen, Toulouse, France) for MLR experiment. Staining antibodies were diluted at 1/200 except specified and cell staining was analyzed with a BD FACS Canto II cytometer (BD Biosciences). The following antibodies were used for studying the IgA-receptor profile of human moDC: Anti-Fc□RI BV510 (BD Biosciences), anti-CD71 FITC (BD Biosciences), anti-Dectin-1 PE (BD Biosciences), anti-DC-SIGN BV421 (BD Biosciences), FITC mouse IgG2a, κ isotype control (BD Biosciences), BV421 mouse IgG1, κ isotype control (BD Biosciences), PE mouse IgG2a, κ isotype control (BD Biosciences), BV510 mouse IgG1, κ isotype control (BD Biosciences). The following antibodies were used for testing maturation and phenotype of human moDC: anti-DC-SIGN/DC-SIGN BV421 (BD Biosciences), anti-CD1a APC-Vio770 (Miltenyi Biotec, Paris France), anti-CD14 PE (Miltenyi Biotec), anti-CD11b PE-Vio770 (Miltenyi Biotec), anti-HLA-DR BV510 (BD Biosciences), anti-CD80-PE-Vio770 (Miltenyi Biotec), anti-CD86-FITC (Miltenyi Biotec), anti-CD40-PE (Miltenyi Biotec). The following antibodies were used for testing maturation and phenotype of DC from human gut: anti-CD68 FITC (BD Biosciences), anti-CD1c PE (BD Biosciences), anti-CD11b APC (BD Biosciences), anti-CD11 PE-Cy7 (BD Biosciences), anti-CD103 BV421 (BD Biosciences), anti-CX3CR1 BV510 (BD Biosciences), anti-HLA-DR APC-H7 (BD Biosciences), anti-CD80 APC (Biolegend, San Diego, USA). The following antibodies were used for testing proliferation and activation of human T cells after MLR: anti-CD3 BV510 (BD Biosciences), anti-CD8 PE-Cy7 (BD Biosciences), anti CD4 APC (BD Biosciences), anti-CD25 PE (BD Biosciences), anti-Ki67 BV421 (BD Biosciences). We followed the "Guidelines for the use of flow cytometry and cell sorting in immunological studies" [51].

Human IgA

Endotoxin-free human monomeric anti-hCD20 mIgA1 and mIgA2 were produced in CHO cells and purified by affinity chromatography with peptide M. (Invivogen, Toulouse, France). The dimeric dIgA1 (Nordic Mubio, Susteren, Netherland) were mAb taken from a patient myeloma with a tested purity around 98% or was purified from IgA1 hybridomas (clone BT1 and BT2 referred as dIgA1 (B) and dIgA1 (C)) immortalized from plasma cells taken from the *lamina propria* of a Crohn's disease patient. The dimeric dIgA2 were mAb obtained from different IgA2 hybridomas (clone HF2, HF3 and HF4 referred as dIgA2 (A-C)) immortalized from plasma cells taken from the *lamina propria* of a Crohn's disease patient (DDXK-HuBBB, Dendritics Lyon, France). Clones BT1, BT2, HF2, HF3 & HF4 supernatants were concentrated in 100K Amicon (Millipore, France), filtered in 0.22µm and purified by affinity chromatography with peptide M agarose (InvivoGen). Secretory IgA (SIgA) were formed by combining equimolar quantity of dimeric IgA and secretory component [52, 53]. The purity of each isoform was tested by Western Blot and always higher than 85%. For all *in vitro* experiments, polymyxin B was added.

Enzyme-linked immunosorbent assay (ELISA) for IgA/receptors affinity

96-well maxisorp plates (ThermoFisher) were coated O/N with either the Fc□RI or the DECTIN-1 receptors-Fc (R&D systems, Lille, France) or with IgA (for the DC-SIGN and CD71 ELISA). Fc□RI and Dectin-1 concentrations began at $6x10^{-7}$ mol/L and serial dilutions were performed at 1/3 whereas IgA concentration was stable at $6x10^{-8}$ mol/L in PBS. After 2 hours of blocking (PBS, tween 0.05%, BSA 1%), the plates were washed three times with PBS supplemented with Tween (0.05%). Either the IgA ($6x10^{-8}$ mol/L) or the DC-SIGN or CD71 (serial dilutions beginning at $4.8x10^{-8}$ mol/L) receptors-Fc were added and incubated during 2h. After three washes, plates were incubated either with an anti-human IgA HRP (Sigma-Aldrich)

or with an anti-human DC-SIGN (Life technologies, Illkirch, France) or with an anti-human CD71 antibody (Life technologies). After three washes, plates previously incubated with the anti-human DC-SIGN or CD71 were incubated with anti-rabbit IgG coupled to horseradish peroxidase (HRP) (Cell signaling technology). Plates were eventually incubated with TMB (Tebu-bio laboratories) after 4 last washes during 30min maximum and the reaction was stopped with hydrochloric acid. The optical density (OD) was read at 450nm (TECAN).

Microscale Thermophoresis

The recombinant receptors FcαRI (R&D systems, Lille, France), Dectin-1 (R&D systems), DC-SIGN (R&D systems) and the human transferrin receptor CD71 (R&D systems) display a N-terminal histidine tag. Coupling of receptor (200nM) with the RED NT-647 (100nM) was performed using « Monolith NT™ His-Tag Labeling Kit RED-tris-NTA » (NanoTemper technologies, München, Germany) following the manufacturer's protocol. Labeled receptors at 25nM final were added separately to a range of human dimeric/monomeric IgA1 or IgA2 2-fold dilutions from 25µM to 0,3nM in PBS, Tween 0.05%, then loaded in standard capillaries (NanoTemper) for MST measurement. The strength of receptor/ligand interaction was measured from the diffusion of the labeled molecule in function of ligand concentration when a temperature gradient was applied on the capillaries, using a thermophoresis reader (Monolith NT.115, NanoTemper). K_D were calculated from the titration curves using the MO.Affinity Analysis Software (NanoTemper).

moDC immunostaining for confocal microscopy

LabTek® slides (Sigma-Aldrich, St Quentin Fallavier, France) were treated with 500µL of Poly-L-lysine (Sigma) and incubated 1hr at 37°C. Slides were washed in PBS and dried 1-2hrs under a safety cabinet. $1x10^6$ moDC/compartment were seeded in complete RPMI medium O/N at

37°C. After 2 gently washes with PBS, cells were incubated with 6µg of antibodies in 200µL of complete RPMI at 37°C during 1hr. After 2 PBS washes, cells were fixed 5min (PBS, 4% formaldehyde), washed again and non-specific sites were blocked (PBS, BSA 1%) during 15min at RT. Cells were permeabilized (PBS, BSA 1%, Triton 0.1%) 2min and washed 2 times with PBS. Primary Ab were added 1hr at 4°C : 5µg/mL of rabbit anti-human CD71 (Thermofisher, Illkirch, France), 20µg/mL of rabbit anti-human DC-SIGN (Thermofisher), 5µg/mL of rabbit anti-human Dectin-1 (Thermofisher), rabbit anti-human Fc□RI (1/500, Abcam, Paris, France), 5µg/mL of goat anti-human IgA Alexa555 (Southern Biotech, Birmingham, USA). Cells were washed 2 times with PBS and incubated 45min at 4°C with 5µg/mL of the secondary antibody goat anti-rabbit IgG Alexa 488 (Southern Biotech). Cells were washed with PBS and the nucleus was stained 5-10 min with Draq5 (1/1000, Abcam). After 2 washes, cells were mounted between slide and slip cover with vectashield (Vector laboratories) and eventually observed with the FLUOVIEW FV1200 laser scanning confocal microscope at RT (Olympus IX83, Tokyo, Japan) and equipped with the FV10-ASW4.1 imaging software (Olympus, Hamburg, Germany). The objective was an Olympus UPlanSApo 60x/1.35 Oil ∞ /0.17/FN26.5. Image processing was performed with ImageJ Software.

Expression profile by quantitative reverse transcription polymerase chain reaction (qRT-PCR)

RNA from frozen pellets of 1-5 x10^5 activated moDC were extracted thanks to a Quick-RNA MicroPrep Kit (Zymo Research). Total RNA quantification was performed with a 2000c nanodrop (Thermos scientific). RNA quality was assessed (Biorad, 700-7103) with the Experion™ system (Biorad, Marnes-La-Coquette, France). Quantification of a RNA panel described in **Suppl. Fig 4** was done with Qiagen kits for Human dendritic cells (330404,

330523, 330231) and the Applied Biosystems® 7500 system. qRT-PCR results were analysed with the data Analysis Center of Qiagen following supplier instructions.

Cytokine and chemokines titration

The evaluation of multiple cytokines/chemokines was performed with a Luminex 100 instrument (Luminex, Austin, Tex) in combination with the personalized Bio-Plex human cytokine panel composed by IL-12p40, IL-12p70, IL-2, IL-4, IL-6, IL-10, IL-21, IL-23 and TGF-β, IFN-α and IFN-β for monomeric forms or IFN-γ, IL-16 for comparison between IgA isoforms (Bio-Rad Laboratories, Hercules, Calif). Dosages were performed as specified by the manufacturer on pure supernatant of activated moDC previously frozen. Cytokine and chemokine concentrations were determined with one measure for each condition. IL-16 secretion in supernatant was determined with an ELISA kit on supernatant in duplicate following the specifications of the manufacturer (Abcam, Paris, France).

***In vitro* priming of antigen-specific CD8$^+$ T-cell precursors**

Naïve precursors specific for the HLA-A2-restricted Melan-A epitope ELA (ELAGIGILTV; Melan-A/MART-1 residues 26–35A27L) were primed *in vitro* using an accelerated dendritic cell coculture protocol as previously published [22]. Briefly, thawed PBMCs were resuspended in AIM medium, supplemented with FLT3L (50 ng/ml; R&D Systems), and plated out at 2.5×10^6 cells/well in a 48-well tissue culture plate. After 24 hours, the ELA-20 peptide was added (1 μM) and the maturation of resident dendritic cells was induced using a cocktail of cytokines including TNF (1000 U/mL), IL-1β (10 ng/mL), IL-7 (0.5 ng/mL) and prostaglandin E2 (PGE2; 1 μM) (R&D Systems). Alternatively, maturation of DC was induced using ssRNA40 (0.5 μg/mL; Invivogen) or 12μg of IgA. On day 2, fetal calf serum (FCS) was added to 10% by volume per well. Fresh RPMI-1640 (Gibco) enriched with 10% FCS was used to

replace the medium every 3 days. ELA-specific $CD8^+$ T-cell frequency and phenotype were determined on day 10 by flow cytometry.

Directly conjugated mAbs were purchased from commercial sources as follows: 1) anti–CD8-APC-Cy7, anti–CCR7-PE-Cy7, and anti–granzyme-BV450 (BD Biosciences); 2) anti–CD27-AlexaFluor 700 (BioLegend); 3) anti–CD45RA-PercP Cy5.5, anti–T-bet-Alexa Fluor 647, Eomes PE-eFluor 610, anti–perforin-FITC (eBiosciences). The amine-reactive viability dye Aqua (Life Technologies) was used to eliminate dead cells from the analysis. Intracellular staining for T-bet and Eomes was performed using the Transcription Factor Buffer Set (BD Biosciences), according to the manufacturer's instructions. Intracellular staining for granzyme B and perforin was compatible with this procedure. Staining with all other reagents was conducted according to standard protocols. Data were acquired using an LSR Fortessa flow cytometer (BD Biosciences) and analyzed with FlowJo software version 9.3.7 (Tree Star).

Statistical analysis

All statistical analyses were performed with InStat software (version 5.02; GraphPad Software, La Jolla, Calif). The normality was tested for each data set with both Shapiro-Wilk and Agostino-Pearson tests. When data could be modeled by a normal distribution, the following tests were performed depending on the comparison: Student t-test (two means comparison), one-way ANOVA (multiple mean comparisons) with Bonferroni correction (comparison of all pair of data sets) or Dunnet's correction (comparison to a control group). Alternatively, non-parametric tests were performed: Mann-Whitney test (two means comparison), Kruskal-Wallis (multiple mean comparison) with or without Dunn's correction (comparison of all pair of data sets). In case of comparison of two independent variables, a two-way ANOVA test was done. Results were represented as Mean ± SEM. P values of less than 0.05(*), less than 0.01(**), and less than 0.001(***) were considered significant. Statistically significant differences between groups are

emphasized by bars connecting the relevant columns. If not, the comparison was automatically with the control group (NS).

Acknowledgments

The authors thank M. Zhiguo for his help with confocal microscopy visualization and analysis. The study was supported by University Jean Monnet, FNS grant #3100-156806 to BC and the Auvergne-Rhône-Alpes region. RG was supported by a fellowship from the ARC1 and MSD (France). This work was financed by research grants from the MSD Avenir program. The authors declare no competing financial interests.

R. Gayet & S. Paul designed and performed the experiments and wrote, reviewed and edited the manuscript. F. Nicoli designed and performed the experiments. B. Chanut performed the experiments. C. Guillon designed the experiments and reviewed the manuscript. L. Papagno designed and performed the experiments and reviewed and edited manuscript. B. Corthesy designed the experiments and reviewed the manuscript. G. Bioley designed the experiments and reviewed and edited the manuscript.

The authors declare no competing interests

Figure legends

Table 1. Effect of different forms of IgA on the expression of activation markers by moDC. Relative modifications of the expression of activation markers induced independently by IgA1 and IgA2 isoforms were compared by flow cytometry analysis. Datas are obtained from four experiments with 3-5 donors per experiment performed in triplicate. Total number of donors was 17 for IgA1 and 8 for IgA2. Arrows represent the increase (up arrows) or decrease (down arrows) tendencies in relative markers expression on either $CD1a^+$ or $CD1a^-$ cells 24hrs after stimulation with 12µg of IgA. Two-way ANOVA with Bonferroni's post-hoc test was used to determine the significance of mean differences. (*) $p \leq 0.05$, (**) $p \leq 0.01$ and (***) $p \leq 0.001$. MFI= Mean fluorescent Intensity.

	mIgA1		mIgA2	
dIgA1	↑	$CD1a^+$	↑	dIgA2
SIgA1	↑	CD80	↑	SIgA2
dIgA1	↓	$CD1a^-$	↓	dIgA2
SIgA1	↓	CD80	↓	SIgA2
dIgA1	↑ (**)	$CD1a^+$	↑	dIgA2
SIgA1	↑ (**)	CD86	↑	SIgA2
dIgA1	↑ (*)	$CD1a^-$	↑	dIgA2
SIgA1	↑ (*)	CD86	↑	SIgA2
dIgA1	↑ (**)	$CD1a^+$	↑ (*)	dIgA2
SIgA1	↑ (**)	HLA-DR	↑	SIgA2
dIgA1	↑	$CD1a^-$	↑ (*)	dIgA2
SIgA1	↑	HLA-DR	↑ (**)	SIgA2
dIgA1	↑ (**)	$CD1a^+$	↑ (*)	dIgA2
SIgA1	↑ (***)	CD40	↑ (**)	SIgA2
dIgA1	↑ (***)	$CD1a^-$	↑	dIgA2
SIgA1	↑ (***)	CD40	↑	SIgA2

Figure 1. Different binding of IgA isotypes and isoforms to IgA receptors on moDC. (A) Confocal microscopy of IgA receptors on monocytes-derived dendritic cells (moDC) upon treatment with 12µg of mIgA1/2, dIgA1/2 (dIgA1 from myeloma & dIgA2 from HF2 hybridoma) or SIgA1/2 (prepared with dIgA1 from myeloma & dIgA2 from HF2 hybridoma). Surface and intracellular Fc□RI, Dectin-1, DC-SIGN and CD71 were stained (green) on moDC after IgA treatment. Colocalizations (yellow) between receptors and IgA (red) were evaluated on live cells stained for their nucleus with Draq 5 (blue). Pictures are representative from two experiments with 3 different donors (total=6). Magnification (x60) Scale bar 10µm. (B) Quantification of binding intensities (Arbitrary Units) of the same IgAs on Fc□RI, Dectin-1, DC-SIGN and CD71. Intensity of co-labeling was estimated on 50 different cells per condition (two experiments with 3 donors performed in triplicate, n=6) and compared with anti-IgA alone. Relative binding intensities were compared with a two-way ANOVA with Dunnett's multiple comparison test (*) $p \leq 0.05$, (**) $p \leq 0.01$ and (***) $p \leq 0.001$. Datas are shown as median +/- SD. (C) After 24hrs of incubation with IgA, moDC were separated depending on the number of IgA-receptors expressed on their surface (Fc□RI, DC-SIGN, Dectin-1 and CD71) by flow cytometry. Data are from three experiments with 2-3 donors per experiment, performed in triplicate (n=8). Kruskal-Wallis with Dunn's multiple comparison test was performed. Datas are shown as median +/- SD (D-G) Thermopheresis analysis of IgA binding to the different receptors. Histidine-tagged receptors were coupled with a fluorochrome and the delay of fluorescence recovery after warming was measured after binding with several concentrations of monomeric IgA1 (red line), IgA2 (green line) or dIgA1 (purple line) or dIgA2 (blue line) to DC-SIGN (D), CD71 (E), Fc□RI (F) and Dectin-1 (G). Measures at each ligand concentration are displayed as mean +/- s.d. of 3 different experiments in duplicate (n=6).

Figure 2. Relation between receptors expression on moDC and IgA internalization. (A-D) Mean Fluorescence Intensity (MFI) of CD71 (A), FcαRI (B), Dectin-1 (C), DC-SIGN (D) receptor expression on IgA^+ moDCs. Expression was analyzed by flow cytometry after 24hrs with an activation cocktail (Cytokines: IL-1β, IL-6, TNF-α) or IgA1/IgA2 isoforms. Measures were normalized relatively to non-stimulated (NS) moDC to reduce intra-donors biases. Data are obtained from 8 donors and experiments were realized in triplicate. Relative expression means were compared with each other thanks to a two-way ANOVA with Dunnett's multiple comparison test. (*) $p \leq 0.05$, (**) $p \leq 0.01$ and (***) $p \leq 0.001$. Datas are shown as median +/- SD.

Figure 3. moDC activation by IgA1 and IgA2 isoforms. (A-D) Flow cytometry analysis of the relative expression of activation markers (CD80, CD40, CD86, HLA-DR) by moDC were obtained by comparing the MFI after 24h of IgA stimulation (12µg/mL) to non-stimulated moDC (NS). A stimulated positive control (Cytokines: IL-1β, IL-6, TNF-α) was used. The increase/decrease of marker expression between them was normalized (percentages displayed on pie chart). Data are from five experiments with 3-5 donors per experiment, performed in triplicate (n=19 for IgA1 and 8 for IgA2). Relative expression means were compared with a two-way ANOVA with with Dunnett's multiple comparison test. (*) $p \leq 0.05$, (**) $p \leq 0.01$ and (***) $p \leq 0.001$. Datas are shown as median +/- SD.

Figure 4. Transcriptomic and cytokine profiles of moDC activated by the various IgA isoforms and isotypes. (A-B-C) RNA expression of moDC from 3 different donors (n=3) stimulated with either mIgA1/mIgA2 isoforms (A), dimeric IgA1/IgA2 isoforms (dIgA1 from myeloma & dIgA2 from HF2 hybridoma) (B) or secretory IgA1/IgA2 (prepared with dIgA1 from myeloma & dIgA2 from HF2 hybridoma) (C). RNA expression was compared to non-stimulated moDC. Analysis of qRT-PCR results was performed with the help of the Qiagen Data Analysis Center in order to determine the correspondence between Ct and genes fold-regulation. Genes displaying 2-fold up- or down-regulated expressions were considered as affected by IgA stimulation. (D-E-F) Cytokine concentrations in the culture supernatant of stimulated moDC with IgA1 isoforms (D) or IgA2 isoforms (E) or stimulated moDCs with dIgA1 or dIgA2 (F) were determined by Luminex or ELISA assays. A one-way ANOVA with Dunnett's multiple comparison test or Kruskal-Wallis with Dunn's multiple comparison test depending on results of normality tests (Shapiro-Wilk and Agostino-Pearson) was used. Cytokine profiles are shown as radar charts; each axis displays the mean quantity (in pg/mL) of each cytokine/chemokine 24hrs after moDC stimulation. Data are from four experiments

with 3-5 donors per experiment, performed in triplicate (n=14). The scale of each axis being different, the values of both minimum and maximum were indicated into brackets [min: max]. (*) $p \leq 0.05$, (**) $p \leq 0.01$ and (***) $p \leq 0.001$.

Figure 5. Activation of cytotoxic CD8 T cells in the presence of mIgA1 or mIgA2. (A, B) Flow cytometry analysis of the activation of $CD4^+$ (A) or $CD8^+$ (B) $CD25^+$ T cells in a mixed lymphocytes reaction with moDC primed with mIgA1 or mIgA2 . Non-stimulated moDC was used as negative control (illustrated by the line at 100%). A Kruskal-Wallis with Dunn's multiple comparison tests was performed. Data are from two experiments with 2-3 donors per experiment, performed in duplicate (n=5). (C, D, E, F, G) Frequencies of MelanA-specific CD8 T cells (C), together with expression of transcription factors T-bet and Emoes (D, E) and Granzym B and Perforin (F, G) were determined by flow cytometry after *in vitro* priming with mIgA1 or mIgA2-stimulated moDC. Data are normalized compared to non-stimulated conditions. We performed a one-way ANOVA with Dunnett's multiple comparison test. Data are from three experiments with 3 donors per experiment, performed in duplicate (n=9). s.d. are indicated on the graphs (*) $p \leq 0.05$, (**) $p \leq 0.01$ and (***) $p \leq 0.001$.

References

1 **Woof, J. M. and Mestecky, J.,** Mucosal immunoglobulins. *Immunol Rev* 2005. **206**: 64-82.

2 **Brandtzaeg, P. and Prydz, H.,** Direct evidence for an integrated function of J chain and secretory component in epithelial transport of immunoglobulins. *Nature* 1984. **311**: 71-73.

3 **Woof, J. M. and Kerr, M. A.,** The function of immunoglobulin A in immunity. *J Pathol* 2006. **208**: 270-282.

4 **Zhou, M. and Ruprecht, R. M.,** Are anti-HIV IgAs good guys or bad guys? *Retrovirology* 2014. **11**: 109.

5 **Kerr, M. A.,** The structure and function of human IgA. *Biochem J* 1990. **271**: 285-296.

6 **Kett, K., Brandtzaeg, P., Radl, J. and Haaijman, J. J.,** Different subclass distribution of IgA-producing cells in human lymphoid organs and various secretory tissues. *J Immunol* 1986. **136**: 3631-3635.

7 **Lu, J., Marjon, K. D., Marnell, L. L., Wang, R., Mold, C., Du Clos, T. W. and Sun, P.,** Recognition and functional activation of the human IgA receptor (FcalphaRI) by C-reactive protein. *Proc Natl Acad Sci U S A* 2011. **108**: 4974-4979.

8 **Moura, I. C., Centelles, M. N., Arcos-Fajardo, M., Malheiros, D. M., Collawn, J. F., Cooper, M. D. and Monteiro, R. C.,** Identification of the transferrin receptor as a novel immunoglobulin (Ig)A1 receptor and its enhanced expression on mesangial cells in IgA nephropathy. *J Exp Med* 2001. **194**: 417-425.

9 **Rochereau, N., Drocourt, D., Perouzel, E., Pavot, V., Redelinghuys, P., Brown, G. D., Tiraby, G., Roblin, X., Verrier, B., Genin, C., Corthesy, B. and Paul, S.,** Dectin-1 is essential for reverse transcytosis of glycosylated SIgA-antigen complexes by intestinal M cells. *PLoS Biol* 2013. **11**: e1001658.

10 **Baumann, J., Park, C. G. and Mantis, N. J.,** Recognition of secretory IgA by DC-SIGN: implications for immune surveillance in the intestine. *Immunol Lett* 2010. **131**: 59-66.

11 **Lycke, N. Y. and Bemark, M.,** The regulation of gut mucosal IgA B-cell responses: recent developments. *Mucosal Immunol* 2017. **10**: 1361-1374.

12 **Heineke, M. H., van der Steen, L. P. E., Korthouwer, R. M., Hage, J. J., Langedijk, J. P. M., Benschop, J. J., Bakema, J. E., Slootstra, J. W. and van Egmond, M.,** Peptide mimetics of immunoglobulin A (IgA) and FcalphaRI block IgA-induced human neutrophil activation and migration. *Eur J Immunol* 2017. **47**: 1835-1845.

13 **Heineke, M. H. and van Egmond, M.,** Immunoglobulin A: magic bullet or Trojan horse? *Eur J Clin Invest* 2017. **47**: 184-192.

14 **Kubinak, J. L. and Round, J. L.,** Do antibodies select a healthy microbiota? *Nat Rev Immunol* 2016. **16**: 767-774.

15 **Bunker, J. J., Erickson, S. A., Flynn, T. M., Henry, C., Koval, J. C., Meisel, M., Jabri, B., Antonopoulos, D. A., Wilson, P. C. and Bendelac, A.,** Natural polyreactive IgA antibodies coat the intestinal microbiota. *Science* 2017. **358**.

16 **Macpherson, A. J., Yilmaz, B., Limenitakis, J. P. and Ganal-Vonarburg, S. C.,** IgA Function in Relation to the Intestinal Microbiota. *Annu Rev Immunol* 2018. **36**: 359-381.

17 **Mkaddem, S. B., Christou, I., Rossato, E., Berthelot, L., Lehuen, A. and Monteiro, R. C.,** IgA, IgA receptors, and their anti-inflammatory properties. *Curr Top Microbiol Immunol* 2014. **382**: 221-235.

18 **Hansen, I. S., Krabbendam, L., Bernink, J. H., Loayza-Puch, F., Hoepel, W., van Burgsteden, J. A., Kuijper, E. C., Buskens, C. J., Bemelman, W. A., Zaat, S. A. J., Agami, R., Vidarsson, G., van den Brink, G. R., de Jong, E. C., Wildenberg, M. E., Baeten, D. L. P., Everts, B. and den Dunnen, J.,** FcalphaRI co-stimulation converts human intestinal CD103(+) dendritic cells into pro-inflammatory cells through glycolytic reprogramming. *Nat Commun* 2018. **9**: 863.

19 **Chang, C. C., Wright, A. and Punnonen, J.,** Monocyte-derived CD1a+ and CD1a- dendritic cell subsets differ in their cytokine production profiles, susceptibilities to transfection, and capacities to direct Th cell differentiation. *J Immunol* 2000. **165**: 3584-3591.

20 **Gogolak, P., Rethi, B., Szatmari, I., Lanyi, A., Dezso, B., Nagy, L. and Rajnavolgyi, E.,** Differentiation of CD1a- and CD1a+ monocyte-derived dendritic cells is biased by lipid environment and PPARgamma. *Blood* 2007. **109**: 643-652.

21 **Pasquier, B., Lepelletier, Y., Baude, C., Hermine, O. and Monteiro, R. C.,** Differential expression and function of IgA receptors (CD89 and CD71) during maturation of dendritic cells. *J Leukoc Biol* 2004. **76**: 1134-1141.

22 **Lissina, A., Briceno, O., Afonso, G., Larsen, M., Gostick, E., Price, D. A., Mallone, R. and Appay, V.,** Priming of Qualitatively Superior Human Effector CD8+ T Cells Using TLR8 Ligand Combined with FLT3 Ligand. *J Immunol* 2016. **196**: 256-263.

23 **Cernadas, M., Lu, J., Watts, G. and Brenner, M. B.,** CD1a expression defines an interleukin-12 producing population of human dendritic cells. *Clin Exp Immunol* 2009. **155**: 523-533.

24 **Monteiro, R. C. and Van De Winkel, J. G.,** IgA Fc receptors. *Annu Rev Immunol* 2003. **21**: 177-204.

25 **Geijtenbeek, T. B., Torensma, R., van Vliet, S. J., van Duijnhoven, G. C., Adema, G. J., van Kooyk, Y. and Figdor, C. G.,** Identification of DC-SIGN, a novel dendritic cell-specific ICAM-3 receptor that supports primary immune responses. *Cell* 2000. **100**: 575-585.

26 **Heystek, H. C., Moulon, C., Woltman, A. M., Garonne, P. and van Kooten, C.,** Human immature dendritic cells efficiently bind and take up secretory IgA without the induction of maturation. *J Immunol* 2002. **168**: 102-107.

27 **Fabiano, R. C., Pinheiro, S. V. and Simoes, E. S. A. C.,** Immunoglobulin A nephropathy: a pathophysiology view. *Inflamm Res* 2016. **65**: 757-770.

28 **Pasquier, B., Launay, P., Kanamaru, Y., Moura, I. C., Pfirsch, S., Ruffie, C., Henin, D., Benhamou, M., Pretolani, M., Blank, U. and Monteiro, R. C.,** Identification of FcalphaRI as an inhibitory receptor that controls inflammation: dual role of FcRgamma ITAM. *Immunity* 2005. **22**: 31-42.

29 **Wehrli, M., Cortinas-Elizondo, F., Hlushchuk, R., Daudel, F., Villiger, P. M., Miescher, S., Zuercher, A. W., Djonov, V., Simon, H. U. and von Gunten, S.,** Human IgA Fc receptor FcalphaRI (CD89) triggers different forms of neutrophil death depending on the inflammatory microenvironment. *J Immunol* 2014. **193**: 5649-5659.

30 **Saha, C., Das, M., Patil, V., Stephen-Victor, E., Sharma, M., Wymann, S., Jordi, M., Vonarburg, C., Kaveri, S. V. and Bayry, J.,** Monomeric Immunoglobulin A from Plasma Inhibits Human Th17 Responses In Vitro Independent of FcalphaRI and DC-SIGN. *Front Immunol* 2017. **8**: 275.

31 **Cruikshank, W. W., Kornfeld, H. and Center, D. M.,** Interleukin-16. *J Leukoc Biol* 2000. **67**: 757-766.

32 **Sadasivan, B., Lehner, P. J., Ortmann, B., Spies, T. and Cresswell, P.,** Roles for calreticulin and a novel glycoprotein, tapasin, in the interaction of MHC class I molecules with TAP. *Immunity* 1996. **5**: 103-114.

33 **Diana, J., Moura, I. C., Vaugier, C., Gestin, A., Tissandie, E., Beaudoin, L., Corthesy, B., Hocini, H., Lehuen, A. and Monteiro, R. C.,** Secretory IgA induces tolerogenic dendritic cells through SIGNR1 dampening autoimmunity in mice. *J Immunol* 2013. **191**: 2335-2343.

34 **Kassiotis, G. and Kollias, G.,** Uncoupling the proinflammatory from the immunosuppressive properties of tumor necrosis factor (TNF) at the p55 TNF receptor level: implications for pathogenesis and therapy of autoimmune demyelination. *J Exp Med* 2001. **193**: 427-434.

35 **Scheller, J., Chalaris, A., Schmidt-Arras, D. and Rose-John, S.,** The pro- and anti-inflammatory properties of the cytokine interleukin-6. *Biochim Biophys Acta* 2011. **1813**: 878-888.

36 **Gillessen, S., Carvajal, D., Ling, P., Podlaski, F. J., Stremlo, D. L., Familletti, P. C., Gubler, U., Presky, D. H., Stern, A. S. and Gately, M. K.,** Mouse interleukin-12 (IL-12) p40 homodimer: a potent IL-12 antagonist. *Eur J Immunol* 1995. **25**: 200-206.

37 **Teng, M. W., Bowman, E. P., McElwee, J. J., Smyth, M. J., Casanova, J. L., Cooper, A. M. and Cua, D. J.,** IL-12 and IL-23 cytokines: from discovery to targeted therapies for immune-mediated inflammatory diseases. *Nat Med* 2015. **21**: 719-729.

38 **Cooper, A. M. and Khader, S. A.,** IL-12p40: an inherently agonistic cytokine. *Trends Immunol* 2007. **28**: 33-38.

39 **Pabst, O.,** New concepts in the generation and functions of IgA. *Nat Rev Immunol* 2012. **12**: 821-832.

40 **Pfeifle, R., Rothe, T., Ipseiz, N., Scherer, H. U., Culemann, S., Harre, U., Ackermann, J. A., Seefried, M., Kleyer, A., Uderhardt, S., Haugg, B., Hueber, A. J., Daum, P., Heidkamp, G. F., Ge, C., Bohm, S., Lux, A., Schuh, W., Magorivska, I., Nandakumar, K. S., Lonnblom, E., Becker, C., Dudziak, D., Wuhrer, M., Rombouts, Y., Koeleman, C. A., Toes, R., Winkler, T. H., Holmdahl, R., Herrmann, M., Bluml, S., Nimmerjahn, F., Schett, G. and Kronke, G.,** Regulation of autoantibody activity by the IL-23-TH17 axis determines the onset of autoimmune disease. *Nat Immunol* 2017. **18**: 104-113.

41 **Milpied, P. J. and McHeyzer-Williams, M. G.,** High-affinity IgA needs TH17 cell functional plasticity. *Nat Immunol* 2013. **14**: 313-315.

42 **Corthesy, B.,** Role of secretory immunoglobulin A and secretory component in the protection of mucosal surfaces. *Future Microbiol* 2010. **5**: 817-829.

43 **Crottet, P. and Corthesy, B.,** Secretory component delays the conversion of secretory IgA into antigen-binding competent F(ab')2: a possible implication for mucosal defense. *J Immunol* 1998. **161**: 5445-5453.

44 **Farache, J., Koren, I., Milo, I., Gurevich, I., Kim, K. W., Zigmond, E., Furtado, G. C., Lira, S. A. and Shakhar, G.,** Luminal bacteria recruit CD103+ dendritic cells into the intestinal epithelium to sample bacterial antigens for presentation. *Immunity* 2013. **38**: 581-595.

45 **Niess, J. H., Brand, S., Gu, X., Landsman, L., Jung, S., McCormick, B. A., Vyas, J. M., Boes, M., Ploegh, H. L., Fox, J. G., Littman, D. R. and Reinecker, H. C.,** CX3CR1-mediated dendritic cell access to the intestinal lumen and bacterial clearance. *Science* 2005. **307**: 254-258.

46 **Cheroutre, H., Lambolez, F. and Mucida, D.,** The light and dark sides of intestinal intraepithelial lymphocytes. *Nat Rev Immunol* 2011. **11**: 445-456.

47 **Bennett, M. S., Trivedi, S., Iyer, A. S., Hale, J. S. and Leung, D. T.,** Human mucosal-associated invariant T (MAIT) cells possess capacity for B cell help. *J Leukoc Biol* 2017. **102**: 1261-1269.

48 **Ludvigsson, J. F., Neovius, M. and Hammarstrom, L.,** Association between IgA deficiency & other autoimmune conditions: a population-based matched cohort study. *J Clin Immunol* 2014. **34**: 444-451.

49 **Rochereau, N., Pavot, V., Verrier, B., Jospin, F., Ensinas, A., Genin, C., Corthesy, B. and Paul, S.,** Delivery of antigen to nasal-associated lymphoid tissue microfold cells through secretory IgA targeting local dendritic cells confers protective immunity. *J Allergy Clin Immunol* 2016. **137**: 214-222 e212.

50 **Rochereau, N., Pavot, V., Verrier, B., Ensinas, A., Genin, C., Corthesy, B. and Paul, S.,** Secretory IgA as a vaccine carrier for delivery of HIV antigen to M cells. *Eur J Immunol* 2015. **45**: 773-779.

51 **Cossarizza, A., Chang, H. D., Radbruch, A., Acs, A., Adam, D., Adam-Klages, S., Agace, W. W., Aghaeepour, N., Akdis, M., Allez, M., Almeida, L. N., Alvisi, G., Anderson, G., Andra, I., Annunziato, F., Anselmo, A., Bacher, P., Baldari, C. T., Bari, S., Barnaba, V., Barros-Martins, J., Battistini, L., Bauer, W., Baumgart, S., Baumgarth, N., Baumjohann, D., Baying, B., Bebawy, M., Becher, B., Beisker, W., Benes, V., Beyaert, R., Blanco, A., Boardman, D. A., Bogdan, C., Borger, J. G., Borsellino, G., Boulais, P. E., Bradford, J. A., Brenner, D., Brinkman, R. R., Brooks, A. E. S., Busch, D. H., Buscher, M., Bushnell, T. P., Calzetti, F., Cameron, G., Cammarata, I., Cao, X., Cardell, S. L., Casola, S., Cassatella, M. A., Cavani, A., Celada, A., Chatenoud, L., Chattopadhyay, P. K., Chow, S., Christakou, E., Cicin-Sain, L., Clerici, M., Colombo, F. S., Cook, L., Cooke, A., Cooper, A. M., Corbett, A. J., Cosma, A., Cosmi, L., Coulie, P. G., Cumano, A., Cvetkovic, L., Dang, V. D., Dang-Heine, C., Davey, M. S., Davies, D., De Biasi, S., Del Zotto, G., Dela Cruz, G. V., Delacher, M., Della Bella, S., Dellabona, P., Deniz, G., Dessing, M., Di Santo, J. P., Diefenbach, A., Dieli, F., Dolf, A., Dorner, T., Dress, R. J., Dudziak, D., Dustin, M., Dutertre, C. A., Ebner, F., Eckle, S. B. G., Edinger, M., Eede, P., Ehrhardt, G. R.**

A., Eich, M., Engel, P., Engelhardt, B., Erdei, A., Guidelines for the use of flow cytometry and cell sorting in immunological studies (second edition). *Eur J Immunol* 2019. **49**: 1457-1973.

52 **Crottet, P. and Corthesy, B.,** Mapping the interaction between murine IgA and murine secretory component carrying epitope substitutions reveals a role of domains II and III in covalent binding to IgA. *J Biol Chem* 1999. **274**: 31456-31462.

53 **Crottet, P., Peitsch, M. C., Servis, C. and Corthesy, B.,** Covalent homodimers of murine secretory component induced by epitope substitution unravel the capacity of the polymeric Ig receptor to dimerize noncovalently in the absence of IgA ligand. *J Biol Chem* 1999. **274**: 31445-31455.

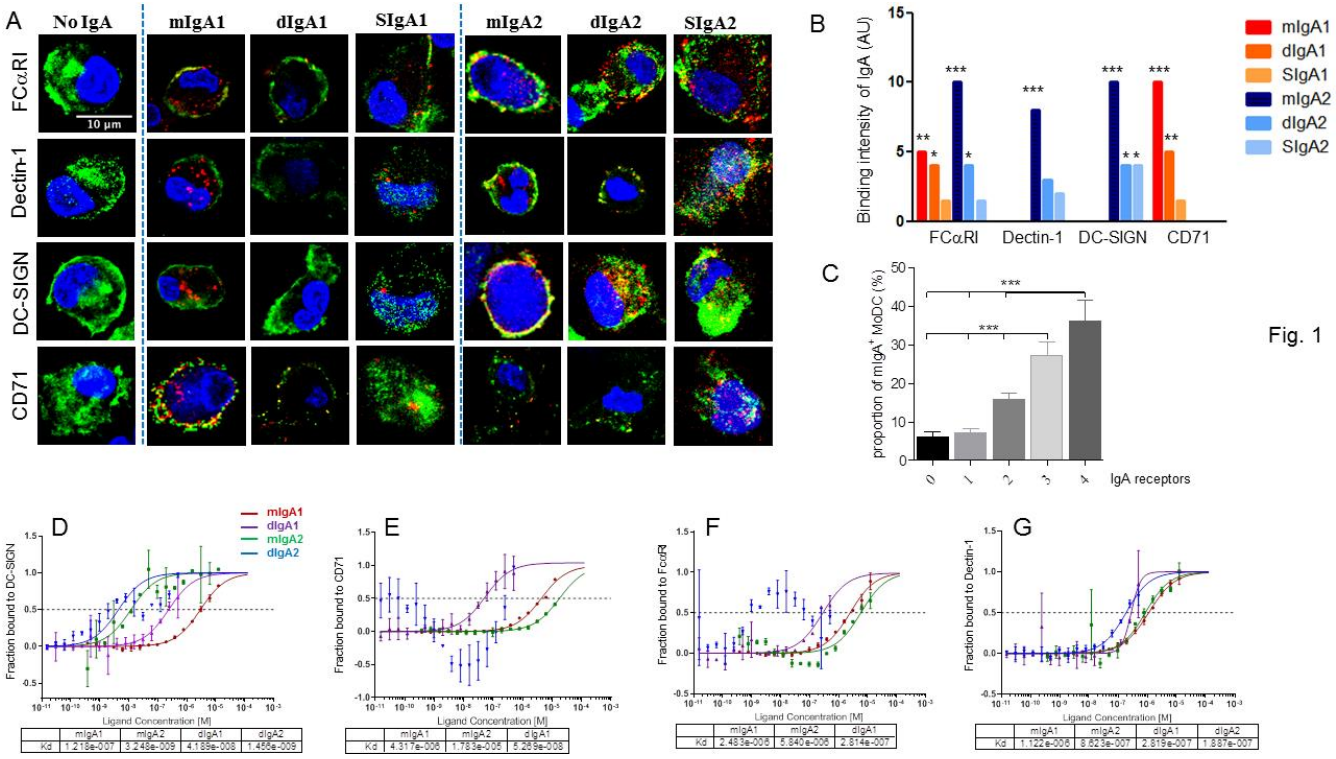
A
No IgA
mIgA1
dIgA1
SIgA1
mIgA2
dIgA2
SIgA2
FCαRI
Dectin-1
DC-SIGN
CD71
10 µm
B
Binding intensity of IgA (AU)
mIgA1
dIgA1
SIgA1
mIgA2
dIgA2
SIgA2
FCαRI
Dectin-1
DC-SIGN
CD71
C
proportion of mIgA+ MoDC (%)
IgA receptors
D
E
F
G
Fraction bound to DC-SIGN
Fraction bound to CD71
Fraction bound to FcαRI
Fraction bound to Dectin-1
Ligand Concentration [M]
mIgA1
dIgA1
mIgA2
dIgA2

Fig. 1

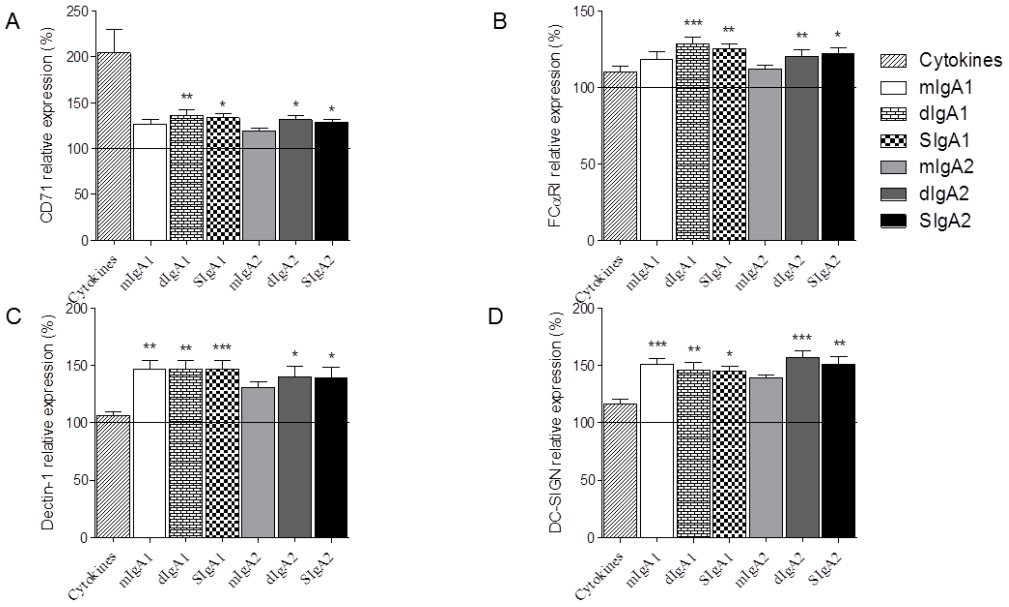
A
CD71 relative expression (%)
B
FCαRI relative expression (%)
C
Dectin-1 relative expression (%)
D
DC-SIGN relative expression (%)
Cytokines
mIgA1
dIgA1
SIgA1
mIgA2
dIgA2
SIgA2

Fig. 2

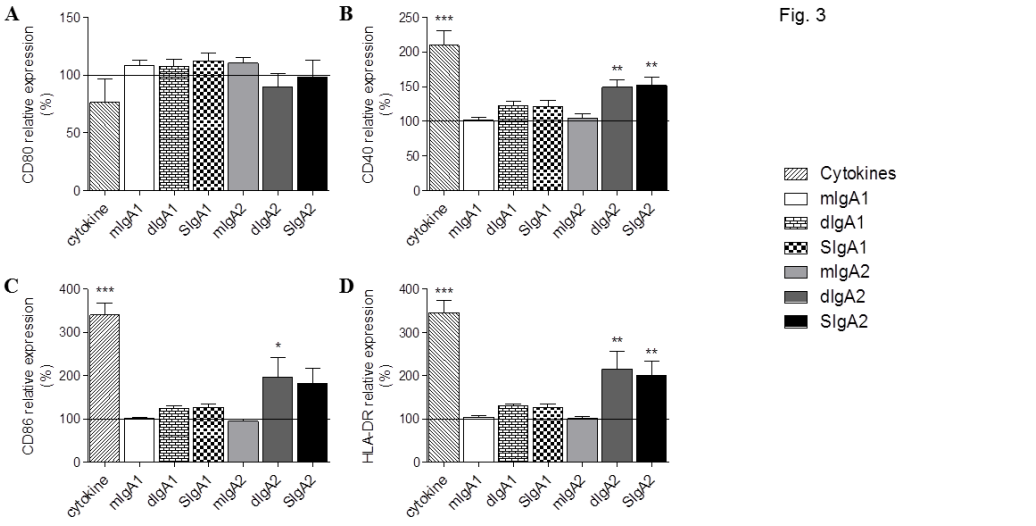
A
CD80 relative expression (%)
150
100
50
0
cytokine
mIgA1
dIgA1
SIgA1
mIgA2
dIgA2
SIgA2
B
CD40 relative expression (%)
250
200
150
100
50
0
***
**
**
C
CD86 relative expression (%)
400
300
200
100
0
***
*
D
HLA-DR relative expression (%)
400
300
200
100
0
***
**
**
Cytokines
mIgA1
dIgA1
SIgA1
mIgA2
dIgA2
SIgA2

Fig. 3

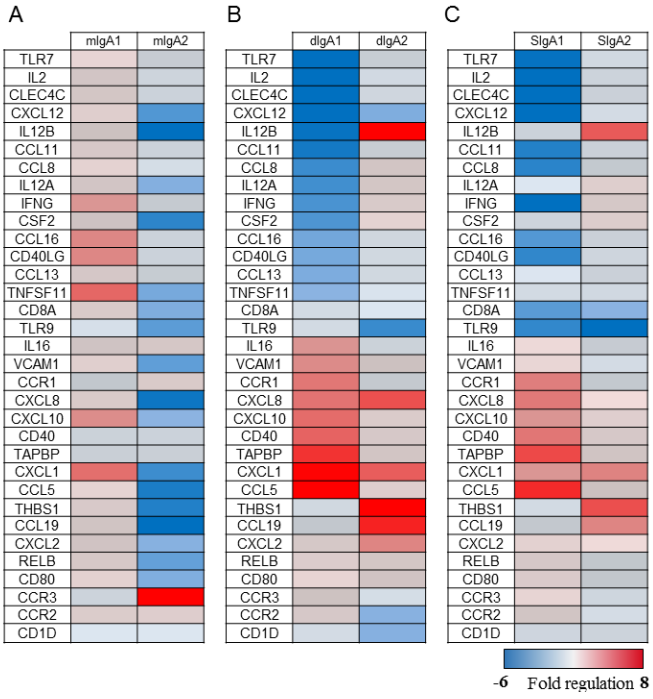
A
mIgA1
mIgA2
B
dIgA1
dIgA2
C
SIgA1
SIgA2
TLR7
IL2
CLEC4C
CXCL12
IL12B
CCL11
CCL8
IL12A
IFNG
CSF2
CCL16
CD40LG
CCL13
TNFSF11
CD8A
TLR9
IL16
VCAM1
CCR1
CXCL8
CXCL10
CD40
TAPBP
CXCL1
CCL5
THBS1
CCL19
CXCL2
RELB
CD80
CCR3
CCR2
CD1D
-6
Fold regulation
8

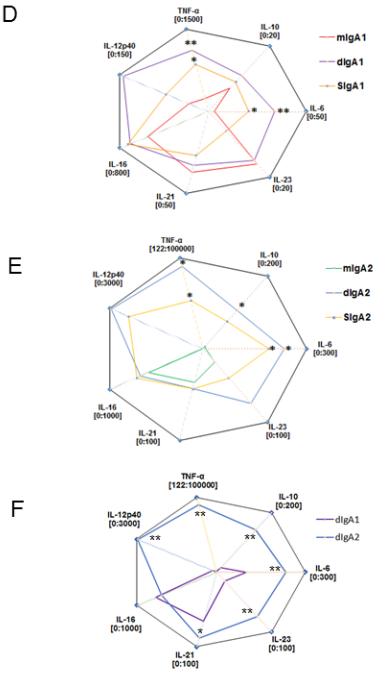
D
TNF-α [0:1500]
IL-10 [0:20]
IL-12p40 [0:150]
IL-6 [0:50]
IL-16 [0:800]
IL-23 [0:20]
IL-21 [0:50]
mIgA1
dIgA1
SIgA1
E
TNF-α [122:100000]
IL-10 [0:200]
IL-12p40 [0:3000]
IL-6 [0:300]
IL-16 [0:1000]
IL-23 [0:100]
IL-21 [0:100]
mIgA2
dIgA2
SIgA2
F
TNF-α [122:100000]
IL-10 [0:200]
IL-12p40 [0:3000]
IL-6 [0:300]
IL-16 [0:1000]
IL-23 [0:100]
IL-21 [0:100]
dIgA1
dIgA2

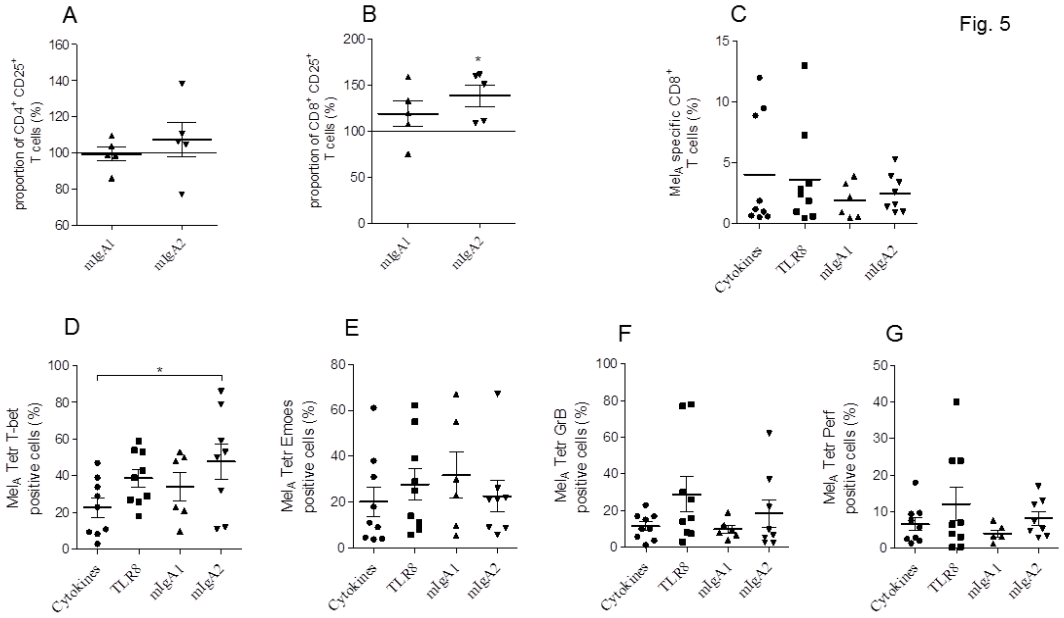
A
proportion of CD4+ CD25+ T cells (%)
mIgA1
mIgA2
B
proportion of CD8+ CD25+ T cells (%)
C
MelA specific CD8+ T cells (%)
Cytokines
TLR8
D
MelA Tetr T-bet positive cells (%)
E
MelA Tetr Emoes positive cells (%)
F
MelA Tetr GrB positive cells (%)
G
MelA Tetr Perf positive cells (%)

Fig. 5

Supplementary document

Supplemental methods

Monocyte derived dendritic cells (moDC) preparation

Human peripheral blood mononuclear cells (PBMCs) were obtained from buffy coats of healthy volunteers (EFS Auvergne-Rhône-Alpes) by density gradient centrifugation over a lymphocyte separation medium (Eurobio; Abcys, Courtaboeuf France). Monocytes ($CD14^+$) were positively sorted from PBMC with magnetic beads according to manufacturer's instructions (Miltenyi Biotec, Paris France). Differentiation of moDC was induced by culture of monocytes with complete RPMI medium (RPMI 1640, 10% FBS, 1% penicilline/streptomycine) supplemented with 100ng/mL of human granulocyte macrophage colony-stimulating factor (GM-CSF) (Miltenyi Biotec) and 50ng/mL of human interleukin (IL)-4 (Miltenyi Biotec) for 6 days with addition of fresh medium at day 3. The monocyte differentiation into moDC ($CD14^-$, $CD11b^+$, DC-$SIGN^+$ and $CD207^-$) was checked by flow cytometry.

moDC maturation

moDC were cultured at $1x10^6$ cells/mL in 24 wells plates in complete RPMI medium. A treatment with 50µg/mL of polymyxin B (InvivoGen) was done except for comparison between mIgA1 and mIgA2 (Fig. 2 and 3). Reagents were then added at indicated concentrations for moDC stimulation during 24hrs: 500ng/mL of Lipopolysaccharides from E. coli (Sigma), cytokines activator cocktail composed by 25ng/mL of human IL-1β (Miltenyi), 100ng/mL of human IL-6 (Miltenyi) and 50ng/mL of human Tumor Necrosis Factor (TNF)-α (Miltenyi), the various IgA at 12µg/mL.

Human intestinal biopsies

With the patient's agreement, ileum and colon biopsies were sampled. Samples were chopped with a scalpel in a petri dish containing complete RPMI medium. After the mechanic digestion, enzymatic digestion was performed with 10 U/mL of collagenase and 1/500 DNase (Sigma Aldrich, St Quentin Fallavier, France) for 20min at 37°C under agitation. Samples were ground in Medicon (BD Biosciences, Erembodegem, Belgium) and 30µm filtered (BD Biosciences) after 3 washes. Cells were centrifuged at 200g for 5min and resuspended into hyper complete RPMI medium (RPMI 1640, 10% FBS, 1% penicilline/streptomycine, 2mM L-glutamine, 1% non-essential amino acids, 10mM Hepes, 1mM sodium pyruvate).

Mixed lymphocyte reaction (MLR)

Negative cells recovered after CD14 sorting of PBMC were cultured in complete RPMI medium with 2,5ng/mL (50 UI/mL) of recombinant human IL-2 (rIL-2, R&D system). The medium was changed every 3 days until the differentiation and activation of moDC. Before incubation with IgA-primed moDC (24h with 12 µg of IgA), cells were assessed to be mostly live T cells ($CD3^+CD8^+$ or $CD3^+CD4^+$) by flow cytometry. In a 96-wells plate, $1x10^5$ activated moDC were cocultured with $5x10^5$ allogenic T cells in complete RPMI medium supplemented with rIL-2. A positive control was performed with T cell incubated without moDC in medium supplemented with phytohemagglutinin (PHA) at 5µg/mL (Sigma Aldrich, L8754). Five days after T cell stimulation, surface CD3, CD4, CD8 and CD25 staining were performed and cells were fixed and permeabilized (BD). A Ki-67 BV421 staining was performed in order to check the proliferation of T cells.

Supplementary Figure 1: Different binding of IgA isotypes and isoforms to IgA receptors on HELA-transfected cells. Confocal microscopy of IgA receptors on HELA-transfected cell lines with pcDNA3-FcRα (generous gift from Pr R. Monteiro), pcDNA3-CD71, pcDNA3-DCSIGN and pcDNA3-Dectin1 upon treatment with 12µg of monomeric (mIgA), dimeric (dIgA) or secretory (SIgA) IgA1 or IgA2. Three dimeric IgA1 (purified from myeloma (A) or BT1/BT2 hybridomas (B and C)) and three dimeric IgA2 (purified from HF2-4 hybridomas) were compared. From top to bottom: surface and intracellular FcαRI, Dectin-1, DC-SIGN and CD71 were stained (green) on HELA-transfected cell lines after one hour of incubation with IgA. Colocalizations (yellow) between receptors and IgA (red) were evaluated on live cells stained for their nucleus with Draq 5 (blue) thanks to merged pictures. Pictures are representative from three experiments with 3 different donors (total =9). Experiments were performed in triplicate. Magnification (x60).

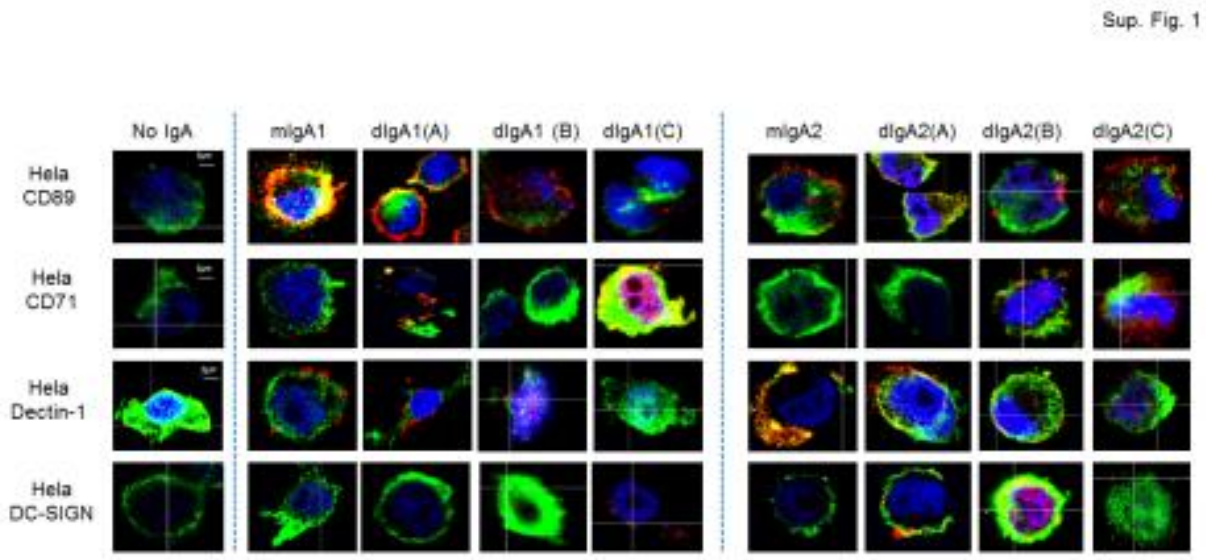

Supplementary Figure 2: Analysis of IgA binding to receptors by *in vitro* imaging and ELISA measurement of IgA affinity to the different receptors. (A) Area containing two moDC after binding with IgA1 (1h) and stained for human IgA (red) and for FCαRI (green). While one DC displayed a double staining, another cell (white dotted square) was stained for IgA but not for the FCαRI (x60). This picture is representative of 3 independent experiments in duplicate (n=6) also performed with DC-SIGN, Dectin-1 and CD71. (B, C, D, E) ELISA assays were performed to compare the binding of mIgA1 (continuous red line) and mIgA2 (continuous green line) with dIgA1 (purified from myeloma, dotted red line) and dIgA2 (purified from HF2 hybridoma, dotted green line) to FcαRI, Dectin-1, DC-SIGN and CD71. Decreasing concentrations of receptors were used with a stable amount of IgA with either a coating with receptors (B and C) or with IgA (D and E). A one site binding site model was determined from two experiments performed in duplicate (n=4) for each receptors/IgA combination using GraphPad® software. s.d. are indicated on the graphs. (*) $p \leq 0.05$, (**) $p \leq 0.01$ and (***) $p \leq 0.001$.

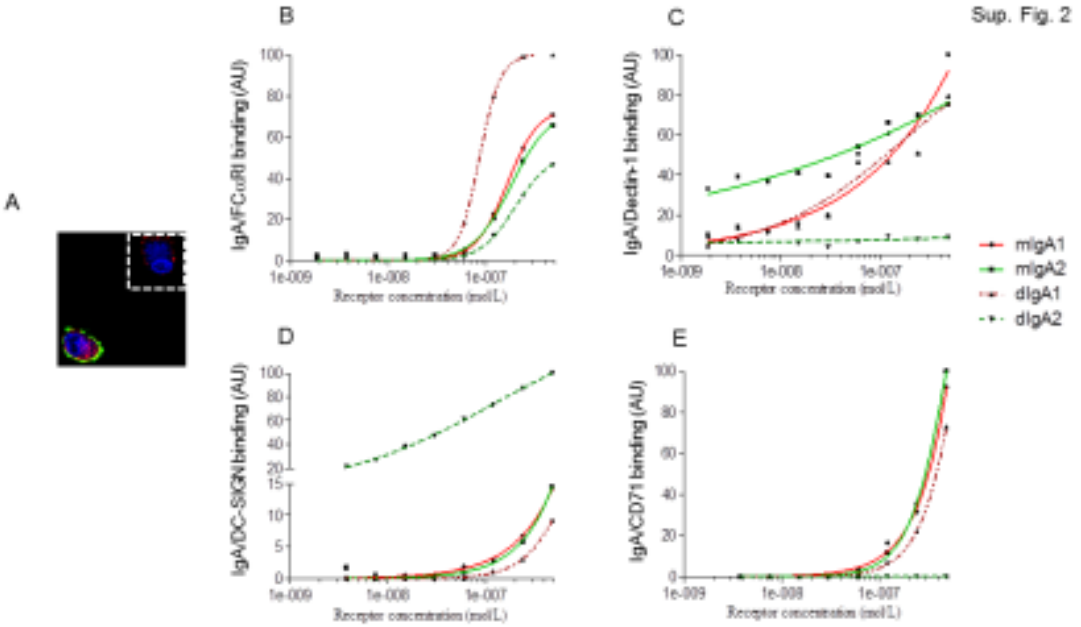

Supplementary Figure 3: IgA modified the expression of their receptors on the surface of CD1a$^-$ and CD1a$^+$ moDC. (A) Uptake/Binding of mIgA1 or mIgA2, dIgA1 or dIgA2 (myeloma and HF2), SIgA1 or SIgA2 were analyzed on different moDCs populations CD71$^+$, FcαRI$^+$(CD89), CD71$^+$/FcαRI$^+$(CD89), Dectin-1$^+$(CD369); DC-SIGN$^+$(CD209) and Dectin-1$^+$(CD369)/DC-SIGN$^+$(CD209) by flow cytometry. After 6 days of differentiation, moDCs were incubated with 6 µg of IgA during 24h. Datas are from two experiments with 4 donors per experiment, performed in triplicate and so the total number of donors is 8. (B) Upregulation of CD71, FcαRI, DC-SIGN and Dectin-1 receptors on CD1a$^+$ or CD1a$^-$ moDCs after IgA stimulation during 24h. MFI obtained for all the conditions were normalized relatively to the non-stimulated condition. Data are from two experiments with 4 donors per experiment, performed in triplicate and so the total number of donors is 8. Relative expression means were compared with a two-way ANOVA with with Dunnett's multiple comparison test. s.d. are indicated on the graphs (*) p≤0.05, (**) p≤0.01 and (***) p≤0.001. (C) The mean fluorescence intensity (MFI) of CD71, FcαRI, DC-SIGN and Dectin-1 expressed on the surface of CD1a$^+$ and CD1a$^-$ moDC was measured by flow cytometry. Normality and Mann-Whitney tests were used to compare the two means obtained. Data are from two experiments with 4 donors per experiment, performed in triplicate and so the total number of donors is 8. Relative expression means were compared with a two-way ANOVA with with Dunnett's multiple comparison test. s.d. are indicated on the graphs (*) p≤0.05, (**) p≤0.01 and (***) p≤0.001.

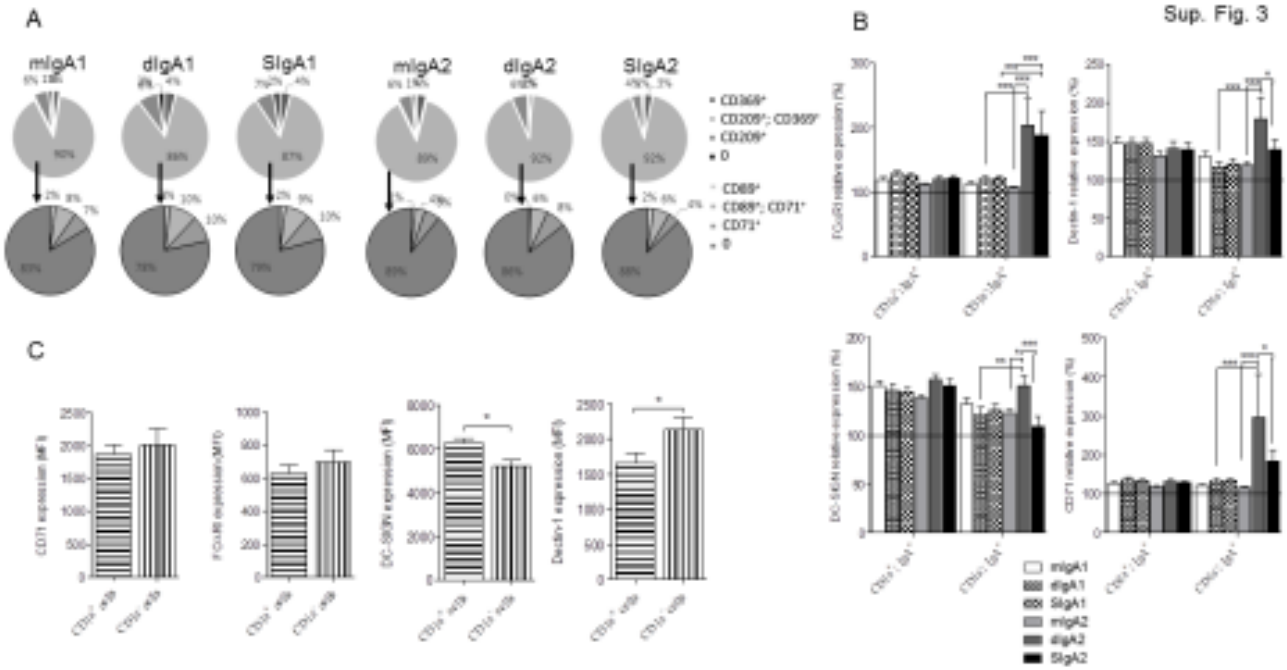

Supplementary Figure 4: Effect of IgA stimulation on mucosal human DCs. DC from gut surgeries of Crohn's disease patients were stimulated 24hrs with 12 µg of dimeric IgA1 (purified from myeloma) or dimeric IgA2 (purified from HF2 hybridoma). Expression of the CD86, HLA-DR, CD40 and CD80 activation markers was measured by flow cytometry and compared/normalized relatively to the non-stimulated (NS) condition (threshold at 100%). Analysis of activation markers were performed on $CD1a^+$ (A-B) or $CD1a^-$ (C) human mucosal DCs. Analysis of mucosal DCs are from five experiments with 2 patients per experiment, performed in triplicate and so the total number of donors is 10. Either one-way ANOVA with Dunnett's multiple comparison test or Kruskal-Wallis with Dunn's multiple comparison test depending on results of normality tests (Shapiro-Wilk and Agostino-Pearson) were performed. (*) $p \leq 0.05$, (**) $p \leq 0.01$ and (***) $p \leq 0.001$.

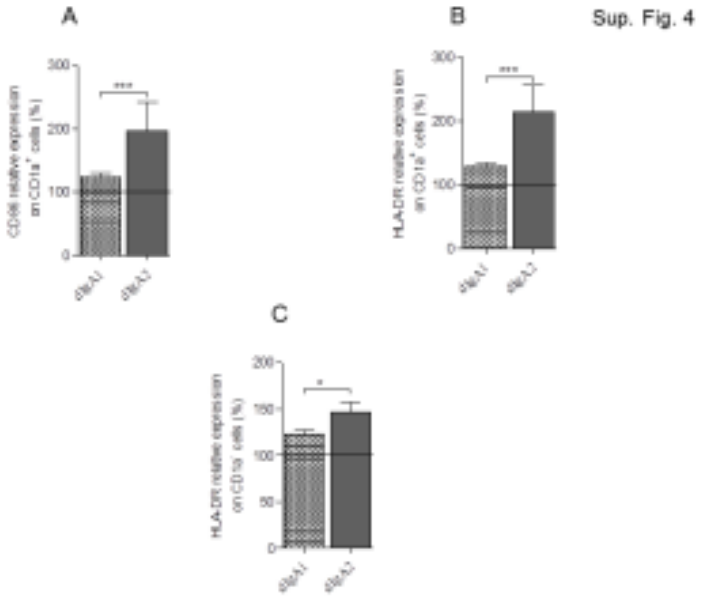

Supplementary Figure 5: Activation of cytotoxic CD8 T cells in the presence of IgA1 or IgA2 isotypes and isoforms. Flow cytometry analysis of the frequencies of Melan-A-specific CD8 T cells, and expression of transcription factors (Tbet) and cytotoxins (Granzyme B or Perforin) after *in vitro* priming in the presence of a cytokine activation cocktail, a TLR8 ligand or mIgA1, mIgA2, dIgA1 (myeloma) or dIgA2 (HF2) in the presence of polymyxin B . These data show results obtained from one representative donor (n=1).

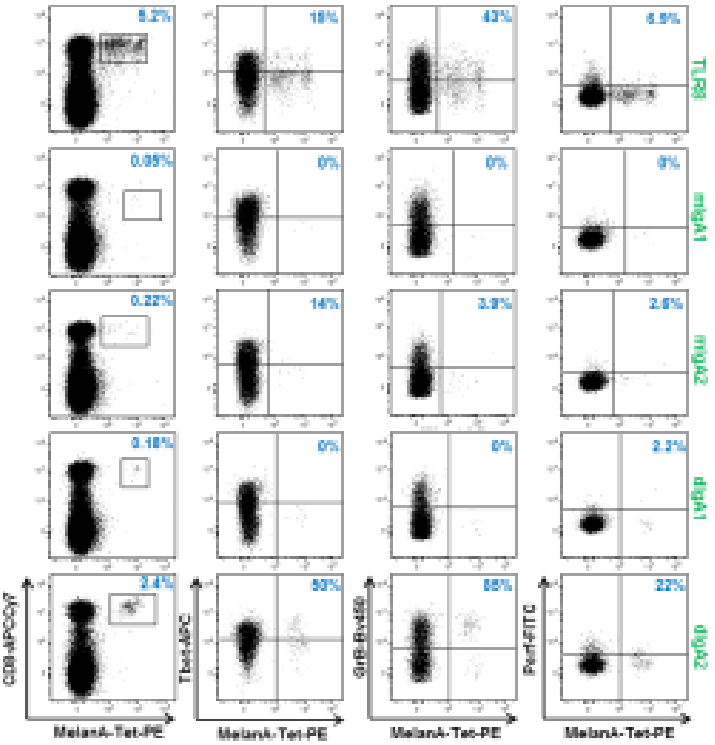

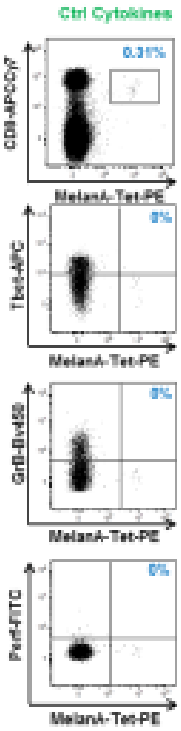

Suppl. Fig. 5

Nous montrons que les IgA, en particulier les formes dimériques, favorisent l'augmentation de l'expression de leurs propres récepteurs, avec un effet particulièrement prononcé pour Dectin-1 et DC-SIGN. L'affinité des IgA1 dimériques (dIgA1) pour les récepteurs FcαRI est particulièrement intéressante : l'IgA1 et l'IgA2 monomériques signalent chacune selon des cascades différentes suite à cette liaison [128]. L'activation de processus pro-inflammatoires par l'association IgA-FcαRI est concomitante à l'activation des voie intracellulaire Erk et Syk, et est observée majoritairement lors de la liaison IgA2-FcαRI[128]. Il serait intéressant d'étudier ce différentiel de réponse, corrélé à une importante sialylation des IgA1 et a un faible niveau de sialylation des IgA2. De plus, au vu de la polarisation des réponses muqueuse par les bactéries de la flore commensale, il serait important d'évaluer l'impact de la liaison à des antigènes commensaux ou du soi comparée à celle des pathogènes (i) sur ces mêmes cascades intracellulaires, (ii) sur le phénotype des moDC et leurs expressions des récepteurs aux IgA. Une étude transcriptomique tout le long du tube digestif, comme cela a déjà été fait pour caractériser la nature des cellules et la diversité épithéliales[11], permettrait d'établir une carte de l'expression des différents récepteurs aux IgA. Un second niveau d'analyse isolant spécifiquement les DCs des différentes sections du tube digestif (par tri cellulaire, par exemple) définirait les populations les plus promptes à fixer les IgA1 ou IgA2 selon le profil d'expression de ces récepteurs. Ce genre d'étude, réalisable chez la souris, reste néanmoins complexe au vu du petit nombre de cellules disponibles.

Nous montrons également que les formes dimériques, en particulier l'IgA2 dimérique, induisent plus fortement la maturation des moDC. De nouveau, il faudra approfondir ces résultats par l'étude du phénotype de ces DC face à des complexes Ig-antigènes. Pour rapprocher ces résultats de l'environnement muqueux, l'impact des complexes et les DC conditionnées par ceux-ci peut être testé directement sur des organoïdes intestinaux. La sécrétion d'IL-33, d'IL-21, de TNF-α, ou encore de PPARα est susceptible d'être activée suivant le type de complexes. Moins ambitieusement, le tri cellulaire sur biopsies et la co-culture des populations T, B, et macrophages avec ces DC permettrait d'établir un profil immun complet associé à un isoforme, une sous-classe, et un complexe formé par les IgA. La production d'IgA elle-même sera affectée par l'ensemble de ces réponses, en particulier du fait que nous montrons une augmentation de l'expression de CD40 dans les moDC. L'utilisation d'ELISPOT, dans lesquels seraient co-cultivés LB (d'hybridomes, par exemple) et ces moDC, ou bien des lysats de PP confirmerait l'importance de la nature de l'Ig dans l'entretien de la

sécrétion des IgA muqueuses. À cet effet, l'expression de BAFF et APRIL devra être monitorée, au vu de leur rôle primordial dans la commutation de classe, ainsi que la maturation, et le maintien, des lymphocytes B.

Notre analyse transcriptomique montre que si les mIgA augmentent la transcription des gènes de l'immunité, celle des dIgA2 induit l'activation de gènes d'activation cellulaire et de chimiotactisme (particulièrement pour les LT, macrophages et neutrophiles) tandis que les dIgA1, par contre, en diminuent l'expression. L'importante production cytokinique par les moDC stimulées par les dIgA2, et notamment celle du TNF-α et de l'IL-6, par rapport aux dIgA1, confirme les résultats précédemment obtenus par d'autres, qui présentent l'IgA2 comme plus inflammatoire que l'IgA1[128,220]. En l'état, cependant, ils ne confirment pas que ce recrutement cellulaire a lieu, aussi il est envisagée de co-cultiver d'une part les IgA (de sous-classe et d'isoforme différente, complexées ou non) avec des neutrophiles et des macrophages humains pour en étudier la réponse cytokinique. D'autre part, ces mêmes macrophage et neutrophiles seront co-cultivés avec des DC conditionnées par ces mêmes Ig. Ce modèle permettrait d'inférer sur l'inflammation muqueuse en réponse aux signaux exogènes intestinaux, par exemple. Pour aller plus loin dans ce sens, reproduire ces conditionnements sur des DC murines, co-cultivées avec des lysats de PP par exemple, permettrait d'avoir une vue *in vivo* de l'impact de ce conditionnement dans la muqueuse.

De plus, les IgA2 induisent une forte activation des LT $CD8^+$ et orientent la réponse immune vers un phénotype Th_1. Il serait donc intéressant de caractériser la réponse IgA et la réponse cytotoxique dans les maladies inflammatoires orientées vers un profil Th_1, comme c'est le cas pour la maladie de Crohn. L'utilisation d'IgA muqueuses, purifiées chez des patients par exemple, sur notre modèle de moDC serait un bon travail préliminaire dans ce sens.

De manière plus générale, notre étude bénéficierait à être reproduite avec des IgA de même spécificité, tests qui élimineraient la possibilité d'une interaction privilégiée. Les IgA n'étant pas les seules Ig sécrétoires ou même polymériques, nous souhaitons étendre l'étude aux IgM, qui existent sous forme monomérique (membranaire), pentamérique, sécrétoire, et hexamèrique. Le conditionnement des DC par ces différentes formes, le profil cytokinique et transcriptomique, ainsi que l'orientation de la réponse immune, sont ainsi peu décrits, en particulier au niveau des muqueuses.

B- Article 2 : Dynamique de transport des SIgM et nouvelles stratégies d'immunisation

1- Article et résumé

L'immunité muqueuse est assurée en première ligne par les IgA sécrétoires, notamment dans l'induction de la tolérance envers la flore commensale. Pour la réponse aux pathogènes, les IgA de haute affinité ciblent les bactéries de la lumière intestinale. Ces complexes immuns sont pris en charge au niveau de la PP par les cellules M du FAE. À la suite de cette reconnaissance par Dectin-1, les complexes SIgA-bactéries sont retro-transportés vers les DC insérées dans la poche de la cellule M pour induire des réponses inflammatoires appropriées. Cependant, le caractère sécrétoire n'appartient pas qu'aux IgA, les IgM possèdent des caractéristiques semblables, à savoir la liaison à la chaîne J et à la pièce sécrétoire, la multimérisation et la sécrétion dans la lumière intestinale *via* la transcytose.

Non montrons ainsi que le récepteur TOSO (FcμR) est exprimé par les cellules M murines et humaines et qu'il médie le transport de l'IgM *in vitro* et dans des expériences de ligatures intestinales chez la souris. De plus, nous démontrons l'immunogénicité de complexes IgM-p24 lorsqu'ils sont injectés au niveau de la muqueuse nasale et intestinale validant leur capacité fonctionnelle à délivrer des antigènes par transcytose inverse.

Essential role of TOSO/FAIM3 in intestinal IgM reverse transcytosis

Nicolas Rochereau[1], Eva Michaud[1], Rémi Gayet[1], Xavier Roblin[1], Gilles Biolley[2], Blaise Corthésy[2], Stéphane Paul[1].

[1] GIMAP/EA3064, Université de Lyon, CIC 1408 Vaccinology, F42023 Saint-Etienne, France; [2]R&D Laboratory of the Division of Immunology and Allergy, CHUV, Centre des Laboratoires d'Epalinges, 1066 Epalinges, Switzerland

* Corresponding author: Stéphane PAUL; stephane.paul@chu-st-etienne.fr
Faculté de médecine de St-Etienne, Laboratoire GIMAP
10 rue de la Marandière, 42270 St Priest-en-Jarez
Tel: +33 (0) 4 77 42 14 84; Fax: +33 (0) 4 77 42 14 86

Abstract

Mucosal immunity is thought to rely mostly on secretory IgA as a first line of defense. They indeed represent the bulk of Ig secretion at mucosal surfaces and can travel to and from the lumen, where they transport antigen to subepithelial dendritic cells DC-SIGN$^+$ (DC). However, they are not the only secretory Ig, as IgM can also multimerize into functional, J-chain- and secretory component (SC)-bound antibodies. While it is already known that both SIgA and SIgM undergo polymeric Ig receptor (pIgR)-mediated transcytosis to be secreted at the mucosal surface, only SIgA has been shown to perform the return trip in receptor-dependent manner through microfold (M) cell of the Peyer's patch (PP). Here we investigated whether SIgM could also be uptaken by M cell in a similar manner. We show that this transport is mediated by TOSO binding at the apical membrane of M cells. We then demonstrated that it can be exploited by SIgM-p24 complexes during immunization experiment in the nasal- or gut-associated lymphoid tissues (NALT, GALT) and confers efficient humoral and cellular recall responses against p24.

Keywords: IgM / secretory IgA / retrograde transport / Microfold cells / *TOSO*

Introduction

The concept of local or mucosal immunity has expanded dramatically over the past decades. The mucosal wall is equipped with a tightly regulated defense system. The intestinal mucosa contains more than 80% of all immunoglobulin producing cells in the human body. Gut-associated lymphoid tissues (GALT) are the primary inductive sites for secretory immunoglobulin, of which secretory IgA (SIgA) is the dominant entity. SIgA has long been recognized as the first line of defense in protecting the intestinal epithelium from enteric pathogens and toxins. It is generally assumed that SIgA acts primarily through receptor blockade, steric hindrance, and / or immune exclusion. Evidence has emerged indicating that SIgA promotes the uptake and delivery of antigens (Ag) from the intestinal lumen to DC subsets located in GALTs. It thusly influences inflammatory responses normally associated with the uptake of highly pathogenic bacteria and potentially allergenic Ags. This particular feature of SIgA, called reverse transcytosis, is mediated by epithelial M cells[1]. Our and previous data have shown that SIgA selectively binds Dectin-1 and Siglec-5 receptors at the apical membrane of Peyer's patches (PP) M cells. This triggers SIgA transport across the epithelium towards underlying DCs of the subepithelial dome (SED) region, inducing their maturation and migration to the interfollicular areas [1]. We also demonstrated that both the Cα1 region and glycosylation, particularly sialic acid residues, are involved in M cell–mediated reverse transcytosis. Finally, oral and nasal administration of an SIgA-bound p24 antigen vaccine candidate was shown to elicit antigen-specific immune responses in both mucosal and systemic compartments, ensureing protection against a recombinant vaccinia virus expressing the gag antigen [2,3]. Although considerable emphasis has been devoted to the role of IgA because of its relative abundance in digestive tract secretions, mucosal functions of SIgM have been comparatively neglected.

Human secreted IgM (SIgM) is the first antibody to be produced during an immune response. Bearing five *N*-linked glycosylation sites on each μ chain[4], SIgM is a J chain-bound pentamer. It is secreted at mucosal surfaces through polymeric Ig receptor (pIgR)-mediated transcytosis, similarly to SIgA[5,6]. To date, two additional Fc receptors, FcμR and Fcα/μR, have been shown to bind to IgM [7] in addition to the pIgR [8]. Both Fcα/μR and pIgR can bind both to IgA and IgM with intermediate affinity. FcμR (TOSO/FAIM3) has been identified the latest as a highly specific receptor for IgM and data suggest that it may serve as an uptake receptor for IgM-opsonized antigens by B cells [9].

Given that SIgA is accepted as the predominant gut antibody, little discussion has been spared for SIgM. However it represents up to 20% of mucosal antibodies in humans [10]. Gut IgM^+ B

cell have been shown to recall efficient anti-commensal recall response *via* SIgM secretion and IgA class-switch recombination (CSR)[11]. Studies in SIgA-deficient patients (SIgAd) show partial functional redundancy between IgA- and IgM-coated commensal bacteria[12,13], thought to limit the induction of dysbiosis. Though it does not recapitulates all typical SIgA functions, human SIgM binds a broader set of commensals than that of SIgA[12,13], activates complement[14] and extensive anti-glycan IgM repertoires protect the neonatal mucosa[15] during early bacterial colonisation. Moreover, SIgM -deficient mice and humans have increased sensitivity to viral, bacterial and protozoal infection[16]. As these studies suggest IgM samples bacterial antigens in the intestinal mucosa, we sought to study whether M cell also transport SIgM from the intestinal lumen to PPs through receptor-specific processes. We demonstrate that SIgM were able to perform reverse transcytosis via M cells both in human *in vitro* models and *in vivo* in mice. We were then able to demonstrate that this relied on to the ability of SIgM to bind TOSO/FAIM3 on M cells. We then showed that SIgM-bound p24, were uptaken by M cells *in vivo* the murine GALT and NALT. Finally, we were able to show that this vaccine formulation was immunogenic.

Methods

Reagents. Pullulan from *Aureobasidium pullulans,* mannan from *Saccharomyces cerevisiae,* Lactose, L-fructose, glycogen from bovine liver, sucrose, curdlan from *Alcaligenes faecalis,* laminarin from *Laminaria digitata* and zymosan from *Saccharomyces cerevisiae* were all purchased from Sigma-Aldrich. Anti-human Dectin-1/CLEC 7A polyclonal Ab (pAb) (goat IgG), anti-human pIgR Ab (goat IgG) and anti-human CD170 mAb (Siglec-5) (mouse IgG1) were purchased from R&D Systems. Anti-human CD206 mAb (mouse IgG1) (mannose receptor) was purchased from Ozyme. Anti-human CD71 mAb (mouse IgG1) was purchased from Cliniscience. Anti-FAIM3 Ab (mouse IgG2b) and Anti-CD351 antibody were purchased from Abcam. All were blocking antibodies and were used according to manufacturers' instructions.

Cell culture. Both the human intestinal cell line Caco-2 cell (clone 1) (obtained from Dr. Maria Rescigno, University of Milan-Bicocca, Milan, Italy)[17] and CHO cells were cultured in Dulbecco's modified Eagle's medium (DMEM) (PAA) supplemented with 10% (v/v) fetal bovine serum (FBS, Thermo-Fisher), 1% (v/v) non-essential amino-acids (PAA), and 1% (v/v) penicillin-streptomycin (PAA). The human Burkitt's lymphoma cell line Raji B (American Type Culture Collection) was cultured in RPMI 1640 supplemented with 10% (v/v) FBS, 1% (v/v) non-essential amino-acids, 1% (v/v) L-glutamine and 1% (v/v) penicillin-streptomycin.

Inverted *in vitro* model of the human FAE. The inverted FAE model has been previously published [1,18]. Inverted Transwell® polycarbonate inserts (12 wells, pore diameter of 3.0 µm, Corning) were coated with Matrigel™ (BD Biosciences) prepared in pure DMEM to a final protein concentration of 100 µg/mL for 1 h at room temperature (RT). The coating solution was removed and inverted inserts washed with 300 µL of DMEM. Caco-2 cells (3 x 10^5), resuspended in 300 µL of supplemented DMEM, were seeded on the lower insert side and cultured overnight. The inserts were then inverted and placed in a 12-well culture dish and kept for 9 days. Raji B cells (5 x 105), were resuspended in supplemented DMEM and then added to the basolateral compartment of the Caco-2 cells, and co-cultures are maintained for 5 days. Mono-cultures of Caco-2 cells, cultivated as above but without the Raji B cells, were used as controls. Both co- and mono-cultures, is controlled by measurement of TEER using an EndohmTM tissue resistance chamber (Endohm-12, World Precision Instruments) connected to a Millicell®-ERS Ohmmeter (Millipore). The resistance of medium alone (9 Ω x cm2) was considered as background resistance and subtracted from each TEER value. Finally, the inserts were inverted in 6-well plates, and a piece of silicon tubing (14 x 20 mm, Labomoderne) was placed on the basolateral side of each insert.

Immunolabelling of *in vitro* model of the human follicle-associated epithelium (FAE). Inserts were washed in HBSS to eliminate residual medium, incubated in 4% paraformaldehyde for 30 min, permeabilized with 0.1% Triton X- 100 (Sigma-Aldrich), and blocked with PBS containing 5% FBS for 15 min at room temperature. Immunolabeling was performed using a combination of PE-IgM, FITC-IgM, anti-human GP2 mAb (MBL), Anti-FAIM3 Ab (Abcam), and mouse anti-human CA19.9 (Dako). Each reagent was diluted to 1/100, and incubated for 2 h at RT. 1/200 dilutions of secondary antibodies labeled with a fluorochrome were incubated for 1 h at room temperature. After two washes, inserts were air-dried, mounted with Fluoprep (BioMerieux), and observed by epifluorescence microscopy (Eclipse Ti, Nikon).

Measure of reverse transcytosis *in vitro*. Transport experiments were performed in HBSS at 37°C for 90 min with 10 mg of IgM (Sigma). Basolateral solutions were then recovered and the number of retro-transcytosed Ab measured by ELISA. Ninety-six-well Maxisorp plates were coated overnight with 50 µL of anti-human IgM (Abliance) (10 µg/mL in sterile PBS). Transported IgM were detected by means of incubation (for 1 hour at 37°C) with horseradish peroxidase–conjugated goat anti-human IgM (Oaris) for 1 hour at 37°C. Results are presented as mean +/- SEM concentrations.

Inhibition experiments. Cell monolayers were first pre-incubated apically with 5 mg of inhibitor in HBSS for 90 min at 37°C, and washed with HBSS, before adding the IgM suspension. All transport experiments were carried out in triplicate.

SiRNA assays. ON-TARGETplus SMARTpool siRNAs (Dharmacon) were transfected at final concentration 5 nM using Silentfect reagent (Bio-Rad) in the inverted *in vitro* model of FAE according to the procedure provided by the manufacturer. The genes targeted in this study were Toso/FAIM3 (L-004451-00-0005), Dectin-1 (L-021476-00-0005), Siglec-5 (L-019522-02-0005), EEA-1 (L-004012-00-0005), pIgR (L-017729-00-0005), Rab5 (L-004009-00-0005), Rab7 (L-010388-00-0005), Rab9 (L-004177-00-0005), Rab11 (L-004726-00-0005), Rab17 (L-006474-00-0005), Rab25 (L-010366-00-0005) (Dharmacon)

Mice. Mouse strains used in this study consisted of 8-week-old female BALB/c mice (Charles River). All animals were housed at the Unité hospitalo-universitaire d'expérimentation animale (Saint-Etienne, France). The protocol was approved by the Ethics Committee of CREEA (Permit number: No. 69387487).

Production of p24–SIgM complexes. Polymeric IgM from the IgMHF5 hybridoma was obtained from culture in CELLline flasks (Integra, 900010) in RPMI 1640) medium supplemented with 10% fetal bovine serum (SVF), 1% streptomycin/penicillin, 2mM L-glutamine (Sigma, G7513), 1% non-essential amino acids (Sigma, M7145), 10 mM Hepes (Sigma, H0887), and 1mM sodium pyruvate (Sigma, S8636). Supernatant containing IgM was purified on a PORO CaptureSelect IgM Affinity Matrix resin (Invitrogen) every week. Purified free human SC was produced in Chinese hamster ovary cells [19]. SIgM were obtained by combining pIgM molecules in PBS with a twofold excess of human SC for 1 h at room temperature as previously described [20]. SIgM complexes were then purified before being covalently linked to p24 at equimolar ratio. p24 antigen was produced in CHO cells (Px Therapeutics, Lyon, France). Covalent association between p24 and SIgM was carried out with the heterobifunctional crosslinker Sulfo-KMUS according to the protocol provided by the manufacturer (Thermo Scientific, Waltham, MA, USA).

IgM Administration into Ligated Loops and NALT. For ileal loop preparation, mice were anesthetized by intraperitoneal injection of a mix of ketamine and xylazine. A total of 100 µL of a 1 mg/mL solution of SIgM diluted in PBS was administered into a 1.5-cm ileal loop containing a PP. Upon completion of the experiment, mice were sacrificed, the loop was removed, embedded in optimal cutting tissue solution and placed on microscope slides.

An identical SIgM solution was administered intranasally and NALT dissection was performed as previously described [2]. Processed tissue was embedded in OCT solution and placed on

microscope slides. Seven micrometer sections (Leica cryostat model CM1950; Leica Microsystem, Wetzlar, Germany) were placed on Ultra Superfrost microscope slides (VWR International, Radnor, Pa). Slides were washed in PBS to eliminate residual OCT and blocked with PBS containing 5% FBS for 30 minutes at room temperature. Immunolabeling was performed with the following primary antibodies (1:200 dilution): anti-human DC-SIGN and anti–Ulex europaeus agglutinin 1 (UEA-1), both were fluorescein isothiocyanate conjugated. Slides were examined by means of immunofluorescence microscopy (Eclipse; Nikon, Tokyo, Japan).

Immunization with p24–SIgM complexes. Mouse oral and nasal immunizations were performed as previously described [2,3]. Immunizations consisted of three administrations of 100 µL each at 1-week intervals, followed by a last boosting immunization 3 weeks later. Groups of five mice were immunized with either PBS, 50 µg of p24 or 50 µg of p24–SIgM at each time point.

Recovery of blood, feces, and vaginal lavages. Biological fluids were recovered prior to- and 1 week after each- immunization to examine their Ab content. Sera were collected by centrifugation at 16,000 × g and stored at −20°C until use. Feces, vaginal lavages, and saliva were incubated with Halt™ protease inhibitor cocktail (Thermo Scientific), centrifuged at 16,000 × g and stored at −20°C until use.

Quantification of p24-specific IgG and IgA. Abs in biological fluids p24-specific IgG/IgA in serum, vaginal lavages, feces and saliva samples were measured by quantitative ELISA. 96-well Maxisorp® plates were coated with 50 µL of p24 antigen solution (5 µg/mL in sterile PBS). Bound or captured Igs were detected by incubation (1 h, 37°C) with HRP-conjugated goat anti-mouse IgG, and bound IgA was detected with biotinylated goat anti mouse IgA followed by streptavidin- HRP. Results are given as the means of concentrations ± SEM and background Ab concentration measured on preimmune samples was subtracted for each animal.

Detection of p24-specific Th1 response by ELISPOT. Mice were sacrificed by cervical dislocation under anesthesia 1 week after the booster immunization. ELISPOT assays were performed with cells isolated from spleen of mice as described[21,22]. ELISPOT assays were performed with the ELISPOTplus kit for mouse IFN-γ according to the procedure provided by the manufacturer (Mabtech, Cincinnati, OH, USA).

Statistical analysis. All statistical analyses were performed with the InStat version 5.02 software from GraphPad Software. A nonparametric Mann–Whitney U-test or one-way ANOVA followed by Bonferroni post hoc test was used where appropriate [23,24]. The p values less than 0.05 (marked by *), or less than 0.01 (**), or less than 0.005 (***) were considered

as significant. Statistically significant differences between groups are emphasized by bars connecting the relevant columns.

Results

SIgM are efficiently uptaken and transported by human M cells in oral and nasal mucosae

One feature of M cells is their ability to transport a broad range of materials including Abs from the lumen to the underlying follicles. Specific retro-transport of IgM was evaluated in an *in vitro* model of human FAE containing M-like cells as previously described [25]. A significant transport of the IgM across the cell monolayer harboring M-like cells was observed (Fig. 1a). No transport was detected in the absence of M cells. Similar results were obtained with either recombinant CD20- or TNF-specific IgM (Fig. 1a). Association with human SC did not increase IgM uptake by M-like cells. Uptake of IgM by M-like cells was also confirmed by colocalizing IgM with CA19-9 and GP2 M-cell markers (Fig. 1b). Specificity of IgM reverse transcytosis was further confirmed *in vivo* after fluorescent IgM administration in ligated murine intestinal loop experiments (Fig. 1c). The number of IgM^+ cells were 8 times more abundant than that of IgG^+- cells in PPs, thus indicating increased transport of IgM trough the FAE (Fig. 1e). The nasal-associated lymphoid tissue (NALT), is separated from the nasal cavity by an epithelium containing M cells [26]. This anatomic similarity with the gastrointestinal tract led us to evaluate the specific retro-transport of IgM after nasal administration in mice (Fig. 1d). Intranasal administration of fluorescent IgM showed colocalization between IgM and UEA-1, a typical murine M-cell marker[27]. The number of IgM^+ cells were 10 times more abundant than that of IgG^+ cells in the NALT (Fig. 1e). These results demonstrate that IgM is uptaken by M cells of the GALT and of the NALT before being retro-transported into lymphoid tissues.

IgM reverse transcytosis is glycosylation-independent.

Influence of N-glycosylation on the uptake of IgA2 by M-like cells has been previously described[25]. To determine whether IgM N-glycosylations could influence their uptake and transport by M-like cells, the *in vitro* reverse transcytosis of enzymatically digested IgM by PNGase and Neuraminidase was tested. First, SDS-PAGE performed under reducing conditions confirmed the expected molecular weight for the light and heavy chains of deglycosylated IgM (Supplementary Fig. 1a). Surprisingly, the efficiency of IgM reverse transcytosis was not dependent on its glycosylation motifs *in vitro.* No decrease of the retro-transport was detected in the presence of M cells either under PNGase or Neuraminidase treatment (Supplementary Fig. 1b), and no binding on M cells were detected by epifluorescence (Supplementary Fig. 1c).

To further explore the possible involvement of glycans in IgM trafficking, blocking experiments were performed using □-glucans, mono- or disaccharides, and sialic acids (Supplementary Fig. 1d). In contrast with IgA2 [1], any inhibition was observed with all sugar family tested, independently of the concentration used.

TOSO is a new M-like cells receptor which bind IgM

To further explore the uptake of IgM in M cells, Abs directed against IgA or IgM receptors that have been described as being involved in their transport were used in blocking experiments (Fig. 2a). In contrast to IgA2[1], the use of an anti-Dectin-1 and anti-Siglec-5 mAb did not influence IgM retro-transport. Similarly, targeting of the human myeloid IgA Fc receptor (CD89) with a specific mAb, or the mannose receptor with an anti-CD206 mAb, did not block the transport of IgM through M-like cells. Other receptors described as being involved in IgA transport such as transferrin receptor (CD71), poly immunoglobulin receptor (PIgR) and Fcα/μ receptor (CD351) showed similar results. The use of an anti-Toso mAb, a novel IgM receptor, led to an almost complete inhibition of IgM reverse transcytosis. Consistently, the binding of IgM on TOSO and the its presence on M-like cells *in vitro* was observed by epifluorescence microscopy (Fig. 2b) and flow cytometry (Fig. 2c). These figures show colocalisation of $GP2^+$ and $Toso^+$ cells and IgM^+ and $Toso^+$ cells only on cocultures, suggesting TOSO might be up-regulated upon M-cell differentiation. To confirm these *in vitro* results, TOSO expression was also analyzed *in vivo* in the murine FAE (Fig. 2d) and *ex vivo* in the human FAE (Fig. 2e). Both panels show colocalization between Toso and M cells markers. Moreover, a significant 9-fold decrease in IgM transport when cells were treated with TOSO siRNA *in vitro* confirms its implication in reverse-transcytosis (Fig 2f), as background levels of IgM retrotransport were not affected after transfection with siRNA knockdown. Indeed, either with or without M-like cells in the polarized monolayer, IgM retrotransport is comparable to that in Fig. 1a (lanes control and random oligoNT). In additional control experiments, both the decrease in the level of targeted proteins and the monolayer integrity (TEER) were systematically monitored after siRNA transfection (Supplementary Fig. 2a and 2b). No significant modifications between controls, knockdown and stimulated cells were observed.

Traditional transport (transcytosis) across polarized epithelial of serosal polymeric Ig into secretions requires polymeric Ig receptor and a plethora of evolutionary well-conserved intracellular proteins including EEA-1, Rab-5, Rab-9, Rab-11, Rab-17, Rab-25[28–30]. As such, Figure 2d shows that EEA-1, Rab-5, Rab-17 siRNA knockdown led to a significant decrease of IgM transport relative to controls.

Reverse-transcytosed SIgM target DC-specific receptors *in Vivo* and *in Vitro*

To measure IgM transport from the intestinal lumen to DCs located in the SED region, we took advantage of previous data showing that SIgA is recognized by DCs *via* DC-SIGN receptor after their transport through M cells [1–3,31]. IgM uptake by DCs was assessed *in vivo* in an intestinal ligated loop model and in the nasal cavity from wt mice using an anti-DC-SIGN-(FITC) and IgM-(PE) specific immunostaining. IgM transported in the GALT and NALT were found in close association with murine DC-SIGN$^+$ DCs (Fig. 3a and 3b). In parallel, HeLa transfectants stably expressing human DC-SIGN added to the basolateral chamber in Caco-2 cells co-cultures were used as surrogates to human DCs populating the SED region of PPs [32]. Control of DC-SIGN expression was demonstrated by the inhibition of gp120 binding on HeLa-DC-SIGN$^+$ cells by specific blocking mAbs (unpublished data). The binding of IgM that had previously crossed the monolayer containing M-like cells was observed by immunostaining of HeLa-DC-SIGN (Fig. 3c), but not with wt HeLa cells. The sum of these data sheds light on the biochemical partners involved in reverse transcytosis of IgM. SIgM is first taken up by M cells via the Toso receptor, and is subsequently targeted to DC-SIGN$^+$ DCs located in the SED region. Such characteristics prompted us to investigate whether oral and nasal immunization with p24-SIgM complexes could induce subsequent p24-specific immune responses.

Oral and nasal administration of p24-SIgM complexes via M cells is highly immunogenic

BALB/c mice were immunized as described in the Methods section. Mucosal and systemic p24-specific humoral immune responses were measured by ELISA in serum and various mucosal compartments, including feces and vaginal lavage samples collected 1 week after the last immunization (Fig. 4a). Immunization with p24-SIgM induced significantly higher p24-specific IgG and IgA titers in serum and feces samples after oral administration compared to p24 alone. p24-IgG and IgA titers were also significantly higher than for p24 alone in vaginal lavages after nasal administration (Fig. 4a). Splenic B lymphocytes recovered from immunized mice were co-cultured with p24 in ELISpot assays. In both oral or nasal immunization routes, B cell populations included significantly higher levels of IgA- and IgG-secreting plasma cells than p24 control samples, indicating specific activation and migration of locally primed cells to distant effector sites (Fig. 4b).

Induction of IFN-γ secreting Th1 cells in the process of fighting mucosal infections, in particular viral infections, is highly relevant. To assess this response, splenocytes from immunized mice were co-cultured with p24 in ELISpot assays. Nasal and oral immunizations

with p24-SIgM both promoted significantly more elevated IFN-γ production in response to p24 (Fig. 4b). Altogether, these results highlight the potential of IgM as a functional and potent vaccine carrier in promotin both humoral and cellular immunity *in vivo.*

Discussion

M cells possess a high transcytosis capacity, allowing for a wide range of materials to be transported into the mucosa, including particulate Ags, soluble macromolecules, and pathogens. The latter are delivered from the intestinal lumen to inductive sites of the mucosal immune system. M cells are also the primary route through which SIgA promote GALT immunity. We previously found that SIgA bound Dectin-1 on M cells and that the ensuing transport of SIgA-bound antigen into nasal and intestinal lymphoid tissue targeted DC-SIGN$^+$ DCs. In the current study, we investigated the transport of SIgM across the murine GALT and NALT. We provide evidence that IgM is uptaken by TOSO$^+$ M cells of both the GALT and the NALT. We also demonstrate that it is then retro-transported towards DC-SIGN$^+$ DC from lymphoid tissues. Finally, we validate these *in vitro* results using *in vivo* analyses of murine tissues, ultimately demonstrating that TOSO-mediated uptake of SIgM-based complexes results in productive mucosal and systemic antigen-specific Ab responses.

We initially studied reverse transcytosis of IgM across human M-like cells using a cell culture model that reproduces features of the FAE tissue. We confirmed that human IgM, with or without SC, selectively bound the apical surface of *in vitro*-differentiated human M-like cells. Oppositely to IgA[1], IgM glycosylation does not appear to impact this retro transport. This difference can be explained by the involvement of another receptor for IgM than that of IgA reverse transcytosis. A recent study shows that IgM-TOSO interaction is critically dependent on the C□4 domain, and specifically on the glutamine at position 510. Although glutamines can be glycosylated, N-glycosylation of IgM are borne by asparagines and regulate post-traductional protein folding[33]. There is, however evidences of atypical glutamine N-glycosylation in human IgG2 that suggest further caracterization of SIgM N-glycans might be required[34]. Sialic acids and SC-borne glycosylation are also involved in SIgA binding to Siglec-5, a co-receptor for reverse transcytosis[25,35]. Siglecs are abundantly expressed at the apical membrane of M cells[27], and may also serve as co-receptor for SIgM transport. Amongst them, CD22 is a likely candidate, as it has already been characterized as an IgM receptor [36]. Its expression by M cells, however, has not been verified.

Our work evidences TOSO expression by M-like cells, together with its involvement in the reverse transcytosis of SIgM. Of note, TOSO holds a critical role IgM homeostasis, B cell survival and humoral responses : it is expressed by CD19$^+$ cells, T cells (CD4$^+$ and CD8$^+$) and CD56$^+$ CD3$^-$ NK cells in human [37,38], murine B cell [39], and is rapidly internalized upon IgM binding [40,41], suggesting enhanced responsiveness of the mucosa that is yet to be demonstrated.

Transcytosis across M cells is known to enable the selective transport of particulate antigens in the absence of any assessable damage [42,43]. This holds true for soluble SIgM, as the transcytosed Ab released by M cells in the human *in vitro* and murine *in vivo* models was still able to specifically target cells expressing DC-SIGN in the basolateral environment (Figure 3a and 3b). In mucosal tissues such as the rectum, uterus, and cervix, DC-SIGN is abundantly expressed by DCs of the *lamina propria* and PPs, further substantiating the importance of the localization of DC-SIGN$^+$ DCs as a first line of defense against viruses and pathogens. Moreover, DC-SIGN, by binding to ICAM-3, favors the generation of antigen-specific suppressive CD4$^+$ T cells, which produce IL-10 [44], a regulatory cytokine that intervenes in both intestinal homeostasis and the production of local secretory Ig to promote commensal mutualism. Delivery in the form of SIgM-based immune complexes may thus promote both antigen-specific responses host-microbe interactions.

References

1. Rochereau, N. *et al.* Dectin-1 Is Essential for Reverse Transcytosis of Glycosylated SIgA-Antigen Complexes by Intestinal M Cells. *PLoS Biol.* 11, e1001658 (2013).
2. Rochereau, N. *et al.* Delivery of antigen to nasal-associated lymphoid tissue microfold cells through secretory IgA targeting local dendritic cells confers protective immunity. *J. Allergy Clin. Immunol.* (2015) doi:10.1016/j.jaci.2015.07.042.
3. Rochereau, N. *et al.* Secretory IgA as a vaccine carrier for delivery of HIV antigen to M cells. *Eur. J. Immunol.* (2014) doi:10.1002/eji.201444816.
4. Arnold, J. *et al.* Human Serum IgM Glycosylation IDENTIFICATION OF GLYCOFORMS THAT CAN BIND TO MANNAN-BINDING LECTIN. *J Biol Chem* 280, 29080–29087 (2005).
5. In, N., Fe, J., H, S. & P, B. Regulation of the formation and external transport of secretory immunoglobulins. *Crit. Rev. Immunol.* 19, 481–508 (1999).
6. Brandtzaeg, P. Transport models for secretory IgA and secretory IgM. *Clin. Exp. Immunol.* 44, 221–232 (1981).
7. Shibuya, A. *et al.* Fc alpha/mu receptor mediates endocytosis of IgM-coated microbes. *Nat. Immunol.* 1, 441–446 (2000).
8. Bournazos, S., Woof, J. M., Hart, S. P. & Dransfield, I. Functional and clinical consequences of Fc receptor polymorphic and copy number variants. *Clin. Exp. Immunol.* 157, 244–254 (2009).
9. Shima, H. *et al.* Identification of TOSO/FAIM3 as an Fc receptor for IgM. *Int. Immunol.* 22, 149–156 (2010).
10. Chen, K., Magri, G., Grasset, E. K. & Cerutti, A. Rethinking mucosal antibody responses: IgM, IgG and IgD join IgA. *Nat. Rev. Immunol.* 1–15 (2020) doi:10.1038/s41577-019-0261-1.
11. Magri, G. *et al.* Human Secretory IgM Emerges from Plasma Cells Clonally Related to Gut Memory B Cells and Targets Highly Diverse Commensals. *Immunity* 47, 118-134.e8 (2017).
12. Catanzaro, J. R. *et al.* IgA-deficient humans exhibit gut microbiota dysbiosis despite secretion of compensatory IgM. *Sci. Rep.* 9, 1–10 (2019).
13. Fadlallah, J. *et al.* Microbial ecology perturbation in human IgA deficiency. *Sci. Transl. Med.* 10, (2018).
14. Michaelsen, T. *et al.* Human secretory IgM antibodies activate human complement and offer protection at mucosal surface. *Scand J Immunol* (2016) doi:10.1111/sji.12508.
15. Xia, L. & Gildersleeve, J. C. Anti-glycan IgM repertoires in newborn human cord blood. *PLOS ONE* 14, e0218575 (2019).
16. Louis, A. G. & Gupta, S. Primary Selective IgM Deficiency: An Ignored Immunodeficiency. *Clin. Rev. Allergy Immunol.* 46, 104–111 (2014).
17. Rescigno, M. *et al.* Dendritic cells express tight junction proteins and penetrate gut epithelial monolayers to sample bacteria. *Nat. Immunol.* 2, 361–367 (2001).
18. des Rieux, A. *et al.* An improved in vitro model of human intestinal follicle-associated epithelium to study nanoparticle transport by M cells. *Eur. J. Pharm. Sci. Off. J. Eur. Fed. Pharm. Sci.* 30, 380–391 (2007).
19. Phalipon, A. *et al.* Secretory component: a new role in secretory IgA-mediated immune exclusion in vivo. *Immunity* 17, 107–115 (2002).
20. Rindisbacher, L., Cottet, S., Wittek, R., Kraehenbuhl, J.-P. & Corthésy, B. Production of Human Secretory Component with Dimeric IgA Binding Capacity Using Viral Expression Systems. *J. Biol. Chem.* 270, 14220–14228 (1995).

21. Lefrançois, L. & Lycke, N. Isolation of mouse small intestinal intraepithelial lymphocytes, Peyer's patch, and lamina propria cells. *Curr. Protoc. Immunol. Ed. John E Coligan Al* Chapter 3, Unit 3.19 (2001).
22. Carvalho, L. H., Hafalla, J. C. & Zavala, F. ELISPOT assay to measure antigen-specific murine CD8(+) T cell responses. *J. Immunol. Methods* 252, 207–218 (2001).
23. Clark, S. R. *et al.* Characterization of platelet aminophospholipid externalization reveals fatty acids as molecular determinants that regulate coagulation. *Proc. Natl. Acad. Sci.* 110, 5875–5880 (2013).
24. Xu, W. & Südhof, T. C. A Neural Circuit for Memory Specificity and Generalization. *Science* 339, 1290–1295 (2013).
25. Rochereau, N. *et al.* Dectin-1 Is Essential for Reverse Transcytosis of Glycosylated SIgA-Antigen Complexes by Intestinal M Cells. *Plos Biol* 11, e1001658 (2013).
26. Date, Y. *et al.* NALT M cells are important for immune induction for the common mucosal immune system. *Int. Immunol.* 29, 471–478 (2017).
27. Mabbott, N. A., Donaldson, D. S., Ohno, H., Williams, I. R. & Mahajan, A. Microfold (M) cells: important immunosurveillance posts in the intestinal epithelium. *Mucosal Immunol.* 6, 666–677 (2013).
28. Fung, K. Y. Y., Fairn, G. D. & Lee, W. L. Transcellular vesicular transport in epithelial and endothelial cells: Challenges and opportunities. *Traffic Cph. Den.* 19, 5–18 (2018).
29. Jing, J. & Prekeris, R. Polarized endocytic transport: The roles of Rab11 and Rab11-FIPs in regulating cell polarity. *Histol. Histopathol.* 24, 1171–1180 (2009).
30. Rojas, R. & Apodaca, G. Immunoglobulin transport across polarized epithelial cells. *Nat. Rev. Mol. Cell Biol.* 3, 944–956 (2002).
31. Baumann, J., Park, C. G. & Mantis, N. J. Recognition of secretory IgA by DC-SIGN: Implications for immune surveillance in the intestine. *Immunol. Lett.* 131, 59–66 (2010).
32. Rochereau, N., Verrier, B., Pin, J.-J., Genin, C. & Paul, S. Phenotypic localization of distinct DC subsets in mouse Peyer Patch. *Vaccine* 29, 3655–3661 (2011).
33. Giannone, C., Fagioli, C., Valetti, C., Sitia, R. & Anelli, T. Roles of N-glycans in the polymerization-dependent aggregation of mutant Ig-μ chains in the early secretory pathway. *Sci. Rep.* 7, 41815 (2017).
34. Valliere-Douglass, J. F. *et al.* Glutamine-linked and Non-consensus Asparagine-linked Oligosaccharides Present in Human Recombinant Antibodies Define Novel Protein Glycosylation Motifs. *J. Biol. Chem.* 285, 16012–16022 (2010).
35. Mathias, A. & Corthésy, B. N-Glycans on secretory component. *Gut Microbes* 2, 287–293 (2011).
36. Adachi, T. *et al.* CD22 serves as a receptor for soluble IgM. *Eur J Immunol* 42, 241–7 (2011).
37. Honjo, K., Kubagawa, Y. & Kubagawa, H. Is Toso/IgM Fc receptor (FcμR) expressed by innate immune cells? *Proc. Natl. Acad. Sci.* 110, E2540–E2541 (2013).
38. Kubagawa, H. *et al.* Identity of the elusive IgM Fc receptor (FcμR) in humans. *J. Exp. Med.* 206, 2779–2793 (2009).
39. Honjo, K. *et al.* Altered Ig levels and antibody responses in mice deficient for the Fc receptor for IgM (FcμR). *Proc. Natl. Acad. Sci.* 109, 15882–15887 (2012).
40. Ouchida, R. *et al.* Critical role of the IgM Fc receptor in IgM homeostasis, B-cell survival, and humoral immune responses. *Proc Natl Acad Sci* 109, E2699–E2706 (2012).
41. Vire, B., David, A. & Wiestner, A. TOSO, the Fcmicro receptor, is highly expressed on chronic lymphocytic leukemia B cells, internalizes upon IgM binding, shuttles to the lysosome, and is downregulated in response to TLR activation. *J Immunol* 187, 4040–50 (2011).
42. Owen, R. L. & Ermak, T. H. Structural specializations for antigen uptake and processing in the digestive tract. *Springer Semin. Immunopathol.* 12, 139–152 (1990).

447 43. Neutra, M. R., Pringault, E. & Kraehenbuhl, J. P. Antigen sampling across epithelial
448 barriers and induction of mucosal immune responses. *Annu. Rev. Immunol.* 14, 275–300 (1996).
449 44. Li, D. *et al.* Targeting self- and foreign antigens to dendritic cells via DC-ASGPR
450 generates IL-10-producing suppressive CD4+ T cells. *J. Exp. Med.* 209, 109–121 (2012).
451
452

453

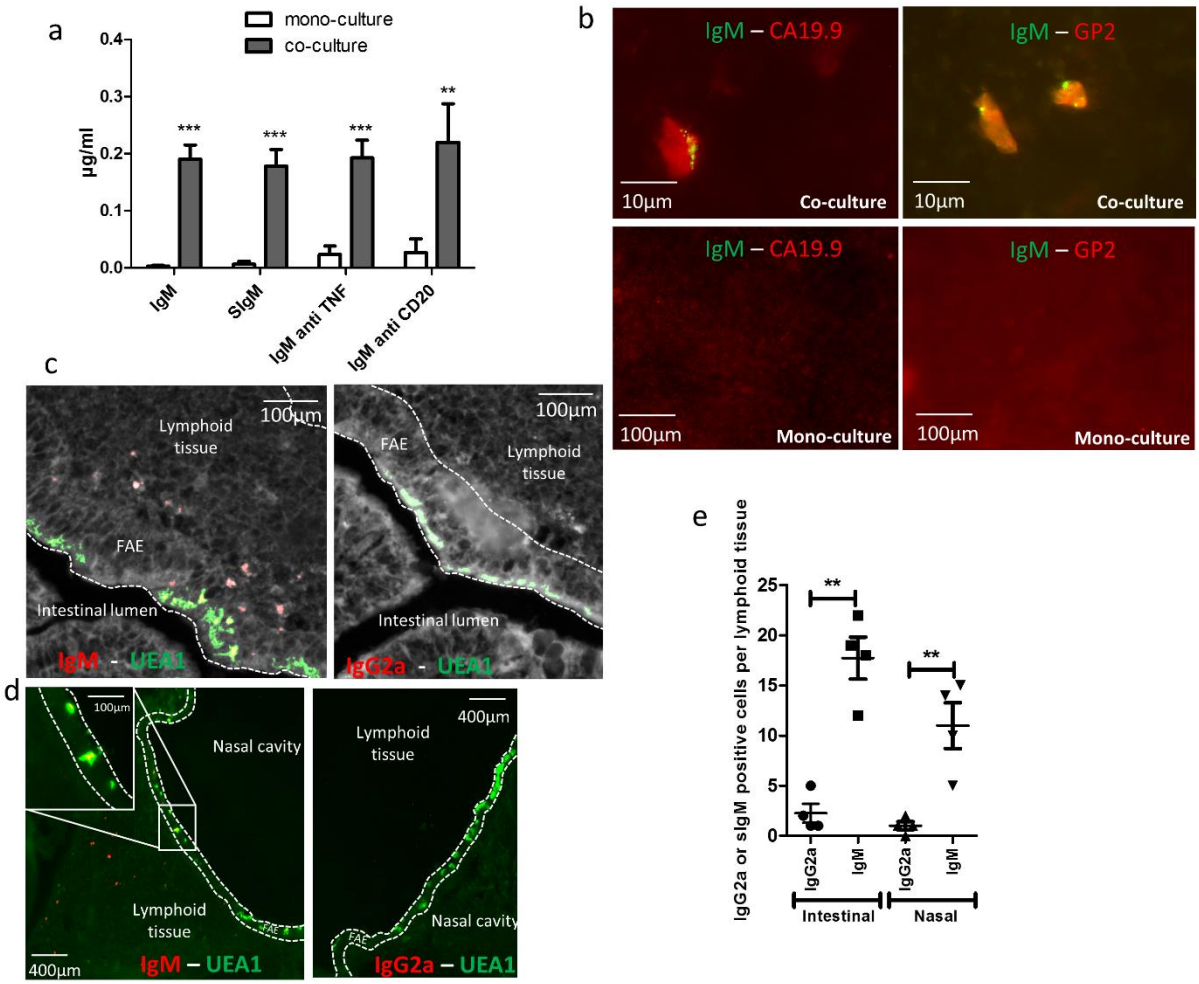

Figure 1: IgM are able to cross through human and murine epithelium *via* M cells. (a) Mono- and co-cultures were incubated for 90 min at 37°C with IgM from murine hybridoma with or without SC and human recombinant TNF or CD20-specific IgM. Transported IgM was evaluated by ELISA (n=4). Vertical bars show the mean value +/- SEM. One-way ANOVA followed by Bonferroni post hoc test was used (*p* values: ** $p < 0.01$; *** $p < 0.005$). (b) Co-localization evaluated by immunofluorescence microscopy of CA19.9-PE or GP2-PE and IgM-GFP indicates binding of the Ab to M-like cells (top view). Mouse SIgM-Cy3 incubated for 60 min in a ligated intestinal loop containing a PP (c) or in NALT (d) was taken up by M cells. Co-localization was observed with both UEA-1-FITC (a1) and SIgM-Cy3. Dotted lines delineate the interface between the intestinal lumen and tissue (side view). (e) Graph shows the number of SIgM- and IgG2a positive cells per lymphoid tissues. One-way ANOVA followed by Bonferroni post hoc test was used. Vertical bars show the mean value ± SEM (** $p < 0.01$).

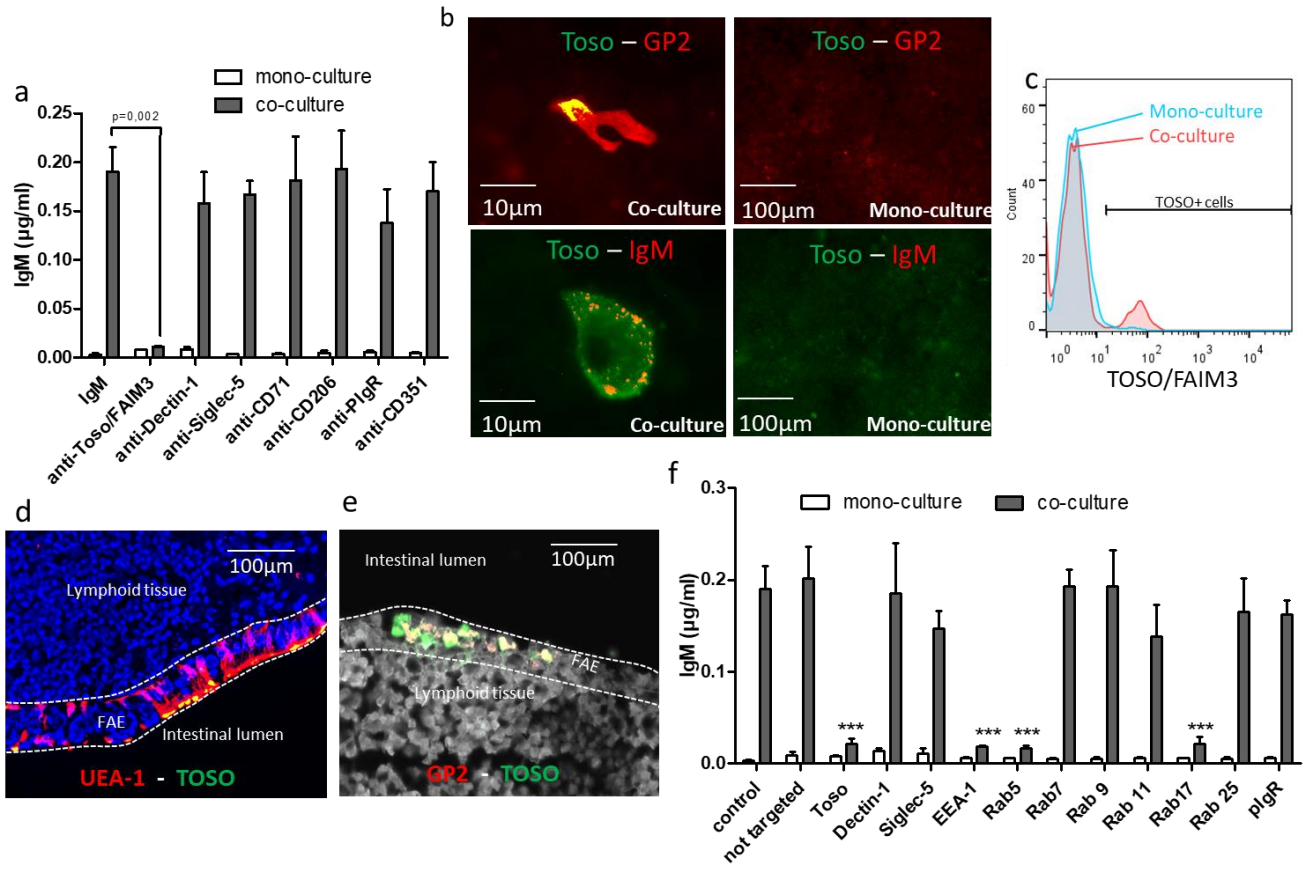

Figure 2: TOSO receptor is involved in IgM reverse transcytosis. (a) Mono- and co-cultures were pre-incubated apically with 10 mg of blocking Abs directed against potential receptors prior to addition of various IgM for 90 min at 37°C. The concentration of transported IgM was evaluated by ELISA (n=4). Vertical bars show the mean value +/- SEM. One-way ANOVA followed by Bonferroni post hoc test was used. Detection of Toso on M-like cells *in vitro* assessed by immunofluorescence (top view) (b) and flow cytometry (c). Tissue section showing a PP obtained from an intestine in mice (d), and from patient biopsy samples taken from terminal ileum (e). Tissue were immunolabeled with PE-UEA-1 and FITC-TOSO (d) and with human PE-GP2 and FITC-TOSO (e) at RT for 2 h. Conspicuous co-localizations between GP2 or UEA-1 with TOSO were observed (n = 2). On all pictures, dotted lines delineate the FAE separating the intestinal lumen and the lymphoid tissue (side view). (f) After siRNA knockdown, IgM transport were quantified in the inverted *in vitro* model of FAE and transported IgM was evaluated by ELISA. Vertical bars show the mean value +/- SEM. n=3 independent experiments. One-way ANOVA followed by Bonferroni post hoc test was used (*p* values: *** $p < 0.005$).

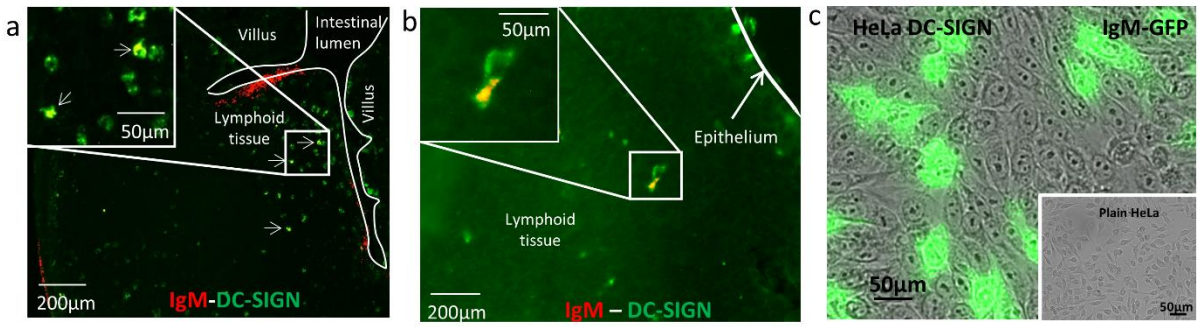

Figure 3: Specific uptake and transport of IgM across murine GALT and NALT. (a) Mouse sIgM incubated for 60 min in a ligated intestinal loop containing a PP was taken up by M cells and DCs in the SED region. (n = 3). (b) Mouse sIgM was intranasally administered and incubated for 60 minutes in the nasal cavity. Co-localization was observed with both UEA-1-FITC (a, b) and DC-Sign-FITC (a, b). (c) HeLa cells expressing DC-SIGN bound GFP-IgM having previously crossed the monolayer containing M-like cells *in vitro*.

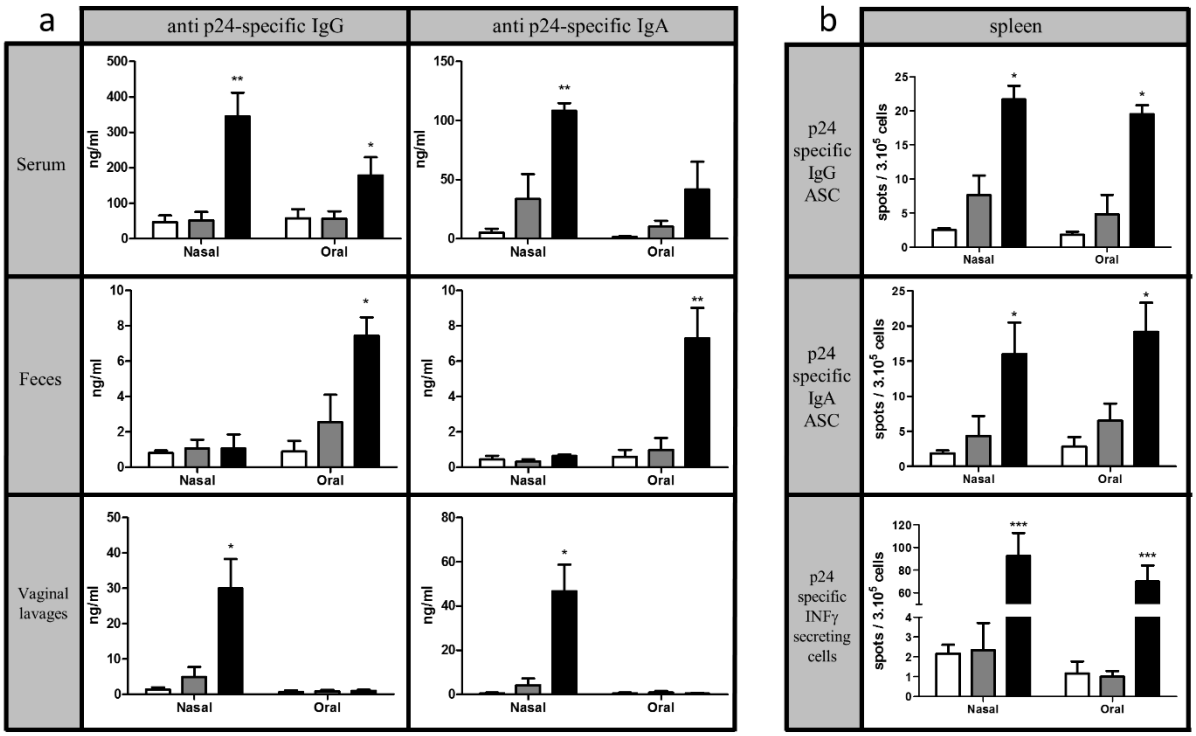

Figure 4: p24-specific IgA, IgG responses after oral and nasal administration of p24-SIgM complexes. (a), Mice were immunized with PBS (white bar), p24 (grey bar), and p24-SIgM (black bar). (a) Serum, feces and vaginal lavage samples were isolated at day 42. (b) Spleens were isolated after 42 days, and ELISpot assays were performed on IgG and IgA antibody-secreting cells (ASC) and IFN-γ–producing cells. Data are shown as means +/- SEMs. ANOVA followed by the Bonferroni post hoc test were performed. *P < 0.05, **P < 0.01, and ***P < 0.005. Data from 2 independent experiments consisting of 5 mice per group showing very close results have been pooled (total n=10).

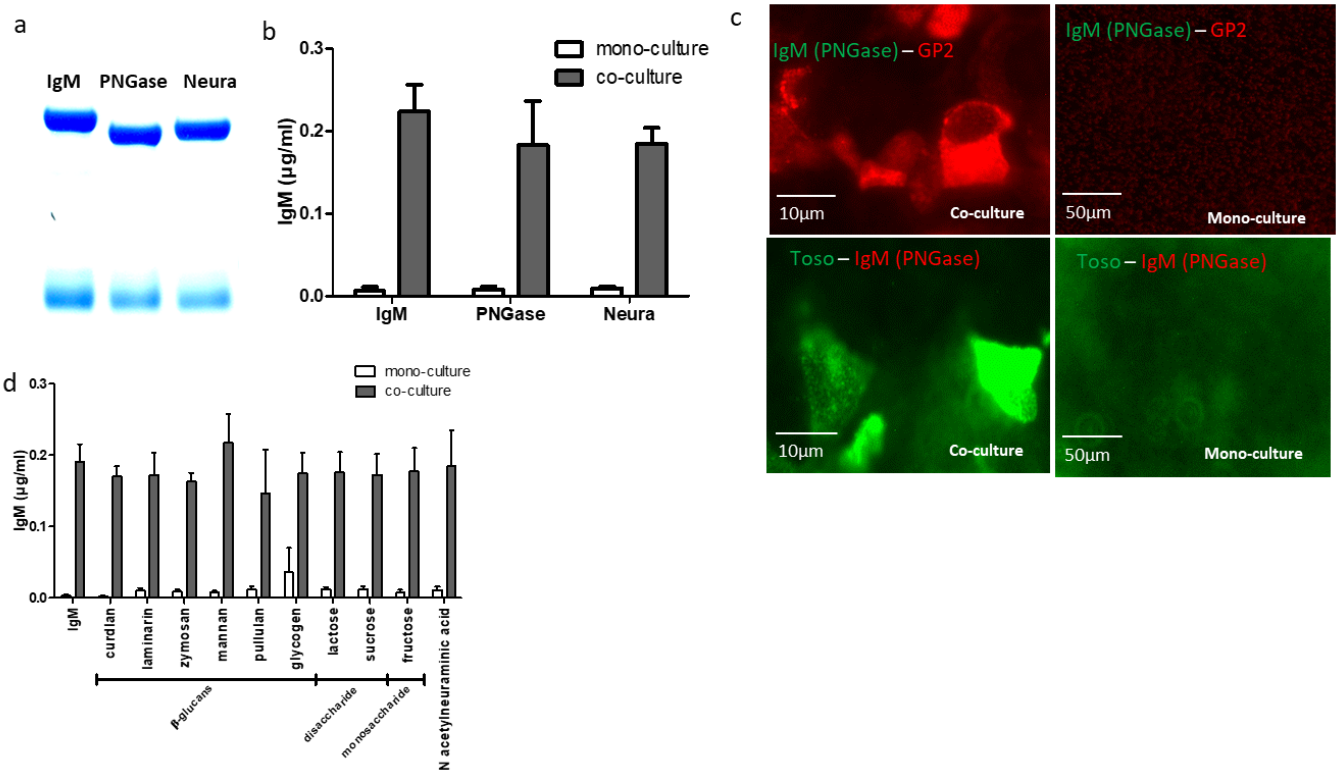

506

507 **Supplementary figure 1: Influence of glycosylation and sialylation on the uptake of IgM**
508 **by M-like cells.** (a) IgM deglycosylation and desialylation was monitored by SDS-PAGE under
509 reducing conditions and stained with Coomassie blue. (b) Mono- and co-cultures were
510 incubated for 90 min at 37°C with enzymatically deglycosylated IgM, and transported IgM was
511 evaluated by ELISA (n = 4). PNGase, Peptide N:glycosidase; Neura, neuraminidase. (c)
512 Detection of deglycosylated IgM on TOSO^{+} or GP2^{+} M-like cells *in vitro* assessed by
513 immunofluorescence (top view). (d) Mono- and co-cultures were pre-incubated apically with 5
514 mg of different mono/polysaccharides and sialic acid, prior to addition of IgM constructs for
515 90 min at 37°C. The concentration of transported IgM was evaluated by ELISA (n=4). Data are
516 shown as means +/- SEMs. ANOVA followed by the Bonferroni post hoc test were performed.

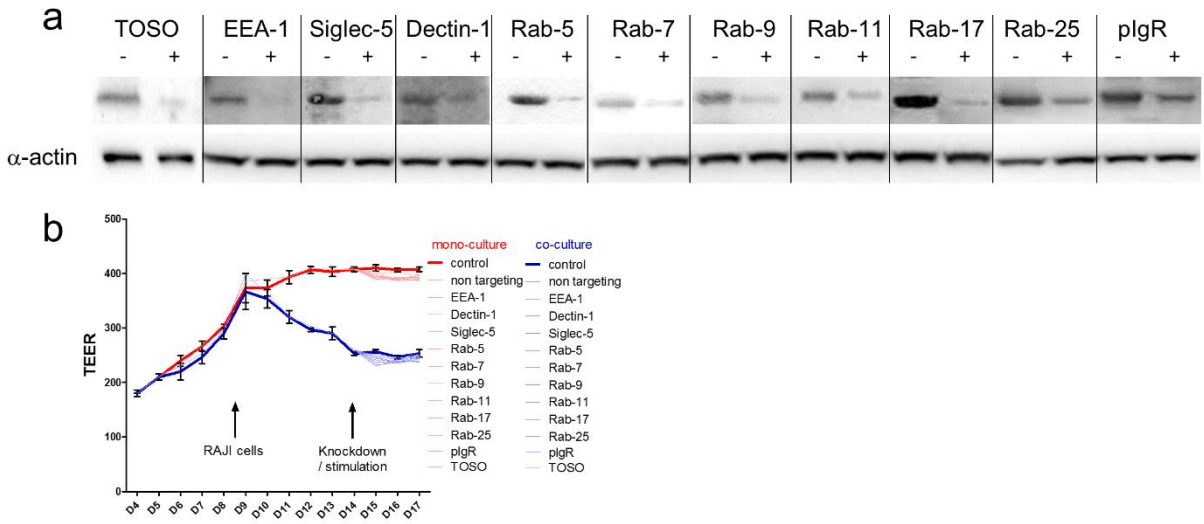

Supplementary figure 2: Confirmation of the effect of siRNA transfection in the inverted *in vitro* model of human FAE. (a) Western Blot show decrease of the amount of proteins between control "-" (no target knockdown) and knocked down cells "+". (b) TEER is measured to detect the monolayer integrity and M cell conversion. No statistical changes between control and knockdown cells have been observed.

Pour la première fois, nous démontrons le rétrotransport des IgM à travers les cellules M *in vitro* et *in vivo,* transport indépendant de la SC. Cela pose la question de l'importance de la SC pour les SIgM muqueuses : est-ce, comme pour les IgA, un moyen de reconnaissance non-conventionnel des bactéries commensales, par exemple par des interactions glycans-glycans ? Pour répondre à cette question, différentes constructions d'IgM, sécrétoires ou non, muqueuses (fécales) ou circulantes, liées à la SC ou non, seront placées en présence de souches bactériennes commensales ou pathogènes dans des expériences d'agglutination bactérienne. L'expérience sera reproduite avec la SC seule, dans un premier temps, puis avec des IgM issues d'hybridomes réalisés à partir de résection chirurgicale chez des patients Crohn. Avec ces dernières nous évaluerons l'effet d'IgM produites en conditions inflammatoires muqueuses, fonction qui n'est pas décrite à ce jour.

Le dynamisme de ce transport sera également à évaluer : comme pour l'article précédent, la question des complexes Ig-antigènes se pose. Puisque le co-récepteur Siglec-5 est recruté pour la RT des SIgA, il serait vraisemblable que d'autres Siglecs, abondants à la membrane apicale des cellules M puissent être impliqués, en particulier pour la reconnaissance de complexes immuns. Les modalités de la RT des SIgM seront donc réévaluées lorsque celles-ci sont liées à différents types d'antigènes (soi, non-soi, commensal, pathogène), et des expériences de co-immunoprécipitation seront également mise en place, en recherchant spécifiquement des protéines de la famille des Siglecs. Pour ceci, CD22, est l'un de nos candidats phare, puisqu'il est déjà impliqué dans la reconnaissance des IgM grâce à laquelle il limite l'engagement du BCR [388]. Il serait également intéressant, comme nous l'avons déjà fait pour le récepteur Dectin-1 de développer un modèle murin TOSO KO et d'y mesurer la RT des IgM *in vivo,* ainsi que l'impact que l'absence de la signalisation TOSO-IgM a sur l'immunité muqueuse. Nous n'avons, jusqu'ici, pas réussi à obtenir de telles souris.

Nous confirmons l'utilisation de ce transport rétrograde des IgM lors d'expérience *in vivo* dans la muqueuse intestinale et la muqueuse nasale murines, et que, comme les SIgA elles peuvent être adressées au récepteur DC-SIGN. Reste donc à caractériser les réponses immunes que cette interaction entraîne : pour cela, il serait intéressant de cultiver des lysats de PP murines avec ces même IgM (complexées ou non) pour évaluer la sécrétion cytokinique et l'état d'activation des différents effecteurs immuns par cytométrie en flux. De plus, directement sur le modèle *in vitro* de FAE, il est possible de récolter les cellules de la monocouche pour en extraire les ARN et analyser les profils transcriptomiques engagés. De plus, nous avons

précédemment montré que les SIgA peuvent être utilisées comme vecteur vaccinal muqueux[389,390]. Au vu de la valence des SIgM et du présent constat qu'elles effectuent la RT, un travail similaire est à envisager, et permettrait l'élaboration de formules vaccinales multivalentes.

Nous faisons le constat surprenant que les glycosylations des SIgM sont dispensables pour la RT, leur rôle reste donc à éclaircir. La production d'IgM augmente de manière compensatoire chez les patients présentant des déficits en IgA (SIgAd)[209,391]. Étudier la structure, et notamment les glycosylations, de ces IgM dans les compartiments sanguins et fécaux, en la comparant à celle d'individu sain permettrait de répondre en partie à cette question. Également, la purification chez des souris SIgAd et l'injection de ces IgM dans des anses intestinales permettraient d'élucider les dynamiques de transport des IgM en conditions physiologiques et en conditions pathologiques. De même, le rôle des SIgM en contexte inflammatoire muqueux, reste inconnu. Une étude similaire chez des patients atteints de MICI et dans des modèles murins de colite est à envisager à la suite de ces premiers résultats. Nous souhaiterions illustrer la fonction de l'IgM comme une alternative, lorsque la fonction des IgA est altérée ou que celles-ci sont absentes.

La RT des IgM est un phénomène récepteur-dépendant, qui requiert la liaison à TOSO (FcμR). Pour caractériser les conséquences de cette liaison et ses modalités, il nous faudra étudier les cascades de signalisation intracellulaire engagées par TOSO pour le recrutement des protéines vésiculaires, par l'utilisation d'inhibiteurs spécifiques des voies canonique intracellulaires. À l'image du FcαRI, pour la liaison duquel IgA1 et IgA2 engagent différentes voies intracellulaires, nous voulons montrer que suivant la forme d'IgM et le complexes immuns, ce recrutement est régulé différemment.

Il nous restera enfin à caractériser les capacités neutralisantes des IgA et IgG produites en réponse à l'immunisation par des complexes IgM-antigènes, et à évaluer la persistance de cette immunité protectrice sur le plus long terme.

Ces travaux mettent en lumière le rôle fondamental des Ig sécrétoires dans la polarisation des réponses immunitaires muqueuses, en conditionnant les DC vers un profil plus ou moins inflammatoire, et en leur acheminant des antigènes *via* la RT. Nous pensons donc que ces mécanismes régulateurs sont affectés par la mise en place de l'inflammation chronique au cours de MICI, et contribuent au maintien de cette inflammation dans la muqueuse.

Chapitre 2 – Rôle pathogénique des IgA sécrétoires

A- Introduction

Les MICI sont des pathologies chroniques du tube digestif auxquelles appartiennent la maladie de Crohn (MC) et la rectocolite hémorragique (RCH). Elles se caractérisent par une inflammation chronique et la perte de la diversité commensale. Cette dernière se traduit par une diminution du ratio *Firmicutes/Bacteroidetes*[341,342]. Les espèces de la flore ont, en conditions saines, pour fonction d'assurer la digestion et la protection de la muqueuse par compétition avec des espèces pathogènes. Elles produisent des métabolites, les SCFA, qui sont essentiels à la cicatrisation, l'énergie, la promotion de la tolérance immune et au renouvellement du mucus [72,81,96,392,393]. Dans les MICI, ces espèces se raréfient, en particulier *Faecalibacterium prausnitzii*[76,394], et les espèces *Roseburia, Blautia, Ruminococcus* et *Bifidobacterium*[306]. En contrepartie, des espèces normalement rares comme les bactéries SFB et des espèces oro-pharyngées comme *Streptococcus salivarius* colonisent la muqueuse[13]. Parmi les nombreuses associations génétiques connues pour les MICI, les polymorphismes sur le gène PRR intracellulaire *NOD2* sont associés au développement de la MC et représentent la plus forte association génétique connue. NOD2 est un senseur bactérien inné impliqué dans la régulation de la voie NF-κB. Ce rôle central dans la détection de pathogènes intracellulaire le place en première ligne dans la réponse à l'invasion des tissus : son inactivation pourrait donc contribuer à la rupture de la barrière intestinale au cours de la MC.

Les SIgA et les SIgM ont pour rôle la sélection du microbiote commensal et la ségrégation des espèces pathogènes[232]. Parmi les deux sous-classes d'IgA humaine, IgA1 et IgA2, seulement l'IgA2 possède la capacité, une fois secrétée et liée à une cible antigénique, d'être transportée depuis la lumière intestinale vers la muqueuse[43]. Ce mécanisme, RT, n'est possible qu'au niveau des cellules M du dôme sous-épithélial après reconnaissance des glycosylations des IgA2 par Dectin-1 et Siglec-5[43]. Le transport de complexe-immuns selon ce mode permet l'activation rapide des DC $CD11c^+$ enchâssées dans la poche de la cellule M et la polarisation de réponses inflammatoires[43,68,200]. Ces sous-classes d'IgA se distinguent structurellement : les IgA1 ont une plus longue région charnière très O-glycosylée et deux sites de N-glycosylation [126], alors que les IgA2 ont une région charnière plus courte et sont majoritairement N-glycosylées [230]. Bien qu'il semble que l'IgA1 occupe une fonction plutôt anti-inflammatoire, et que son niveau de sialylation régule cette fonction[128,220], l'impact de la structure et de la sous-classe d'IgA sur l'orientation de la réponse muqueuse ou sur la dysbiose est encore peu défini. Une forte opsonisation des bactéries par ces IgA est associée à un amoindrissement de la diversité commensale dans la MC[302]. D'autre part, les premières lésions

liées à l'inflammation de la MC sont observées au niveau du FAE de la PP[395]. Ici, nous supposons que cette inflammation est entretenue par une augmentation du transport de ces complexes IgA-bactéries au niveau des cellules M. Nous évaluons également la possibilité que ce transport soit régulé par NOD2. En parallèle, nous avons souhaité étudier le microbiote spécifiquement associé aux IgA1 et les IgA2 intestinales dans les MICI.

A l'aide de biopsies de PP de patients avec et sans polymorphisme NOD2, nous montrons une augmentation du transport d'IgA. Plus encore, il apparait que NOD2 régule négativement l'expression membranaire de Dectin-1 et Siglec-5 sur la cellule M. Ces résultats inédits suggèrent que NOD2, au-delà de son rôle de senseur, occupe également un rôle crucial dans la régulation des réponses envers le microbiote intestinal, en tempérant les réponses innées envers la flore. De plus, nous montrons que la MC est caractérisée par une sélection accrue par les IgA1 d'espèces bénéfiques, dont *Faecalibacterium* qui pourrait être à l'origine de la disparition de ces espèces dans le microbiote des patients. Ce défaut s'accompagne d'une propension des IgA1 à effectuer la RT selon un mode Dectin1-dépendant, processus normalement réservé aux IgA2. La RCH est caractérisée par une perte de fonction des SIgA : ni les SIgA1 ni les SIgA2 ne peuvent effectuer la RT, malgré une diversité microbienne dans les fractions IgA^+ similaires au groupe contrôle. Elles ont, de plus, perdu significativement leur réactivité contre les glycans communs du soi et de la flore qui caractérisent les réponses IgA muqueuses anti-inflammatoire en conditions saines.

B- Article 3 : Rôle des polymorphismes NOD2 dans la régulation de la transcytose inverse des IgA dans la maladie de Crohn .

NOD2-dependent influence of secretory IgA complexes in inducing GALT inflammation in Crohn's disease (Sous presse, *Nature Communication*)

Authors : Nicolas Rochereau[1], Xavier Roblin[1], Eva Michaud[1], Rémi Gayet[1], Blandine Chanut[1], Fabienne Jospin[1], Blaise Corthésy[2] & Stéphane Paul[1*]

Affiliations:

[1] GIMAP/EA3064, Université de Lyon, CIC 1408 Vaccinology, F42023 Saint-Etienne, France;

[2]R&D Laboratory of the Division of Immunology and Allergy, CHUV, Centre des Laboratoires d'Epalinges, 1066 Epalinges, Switzerland

* Corresponding author / Lead contact: Dr. Nicolas Rochereau ; nicolas.rochereau@univ-st-etienne.fr
Faculté de médecine de St-Etienne, Laboratoire GIMAP
10 rue de la Marandière, 42270 St Priest-en-Jarez
Tel: +33 (0) 4 77 42 14 84; Fax: +33 (0) 4 77 42 14 86

Abstract

Intestinal microfold cells (M cells) are the primary pathway for translocation of secretory IgA (SIgA)-pathogen complexes to gut-associated lymphoid tissue (GALT). Uptake of secretory IgA/commensals complexes is important for priming adaptive immunity in the mucosa. This study aims to explore the effect of SIgA retrograde transport of immune complexes in Crohn's disease (CD). A significant increase of SIgA transport in CD patients with *NOD2*-mutation compared to CD patients without *NOD2* mutation and/or healthy individuals has been observed. NOD2 has a direct effect in the IgA transport through human and mouse M cells by downregulating Dectin-1 and Siglec-5 expression, two receptors involved in retrograde transport. These findings define a new mechanism of NOD2-mediated regulation of mucosal responses to intestinal microbiota, which is involved in CD intestinal inflammation and dysbiosis.

Keywords: Crohn's disease, secretory IgA, retrograde transport, Microfold cells, *NOD2*

Introduction

The ability of the host immune system to discriminate between pathogens and commensals is essential to maintain mucosal homeostasis [1,2]. The critical importance of maintaining a mucosal homeostatic mechanism in the intestine is highlighted when functional or genetic deficiencies exist. An example of such failure in maintaining finely balanced immune response is the development of chronic intestinal inflammation, such as Crohn's disease (CD). CD is an idiopathic, chronic regional enteritis that most commonly affects the terminal ileum but has the potential to affect any part of the gastrointestinal tract from mouth to anus. CD is thought to occur as a result of breakdown in self-recognition of commensal bacteria together with mucosal barrier dysfunction in individuals with a given genetic background [3–5]. The most strongly associated genetic risk factor for CD in Western populations remains NOD2, an intracellular pattern recognition receptor important in immune defense against intracellular microbes [6–8]. NOD2 is known to regulate the intestinal barrier function, limiting the transcellular permeability and bacterial translocation [9,10]. The CD-associated mutation in *NOD2* (Leu1007fsinsC, Gly908Arg, and Arg702Trp) [10], located within the LRR region of the protein, results in loss of NF-κB activation in response to muramyl dipeptide (MDP). However, the reasons why inactivation of *NOD2* can result in chronic colitis remain largely speculative.

Secretory IgA (SIgA), the most abundantly secreted antibody isotype in mammals, has long been recognized as a first line of defense in protecting the intestinal epithelium from enteric pathogens and toxins [11–16]. Recognition of enteric pathogens by the intestinal immune system results in the production of high affinity, T-cell-dependent, pathogen-specific IgA, which is "transcytosed" into the intestinal lumen. In recent years, evidence has emerged indicating that SIgA2, promotes the uptake and delivery of antigens (Ags) from the intestinal lumen to dendritic cell (DC) subsets located in gut-associated lymphoid tissues (GALTs), and influences inflammatory responses normally associated with the uptake of highly pathogenic bacteria and

potentially allergenic Ags [17]. This particular feature of SIgA, called retrograde transport (or reverse transcytosis), is mediated by epithelial M cells [18–21]. Both the Cα1 domain of SIgA2 and its associated Sialic acid (Sia) residue glycosylation are involved in M-like cell-mediated reverse transcytosis. Dectin-1 and Siglec-5 have been identified as essential receptors for SIgA uptake on M-cells [19]. Finally, Dectin-1/Siglec 5-mediated uptake of SIgA-based complexes results in productive mucosal and systemic Ags-specific Ab responses [19]. However, although the potentially useful properties of M cells on SIgA uptake are now well known, the regulation and pathway(s) whereby SIgA is transported across M cells remains elusive.

Increase of the intestinal permeability has for many years been recognized as a pathogenic factor in CD. An abundance of clinical, epidemiologic, and animal model studies have assessed the impact of various commensal and potentially pathogenic enteric bacteria that may trigger or exacerbate IBD [22,23]. In a population-based cohort study, an increased risk of IBD was demonstrated in individuals notified in laboratory registries with an episode of *Salmonella* gastroenteritis [24]. This finding promotes the concept that pathogens that cause acute intestinal inflammation may predispose individuals to later development of CD, perhaps by causing initial intestinal inflammation or alterations of the intestinal microbiota to promote the formation of colitogenic microbes. We hypothesized that the mucosal inflammation observed in CD patient could be due to an increasing transport of IgA-pathogen complexes from lumen to Peyer's patches (PP) immune cells through M cells. Indeed, after reverse transcytosis, bacteria-IgA complexes are taken up by $CD11c^+$ DCs, and can induce inflammatory responses [18,19]. Moreover, intestinal bacteria selected on the basis of high coating with IgA is associated with reduced gut microbial diversity in human [25] and conferred dramatic susceptibility to colitis in germfree mice [12,26]. The earliest observable CD lesions are reported to occur in the follicle associated epithelium (FAE), where M cells are abundant [27], where the PPs are more numerous, and where IgA2 predominates [28]. *NOD2* mutations associated with CD primarily predispose to

the development of lesions in the ileal compartment [29], indicating that disease susceptibility is increased by altering signaling interactions between intestinal microbiota and the mucosal innate immunity. Hence, we next hypothesized that *NOD2* regulates IgA retrograde transport might explain the dysregulation observed in patients with *NOD2* mutations.

We observe an increasing transport of IgA in human PP biopsies obtained from CD patients with or *NOD2* mutations. We demonstrate that *NOD2* has a regulatory effect in the IgA transport through human and mouse M cells by decreasing the Dectin-1 and Siglec-5 expression on M cells, already identified to act as co-receptors in this process. Our findings define a new mechanism of NOD2-mediated regulation of innate immune responses to intestinal microbiota which is involved in the initiation and/or perpetuation of the mucosal inflammation observed in CD patients.

Results

NOD2 mutation significantly increases SIgA reverse transcytosis in Crohn's disease patients

We initially examined whether the transport of SIgA was modified as a consequence of the disease, and second refined the analysis to samples collected from CD patients with or lacking *NOD2* mutations. To address this question, we first determined NOD2 genotypes from PP biopsies in the terminal ileum from healthy (n=8) or CD (n=20) followed by quantification of SIgA-positive cell numbers. The mean fold-increase of SIgA-positive cells per PP was 2.8 in CD patients expressing *NOD2* frameshift polymorphisms (n=10) compared to healthy individuals (n=8) and CD patients expressing wild type (WT) *NOD2* (n=10). A first, colocalization (Fig. 1b) with anti-IgA Ab and anti-secretory component (SC) Ab confirm that IgA was not enriched from inside (interstitial fluids) but from the lumen (retrotranslocation of SIgA from the lumen to the Peyer's patches). Colocalization IgA^+/SC^+ was observed in all

tested biopsies (healthy n=8; CD patients with *NOD2* frameshift polymorphisms n=10; CD patients with WT *NOD2* n=10). A second colocalization $IgA2^+$/DC-$SIGN^+$ (Fig. 1b) indicate that counted $SIgA^+$ cells derived from the retrograde transport of SIgA through M cells followed by their DC uptake. Increase of SIgA retrotransport is not observed in segments of the intestine lacking PPs (Fig. 1a and b). Weak differences in numbers of $SIgA^+$ cells were measured in patients with *NOD2* polymorphisms R702W (n=4) or FS1007insC (n=3) or R702W/G908R (n=3) (Fig. 1a). The sum of the data demonstrates an increase in PP-associated SIgA in the subset of CD patients displaying mutated *NOD2* gene solely.

NOD2 deficiency significantly increases IgA retrograde transport in murine Peyer's patches

In the absence of *NOD2*, PPs present a higher level of CD4+ T cells and M cells in the FAE and increased levels of Th1 (IFN-γ, TNF-α and IL-12) and Th2 (IL-4) cytokines. These immune alterations are associated with an increase of paracellular permeability and yeast/bacterial translocation [30,31]. Hence, we next hypothesized that at steady-state, the dysregulation observed in CD patients with *NOD2* mutations may favor SIgA reverse transcytosis, and ultimately lead to excessive uptake of bacteria-SIgA complexes.

To this aim, we sought to determine whether the loss of *NOD2* expression affected transport of SIgA in a *NOD2* knock-out (KO) mouse model. Transport of fluorescently labeled SIgA was compared between *NOD2* KO mice and WT mice by examining the fate of the antibody molecule after administration into a ligated intestinal loop containing a PP. As observed in human gut biopsies obtained from patients with NOD2 polymorphisms, the mean fold-increase (2.3) of SIgA transport from lumen into the PP in *NOD2* KO mice (112.4 ± 14.5) was significantly different when compared to WT mice (49.4 ± 7.6). This significant increase of IgA transport, together with a significant decrease after MDP-PAM treatment demonstrate the

implication of *NOD2* in the process of transcytosis (Fig. 2a). Cy3 administered per se in the ligated intestinal loop did not yield any fluorescent signal in tissue sections (data not shown). Finally, we did not observed any retrotranscytosis of negative controls as BSA or an irrelevant mouse IgG using a ligated intestinal loop model suggesting that the effect is SIgA-dependant (Fig. 2a).

Oral administration of HIV p24 in association with SIgA to littermate WT mice leads to the generation of a robust immune response against the viral antigen. In this experimental setting, SIgA serves as a delivery system carrying an intact HIV p24 antigen into intestinal M cells in PPs [20]. We thus speculated that the increased retro-transport of SIgA observed in *NOD2* KO mice would result in improved p24-specific reactivity after oral immunization as compared to littermate WT mice. First, we confirmed the same ability of IgA to bind to the same microbiota pattern in littermate or NOD2 KO mice, as previously described [33] (Fig 2c). It was also confirmed by quantification of IgA^+ bacteria with flow cytometry (Fig 2b). As oral immunization is well known to induce both systemic and mucosal responses, antigen-specific response was measured in both serum and feces samples 1 week after the last immunization. Systemic p24-specific IgG and fecal IgA titers were significantly increased in *NOD2* KO mice as compared to littermate WT mice (Fig. 2d and 2e). Oral delivery of an equivalent amount of p24 alone was not sufficient to induce a specific Ab responses in either KO or littermate WT animals (Fig. 2d and 2e). Because the local tissue-dependent nature of immune responses relies highly on the controlled production of cytokines, a panel of them was measured by Luminex in serum and feces obtained 24 h after the last immunization. In comparison with p24 alone, p24-SIgA was a potent inducer of all the tested cytokines in serum but also TNF-α, INF-γ and IL-17 measured in feces of *NOD2* KO mice (Fig. 2f). Immunization with SIgA alone has no effect on the production of cytokines. Except for IL-10, no difference in cytokine secretion was observed between littermate WT and *NOD2* KO mice. The increase of IL-10 in serum after

immunization with p24-SIgA in the *NOD2* KO mice may indicate regulation of the systemic inflammatory process following initial priming of the specific Th cell response. Taken together, these results indicate that transport of p24-SIgA complexes is dependent on functional *NOD2* and results in the regulated passage of the hooked Ag, which is subsequently processed to trigger the onset of mucosal and systemic antibody and cytokine responses.

SIgA-*Salmonella* immune complexes amplify *Salmonella*-induced colitis in mice.

The demonstration that SIgA reverse transcytosis in *NOD2* KO mice favors the transport of a bound Ag, as reflected by the detection of specific immune responses, suggests that such a mechanism may be involved in the pathogenesis of chronic colitis. To address this hypothesis, KO mice displaying opposed effects on intestinal SIgA retrograde transport (i.e. *NOD2* KO mice identified as promoting intestinal retrograde transport (this study), and *Dectin-1* KO mice known to abrogate reverse transcytosis [19]) were used and compared with WT littermate animals. The disease condition was triggered upon administration of dextran sodium sulfate (DSS) in drinking water (positive control), or after oral delivery of *Salmonella* Typhimurium alone (*Salmonella*-induced colitis model) or in association with murine *Salmonella*-specific SIgASal4 (working hypothesis). In control experiments, oral administration of the Dectin-1 antagonist laminarin, known to suppress the development of DSS-colitis [34], was used to further verify the impact of SIgA retrograde transport inhibition.

In comparison with the PBS control group, oral administration of *Salmonella* alone in littermate WT mice resulted in a significant increase of inflammation severity, as determined by the measurement of the Disease Activity Index (DAI) (Fig. 3a). Oral delivery of *Salmonella*-SIgASal4 complexes led to a weak, yet statistically significant further increase in DAI at day 5 (Fig. 3a). DSS-treated littermate WT mice showed the highest signs of disease. Blocking of Dectin-1, and thus reduction of SIgA reverse transcytosis by addition of laminarin in the

drinking water, markedly decreased the severity of colitis. In support of our working hypothesis, *NOD2* KO mice with increased SIgA reverse transcytosis and thus higher intestinal transport of *Salmonella* exhibited a DAI resembling that of DSS-treated animals (Fig. 3a), well above the index observed in the *Salmonella* alone condition. Such a colitis-preventing effect was impaired upon delivery of laminarin to mice (Fig. 3a). The "clinical" progression of colitis was also confirmed by quantifying neutrophil infiltration in the *lamina propria* (Fig. 3b), according to the Nancy histological score (Fig. 3c), by measuring weight loss (Supplementary Fig. 1a), serum IL-6, CRP and Lipopolysaccharide (LPS) (Supplementary Fig. 1b). The high level of blood LPS in *Salmonella*-IgA treated mice reflect the IgA-based retrotranscytosis of *Salmonella* through the intestinal epithelium. This seems to demonstrate the inability of Sal4 IgA to neutralize *Salmonella* under our experimental conditions as previously described [35]. To confirm this point, we measured the aggregation of S*almonella* Typhimurium after SIgASal4 binding [35]. We did not observed *in vitro* a significant increase in *Salmonella* aggregates after SIgA binding (Supplementary Fig. 1c). The absence of aggregates confirms the non-neutralizing character of Sal4 IgA in our experimental conditions. This could indicate that these aggregates are only capable of forming *in vivo* and do not alter the retrotranscytosis ability of IgA.

SIgA-*Salmonella* treated mice without laminarin have been isolated, plotted and significantly highlighted by comparing littermate WT and Nod2KO mice (Supplementary Fig. 1d). The significative difference of DAI at day 5 after SIgA-*Salmonella* administration clearly confirms the role of Nod2 in SIgA-*Salmonella* transport. This statement was also observed using a *Salmonella*-GFP bound with SIgA administered into a ligated intestinal loop containing a PP in *NOD2* KO mice and WT littermate mice (Supplementary Fig 1e). Results obtained by blocking Dectin-1 by addition of laminarin in the drinking water were similar by using *Dectin-1* KO mice (Supplementary Fig. 1f) and are consistent with previous reports [34]. Thus, SIgA

reverse transcytosis seems to play a role in colitis induction by a *NOD2*-mediated increased transport of pathogens.

NOD2 modulates the expression of Dectin-1 and Siglec-5 receptors involved in IgA reverse transcytosis

In the mouse intestine, selective IgA reverse transcytosis across the epithelium has been shown to depend on the expression of Dectin-1 and to a lesser extent Siglec-5 on M cells [19]. IgA reverse transcytosis can be recapitulated in the *in vitro* model of FAE comprising human polarized Caco-2 cells and M-like cells. Traditional transport (transcytosis) across polarized epithelial of serosal polymeric IgA into secretions requires polymeric Ig receptor and a plethora of evolutionary well-conserved intracellular proteins including EEA-1, Rab-5, Rab-9, Rab-11, Rab-17, Rab-25. Because the regulation of vesicle trafficking along the retro-transcytotic pathway is unknown, we found it important to determine whether *NOD2* may somehow contribute to fine-tune the expression of either one of the two receptors and/or the putative organelle-specific proteins.

In order to address the nature of possibly involved proteins, we took advantage of the *in vitro* model of FAE. In the absence of M-like cell conversion, the plain Caco-2 cell polarized monolayer (mono-culture) allowed weak retrotranscytosis of the reporter IgA-luciferase fusion protein (IgA-Luc), in agreement with previous data [19]. This background level was not affected after transfection with siRNA targeting a selection of extra- and intracellular proteins, as indicated in Fig. 4a. In the presence of interspersed M-like cells in the polarized monolayer (co-culture), SIgA reverse transcytosis of IgA-Luc was increased by a factor of 4 (Fig. 4a, lanes control and random non targeting oligo). Among the assayed candidates, the targeting of EEA-1, Rab-5, Rab-17, as well as SYK and TAK1 proteins involved in Dectin-1 signaling pathway led to a significant 3-fold decrease of SIgA-Luc transport, as compared to controls (Fig 4a).

This decrease compares with that resulting from the targeting of Dectin-1 and Siglec-5 used as positive controls. A significant 2-fold increase of IgA transport in cells treated with *NOD2* siRNA, together with a significant 3-fold decrease after MDP-PAM treatment confirm the implication of *NOD2* in the process of transcytosis, and indirectly validates the results obtained via the FAE model (Fig 4a). Western Blot (Supplementary Fig. 2a) or quantitative RT-PCR was performed to correlate the decrease of mRNA level and its expected increase after MDP/PAM treatment, (Supplementary Fig. 2b). In additional control experiments, both the decrease in the level of targeted proteins and the monolayer integrity (TEER) were systematically monitored after siRNA transfection (Supplementary Fig. 2c). No significant modifications between controls, knockdown and stimulated cells were observed. Staining of tight junctions using ZO-1 detection confirmed the monolayer integrity after siRNA transfection (Supplementary Fig. 2d). Finally, the retrotransport of cholera toxin (CT), which is known to use the Rab-5 pathway [36], has been use as a positive apical-to-basal transport control to test the efficacy of siRNA knockdown on either monoculture or coculture conditions (Supplementary Fig. 2e). After Rab-5 siRNA knockdown, CT transport is significantly reduced in our inverted *in vitro* model, confirming the role of Rab-5 in CT transport and the efficacy of siRNA knockdown.

To identify if EEA-1, Rab-5, Rab-17, Dectin-1 and Siglec-5 as key partners in IgA reverse transcytosis, IgA2 was added apically in the *in vitro* model of FAE for 30 or 60 min, and IgA2-associated proteins complexes were recovered after immunoprecipitation with protein M-agarose beads. Association between IgA2 and EEA-1, Rab-5, Rab-17, Dectin-1 and Siglec-5 was revealed by immunodetection with a battery of specific antibodies (Fig. 4b). Specific colocalizations $IgA^+/EEA\text{-}1^+$, $IgA^+/Rab\text{-}5^+$, and $IgA^+/Rab\text{-}17^+$ were also confirmed by immunofluorescence. No colocalization was observed with Rab-7, Rab-9, Rab-11, Rab-25 and pIgR with IgA (Fig. 4c).

The role of *NOD2* in modulation of protein expression associated with SIgA reverse transcytosis was investigated next. The *in vitro* model containing M-like cells (co-culture) or not (mono-culture) was used as such, or following of *NOD2* knockdown with siRNA. Proteins were recovered from whole cell lysates and their relative abundance was assessed by Western blot (Fig. 5a). The expression of Dectin-1 and Siglec-5 was significantly increased after *NOD2* knockdown, whereas no relevant changes were observed upon analysis of the endosomal proteins tested. MDP-PAM treatment led to a decrease of expression of the two IgA receptors (Fig. 5b). When examining specifically the expression of Dectin-1 and Siglec-5 in $GP2^+$ M-like cells, as tested by flow cytometry, a consistent 3-fold increase of either receptor occurred in *NOD2* knockdown cells was confirmed as compared to unconverted cells with an enterocyte phenotype (Fig. 5c). In support of data in Fig. 5b, MDP-PAM treatment did not result in any significant changes in expression of either receptor. Dectin-1 and/or Siglec-5 expression has not been detected on enterocytes. This observation has been confirmed in NOD2 KO mice where Dectin-1 expression is increased on Peyer's patches M cells compared to WT mice (Fig. 5d). Finally, we investigate the involvement of NOD2 in other stages of the mucosal IgA pathway, such as production. Figure 5e clearly shows no significant difference in IgA concentration observed in serum or feces between NOD2KO mice and littermate WT mice. The sum of the data implicates NO*D2* in M-like cells as the plausible player involved in Dectin-1 and Siglec-5-mediated facilitated retrograde transport of IgA across a tight epithelial mimic.

Discussion

So far, the mechanisms involved in the loss-of-function polymorphisms on downstream *NOD2* signaling and the pathogenesis of CD remain largely unknown. A commonly recognized finding is that defects in *NOD2* result in a constitutively weak inflammatory response that can lead to increased intestinal bacterial load and with time to chronic intestinal inflammation observed in

CD [8,37]. Here we demonstrate for the first time that the mucosal inflammation observed in CD patients is could be due to an increased transport through M cells of IgA-bacteria complexes from the lumen to immune cells present in the PP. First, we found that IgA reverse transcytosis was significantly increased through human (Figure 1) and mouse (Figure 2) M cells when *NOD2* is mutated or absent. At steady state, *NOD2* seems to down-regulate the IgA retrograde transcytosis through M cells. In CD or colitis mouse models, the absence of *NOD2* could increase the transport of IgA-bacteria complexes inducing mucosal inflammation. It is well established that polymorphism of the *NOD2* gene is a major risk factor in CD. However, a molecular explanation of how such loss of function leads to increased susceptibility to CD remains unclear. Hedl *et al.* have shown that NOD2 signaling activates the mTOR pathway which induce the upregulation of anti-inflammatory mediators and simultaneously the downregulation of pro-inflammatory cytokines [38]. These data support the idea that *NOD2* modulates innate immune responses to intestinal microflora and thus suggest that the absence of such regulation leads to increased susceptibility to CD.

The role of the IgA reverse transcytosis in the pathogenesis of chronic colitis was identified in Dectin-1 KO mice and littermate WT mice using the well-known *Salmonella* colitis model [39,40]. Dectin-1 signalling has been described to regulate intestinal inflammation by controlling commensal Lactobacillus-mediated colonic regulatory T cells [34]. It seems that the transport of IgA-bacteria complexes through M cells *via* Dectin-1 receptor [19] induces intestinal inflammation, suggesting some degrees of the correlation between the abundance of M cells and chronic intestinal inflammation. In this respect, Bennet *et al*. found that in both the dextran sodium sulfate and *Citrobacter rodentium* models of colitis, significantly increased numbers of PP M cells were induced at the peak of inflammation in the colonic epithelium [41]. Using KO mice, we demonstrate that *NOD2* acts as an immune regulator of IgA reverse transcytosis. Indeed, *NOD2* KO mice administered with *Salmonella*-IgA complexes exhibit an increase of

the inflammation's severity as compared to littermate WT mice. This observation is supported by studies showing that NOD2 can modulate inflammation and mediate efficient clearance of bacteria from the mucosal tissue during *Salmonella* colitis [42,43].

We next investigated the molecular mechanisms which could explain how *NOD2* modulates IgA retrograde transport. Using specific siRNA knockdown approach in the *in vitro* model containing M-like cells, the involvement of *NOD2* as a regulator of IgA transport was confirmed. The role of endosomal proteins already known to be involved in the IgA transport through enterocytes was also studied [44]. Our data reveal that IgA reverse transcytosis through M cells seems to be mediated by EEA-1, Rab-5 and Rab-17 endosomal proteins as it has been previously described for epithelial IgA transcytosis. The role of Dectin-1 and Siglec-5 in IgA reverse transcytosis was also confirmed [19]. *NOD2* has also been shown to influence MHC cross-presentation [29], autophagy induction and resistance to intracellular bacterial infection [45,46]. Thus, while principally well-known for its acute signaling effects, NOD2 activation causes a variety of cellular changes *in vivo* that are also likely important for immune homeostasis. SYK and TAK1 proteins from the Dectin-1 signaling pathway are also involved in the blocking of IgA reverse transcytosis. The role of NOD2 interaction with TAK1 through its leucine-rich repeat (LRR) region to exert its inhibitory effect on TAK1-induced NF-κB activation has been published [47]. This suggests that NOD2 inhibits TAK1-induced NF-κB activation, which results in the downregulation of IgA transport. A significant decrease of Dectin-1 and Siglec-5 expression after *NOD2* knockdown in M cells is observed in the current study, suggesting that NOD2 contributes to regulate the expression of these two receptors for SIgA (graphical abstract). Of interest in the more global context of intestinal diseases, *NOD2* has been identified as a negative regulator of TLR2 [48] and of TLR4 in necrotising enterocolitis [49].

Our finding should be interpreted with caution, as the etiology of CD involves a combination of genetic, environmental, and microbial factors [37]. Hence, we find it fair to underline that the

SIgA-dependent route identified in the study is likely to be one among other mechanism that eventually initiates and/or perpetuates mucosal inflammation observed in CD. In any case, our data confirm and extend the knowledge that the *NOD2* genotype status is currently the strongest genetic marker associated with a severe CD course. In figure 1, *NOD2* mutations of the studied population (R702W, 1007fs and R702W/G908R) were compared and no differences were observed in IgA-positive cells distribution in PP. These results are consistent with the study of Hugot *et al*, which provided strong evidence that the penetrance of the most at-risk genotypes is low. They found no clear relationship between mutation frequencies and the disease incidence in their studied populations and no significant deficit of double-dose mutation carriers among healthy controls [50]. However, another study predict an 8% increase in the risk for complicated disease with presence of a single *NOD2* mutation, and a 41% increase with 2 mutations [51]. Nevertheless, these two studies confirm that CARD15/*NOD2* acts in interaction with other unknown risk cofactors.

A newly developed theory proposes that antibodies generated in response to microbial colonization of the intestine shape the microbiota composition to benefit the health of the host through a process called antibody mediated immunoselection (AMIS) [52]. Immunoselection refers to a process of natural selection within a host organism that is mediated by the immune system to influence microbial fitness and hence microbial ecology and evolution. A significant fraction of commensal bacteria is heavily coated with IgAs [26,53,54]. However, such coating seems to be non-specific, as there is a significant overlap of bacterial species between IgA-coated and non-coated fractions. Under such conditions the bacteria diversity was significantly reduced. Thus, it seems that reduced affinity maturation of IgAs is associated with reduced diversity and skewed microbiota and abundant coating of bacteria with natural IgAs. A recent paper goes further by saying that bacteria recognized by human SIgM were dually coated by SIgA and showed increased richness and diversity compared to IgA-only-coated or uncoated bacteria [55].

This bacterial selection mechanism could be a causal agent for CD development or other IgA-based diseases where IgA reverse transcytosis could play a role. Indeed, CD patients have several features in common with IgA nephropathy and celiac disease. Increased small intestinal mucosal permeability has been demonstrated in these pathologies [56,57]. In IgA nephropathy, this may allow the influx of food and bacterial Ags resulting in immune complex formation and deposition. In celiac disease, the alteration of para- and transcellular pathways has been proposed to explain the retrograde transport of intact peptides, and notably the apico-to-basal translocation of SIgA ensured by the transferrin receptor [58].

The better understanding of molecular mechanisms driving chronic gut inflammation has led over the past two decades to novel therapeutic strategies with major impacts for the current management of IBD [59,60]. However, despite spectacular successes mainly attributable to the anti-TNF therapy, not all patients respond to the newer drugs and about one third of the responders relapse within a short period of time. Further works are therefore needed to identify novel therapeutic molecules in IBD. In the present study, we demonstrated that IgA retro-transport is involved in promoting inflammation in CD by acting on the transport of IgA-bacteria immune complexes in the PP through M cells. Novel therapeutic strategies aiming at blocking IgA reverse transcytosis during acute phase of CD may be considered to design new efficient immunotherapeutic strategies.

Methods

Immunolabeling of human Peyer's patches *ex vivo*. Informed and consenting CD patients or healthy individuals who had undergone lower endoscopy for routine diagnostic purposes with normal intestinal mucosa provided two biopsy samples from the terminal ileum. Biopsies were fixed for 2 h in 3% paraformaldehyde and included in OCT embedding solution, before being cryosectioned using a Leica cryostat model CM1950. 7-µm sections were captured on Ultra+ Superfrost microscope slides and stained for M cells. Slides were washed in PBS to eliminate residual OCT embedding solution, and blocked with PBS containing 5% FBS for 30 min at room temperature. Immunolabeling was performed using a combination of GFP-IgA2 (Invivogen), anti-human PE-GP2 mAb (MBL), anti-human PE-DC-SIGN mAb (ThermoFisher scientific), and mouse anti-IgA secretory component Ab (Abcam) followed by goat anti-mouse PE-IgG (Abcam) diluted to 20 µg/ml for 2 h at room temperature. The slides were then washed in PBS, air-dried and mounted with Fluoprep (Biomérieux). Slides were observed by immunofluorescence microscopy (Eclipse, Nikon).

Oligonucleotide Sequences for *NOD2* Polymorphism PCR. *NOD2* genotyping has been previously reported [61], PCR of *NOD2* polymorphisms (R702W, G908R, FS1007insC) were performed on DNA extracted from human biospies with a commercial extraction kit (QIAamp DNA mini kit, Qiagen, Hilden, Deutschland). The following primers were used to identify specific mutations: R702W: forward, 5'-GAA TTC CTT CAC ATC ACT TTC CAG T -3' and reverse, 5'- GTC AAC TTG AGG TGC CCA ACA TT -3'; G908R: forward, 5'- CCC AGC TCC TCC CTC TTC -3' and reverse, 5'- AAG TCT GTA ATG TAA AGC CAC -3'; FS1007insC: forward, 5'- CTG AGC CTT TGT TGA TGA GC -3' and reverse, 5'- TCT TCA ACC ACA TCC CCA TT -3'. We purified PCR products with a PCR purification kit (Qiagen) before sequencing (Eurofins).

Mice. *NOD2* KO mice were obtained from Gabriel Nunez (University of Michigan, USA). Dectin-1 KO mice were obtained from Gordon D. Brown (University of Aberdeen, UK). Littermate mice were obtained from Nod2-heterozygous crosses. All mice were hosted at the University Hospital Unit for animal testing (Saint-Etienne, France) in the same conditions. The experimental procedures followed the protocol of the Ethics Committee of CREEA (Permit Number No. 69387487).

SIgA administration into ligated loops. For ileal loop preparation, mice were starved overnight, anesthetized by intra-peritoneal injection of a mix of ketamine and xylazine (100 and 10 mg/kg animal weight, respectively) and kept warm at 37°C throughout the surgical procedure. 100 µl of a 1 mg/ml solution of SIgA-Cy3 diluted in PBS or *Salmonella*(GFP)-SIgASal4 immune complexes (see model of mouse colitis), BSA (Sigma), or mouse IgG (anti-human TAK1 mAb (R&D System) were administered into a 1.5-cm ileal loop containing a PP. *Salmonella* enterica subsp. enterica serovar Typhimurium GFP were obtained from ATCC® (14028GFP™). Upon completion of the experiment, the mice were sacrificed by cervical dislocation and the piece of intestine was removed, extensively washed with PBS, fixed for 2 h in 3% paraformaldehyde, and included in optimal cutting tissue (OCT) embedding solution. 7-µm sections (Leica cryostat model CM1950, Leica Microsystems) were captured on Ultra+ superfrost microscope slides (VWR International). Slides were observed by immunofluorescence microscopy (Eclipse, Nikon). The protocol followed the guidance of the regional Ethics Committee for animal testing, CREEA (Permit number: No. 69387487).

Mice stimulated by MDP-PAM were administered with MDP-PAM in the ligated loop, two hours before SIgA-Cy3 administration.

To measure mouse SIgA retrotranscytosis, a polymeric IgA Ab (clone IgAC5 specific to S. flexneri serotype 5a LPS [62]) was obtained as previously described [63]. Purified free human SC was produced in Chinese Hamster Ovary cells [64]. SIgA were obtained by mixing in PBS pIgA

molecules with a 2-fold excess of human SC for 2 h at room temperature according to the conditions described previously [65]. Cy3-SIgA complexes were obtained by conjugation with indocarbocyanine (Cy3) using the FluoroLink mAb Cy3 labeling kit (Amersham Biosciences).

Study of IgA/fecal microbiota interactions. The ability of fecal IgA to bind gut microbiota has been measured by western blot as previously reported [33]. Shortly, lysed bacteria were used as the target antigens in a western blot assay. Serum or fecal supernatant from WT or Nod2KO mice were used as primary antibody and anti-IgA-HRP as secondary antibody. This experiment was repeated on 4 mice per group. The quantity of IgA already bound with fecal bacteria were also quantified by flow cytometry. Fecal supernatant from WT and Nod2KO mice were stained with anti-IgA-FITC and the MFI were calculated on IgA-bacteria. This experiment was analysed using 4 mice per group.

Immunization with p24-SIgA complexes. Mouse oral immunizations, recovery of blood and feces, and quantification of p24-specific IgG, IgA, cytokines and chemokines were performed as previously described [20].

***In Vivo* Delivery of HIVp24-SIgA and measurement of p24-Specific Abs**. Immunization with HIVp24-SIgA complexes and measurement of HIVp24-specific IgG and IgA Abs in serum and feces has been already described as well as the measure of cytokine panels [19–21].

Model of mouse colitis. The virulent streptomycin resistant *Salmonella enterica* serovar Typhimurium strain SL1344 was cultured in LB (LB Broth, Sigma) supplemented with 90µg/ml of streptomycin (LB-St). A day before infection, a SL1344 colony was cultured overnight at 37°C, 100rpm in 3 ml of LB-St. Mouse IgASal4, specific for *Salmonella* Typhimurium surface carbohydrates was produced as described previously and used to treat mice with SigA-*Salmonella* complexes. In other experiments, colitis was also induced by giving 5% dextran sodium sulfate solution in drinking water *ad libitum* for 7 days as previously described [66]. Body weight and disease activity index were monitored each days.

NOD2 KO (n=5), Dectin-1 KO (n=5) and littermate WT (n=5) mice were given either *Salmonella*-SigASal4 complexes or S*almonella* alone (i.e., 10^6 CFU/mouse) in 100 µl PBS by orogastric intubation with polyethylene tubing under light anesthesia with isoflurane (Halocarbon Laboratories). Mice were not pre-treated with streptomycin as we would like to measure the role of SigA reverse transcytosis in the context of a normal microbiota. Infectivity and dissemination of *Salmonella* SL1344 were fist tested at different doses. A dose of 1.10^6 CFU/mouse was used as it was not lethal but induce strong inflammation.

Induction of colitis were compared in *NOD2* KO (n=5), Dectin-1 KO (n=5) and littermate WT (n=5) mice after adding 5% laminarin in drinking water for 3 days before colitis induction as previously described [34].

Assessment of colitis severity

- **Disease activity index (DAI).** During the duration of the experiment, the DAI score was monitored daily to evaluate the clinical progression of colitis [67]. The DAI score combines read-outs including: weight loss compared to initial weight, stool consistency, and rectal bleeding. Scores were defined as follows: weight loss: 0 (no loss), 1 (1-5%), 2 (5-10%), 3 (10-20%), and 4 (>20%); stool consistency: 0 (normal), 2 (loose stool), and 4 (diarrhoea); and rectal bleeding: 0 (no blood), 2 (visual pellet bleeding), and 4 (gross bleeding, blood around anus). The experimental endpoint was reached when mice exhibited weight loss greater than 20% of initial weight with dehydration and diarrhoea had to be euthanized by cervical dislocation following inhalation of isoflurane.

- **Histology.** To evaluate histological damages reflecting colitis severity, a small fragment (0.5 cm) of the colon was cut, embedded in OCT, and frozen in isopentane cooled with liquid nitrogen. 7-µm sections were prepared as previously described and stained with hematoxylin/eosin using the published procedures [68]. Scoring of neutrophil infiltration was

performed using a standard microscope, based on the method described previously [69]. Nancy histological score has been also evaluated by a blinded pathologist.

- Serum IL-6, LPS and CRP Assays. Mice were bled 5 days after treatment through retro-orbital plexus. The presence of IL-6, LPS and CRP in sera was assessed by ELISA (Mouse IL-6 ELISA MAX, Biolegend, San Diego, CA; Mouse Lipopolysaccharide ELISA Kit, ELISAgenie, London, UK; Mouse C-Reactive Protein/CRP DuoSet ELISA, R&D system, USA).

IgA-*Salmonella* agglutination assay. *Salmonella* aggregates formed by IgASal4 has been quantified before oral challenge as previously described [35].To test the *in vitro* agglutination of S. typhimurium by IgASal4 antibodies, 0.1 ml of hybridoma culture supernatants (1 µg) was added to 0.1 ml of an overnight culture of bacteria and incubated in round-bottom ELISA plates. Unrelated IgA hybridoma supernatant (anti-V. cholera[70]) or fresh culture medium was used as a control. Agglutination was measured by flow cytometry after 3h at 23°C.

Cell culture. The human intestinal cell line Caco-2 (clone 1) (obtained from Dr. Maria Rescigno, University of Milan-Bicocca, Milan, Italy) [71] was cultured in Dulbecco's modified Eagle's medium (DMEM) (PAA) supplemented with 10% (v/v) fetal bovine serum (FBS, Thermo-Fisher), 1% (v/v) non-essential amino-acids (PAA), and 1% (v/v) penicillin-streptomycin (PAA), referred to as complete DMEM. The human Burkitt's lymphoma cell line Raji B (American Type Culture Collection), was cultured in RPMI 1640 supplemented with 10% (v/v) FBS, 1% (v/v) non-essential amino-acids, 1% (v/v) L-glutamine and 1% (v/v) penicillin-streptomycin.

Inverted *in vitro* model of the human FAE. The inverted FAE model has been previously reported [19,72]. Inverted Transwell® polycarbonate inserts (12 wells, pore diameter of 3.0 µm, Corning) were coated with Matrigel™, a basement membrane matrix (BD Biosciences) prepared in pure DMEM to a final protein concentration of 100 µg/mL for 1 h at room

temperature. The coating solution was removed and inverted inserts were washed with 300 µl of DMEM. Caco-2 cells (3 x 10^5), suspended in 300 µL of complete DMEM, were seeded on the lower insert side and cultured overnight. The inserts were then inverted and placed in a 12-well culture dish and kept for 9 days. Raji B cells (5 x 10^5) were resuspended in complete DMEM and then added to the basolateral compartment of the Caco-2 cells, and co-cultures were maintained for 5 days. Mono-cultures of Caco-2 cells, cultivated as above but without back-addition of Raji B cells, were used as controls. Establishment of polarized co- and mono-cultures was controlled by measurement of TEER using an EndohmTM tissue resistance chamber (Endohm-12, World Precision Instruments) connected to a Millicell®-ERS Ohmmeter (Millipore). The mean TEER value of medium alone (9 Ω per cm^2) was subtracted from each measurement. In random samples, the barrier integrity of the tight junctions was confirmed by zonula occludens-1 (ZO-1) immunolabeling [73]. For transcytosis analyses, inserts were inverted prior to incubation in a 6-well plate, and a piece of silicon tubing (14 (height) x 20 (diameter) mm, Labomoderne) serving as a medium reservoir was placed on the surface facing the basolateral pole of the cell monolayer.

Gene inhibition by small interfering (si) RNA. Cells in the inverted *in vitro* model of FAE were transfected at a final concentration of 5 nM with ON-TARGETplus SMARTpool siRNAs (Dharmacon) using Silentfect reagent (Bio-Rad) according to the procedure provided by the manufacturer. The reference numbers for gene targeting were as follows: Dectin-1: L-021476-00-0005; Siglec-5: L-019522-02-0005; EEA-1: L-004012-00-0005; pIgR: L-017729-00-0005; Rab-5: L-004009-00-0005; Rab-7: L-010388-00-0005; Rab-9: L-004177-00-0005; Rab-11: L-004726-00-0005; Rab-25: L-010366-00-0005; Syk: L-003176-00-0005; *NOD2*: L-003464-00-0005. TAK-1 was silenced by using sequence 6317S (Cell Signaling Technology).

Treatment with muramyl dipeptide - Pam3Cys (MDP-PAM). In order to specifically activate *NOD2*, the inverted *in vitro* model of FAE was exposed to 1 μg/ml muramyl dipeptide and 1 μg/ml Pam3Cys-Ser-(Lys)4 hydrochloride (Invivogen) for 24 h.

Immunoprecipitation and Western Blot. 10 μg of IgA2 (Invivogen) were added to the apical compartment of the *in vitro* model of FAE. And the cells were incubated for 30 or 60 min at 37°C. After two washes with PBS, the cells were lysed with Mammalian Protein Extraction Reagent (Thermo Scientific). The lysate was cleared by centrifugation and the protein concentration was brought to 5 μg/ml. IgA2 (and bound proteins) were concentrated by immunoprecipitation with protein M-agarose beads (Invivogen). Post washes, elution was performed with 0,1 m glycine (pH 3.0), with immediate neutralization by 1 M Tris buffer (pH 8.0). The eluted material was subjected to SDS-PAGE followed by transfer onto a hybond ECL nitrocellulose membrane (GE Healthcare Life Science). Immunodetection of targeted proteins was performed with a selection of Abs/antisera including: Goat anti-human Dectin-1/CLEC 7A serum, anti-human CD170 (Siglec-5) mAb (mouse IgG1, Clone #194128), sheep anti-human EEA-1 serum, anti-human pIgR mAb (Mouse IgG3, Clone # 825724), anti-human SYK mAb (mouse IgG1, Clone # 720402), anti-human TAK1 mAb (mouse IgG1, Clone # 491840) were purchased from R&D System, and rabbit anti-human Rab-5 serum, anti-human Rab-7 mAb (mouse IgG2b, Clone # Rab-7-117), anti-human Rab-9 mAb (mouse IgG1, Clone # Mab9), rabbit anti-human Rab-11 serum, anti-human Rab-25 mAb (Rabbit IgG, Clone EPR18353) were obtained from Abcam. Appropriate HRP-coupled secondary Abs were used for detection with the “Clarity Western ECL Substrate” (Biorad).

Immunofluorescence staining. 10 μg of IgA2 (Invivogen) were added to the apical compartment of the *in vitro* model of FAE. The cells were incubated for 60 min at 37°C. Inserts were washed in HBSS to eliminate residual medium, incubated in 4% paraformaldehyde for 30 min, permeabilized with 0.1% Triton X-100 (Sigma-Aldrich), and blocked with PBS containing

5% FBS for 15 min at room temperature. Immunolabeling was performed using a combination of same anti-rabs and anti-EEA-1 mAbs described in the previous section. Each reagent was diluted to 1/100, and incubated for 2 h at room temperature. A corresponding secondary antibodiy labeled with a PE were incubated for 1 h at room temperature. After two washes, inserts were air-dried, mounted with Fluoprep (BioMerieux), and observed by Immunofluorescence microscopy (Eclipse Ti, Nikon).

***NOD2* RT-qPCR.** *NOD2* RT-qPCR has been previously reported [74]. Briefly, total RNA was extracted using TRIZOL (Invitrogen). Reverse transcription was performed using the PrimeScript® RT reagent kit (TaKaRa Biotechnology, Dalian, PRC). The SYBR® Premix Ex Taq™ II kit (TaKaRa Biotechnology) was used to amplify *GAPDH* and *NOD2* gene products. The oligonucleotide primers used were as follows: *NOD2*: forward, 5′- CTG AAG AAT GCC CGC AAG GT -3′ and reverse, 5′- GTC TCT TGG AGC AGG CGG ATG -3′ ; *GAPDH*: forward, 5'- TGC ACC ACC AAC TGC TTA GC -3' and reverse, 5'- GGC ATG GAC TGT GGT CAT GAG -3'. The double standard curve method was used to analyze the relative gene expression [75].

IgA RT experiment. After 48 h of siRNA mediated gene knockdown or 24h of MDP-PAM stimulation, 10 µg of Ab conjugated with luciferase (Luc) or colostrum IgA or 1 µg of CT from V. cholerae (sigma) were added to the apical side of the *in vitro* model of FAE at 37°C for 90 min, as previously described [19]. Basolateral solutions were then recovered and the number of retro-transcytosed Ab-Luc measured by luminometry using the Gaussia Luc Assay Kit (Biolux) according to the procedure provided by the manufacturer. Transported colostrum IgA and CT was detected by ELISA using respectively biotinylated goat anti-human IgA (Southern Biotech) and biotinylated rabbit anti-CT pAb (Invitrogen) followed by streptavidin-HRP (Amersham).

Statistical Analysis. Statistical analyses were performed using the InStat version 2.01 from the GraphPad Software. A nonparametric Mann-Whitney U-test or one-way ANOVA followed by

570 Bonferroni post hoc test was used where appropriate [76,77]. The limit of significance for p values
571 was set at 0.05 (marked by * in the plot); ** indicates p values ≤ 0.01, and *** stands for p
572 values ≤ 0.005. Statistically significant differences between groups are emphasized by bars
573 connecting the relevant columns under comparison.
574
575 **Author Contributions.** Nicolas Rochereau, Eva Michaud, Rémi Gayet, Blandine Chanut, and
576 Fabienne Jospin carried out the experiment. Nicolas Rochereau wrote the manuscript with
577 support from Xavier Roblin, Blaise Corthésy and Stéphane Paul. Blaise Corthésy and Stéphane
578 Paul supervised the project.
579 **Acknowledgments.** N. Rochereau was supported by a post-doc fellowship from the Sir Jules
580 Thorn Charitable Trust and subsequently by a post-doc fellowship from Region Rhone-Alpes
581 and also from ANRS (France). The laboratory of S. Paul is supported by research grants from
582 ANRS, Sidaction and MSD Avenir, and that of B. Corthésy by grant No. 3100-156806 from
583 the Swiss Science Research Foundation. We would like to thank the staff of the "Unité
584 Hospitalo-Universitaire d'expérimentation animale" technical platforms of IFR143 for help in
585 sample analysis.
586 **Declaration of Interests**. The authors have declared that no conflict of interest exists.
587

References

1. van den Elsen, L. W., Poyntz, H. C., Weyrich, L. S., Young, W. & Forbes-Blom, E. E. Embracing the gut microbiota: the new frontier for inflammatory and infectious diseases. *Clin. Transl. Immunol.* **6**, e125 (2017).
2. Kayama, H. & Takeda, K. Functions of innate immune cells and commensal bacteria in gut homeostasis. *J. Biochem. (Tokyo)* **159**, 141–149 (2016).
3. Castro-Dopico, T. *et al.* Anti-commensal IgG Drives Intestinal Inflammation and Type 17 Immunity in Ulcerative Colitis. *Immunity* **50**, 1099-1114.e10 (2019).
4. de Jong, R. J. & Ohnmacht, C. Defining Dysbiosis in Inflammatory Bowel Disease. *Immunity* **50**, 8–10 (2019).
5. Parikh, K. *et al.* Colonic epithelial cell diversity in health and inflammatory bowel disease. *Nature* **567**, 49–55 (2019).
6. Dragasevic, S. *et al.* Genetic and environmental factors significant for the presentation and development of inflammatory bowel disease. *Eur. J. Gastroenterol. Hepatol.* **29**, 909–915 (2017).
7. Goethel, A. *et al.* Nod2 influences microbial resilience and susceptibility to colitis following antibiotic exposure. *Mucosal Immunol.* **12**, 720–732 (2019).
8. Ramanan, D., Tang, M. S., Bowcutt, R., Loke, P. & Cadwell, K. Bacterial sensor Nod2 prevents inflammation of the small intestine by restricting the expansion of the commensal Bacteroides vulgatus. *Immunity* **41**, 311–324 (2014).
9. Shawki, A. & McCole, D. F. Mechanisms of Intestinal Epithelial Barrier Dysfunction by Adherent-Invasive Escherichia coli. *Cell. Mol. Gastroenterol. Hepatol.* **3**, 41–50 (2017).

10. Kennedy, N. A. *et al.* The Impact of NOD2 Variants on Fecal Microbiota in Crohn's Disease and Controls Without Gastrointestinal Disease. *Inflamm. Bowel Dis.* **24**, 583–592 (2018).
11. Bunker, J. J. *et al.* Natural polyreactive IgA antibodies coat the intestinal microbiota. *Science* **358**, (2017).
12. Hansen, I. S., Baeten, D. L. P. & den Dunnen, J. The inflammatory function of human IgA. *Cell. Mol. Life Sci. CMLS* (2018) doi:10.1007/s00018-018-2976-8.
13. Heineke, M. H. & van Egmond, M. Immunoglobulin A: magic bullet or Trojan horse? *Eur. J. Clin. Invest.* **47**, 184–192 (2017).
14. Macpherson, A. J., Yilmaz, B., Limenitakis, J. P. & Ganal-Vonarburg, S. C. IgA Function in Relation to the Intestinal Microbiota. *Annu. Rev. Immunol.* (2018) doi:10.1146/annurev-immunol-042617-053238.
15. Melo-Gonzalez, F. *et al.* Antigen-presenting ILC3 regulate T cell-dependent IgA responses to colonic mucosal bacteria. *J. Exp. Med.* **216**, 728–742 (2019).
16. Neumann, C. *et al.* c-Maf-dependent Treg cell control of intestinal TH17 cells and IgA establishes host-microbiota homeostasis. *Nat. Immunol.* **20**, 471–481 (2019).
17. Hansen, I. S. *et al.* FcαRI co-stimulation converts human intestinal CD103+dendritic cells into pro-inflammatory cells through glycolytic reprogramming. *Nat. Commun.* **9**, 863 (2018).
18. Corthésy, B. Roundtrip ticket for secretory IgA: role in mucosal homeostasis? *J. Immunol. Baltim. Md 1950* **178**, 27–32 (2007).
19. Rochereau, N. *et al.* Dectin-1 Is Essential for Reverse Transcytosis of Glycosylated SIgA-Antigen Complexes by Intestinal M Cells. *PLoS Biol.* **11**, e1001658 (2013).
20. Rochereau, N. *et al.* Secretory IgA as a vaccine carrier for delivery of HIV antigen to M cells. *Eur. J. Immunol.* (2014) doi:10.1002/eji.201444816.

21. Rochereau, N. *et al.* Delivery of antigen to nasal-associated lymphoid tissue microfold cells through secretory IgA targeting local dendritic cells confers protective immunity. *J. Allergy Clin. Immunol.* (2015) doi:10.1016/j.jaci.2015.07.042.
22. Eom, T., Kim, Y. S., Choi, C. H., Sadowsky, M. J. & Unno, T. Current understanding of microbiota- and dietary-therapies for treating inflammatory bowel disease. *J. Microbiol. Seoul Korea* **56**, 189–198 (2018).
23. Nishida, A. *et al.* Gut microbiota in the pathogenesis of inflammatory bowel disease. *Clin. J. Gastroenterol.* **11**, 1–10 (2018).
24. Schultz, B. M. *et al.* A Potential Role ofSalmonellaInfection in the Onset of Inflammatory Bowel Diseases. *Front. Immunol.* **8**, 191 (2017).
25. Jørgensen, S. F. *et al.* Selective IgA deficiency in humans is associated with reduced gut microbial diversity. *J. Allergy Clin. Immunol.* (2019) doi:10.1016/j.jaci.2019.01.019.
26. Palm, N. W. *et al.* Immunoglobulin A coating identifies colitogenic bacteria in inflammatory bowel disease. *Cell* **158**, 1000–1010 (2014).
27. Bosca-Watts, M. M. *et al.* Pathogenesis of Crohn's disease: Bug or no bug. *World J. Gastrointest. Pathophysiol.* **6**, 1–12 (2015).
28. Lin, M., Du, L., Brandtzaeg, P. & Pan-Hammarström, Q. IgA subclass switch recombination in human mucosal and systemic immune compartments. *Mucosal Immunol.* **7**, 511–520 (2014).
29. Corridoni, D. *et al.* Genetic deletion of the bacterial sensor NOD2 improves murine Crohn's disease-like ileitis independent of functional dysbiosis. *Mucosal Immunol.* (2016) doi:10.1038/mi.2016.98.
30. Jung, C., Hugot, J.-P. & Barreau, F. Peyer's Patches: The Immune Sensors of the Intestine. *Int. J. Inflamm.* **2010**, 823710 (2010).

31. Graziani, C. *et al.* Intestinal permeability in physiological and pathological conditions: major determinants and assessment modalities. *Eur. Rev. Med. Pharmacol. Sci.* **23**, 795–810 (2019).
32. Henckaerts, L. & Vermeire, S. NOD2/CARD15 disease associations other than Crohn's disease. *Inflamm. Bowel Dis.* **13**, 235–241 (2007).
33. McCarthy, D. D. *et al.* Mice overexpressing BAFF develop a commensal flora–dependent, IgA-associated nephropathy. *J. Clin. Invest.* **121**, 3991–4002 (2011).
34. Tang, C. *et al.* Inhibition of Dectin-1 Signaling Ameliorates Colitis by Inducing Lactobacillus-Mediated Regulatory T Cell Expansion in the Intestine. *Cell Host Microbe* **18**, 183–197 (2015).
35. Mantis, N. J. & Forbes, S. J. Secretory IgA: arresting microbial pathogens at epithelial borders. *Immunol. Invest.* **39**, 383–406 (2010).
36. Cho, J. A. *et al.* Insights on the trafficking and retro-translocation of glycosphingolipid-binding bacterial toxins. *Front. Cell. Infect. Microbiol.* **2**, (2012).
37. Ramos, G. P. & Papadakis, K. A. Mechanisms of Disease: Inflammatory Bowel Diseases. *Mayo Clin. Proc.* **94**, 155–165 (2019).
38. Hedl, M. & Abraham, C. Secretory mediators regulate Nod2-induced tolerance in human macrophages. *Gastroenterology* **140**, 231–241 (2011).
39. Sinha, R. *et al.* Retinoic acid decreases the severity of Salmonella enterica serovar Typhimurium mediated gastroenteritis in a mouse model. *Immunobiology* (2016) doi:10.1016/j.imbio.2016.01.011.
40. Lo, B. C. *et al.* IL-22 Preserves Gut Epithelial Integrity and Promotes Disease Remission during Chronic Salmonella Infection. *J. Immunol. Baltim. Md 1950* **202**, 956–965 (2019).

41. Bennett, K. M. *et al.* Induction of Colonic M Cells during Intestinal Inflammation. *Am. J. Pathol.* **186**, 1166–1179 (2016).
42. Claes, A.-K. *et al.* Salmonella enterica serovar Typhimurium ΔmsbB Triggers Exacerbated Inflammation in Nod2 Deficient Mice. *PLOS ONE* **9**, e113645 (2014).
43. Robertson, S. J., Geddes, K., Maisonneuve, C., Streutker, C. J. & Philpott, D. J. Resilience of the intestinal microbiota following pathogenic bacterial infection is independent of innate immunity mediated by NOD1 or NOD2. *Microbes Infect.* **18**, 460–471 (2016).
44. Garcia-Castillo, M. D., Chinnapen, D. J.-F. & Lencer, W. I. Membrane Transport across Polarized Epithelia. *Cold Spring Harb. Perspect. Biol.* a027912 (2017) doi:10.1101/cshperspect.a027912.
45. Boyle, J. P., Parkhouse, R. & Monie, T. P. Insights into the molecular basis of the NOD2 signalling pathway. *Open Biol.* **4**, (2014).
46. Cadwell, K. Crosstalk between autophagy and inflammatory signalling pathways: balancing defence and homeostasis. *Nat. Rev. Immunol.* **16**, 661–675 (2016).
47. Chen, C.-M., Gong, Y., Zhang, M. & Chen, J.-J. Reciprocal cross-talk between Nod2 and TAK1 signaling pathways. *J. Biol. Chem.* **279**, 25876–25882 (2004).
48. Watanabe, T., Kitani, A., Murray, P. J. & Strober, W. NOD2 is a negative regulator of Toll-like receptor 2-mediated T helper type 1 responses. *Nat. Immunol.* **5**, 800–808 (2004).
49. Richardson, W. M. *et al.* Nucleotide-binding oligomerization domain-2 inhibits toll-like receptor-4 signaling in the intestinal epithelium. *Gastroenterology* **139**, 904–917, 917.e1–6 (2010).
50. Hugot, J.-P. *et al.* Prevalence of CARD15/NOD2 mutations in Caucasian healthy people. *Am. J. Gastroenterol.* **102**, 1259–1267 (2007).

51. Adler, J., Rangwalla, S. C., Dwamena, B. A. & Higgins, P. D. R. The prognostic power of the NOD2 genotype for complicated Crohn's disease: a meta-analysis. *Am. J. Gastroenterol.* **106**, 699–712 (2011).
52. Kubinak, J. L. & Round, J. L. Do antibodies select a healthy microbiota? *Nat. Rev. Immunol.* **16**, 767–774 (2016).
53. Sutherland, D. B., Suzuki, K. & Fagarasan, S. Fostering of advanced mutualism with gut microbiota by Immunoglobulin A. *Immunol. Rev.* **270**, 20–31 (2016).
54. Pabst, O., Cerovic, V. & Hornef, M. Secretory IgA in the Coordination of Establishment and Maintenance of the Microbiota. *Trends Immunol.* **37**, 287–296 (2016).
55. Magri, G. *et al.* Human Secretory IgM Emerges from Plasma Cells Clonally Related to Gut Memory B Cells and Targets Highly Diverse Commensals. *Immunity* **47**, 118-134.e8 (2017).
56. Clément, B.-J., Lebreton, C., Malamut, G. & Cerf-Bensussan, N. Perméabilité intestinale et maladie cœliaque. *Médecine Mal. Métaboliques* **9**, 19–26 (2015).
57. König, J. *et al.* Human Intestinal Barrier Function in Health and Disease. *Clin. Transl. Gastroenterol.* **7**, e196 (2016).
58. Lebreton, C. *et al.* Interactions among secretory immunoglobulin A, CD71, and transglutaminase-2 affect permeability of intestinal epithelial cells to gliadin peptides. *Gastroenterology* **143**, 698-707.e1–4 (2012).
59. Bilsborough, J., Targan, S. R. & Snapper, S. B. Therapeutic Targets in Inflammatory Bowel Disease: Current and Future. *Am. J. Gastroenterol. Suppl.* **3**, 27–37 (2016).
60. Narula, N., Rubin, D. T. & Sands, B. E. Novel Therapies in Inflammatory Bowel Disease: An Evaluation of the Evidence. *Am. J. Gastroenterol. Suppl.* **3**, 38–44 (2016).
61. Cooney, R. *et al.* NOD2 stimulation induces autophagy in dendritic cells influencing bacterial handling and antigen presentation. *Nat. Med.* **16**, 90–97 (2010).

734 62. Phalipon, A. *et al.* Monoclonal immunoglobulin A antibody directed against serotype-
735 specific epitope of Shigella flexneri lipopolysaccharide protects against murine
736 experimental shigellosis. *J. Exp. Med.* **182**, 769–778 (1995).
737 63. Favre, L. I., Spertini, F. & Corthésy, B. Simplified procedure to recover recombinant
738 antigenized secretory IgA to be used as a vaccine vector. *J. Chromatogr. B Analyt.*
739 *Technol. Biomed. Life. Sci.* **786**, 143–151 (2003).
740 64. Phalipon, A. *et al.* Secretory component: a new role in secretory IgA-mediated immune
741 exclusion in vivo. *Immunity* **17**, 107–115 (2002).
742 65. Rindisbacher, L., Cottet, S., Wittek, R., Kraehenbuhl, J.-P. & Corthésy, B. Production of
743 Human Secretory Component with Dimeric IgA Binding Capacity Using Viral
744 Expression Systems. *J. Biol. Chem.* **270**, 14220–14228 (1995).
745 66. Nyuyki-Dufe, K., Cluny, N. L., Sharkey, K. A., Swain, M. G. & Pittman, Q. J.
746 Behavioral Comorbidities in Dextran Sulphate Sodium (DSS) Colitis, an animal model
747 of Inflammatory Bowel Diseases. *FASEB J.* **30**, lb637–lb637 (2016).
748 67. Schippers, A. *et al.* β7-Integrin exacerbates experimental DSS-induced colitis in mice by
749 directing inflammatory monocytes into the colon. *Mucosal Immunol.* **9**, 527–538 (2016).
750 68. Fischer, A. H., Jacobson, K. A., Rose, J. & Zeller, R. Hematoxylin and Eosin Staining of
751 Tissue and Cell Sections. *Cold Spring Harb. Protoc.* **2008**, pdb.prot4986 (2008).
752 69. Marchal-Bressenot, A. *et al.* Development and validation of the Nancy histological
753 index for UC. *Gut* **66**, 43–49 (2017).
754 70. Winner, L. *et al.* New model for analysis of mucosal immunity: intestinal secretion of
755 specific monoclonal immunoglobulin A from hybridoma tumors protects against Vibrio
756 cholerae infection. *Infect. Immun.* **59**, 977–982 (1991).
757 71. Rescigno, M. *et al.* Dendritic cells express tight junction proteins and penetrate gut
758 epithelial monolayers to sample bacteria. *Nat Immunol* **2**, 361–367 (2001).

72. des Rieux, A. *et al.* An improved in vitro model of human intestinal follicle-associated epithelium to study nanoparticle transport by M cells. *Eur. J. Pharm. Sci. Off. J. Eur. Fed. Pharm. Sci.* **30**, 380–391 (2007).

73. Váradi, J. *et al.* Alpha-Melanocyte Stimulating Hormone Protects against Cytokine-Induced Barrier Damage in Caco-2 Intestinal Epithelial Monolayers. *PloS One* **12**, e0170537 (2017).

74. Brain, O. *et al.* The Intracellular Sensor NOD2 Induces MicroRNA-29 Expression in Human Dendritic Cells to Limit IL-23 Release. *Immunity* **39**, 521–536 (2013).

75. Larionov, A., Krause, A. & Miller, W. A standard curve based method for relative real time PCR data processing. *BMC Bioinformatics* **6**, 62 (2005).

76. Clark, S. R. *et al.* Characterization of platelet aminophospholipid externalization reveals fatty acids as molecular determinants that regulate coagulation. *Proc. Natl. Acad. Sci.* **110**, 5875–5880 (2013).

77. Xu, W. & Südhof, T. C. A Neural Circuit for Memory Specificity and Generalization. *Science* **339**, 1290–1295 (2013).

Figure and legends

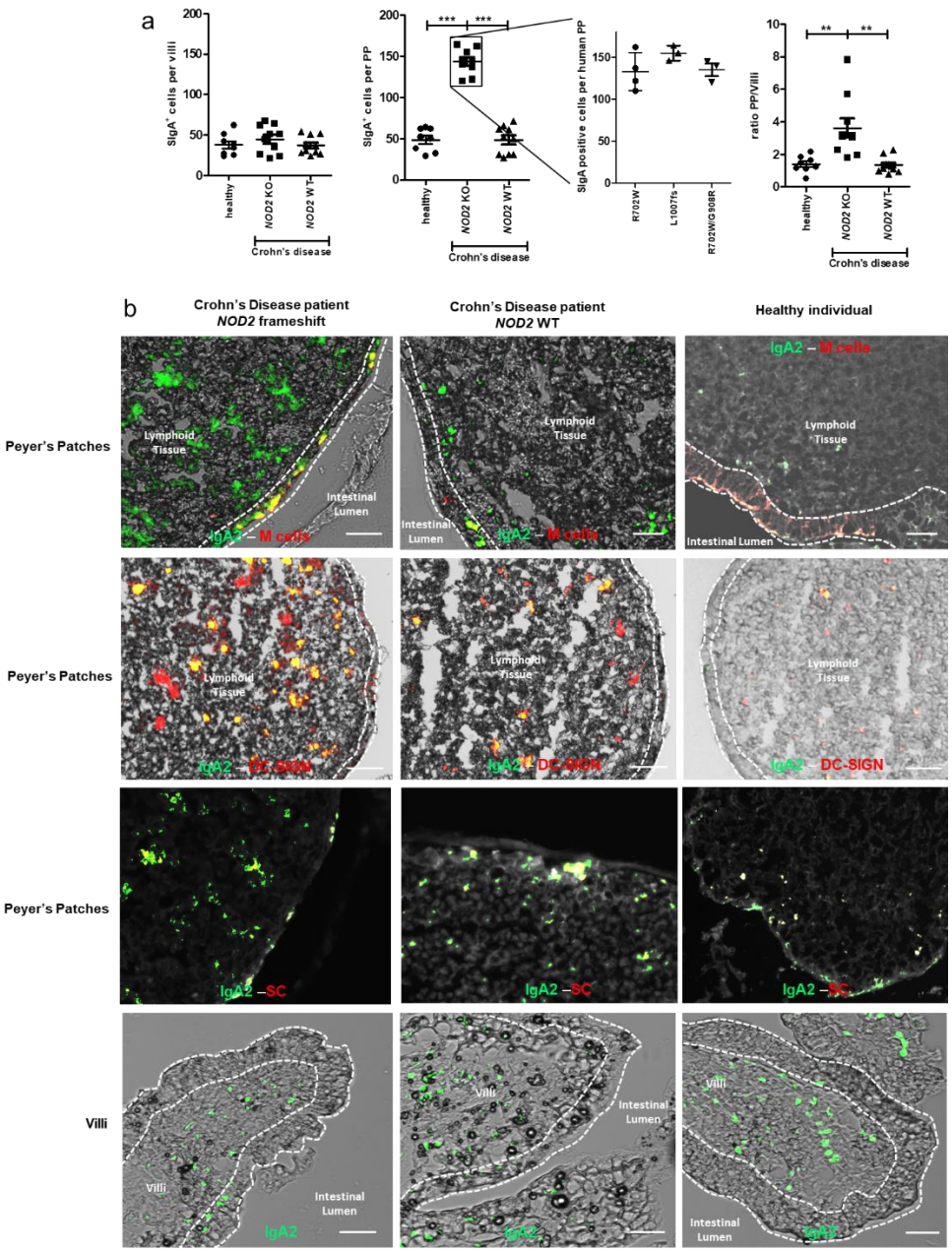

Figure 1: *NOD2* mutation significantly increases SIgA reverse transcytosis in Crohn's disease patients. (a) The two first graph compares frequency of IgA-positive cells between healthy donors, CD WT *NOD2* patients and CD patients expressing *NOD2* polymorphisms in PP and in villi. The 3rd graph shows the number of IgA positive PP cells in patients expressing different NOD2 polymorphisms. NOD2 polymorphisms (R702W, G908R, FS1007insC) were determined by qPCR and sequencing. The last graph show the ratio PP/villi. Vertical bars show the mean value ± SEM (** $p < 0.01$*** $p < 0.005$). (b) Images obtained from patient biopsy samples taken from the terminal ileum. Biopsies were labeled with anti-human GFP-IgA2 and PE-GP2 to label M cells or PE-DC-SIGN or PE anti-human SC at room temperature for 2 h. The left panels show representative images from CD patients expressing *NOD2* polymorphism, the middle panels, CD patients with WT *NOD2*, and the right panels depict images from healthy donors. Bars: 200 µm. On all pictures, dotted lines delineate the follicle–associated epithelium (FAE) separating the intestinal lumen and the lymphoid tissue (side view). Source data are provided as a Source Data file.

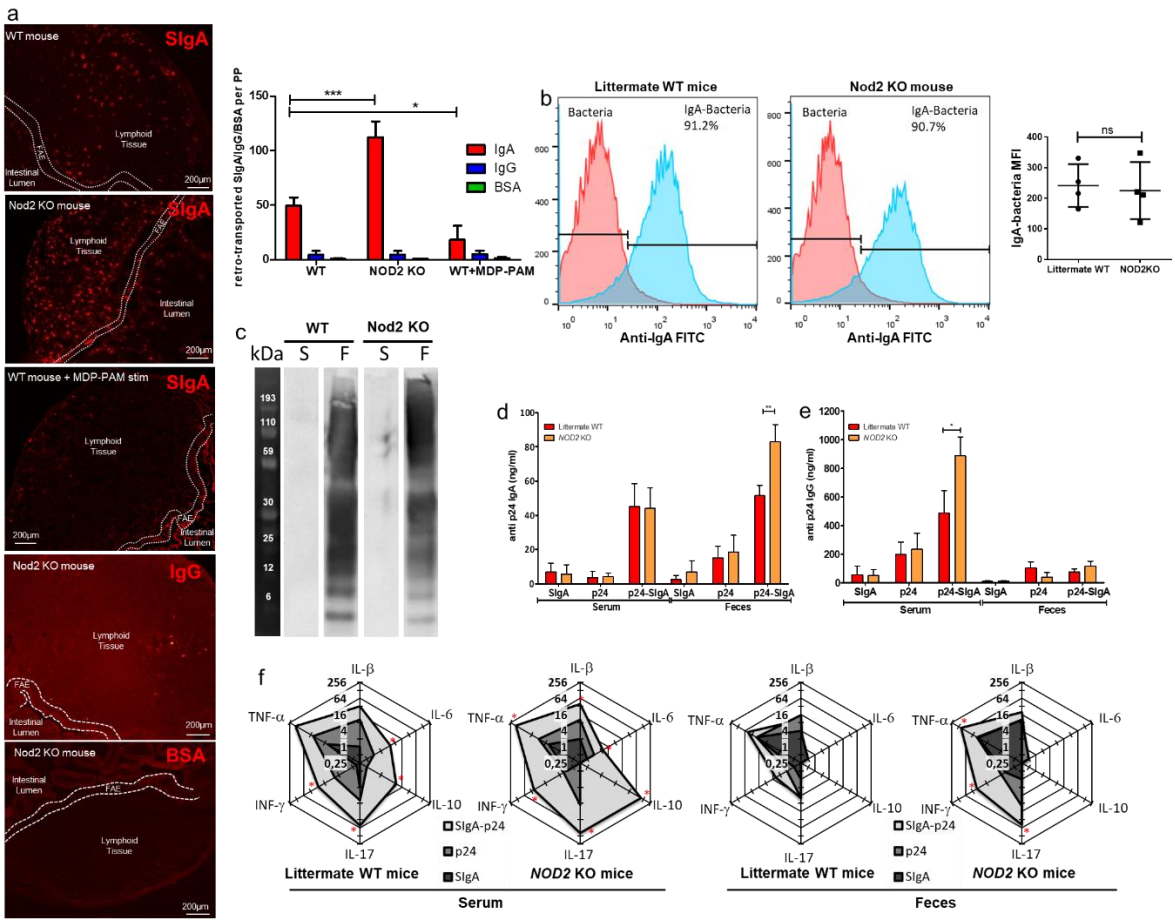

Figure 2: *NOD2* deficiency significantly increases IgA retrograde transport in murine Peyer's patches. (a) Tissue section showing a PP obtained from a ligated intestinal loop WT , *NOD2* KO or WT mice after MDP-PAM stimulation following exposure to SIgA-Cy3 for 60 min. Mouse IgG and the BSA were used as negative controls. Graph shows the number of SIgA-positive cells per PP. This experiment was repeated on 6 mice per group and the average of 3 PP per mouse was done. (b) Fecal bacteria from WT or Nod2KO mice were stained with anti-IgA-FITC and the MFI were calculated on IgA-bacteria. This experiment was repeated on 4 mice per group. (c) Lysed bacteria were used as the target antigens in a western blot, using serum (S) or fecal (F) supernatant from WT or NOD2 KO mice as primary antibody and anti–IgA-HRP as secondary antibody. This experiment was repeated on 4 mice per group. *NOD2* KO and littermate WT mice were immunized orally with p24-SIgA. (d) Levels of Ag specific mucosal IgA and (e) levels of serum IgG in littermate WT or *NOD2* KO mice were shown. Samples were collected 1 week after the last immunization and Ab production was measured by ELISA. Vertical bars show the mean value +/- SEM. (f) Cytokine concentrations in serum and feces were determined in duplicate by Luminex-multiplex cytokine assay. Cytokine profiles are shown as radar charts; each axis displays the mean quantity (pg/ml) of each cytokine after immunization with p24-SIgA, p24 and PBS. The values of each axis were joined to form the central polygon area, which represents the overall cytokine balance. Increasing or decreasing central polygon areas reflect higher or lower expression of the protein under analysis. The experiment was repeated twice with 3 mice for each group showing similar results. *P* values have been calculated by comparing the p24-SIgA group with the p24 group; * $p < 0.05$. Source data are provided as a Source Data file.

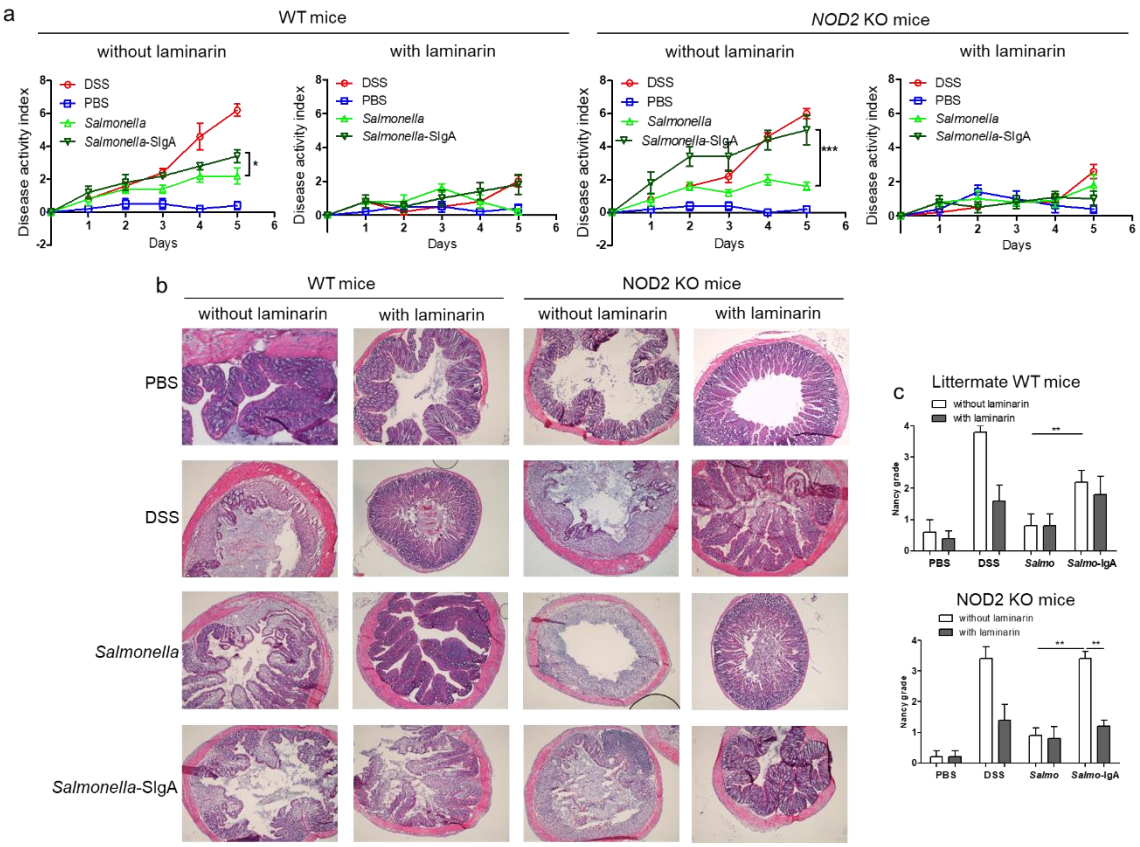

Figure 3: SIgA-*Salmonella* immune complexes amplify *Salmonella*-induced colitis in mice. Mice were challenged orally either with DSS, PBS, *Salmonella* Typhimurium or *Salmonella* Typhimurium bound with murine IgA. They were left untreated or treated with 5% laminarin in drinking water for 3 days prior to colitis challenge. (a) Disease activity index (DAI) score was undertaken daily to evaluate the clinical progression of colitis. The DAI was the combined score of weight loss compared to initial weight, stool consistency, and bleeding. Vertical bars show the mean value +/- SEM (* $p < 0.05$; *** $p < 0.005$). (b) Sections from colon of mice showing neutrophil infiltrates in the lamina propria. (c) Nancy histological score *(61)* applied in each colon section for littermate and *NOD2* KO mice. Source data are provided as a Source Data file.

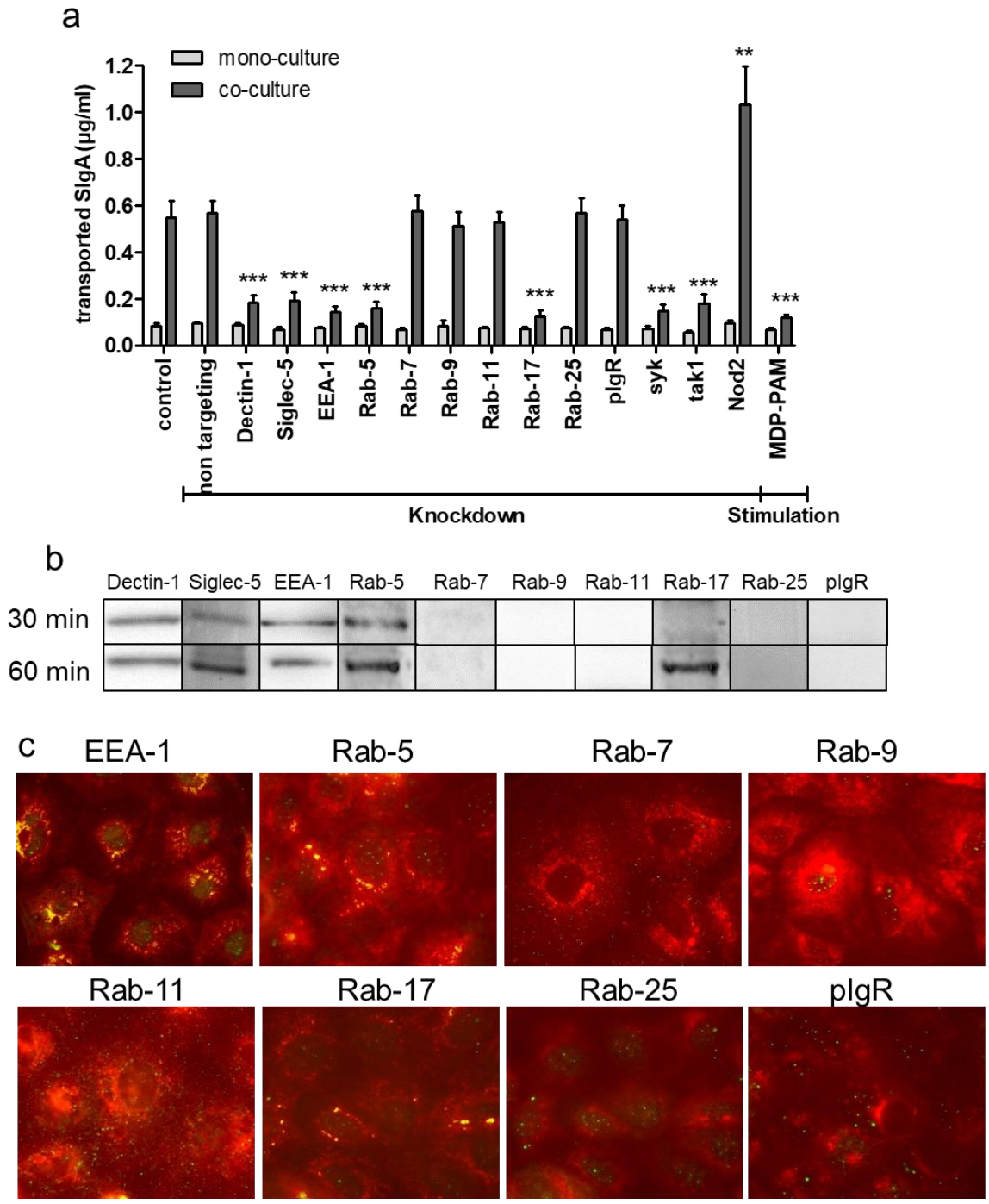

Figure 4: IgA reverse transcytosis after protein inhibition or stimulation. After siRNA knockdown or muramyl dipeptide - Pam3Cys (MDP-PAM) stimulation, IgA2 conjugated with luciferase (a) transport were quantified in the inverted *in vitro* model of FAE. (b) Immunoprecipitation made 30 or 60 min after IgA incubation. (c) Immunofluorescence staining after IgA incubation (60 min), with FITC anti-human IgA and anti-Rabs mAbs or anti-EEA-1 mAbs followed by corresponding PE secondary Abs. Colocalization between IgA and endosomal proteins resulted in yellow dots present in EEA-1, Rab-5 and Rab-17 images. Vertical bars show the mean value +/- SEM (** $p < 0.01$; *** $p < 0.005$). Source data are provided as a Source Data file.

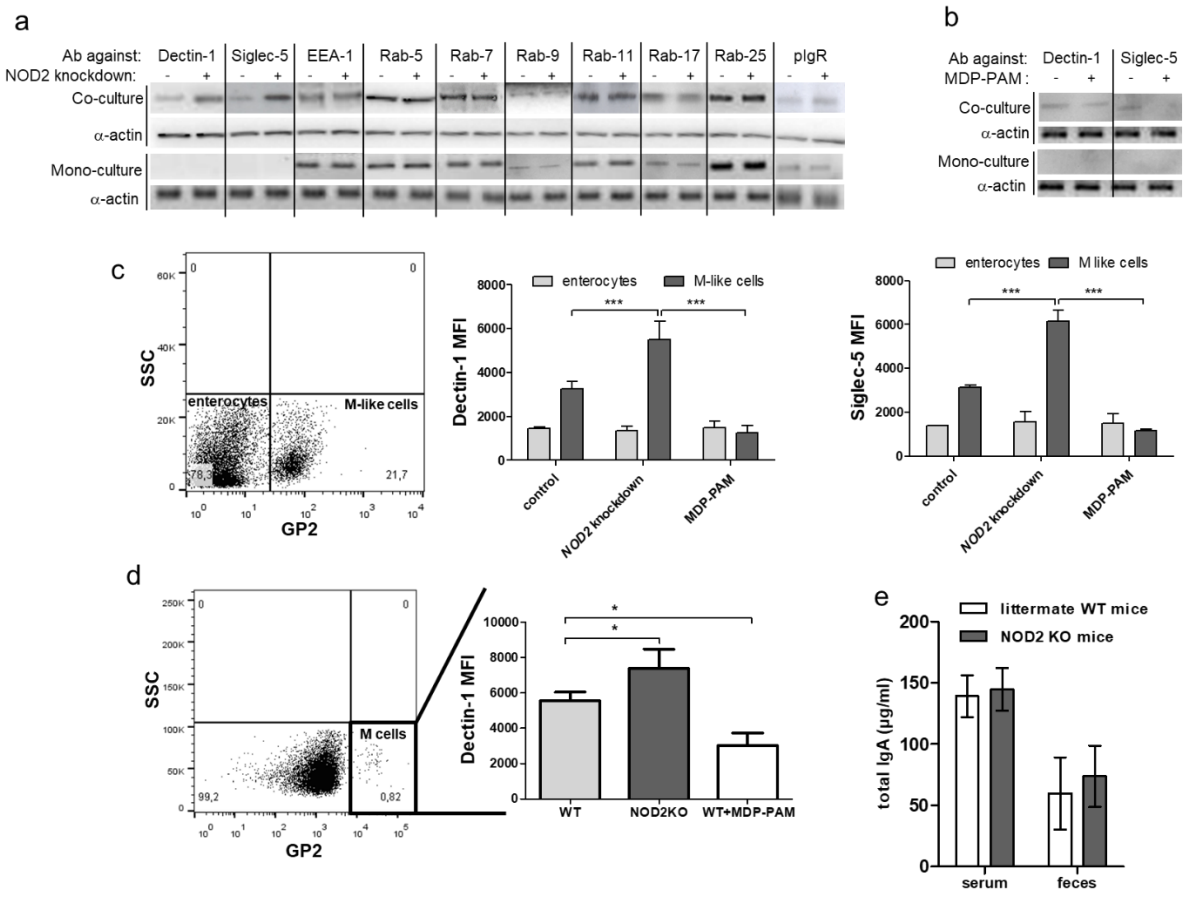

Figure 5: *NOD2* modulates the expression of Dectin-1 and Siglec-5 receptors involved in IgA reverse transcytosis. Western blot showing the expression of proteins in an *in vitro* model containing (co-culture) or not (mono-culture) M like cells before "-" or after "+" NOD2 blocking of transcription with siRNA knockdown (a) or NOD2 stimulation with MDP-PAM treatment (b). Flow cytometry was used to examine the role of NOD2 on Dectin-1 and Siglec-5 expression in M like cells *in vitro* (c) and *in vivo* (d). (e) Total IgA concentration were determined by ELISA in serum and faeces of NOD2KO mice and littermate WT mice. Vertical bars show the mean value ± SEM (* $p < 0.05$;*** $p < 0.005$). kd: knockdown; stim: stimulation. Source data are provided as a Source Data file.

C- Article 4 : Fonctions des sous-classes d'IgA et impact sur la dysbiose au cours de MICI

Alterations in SIgA functionality and reactivity towards the microbiota caracterise distinct profiles in IBD

Eva Michaud[1], Rémi Gayet[1], Blandine Chanut[1], Fabienne Jospin[1], Kathel Bathany[2], Magali Monnoye[3], Coraline Genet[4], Amelie Prier[1], , Caroline Totarski[2], Phillipe Gérard[4], Xavier Roblin[1], Nicolas Rochereau[1], Stéphane Paul[1*].

[1] GIMAP/EA3064, Université de Lyon, CIC 1408 Vaccinology, F42023 Saint-Etienne, France;
[2] Université de Bordeaux, CNRS, Bordeaux INP, Chimie et Biologie des Membranes et des Nano-objets (UMR 5248), Pessac, France
[3] Micalis Institute, INRAE, AgroParisTech, Université Paris-Saclay, 78350 Jouy-en-Josas, France
[4] Inserm UMR 1098 Right, Université Bourgogne Franche-Comté, France

*Corresponding author: Stéphane PAUL
stephane.paul@chu-st-etienne.fr
Faculté de médecine de St-Etienne, Laboratoire GIMAP
10 rue de la Marandière, 42270 St Priest en Jarez
Tel: +33 (0) 4 77 42 14 84; Fax: +33 (0) 4 77 42 14 86

Abstract

Secretory immunoglobulins A (SIgA) play a critical in sampling the commensal flora and identifying pathogens. They transport antigens below the sub-epithelial dome of Peyer Patches through M cells of the follicle-associated epithelium (FAE), a process termed ‘reverse transcytosis’ (RT). Of the two human SIgA1 et SIgA2 subtypes, only SIgA2 can undergo RT in a Dectin-1-dependant manner. Current knowledge on IgA1 and IgA2 suggest IgA1 tends to be tolerogenic, notably through IL-10 induction, while IgA2 selects a broader spectrum of commensal bacteria and induces potent T cell responses against pathogens and opportunistic bacteria.

Inflammatory Bowel Diseases (IBD) are characterized by a loss of commensal tolerance through pathways that are still poorly described. Patients display severe dysbiosis concurrent with extensive activation of inflammatory pathways. The role of SIgA in the establishment of such remains largely unknown at the subclass level. Here we show that IgA1 select beneficial strains in Crohn’s disease (CD), has increased reactivity towards common glycans, and gains the ability to undergo RT. In ulcerative colitis (UC) we observed complete loss of IgA transport through M cell and extensive loss of reactivity towards self and commensal glycans.

Keywords : SIgA, mucosal, immunity, Crohn’s disease, Ulcerative colitis,

Introduction

Mutualism between host immunity and microbial communities at the gut mucosal surface is critical for the education of the immune system and the processing of digested foods. To that end, the mucosa integrates a multitude of signals that converge towards commensal selection and pathogen elimination. In this regard, epithelial cells secrete anti-microbial peptides, mucus, and favor the transcytosis of secretory IgA (SIgA) to promote the maintenance of beneficial taxa. In response, microbes signal through the production of metabolites that induce regulatory T cells (T_{reg}) expansion (1), dampen B cell class-switch recombination and high affinity maturation, and promote the growth of other beneficial species.

SIgA promotes the establishment of bacterial networks (2,3) through both glycan-glycan interactions (4,5) and Fab binding (6), a process known as antibody-mediated immune selection (AMIS). SIg are characterized by J-chain-mediated multimerization and secretory component (SC) binding, enabling their efficient trafficking to and from the mucosal surface (7). Commensal selection is thought to rely on TI-induced low affinity SIgA and requires ILC intervention and TLR signaling. Oppositely, high affinity TD-produced SIgA selectively identifies fast-replicating bacteria as pathogenic and drives clump formation. SIgA are heavily glycosylated themselves, which favors mucus entrapment of SIgA-bound bacteria. However, the two human IgA subclasses, IgA1 and IgA2, have distinct patterns of glycosylation wherein IgA1 is mostly O-glycosylated (8,9), and IgA2 is mostly N-glycosylated (10). That affects their trafficking, as SIgA2 is the only of the two than can perform reverse-transcytosis (RT), a process by which antigen-bound SIgA travel from the lumen towards the subepithelial dome of Peyer Patches by binding Dectin-1 receptors on M-cells (11). They share two sites of N-glycosylation, on which sialylation of IgA1 dampens its pro-inflammatory effects (10). Moreover, anti-commensal IgA1 signaling tends to elicit tolerogenic signals such as T_{reg} induction and IL-10 secretion (6). In mice, highly glycosylated IgA coating of mucus-resident bacteria lowers susceptibility to chemically induced colitis, and promotes symbiotic *Firmicute* growth (12). In humans, despite IgA1 binding to bacteria usually being concomitant to that of IgA2, IgA1 displays a preference towards *Actinobacteria* selection while IgA2 identification favors *Bacteroidetes* selection (6), suggesting dual contributions to microbiome diversity.

A ‘healthy’ microbiome can be defined by its propensity to use and produce beneficial metabolites (13). The production and metabolism of short-chain fatty acids (SCFA) is amongst the most sought out by commensal microbes, such as members of the *Faecalibacterium* (14), *Roseburia* (15), *Blautia* or *Oscillospira* species. Optimal composition of the commensal microbiota may be measured by the *Firmicutes/Bacteroidetes* ratio, the two main phyla in

which, at the mucosal surface, SCFA producers dominate.Strong evidence support that dysbiosis within the intestinal microbiota – that is the alteration of resident commensal ecosystems in favor of non-beneficial communities – is responsible for Inflammatory Bowel Diseases (IBD) defects(16,17). In both Crohn's disease (CD) and ulcerative colitis (UC), T_{reg} tend to be decreased, anergized, or absent (18) and the *Firmicutes/Bacteroidetes ratio* decreases (19–22). In CD this is mostly attributed to reduced diversity amongst *Firmicutes*, the resurgence of atypical species such as segmented filamentous bacteria (SFB) and the colonization of the mucosa by oropharyngeal species (23,24). A such, CD has been strongly and extensively associated to the loss of SCFA producers such as *Faecalibacterium prausnitzii* (25), *Eubacterium rectale* (23) , *Blautia faecis, Roseburia inulinovorans* and *Ruminococcus torque* (26,27). *Faecalibacterium, Blautia* and *Ruminococcaceae* abundance are also significantly associated to functional defects of the mucosa, in that they correlate with pathogenic Paneth cells profiles (28). Dysbiosis in UC is associated to the reduction of both *Firmicutes* and *Bacteroidetes* abundance, despite a higher diversity than in CD (26). Reduction in *Roseburia* and *Faecalibacterium*(29) abundance correlates with disease occurrence(30). A noticeably lower representation of the phylum *Verrucomicrobia,* of which are *Akkermansia* species, was also evidenced in UC patients compared to healthy controls (31–33). *Akkermansia* species are mucolytic bacteria that would be involved in the maintenance of an optimal gut barrier health. Coincidentally, IBD patients' stools show increased levels of IgA-bound bacteria (24), either commensal or opportunistic, and shift from dimeric IgA secretion towards monomeric IgA secretion.

It is very likely that SIgA repertoires are affected over the course of IBD, resulting in aberrant responses to normally tolerated strains that leave room for opportunistic species to colonize niches they do not normally have access to. There is, however, little to no information on how IgA1 or IgA2 interactions with the gut microbiota affect their functional dynamics in a chronic inflammatory context. We have previously shown that SIgA2 requires optimal sialylation and N-glycosylation to undergo RT (11) as it is critical for Dectin-1 recognition, and that CD patients tend to have higher levels of RT (NR). Here, we investigate the functional abilities of human secretory IgA1 and IgA2 in terms of receptor binding, trafficking and microbiota association in CD and UC. We have thus purified IgA1 and IgA2 from IBD and non-IBD patients stool and performed sequencing of the 16S rDNA genes of IgA1- of IgA2-associated bacteria. We show that these SIgA are abnormally reactive to self and commensal glycans> This is combined observations of specific IgA1-associated and IgA2-associated microbial

profile in both CD and UC. Moreover, the loss of beneficial taxa in CD appears to originate from extensive IgA1 selection in CD, while UC IgA1 and IgA2 display a striking loss in both functionality and reactivity.

Materials and methods

Stool samples

Stool from either CD, UC or healthy individuals were collected prospectively from informed and consenting non-IBD, CD, and UC patients (Centre National Informatique et Liberte CNIL, approbation number: 1849323; Ethic committee of the CHU Saint-Etienne, Terre d'Ethique)then transferred to our facility. Briefly, samples were homogenized in Phosphate-Buffer Saline (PBS)-Tween 0,5% at a 0.1g/mL concentration then centrifuged at 1500g at 4°C for 20 min. Supernatant was collected then centrifuged at 10 000g at 4°C for 10 min. Supernatant was again collected, aliquoted, then stored at -20°C. Pellets were resuspended in 3mL of PBS-Tween 0.5% and stored at -20°C for magnetic cell separation.

IgA1 and IgA2 purification

IgA purification were performed as described by Moor, *et al.*(34). Briefly, a 10mL aliquot of homogenized stool was thawed, filtered on a 20µm filter and loaded on a peristaltic pump connected to a Peptide-M-Agarose (Invivogen) filled column (ref C10/10, GE Healthcare) and left running on a closed loop at 4°C overnight. Bound IgA was eluted on an AktaSTART HPLC (GE Healthcare) with pH 2-3 0,1M Glycine. The resulting eluate was neutralized with pH 7.5 Tris-HCl 1M, then placed to run on a Jacalin-Agarose (Pierce) column. Elution was carried out using α-D-Galactose, 1M (Sigma). Samples were then loaded onto 50kDa Amicon (ThermoFisher) and buffer-exchanged in PBS 1X for storage at -20°C in low retention tubes (ThermoFisher).

IgA and SC ELISAs

Nunc Maxisorp 96 well plates (Fisher) were coated with either anti-human IgA (Sigma I1261), antibodies or mouse anti-hSC (courtesy of B. Corthésy) in carbonate buffer (pH 9,6). Plates were sealed and incubated overnight at 4°C. Wells were saturated with BSA 1% in PBS-tween 0.05% (PBST) at room temperature (RT) for 90 min, then washed 3 times with PBST; stool samples were added at a 1/100 first dilution and incubated at RT for 1h30. Plates were then washed with PBST, then rabbit anti-human SC (courtesy of B. Corthésy), or biotinylated anti-

human IgA1 (Southern Biotech, 9130-08) or anti-human IgA2 (Southern Biotech, 9140-08) were incubated at RT for 1h30. After washing in PBST, streptavidin-HRP (BD, 554066) or anti-rabbit IgG-HRP (ThermoFisher, G-21234) were added for 1h. Revelation through addition of TMB in wells for 3 to 10 minutes was stopped with 1N HCl. Plates optical density (OD) were read at 450 nm (Sunrise TECAN microplate reader).

IgA binding assay to Dectin-1

Recombinant Fc-Dectin-1 (R&D Systems) was coated overnight at room temperature in Nunc Maxisorp 96 wells plates (Fisher). Concentrations were adjusted so that purified IgA could be used at 10 receptors per 1 IgA ratio later on. Wells were washed 3 times with PBST, and stool-purified IgA was added to the wells and incubated two hours with slight agitation at RT. After three washes with PBST, wells were incubated with biotinylated anti-human IgA1 (Southern Biotech, 9130-08) or anti-human IgA2 (Southern Biotech, 9140-08) diluted at 1/2500 and incubated at RT for 90 min. After washing in PBST, streptavidin-HRP (BD, 554066) was added for 60 min nb. Revelation through addition of TMB in wells for 10 to 20 minutes was stopped with 1N HCl. Plates optical density (OD) were read at 450 nm (Sunrise TECAN microplate reader).

In vitro model of human FAE and reverse-transcytosis assay

The model was set-up as previously published by our team (REF). Briefly, transwells inserts (Corning, 1402) were reversed and 300µL of Matrigel-enriched DMEM high-glucose medium was incubated at 37°C for 30min. After removal of excess liquid, $3{,}3.10^5$ Caco2 cells were seeded on the still reversed insert and incubated at 37°C overnight. Inserts were then placed in 12-wells plates and both inside and outside chambers were filled with complete DMEM high glucose medium and cultured for 7 to 9 days. When trans-epithelial resistance (TER) reached about 350 Ohms, 1.10^5 Raji cells were added to the inner chamber and the culture was monitored for a 100-150 Ohm TER drop over the next 2 to 4 days. Once ready, inserts were fitted in a silicone tube and both top and bottom chambers were filled with HBSS buffer. Samples were added to the top chamber and incubated for 90min at 37°C. The bottom chamber was collected and tested for Ig passage by ELISA.

MACS purification of SIgA1 and SIgA2

Resuspended pellets from stool homogenization were divided into two 1.5mL fractions. Each were centrifuged at 10.000g for 6 minutes and washed twice in MACS buffer (Miltenyi). Pellets

were resuspended in 500µL of MACS buffer and incubated with biotinylated anti-IgA1 or anti-IgA2 Abs (Southern Biotech) at 4°C with slight agitation for 40 minutes. after two washes, they were resuspended in 500µL To which 50µL of magnetic streptavidin beads (Miltenyi) were added, and incubated at 4°C for 20 minutes. Magnetic separation was then performed on LS columns with a MACS Magnet (Miltenyi) according to the manufacturer's instruction. Eluted fractions were pelleted at 10,000g for 10 minutes, andpellets were stored at -20°C for 16S-sequencing.

Analysis of the IgA1- and IgA2-coated microbial community using sequencing

Extraction of total bacterial DNA from purified IgA1 and Iga2 was performed using the QIAamp PowerFecal DNA Kit (Qiagen) and the mechanical bead-beating disruption method as previously described (35) . The V3-V4 region of the 16S rRNA genes was amplified using MolTaq (Molzym, Plaisir, France) and primers V3F: TACGGRAGGCAGCAG and V4R: ATCTTACCAGGGTATCTAATCCT. The purified amplicons were sequenced using Miseq sequencing technology (Illumina) at the GeT-PLaGe platform (Toulouse, France). Paired-end reads obtained from MiSeq sequencing were analyzed using the Galaxy-supported FROGS (Find, Rapidly, OTUs (Operational Taxonomic Units) with Galaxy Solution) pipeline (36). For preprocessing, reads with length ≥ 380 bp were kept. Clustering and chimera removal steps followed the FROGS guidelines. Assignation was performed using SILVA 16S. OTUs with abundances lower than 0.005% of the total read set were removed prior to analysis. Then, 16S sequencing data were analyzed using the Phyloseq and ggplot2 R packages in addition to custom scripts as previously described (37).

Analysis of IgA-coated microbiota by flow cytometry

2 mL of stool homogenate were thawed and centrifuged at 10 000g for 6min. Pellets were washed twice in 1mL FACS buffer (PBS 1X, 2% FBS, 10mM EDTA) then stained with mouse anti-human IgA1-PE (Southern Biotech, 9130-09) and mouse-anti-human IgA2-AlexaFluor647 (Southern Biotech, 9140-31) at 4°C in the dark for 30 min. Cells were washed in FACS buffer once, then re-suspended in 300µL of FACS buffer. Samples were then analyzed on a BD FACS Canto II cytometer (BD Bioscience) and resulting data were analyzed using the FlowJo Software.

IgA reactivity using glycan arrays

Glycan arrays (Raybiotech) were used according to the manufacturer's instruction. Arrays were blocked for 30 minutes at room temperature, then stool-purified IgA1 or IgA2 were incubated overnight at 4°C a final concentration of 50µg/mL. After washing the slides, biotinylated mouse anti-human IgA1 or IgA2 (Southern Biotech) diluted 1/500 were incubated at room temperature under slight agitation for 2 hours. Slides were washed then the Streptavidin-Cy3-equivalent reagent (Raybiotech) was added for 1 hour, after which slides were washed, air-dried, and stored at -20°C until Cy3-fluroescence readings could be performed (Tebu-bio).

Combined FISH-IF staining

Biopsies from 6 active and 4 inactive CD patients were harvested during routine exploratory colonoscopy and immediately placed in complete cold RPMI medium for transport. They were fixed in 4% paraformaldehyde overnight then embedded and frozen in OCT. 6 µm thick sections were cut, then rinsed in PBS three times to eliminate OCT. Tissue permeabilization was performed by incubating slides in 0.6% Triton for 5 min, then incubated in 2X Saline Sodium Citrate (SSC) buffer for 25 minutes. Slides were washed in DEPC-treated water (10 dips), then in 0.065M trietanolamine (TEA, Sigma) (10 dips), and finally twice in 2X SSC. Tissues were hybridized with 150µLof 16S-probes (50pM final) (**Suppl. Table 1**) overnight, at room temperature. Slides were washed in successive baths of decreasing SSC concentrations (4X, 2X, 1X, 0,5X, 0,1X) then blocked for one hour in a 1% BSA, 5% FBS, 0.3% Triton-X100 PBS solution. All subsequent washing steps were carried out in PBS. Mouse anti-human IgA2 antibodies (Southern Biotech, 9140-01) were deposited over each section at a 1/500 dilution and incubated for 2 hours at room temperature. Slides were washed and secondary antibodies (goat anti-mouse IgG-AF488, abcam) were then added for one hour. Slides were washed in PBS then distilled water, air-dried, and sealed with Vectashield (Vectra, H1000) for confocal microscopy.

Statistics

Statistical analyses were performed using the InStat version 2.01 from the GraphPad Software. A nonparametric Mann-Whitney U-test or Kruskal-Wallis test followed by Dunn's correction post hoc test were used where appropriate. The limit of significance for p values was set at 0.05 (marked by * in the plot); ** indicates p values ≤ 0.01, and *** stands for p values ≤ 0.005. Statistically significant differences between groups are emphasized by bars connecting the relevant columns under comparison.

Results

Patients with IBD have altered secretory antibodies levels

Non-IBD, CD and UC stool samples were compared for total IgA, IgA1 and IgA2 concentrations. Interestingly, IgA1 and IgA2 concentrations tended to increase in CD (**Fig. 1A, B**). There was, however, a significant decrease in both Ig concentrations in UC compared to CD patients (**Fig. 1C**) and a tendency towards lower total Secretory Component (SC) levels as well (**Fig. 1D**). Moreover, disease activity at the time of sample collection correlated with IgA2 stool concentrations (**Fig. 1E, F**). As seen in **Fig. 1F**, CD IgA2 concentration tended to be higher in patients with active disease, and a significant decrease in active UC IgA2 stool concentration was also evidenced. Thus, while overall IgA levels seem unaffected by the pathology, UC is affected by specific subclass-related alterations while CD IgA2 levels correlated with disease activity.

Levels of IgA1 and IgA2-coated microbiota fractions correlate with UC disease status

To evaluate the general level of stool microbiota bound to either IgA1, IgA2 or both, we performed flow cytometry analysis on stool homogenates. There were no differences in the levels of total $IgA1^+$-or total IgA^+-bound stool microbiota (**Fig. 2A, B**) between either group of IBD and non-IBD individuals. That could be attributed to high and low IgA-binding clusters within the IBD groups (**Fig. 2A, B**). To explain this clustering, we separated single-Ig-bound from double-positive bacteria (**Fig. 2C**). While no differences between CD and non-IBD groups were evidenced, $IgA1^-$ $IgA2^+$-coated bacteria levels were lower in UC than non-IBD patients (**Fig. 2C**) suggesting IgA2 coating of microbiota is critically altered in UC patients. Further segregation according to disease activity at the time of stool collection (**Fig. 2 D-F**) shows that active UC tended to higher levels of $IgA1^-$ $IgA2^+$- and $IgA1^+$ $IgA2^+$- bound bacteria than inactive UC (**Fig. 2E, F**). Inactive CD had higher levels of $IgA1^+$ $IgA2^+$-bound microbiota than inactive UC patients had, and inactive UC had lower levels than active UC for this fraction (**Fig. 2F**), all of which indicates that quiescent CD inflammation does not return to its homeostatic level of Ig-microbe interaction while that of UC does.

CD is characterized by IgA1-driven microbiota selection defects

Magnetically separated IgA1- and IgA2-bound fractions of the stool microbiota were analyzed using 16S sequencing. ChaO1 and Shannon diversity indices were not different in CD, UC and non-IBD, indicating similar bacterial richness (**Fig. 3A**). Likewise, principal-coordinate analysis of the Jaccard distances did not separate CD, UC and non IBD microbial profiles

indicating similar global community structure (**Fig. 3B**). Nevertheless, at the phylum level, composition appeared to be different in CD patients compared to the two other groups, with higher proportion of Bacteroidetes and lower proportion of Proteobacteria (**Fig. 3C**). Interestingly, analysis at the family level showed that reduced Proteobacteria was mainly due to lower proportion of Enterobacteriaceae (**Fig. 3D, Suppl. fig. 2A**) which are known to include pathobionts and opportunistic species like *Escherichia*, *Enterobacter* and *Shigella* species which are normally present at very low levels in healthy gut microbiota. Their decreased selection by IgA1 suggests they might be allowed to expend which coincides with previous findings that Proteobacteria abundance generally increases in CD. Concurrently, the increase in Bacteroidetes was mainly due to the family Bacteroidaceae (**Fig. 3D, Suppl. Fig 2B**) which includes commensal species normally found in healthy microbiota.

13 species were found differentially abundant between CD and Non-IBD groups, and included *Bacteroides, Lachnoclostridium, Anaerostipes, Blautia,* and *Bifidobacterium* species (**Table 1**). More importantly, they included butyrate producers (two *Ruminococcus* species, *Butyricicoccus* and *Faecalibacterium*), and one oropharyngeal species, *Streptococcus salivarius*. Butyrate producers and opportunistic bacteria alike are thus highly selected by IgA1 in CD. When we assessed the impact of the most abundant species within these 13 species, two unknown *Bacteroides,* an *Anaerostipes,* a *Bifidobacterium* and a *Faecalibacterium* species were significantly more abundant in the $IgA1^+$ fraction of CD patients' microbiota relative to non-IBD (**Fig. 3E**). In contrast, no specific enrichment was observed in the $IgA1^+$ fraction of UC patients' microbiota compared to either Non-IBD individuals. The UC $IgA1^+$ fraction was, however, enriched in three *Ruminicoccaceae* species, two unknown *Aerotruncus* and *Ruminiclostridium* species and *Massilioclostridium coli* compared to CD patients but these species did not pass our statistical abundance filters (data not shown).. Taken together, these results suggest that IgA1 binding mostly affects CD dysbiosis, possibly through the elimination of beneficial SCFA-producing species.

IgA2-coated microbiota is partially preserved in IBD

We next performed a similar analysis in the $IgA2^+$ fraction of non-IBD and IBD microbiota. Similar to IgA1, ChaO1 and Shannon diversity indices of the $IgA2^+$ fraction were not different in CD, UC and non-IBD (**Fig. 4A**). Moreover, no clustering of the different groups was obtained by principal-coordinate analysis of the Jaccard distances (**Fig. 4B**). At the phylum level, $IgA2^+$ fraction microbial profiles were close to that of the $IgA1^+$ fraction and were also characterized

by a higher proportion of *Bacteroidetes* and lower proportion of *Proteobacteria* in CD patients (**Fig. 4C**).

Contrary to IgA1, there was no significantly enriched *taxa* in the $IgA2^+$ fraction of the stool microbiota in CD patients compared to non-IBD individuals. One unknown species of *Bacteroides* was enriched in the $IgA2^+$ fraction of UC compared to that of non-IBD individuals (**Fig. 4D**). Moreover, one *Lachnospiraceae* species was also more abundant in UC $IgA2^+$ fraction relative to CD individuals (**Fig. 4E**). IgA2 might thus tends to deplete beneficial commensals. However, despite these alterations affecting taxa known to include SCFA producers, IgA2 selection of the microbiota appears to be more robustly maintained in IBD than that of IgA1.

In CD, IgA2-coated species correlate with disease activity

The surprising absence of altered abundance in the IgA2-bound fraction of the microbiota, given the major role IgA2 plays in antigen sampling under homeostatic conditions, led us to hypothesize that IgA2-induced microbial alterations might trigger flares but not participate in the overall maintenance of the inflammation. As IgA2 levels tended to follow disease activity in CD patients (**Fig. 1F**), we evaluated its patterns of selection *in situ* by co-staining colonic biopsies from patients with either active or quiescent disease with a panel of ten 16S rRNA probes and anti-IgA2 fluorescent antibodies (**Fig. 5A**). Due to the extreme friability of their colonic mucosa, no biopsies could be obtained from UC patients. Quantitative analysis of the images acquired from CD patients' biopsies showed significant changes in two groups : the total abundance *Collinsella aerofaciens* was lower, and that of *Prevotella* species was higher, in patients with quiescent disease compared to those with active disease (**Fig. 5B)**. Co-occurrence analysis between 16S probes and IgA2 staining did not recapitulate these differences but showed that quiescent disease was associated to lower IgA2 binding of *Bifidobacteria* (**Fig. 5C**). Hence, IgA2 binding, while overall not displaying significantly altered selection of the microbiota in CD, still has altered patterns of selection in active disease.

Modification of SIgAs functions in IBD

As SIgA1 and SIgA2 from IBD patients displayed significantly altered selectivity trends compared to non-IBD individuals, we asked whether their trafficking dynamics might also be dysregulated. Purification of stool IgA1 and IgA2 via two consecutive HPLC steps (10,34) lead to the efficient segregation between the two isotypes. Using a previously described *in vitro* model of FAE (11), we evaluated the reverse transcytosis (RT) potential separately for IgA1

and IgA2. In non-IBD patients, we confirm that only IgA2 could perform RT (**Fig. 5B**), as IgA1 RT activity was negligible (**Fig. 6A**). Interestingly, purified CD IgA1 but not UC IgA1 was also able to undergo RT (**Fig. 6A**). Moreover, UC IgA2 did not behave as expected, as no RT could be evidenced in those samples (**Fig. 6B**). As RT activity is associated to IgA2 binding to Dectin-1, we evaluated the Dectin-1-IgA interaction with patients-purified IgA. IgA1 could bind Dectin-1 in all groups without apparent discrepancy in its binding levels between groups (**Fig. 6C**). IgA2 from UC patients, however, had a significantly lower affinity for Dectin-1 compared to both non-IBD and CD individuals (**Fig. 6D)**, suggesting the lower levels of RT observed in UC could be attributed to defective Dectin-1 recognition. Overall, it appears that IgA gain functions in CD and loses these functions over the course of UC.

IgA interactions with Dectin-1 in IBD are altered in Crohn's disease.

We next asked whether the strength of Dectin-1 binding influenced the levels of RT. In non-IBD patients, IgA2 binding was consistently associated with higher RT percentages compared to IgA1 (**Suppl. fig. 3A**). In CD, this remained true for weak binding to Dectin-1 as RT levels were higher for IgA2 than for IgA1 (**Suppl. fig. 3B**). However, strong IgA1 binding to Dectin-1 correlated to higher levels of RT than those of strong IgA2 binding (**Suppl. fig. 3B**). Of note, weak Dectin-1 IgA1 binders in CD, while not displaying high RT levels, still retained a significantly higher ability to travel through M cells than non-IBD IgA1 (**Fig. 7A**). This was even more pronounced in strong IgA1 binders, as high levels of IgA1 RT still correlated with high binding affinity to Dectin-1 (**Fig. 7B, Suppl. Table 2**).Neither non-IBD nor CD IgA2 showed such association (**Fig. 7C, 7D, Suppl. Table 2**). Moreover, non-IBD and CD IgA2 displayed high levels of RT regardless of the affinity for Dectin-1 (**Fig. 7C, D**). One major event thus occurs in CD : IgA1 gains RT ability that is dependent on Dectin-1 binding strength and is more potent than that of IgA2, which would potentially contribute to the aggravation of inflammatory processes. There were no strong IgA1 or IgA2 binders in UC, which further suggest defective recognition for IgAs in UC (**Fig. 7A-D, Suppl. fig. 3C**).

Glycan-reactivity of SIgA from IBD patients is altered.

IgA functionality does not rely solely on antigen transport across mucosal surfaces so we evaluated SIgA reactivity in IBD by testing purified IgA1 and IgA2 from each group against a library of 100 commonly-known glycans. As intestinal IgA have a broad but low affinity for glycosylated bacterial antigens, we meant to correlate structural and functional alterations to differential patterns of antigen recognition. UC samples clustered separately from CD and

control in a principal component analysis of glycan micro-arrays for IgA1 and IgA2 combined (**Suppl. Fig.4A**). UC and CD did not have similar pattern of glycan recognition, which to our knowledge has not been evidenced before. Comparison between CD and controls with both IgA1 and IgA2 combined revealed that one glycan, Neu5Ac-2,3-Gal-1,4-Glc-Sp1, was significantly less targeted. This glycan is notably expressed by laminins of the epithelial extracellular matrix of basal membranes and recognized by bacterial lectins (38) (**Suppl.table 3**). Two others, also sialylated, were significantly more targeted (**Suppl.table 3**) : SGP and Neu5Ac-2,3-Gal-1,4-(Fuc-1,3)-Glc-[3-Sialyl-3-fucosyllactose/F-SL]. UC samples presented a strikingly different profile compared to both control and CD samples with more than 45 glycans significantly less targeted by UC IgAs (**Suppl. Fig 4E**).

Separately analysing of IgA1 and IgA2 reactivity showed IgA1 from CD patients tended to a lower affinity towards one disaccharide, 4-P-GlcNac-1,4-Man-Sp, one α-Gal, Gal-1,4-Gal-1,4-Glc, and a higher affinity towards one sialylated oligosaccharide, Gal-1,3-(Neu5Ac-2,6)-GalNac ($p<0.1$) (**Fig. 9A, Suppl. Table 3**) when compared to controls. In contrast, UC IgA1 was again leaning towards significantly lower affinity for 34 glycan species (**Fig. 9B**). More broadly, CD IgA1 displayed a higher fluorescence intensity for all groups of glycans than non-IBD IgA1 (**Fig. 9C**), suggesting increased self-recognition that might affect the inflammatory status of these patients, while UC IgA1 had lower affinity for all glycans. Similar observations were made for IgA2 in both CD and UC (**Fig. 10 A-C**) ; CD IgA2 had a general higher affinity towards commonly targeted glycans (**Fig. 10C**), with three motifs being significantly differentially targeted (**Suppl. Table 3**). Amongst those, the previously mentioned oligosaccharide Neu5Ac-2,3-Gal-1,4-(Fuc-1,3)-Glc-[3-Sialyl-3-fucosyllactose/F-SL] and maltotetraose were more targeted. For the former, it suggests that the increased reactivity observed with both IgA subclasses combined could be attributed to IgA2 reactivity. Maltotetraose, a common plasma glycopeptide, also characterizes starch-degrading bacteria (39) and its targeting could participate in the dysregulation of commensal homeostasis. Oppositely, Neu5Ac-2,3-Gal-1,4-Glc, which was previously significantly less targeted by all IgA combined in CD, was again less bound by CD IgA2, suggesting this decreased reactivity could be attributed to IgA2.

On the other hand, UC IgA2 again presented a loss of reactivity towards more that 40 glycans structures (**Fig. 10B, C**). Overall, these results highlight distinct reactivity profile for CD and UC IgA, with the latter displaying a general loss of affinity towards common glycans.

Discussion

We aimed at assessing the impact of structural and functional SIgA defects in IBD. We have previously shown that human SIgA2 but not SIgA1 had different functional abilities (ref), and notably highlighted that CD patients had higher levels of IgA RT (Papier NR Crohn). The present study shows distinct SIg profiles for CD and UC. UC patients had lower stool IgA concentrations, no ability to perform RT and generally targeted less antigens than CD or control samples, generally arguing for functional losses in UC secretory immunity. To our knowledge, such alterations have not been described yet. On the other hand, CD stool SIgA seemed to have gained functions, as both IgA1 and IgA2 underwent high rates of RT, were more reactive to common glycan motifs, and were generally more N-glycosylated. This is consistent with preexisting data showing that IgA1, because it is mostly O-glycosylated and not N-glycosylated, cannot bind RT receptors Dectin-1 (11), and thus does not undergo RT in healthy individuals.

Our results also demonstrate a clear pattern of IgA1-associated selection of the microbiota in CD that could contribute to the establishment and/or the maintenance of dysbiosis (**Fig. 3D, Table 1**). Loss of *Faecalibacterium*, especially *Faecalibacterium prausnitzii*, is critically associated with CD and its severity (16,26,29). Its enrichment in the $IgA1^{+}$ fraction of CD patients' microbiota suggests that IgA1 identification is pathogenic, and could contribute to its elimination, possibly through neutralization. *Anaerostipes, Bifidobacterium,* and *Peptostreptococcaceae*, which were also enriched in that fraction decreased in treatment naïve CD patients (40), further suggesting that IgA1 selection contributes to the elimination of beneficial taxa. Here we also highlight that IgA2, while not displaying an overall altered microbial profile can influence the onset of flares, as the loss of *Bifidobacterium* selection was associated with quiescent disease, suggesting IgA2-binding also has pathogenic potential that may be drowned in the overall signals when the analysis comprises all patients.

In terms of general *in situ* abundance, *Prevotella* specieswere less represented in active disease biopsies; they areassociated to Th17-oriented diseases (41), which CD also qualifies as, in that they promote Th17 inflammation through pathways that are still unclear (42). Our observation thus suggests latent pro-inflammatory microbial expansion that might promote flares However, there was also a decrease in *Colinsella* abundance in biopsies from quiescent disease patients, while these species were shown to be decreased in CD (40). These results were obtained from stool samples, whereas ours were observed directly in the mucosa : *Colinsella* could be decreased in stool simply because they retain better adherence to the colonic mucus in CD.

A caveat of our study is that while we separated IgA1- from IgA2-bound microbiota, flow cytometry analysis showed that IgA1 was mostly found in dual binding with IgA2, suggesting a large portion of that $IgA1^+$ fraction may actually be $IgA1^+ IgA2^+$. This separation thus at least gets rid of the $IgA1^-IgA2^+$ fraction, and shows that IgA1 binding effectively shifts commensal selection in CD. On the other hand, IgA2 separation only gets rid of the $IgA1^+IgA2^-$, which is minimal as shown by flow cytometry. In this Ig-bound fraction, few discrepancies were noted between CD and non-IBD samples, suggesting this lost $IgA1^+$ fraction of the microbiota might still represent the driving force behind the aforementioned alterations. Previous work on stool anti-commensal IgA1 and IgA2 in healthy individuals showed that IgA1 and IgA2 dual opsonization of the microbiota tends to segregate Actinobacteria, whereas IgA2 identification mostly promotes *Bacteroidetes* selection (6). In this study, the authors also showed that IgA1 preferentially induce an IL-10 oriented micro-environment suggesting steady state IgA1 secretion in the gut promotes tolerance to commensals. Our own results thus propose that this property might be abrogated over the course of CD, either as the cause or the consequence of disorganized commensal selection. Indeed, the elimination of SCFA producers is known to promote cytokine imbalance that favors inflammatory responses (1). Moreover, the loss of Proteobacteria selection in both $IgA1^+$ and $IgA2^+$ fractions of CD microbiota suggests that opportunistic species are no longer controlled by SIgA and might support the maintenance of dysbiosis.

In UC, Ig-microbiota alterations were less obvious, despite distinct profiles from CD: there was a differential but not significant enrichment in the IgA1 fraction for three *Ruminicoccaceae* species, unknown *Anaerotruncus* and *Ruminiclostridium* species and *Massilioclostridium coli*. *Ruminococcus* abundance is generally positively associated to T_{reg} levels (43) but species like *Ruminococcus gnavus* produce a pro-inflammatory polysaccharidic capsules, suggesting glycan reactivity might indeed trigger inflammatory cascades (44), and that IgA1 could lose its tolerogenic properties by actively targeting these species. *Ruminiclostridium* colonization was shown to re-merge after treatment intervention with 5-ASA (45) and generally argues for the re-emergence of *Firmicutes* as a positive marker for therapeutic success. Here, IgA1 identification of these taxa once again enforces that the binding becomes pathogenic over the course of UC. Moreover, one *Bacteroides* was also specifically enriched in the IgA2-fraction of the microbiota, suggesting that IgA2 contributes to *Bacteroidetes* elimination, and IgA1 to that of *Firmicutes*, in UC. Specific functional defects that are directly attributed to SIgA physiology in the gut in both diseases were also observed. Under homeostatic conditions, only

IgA2 is able to transport immune complexes within M cells and towards DC of the PP in healthy individuals. In CD patients, SIgA1 has gained RT abilities, which correlates with the strength of Dectin-1 binding. As this interaction relies on N-glycosylation and sialic acid enrichment (11), we believe that CD IgA1 undergoes extensive dysfunctional post-traductional modifications. Oppositely, all transport, either by IgA1 or IgA2, was inexistent when we tested UC fecal Igs. To our knowledge, no data exist regarding such alterations in IBD, and they suggest that CD inflammation might be driven by increased transport of immune complexes, while UC inflammation might be attributed to their absence. Consequently, IgA1 and IgA2 in CD had an overall increased reactivity towards common glycans, suggesting autoimmune features that might be related to other Th17-oriented disease. UC IgAs, on the other hand, presented a general loss of reactivity, implying defects that impact antigen as well as receptor recognition. In the absence of IgA-induced tolerogenic signals, immune equilibrium could thus break resulting in typical Th2 inflammation in UC. In healthy individuals, IgA2 tends to favor the selection of terminal αGal and Neu5Ac motifs (6), which was not the case either in the CD or in the UC cohorts.

Maltotetraose is abnormally elevated in cases of Pompe disease (46), a genetic defect in the enzyme that converts glycogen into glucose, and its increased targeting by CD IgA2 suggests IgA2-driven dysregulation of glucose metabolism at the mucosal level. Maltotetraose also inhibits TNF-α-induced expression of intercellular adhesion molecule-1 (ICAM-1) in mouse smooth muscle cells (VSMCs) transfected with an ICAM-1 reporter (47). This posits that neutralization by IgA2 in the gut would amplify TNF-α signaling and immune effectors recruitment, thusly maintaining the inflammatory loop.

Sisomicin sulfate tended to be over selected by CD IgA (**Suppl. Table 3**); it is an aminoglycoside antibiotic generally isolated from *Micronopora inyoensis*, and is effective against several *Klebsiella E. coli, P. aeruginosa, Enterobacter* species, and *Pseudomonas,* all of which being opportunistic species belonging to Proteobacteria (48,49). IgA targeting of this regulatory glycan would thus affect the overall ecology of the commensal microbiota. Moreover, several of the significantly less targeted glycans are found in pathogenic species: the Gal-1,4-Gal-1,4-Glc motif is borne by *H. influenzae* glycans and normally recognized by agglutinins.(50). This suggests inadequate responses towards pathogens.

Most of the differentially targeted glycans were sialylated antigens; increased reactivity towards these motifs, given they are also recognized by Siglecs at the apical membrane of M cells (11), could participate in the enhanced reverse-transcytosis observed in CD (Ref NR Crohn). The rest of these antigens were natural oligosaccharides, blood antigens or milk polysaccharides,

suggesting both altered self-reactivity and reactivity towards dietary antigens, which could explain the auto-immune features observed in CD. The loss of reactivity for UC IgA, regardless of subclass, demonstrates a clear loss in functionality in the mucosal compartment, distinctive from our observations in CD.

Those results remain preliminary, and would of course benefit from a larger cohort, which we are currently working on.

Although CD and UC are classified together as IBD, they not only present very different physiological features, but also distinct immune responses. In this study, we observe that dysbiosis in both diseases might also have different causes, namely that CD seems to have gained inflammatory properties towards the microbiota, whereas UC appears to have lost its regulatory potential. Both these assumptions could correlate with immune profiles currently accepted as representative of both diseases: CD is mostly Th1/Th17-oriented whereas UC is mostly Th2-oriented. Such cellular responses are consistent with these humoral defects and more investigation on the pathways involved in the communication between these two compartments of adaptive immunity in IBD should be envisioned. Our observations could also explain the extreme variability in outcomes after fecal transplants trials in CD.(51,52) In UC however, fecal transplants seem to get better results(51,53,54). Taking our findings into account, the lack of immune secretory response to the microbiota could provide a favorable terrain for engraftment, but correlates with the observation that UC patients do not present lasting engraftments and will eventually lose beneficial taxa over time. These findings thus offer new directions on the design of new therapeutic strategies, for example by specifically blocking IgA RT to lower the inflammatory burden during acute episodes.

Aknowledgment

We would like to thank Blaise Corthésy for the use of his reagents, and Mélanie Dhayer for her extensive help in the setting up of confocal microscopy observations.

This work is funded by the ARC1-Santé grant of the Région Rhone-Alpes and by the MSD-Avenir grant.

Author Contributions.

EM, FJ, BC, AP, CG, KB, MM performed the experiments. EM, MM, PG performed the analysis. EM, NR, SP, PG, and XR wrote the manuscript.

The authors declare no conflicts of interests.

Figure legends

Figure 1 – Fecal IgA levels distinguish CD from UC but are not affected by disease status

ELISA assay of fecal IgA1 (**A**), IgA2 (**B**), total IgA (**C**), and secretory component (**D**) levels from non-IBD (n= 7), CD (n=18), and UC (n=12) patients' stool. Data were further separated according to disease activity for IgA1 (**E**) and IgA2 (**F**).

All data were analyzed using the Kruskall-Wallis test. * : p-value < 0,05; **: p-value < 0,01.

Figure 2 – Ig-bound bacteria are mostly $IgA1^+$ $IgA2^+$ in IBD and non-IBD stool.

Flow cytometry analysis of total IgA1-bound (**A**) and IgA2-bound (**B**) fecal microbiota. (**C)** Flow cytometry analysis of stool $IgA1^+$ $IgA2^-$ bacteria (grey dots), $IgA1^-$ $IgA2^+$ bacteria (black dots) and $IgA1^+$ $IgA2^+$ bacteria (empty dots). (**D**) Flow cytometry analysis of total $IgA1^+$ $IgA2^-$ bound bacteria according to disease status at the time of collection (**E**) Flow cytometry analysis of total $IgA1^-$ $IgA2^+$ bound bacteria according to disease status at the time of collection. (**F)** Flow cytometry analysis of $IgA1^+$ $IgA2^+$ bacteria according to disease status at the time of collection. Data were analyzed using the Kruskall-Wallis test. * : p-value < 0,05

Non-IBD : n= 7, CD : n= 18 ; UC : n=12.

Figure 3 – CD IgA1 displays biased selectivity towards beneficial members of the commensal microbiota.

(**A**) Shannon and Chao1 diversity indices of IgA1-bound microbiota in Control, CD and UC. (**B**) PCoA plot based on the Jaccard distance between samples. (**C**) Phylum-level composition of IgA1-bound microbiota in Control, CD and UC. (**D**) Boxplots of OTUs whose abundance was significantly different between Control and CD. OTUs present in less than 25% of samples or with read count lower than 50 were filtered out. Differential abundance was tested using negative binomial model implemented in DESeq2 and p-values corrected with False Discovery Rate (FDR) procedure.

Figure 4 – IgA2-driven selection of the microbiota presents less alterations than that of IgA1 in IBD.

(**A**) Shannon and Chao1 diversity indices of IgA1-bound microbiota in Control, CD and UC. (**B**) PCoA plot based on the Jaccard distance between samples. (**C**) Phylum-level composition of IgA1-bound microbiota in Control, CD and UC. (**D**) Boxplots of OTUs whose abundance was significantly different between CD and UC, and between Control and UC, respectively..

OTUs present in less than 25% of samples or with read count lower than 50 were filtered out. Differential abundance was tested using negative binomial model implemented in DESeq2 and p-values corrected with False Discovery Rate (FDR) procedure.

Figure 5 – CD IgA2 displays biased selectivity in active CD patients.

(**A**) Combined FISH-IF stainings for each probe. (**B**) Total fluorescence detected per probe and per biopsy. (**C**) Percent of co-occured IgA2 and FISH-bound particles.

* : p-value < 0,05 (Two-Way ANOVA). Active CD : n= 6 ; Inactive CD : n=4.

Figure 6 – Purified fecal IgA1 and IgA2 from IBD patients have altered functionality.

In vitro assay of Ipurified gA1 (**A**) and IgA2 (**B**) reverse-tanscytosis abilities on an inverted model of FAE from Caco2 and Raji cells co-culture. (**C**) ELISA assay of IgA1-Dectin-1 binding, at a rate of one receptor per 10 IgA; (**D**) ELISA assay of IgA1-Dectin-1 binding, at a rate of one receptor per 10 IgA; (**E**) Immunofluorescent staining of IgA1 (green, AF-488) binding to Dectin-1 (AF-555, red) on transformed Hela cells ; (**F**) ELISA assay of IgA2-Dectin-1 binding, at a rate of one receptor per 10 IgA; Non-IBD : n= 6; CD : n= 8 ; UC : n=5. All data were analyzed using the Kruskall-Wallis test. * : p-value < 0,05.

Figure 7 – Strong Dectin-1 binding correlates with increased IgA reverse-transcytosis in CD.

Percent of IgA1 (**A, B**) and IgA2 (**C, D**) reverse-transcytosis for weak (**A, C**) and strong (**B, D**) Dectin-1 binding. Of note, there were no UC IgA1 strong binders. Data were analyzed using the Kruskall-Wallis test when possible, or the Mann-Whitney test. * : p-value < 0,05. Non-IBD : n= 6; CD : n= 8 ; UC : n=5.

Figure 8 – IgA1 and IgA2 from IBD patients have distinct N-glycosylation profiles.

(**A**) Number of O-glycosylation motifs on IgA1 hinge region (**B**)) Number of N-glycosylation motifs on IgA1 (left) and IgA2 (right) wherein N131/144 and N340/327 overlap (**C**) Composition in N-glycosylation motifs on IgA1 at N131/144 and N340/327. (**D**) Composition in N-glycosylation motifs on IgA2. Data were analyzed using the Kruskall-Wallis test. * : p-value < 0,05

CD : n= 5 ; UC : n=3.

Figure 9 – CD and UC IgA1 have distinct reactivity profiles towards common glycans.

CD (**A**) and UC (**B**) fold change reactivity compared to non-IBD IgA1. (**C**) Relative fluorescence intensity (arbitrary units) over glycan-100 arrays.

* : p-value < 0,05

Non-IBD : n= 6; CD : n= 6 ; UC : n= 6.

Figure 10 – IgA2 reactivity to towards common glycan mirrors that of IgA1 in IBD.

CD (**A**) and UC (**B**) fold change reactivity compared to non-IBD IgA1. (**C**) Relative fluorescence intensity (arbitrary units) over glycan-100 arrays.

* : p-value < 0,05

Non-IBD : n= 6; CD : n= 6 ; UC : n= 6.

Supp. Fig. 2 – Detailed phylum composition in $IgA1^+$ and $IgA2^+$ fraction of the microbiota

(**A**) Proteobacteria composition in the $IgA1^+$ fraction, (**B**) Bacteroidete composition in the $IgA1^+$ fraction (**C**) Proteobacteria composition in the $IgA2^+$ fraction (**D**) Bacteroidete composition in the $IgA2^+$ fraction.

Supp. Fig. 3 – Comparison of weak and strong IgA binders RT within non-IBD and IBD groups

(**A**) Percentage of RT in Non-IBD weak (left) and strong (right) IgA1 and IgA2 binders (**B**) Percentage of RT in CD weak (left) and strong (right) IgA1 and IgA2 binders (**C**) Percentage of RT in UC weak (left) and strong (right) IgA1 and IgA2 binders

Supp. Fig. 4 – Principal component analysis of IgA reactivity towards common glycans

Principal component analysis on (**A**) All IgA, (**B**) IgA1, and (**C**) IgA2, purified from patients' stool and tested for glycan reactivity on glycan micro-arrays. (**A-C**) Changes in the shape of data points indicate a different micro-array plate. (**D**) CD and (**E**) UC fold change in the reactivity towards Glycan-100 compared to non-IBD IgA.

References

1. Bhaskaran N, Quigley C, Paw C, Butala S, Schneider E, Pandiyan P. Role of Short Chain Fatty Acids in Controlling Tregs and Immunopathology During Mucosal Infection. Front Microbiol. 2018;9:1995.
2. Rios D, Wood MB, Li J, Chassaing B, Gewirtz AT, Williams IR. Antigen sampling by intestinal M cells is the principal pathway initiating mucosal IgA production to commensal enteric bacteria. Mucosal Immunol. 2016;9(4):907-16.
3. Mathias A, Pais B, Favre L, Benyacoub J, Corthésy B. Role of secretory IgA in the mucosal sensing of commensal bacteria. Gut Microbes. 2014;5(6):688-95.
4. Perrier C, Sprenger N, Corthésy B. Glycans on secretory component participate in innate protection against mucosal pathogens. J Biol Chem. 19 mai 2006;281(20):14280-7.
5. Rollenske T, Szijarto V, Lukasiewicz J, Guachalla LM, Stojkovic K, Hartl K, et al. Cross-specificity of protective human antibodies against Klebsiella pneumoniae LPS O-antigen. Nat Immunol. 2018;19(6):617-24.
6. Sterlin D, Fadlallah J, Adams O, Fieschi C, Parizot C, Dorgham K, et al. Human IgA binds a diverse array of commensal bacteria. J Exp Med. 2 mars 2020;217(3).
7. Brandtzaeg P. Transport models for secretory IgA and secretory IgM. Clin Exp Immunol. mai 1981;44(2):221-32.
8. Novak J, Julian BA, Mestecky J, Renfrow MB. Glycosylation of IgA1 and pathogenesis of IgA nephropathy. Semin Immunopathol. mai 2012;34(3):365-82.
9. Ohyama Y, Yamaguchi H, Nakajima K, Mizuno T, Fukamachi Y, Yokoi Y, et al. Analysis of O -glycoforms of the IgA1 hinge region by sequential deglycosylation. Sci Rep. 20 janv 2020;10(1):1-11.
10. Steffen U, Koeleman CA, Sokolova MV, Bang H, Kleyer A, Rech J, et al. IgA subclasses have different effector functions associated with distinct glycosylation profiles. Nat Commun. 8 janv 2020;11(1):1-12.

11. Rochereau N, Drocourt D, Perouzel E, Pavot V, Redelinghuys P, Brown G, et al. Dectin-1 Is Essential for Reverse Transcytosis of Glycosylated SIgA-Antigen Complexes by Intestinal M Cells. Plos Biol. 2013;11(9):e1001658.
12. Nakajima A, Vogelzang A, Maruya M, Miyajima M, Murata M, Son A, et al. IgA regulates the composition and metabolic function of gut microbiota by promoting symbiosis between bacteria. J Exp Med. 06 2018;215(8):2019-34.
13. Wang G, Huang S, Wang Y, Cai S, Yu H, Liu H, et al. Bridging intestinal immunity and gut microbiota by metabolites. Cell Mol Life Sci CMLS. oct 2019;76(20):3917-37.
14. Benus RFJ, van der Werf TS, Welling GW, Judd PA, Taylor MA, Harmsen HJM, et al. Association between Faecalibacterium prausnitzii and dietary fibre in colonic fermentation in healthy human subjects. Br J Nutr. sept 2010;104(5):693-700.
15. Duncan SH, Hold GL, Barcenilla A, Stewart CS, Flint HJ. Roseburia intestinalis sp. nov., a novel saccharolytic, butyrate-producing bacterium from human faeces. Int J Syst Evol Microbiol. sept 2002;52(Pt 5):1615-20.
16. Joossens M, Huys G, Cnockaert M, De Preter V, Verbeke K, Rutgeerts P, et al. Dysbiosis of the faecal microbiota in patients with Crohn's disease and their unaffected relatives. Gut. mai 2011;60(5):631-7.
17. Ni J, Wu GD, Albenberg L, Tomov VT. Gut microbiota and IBD: causation or correlation? Nat Rev Gastroenterol Hepatol. oct 2017;14(10):573-84.
18. Huibregtse IL, van Lent AU, van Deventer SJH. Immunopathogenesis of IBD: insufficient suppressor function in the gut? Gut. avr 2007;56(4):584-92.
19. Pascal V, Pozuelo M, Borruel N, Casellas F, Campos D, Santiago A, et al. A microbial signature for Crohn's disease. Gut. 18 janv 2017;gutjnl-2016-313235.

687 20. Fuentes S, Rossen NG, van der Spek MJ, Hartman JH, Huuskonen L, Korpela K, et al.
688 Microbial shifts and signatures of long-term remission in ulcerative colitis after faecal
689 microbiota transplantation. ISME J. 2017;11(8):1877-89.
690 21. Mariat D, Firmesse O, Levenez F, Guimarães V, Sokol H, Doré J, et al. The
691 Firmicutes/Bacteroidetes ratio of the human microbiota changes with age. BMC
692 Microbiol. 9 juin 2009;9:123.
693 22. Ni J, Wu GD, Albenberg L, Tomov VT. Gut microbiota and IBD: causation or
694 correlation? Nat Rev Gastroenterol Hepatol. oct 2017;14(10):573-84.
695 23. Yamada T, Hino S, Iijima H, Genda T, Aoki R, Nagata R, et al. Mucin O-glycans
696 facilitate symbiosynthesis to maintain gut immune homeostasis. EBioMedicine. 1 oct
697 2019;48:513-25.
698 24. Rengarajan S, Vivio EE, Parkes M, Peterson DA, Roberson EDO, Newberry RD, et al.
699 Dynamic immunoglobulin responses to gut bacteria during inflammatory bowel disease.
700 Gut Microbes. 16 juin 2019;1-16.
701 25. Quévrain E, Maubert MA, Michon C, Chain F, Marquant R, Tailhades J, et al.
702 Identification of an anti-inflammatory protein from Faecalibacterium prausnitzii, a
703 commensal bacterium deficient in Crohn's disease. Gut. mars 2016;65(3):415-25.
704 26. Yilmaz B, Juillerat P, Øyås O, Ramon C, Bravo FD, Franc Y, et al. Microbial network
705 disturbances in relapsing refractory Crohn's disease. Nat Med. févr 2019;25(2):323-36.
706 27. Takahashi K, Nishida A, Fujimoto T, Fujii M, Shioya M, Imaeda H, et al. Reduced
707 Abundance of Butyrate-Producing Bacteria Species in the Fecal Microbial Community
708 in Crohn's Disease. Digestion. 2016;93(1):59-65.
709 28. Liu T-C, Gurram B, Baldridge MT, Head R, Lam V, Luo C, et al. Paneth cell defects in
710 Crohn's disease patients promote dysbiosis. JCI Insight. 02 2016;1(8):e86907.

29. Machiels K, Joossens M, Sabino J, De Preter V, Arijs I, Eeckhaut V, et al. A decrease of the butyrate-producing species Roseburia hominis and Faecalibacterium prausnitzii defines dysbiosis in patients with ulcerative colitis. Gut. août 2014;63(8):1275-83.
30. Mirsepasi-Lauridsen HC, Vrankx K, Engberg J, Friis-Møller A, Brynskov J, Nordgaard-Lassen I, et al. Disease-Specific Enteric Microbiome Dysbiosis in Inflammatory Bowel Disease. Front Med. 2018;5:304.
31. Lopez-Siles M, Enrich-Capó N, Aldeguer X, Sabat-Mir M, Duncan SH, Garcia-Gil LJ, et al. Alterations in the Abundance and Co-occurrence of Akkermansia muciniphila and Faecalibacterium prausnitzii in the Colonic Mucosa of Inflammatory Bowel Disease Subjects. Front Cell Infect Microbiol. 2018;8:281.
32. den Besten G, van Eunen K, Groen AK, Venema K, Reijngoud D-J, Bakker BM. The role of short-chain fatty acids in the interplay between diet, gut microbiota, and host energy metabolism. J Lipid Res. sept 2013;54(9):2325-40.
33. Moor K, Diard M, Sellin ME, Felmy B, Wotzka SY, Toska A, et al. High-avidity IgA protects the intestine by enchaining growing bacteria. Nature. avr 2017;544(7651):498-502.
34. Moor K, Fadlallah J, Toska A, Sterlin D, Balmer M, Macpherson A, et al. Analysis of bacterial-surface-specific antibodies in body fluids using bacterial flow cytometry. Nat Protoc. 2016;11(8):1531-53.
35. Lemaire M, Dou S, Cahu A, Formal M, Le Normand L, Romé V, et al. Addition of dairy lipids and probiotic Lactobacillus fermentum in infant formula programs gut microbiota and entero-insular axis in adult minipigs. Sci Rep. 3 août 2018;8(1):1-16.
36. Escudié F, Auer L, Bernard M, Mariadassou M, Cauquil L, Vidal K, et al. FROGS: Find, Rapidly, OTUs with Galaxy Solution. Bioinforma Oxf Engl. 15 2018;34(8):1287-94.

735 37. Safari Z, Bruneau A, Monnoye M, Mariadassou M, Philippe C, Zatloukal K, et al.
736 Murine Genetic Background Overcomes Gut Microbiota Changes to Explain Metabolic
737 Response to High-Fat Diet. Nutrients. 21 janv 2020;12(2).
738 38. Sialic Acid Derivative - an overview | ScienceDirect Topics [Internet]. [cité 22 mars
739 2020]. Disponible sur: https://www.sciencedirect.com/topics/neuroscience/sialic-acid-
740 derivative
741 39. Yan Z, She X, Li M, Zhang S. Screening of bacterial strains producing maltotetraose-
742 forming amylase and the conditions for enzyme production. Chin J Biotechnol.
743 1992;8(3):211-8.
744 40. Gevers D, Kugathasan S, Denson LA, Vázquez-Baeza Y, Van Treuren W, Ren B, et al.
745 The treatment-naive microbiome in new-onset Crohn's disease. Cell Host Microbe. 12
746 mars 2014;15(3):382-92.
747 41. Larsen JM. The immune response to Prevotella bacteria in chronic inflammatory disease.
748 Immunology. 1 août 2017;151(4):363-74.
749 42. Grosserichter-Wagener C, Radjabzadeh D, van der Weide H, Smit KN, Kraaij R, Hays
750 JP, et al. Differences in Systemic IgA Reactivity and Circulating Th Subsets in Healthy
751 Volunteers With Specific Microbiota Enterotypes. Front Immunol [Internet]. 2019 [cité
752 9 janv 2020];10. Disponible sur:
753 https://www.frontiersin.org/articles/10.3389/fimmu.2019.00341/full
754 43. Shimizu J, Kubota T, Takada E, Takai K, Fujiwara N, Arimitsu N, et al. Propionate-
755 producing bacteria in the intestine may associate with skewed responses of IL10-
756 producing regulatory T cells in patients with relapsing polychondritis. PLoS ONE
757 [Internet]. 20 sept 2018 [cité 9 mars 2020];13(9). Disponible sur:
758 https://www.ncbi.nlm.nih.gov/pmc/articles/PMC6147427/

759 44. Henke MT, Kenny DJ, Cassilly CD, Vlamakis H, Xavier RJ, Clardy J. Ruminococcus
760 gnavus, a member of the human gut microbiome associated with Crohn's disease,
761 produces an inflammatory polysaccharide. Proc Natl Acad Sci U S A. 25 juin
762 2019;116(26):12672-7.
763 45. Xu J, Chen N, Wu Z, Song Y, Zhang Y, Wu N, et al. 5-Aminosalicylic Acid Alters the
764 Gut Bacterial Microbiota in Patients With Ulcerative Colitis. Front Microbiol [Internet].
765 13 juin 2018 [cité 9 mars 2020];9. Disponible sur:
766 https://www.ncbi.nlm.nih.gov/pmc/articles/PMC6008376/
767 46. An Y, Young SP, Kishnani PS, Millington DS, Amalfitano A, Corz D, et al. Glucose
768 tetrasaccharide as a biomarker for monitoring the therapeutic response to enzyme
769 replacement therapy for Pompe disease. Mol Genet Metab. août 2005;85(4):247-54.
770 47. Shin SY, Jung YJ, Yong Y, Cho HJ, Lim Y, Lee YH. Inhibition of PDGF-induced
771 migration and TNF-α-induced ICAM-1 expression by maltotetraose from bamboo stem
772 extract (BSE) in mouse vascular smooth muscle cells. Mol Nutr Food Res.
773 2016;60(9):2086-97.
774 48. Waitz JA, Moss EL, Drube CG, Weinstein MJ. Comparative Activity of Sisomicin,
775 Gentamicin, Kanamycin, and Tobramycin. Antimicrob Agents Chemother. 1 déc
776 1972;2(6):431-7.
777 49. Stewart D, Bodey GP. IN VITRO ACTIVITY OF SISOMICIN, AN
778 AMINOGLYCOSIDE ANTIBIOTIC, AGAINST CLINICAL ISOLATES. J Antibiot
779 (Tokyo). 1975;28(2):149-55.
780 50. Kalograiaki I, Euba B, Fernández-Alonso M del C, Proverbio D, Geme JWS, Aastrup T,
781 et al. Differential recognition of Haemophilus influenzae whole bacterial cells and
782 isolated lipooligosaccharides by galactose-specific lectins. Sci Rep. 2 nov
783 2018;8(1):1-12.

51. Allegretti J, Eysenbach LM, El-nachef N, Fischer M, Kelly C, Kassam Z. The Current Landscape and Lessons from Fecal Microbiota Transplantation for Inflammatory Bowel Disease: Past, Present, and Future. Inflamm Bowel Dis. 1 oct 2017;23(10):1710-7.
52. Bak SH, Choi HH, Lee J, Kim MH, Lee YH, Kim JS, et al. Fecal microbiota transplantation for refractory Crohn's disease. Intest Res. avr 2017;15(2):244-8.
53. Ishikawa D, Sasaki T, Takahashi M, Kuwahara-Arai K, Haga K, Ito S, et al. The Microbial Composition of Bacteroidetes Species in Ulcerative Colitis Is Effectively Improved by Combination Therapy With Fecal Microbiota Transplantation and Antibiotics. Inflamm Bowel Dis. 29 2018;24(12):2590-8.
54. Shi Y, Dong Y, Huang W, Zhu D, Mao H, Su P. Fecal Microbiota Transplantation for Ulcerative Colitis: A Systematic Review and Meta-Analysis. PloS One. 2016;11(6):e0157259.

797

798

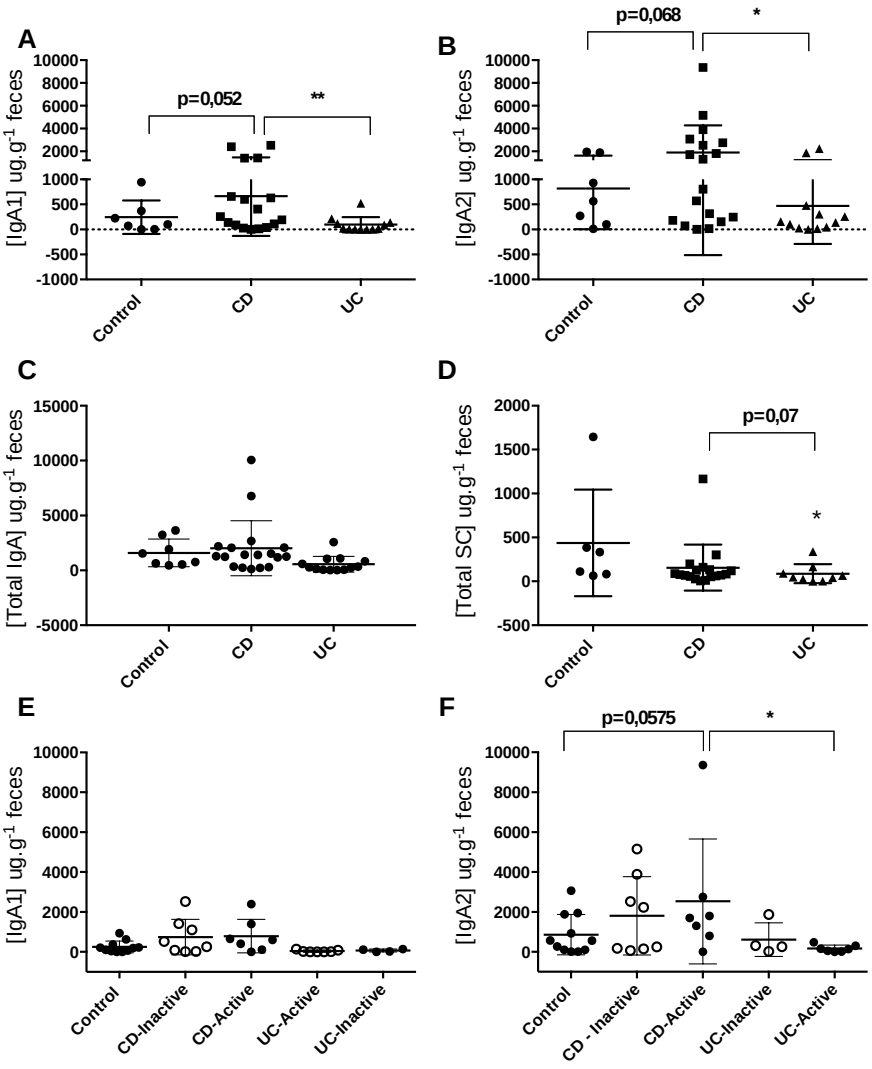
A
[IgA1] ug.g-1 feces
p=0,052
**
Control
CD
UC
B
[IgA2] ug.g-1 feces
p=0,068
*
C
[Total IgA] ug.g-1 feces
D
[Total SC] ug.g-1 feces
p=0,07
*
E
[IgA1] ug.g-1 feces
Control
CD-Inactive
CD-Active
UC-Active
UC-Inactive
F
[IgA2] ug.g-1 feces
p=0,0575
*
CD - Inactive
UC-Inactive
UC-Active

Fig. 1

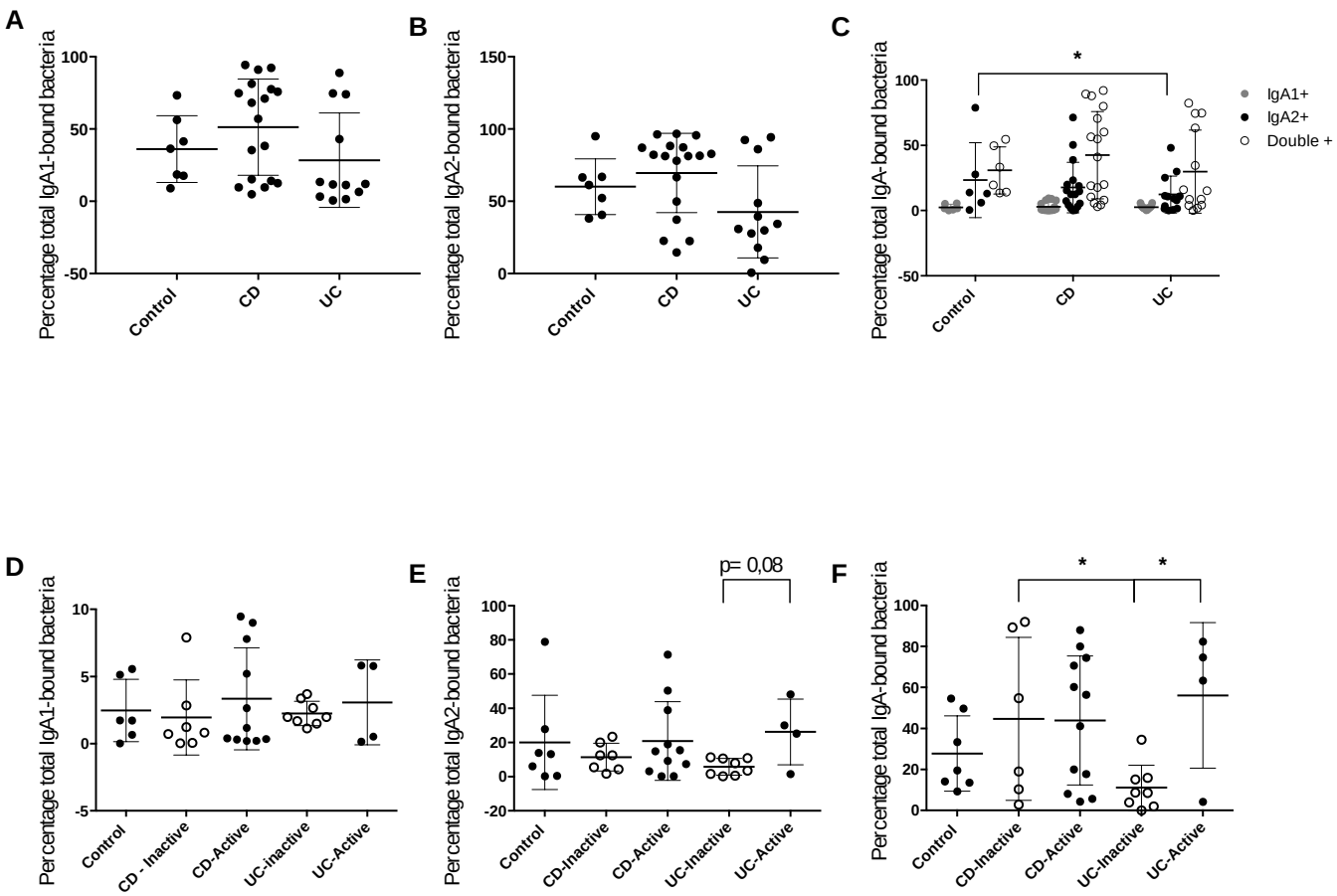
A
Percentage total IgA1-bound bacteria
100
50
0
-50
Control
CD
UC
B
Percentage total IgA2-bound bacteria
150
100
50
0
Control
CD
UC
C
Percentage total IgA-bound bacteria
*
100
50
0
-50
Control
CD
Uc
IgA1+
IgA2+
Double +
D
Percentage total IgA1-bound bacteria
10
5
0
-5
Control
CD - Inactive
CD-Active
UC-inactive
UC-Active
E
p= 0,08
Percentage total IgA2-bound bacteria
100
80
60
40
20
0
-20
Control
CD-Inactive
CD-Active
UC-Inactive
UC-Active
F
* *
Percentage total IgA-bound bacteria
100
80
60
40
20
0
Control
CD-Inactive
CD-Active
UC-Inactive
UC-Active

Fig. 2

800

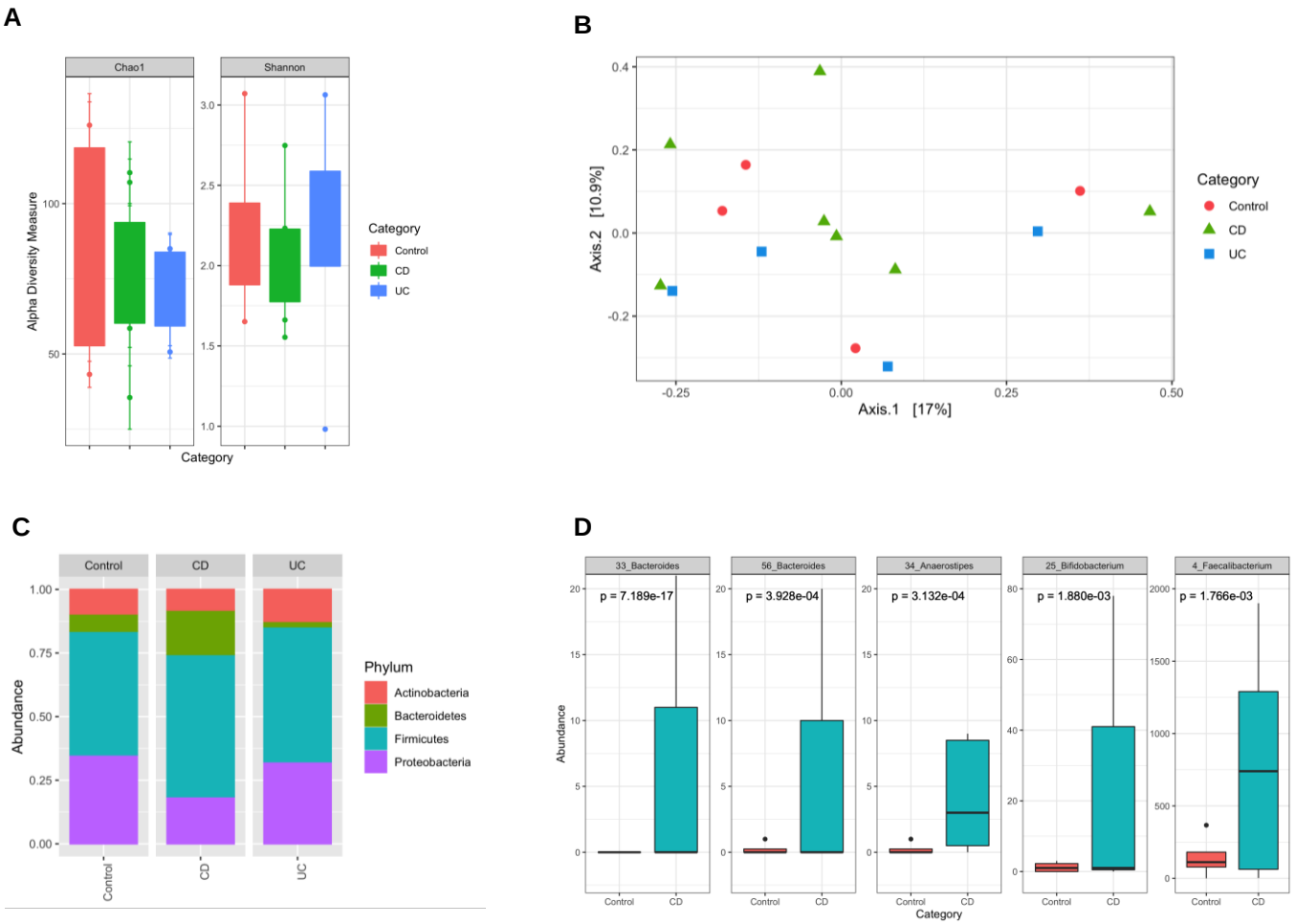
A
Chao1
Shannon
Alpha Diversity Measure
Category
Control
CD
UC
B
Axis.2 [10.9%]
Axis.1 [17%]
Category
Control
CD
UC
C
Control
CD
UC
Abundance
Phylum
Actinobacteria
Bacteroidetes
Firmicutes
Proteobacteria
D
33_Bacteroides
56_Bacteroides
34_Anaerostipes
25_Bifidobacterium
4_Faecalibacterium
p = 7.189e-17
p = 3.928e-04
p = 3.132e-04
p = 1.880e-03
p = 1.766e-03
Abundance
Category

Fig. 3

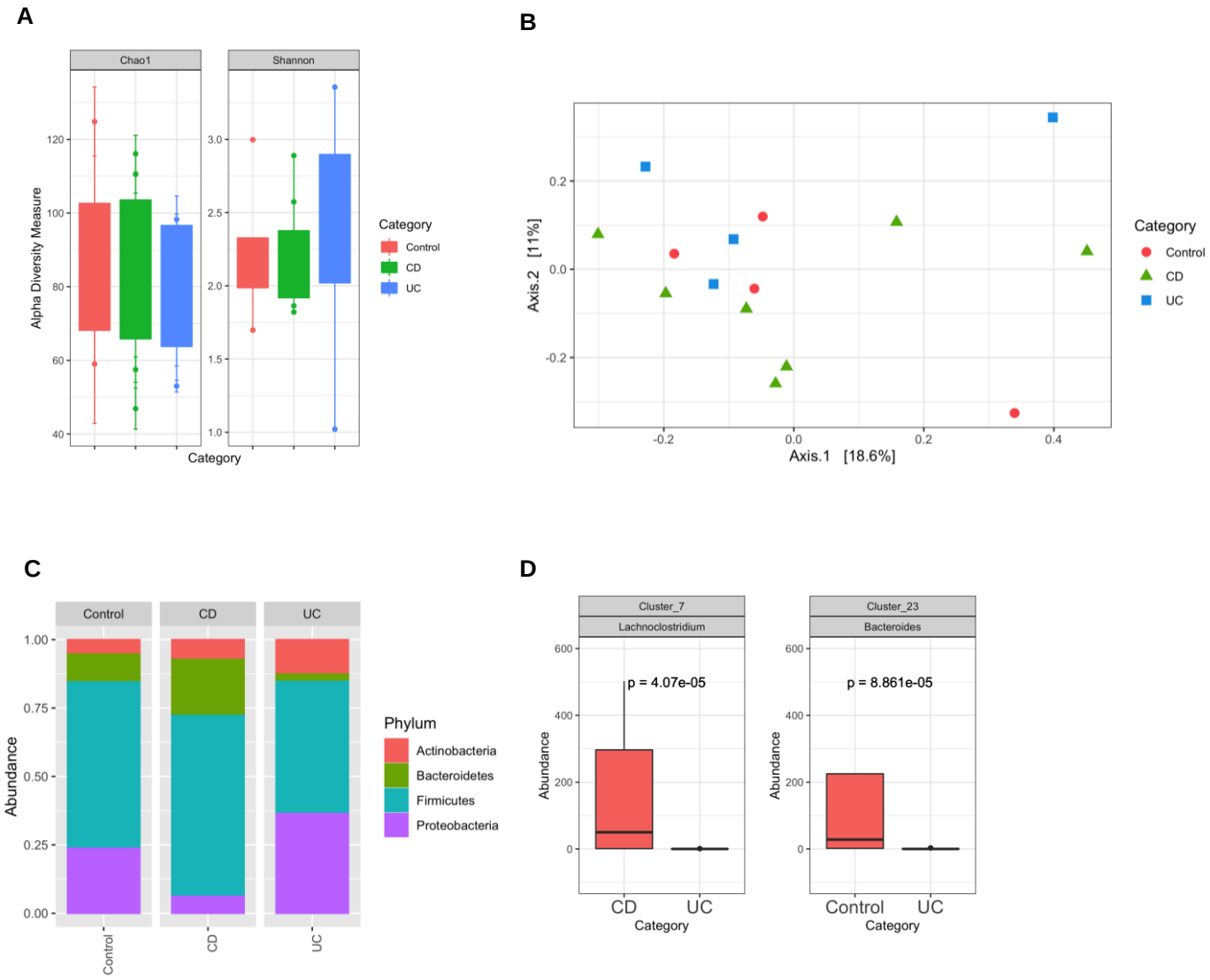
A
Chao1
Shannon
Alpha Diversity Measure
Category
Control
CD
UC
B
Axis.2 [11%]
Axis.1 [18.6%]
Category
Control
CD
UC
C
Control
CD
UC
Abundance
Phylum
Actinobacteria
Bacteroidetes
Firmicutes
Proteobacteria
D
Cluster_7
Lachnoclostridium
p = 4.07e-05
Cluster_23
Bacteroides
p = 8.861e-05
Abundance
CD
UC
Control
Category

Fig. 4

801

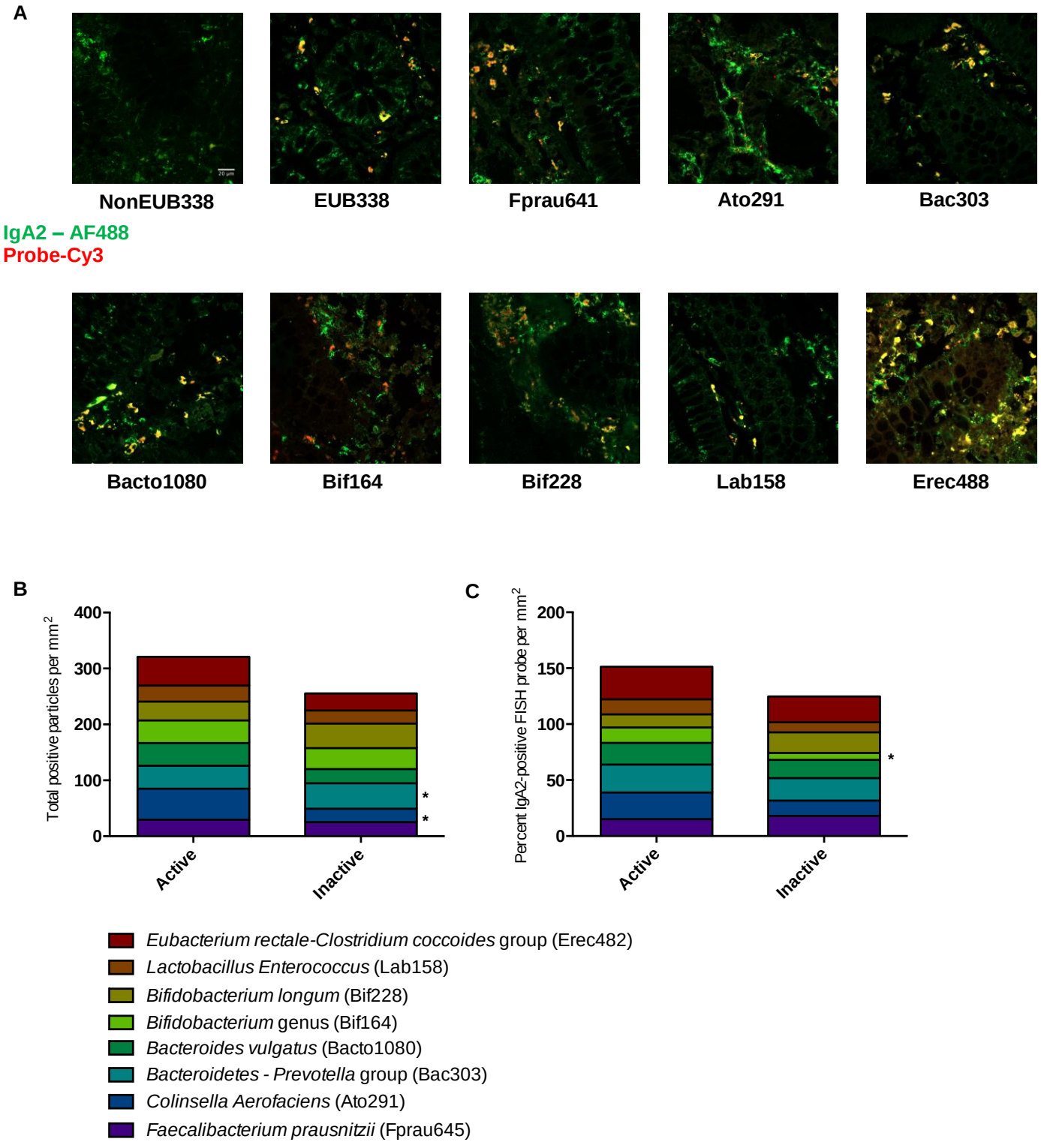
A
NonEUB338
EUB338
Fprau641
Ato291
Bac303
IgA2 – AF488
Probe-Cy3
Bacto1080
Bif164
Bif228
Lab158
Erec488
B
Total positive particles per mm2
400
300
200
100
0
Active
Inactive
*
*
C
Percent IgA2-positive FISH probe per mm2
200
150
100
50
0
Active
Inactive
*
Eubacterium rectale-Clostridium coccoides group (Erec482)
Lactobacillus Enterococcus (Lab158)
Bifidobacterium longum (Bif228)
Bifidobacterium genus (Bif164)
Bacteroides vulgatus (Bacto1080)
Bacteroidetes - Prevotella group (Bac303)
Colinsella Aerofaciens (Ato291)
Faecalibacterium prausnitzii (Fprau645)

Fig. 5

803

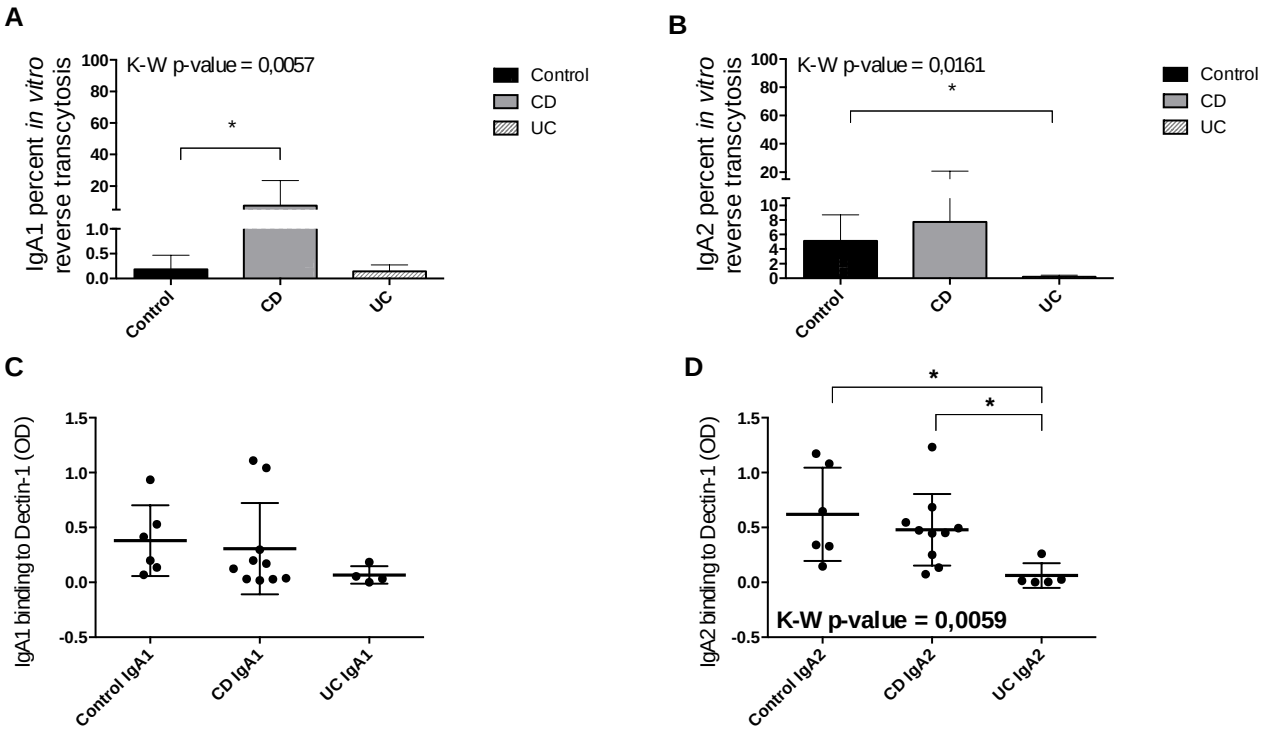

Fig. 6

804

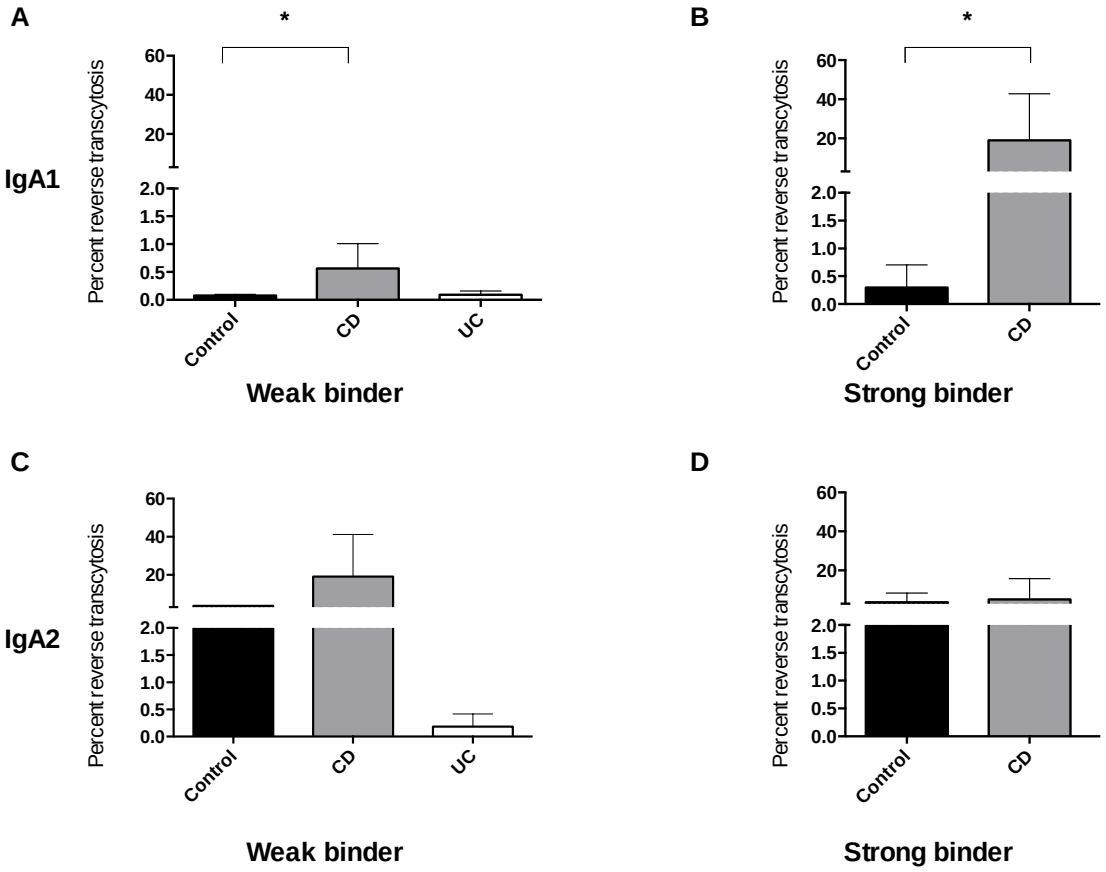

Fig. 7

805

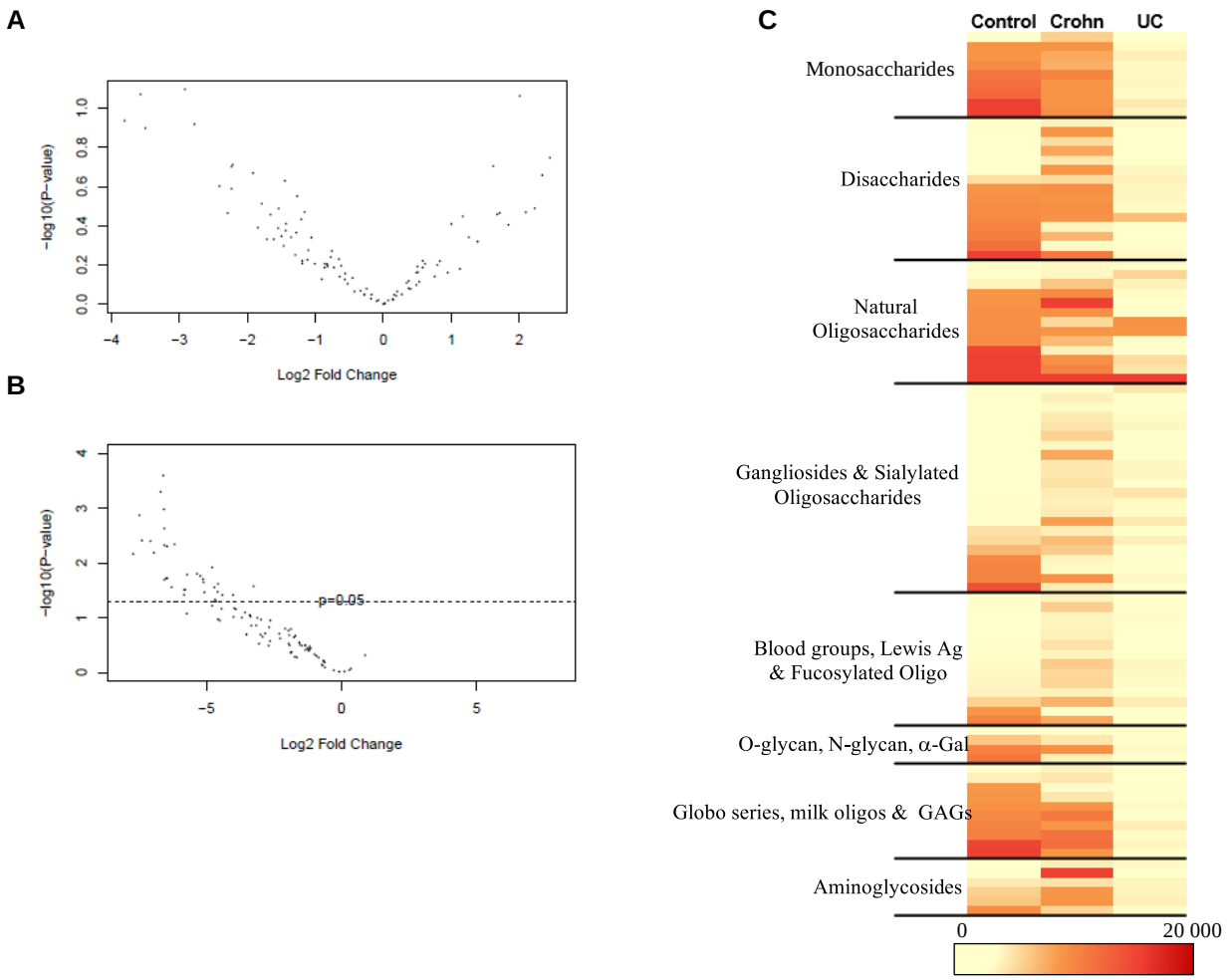
A
−log10(P−value)
Log2 Fold Change
B
−log10(P−value)
p=0.05
Log2 Fold Change
C
Control
Crohn
UC
Monosaccharides
Disaccharides
Natural Oligosaccharides
Gangliosides & Sialylated Oligosaccharides
Blood groups, Lewis Ag & Fucosylated Oligo
O-glycan, N-glycan, α-Gal
Globo series, milk oligos & GAGs
Aminoglycosides
0
20 000

Fig. 9

806

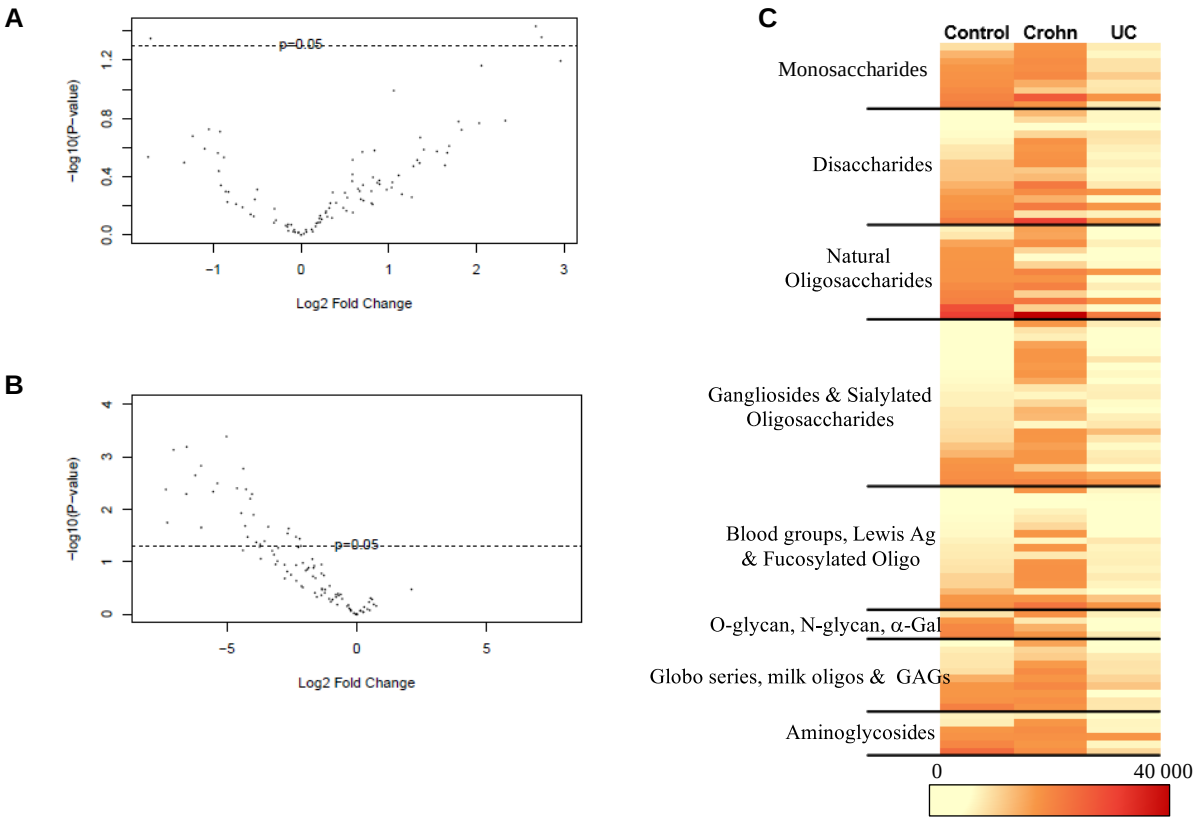
A
p=0.05
−log10(P−value)
Log2 Fold Change
B
p=0.05
−log10(P−value)
Log2 Fold Change
C
Control
Crohn
UC
Monosaccharides
Disaccharides
Natural Oligosaccharides
Gangliosides & Sialylated Oligosaccharides
Blood groups, Lewis Ag & Fucosylated Oligo
O-glycan, N-glycan, α-Gal
Globo series, milk oligos & GAGs
Aminoglycosides
0
40 000

Fig. 10

Table 1 – Differentially recognised species in the IgA1^{+} fraction of the CD stool microbiota

Genus, Species (Order, Cluster)	Abundance ?	p-value
Bacteroides, Unknown (*Bacteroidales*, 33)		$5.97.10^{-15}$
Bacteroides, Unknown (*Bacteroidales*, 56)		0,011
Lachnoclostridium, Unknown (*Clostridiales*, 122)		0,019
Unknown *Lachnospirceae,* Unknown (*Clostridiales*, 136)		0,019
Lachnoclostridium, Unknown (*Clostridiales*, 275)		0,042
Anaerostipes, Unknown (*Clostridiales*, 34)		0,011
Blautia, Unknown (*Clostridiales*, 239)		0,042
Lachnospira, Unknown (*Clostridiales*, 245)		0,027
Bifidobacterium, Unknown (*Bifidobacteriales*, 25)		0,019
Butyricicoccus, Unknown (*Clostridiales*, 68)		0,019
Blautia, Unknown (*Clostridiales*, 102)		0,019
Faecalibacterium, Unknown (*Clostridiales*, 4)		0,019
Streptococcus, Streptococcus salivarius (*Lactobacillales*, 275)		0,043

839 **Supplementary figures.**

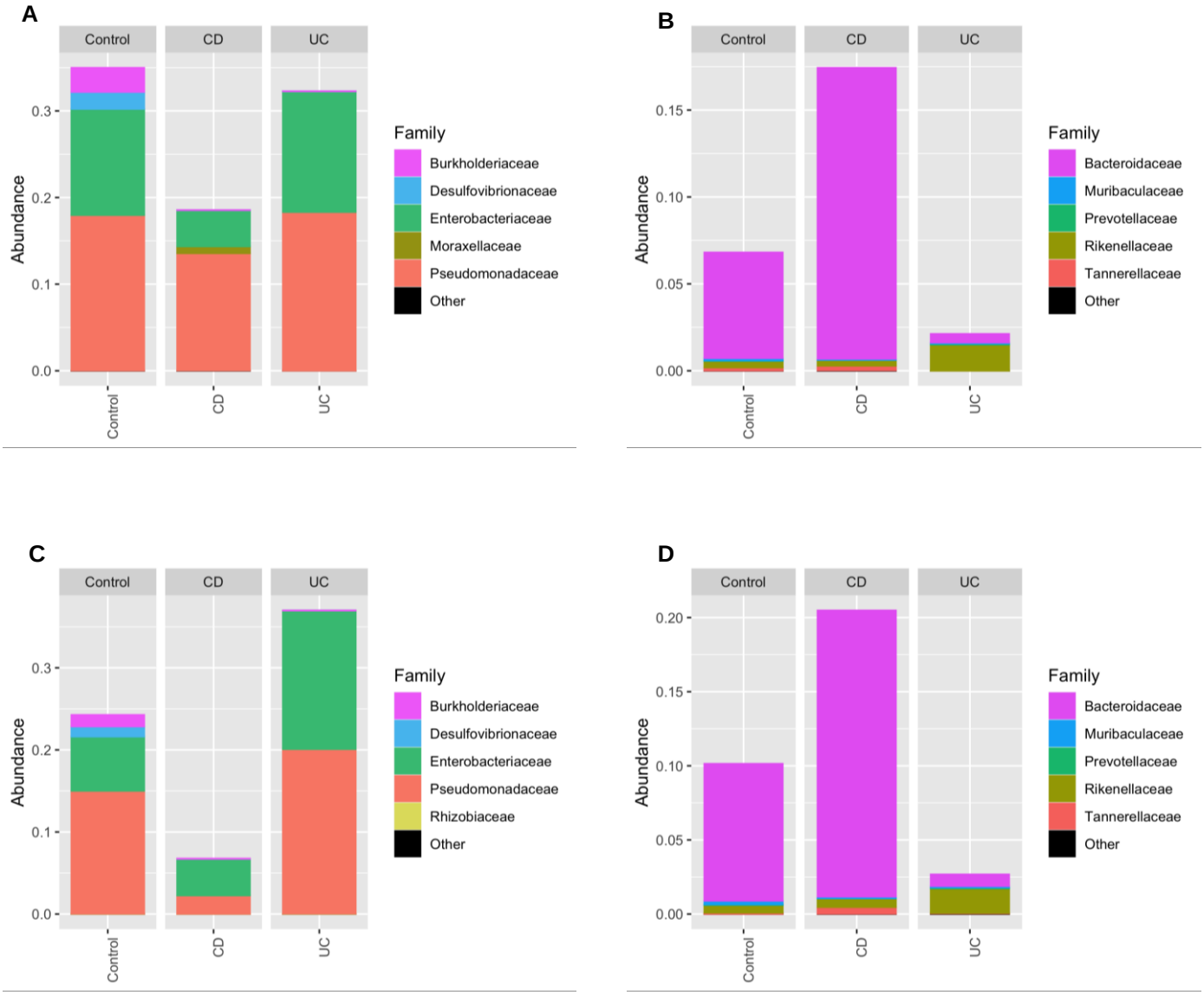

Supp. Fig. 2

840

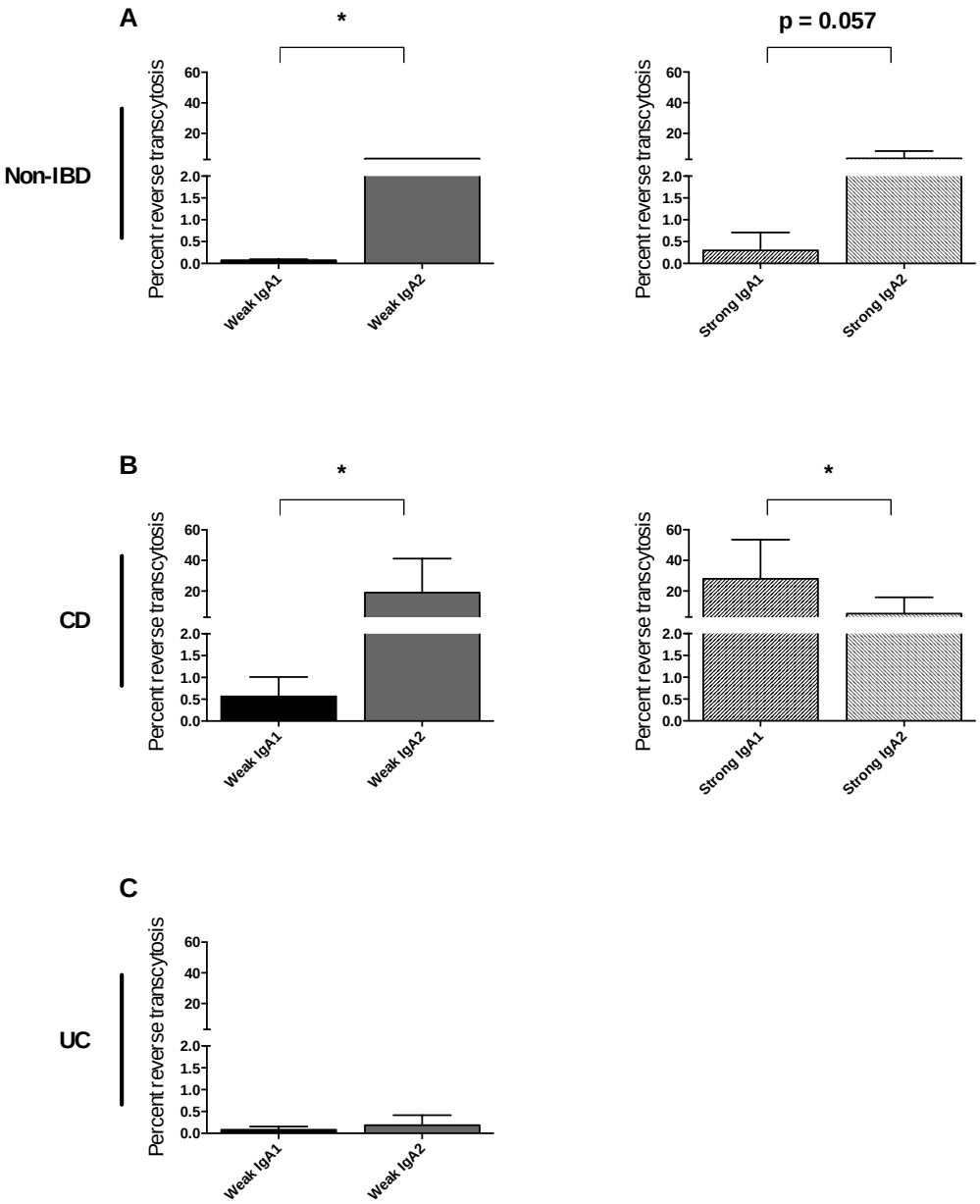

Supp. Fig. 3

841

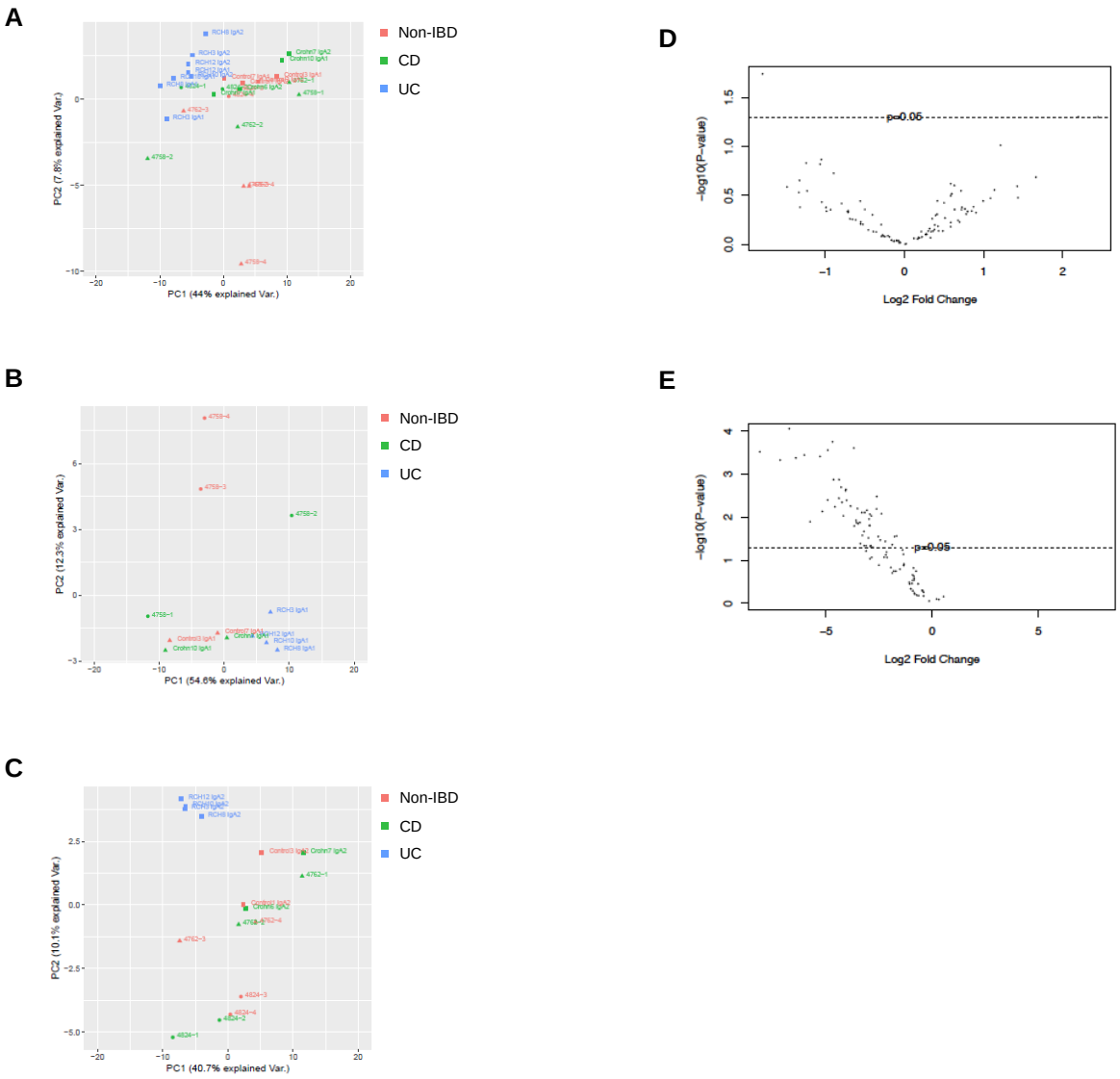

Supp. Fig. 4

Supp. Table 1 – FISH probe sequences

Name	Sequence
NonEUB 338 (Negative control)	ACATCCTACGGGAGGC
EUB338 (Positive control)	GCTGCCTCCCGTAGGAGT
Ato291 (*Collinsella aerofasciens*)	GGTCGGTCTCTCAACCC
Bac303 (*Bacteroides – Prevotella* group)	CCAATGTGGGGGACCTT
Bacto1080 (*Bacteroides vulgatus*)	GCACTTAAGCCGACACCT
Bif164 (*Bifidobacterium* genus)	CATCCGGCATTACCACCC
Bif228 (*Bifidobacterium longum*)	GATAGGACGCGACCCCAT
Erec482 (*Eubacterium rectale-Clostridium coccoides* group)	GCTTCTTAGTCARGGTACCG
Fprau645 (*Faecalibacterium prausnitzii*)	CCTCTGCACTACTCAAGAAAAAC
Lab158 (*Lactobacillus – Enterococcus* group)	GGTATTAGCAYCTGTTTCCA

842
843

Supp. Table 2 – Correlation between percent IgA1 or IgA2 reverse transcytosis and Dectin-1 binding

Group	Spearman's ρ	P-value
CTR IgA1 – Dectin-1 binding	0,698	0,506
CD IgA1 – Dectin-1 binding	**0,738**	**0,046**
CTR IgA2 – Dectin-1 binding	0,927	0,244
CD IgA2 – Dectin-1 binding	-0,485	0,180
UC IgA2 – Dectin-1 binding	0,070	0,930

Supp. Table 3 – Glycan motifs recognition by CD IgAs

Ig	Motif	LogFC	p-value
All IgA	Neu5Ac-2,3-Gal-1,4-Glc-Sp1	**-1,80**	**0.019**
	SGP	**2,12**	**0.049**
	Neu5Ac-2,3-Gal-1,4-(Fuc-1,3)-Glc-[3-Sialyl-3-fucosyllactose/F-SL]-Sp1	2,45	0.050
	Sisomicin Sulfate	1,22	0.096
IgA1	Gal-1,4-Gal-1,4-Glc-Sp	-2,92	0.080
	4-P-GlcNac-1,4-Man-Sp	-3,57	0.085
	Gal-1,3-(Neu5Ac-2,6)-GalNac-Sp	2,01	0.086
IgA2	Neu5Ac-2,3-Gal-1,4-(Fuc-1,3)-Glc-[3-Sialyl-3-fucosyllactose/F-SL]-Sp1	**2,68**	**0.037**
	Maltotetraose-Sp1	**2,74**	**0.044**
	Neu5Ac-2,3-Gal-1,4-Glc-Sp1	**-1,71**	**0.045**
	Gal-1,3-GalNac-1,4-(Neu5Ac-2,3)-Gal-1,4-Glc-Sp1	2,96	0.064
	GalNAc-1,3-Gal-1,4-Gal-1,4-Glc-Sp	2,06	0.068

D- Conclusions et perspectives.

Pour la première fois, nous mettons en évidence plusieurs altérations fondamentales de la fonction des IgA sécrétoires dans les MICI : (i) NOD2 régule la RT des IgA négativement et les polymorphisme sur le gène *NOD2* entraînent une augmentation de celle-ci, (ii) les IgA1 de patients atteints de la MC sélectionne des espèces bénéfiques et pourraient contribuer à leur élimination, (iii) ces IgA1 acquièrent la capacité d'effectuer la transcytoses inverse, (iv) les IgA dans la MC ont une réactivité anti-glycan accrue, et enfin (v) les IgA dans la RCH sont caractérisées par une absence de RT et une perte de réactivité contre ces même glycans. Plusieurs aspects de ces dynamiques restent cependant à confirmer.

Dans un premier temps, les résultats de notre étude du microbiote (Chapitre 2, Article 2) seront à approfondir par l'inclusion d'un plus de grand nombre de sujets, notamment pour palier à l'importante variabilité intra-groupe observée lors du séquençage 16S et des expériences de cytométrie en flux.

La poursuite de cette recherche bénéficierait de la mise en culture des biopsies intestinales de patients NOD2 en présence de différents types d'antigènes, commensaux ou pathogènes, ainsi que de l'analyse des métabolites bactériens produits au cours de cette culture, afin d'évaluer l'orientation de la réponse immune muqueuse par cytométrie en flux. De plus, des clones circulants de LB produisant des Ig (A, M, et G) anti-commensales sont retrouvés chez l'individu sain et les patients atteints de MICI[220,357,396]. Les résultats obtenus dans nos études mériteraient donc d'être complétés par une étude du répertoire et de la réactivité des Ig circulantes chez ces mêmes patients. À cet effet, nous avons immortalisé des LB issus de résections chirurgicales iléales de patients atteints de MC. Après dilution clonale, les LB sécrétant des IgA1, IgA2, IgM et IgG ont été conservés et leurs Ig purifiées pour l'analyse de la liaison au microbiote. Nous souhaitons, et c'est en cours, extraire les ARN de ces clones pour séquencer les régions variables des transcrits et analyser le répertoire Ig muqueux. Nous recherchons d'éventuels défauts de maturation d'affinité, une restriction de la variabilité directement au niveau des séquences VH, ou une spécificité accrue pour certains motifs commensaux. Au moment de la rédaction de cette thèse, plus de 300 clones (toute Ig confondues) ont été isolés (**Tableau 4**). La RT-PCR pour l'amplification des gène Ig (**Fig. 29**) a été mise au point et tous les clones ont à ce jour été amplifiés selon cette méthode.

Tableau 4 – Nombre de clones immortalisés par pièce chirurgicales (A, B, C).
Chaque pièce a été prélevée sur un patient différent atteint de la maladie de Crohn. Les tissus ont été broyés et digéré à la collagénase, puis les cellules ont cocultivées avec l'EBV. Lorsque des amas cellulaires ont commencé à se former, les cellules ont été repiquées par dilution clonale. La sécrétion d'Ig a été mesurée par ELISA.

Patient	IgM	IgA1	IgA2	IgG	TOTAL	Nb de cellules initial par puit
A	12	7	3	3	**25**	$2{,}2.10^3$
B	46	11	4	15	**76**	$1{,}1.10^4$
C	92	86	27	90	**295**	$1{,}98.10^4$

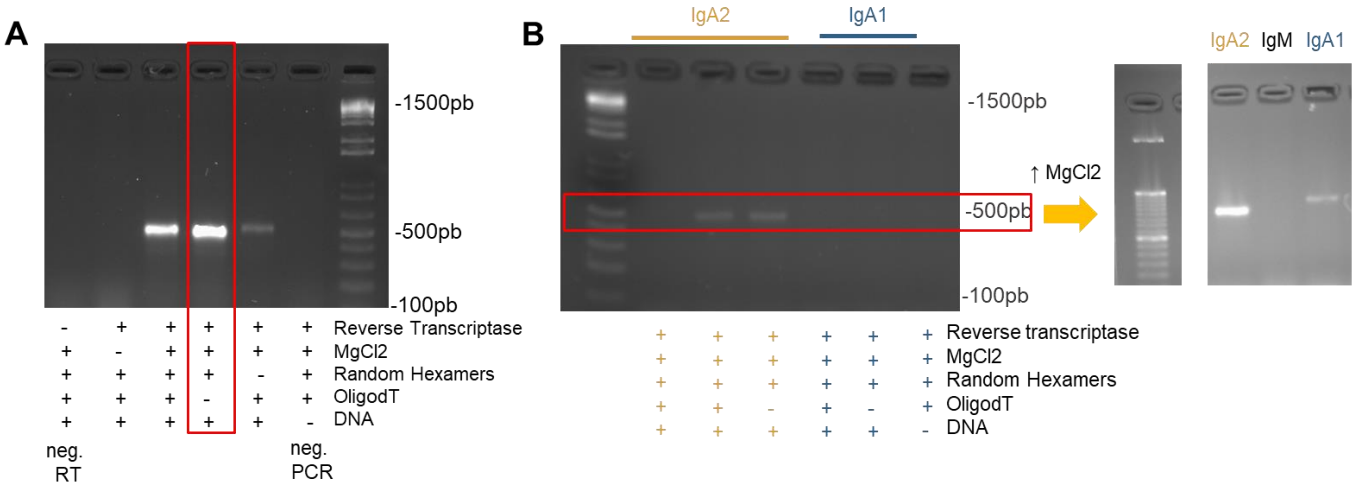

Figure 29 – Mise au point de la PCR d'amplification des région variables des gènes des chaînes lourdes des Ig.
(A) Electrophorèse sur gel des produits PCR après les two-step RT-PCR sur pour le gène Cμ. L'encadré rouge est la fornulation du mix PCR sélectionnée à l'issue des mises au point. (B) Two-step RT-PCR sur pour le gène Cα. Dans un premier temps, les quantités ont été conservées selon celles choisies pour les RT-PCR IgM. La mise au point a été faite sur un clone àa IgA2 (jaune) et un clone à IgA1 (bleu). Pour augmenter la qualité de l'amplification (encadré rouge), les concentrations de MgCl2 ont été augmentées (flèche jaune).

Nous montrons également des biais de sélection de la flore microbienne dans les MICI, cependant la nature des IgA qui sélectionnent ce microbiote n'est pas élucidée : ces IgA peuvent être issues de processus T-dépendants, et sont généralement de haute affinité, ou bien de processus T-indépendants, et donc polyréactives. Si la polyréactivité a été testée en partie par les *glycan array*, il est également envisageable de déglycosyler nos IgA purifiées et de vérifier quelles bactéries restent sélectionnées. Nous supposons que cette déglycosylation limitera la sélection d'espèces commensales mais pas celle d'espèces pathogènes.

En termes de mécanistique, il faudra mettre en évidence que les IgA1 de la MC effectuent bien la transcytose inverse grâce à la liaison à Dectin-1. Pour cela, nous prévoyons de reproduire les traitements par siRNA utilisée pour démontrer la transcytose des IgA2 [43] et le recrutement des protéines vésiculaires (**Chapitre 2, Article 1**) sur le modèle *in vitro* de FAE dans nos précédents travaux. Ce dispositif permettra également d'établir le rôle de Siglec-5 dans ce transport. En complément, les expériences de liaison à Dectin-1 par ELISA seront reproduites entre Siglec-5 et les IgA de patients atteints de MICI et d'individus non-MICI.

De plus, NOD2 interagit avec Dectin-1 et Siglec-5, mais aussi avec les protéines de transport vésiculaire Rab-5, Rab-7 et EEA-1. Il semble également que la signalisation *via* Syk et TAK1 intervienne dans la RT des IgA. Si la présence de Syk et TAK1 dans la signalisation de Dectin-1 est connue[397], leur rôle dans la RT n'a jusqu'ici pas été illustré. Puisque Syk et TAK1 convergent toutes deux sur la voie NF-κB, il serait intéressant de reproduire nos observations avec des effecteurs de cette voie tels que IKK, ou les sous-unités de NF-κB. NOD2 pourrait, dans ce contexte, agir comme une plateforme d'interaction moléculaire.

NOD2 est également impliqué dans la régulation des TLR2 et 4, en conditions inflammatoires[398], ce qui implique que la détection des signaux commensaux sera altérée, et peut entraîner une dérégulation des niches microbiennes intestinales. Dans nos modèles murins, il faudrait donc comparer la diversité bactérienne fécale des animaux NOD2 KO et des animaux sauvages. Puisque qu'il y a une RT accrue des IgA chez les animaux NOD2 KO, il serait également intéressant de comparer la diversité de la fraction microbienne IgA^+ entre animaux KO et animaux sauvages. De même, pour démontrer la causalité entre les défauts de sélection du microbiote par IgA1 et IgA2 et l'installation d'une l'inflammation latente liée à la dysbiose, nous aimerions inoculer ces fraction $IgA1^+$ et $IgA2^+$ de patients atteints de MICI à des souris axéniques. Nous voulons corréler l'orientation vers un profil Th_1-Th_{17} à l'inoculation du microbiote de patients MC, avec comme hypothèse principale que la fraction $IgA1^+$ fera

pencher la balance plus rapidement vers l'inflammation que la fraction $IgA2^+$ seule. Selon ce même schéma, l'accumulation et l'activation des Th_9 et des Th_2 y serait corrélée au microbiote issu de patients atteints RCH. Ces corrélations peuvent, dans un premier temps, se faire sur notre modèle de moDC, en conditionnant celles-ci avec nos IgA purifiées ou complexées, et en les plaçant au contact de LT $CD4^+$ autologues, dont le phénotype sera analysé par cytométrie en flux puis par analyse de la production cytokinique par technologie Luminex.

De plus, et comme nous l'avons mentionné dans l'introduction, le rôle compensatoire des SIgM lorsque la sécrétion d'IgA est défectueuse est connu[209,391]. Aussi il semble approprié de reproduire l'ensemble de l'étude (liaison au microbiote, transcytose inverse avec et sans polymorphismes NOD2, liaison au récepteur de RT TOSO, réactivité anti-glycan) sur des IgM purifiées de selle de patients.

Chapitre 3 – Inhibition de la transcytose-inverse en conditions physiopathologiques

A- Résumé et article 5 : Compétition pour la transcytose inverse des IgA in vivo *au cours de colite à Salmonelle*

Les MICI sont caractérisées par une inflammation chronique, de la dysbiose microbienne [308,399–402], et une augmentation de la perméabilité intestinale[288,403]. Les traitements actuels ciblent l'induction et le maintien de la rémission, en l'absence de traitement curatif. Ils visent à limiter l'impact de la sécrétion de TNF-α sur les muqueuses et à limiter le recrutement d'effecteurs cellulaires. Ainsi, l'utilisation d'anticorps monoclonaux anti-TNF-α[404], d'inhibiteurs des intégrines α4β7[405] ou des calcineurines[406], et désormais d'inhibiteurs de Jak[407] a considérablement amélioré la prise en charge des MICI. L'effet de ceux-ci peut être complété par l'administration d'antibiotiques, de thiopurines ou de corticostéroïdes [288,403]. Malgré ces progrès, les échecs thérapeutiques sont nombreux, environ 40% des patients ne répondent pas aux anti-TNF. De récentes données soulignent également qu'un microbiote dysbiotique promeut l'échec thérapeutique aux anti-TNF-α [404] ou aux anti-intégrines [405]. De plus, l'ensemble de ces traitements est à l'origine de très lourds effets secondaires (**Tableau 3**), ce qui appelle au développement de nouvelles approches thérapeutiques.

Au vu du rôle prédominant du microbiote dans la pathogenèse des MICI, plusieurs dérivés microbiens ont été utilisés par de récents travaux pour limiter l'inflammation intestinale. Ainsi, les α- et β-glucans fongiques sont utilisés avec succès chez la souris au cours de colites au DSS ou des HFD, où ils limitent la sévérité de l'inflammation[408–411]. Les glucans fongiques sont reconnus dans la muqueuse intestinales par les CLR Dectin-1, -2, et -3. Alors que Dectin-1 reconnait les β-glucans, Dectin-2 lie les α-glucans ; ils induisent respectivement une immunité de type Th_1-Th_{17}[42,44,412,413] et Th_{17}-Th_2[47,414,415].

Nous avons également montré que Dectin-1 permet la RT des IgA au niveau des cellules M de la PP[43], et que le taux de RT des IgA augmente dans la maladie de Crohn. D'autres maladies intestinales, comme la maladie cœliaque, mettent en jeu le retro-transport des complexes IgA-antigènes pour la promotion de l'inflammation[163,416]. Aussi, nous avons souhaité évaluer si le blocage du transport de ces complexes IgA-médiés permettrait de limiter l'établissement de boucles inflammatoires muqueuses au cours de colite à *Salmonelle* (**Article 5).**

Nous montrons que parmi les glucans testés, le β-glucan zymosan et l'α-glucan pullulan, permettent de limiter ou de retarder les effets d'une colite infectieuse à Salmonelle. L'activité du zymosan dépend notamment de sa capacité à activer les TLR. L'injection de zymosan ou de

pullulan limite la pénétration bactérienne dans les tissus et est, de plus, corrélée à une moindre réabsorption des IgA dans la PP.

Oral administration of microbial glucans prevents IgA-mediatedbacterial translocation into Peyer's patches and limit exacerbation of *Salmonella*-induced colitis in mice

Eva Michaud[1], Rémi Gayet[1], Blandine Chanut[1], Fabienne Jospin[1], Xavier Roblin[1], Nicolas Rochereau[1], Stéphane Paul[1].

[1] GIMAP/EA3064, Université de Lyon, CIC 1408 Vaccinology, F42023 Saint-Etienne, France;

Corresponding author: Stéphane PAUL
stephane.paul@chu-st-etienne.fr
Faculté de médecine de St-Etienne, Laboratoire GIMAP
10 rue de la Marandière, 42270 St Priest en Jarez
Tel: +33 (0) 4 77 42 14 84; Fax: +33 (0) 4 77 42 14 86

Abstract

Inflammatory Bowel Diseases (IBD) are characterised by chronic inflammation of various origins with increasing incidence world widely. Evidences of severe dysbiosis over the course of IBD suggest the microbiota could influence responses to current treatments as well as promote the orientation of the immune response towards either tolerance or inflammation.

Previous studies have indicated that microbial glucans, especially fungal β- and α-glucan favor targeted delivery of current treatment, and promote the restoration of microbiota diversity during colitis. We have previously shown that decitn-1, a receptor for fungal β-glucans in the gut, favors IgA trafficking in the gut. As IgA select commensal microbiota and increased retrotransport of IgA has been observed in IBD, we aim to limit the translocation of IgA-bacteria complexes *n vivo* by competing for Dectin recognition in the gut. We show that the β-glucan zymosan and α-glucan pullulan both limit IgA-*Salmonella* complexes translocation into murine Peyer's patches. Both promote enhanced survival and zymosan favors lower inflammation in a TLR-dependent manner.

Keywords : Secretory, IgA, glucans, fungi, colitis, Dectin

Introduction

Inflammatory Bowel Disease (IBD) are characterized by chronic inflammation, dysbiosis[1–5], and increased intestinal permeability [6,7], the causes of which are various and multi-faceted. IBD occur in episodic flares that can be triggered by stress, dietary antigens, infections, and antibiotic consumption [26,27]. Increased level of TNF-α are observed in the mucosa of patients with IBD[28,29], and intestinal immunity shifts towards Th17, Th1 or Th2 cytokine production[26,30–33]. Defects in IgA selection of the microbiota, to the benefit of anti-commensal IgG[4,33–35], are also thought to promote dysbiosis in IBD. Despite progress in the characterisation of immune and microbial parameters of IBD, the full understanding of the pathogenesis of IBD remains elusive.

As no curative treatment exists yet, current therapeutic options aim at inducing and maintaining remission. As such, conventional treatments rely on anti-inflammatory and immunosuppressive biological agents : anti-TNF monoclonal antibodies were thus a tremendous progress for IBD. Approximately one-third of patients remains unresponsive to such therapies, while in patients in which they are effective, high doses are required[8]. Other agents such as antibiotics, thiopurines and corticosteroids enhance the effect of anti-TNF therapies[36–38]. However, treatments with most of these drugs are associated to long lists of adverse effects that have yet to be overcome. Consequently, this large number of treatment failure prompts for a rethinking of current approaches. Novel approaches under study include dietary therapy, injection of allogeneic expanded adipose stem cells, anti-a4b7 integrins as well as anti-IL-12 and IL-23 monoclonal antibodies, and gut-specific JAK inhibitors[11,39,40]. However, low microbiota diversity and loss of short chain fatty acids (SCFA)-producing taxa is associated with anti-TNF and anti-integrin failure in IBD [9,41]. It is thus to be be expected that commensal diversity and the nature of its species will impact the response to these treatments as well.

Because the microbiota plays a significant role in the maintenance of homeostasis and it is disturbed in IBD, recent investigations for IBD treatment aim at manipulating bacterial diversity concurrently to lowering inflammatory parameters to promote gut healing and regulatory effectors expansion. Studies on safer and milder treatment delivery systems have thus highlighted the role of microbial glucans either to lower colitis-induced inflammation or as drug delivery systems. In mice, fungal polysaccharides lower the severity of dextran sulfate sodium (DSS)-induced colitis[12–14] and alleviate dysbiosis during a high-fat diet (HFD)[42]. The use of fungal β-glucan-derived nanoparticles, to deliver and maintain sufficient concentration

of anti-TNF treatment or methotrexate within the intestinal tissues are successfully uptaken by macrophages, promote high local drug concentrations and lower the effects of colitis[43,44].

Given increasing evidences of fungal dysbiosis in IBD[45–47], it is thus likely that fungal particles might partially restore microbial homeostasis in the gut during inflammation. Fungal sensing in the gut is ensured through recognition of antigens by Dectin receptors. Dectin-1 is a C-type lectin-like receptor (CLR), the natural ligand of which are usually microbial – especially fungal – β-glucans [48]. CLRs Dectin-2 and 3 are also specialized in anti-fungal immunity [49]. While Dectin-1 signalling tends to elicit Th1, Th9 and Th17 responses [16–19], that of Dectin-2 is thought to induce Th17- and Th2-oriented inflammation [20–22], promote neutrophil recruitment and NETosis[50,51] and trigger NLRP3 activation [52,53] in response to fungal α-mannans [54].

We have previously evidenced Dectin-1 expression at the apical membrane of microfold (M) cells of the follicle-associated epithelium (FAE) of Peyer's patches (PP)[23]. Not only can it sample microbial glucans, we also show that secretory IgA is recognized by Dectin-1 and internalized by M cells[23], a process termed reverse transcytosis (RT), after which it can bind DC-SIGN$^+$ dendritic cells (DC) [23,55] of the intra-epithelial pocket of M cells. Similar retro-transports are also evidenced in coeliac disease, wherein SIgA-antigen complexes are uptaken through FcαRI binding and promote inflammation[24,25]. Secretory IgA (SIgA) are responsible for the optimal segregation of commensal and pathogenic bacteria [56–58]. In IBD, alterations of such IgA-driven selection of the microbiota[34,59], and increases in reverse transcytosis activity (Rochereau, *et al.* Nature communication, 2020, *in press*) have been observed. We have thus evaluated a novel strategy to limit IgA RT by competing for Dectin availability *in vivo.* After screening for possible microbial ligands, we show that *Salmonella*-induced colitis can be attenuated through the administration of two fungal glucans, zymosan and pullulan. Both these compounds limited the reabsorption of IgA-bacteria complexes into the PP and enhanced survival during experimental colitis. We highlight that zymosan lowers murine DC responsiveness *in vitro* and relies on TLR activation to promote low inflammation levels *in vivo*. This suggest disruption of IgA RT might be a potentially new therapeutic strategy for IBD.

Materials and methods

Reagents

Zymosan depleted (Invivogen, tlrl-zyd), zymosan (Invivogen, tlrl-zyn) and pullulan from *Aureobasidium pullulans* (Sigma-Aldrich, P4516), curdlan from *Alcaligenes faecalis* (Sigma-Aldrich, C7829), laminarin from *Laminaria digitata* (Sigma-Aldrich, L9634) were reconstituted per manufacturer's instructions at a stock concentration of 5 $mg.mL^{-1}$ under sterile conditions.

IgAC5 and IgA-Sal4

Murine *Shigella flexneri* LPS-specific IgAC5 serotype 5a and *Salmonella typhimurium* carbohydrate-specific IgASal4 were produced as previously described [60]. Polymeric isoforms were obtained by steric exclusion chromatography and secretory component (SC) was purified from 2H2 hybridoma culture by affinity chromatography [61]. SC was added to IgAC5 or IgASal4 in equimolar concentrations in PBS for 30 minutes at room temperature (RT) then stored at 4°C.

In vitro model of FAE and reverse-transcytosis assay

The model was set-up as previously published by our team [23]. Once ready, inserts were fitted in a silicone tube and both top and bottom chambers were filled with HBSS buffer. Samples (10 μg of IgA) were added to the top chamber and incubated for 90min at 37°C. The bottom chamber was collected and tested for Ig passage by ELISA.

Salmonella cultures

SL1344 *Salmonella enterica* Typhimurium isolates were provided by Dr. Blaise Corthésy. After a 24h culture at 37°C on streptomycin agars (90ug/mL), 5% CO_2, one colony was transferred to 3mL of liquid LB_{strep} broth (Streptomycin 90 μg/mL) for another 24h at 37°C, 5% CO_2 and under slight agitation. Approximately 100μl of the resulting culture were diluted into another 3mL of liquid LB_{strep} broth, to get to a 0.1 optical density (OD_{600nm}). OD_{600nm} measurements were performed in parallel with gel titration so that bacteria can be administered in their exponential phase during our experiments (CFU). *Salmonella enterica* Typhimurium GFP were obtained from ATCC (14028GFP) and cultured similarly, except all media included both streptomycin and ampicillin (90 $\mu g.mL^{-1}$).

Model of mouse colitis.

6 weeks-old Balb/cByJ female mice were purchased from Charles River and hosted at our facility for 10 days prior to any experiments. Mice were gavaged with 1mg of either depleted zymosan, zymosan or pullulan two hours prior to *Salmonella* infection. SL1344 was then orally administered (10^6 CFU/mouse) in 100 µl PBS. Mice were not pre-treated with streptomycin as we aimed to measure the role of SIgA reverse transcytosis in the context of a normal microbiota. Body weight and disease activity index (DAI) were monitored each day.

Assessment of colitis severity

Disease activity index (DAI). DAI score was monitored daily to evaluate the clinical progression of colitis [62]. The DAI score combines the percentage of weight loss, stool consistency, rectal bleeding, and altered behavior. Scores were defined as described in **Suppl. Table 1**. Experimental endpoint was reached when mice exhibited weight loss greater than 20% or a DAI above 9.

Serum IL-6 assay. Mice were bled one day before the experiments began, 4 days after treatment, and on the day of sacrifice, through the retro-orbital plexus. Serum concentrations of IL-6 were assessed by ELISA (Mouse IL-6 ELISA MAX, Biolegend, San Diego, CA).

Fecal Lipocalin assay. Stools were collected one day before the experiments began, 4 days after treatment, and on the day of sacrifice. When collection was impossible due to diarrhoea, intestinal washes after harvesting colon and coecum were performed. Fecal concentration of the inflammatory marker lipocalin2 was assessed by ELISA (Mouse Lipocalin-2/NGAL DuoSet ELISA, R&D systems)

SIgA administration into ligated loops

For ileal loop preparation, mice were starved overnight, anesthetized by intra-peritoneal injection of a mix of ketamine and xylazine (100 and 10 mg/kg, respectively) and kept warm at 37°C throughout the surgical procedure. 100 □l of a 5 mg/ml zymosan depleted, zymosan, pullulan, or each glucan combined with 10^5 CFU *Sal*-GFP were administered into a 1 cm ileal loop containing a PP. For some experiments, mice were gavaged with either PBS or 1mg of glucan 2 hours prior to ileal loop experiments and only Sal-GFP was injected. After the mice were sacrificed by cervical dislocation, the loop was harvested, washed with sterile PBS, fixed overnight in 4% paraformaldehyde, and included in optimal cutting tissue (OCT) embedding solution. 7-µm sections (Leica cryostat model CM1950, Leica Microsystems) were deposited on Ultra+ superfrost microscope slides (VWR International). The protocol followed the

guidance of the regional Ethics Committee for animal testing, CREEA (Permit number: No. 69387487).

Immunofluorescence stainings

PP sections were washed in PBS three times then permeabilized in a 0.1% Triton, 1% BSA solution for 2 minutes, then washed once more in PBS. Biotinylated rat anti-mouse IgA (1/500 dilution, BD 556978) antibodies were added to each section for 90 minutes. After three PBS washes, Streptavidin-AF555 (1/1000, Fisher) was added and incubated at room temperature for 60 minutes. Slides were mounted in DAPI-fluoroshield (Sigma-Aldrich, F6057) and observed by epifluorescence microscopy (Eclipse, Nikon).

Anti-mouse IgA ELISAs

Anti-mouse κ and λ light chains antibodies (Fisher, 11505040, PISA510216) were coated (1/1000) in Nunc Maxisorp 96-wells plates (Fisher) in carbonate buffer (pH 9.6) overnight at 4ºC. Wells were saturated with BSA 1% in PBS-tween 0.05% (PBST) at room temperature (RT) for 90 min, then washed 3 times with Phosphate-Buffer Saline (PBS)-Tween 0,05% (PBST). stool samples were added at a 1/10 and 1/100 dilution and incubated at RT for 1h30. Plates were then washed with PBST, then biotinylated secondary antibodies (1/500 dilution, BD 556978) were incubated at RT for 1h30. After washing in PBST, streptavidin-HRP (BD, 554066) was added for 60 min. Revelation through addition of TMB in wells for 3 to 10 minutes was stopped with 1N HCl. Plates optical density (OD) were read at 450 nm (Sunrise TECAN microplate reader).

PP lysates co-culture in vitro

10 PP per mouse were harvested as previously described [63], ground on 100 μm cell strainer, then cell viability was assessed by trypan blue exclusion. 5.10^5 cells in 100 μl of the complete medium supplemented with 5 $\mu g.mL^{-1}$ of concanavalin A (Sigma, St. Louis, MO, U.S.A.) and 50 $\mu g.mL^{-1}$ of lipopolysaccharide (LPS, Sigma) were added 96-well tissue culture plates (BD Biosciences), with or without zymosan, zymosan depleted or pullulan (100 $\mu g.mL^{-1}$). After 24 h of incubation at 37 °C cells were harvested for flow cytometry staining.

Flow cytometry

Cells were washed in FACS buffer (PBS, 2% FBS, 1 mM EDTA). A DC antibody panel was added for 30 min in 100 μL of FACS buffer. The panel included: anti-CD103 (Miltenyi, 130-102-479), anti-CD11c (BD, 562949), anti-CD40 (BD, 562846), anti-CD80 (BD, 553769), anti-CD86 (BD, 560582), anti-I-A/I-E (BD, 565254) antibodies. Cells were washed twice in FACS buffer and resuspended in 300 μL of FACS buffer for analysis of $CD11c^+$ DC on a FACS Canto Cytometer (BD).

Results

Zymosan inhibits murine IgA reverse-transcytosis

We have previously evaluated Dectin-1 inhibition in vitro to screen for possible mirobial candidate for *in vivo* administration[23]. To evaluate the ability of an α-glucan and a β-glucan to affect murine IgA reverse transcytosis, we set up an *in vitro* model of the FAE by co-coculturing Caco2 cells with Raji cells. We tested the RT of two murine IgA bound to the secretory component to mimic SIgA structure. Co-administration of murine IgAs withzymosan into the top chamber of the model shows an almost complete inhibition of IgA reverse-transcytosis (**Fig. 1A, B**). This was observed with IgASal4, which is specific for *S.* Typhimurium carbohydrates (**Fig. 1A**) and IgAC5, which is specific for *S. flexneri* LPS (**Fig. 1B**). In both these cases, monoculture of only Caco2 did not lead to any RT (**Fig. 1A, B**) suggesting IgA passage and its inhibition were dependent on M-cell differentiation. Pullulan administration, as previously described [23], did not impact IgA RT (**Fig. 1A, B**). Under homeostatic conditions, IgA and particles that have undergone RT interact with DC of the M-cell pocket. Thus, we wanted to test whether zymosan or pullulan had any effect on DC phenotype. To that end, we cultured PP lysates with zymosan and pullulan for 24 hours and analysed their phenotype by flow cytometry. Compared to both unstimulated and LPS-ConA-stimulated cells, zymosan induced a significant decrease in MHC class II(MHC-II) (**Fig. 1C**), CD86 (**Fig. 1D**), and CD40 (**Fig. 1F**), while CD80 was not affected by either zymosan or pullulan addition. Surprisingly, pullulan had no significant effect on any of these markers (**Fig. 1C-F**), despite a slight tendency to decrease MHC-II expression (**Fig. 1C**). Overall, while both these molecules do inhibit murine IgA RT, these results also suggest zymosan limits DC responsiveness and co-stimulatory ability, with possible consequence for both T and B cell activation.

Zymosan and pullulan inhibit IgA-bacteria complexes penetration into PP

We also studied the local effect of both molecules by injecting them with *Salmonella*-GFP into mouse ligated loops. First, we confirmed that ligated loop injection with *Salmonella* efficiently allowed for *Salmonella* invasion of murine PP (**Fig. 2A**). When mice were gavaged with zymosan or pullulan prior to Salmonella injection however, we observed a significant decrease in intra-PP staining with GFP (**Fig. 2B**) with both molecules. This indicates at least that zymosan and pullulan competed for *Salmonella* tissue invasion. Moreover, we also evaluated *Salmonella* invasion capacities when it was co-injected with zymosan or pullulan. We show that GFP intensity was notably lower in zymosan and pullulan treated loops (**Fig. 2C**) and that this corresponded to a significantly lower percentage of infiltrated bacteria within the PP (**Fig.**

2D). To demonstrate the involvement of IgA in this process, we next stained for mouse IgA in ligated loops. First, we observed an overall lower level of IgA in the PP of animals treated with zymosan and pullulan (**Fig. 2E**). Finally, IgA-*Salmonella* complexes appeared less frequent within PP of zymosan- or pullulan-treated animals, as less IgA-*Salmonella* complexes were observed in those PP (**Fig. 2F**). *In vitro* and ligated loop experiments with other glucan such as curdlan or laminarin resulted in either low RT inhibition or no inhibition of PP invasion (data not shown), so only zymosan and pullulan were tested in the following *in vivo* experiments. These results suggest that treatment with either a β-glucan or an α-glucan limit immune complexes retrotransport within the PP, which could contribute to lower disease burden during colitis.

Zymosan protects against colitis in a TLR-dependent manner

Given both zymosan and pullulan appeared to limit IgA entry into PP, we sought to evaluate their effect over the course of a *Salmonella*-induced colitis. Mice were thus gavaged with 1mg either molecule, then with 10^6 CFU of the *S.* Typhimurium strain SL1344.Survival curves for zymosan administration (**Fig. 3A**) show that zymosan protected mice efficiently from death, as 80% of animals survived. Up until day 7, both PBS- and Zymosan-administered animals displayed a similar progression in terms of weight loss percentages and disease activity index (DAI) (**Fig. 3B, C**), after which zymosan-treated mice resisted death while PBS-treated animals did not. Correspondingly, IL-6 levels were lower at the day of sacrifice in zymosan-treated mice (**Fig. 3D**), suggesting low or absent loss of intestinal permeability in these animals relative to the PBS group. Lipocalin-2, which is a faecal inflammation marker, tended to decrease in zymosan-treated mice (**Fig. 3E**). Moreover, faecal IgA levels appeared unaffected by the zymosan treatment (data not shown). When repeated with depleted zymosan, which cannot activate TLR signalling pathways, the experiment shows that this protective effect was lost as only 30% of animals survived (**Fig. 3F**). Similarly, both DAI, weight loss, and serum IL-6 became comparable to those of the PBS group (**Fig. 3G, H, I**). Taken together, these results suggest that zymosan limits the exacerbation of *Salmonella*-induced colitis and the ensuing increased permeability of the intestinal mucosa, a function that relies on TLR activation in the intestinal mucosa.

Pullulan protects against Salmonella-induced colitis

We initially included pullulan in the *in vivo* experiments as a non-Dectin-1 binding control. Surprisingly, while it did not affect IgA RT *in vitro*, the results show that pullulan treatment

tended to protect animals from death (**Fig. 3J**). However, despite this protective tendency, we still observed no difference between treated and untreated groups regarding either weight loss (**Fig. 3K**), DAI (**Fig. 3L**) or serum IL-6 levels (**Fig. 3M**). Neither IgA nor faecal lipocalin-2 levels were altered in treated animals (**Fig. 3N**). However, lipocalin-2 levels were positively correlated to IgA levels (**Fig. 3N**), indicating pullulan might affect IgA function, which could regulate local inflammation.

Discussion

Given the extensive body of literature describing IgA-mediated selection of the microbiota and IgA induction of intestinal immunity, we investigated whether these regulatory pathways could be disrupted during colitis and improve its outcome. We first investigate IgA reverse-transcytosis in the presence of two microbial glucans : the β-glucan zymosan, derived from *S. cerevisiae* cell wall, and the α-glucan pullulan, purified from *A. pullulans*. Pullulan was initially used as a non-Dectin-1-binding glucan control, and turned out to be surprisingly protective during *Salmonella*-induced colitis (**Fig. 3J**), despite its lack of effect on IgA RT *in vitro* (**Fig. 1A, B**). To our knowledge, such observations have not been made before. The pathways involved can thus only be hypothesized. Pullulan has highly adhesive properties and has been used for drug delivery and explant seeding [64], wherein it invokes Dectin-2 up-regulation [64]. Matching with our observation that both IgA and *Salmonella* penetration in the PP were limited by pullulan injection (**Fig. 2E, F**), pullulan could force the agglutination of both bacteria and immunoglobulin, thereby retaining them in the lumen where they would be eliminated by intestinal flow. Dectin-2 activation, which was not tested in our model might be involved and should thus be investigated, as it is also known to regulate inflammatory lymphocytes expansion and DC activation[21,52]. Its activation might explain why no improvement in inflammatory parameters was observed in our *in vivo* experiments (**Fig. 3, J-M**).

On the other hand, zymosan administration proved to be inhibitory for IgA RT (**Fig. 1C-F**) and for DC responsiveness *in vitro* (**Fig. 1C-F**), which suggested regulatory properties that might affect inflammation. *In vivo,* it was indeed beneficial during *Salmonella*-induced colitis, where it lowered IL-6 levels and attenuated weight loss and clinical scores (**Fig. 3A-D**). Those effects were lost when zymosan was depleted of its TLR-activating properties and suggest TLR synergy with Dectin-1 is required for protection against *Salmonella* infection. Synergy between TLR2 and Dectin-1 for IL-12 and TNF-α production is a known mechanism [65,66], and studies also show enhanced IL-2 and IL-10 secretion in zymosan-stimulated DC (ref3) that is

dependent on intracellular Syk activation [67]. Competition for Dectin-1 binding, and thus internalization, might thus polarize DC of the M cell pocket towards immunosuppressive phenotypes. This is supported by findings that zymosan can induce both tolerogenic and inflammatory DC, thusly triggering both Th17 and T_{reg} responses[67–69]. Zymosan also favors polymorphonuclear neutrophils accumulation and expansion via this TLR2-Dectin-1 dual activation [70]). The lack of TLR signalling might thus (i) not induce zymosan internalisation, or (ii) stimulate only one of those pathways, possibly the most inflammatory one. A study of M-cell intracellular cascades upon zymosan stimulation, with and without TLR activity, would resolve such questions.

Zymosan induces systemic metabolic changes, in that it lowers glycolysis and TCA metabolites production, while it increases fatty acid β-oxidation both locally and systemically [71]. In the intestinal microbiota, optimal glycolysis and TCA function ensure the maintenance of microbial networks and of host-microbe interactions[72–74]. Moreover, commensal signals are integrated *via* TLR activation by epithelial cells under both homeostatic and inflammatory conditions[75–77]. In an inflammatory context, such as *Salmonella*-induced dysbiosis, limiting the utilization of glucose and bacterial metabolism might also benefit commensal population as it would slow *Salmonella* invasion and allow for commensals to maintain their dominance in the lumen.

Competing for Dectin-1 binding thus appears as a new potential strategy to limit dysbiosis-related inflammation in the gut. Here, given the low IgA levels within PP following zymosan treatment, we hypothesize the immune complexes cannot be transported into the PP, and thus lowers *Salmonella* invasion of tissues. As this is not the only *Salmonella* can penetrate the mucosa, we also believe that this protective effect can be attributed to an enhanced response towards the fungal microbiota through zymosan stimulation. Fungal dysbiosis is a feature of IBD [45,78], and increased abundance of fungal species in Crohn's Disease [45] might put commensal bacteria at a disadvantage. Moreover, optimal recognition of fungi by the CLR SIGNR3 is critical for the severity of experimental colitis [79], suggesting both fungi and CLR promote host-microbe homeostasis. Restoring responses towards fungal species during colitis would thus also allow for a return to microbial homeostasis in such pathological contexts.

Other studies have found that zymosan, and β-glucans in general, are detrimental during colitis [80]. However, two parameters differ between our study and those already published : (i) the colitis model is Dextran Sulfate Sodium (DSS)-induced, (ii) mice genotypes, differ from ours, as they were C57BL/6. Both these choices are important sources of variation, as DSS, while ultimately inducing dysbiosis, is an aggressive compound that requires cyclic administration.. While it recapitulates features of the dysbiotic intestine, we feel bacteria-induced dysbiosis is

closer to human physiology as *Salmonella* (and *Campylobacter*) are known risk factors for IBD onset or flares [81]. We have also evaluated the effect of zymosan and pullulan under DSS treatment, which required glucan administration every two days for a similar effect (data not shown). We believe the rapid effect that DSS has on the deterioration of the mucosa presents the observation of early protective glucan-induced effects and the establishments of such effects. In C56BL/6 mice, intra peritoneal injection of zymosan induces up-regulation of TLR2, TLR4 and TNF-α mRNA, concomitant with TNF-α release [65], in peritoneal macrophages. Similarly, zymosan-induced TLR2 activation protects against radiation, via IL-6, IL-12 and TNF-α production [66]. This suggests zymosan-induced recruitment of inflammatory effectors to switch from immunosuppression tolerance towards inflammation. Our results thus suggest that genetic background, and especially latent humoral responses, will affect the uptake of zymosan and, henceforth, the outcome of colitis. The blocking of IgA translocation thus appears to be associated to milder disease course, and to efficient restriction of *Salmonella* entero-invasive properties. Glucan administration was also restorative during HFD feeding[42] and in type 1 diabetes [82], reduced Cox-2, IL-1β and TNFα on caco2 cells and goblet cell-like LS174T *in vitro* [83]. Microbial glucans thus offer new therapeutic avenues for future research on IBD but also on other microbiota- and inflammation-mediated diseases.

Figure legends

Figure 1 – Zymosan and pullulan limit IgA RT and DC responsiveness *in vitro*.

(**A**) Inverted model of FAE in which IgA-Sal4 RT was monitored alone (co-culture) or in the presence of zymosan (Z) or pullulan (P). (**B**) Inverted model of FAE in which SIgAC5 RT was monitored alone (co-culture) or in the presence of zymosan (Z) or pullulan (P). * = $p < 0.05$ (against co-culture), n= 4. (**C-F**) Expression of MHC-II (I-A/I-E) (**C**), CD86 (**D**), CD80 (**E**), and CD40 (**F**) by DC ($CD11c^+$) from PP lysates co-cultured with or without Zymosan or pullulan. * = $p < 0.05$ (against unstimulated); ^{o} = $p < 0.05$ (against LPS-conA); n = 6.

Figure 2 – Zymosan and pullulan limit IgA and *Salmonella* translocation into PP.

(**A**) Immunofluorescence of *Salmonella*-GFP (green arrows) within a Peyer's patch (white line) and quantification of mean *Salmonella* counts per PP (graph) (**B**) Mean *Salmonella* counts per PP when intestinal loops were injected with 10^5 CFU of *Salmonella*-GFP in mice gavaged with either PBS, or 1mg of zymosan or pullulan. (**C**) Mean GFP fluorescence intensity per PP when intestinal loops were co-injected with 10^5 CFU of *Salmonella*-GFP and either PBS, or 1mg of zymosan or pullulan (**D**) Mean *Salmonella* counts per PP when intestinal loops were co-injected with 10^5 CFU of *Salmonella*-GFP and either PBS, or 1mg of zymosan or pullulan. (**E**) Percentage of anti-IgA-AF555 fluorescent area of PP co-injected with 10^5 CFU of *Salmonella*-GFP and either PBS, or 1mg of zymosan or pullulan. (**F**) Percent of co-localized anti-IgA-AF555 and GFP signals in PP co-injected with 10^5 CFU of *Salmonella*-GFP and either PBS, or 1mg of zymosan or pullulan. * = $p<0.05$; ** = $p<0.01$ (against PBS), n= 12.

Figure 3 – Zymosan and pullulan promote survival during *Salmonella*-induced colitis.

(**A-E**) Treatment of mice with either zymosan or PBS, * = $p<0.05$; ** = $p<0.01$ (against PBS), n= 2. (**F-I**) Treatment of mice with either TLR-depleted zymosan or PBS, * = $p<0.05$; ** = $p<0.01$ (against PBS), n= 2. (**J-N**) Treatment of mice with either pullulan or PBS. * = $p<0.05$; ** = $p<0.01$ (against PBS), n= 2.

(**A, F, J**) Percent survival of mice ten days after *Salmonella* infection. (**B, G, K**) Percent weight loss and (**C, H, L**) disease activity scores over the ten days following infection. (**D, I, M**) ELISA dosage of serum IL-6 levels at the day of sacrifice. (**E, N**) ELISA dosage of faecal Lipocalin-2 levels at the day of sacrifice and Spearman's correlation between faecal lipocalin-2 and IgA levels at the day of sacrifice.

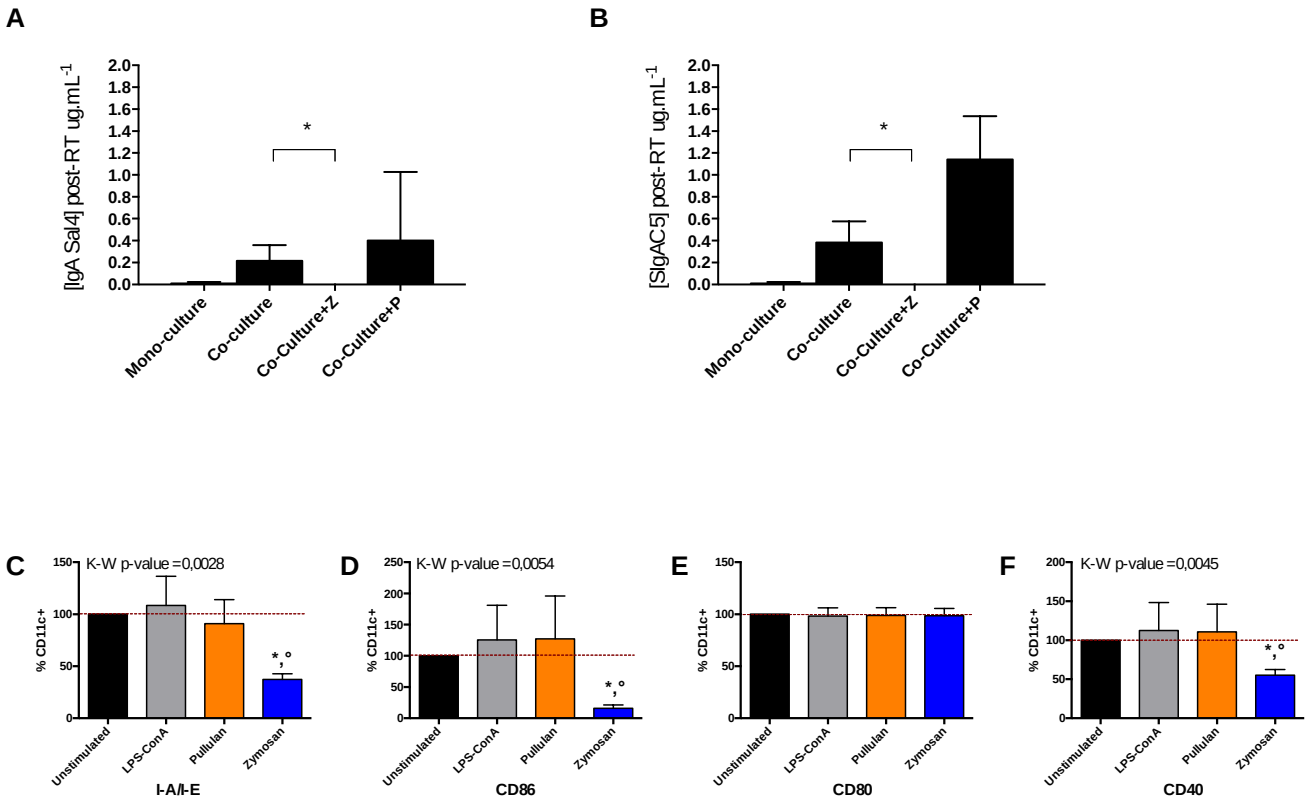
A
[IgA Sal4] post-RT ug.mL-1
2.0
1.8
1.6
1.4
1.2
1.0
0.8
0.6
0.4
0.2
0.0
*
Mono-culture
Co-culture
Co-Culture+Z
Co-Culture+P
B
[SIgAC5] post-RT ug.mL-1
2.0
1.8
1.6
1.4
1.2
1.0
0.8
0.6
0.4
0.2
0.0
*
Mono-culture
Co-culture
Co-Culture+Z
Co-Culture+P
C
K-W p-value =0,0028
% CD11c+
150
100
50
0
*, °
Unstimulated
LPS-ConA
Pullulan
Zymosan
I-A/I-E
D
K-W p-value =0,0054
% CD11c+
250
200
150
100
50
0
*, °
Unstimulated
LPS-ConA
Pullulan
Zymosan
CD86
E
% CD11c+
150
100
50
0
Unstimulated
LPS-ConA
Pullulan
Zymosan
CD80
F
K-W p-value =0,0045
% CD11c+
200
150
100
50
0
*, °
Unstimulated
LPS-ConA
Pullulan
Zymosan
CD40

Fig. 1

Fig. 2

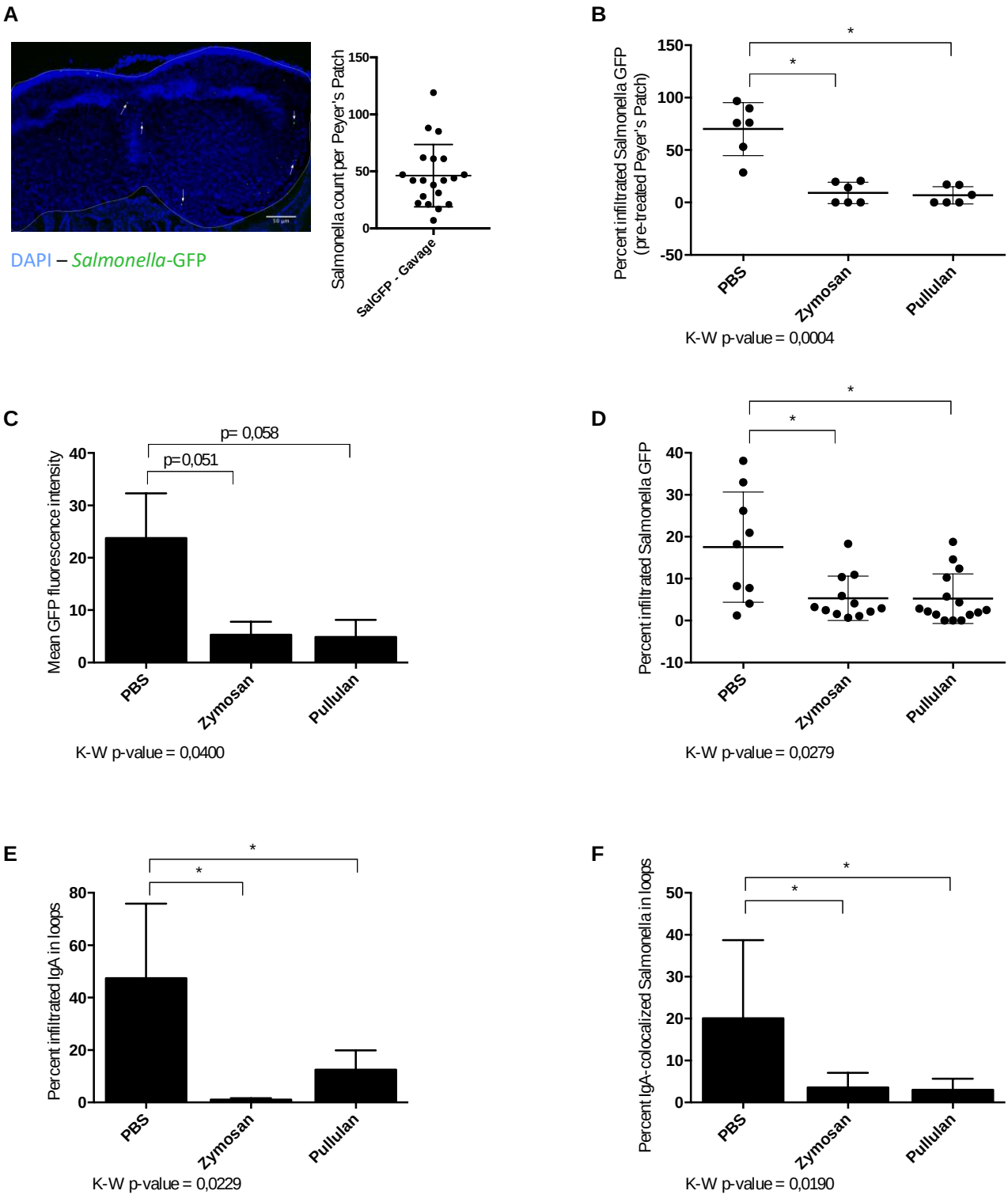
A
DAPI – Salmonella-GFP
Salmonella count per Peyer's Patch
SalGFP - Gavage
B
Percent infiltrated Salmonella GFP (pre-treated Peyer's Patch)
PBS
Zymosan
Pullulan
K-W p-value = 0,0004
C
Mean GFP fluorescence intensity
p= 0,058
p=0,051
K-W p-value = 0,0400
D
Percent infiltrated Salmonella GFP
K-W p-value = 0,0279
E
Percent infiltrated IgA in loops
K-W p-value = 0,0229
F
Percent IgA-colocalized Salmonella in loops
K-W p-value = 0,0190

Fig. 3

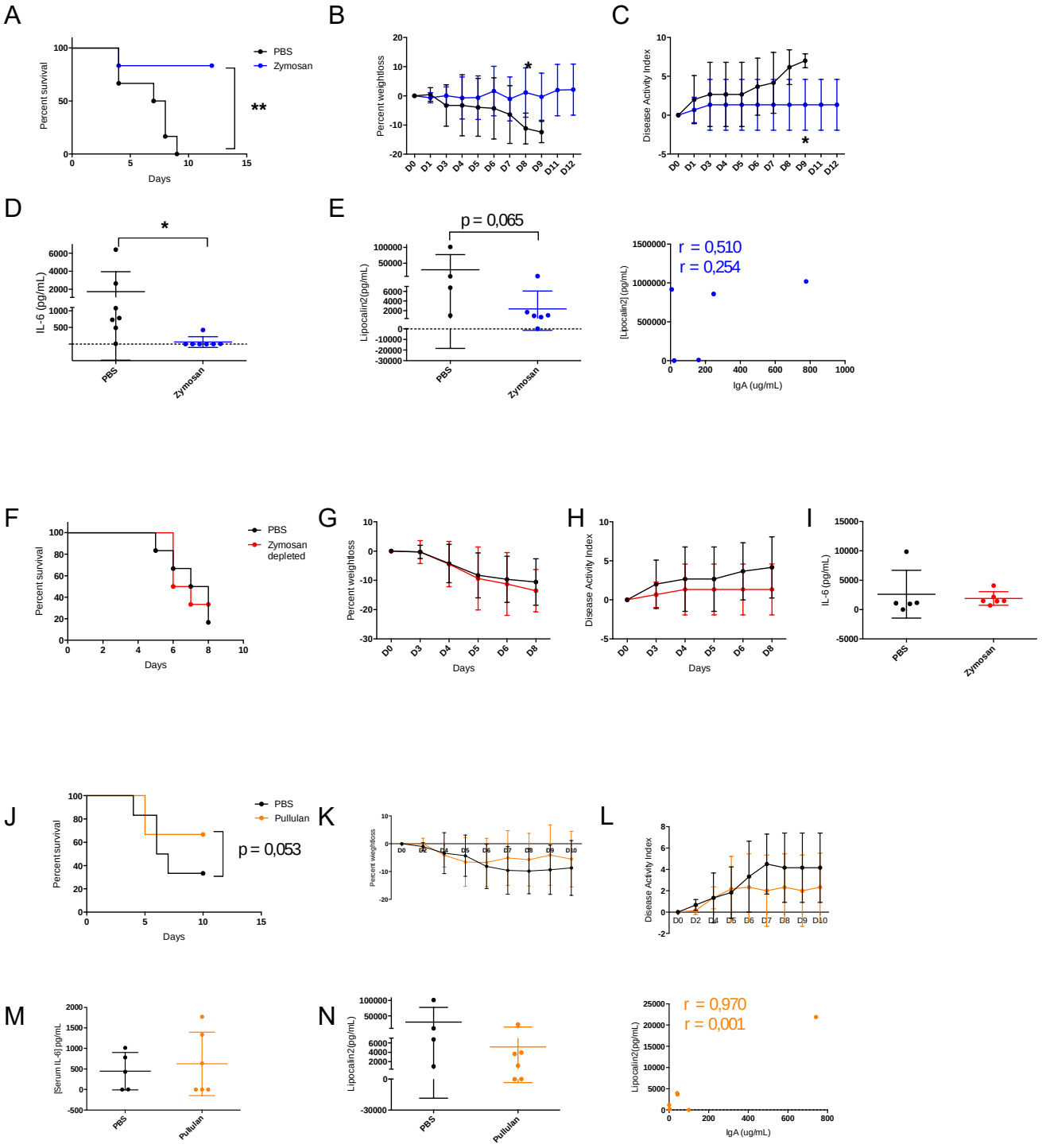
A
Percent survival
PBS
Zymosan
**
Days
B
Percent weightloss
*
C
Disease Activity Index
*
D
IL-6 (pg/mL)
*
PBS
Zymosan
E
p = 0,065
Lipocalin2(pg/mL)
r = 0,510
r = 0,254
[Lipocalin2] (pg/mL)
IgA (ug/mL)
F
Percent survival
PBS
Zymosan depleted
Days
G
Percent weightloss
Days
H
Disease Activity Index
Days
I
IL-6 (pg/mL)
J
Percent survival
PBS
Pullulan
p = 0,053
Days
K
Percent weightloss
L
Disease Activity Index
M
[Serum IL-6] pg/mL
PBS
Pullulan
N
Lipocalin2(pg/mL)
r = 0,970
r = 0,001
IgA (ug/mL)

B- Conclusions et perspectives

Nous montrons que la compétition pour la liaison a Dectin-1 limite le passage des SIgA dans la muqueuse en parallèle d'une amélioration des symptômes de la colite à Salmonelle grâce à l'utilisation du zymosan. Néanmoins, les mécanismes d'action du zymosan ainsi que leurs effets sur l'orientation de la réponse immune muqueuse ne sont pas connus. Ainsi, d'autres travaux montrent que son administration est délétère au cours de colites au DSS [417]. Le différentiel d'effet peut s'expliquer par un choix de fond génétique et de mode d'induction de la colite différent. Par ailleurs, d'autres données suggèrent que le zymosan induit la sécrétion d'IL-10 dans des macrophages *in vitro* [418]. Le zymosan, en liant Dectin-1 à la surface de macrophages déclenche l'activation de la voie MAPK selon une cascade calcium-dépendante[418]. Le calcium, au niveau de l'intestin est un ion crucial, en témoigne l'effet anti-inflammatoire des inhibiteurs de calcineurines dans les MICI[233]. Dans notre modèle de co-culture de lysat de PP, il serait donc intéressant de tester l'utilisation du calcium dans le surnageant de culture et la transcription d'effecteurs des cascades dépendantes du calcium dans les cellules. Dans un second temps, nous pourrions trier les cellules de ce lysat pour évaluer la réponse calcique en fonction d'un type cellulaire et corréler celle-ci à la sécrétion de cytokines pro- ou anti-inflammatoires. Pour aller plus loin, l'effet de la co-administration de zymosan avec des SIgA devrait également être vérifié dans ces cultures. De même, il faudra inclure des conditions expérimentales où l'IgA est délivrée seule, puis complexée à la souche SL1344. En comparant la réponse immune selon que les cellules reçoivent également du zymosan, nous vérifierions ainsi qu'en conditions infectieusesf, le zymosan limite l'inflammation. Sur un modèle humain, nous pourrions reproduire les expériences de Steffen, *et al.*, qui ont testé le recrutement de macrophage et de neutrophiles et leur sécrétion cytokinique selon qu'ils sont co-cultivés avec des IgA1 ou des IgA2[128] : nous administrerions nos IgA purifiées d'individus non-IBD avec et sans zymosan, pour évaluer le recours au métabolisme du calcium dans ce modèle et le phénotype d'activation général des cellules.

Pour parfaire notre analyse, il faudra démontrer la compétitivité vraie entre le zymosan et l'IgA par des calculs de constante de dissociation (K_D) et fonction de la présence ou nom de zymosan dans des tests ELISA de compétitivité, dans un premier temps. Dans un second temps, nous pourrions utiliser la thermophorèse comme cela a été fait pour l'article 1, et comparer (1) la force de liaison ligand-récepteur entre le zymosan et les IgA1 et IgA2 humaine, puis (2) mesurer cette force de liaison lorsque les IgA et le zymosan sont tous les deux en solution et compétitionnent pour la liaison à Dectin-1.

Le pullulan, pour lequel nous n'attendions pas initialement de réponses protectrices, s'est cependant montré prometteur, en promouvant la survie des souris. Bien que les symptômes inflammatoires soient restés comparables entre les groupes traités au pullulan et les groupes contrôles, l'administration de pullulan limitait l'invasion bactérienne de la PP et la translocation d'IgA au niveau de celle-ci. Plusieurs mécanismes, probablement complémentaires, sont envisageables : (1) des données montrent que le pullulan favorise l'expression et l'activation de Dectin-2, ce qui suggère potentiellement une réorientation de la muqueuse vers un profil Th_{17}- Th_2 [47,414,415], plutôt que Th_{17}-Th_1, promue par Dectin-1 [42,44,412,413]. (2) Le pullulan favorise l'adhérence cellulaire lors de culture d'explant[419], aussi il est possible qu'il promeuve l'agglutination bactérienne (complexée ou non aux IgA) dans la lumière intestinale, ce qui créerait une gène stérique limitant l'entrée de ces complexes dans la PP. L'agglutinat immun serait ensuite drainé par le flux intestinal. Pour vérifier cette hypothèse, des expériences d'agglutination des Salmonelle seront réalisées en présence ou non d'IgA murines, puis humaines. Il faudra également démontrer l'interaction pullulan-Dectin-2, si elle a lieu dans notre modèle. Pour ceci, une co-immunoprécipitation à partir de culture de lysat de PP dans lesquelles le pullulan est délivré sera mise e place, et ciblera Dectin-2 ainsi que les effecteurs de sa voies de signalisation, dont fait partie l'inflammasome NLRP3 [48,420]. Des expériences permettant de vérifier l'expression de Dectin-2 dans notre modèle *in vitro* pourraient permettre de vérifier son expression par les cellules M, et de vérifier si, seul, il est internalisé par celles-ci. Des expériences subséquentes de siRNA dans ce modèle nous permettrons de caractériser la signalisation mise en jeu par le pullulan dans notre modèle. Bien qu'il n'inhibe pas la RT des IgA, nous supposons qu'il possède une signature immune spécifique qui n'est pas caractérisée.

Pour conclure, il faudra répéter les expériences *in vivo* sur le modèle de colite à Salmonelle, mais aussi dans des modèles de colites spontanées liées à des KO géniques (*Il10r2*$^{-/-}$*Tgfbr2*$^{-/-}$, *Tbx21*$^{-/-}$*Rag2*$^{-/-}$, *Il12*$^{-/-}$, *Il10*$^{-/-}$) ou dans des modèles récapitulant des polymorphismes géniques associés aux MICI (NOD2 KO, Dectin-1 KO)[194]. L'inhibition, ou la compétition pour la RT des IgA est une voie qui n'est pas encore utilisée pour rompre la boucle inflammatoire qui s'établit au cours de MICI, et qui présente des résultats prometteurs pour l'élaboration de nouvelles stratégies thérapeutiques.

DISCUSSION GÉNÉRALE

Les SIgA assurent la première ligne de défense des muqueuses notamment par leurs capacités à réguler la croissance d'espèces de la flore au potentiel opportuniste et à identifier des espèces d'entéro-pathogènes. L'orientation de réponses adaptatives appropriées est régie à la fois grâce à cette ségrégation par les IgA, et également par les différents mécanismes d'échantillonnages par les PRR muqueux. Mon travail de thèse montre pour la première fois l'importance de la sous-classe et de la structure d'IgA dans le maintien du mutualisme commensal. En parallèle de cela, mes recherches ont mis en évidence le mode d'action complémentaire des IgM. Ces données soulignent l'importance du transport optimal des SIgs à travers la muqueuse intestinale et illustrent d'importants défauts fonctionnels des SIgs au cours de maladies inflammatoires comme les MICI.

En conditions physiologiques, mes travaux montrent que des IgA monomériques activent des voies transcriptionnelles liées aux gènes de l'inflammation, mais que les IgA1 et IgA2 dimériques induisent respectivement une diminution et une augmentation de ces gènes. Ce constat est cohérent avec de précédents travaux dans lesquels des IgA monomériques ont été préalablement agglutinées pour mimer un complexe immun puis testées *in vitro* en co-culture avec des neutrophiles ou des macrophages[128]. Dans ce modèle, où les fonctions effectrices des IgA sont associées à la liaison au FCαRI (CD89), le recrutement accru des neutrophiles, la NETose, et l'augmentation de la sécrétion d'IL-8 et des ROS, sont particulièrement associés à l'activation de la voie intracellulaire induites par les kinases *Syk* et *Erk* lors de la liaison IgA2-FcαRI. Cette étude, l'une des rares comparant les sous-classes d'IgA et leurs fonctions, semble indiquer que l'éventuelle activité inflammatoire des IgA1 est inhibée par l'activation de la phosphatase *Shp-2*. D'autre travaux impliquent le facteur STAT3 dans l'exacerbation de l'inflammation IgA1-dépendante [421].

Les fonctions effectrices de l'IgA1 sont également inhibées par les sialylations portées sur les sites de N-glycosylation N144 et N340 [128]. Ces deux sites sont partagés par les IgA2 (N144/N131 et N340/327).La régulation des sialylations des IgA1 et IgA2 pourrait ainsi constituer un mode de régulation fonctionnelle permettant de basculer rapidement d'une immunité IgA1-dépendante à une immunité IgA2-dépendante selon le contexte inflammatoire. Des fonctions inhibitrices des sialylations, décrites pour les IgM[422], suggèrent que les

modifications post-traductionnelles modifient en effet l'orientation des réponses immunes. De plus, le résidu N58 du FcαRI, lui aussi extensivement sialylé, est critique pour la fonctionnalité du FcαRI et la liaison des IgA par celui-ci [423]. Ainsi, sa désialylation induit une augmentation de la liaison aux IgA[423]. La dérégulation de son fonctionnement est observée dans plusieurs maladies auto-immunes dont le virus de l'immuno-déficience humaine (VIH), le syndrome Henoch-Purpura, et les néphropathies à IgA[424]. Ces maladies présentent, respectivement, une altération de la production d'IgA[425], une dysbiose microbienne[426], et des dépôts d'IgA1 accompagné d'altération de la diversité microbienne[162,427]. Ces dérèglements suggèrent donc que les glycosylations et la biologie du FcαRI occupent un rôle primordial au niveau muqueux. Le comportement et l'expression de ce dernier au cours de MICI, par exemple, ne sont pas décrits.

La MC et laRCH sont associées à une sécrétion accrue d'IL-17 en réponse à des antigènes commensaux[357,428,429]. Or, une étude *in vitro* montre que l'IL-17 peut induire une sécrétion d'IgA1 sous-glycosylées[430]. Les IgA1 potentialisent le recrutement de l'immunité Th_{17} dans les néphropathies à IgA *via* la chimiokine CCL20[431]. Les sialylations semblant inhibitrices, l'étude du profil de glycosylation des IgA utilisées au cours de nos travaux est actuellement en cours auprès de nos collaborateurs du CBMN (CNRS, Université de Bordeaux). Elle devrait permettre d'établir si de tels défauts sont retrouvés chez les patients, et s'ils peuvent être corrélés au profil d'inflammation. Des données préliminaires que nous avons obtenues semblent l'indiquer.

Nous observons dans la MC un enrichissement de la fraction $IgA1^+$ du microbiote en espèces bénéfiques telles que *Bacteroides, Bifidobacterium* et *Faecalibacterium*. L'abondance fécale de ces taxa diminue chez les patients et coïncide avec la sévérité de la maladie[401,432,433]. Ceci suggère un rôle pathogénique de la sélection par les IgA1 dans la MC, et plus encore un basculement fonctionnel des IgA1 vers la promotion de l'inflammation. En conditions homéostatiques, ces dernières sont plutôt associées à la tolérogénisation des muqueuses, notamment *via* la stimulation de la sécrétion d'IL-10, et à l'enrichissement en actinobactéries du microbiote[220]. Par ailleurs, les plasmocytes $IgA1^+$ sont principalement retrouvés dans l'iléon tandis que ceux $IgA2^+$ sont retrouvées majoritairement au niveau de la muqueuse colique [434]. Comme il y a peu de données suggérant un basculement depuis une sous-classe IgA1 vers IgA2 en conditions homéostatiques[434], l'hypothèse qu'un tel basculement ait lieu dans les MICI reste à explorer. En effet, des populations mémoires IgM^+, IgG^+, $IgA1^+$ et $IgA2^+$ sont retrouvées tout le long du GALT[434]. Il y existe un répertoire à IgA distinct spécifiquement associé soit à l'iléon

et soit au colon[434]. Ceci indique une sélection des antigènes qui peut correspondre avec une colonisation différentielle de la muqueuse par la flore commensale sur ces deux sites[435]. Les formes coliques de MC et la RCH présentent de nombreuse similarités, en particulier une association génétique avec des polymorphismes sur les gènes du HLA[436,437]. Il serait donc intéressant de comparer la fonctionnalité des IgA et du répertoire dans ces compartiments au cours de MICI. J'ai pu démarrer ce travail notamment en mettant en place dans le laboratoire la génération d'hybridomes LB en grand nombre à partir de résections iléales de patients atteints de MC, et pour lesquelles les résultats de séquençage ne sont pas disponibles au moment de la conclusion de cette thèse.

La sécrétion défectueuse des IgA a été décrite chez les patient atteints de RCH[351]. Nos résultats montrent que les IgA produites sont de plus incapables d'effectuer la RT et présentent une perte généralisée de leur réactivité anti-glycans. Les clones LB issus d'ILF représentent la majorité du répertoire colique [434]. Cet adressage vers le colon parait assuré par l'expression différentielle des récepteurs de domiciliation CCR9 (adressage vers l'iléon) et GPR15 (adressage vers le colon)[434]. La formation d'ILF chez les patients atteints de MICI n'a pas été investiguée. Au-delà de la structure et de la fonction des Ig produites au cours des MICI, les dynamiques de migration et de recirculation des LB les produisant devraient donc être prises en compte. Dans un premier temps, le phénotypage par cytométrie en flux de l'expression membranaire des récepteurs de domiciliation (dont CCR9 et GRP15) par les LT et les LB pourrait être réalisé à partir de biopsies. Il a été démonté, par exemple, que les intégrines αEβ7 induisent la migration de population LT $CD4^+$ inflammatoires vers le colon au cours de la RCH[429]. De plus, une étude dans la RCH fait état d'une augmentation de la recirculation des T_{fh} chez les patients dont la maladie est active[438]. Les T_{fh}, *via* la sécrétion d'IL-21 (elle aussi augmentée dans la RCH[438]), favorisent la CSR des LB. En parallèle de ces résultats, s'observe une élévation du taux sérique d'IgG[438], rejoignant donc les observations d'augmentation du taux fécal d'IgG anti-commensales[8]. La perte fonctionnelle des IgA pourrait être ainsi à l'origine d'une sélection préférentielle des plasmocytes à IgG. Cette hypothèse pourrait être vérifiée dans les populations B mémoires intestinales, par séquençage des transcrit germinaux de CSR sur les gènes des chaînes lourdes μ, α, et γ. De cette manière, Magri, *et al* démontrent que les clones mémoires IgM^+ intestinaux re-circulent entre l'iléon et le colon avant d'effectuer leur différentiation terminale ou bien la CSR vers l'istoype IgA dans les centres germinatifs [133]
.

La RT des IgA requiert la liaison à Dectin-1[43,180]. Nous montrons d'une part que Dectin-1 (et son corécepteur Siglec-5) est régulée négativement par le PRR NOD2 *in vitro* et que les patients atteints de MC avec des polymorphismes NOD2 présentent une augmentation de la RT. D'autre part, l'affinité des IgA1 pour Dectin-1 corrèle avec la capacité d'effectuer la RT dans la MC, fonction réservée aux IgA2 en conditions physiologiques. Dectin-1 semble donc occuper une fonction centrale dans la MC. Si aucune étude n'a identifié d'association génétique entre la MC et le gène *clec7a* (Dectin-1)[439], d'autres ont été identifiée entre la MC et *CARD9,* codant pour l'un des effecteurs clés de la voie de signalisation Dectin-1-dépendante [440,441].

Les ligands naturels de Dectin-1 sont les β-glucans fongiques[442]. L'expression de Dectin-1 par la cellule M[43] suggère donc une position privilégiée dans la régulation du microbiote fongique. Des polymorphismes génétiques sur le gène codant pour Dectin-1 sont associés au développement de formes sévères de la RCH[442]. Dans les MICI, les altérations dans la diversité fongique sont également très marquées. L'abondance des espèces *Exophiala, Alternaria, Emericella, Epicoccum, Acremonium, Trametes,* et *Penicillium* diminue, tandis que celle des *Aspergillus, Sterigmatomyces,* et *Candida* augmente[443]. Ce « mycobiote » joue donc un rôle dans le maintien de l'homéostasie intestinale. Bien que minoritaire chez l'adulte au bénéfice de populations bactériennes, l'abondance de ces champignons est importante dans l'enfance[444]. Parmi les membres les plus fréquents du microbiote fongique se trouvent les espèces *Candida albicans, Candida galabriata,* et *Saccharomyces cerevisiae.* Leur caractère opportuniste est limité par les lactobacilles de la flore commensale[444]. Dans les MICI, une augmentation du *ratio Basidiomycota/Ascomycota* est observée, ainsi qu'une diminution de l'abondance des *Saccharomyces cerevisiae* et une augmentation de celle des *Candida albicans*[350]. La dysbiose bactérienne, et la perte de ces lactobacilles, au cours des MICI [445] pourrait donc contribuer à l'expansion incontrôlée des espèces fongiques. Dans la MC, l'environnement microbien semble favoriser la croissance des espèces fongiques plutôt que bactériennes[350]. La dérégulation de l'expression de Dectin-1, notamment chez les patients présentant des polymorphismes NOD2 devra donc être évaluée et corrélée à ces défauts de diversité fongique. L'analyse de la diversité de ces espèces fongiques dans les fractions $IgA1^+$ et $IgA2^+$ de notre cohorte serait par ailleurs une mesure complémentaire importante de l'implication des IgA muqueuses dans la dysbiose intestinale.

Mes travaux de thèse décrivent l'impact des IgA et de leur structure sur la polarisation de réponses immunes en conditions physiologiques et inflammatoires. Pourtant, nous montrons également que les IgM fonctionnent selon un mode similaire aux SIgA en termes de trafic dans l'épithélium et de présentation d'antigènes. Également capables de lier la pièce sécrétoire et d'effectuer la transcytose, la fonction muqueuse des SIgM reste cependant peu connue. Quantitativement, la sécrétion d'IgM est minoritaire dans l'intestin[391]. Des études de la sécrétion de la diversité microbienne associée aux SIgM chez les patients déficients en IgA (SIgAd) montrent **1)** que les SIgM sont plus abondantes chez les patients SIgAd, et **2)** que la liaison des SIgM permet de maintenir partiellement le microbiote normalement associé aux IgA[209,391]. La sécrétion d'IgM semble donc complémentaire à celle des IgA, limitant les phénomènes inflammatoires en son absence, et compensant partiellement ses fonctions d'opsonisation[446]. Cependant, comme pour les IgA, il n'est pas à exclure que les isoformes d'IgM aient un impact différent sur la réponse. Ainsi, la forme hexamèrique serait le résultat d'une production aberrante d'IgM [447,448]. Elle serait également produite lorsqu'une forte activation du complément est requise [447,448]. Le nombre et la nature des N-glycosylation variant entre la forme pentamérique et hexamèrique [448], il est probable que ces différences affectent les fonctions effectrices des IgM. Les MICI étant un terrain où des défauts de sécrétion des Ig sont mis en évidence[312,351,402,449,450], de telles altérations sont fortement probables. Chez l'homme, les IgA et IgM dérivées du plasma et liées à la SC induisent toutes deux l'agrégation et la neutralisation de *S. enterica* Typhimurium *in vitro*[185], et suggèrent une fonction anti-inflammatoire des SIgM[451]. Il reste à investiguer dans quelles mesures cette liaison contribue à la diversité microbienne intestinale. La liaison SIgM-commensale[209] et la génération de plasmocytes IgM^+ résidents [133] qui ont bien été observées, n'indiquent pas si l'IgM intestinale sélectionne sa propre fraction du microbiote, ou si elle co-sélectionne le microbiote IgA^+. Les interactions IgM-microbiote fongique n'ont à ce jour pas été démontrées. De plus, les clones mémoires intestinaux IgM^+ répondant aux signaux commensaux effectuent la CSR vers l'IgA en réponse aux signaux TI et TD[133]. Ils présentent une signature génique proche des LB IgM^+ et IgA^+ circulants[133], ce qui suggère une importante redondance fonctionnelle. De fait, l'état actuel de la littérature suggère plutôt qu'en conditions physiologiques, IgA et IgM partagent les mêmes cibles microbiennes[133]. De plus, l'enrichissement en espèces bénéfiques tels que *Lachnospira* et *Ruminococcaceae* dans les fractions IgM^+ du microbiote implique une préférence vers la promotion de la tolérance muqueuse plutôt que l'identification de pathobiontes[133]. Il serait donc particulièrement intéressant de comparer les fractions IgM^+ des

microbiotes des patients atteints de MICI dont la maladie est active avec ceux pour qui elle est quiescente afin de vérifier si les IgM peuvent favoriser ce retour à l'homéostasie en compensant les défauts associés aux IgA. Cette analyse serait d'autant plus informative que nous avons observé une diminution de la sécrétion d'IgA et une perte de la réactivité et des capacités de transport de ces dernières chez les patients atteints de RCH. Comparer la réponse IgA et IgM chez ces patients pourrait être un marqueur biologique précieux potentiellement pronostique. Par ailleurs, la fonction « inflammatoire » muqueuse des SIgM reste à étudier. Ainsi, dans la maladie cœliaque, les patients non-traités présentent une opsonisation accrue des bactérie de la flore, dont *F. prautzinii* et *Bifidobacterium sp,* par les SIgA et les SIgM.[400]. Chez des enfants atteints du syndrome Henoch-Schönlein, la dysbiose orale est corrélée au taux local d'IgM [94]. Ce même taux est aussi corrélé à l'abondance des espèces *Prevotella*, promotrices d'inflammation[94]. De fait, nous allons également évaluer si la sécrétion de SIgM intestinales favorise la mise en place de la dysbiose dans les MICI

Outre les MICI, d'autres maladies présentent des altérations de la diversité microbienne comme l'obésité ou le diabète de type 2[452]. Ainsi, un régime HFD augmente le taux de bactéries IgA^+ chez la souris[228]. Ces souris présentent une déficience en IgA, et elles développent également des troubles de la régulation du glucose et une augmentation de l'inflammation dans l'intestin et le tissus adipeux[228] qui suggèrent que l'IgA régule indirectement la résistance à l'insuline . Chez des animaux sauvage, le gène *P2x7* code pour un récepteur régulateur de l'expansion de T_{fh}. Lorsqu'il est absent chez les souris, la production de SIgA augmente et celles-ci opsonisent massivement les lactobacilles de la flore intestinale [147]. L'administration de lactobacilles de ces souris $P2x7^{-/-}$ à des animaux sauvages entraîne une dérégulation du métabolisme du glucose et une augmentation du stockage d'acide gras [147], qui pourrait expliquer les dérèglements microbiens observés chez les patients obèses et/ou diabétiques. Il serait donc intéressant de corréler cette observation à un trafic altéré des complexes SIgA-lactobacilles à travers l'épithélium. L'administration d'une souche de lactobacille opsonisée par les SIgA humaines à des souris pendant un HFD entraîne une diminution de l'inflammation, notamment par une baisse de la sécrétion d'IL-6 et de TNF-α [215]. L'utilisation de souches bactériennes bénéfiques ciblées afin de traiter un microbiote dysbiotique offre donc de nouvelle voie thérapeutique dans la prise en charge de maladies métaboliques.

Dans les cas d'inflammations liées à des antigènes alimentaires, comme les allergies alimentaires ou la maladie cœliaque, la sécrétion d'IgA est l'élément inducteur de dysbiose[226,400,416]. Ainsi, un mode de retro-transport FcαRI-dépendant de complexes gliadine-SIgA1 et des SIgA1 seules a été proposé pour expliquer la pathogenèse de la maladie cœliaque [416,453]. Ce mécanisme peut être corrigé en stimulant le microbiote par l'administration de probiotiques dérivés de *Saccharomyces boulardii* [416]. Cette interaction muqueuse IgA1-FcαRI a sans doute également lieu dans la MC et devra être vérifié dans notre modèle. Cela dit, il reste difficile de trancher quant aux fonction protectrices ou aggravantes des SIg en condition pathologiques. Par exemple, des taux sériques élevés de SIgA sont associés à une baisse d'activité dans des maladies arthritiques (arthrite et spondylarthrite) [454]. Cela dit, ce que cette étude décrit comme « SIgA » est sans doute l'IgA monomérique circulante, qui peut alors occuper une fonction tolérogène. A l'opposé, une forte opsonisation d'*E. coli* par les IgA fécales est associée au développement de spondylarthrite dans la MC[312]. Le taux de SIgA augmente dans la maladie alcoolique du foie[455] et suggère que la compartimentation de la sécrétion d'IgA et les liens qui sous-tendent sa régulation restent à définir. De plus, les IgG anti-commensales dirigées contre *Saccharomyces cerevisiae* augmentent également dans la maladie alcoolique du foie [455]. Une reconsidération du rôle des IgG anti-commensale muqueuse est proposée par de plus en plus de travaux. De fait, le taux d'IgG anti-*Streptococcus gallolyticus* est corrélé au risque de cancer colorectal [456]. De même, l'augmentation de l'abondance fécale de *Ruminococcus gnavus* est associée à un forte réponse IgG systémique envers cette bactérie commensale dans le lupus systémique érythémateux (SLE) [456]. Un faible taux IgG anti-commensale dans la petite enfance jouerait également un rôle dans le développement des allergies [456]. La sécrétion d'Ig muqueuse régule différemment – et est régulée par – les interactions hôte-microbiote selon le compartiment muqueux et le stade développemental d'un individu.

L'ensemble de nos travaux vise à caractériser les enjeux des interactions IgA-microbiote au cours des MICI dans l'espoir d'y trouver de nouvelles stratégies thérapeutiques. Parmi celles-ci nous avons mis en évidence plusieurs ligands bactériens limitant le transport des IgA dans la PP chez la souris et favorisant la rémission suite à l'infection par *Salmonella* Typhimurium. Ces résultats préliminaires semblent dépendants du fond génétique murin et feront l'objet d'une caractérisation plus précise. Chez l'homme, la transplantation fécale (FMT) semble très prometteuse. Si elle offre d'excellents résultats dans la résolution d'infections chroniques à *Clostridium difficile* [457,458] les essais chez les patients atteints de MICI donnent

des résultats très variables et mitigés. Ainsi, elle semble fonctionner chez les formes pédiatriques de la RCH et beaucoup moins chez les adultes[459]. Chez ces derniers, une répétition de la FMT et l'adéquation donneur-receveur favorisent le succès de la thérapie[459]. Dans la MC, la grande variabilité des résultats ne permet pas de conclure quant à l'efficacité de la FMT, bien que les patients en ayant bénéficié rapportent une amélioration de leur qualité de vie. À la lumière de nos résultats, cela pourrait s'expliquer peut-être une inadéquation entre les fractions IgA^+ (et même $IgA1^+$) entre le microbiote du donneur et celui du receveur, qui n'est pour le moment pas évoquée par les essais actuels. De même, le rôle des IgM et des IgG dans la compatibilité donneur-receveur serait à évaluer. Dans l'hypothèse selon laquelle les SIg des patients recevant ces traitements sont conditionnées pour éliminer les espèces bénéfiques, comme cela semble être le cas dans mes travaux, il apparait nécessaire de bloquer ces interactions néfastes en même temps que l'administration de la flore greffée. L'inhibition de la CSR des IgA, et la co-administration de probiotiques pourraient ainsi s'avérer bénéfiques. Des effets secondaires, notamment l'induction de poussées dans les MICI, ont également été observés après FMT, et suggèrent que cette pratique nécessite une plus ample connaissance des interactions bactériennes et de la compatibilité donneur-receveur.

L'étude des SIg est critique pour l'élaboration de nouvelles stratégies thérapeutiques muqueuses, et plus fondamentalement pour la compréhension de la compartimentation des muqueuses. La capacité des IgA et des IgM sécrétoires à traverser efficacement les muqueuses monostratifiées, nous ont poussé à utiliser les IgA comme vecteurs d'adressage vaccinal d'antigènes pour la protection contre des pathogènes ayant un réservoir muqueux, tels que le VIH[389,460]. Ainsi, l'immunisation nasale par des IgA complexée à la p24 génère une immunité protectrice orale, vaginale, et intestinale[389]. Enfin, l'immunisation muqueuse par des SIgA spécifique de microbe associés à des maladies métaboliques comme *Clostridium ramnosum* , associé à la dysbiose HFD-induite limite l'induction de l'obésité et de ses co-morbidités chez la souris[177]. Ces essais promoteurs ont le potentiel de devenir de nouvelles thérapies non-invasives et personnalisées pour le soin et la prise en charge des maladies inflammatoires muqueuses.

CONCLUSION GÉNÉRALE

Mon travail de thèse permet d'alimenter une réflexion en plein essor sur l'importance des interactions microbiote-immunité au stade physiologique (AMIS) mais aussi dans la prise en charge et l'étude des MICI. Si les défauts immuns et les défauts microbiens existant dans ces maladies sont, de manière générale, connus, ils n'en restent pas moins au stade d'observation. Le lien de cause à effet entre sélection de la flore par les IgA et mise en place de boucles inflammatoires associées à la dysbiose reste à caractériser. En ce sens, nos résultats montrent clairement **(1)** que les IgA1 et les IgA2 exercent des fonctions respectivement anti- et pro-inflammatoire en conditions physiologiques, **(2)** que les IgA1 humaines acquièrent une fonction de transport dans la MC, fonction promue par les polymorphisme génétique NOD2 et **(3)** que la RCH se caractérise par une perte fondamentale de ces fonctions de transport et de la poly-réactivité des IgA. De plus, il reste à définir précisément le rôle et le comportement des SIgM et des IgG muqueuses en conditions physiologiques et en conditions de dysbiose.

Les approchent thérapeutiques visant à rééquilibrer la diversité microbienne dans les MICI ne prennent actuellement pas en compte cette composante humorale du mutualisme commensal. C'est peut-être là la raison des échecs thérapeutiques liés aux thérapies nutritionnelles et de la FMT. Neutraliser les réponses aberrantes des SIg envers la flore devrait ainsi être une démarche concomitante à l'administration de flore bactérienne de donneurs sains. Ces résultats peuvent, de plus, être exploités pour l'étude d'autre maladies immunitaires (telles que les allergies alimentaires), auto-immunes (telles que la polyarthrite rhumatoïde ou le SLE, Annexe 3) et métaboliques (telles que le diabète, l'obésité) où il est maintenant prouvé que le microbiote est altéré.

Annexe 1 – Revue sur les IgM sécrétoires

Trends in Immunology

CellPress REVIEWS

Review

Human Secretory IgM: An Elusive Player in Mucosal Immunity

Eva Michaud,[1] Carmelo Mastrandrea,[2] Nicolas Rochereau,[1,3] and Stéphane Paul[1,3,*]

Secretory IgMs (SIgMs) were amongst the first identified immunoglobulins. However, their importance was not fully understood and recent advances have shown they play a key role in establishing and promoting commensal gut tolerance in mice and humans. The true interactions between SIgMs and the microbiota remain controversial and we aim to consolidate current knowledge in this review. Through comprehensive examination of SIgMs and their corresponding B cell secretors in several different pathological immunological contexts, we review the presumed role of these molecules in gut tolerance, inflammatory bowel diseases, and lung immunity. As SIgMs harbor a mostly tolerogenic function, we posit that their inclusion in further immunological research is paramount.

Highlights

Human secretory immunoglobulin-M (SIgM) is mostly natural IgM and shapes the colonization of mucosal surfaces.

SIgMs can selectively bind commensal bacteria at mucosal surfaces and may have overlapping functions with SIgAs in healthy humans and mice.

SIgM can regulate B cell development.

SIgMs can promote central and mucosal tolerance, which might influence the development and outcomes of autoimmune conditions in mice and humans.

The B-1 cell pool produces the bulk of natural IgM and has regulatory functions in the establishment of tolerance in mice.

If robustly elicited, SIgM might be potentially beneficial in helping to treat certain pathologies such as infections or autoimmune diseases, although robust testing is still warranted.

Immunoglobulins and Mucosal Immunity: Where Do We Stand?

Mucosal immunity has mostly focused on the study of secretory immunoglobulin-A (SIgA). With the rising awareness that mucosal barriers and their allocated microbiota represent a key cornerstone in the establishment and maintenance of an efficient immune response, there comes the need for a better understanding of the interplay between Ig, secretory pathways, and microbiota at mucosal surfaces. However, SIgAs are not the only Igs to be secreted, let alone at mucosal surfaces. Indeed, secretory IgM (SIgM) and SIgA alone share key features of secreted Igs: they exist as functional secreted multimers and can bind both the J-chain and the secretory component (SC) [1] (see Figure I in Box 1). Higher concentrations of SIgMs have been found in individuals with decreasing or absent secretory IgA production relative to healthy individuals, suggesting immunological redundancy [2,3].

Depending on their binding abilities/lineages, antibodies have been further categorized into natural or antigen-specific (or 'immune') Igs. Most secreted IgM belongs to the **natural antibody** (see Glossary) pool, and natural B cells have been extensively studied in mouse models of parasitic infections [4], autoimmune pathologies [5,6], and gastrointestinal infections [7,8]. Reports vary regarding the protective or deteriorating effects of natural IgM (nIgM) on the evolution of such conditions. In humans, similar studies and the characterization of B cell pools remain difficult. This review aims to sort these different results, highlighting the potential of SIgMs in the regulation of B cell fates. We also discuss sIgMs interactions with the microbiota and their possible roles in compensating for human gut Ig defects.

B Cell Subsets Producing Natural and 'Immune' SIgMs: A True Dichotomy?

Murine Data

nIgM is polyreactive, but of low affinity [9], harboring low levels of **somatic hypermutation**, mostly directed against broadly conserved antigens and auto-antigens [10]; it is believed to hold mostly house-keeping functions. In mice, it potentiates both T-dependent responses and **class-switch recombination (CSR)** upon antigenic challenge [11]. Relative to wild type (WT) mice, mice deficient in SIgM, but not membrane-bound IgM ($\mu_S^{-/-}$ mice) [12], present impaired maturation of splenic germinal centers, lower amounts of IgG with concomitant impaired IgG

[1]GIMAP/EA3064, Université de Lyon, CIC 1408 Vaccinology, Saint-Etienne, France
[2]LBTO/UMR1059, Université de Lyon, Saint-Etienne, France
[3]These authors contributed equally to this work

*Correspondence: stephane.paul@chu-st-etienne.fr (S. Paul).

© 2019 Elsevier Ltd. All rights reserved.

antibody responses, and reduced counts of B-1 cells in **serous cavities** [12–14]. In addition, increased numbers of anergic B-2 cells and significantly lower counts of **transitional B cells** in the bone marrow and spleen of $\mu_s^{-/-}$ mice have been noted [12,15]; these findings overall suggest that there may be crosstalk between nIgM and the differentiation of both B-1 and B-2 cell subsets. In mice, B-1 (B-1a and B-1b) are distinguished from B-2 by CD5 expression, while B-2 lymphocytes are categorized into **follicular B cells (FoB)** and **marginal zone B cells (MZB)** [16] (Figure 1, left). In terms of biological functions and antigenic responses, MZB appear to be closer to B-1 cells, as evidenced by the strong IgM response to lipopolysaccharide (LPS) in MZB [28] and the general innate-like reactivity towards commensal flora polysaccharides [29,30]. Murine nIg were shown to originate from both B-1 and MZB cells [31] (Figure 1, left). FoB were not initially identified as nIg or SIgM producers, which might be due to incomplete repertoire characterization. Hence, FoB previously established as naïve, expressed secretory IgM mRNA, but mounted antigen-specific IgM responses to splenic antigenic signals [32]. Thus, separating local IgM production into nIgM or 'immune' IgM remains difficult. At the mucosal level, ambiguous phenotypes of mature B cells have been described in the gut lamina propria, namely IgA- and IgM-producing plasma cells with a functional B cell receptor (BCR) (see Figure I in Box 2) [33]. **CyTOF** approaches [34] and in-depth repertoire sequencing [35] have identified gut-originating IgM^+ **memory B cells (MBC)** with clonal relatedness to circulating antibody secreting cells. There is also evidence that antibacterial mucosal IgM^+-MBC of splenic B-2 descent accumulate with age and require constant output from the commensal flora and luminal antigens for maintenance [36]. Thus, these MBC subsets can diversify from gut antigens and offer systemic protection to pathogenic strains from crossreactive antigens. However, how and if B-2 and B-1 cells collaborate for the establishment of long-lasting mucosal memory is unknown, as is the precise role of SIgM. Indeed, the purported communication between tissue-resident and splenic pools of IgM^+ B-cells, as well as the descent of the ensuing MBC, has been largely discussed and incorporates several contradictory findings [37,38]. A large network of regulatory mechanisms between B-1 and B-2 cells remains unknown, as is the origin of mucosal SIgM B cells in mice. Which interactions preclude the establishment of such niches (microbiota, local immunity, pathological pathways, or possibly all three) is also an elusive question. As MBC diversification seems directly related to the secretory antibody response

Box 1. Structure of Secretory IgM

IgM comprises two heavy chains assembled into a homodimer, each bearing one light chain linked through disulfide bounds (Figure IA). The μ heavy chain (60 kDa) folds into four domains, of which the Cμ4 domain enables membrane-bound IgM and serves as the antigen-binding part of the B cell receptor (BCR) as well as a complement activator [102].

IgM tends to be either pentameric or hexameric. Assembly into pentamers is ensured by the J-chain [103], bridging disulfide bonds (Figure IB), while hexameric IgM does not require it [104]. The role of hexameric IgM remains elusive and might only be the result of cells defective for the J-chain gene, mutant for the μ chain, or pathological situations [105]. Association of the J-chain does not only hold a mechanical function for polymeric IgM, but also facilitates the transport of pentameric IgM across mucosal epithelia [1] and facilitates receptor binding (Box 2).

SIgM, as SIgA, requires binding to the secretory component (SC) (Figure IC). This interaction is less stable than that with SIgA [106] and the J-chain is influential in its binding [59]. The general role of the SC, especially in the context of mucosal immunity, is to increase Ig stability and resist against proteolytic cleavage [107]. As such, the J-chain and the SC constitute the main structural characteristics distinguishing SIg from 'common' Ig and enable optimal secretion at mucosal surfaces.

Secretory IgM is highly *N*-glycosylated at five sites on the μ chain and one on the J-chain [108] (Figure I), the N563 position being critical for functional SIgM formation [109]. Other than strictly impacting IgM structure, glycosylation and sialylation also influence IgM functions. Lack of *N*-sialylation in commercially available IgM from myeloma donors prevents the IgM inhibitory effect on T cell activation [110]. Given that high concentrations of IgM-bound sialic acid were detected in the sera of certain cancer patients [111] and low concentrations of sialylation were shown to correlate with inflammation in multiple myeloma [112], IgM sialylation might act as a putative biomarker and/or as a regulator. *N*-glycans also condition optimal pentamer formation, as mutant μ-chain lacking *N*-glycans aggregate in the cell and cannot be secreted [109]. As glycosylations affect SIgA dynamics in the intestinal mucosa and receptor recognition [68], it remains to be defined whether post-translational handling of SIgM has biological consequences. Consequently, the use of *in vitro* models of trafficking across mucosal epithelia [68] might be used for further approaches to elucidate the immunological function of IgM glycosylations.

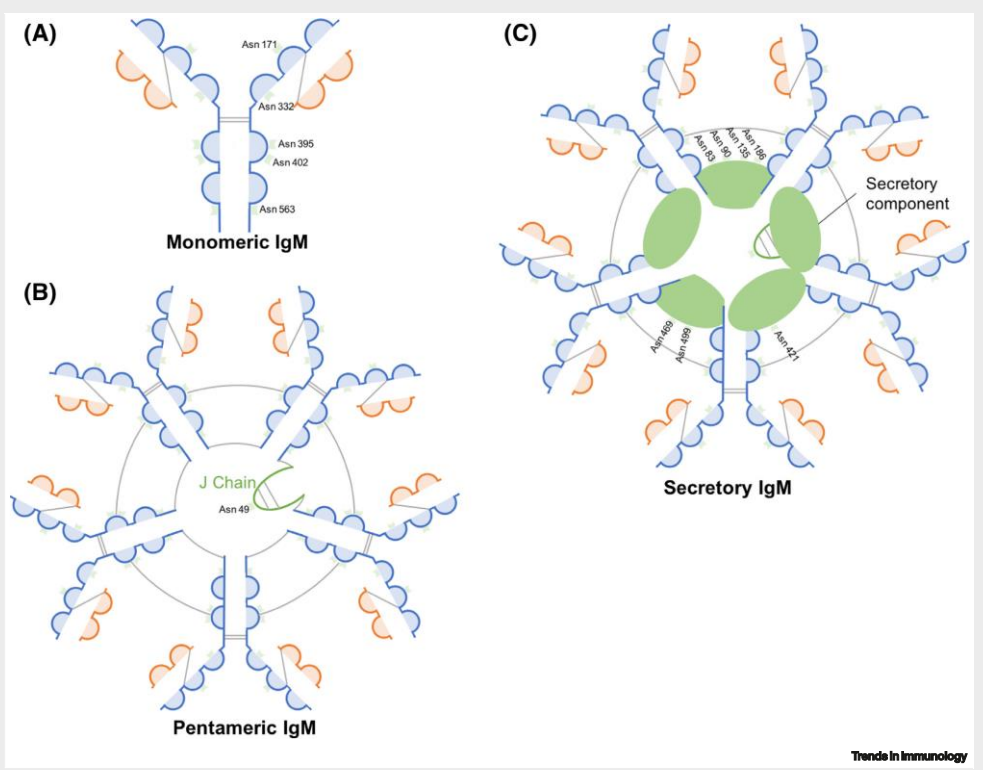

Figure I. Structure and Polymerization of Human IgM. (A) Monomeric IgM comprises two heavy chains (blue line), two variable chains (orange lines), and has five *N*-glycosylation sites. (B) Pentameric IgM is the most encountered form and is assembled by five IgM units joined through the J-chain. (C) Secretory IgM requires pentameric IgM binding to the secretory component, which is also *N*-glycosylated. *N*-glycosylation, light green boxes (as reported in UNIPROT and in [113]). Grey lines, disulfide bonds.

to the commensal flora [39], the influence of microbiota in promoting the establishment of these memory pools should be a focus of further research.

Human Data

Differentiating B-1 from B-2 cells in humans has been difficult because CD5 is expressed by several B-2 cell populations [18] (Figure 1, right). However, a study identified a subset of cells from human cord blood that shared B-1 characteristics: cells that spontaneously produced Ig could elicit T cell stimulation and displayed chronic intracellular signaling [17]. Later, adult human circulating $CD20^+$ $CD27^+$ cells coexpressing CD43 were shown to spontaneously and continuously secrete IgM [17]. Most of this human IgM from 'B-1' cells could also bind common antigens, such as phosphatidylcholine and phosphorylcholine, suggesting that it might also harbor a house-keeping function in humans [10]. Moreover, mice bearing humanized immune systems resort to $CD20^+$ $CD27^+$ $CD43^+$ cells to respond to infections that murine $CD5^+$ B-1 cell would

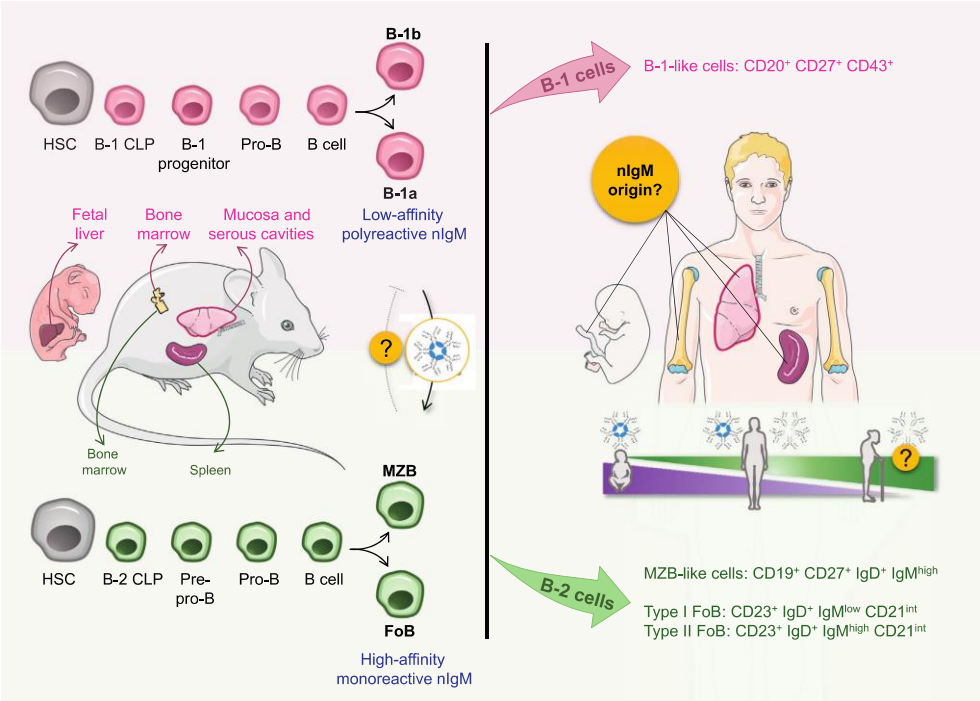

Figure 1. Current Categorization of Murine IgM-Secreting B Cells. In mice (left), two pools of B cells produce IgM in mice, B-1 cells and B-2 cells. Both subsets originate from bone marrow hematopoietic stem cells (HSC) that either differentiate into B-1 common lymphoid progenitor (CLP) in the fetal liver and serous cavities (B-1 cells) or into B-2 CLP in the spleen (B-2 cells) [10]. Both can be further divided into two subsets. B-1 cells can either be B-1a or B-1b; both produce natural IgM (nIgM) [11]. B-2 cells either differentiate into marginal zone B cells (MZB) or follicular B cells (FoB) [16]. nIgM produced by the B-1 pool has positive regulatory functions over B-2 cell expansion [9–12,15]. B-2 regulation by the B-1 cell pool is suspected, but not proven. In humans (right), a $CD20^{+}CD27^{+}CD47^{+}$ subset was characterized as a possible B-1 homolog [17]; CD5 expression cannot distinguish human 'B-1' from B-2 cells [18]. MZB-cells have been identified as $CD19^{+}$ $CD27^{+}$ IgD^{+} IgM^{high} [19,20] and also secrete IgM [20]. FoB cells, however, exist as two types in humans: type I are generally defined as $CD23^{+}$ IgD^{high} IgM^{low} $CD21^{int}$ and type II as $CD23^{+}$ IgD^{high} IgM^{high0} $CD21^{int}$ [16,21]. Early infancy in humans is marked by protection of the mucosa via nIgM production [22–26], while the elderly show a progressive loss of tolerance marked by a rise of autoantibodies that might be attributed to defects in secretory immunity [27].

normally clear [40]. As in mice, human 'B-1' cell counts decline with age, resulting in reduced immune protection, which might coincide with age-related conditions. Specifically, human 'B-1' cells have been shown to be more abundant at early stages of human development, with 30% of these cells spontaneously expressing IgM and IgD [41]. Human marginal zone (MZ)-like B cells have been identified as $CD19^{+}$ $CD27^{+}$ IgD^{+} IgM^{high} [19,20] and recently shown to be major circulating producers of IgM [20]. This specific population appears to decrease in circulation during **autoimmune vasculitis** compared with healthy controls [20]; this suggests that it might bear important regulatory functions in peripheral tolerance induction. As in mice, it thus seems that there are two phenotypes that might continuously secrete SIgM: 'B-1'-like cells, originating from an early lineage, and MZ-like B cells, taking over, or

Box 2. IgM Receptors

Several IgM receptors have been characterized. Amongst them, FcμR (or TOSO/FAIM3) is a regulator of B cell survival and, consequently, IgM responses [114]. In mice, IgM binding induces its rapid internalization, and FcμR expression at the cell surface is highly increased under pathological conditions and following BCR stimulation [114,115]. In addition, mice lacking FcμR display impaired germinal center formation, lower antimicrobial responses, and substantial increases in autoantibodies [114,116], suggesting that it might play a role in the regulation of self-tolerance. In fact, the murine phenotype for FcμR deficiency strongly resembles that of SIgM-deficient mice [15,117]. In contrast with other IgM receptors, in humans, FcμR solely recognizes IgM [88].

SIgM is also recognized by the polymeric Ig receptor (pIgR), expressed at the basal membrane of mucosal epithelium and exocrine glands [42]. It can recognize both IgM and IgA [69] and mediates the baso-lateral transport of secretory immunoglobulins in human mucosa [69]. Upon reaching the apical membrane, pIgR undergoes a proteolytic cleavage resulting in the attachment of the secretory component (SC) to IgM or IgA.

Finally, the Fcα/μreceptor (Fcα/μR) is expressed in mice by nonhematopoietic and B-2 cells [118], specifically, marginal zone B cells (MZB) [119,120]. The murine Fcα/μR also participates in endocytosis of IgM-antigen complexes *in vitro* [118]. In response to IgM binding, the Fcα/μR induces TLR activation [119] and proinflammatory cytokine production [119,120].

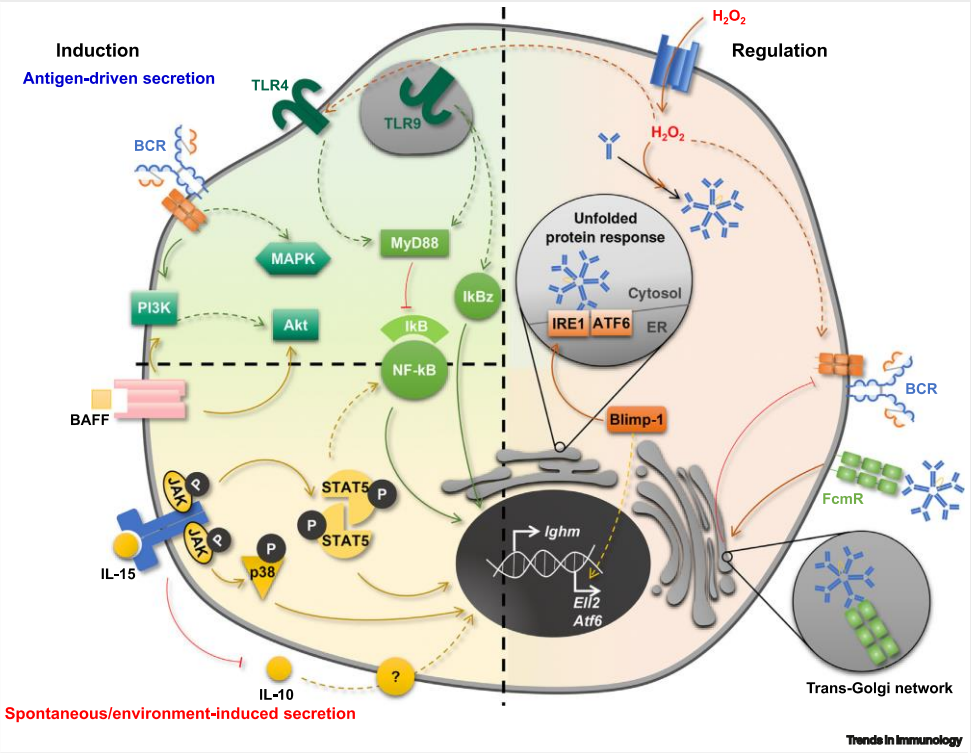

Figure I. Induction of Secretory IgM (SIgM) (Left) Can Be Initiated by Both Antigen Binding and Cytokine Stimulation. B cell receptor (BCR) and/or patter recognition receptor (PRR) (mostly TLR4 and 9) activation triggers converging cascades, activating NF-κB, which translocates to the nucleus. Cytokine-induced IgM has many origins; depicted are IL-15 and IL-10. IL-15 relies on JAK-STAT phosphorylation cascade for STAT5 migration to the nucleus [123], while IL-10 in the mucosal context remains to be defined [128]. Regulation of SIgM assembly relies mainly on IgM itself, acting as its own negative regulator. Interaction with the FcμR in the trans-Golgi network limits BCR signaling [133]. Meanwhile, Blimp-1 can regulate adequate assembly through control of the unfolded protein response effectors, IRE1 and ATF6 [131]. Generally, small molecule regulators such as H_2O_2 can also play a role in both induction and regulation of secreted IgM [131]. Broken lines indicate nondepicted pathways of signal transduction. Abbreviation: ER, endoplasmic reticulum.

complementing the former, as the individual ages. There is, however, scant information on a mucosal role for IgM-secreting cells.

Biological Significance of SIgM

SIgM in Development and Tolerance

In the context of mucosal immunity, SIgM was first studied in cartilaginous and bony fish, in which it has a crucial host defense and tolerogenic functions [42], a feature that, along with its general structure, seems to be broadly conserved amongst species. In mammals, the education of the immune system via the colonization of mucosal surfaces by various commensal species is amongst the first immune events to occur [22]. In human newborn B cells, **TLR4** and **TLR9** are more expressed than in adult and coincide with increased IgM secretion and reduced ability for CSR [23]. A study on human newborn cord blood also characterized an IgM antiglycan repertoire, directed against both human and non-human glycan structures, that was distinct from matched maternal counterparts [24]. Hence, tolerance towards future members of the microbiome might stem from an early temporary restriction on CSR to facilitate increased innate immune signals. In addition, the transfer of IgA and IgM through breast milk induces a largely tolerogenic environment in mice [43,44] and humans [25,26] that may also favor such colonization. This is reinforced by recent work on saliva IgM, where salivary SIgM concentrations increased only after the first 2 weeks of life [45], suggesting that maternal Ig could compensate for this low host response. Of relevance, a cohort of human preterm and term infants showed increased gastric stability of maternal SIg (both IgA and IgM) [46] in the preterm group, possibly to compensate for an immature immune system. Correlating IgM-bound bacterial diversity to immunological responsiveness in preterm or term infants may help define the specific role of early-secreted nIgM. It also appears that local SIgM secretion also plays a role in dampening mucosal immunity, as evidenced by an association between decreased salivary IgM and IgG concentrations and a higher occurrence rate of **oral mucositis** in immunosuppressed children relative to healthy controls [47].

In contrast with the early years of life, the mammalian aging immune system exhibits a proclivity towards general loss of self-tolerance [27] that may involve IgM-secreting B cells [48]. Indeed, a pool of accumulated B cells termed '4BL' that induce potent cytotoxic $CD8^+$ T cells (CTL) responses has been described in aged humans, mice, and macaques [49]. In aging mice, B-1a cells can drift towards a 4BL phenotype, thus inducing large amounts of granzyme B secretion and engaging T cell costimulatory signals that preclude a change from immunosuppression to immunoactivation (via CTLs) not observed in young controls [50]. Together, these findings suggest that early mucosal IgM secretion during development is relevant for establishing proper commensal tolerance. Potentiating tolerance responses at mucosal surfaces would be the result of the maternal selection of antigens through breast-milk and of the newborn-intrinsic negative regulatory mechanisms limiting immune activation. The mechanisms pertaining to these functions have not been specifically defined, but may rely on increased innate immune signals along with a temporary hold on adaptive immunity. This ability to respond to broad immune signals may turn on itself in the aging immune system. This type of immunomodulation might potentially contribute to a breach in self-tolerance with aging and should be further investigated in human studies.

SIg Deficiencies Illustrate Novel Mucosal Roles for SIgM

Further information on IgM mucosal functions comes from studies on **selective IgA deficiency (SIgAd)** and **selective IgM deficiency (SIgMD)**. Because most patients with SIgAd remain asymptomatic most of their lives, the IgA defect is deemed to be compensated by IgM [51]. Indeed, compensatory IgM secretion in cases of IgA deficiency was documented by a recent study in a human cohort of SIgAd patients: flow cytometry analysis of stool microbiota showed

Glossary

Antibody-mediated immune selection: a process by which antibodies distinguish commensal from pathogenic strains of bacteria.
Autoimmune vasculitis: inflammation of blood vessels associated with increased amounts of autoantibodies.
Class-switch recombination (CSR): genetic rearrangement within activated B cells that leads to a switch in constant Ig regions.
Complement cascade: innate molecular assembly pathway at the surface of pathogens leading to immune activation and/or to the targeted membrane disruption.
Crohn's disease: chronic inflammation of the deeper layers of the digestive tube.
CyTOF: technique in which cellular targets are stained with antibodies coupled to pure elements, nebulized, and analyzed via regular time of flight determination.
Dysbiosis: loss of microbial homeostasis at mucosal surfaces.
Fat-associated lymphoid clusters (FALC): atypical lymphoid tissues associated with mucosal surfaces and serous cavities.
Follicular B cells (FoB): part of the B-2 cell pool that mostly produce antigen-specific IgM.
Henoch-Schönlein purpura: common inflammatory disease in children causing leakages in skin, intestine, or kidney small blood vessels.
Innate-like B cell: unconventional B cell populations that respond to innate immunity signals, comprising the murine B-1 and MZB cells.
Ischemia-reperfusion injury: tissue damage occurring after blood flow is reinstated in a tissue following a lack of oxygen (ischemia).
Marginal zone B cell (MZB): part of the B-2 cell pool that produces both nIgM and immune IgM.
Memory B cells (MBC): long-lived B cell subtype generated in germinal centers following primary infection.
Natural antibodies: (immunoglobulins); pre-existing pool of antibody of low but broad affinity to common pathogens.
Oral mucositis: common complication of cancer therapy caused by limited epithelial cell division.
Regulatory B cells: small human immunosuppressive populations of B lymphocytes.

a significant increase in IgM bacterial binding compared with healthy individuals, the latter presenting little to no signal [52]. However, this bound SIgM did not identify all typical IgA targets, suggesting that although the latter may be a natural back-up option at mucosal surfaces, SIgA and SIgM may also have distinct patterns of microbial selection. Similarly, another study reported that despite compensatory IgM secretion in the gut, patients with SIgAd still displayed mild **dysbiosis** [53], highlighting that although SIgM is efficient when secreted, it only appears to dampen the consequences of IgA loss and cannot replace all IgA functions.

The prevalence of SIgMD is underestimated given that its symptoms share great similarity to those of allergy, respiratory infections, and certain autoimmune diseases [54]. In mice, SIgM deficiency leads to unresponsive splenic B cells and B-2 cell anergy in body cavities [15]; flow cytometry analysis of whole blood samples from human SIgMD patients showed a significant increase in **regulatory B cells**, concomitant with significantly decreased IgM^+ memory cells, plasmablasts, and $CD21^{lo}$ cells, compared with healthy individuals [55]. Thus, it appears that IgM may be an important regulator in the establishment of different B cell pools. High counts of transitional B cells, but decreased switched and nonswitched IgM memory B cells in SIgMD patients relative to healthy controls [56], indicate that SIgM deficiency may condition both differentiation and functionality of peripheral B cell pools. FcμR expression on MZB cells is also significantly diminished in patients with SIgMD [57], which suggests regulatory feedbacks between IgM secretion and its receptor. However, there is no clear map of these regulatory cascades, whether for B cell development or for intrinsic B cell metabolism, both of which should be clarified (Box 3).

The function of SIgM at mucosal surfaces in patients with both SIgAd and SIgMd could be easily investigated, by correlating defects to microbial diversity, to examine its consequences on microbiota–immunity interactions. For example, a cohort study in patients with primary IgA and

Selective IgA deficiency (SIgAd): common primary antibody deficiency characterized by low or absent amounts of IgA.
Selective IgM deficiency (SIgMd): common primary antibody deficiency characterized by low or absent amounts of IgM.
Serous cavities: coelomic cavity without interaction with the outside of the body.
Somatic hypermutation: accumulation of mutations in the variable regions of immunoglobulin genes to favor increased affinity for an antigen.
TLR4: Toll-like receptor 4; pattern recognition receptor, a broad sensor of innate immune signals that is triggered by LPS.
TLR9: Toll-like receptor 9, pattern recognition receptor, a broad foreign DNA sensor.
Transitional B cell: intermediate stage of B cell development before fully matured splenic B cells.
Ulcerative colitis: chronic inflammation of the upper layers of the colon.

Box 3. Regulation of IgM Secretion: Recent Findings

Signal transduction pathways following antigen recognition converge towards the NF-κB cascade, essential for long-term survival of murine MZB cells and B-1 cells [121]. In humans, patter recognition receptor (PRR) stimulation has been associated with IgM induction, as TLR4 and TLR9 protein concentrations have been reported to be more elevated in infants than in adults, coinciding with increased IgM secretion [23]. More in-depth studies have led to correlations between TLR9 stimulation and IgM secretion through IκBζ-dependent induction [122].

In mice, other signals can drive IgM secretion, such as IL-15 [123], IL-33, APRIL [124,125] BAFF [126], and IL-10 [23,122]. Specifically, IL-15 was shown to boost IgM production in mice, which required JAK-STAT phosphorylation and converged towards NF-kB induction [123]. In mice, both IL-15 and IL-10 intertwine to govern B-1a cell fate and. thus, the general immune equilibrium in this pool [127]. In addition, in humans, autocrine and paracrine IL-10 stimulation, including TLR9-derived, can drive B cell differentiation to IgM-secreting plasma cells [128].

Recent work identified transcription factor Blimp-1 as a regulator of murine IgM secretion, favoring natural antibody secretion in B-1 cells, but dispensable in the spleen and bone marrow [129,130]. In mice, Blimp-1 has also been implicated in the regulation of the unfolded protein response (UPR) of IgM [131]. Indeed, Blimp-1 has influenced IgM transition, from the membrane-bound to the secreted form of IgM, as evidenced from altered mRNA and protein expression of *Atf6* and *Ell2* and several downstream effectors of the UPR response in Blimp-1-deficient plasma cells relative to controls [131]. This has been associated with lower concentrations of secreted IgM and IgA, despite normal membrane-bound Ig expression in those cells [131]. In mice deficient for an essential H_2O_2 transporter, stimulation with LPS did not initiate the transition from membrane-bound IgM expression to SIgM secretion, as it normally does under LPS-TLR4 signaling [132]. Thus, IgM polymerization could be associated with H_2O_2 import into the cytosol, possibly complementing or amplifying BCR signaling and TLR4 potency. In mice, the FcμR is a regulator of secreted and membrane-bound IgM: interaction between either form of IgM and FcμR in the trans-Golgi network generates a negative feedback loop limiting BCR signaling and dampening nIgM secretion [133]. These findings suggest mutual feedback relationships between the FcμR, BCR, and UPR cascades governing the release of SIgM; this might be potentially disrupted, contributing to autoimmune or metabolic disorders, although this remains to be directly tested. Less information on human heterologs and pathway interactions regulating IgM secretion is available.

IgM deficiencies showed that low concentrations of both IgM and IgA correlated with a higher prevalence of bronchiectasis than in groups with normal concentrations of either of the two [58]. Moreover, physiologic concentrations of either IgA or IgM were sufficient to maintain intact immune responses, as this prevalence was unchanged in groups lacking only one of the two [58]. Again, this seems to suggest the existence of compensatory mechanisms and dual mucosal immune functions between these two Igs. It is thus reasonable to speculate that the use of IgM-enriched therapies for the treatment of certain immunodeficiencies might be potentially beneficial.

These observations and studies of SIgAd and SIgMd phenotypes support the notion that IgM may have a role to play in both peripheral and mucosal immunity. However, separate functions seem to emerge in humans and mice, namely, the regulation of B cell differentiation and the selection of a separate pool of beneficial Ig species. The latter might be overlooked in a healthy host because SIgA secretion is mostly dominant in various human mucosal surfaces.

Mucosal Functions of SIgM

The current consensus regarding secretory IgM is that it harbors a regulatory function when locally secreted. SIgM can activate **complement cascades** *in vitro* in a fashion similar to its 'classical' serum counterpart [59]. Additional functions for SIgM have been reported to occur locally in the lung, gut, liver, and adipose tissue.

Role of SIgM in the Lungs

Several findings support the notion that pulmonary immunity relies on B-1 cells in mice. Infection of B cell deficient mice (μMT mice) with *Escherichia coli* or *Streptococcus pneumoniae* led to a higher and faster mortality rate than in WT groups [60]. Isolated B-1a cells from the pleural cavity of WT mice secreted large amounts of SIgM [60] and transfer of WT B-1a cells into the pleural space rescued this previous defect [60]. However, transfer of granulocyte-macrophage colony-stimulating factor (GM-CSF)-deficient B cells (from *Csf2*$^{-/-}$ mice) into WT mice pleural space did not protect against the infection [60], placing GM-CSF as a key regulator of the respiratory SIgM response [60]. In a mouse model of *Francisella tularensis* infection, another study showed that peritoneal and splenic B-1a B cells were also critical for protective anti-LPS nIgM production in response to infection, this time under the regulation of IL-1β [61]. In *Il1b*$^{-/-}$-mice, tending towards a higher mortality rate than WT mice, lower concentrations of serum nIgM, and B-1a cell counts in the spleen and peritoneal cavity were observed relative to WT mice [61]. Both of these studies highlight the importance of serous cavities in recruiting B-1a cells to counteract bacterial infections in the lung. Moreover, a mouse model of parasitic infection (*Litomosoides sigmodontis* and *Alternaria alternata* nematodes) showed that B-1 cell activation in **fat-associated lymphoid clusters (FALC)** of the pleural cavity was a prerequisite for SIgM secretion in the lungs [4]. This was concomitant with local IL-33 secretion and depended on IL-5 production, as anti-IL-5 injection in the pleural cavity of WT mice impaired both IgM and IL-33 local secretion [4]. During a *Haemophilus influenzae* murine infection, IL-5 secretion itself was negatively regulated by PD-L2 expression on splenic B-1 cells (one of the PD-1 ligands), as PD-L2$^{-/-}$-mice (*Pdcd1lg2* deficient) exhibited higher counts of splenic B-1a cells and increased IL-5 and anti-PC nIgM concentrations than their WT counterparts [62].

Moreover, high SIgM secretion and enhanced local IgM binding to bacteria were also noted during respiratory pneumococcal infection in mice [63]. Indeed, efficient antimicrobial SIgM responses in the lung may rely on the preceding relocation of **innate-like B cell** subsets from serous cavities to the lung parenchyma, as well as circulatory B-1a cell activation and IL-5 signaling. Moreover, recent work in mice infected with the influenza virus shows that SIgM can support antiviral antibody production and clonal expansion via an FcuR-dependent mechanism (assessed

using B cell-specific *Fcmr*$^{-/-}$ mice) [64]. Hence, SIgM can sustain both natural and antigen-specific responses, requiring migratory signals and optimal FcuR signaling [4,60–65].

In humans, however, the identification of pulmonary IgM-secreting B cell subsets remains incomplete due to undefined markers for B-1a and B-1b cells. A recent study described a regulatory B cell subset in response to respiratory syncytial virus infection in human lungs, termed nBreg cells, secreting IgM with a shorter CDR3 region than previously published [66]. This finding, in addition to other studies indicating that IgM-deficient individuals tend to be more sensitive to opportunistic respiratory infections than healthy individuals [39], suggest that in addition to IgA, SIgM might also be important for pulmonary mucosal barrier homeostasis. As human studies in the lung are difficult, further preclinical models and studies on SIgM should aim to be robustly standardized.

Role of SIgM in the Gut and Liver

Both SIgM and SIgA, due to J-chain recognition, are secreted into the intestinal lumen by epithelial cells, where they may bind commensal or pathogenic organisms [67], in a process named transcytosis. Bound SIgA can then pass back through M cells of the epithelium upon Dectin-1 and Siglec-5 binding, a process known as reverse-transcytosis (RT) [68]. This requires optimal *N*-glycosylation and sialylation and SC binding [68], two criteria that SIgM also meets. It is thus suspected, that SIgM might also undergo RT (Figure 2).

In mouse, one caveat is that the murine gut produces little SIgM under homeostatic conditions (Table 1) [78]. There is, however, proof of intestinal nIgM secretion in the murine liver and small intestine [70]. In a murine model of **ischemia-reperfusion injury**, nIgM was produced in response to the inflammation and originated from B-1a cells, as B cells lacking CD6, from CD6$^{-/-}$-mice, did not elicit such a response [83]. It could be proposed that B-1a cells are also engaged in IgM secretion in the murine gut and depend on CD6 signaling to relocate to the peritoneal cavity and/or the gut; indeed, in this study, CD6^{+} B-1 cells accumulated outside the bone marrow and into the peritoneal cavity of WT mice [83]. It thus seems that gut immunity, as does pulmonary immunity, might also rely on B-1 cells relocating from serous cavities towards local tissues. However, studies on ethanol-fed mice offer contradictory findings of both protective or aggravating functions of SIgM: namely, ethanol-fed *Iga*$^{-/-}$-mice exhibit increased compensatory intestinal and plasma IgM secretion in the gut relative to WT littermates, despite similar disease courses [84]. SIgM was also shown to facilitate C1q and C3 complement protein accumulation in the liver of WT ethanol-fed mice relative to controls [85], thereby promoting inflammation. SIgM function in the gut remains to be fully defined, but might potentially compensate for SIgA loss.

In humans, plasma-derived IgA and IgM bound to the SC, induced striking *Salmonella enterica* serovar Typhimurium aggregation *in vitro* [7]; this indicated that Ig interaction with enteropathogens, and their neutralization, can occur via human SIgM binding, with a possibly higher protective potency than SIgA [86]. Hence, a key question is whether or not intestinal SIgM binding to the gut microbiota is influential for gut homeostasis. There are observations of specific human SIgM binding commensal bacteria in the healthy gut [52], but also of SIgM from local IgM^{+} plasma cells binding to SIgA-coated bacteria [35], suggesting partial redundancy of SIgA. Indeed, it is unclear whether SIgM influences the selection of a specific pool of commensals upon binding, or if SIgA and SIgM share similar trends of selectivity. Moreover, an *in vivo* study in rainbow trout introduced a model in which the binding of SIgM heterologs to skin commensals might depend on whether either free or bound SC first targeted the bacteria [87]. Given the conserved SIgM structure between mammals and fish [88], this mode of bacterial selection should be further investigated in mammals. Consequently, although still in its infancy, knowledge regarding

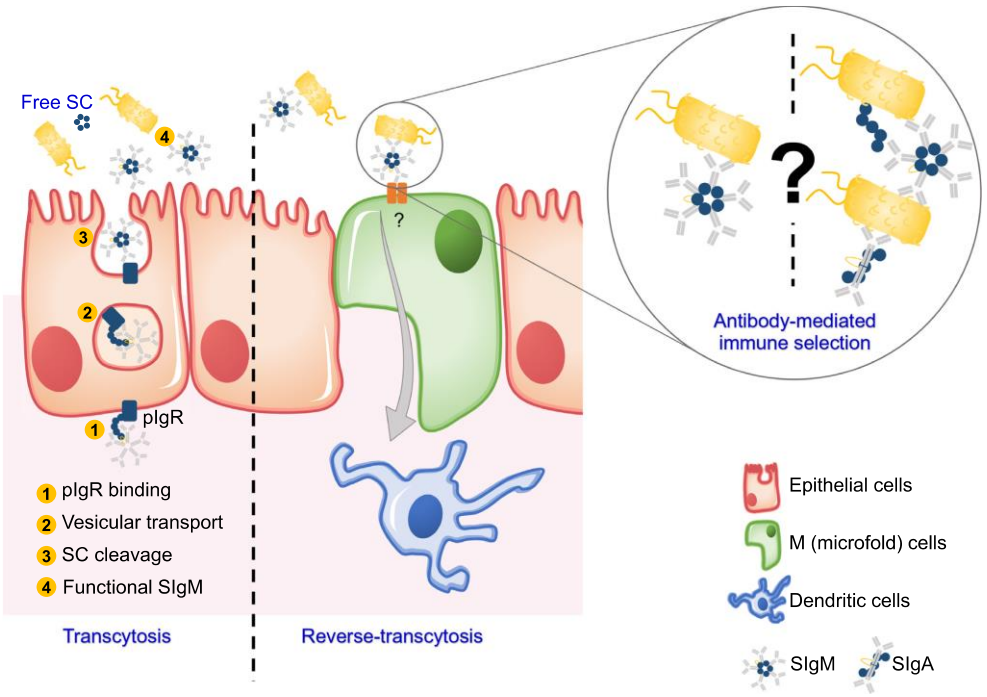

Figure 2. Hypothetical Model of Selective IgM Deficiency (SIgM) at Mucosal Surfaces. Similarly to SIgA, secretion of SIgM to the mucosal surface occurs via transcytosis (left) and requires polymeric Ig receptor (pIgR) binding at the basal membrane of epithelial cells [67,69,70]. Upon recognition, the SIgM-pIgR complex is internalized and transported towards the apical membrane in vesicles [67]. SIgM is secreted via exocytosis, upon which the SIgM-binding part of pIgR is cleaved and remains attached to SIgM as the secretory component (SC) [67]. SC can also be secreted as a free entity in the mucosa but its role is unclear. After antigen binding, SIgM, like SIgA, might undergo reverse-transcytosis (right) at the surface of M (microfold) cells in a possible receptor-dependent manner [68]. SIgM and its antigen are then internalized and transferred below the mucosa to activate immune cascades. The latter remain undefined (not depicted). It remains to be investigated whether SIgM has a distinct repertoire or whether it simply complements and enhances SIgA binding; it is unclear if SC plays a role in SIgM binding to the microbiota (zoom).

Table 1. Physiologic IgM Concentrations in Mucosal Secretions in Humans and Mice[a]

		Salivary ($\mu g.ml^{-1}$)	Digestive ($mg.g^{-1}$ feces)	Breast milk ($mg.ml^{-1}$)	Nasal secretions ($\mu g.ml^{-1}$)	Respiratory tract ($\mu g.ml^{-1}$)	Tears ($\mu g.ml^{-1}$)	Serum ($mg.ml^{-1}$)	Refs
Humans	Infancy	3.60 ± 12.40	0.2–15.5	–	87 ± 74	?	?	1.07 ± 0.29	[45,71,72]
	Adulthood	1.21 ± 0.32	5.9 ± 1.9 ug/ml	14.05-0.37 (0.5–7 days pp)	?	0.22 ± 0.03 (BAL)	5.6	1.47 ± 0.84	[53,73–77]
Mice	Infancy	?	?	–	?	?	?	?	
	Adulthood (Strain)	0.002–0.14	~$0.02.10^{-3}$ (Balb/c)	<0.012 (CBA) <0.02 (C57/BL6)	?	<0.009	Trace	0.22 (C57/BL6)	[78–82]

Abbreviations: BAL, Bronchoalveolar lavages; pp, post-partum.
[a]Data from listed references were converted to comparable units when necessary. '?' was used when no data could be found.

the roles of SIgM in the gut and liver, and ensuing IgM-induced immune responses, merits further attention and might lead to new questions regarding intestinal and/or metabolic diseases.

Selection of the Microbiota

Selection of Commensal Bacteria

In a healthy Chinese middle-aged human cohort, a negative correlation between circulating IgM concentrations and stool Firmicutes enrichment was identified [89]. In that group, general positive correlations between the Bacteroidetes/Firmicutes ratio and serum IgM concentrations were also documented. However, both of those relationships were lost in an elderly cohort from the same study, despite comparable serum IgM concentrations [89], suggesting that aging might trigger a general loss of IgM functions and lead to mild dysbiosis. There was, moreover, a negative correlation between gut Verrucomicrobia (genus *Akkermansia*) abundance and circulating $CD4^+$ and $CD8^+$ T cell percentages in the elderly cohort [89]. As murine B-1a cells can drift towards the 4BL phenotype, which strongly potentiates $CD8^+$ T cells cytotoxicity, IgM–microbiota interactions, or lack thereof, the 4BL phenotype might also have an indirect effect on the polarization of human T cell responses. This scenario might hypothetically favor the development of metabolic disorders or autoimmunity, although this was not directly tested. In this context, an association between nIgM concentrations and Synergistetes abundance in the human gut was reported in patients with systemic lupus erythematosus, and negatively correlated with lower inflammatory parameters in the patients relative to healthy controls [6]. Studies of autoimmune disorders, in conjunction with those of the gradual loss of tolerance in aging populations, have suggested a link between nIgM production with its presumed protective effects in the human intestinal mucosa [9,134]. Healthy human gut SIgA and SIgM have similar commensal targets but SIgM secretion varies between individuals and location within the digestive tract [35]. Of the overall IgM^+ fraction, a general trend towards Firmicutes enrichment has been observed [35]. In addition, the presence of beneficial taxa such as Lachnospiraceae and Ruminococcaceae has suggested an IgM-mediated preference towards gut health promotion via commensal selection rather than pathobiont selection, although further testing is warranted [35]. Analysis of human gut commensals from SIgAd patients have shown a significant bias towards *Clostridium* sp. and *Pseudomonas* sp. in IgM^+ fractions of the gut microbiota relative to healthy individuals [52]. SIgAd patients have also displayed higher abundances of Enterobacteriaceae and Prevotellaceae relative to healthy controls; these frequencies were not found in the case of SIgM, suggesting that IgM might only partially compensate for IgA loss [52]. Rather, a significant association was observed between IgM binding and Actinobacteria in the gut, independently from SIgA titers [52]. Thus, there is still much to learn regarding the associations of intestinal IgM and the composition of the microbiome. Evidently, geographical and demographical differences between different cohorts would affect microbiota composition and hence, presumably IgM–microbiota interactions.

IgM Functions in Dysbiosis

In a mouse model of experimental autoimmune encephalomyelitis (EAE), high fecal concentrations of IgM positively correlated with the spontaneous occurrence of EAE in susceptible mice. In the latter, the IgM coating of fecal bacteria correlated with dysbiosis and with the exacerbation of disease symptoms [90]. IgM^{hi} coated bacteria were predominantly Bacteroidaceae in both EAE and non-EAE mice, a pattern of selection that persisted with age in both groups, suggesting that potential IgM-associated long-lasting changes in microbial ecology could occur [90]. In another study, *Il10*$^{-/-}$ mice were more susceptible to *Helicobacter*-induced dysbiosis and exhibited increased numbers of peritoneal MZB cells than their WT counterparts [91]. As IL-10 deficiency led to higher serum IgM concentrations [91], we speculate that, under homeostatic conditions, IL-10 normally downregulates IgM secretion in the circulation. IgM could either be secreted by

MZB cells, which are regulated by IL-10, or IL-10 could regulate IgM secretion, a limiting signal for MZB cell accumulation in the peritoneal cavity.

Despite its low and controverted abundance in the murine gut, secreted IgM may still have protective functions. Specifically, in a dextran sodium sulfate (DSS)-induced colitis model, *Myd88*$^{-/-}$ mice exhibited a lower survival rate and colonic damage than their WT counterparts [92]. These mice also harbored lower local SIgM, but not SIgA, concentrations compared with WT mice. As MyD88 signaling is a known IgM-governing pathway, this suggests that IgM could be elicited through a Myd88-driven pathway to limit commensal dissemination in the case of mucosal injury [92]. It could be directly attributed to B cells, as specific depletion of MyD88 signaling in murine B cells but not elsewhere led to similar results [92]. Moreover, patients with MyD88 deficiencies present depletion of circulating IgM^{+}IgD^{+}CD27^{+} B cells compared with patients without mutation or defects in MyD8 and this depletion has been correlated with lower concentrations of IgM-binding to bacterial carbohydrates in the sera of these patients [93]. Such findings support the link between MyD88, IgM secretion, and the regulation of circulating B cell pools in humans. Moreover, as IgM^{+}IgD^{+}CD27^{+} B cells are important in mounting T-independent IgM responses [29], defects in bacterial antigen recognition suggest that MyD88 is a crucial pathway for the development of nIgM immunity. More work on the mucosal consequences of MyD88 deficiencies in this cohort, perhaps through analysis of stool microbiota and their bound Ig, could have further complemented this study.

For humans with diseases in which there is evidence of dysbiosis, an in-depth study of SIgM/SIgA dynamics and functionality might be beneficial. For example, untreated celiac disease patients have displayed lower concentrations of beneficial taxa such as *Faecalibacterium prausnitzii* or *Bifidobacterium* sp., accompanied by higher concentrations of both IgA- and IgM-coated stool bacteria, relative to either treated, or control individuals [94]. SIg coating of bacteria, including SIgM, can thus be associated with latent gut dysbiosis in the absence of treatment, the cause of which needs to be further studied. In children with **Henoch-Schönlein purpura**, IgM concentrations have been associated with oral dysbiosis and negatively correlated with *Haemophilus* sp. but positively correlated with *Prevotella* sp. [95]. And, as several *Prevotella* species have been associated with promoting inflammation [96], it appears that IgM might exert an adverse influence on dysbiotic mucosae in humans. Because healthy splenectomized patients have exhibited comparable defects to MyD88-deficient patients [57], it is possible that the IgM^{+}IgD^{+}CD27^{+} B cell subset could constitute a human counterpart to the murine MZB cell subset [19,20].

Moreover, few studies have focused on this SIgM/SIgA ratio in inflammatory bowel diseases (IBD) and, to our knowledge, there are no data investigating SIgM in the gut of IBD patients, in whom dysbiosis is common [97–99]. In blood samples from **ulcerative colitis** patients, flow cytometry analysis revealed that the IgM^{+}IgD^{+}CD27^{+} B cell subset was increased compared with non-IBD controls [100], suggestive of undocumented IgM functions in a human dysbiotic context. This has been supported by a recent report in which **Crohn's disease** patients in remission harbored higher counts of IgM^{+} B cells in the lamina propria than active Crohn's disease patients [101]; however, this was, once again, not investigated in parallel to an analysis of microbiota composition.

While there is evidence in mice of a correlation between SIgM concentrations and dysbiosis, the question remains unresolved in humans. The few clues regarding SIgM amounts only provide contradictory evidence regarding the benefits of IgM secretion under pathological circumstances. In both mice and humans, however, there seems to be an involvement of MZB or MZB-like cells and IgM secretion, suggestive of regulatory feedbacks between circulating and local B cell pools and mucosal homeostasis.

Concluding Remarks

Although SIgA is believed to play the greatest part in the selection of the commensal flora in mammals, SIgM may not be a secondary participant. Its role in **antibody-mediated immune selection** remains to be fully defined, but SIgM has definite interactions with the gut microbial community and can protect mucosae against pathogenic bacterial strains. Moreover, dysregulated IgM functions can accompany autoimmune manifestations, suggesting that SIgM, and especially nIgM, may be critical regulators in the maintenance of general self-tolerance, although further studies are warranted to fully establish this. Nevertheless, because of these features, SIgM may hold therapeutic potential that will require further in-depth investigations (see Outstanding Questions). IgM, as a potential complementary treatment for certain autoimmune diseases and immunodeficiencies, or even oral vaccination strategies, may be an option that should be more broadly reviewed. Finally, investigating ways to elicit secretory antibodies in the putative treatment of IBD merits further attention. The characteristic dysbiosis observed in IBD is likely to have effects on secretory immunity dynamics that have not yet been documented. Given certain compensatory mechanisms between IgA and IgM, it is reasonable to speculate that IgM secretion might be modulated in a similar fashion to IgA during the humoral response and/or recruited to correct IgA defects. However, to our knowledge, no approach has studied either IgA or IgM repertoires in such inflammatory contexts. Hence, the biological consequences of IgA and IgM secretion on microbial equilibrium in mucosal tissues are still being questioned.

Outstanding Questions

Can structural changes in SIgM impact its functionality and immune feedback circuits, if any? How important is SIgM glycosylation in mucosal homeostasis?

How does mucosal immunity, and especially human 'B-1' cells, evolve in IgM-related pathologies such as SIgMd or hyper-IgM syndromes? Does this translate into, or accompany changes in the microbiota composition?

Does SIgM contribute to the selection of a specific pool of microbiota or does it only complement SIgA binding? And if so, how do SIgM binding dynamics change in cases of dysbiosis, such as in IBD?

Does free SC play a role in 'pre-identifying' bacterial strains at mucosal surfaces for SIgM the way it does in other vertebrates? What is its biological significance in humans?

Can long-lasting secretory immunity be generated through SIgM immunization against enteropathogen(s)? Can it be generated in the context of therapeutic vaccines to presumably treat autoimmune disorders? Given its pentameric nature, how relevant is the use of SIgM as a vaccine carrier and what is its potency?

Acknowledgments

This work is supported by La Région Auvergne-Rhône-Alpes through the ARC1-Santé grant and by the MSD-Avenir foundation grant.

References

1. Brandtzaeg, P. and Prydz, H. (1984) Direct evidence for an integrated function of J chain and secretory component in epithelial transport of immunoglobulins. *Nature* 311, 71–73
2. Norhagen, G. *et al.* (1989) Immunoglobulin levels in saliva in individuals with selective IgA deficiency: compensatory IgM secretion and its correlation with HLA and susceptibility to infections. *J. Clin. Immunol.* 9, 279–286
3. Ammann, A.J. and Hong, R. (1971) Selective IgA deficiency: presentation of 30 cases and a review of the literature. *Medicine (Baltimore)* 50, 223–236
4. Jackson-Jones, L.H. *et al.* (2016) Fat-associated lymphoid clusters control local IgM secretion during pleural infection and lung inflammation. *Nat. Commun.* 7, 12651
5. Sun, J. *et al.* (2018) IgM antibodies against phosphorylcholine promote polarization of T regulatory cells from patients with atherosclerotic plaques, systemic lupus erythematosus and healthy donors. *Atherosclerosis* 268, 36–48
6. López, P. *et al.* (2016) Th17 responses and natural IgM antibodies are related to gut microbiota composition in systemic lupus erythematosus patients. *Sci. Rep.* 6, 1–12
7. Bioley, G. *et al.* (2017) Plasma-derived polyreactive secretory-like IgA and IgM opsonizing *Salmonella enterica* Typhimurium reduces invasion and gut tissue inflammation through agglutination. *Front. Immunol.* 8, 1043
8. Pandya, K.D. *et al.* (2018) An unmutated IgM response to the Vi polysaccharide of *Salmonella typhi* contributes to protective immunity in a murine model of typhoid. *J. Immunol.* 200, 4078–4084
9. Grönwall, C. *et al.* (2012) Protective roles of natural IgM antibodies. *Front. Immunol.* 3, 66
10. Rothstein, T.L. *et al.* (2013) Human B-1 cells take the stage. *Ann. N. Y. Acad. Sci.* 1285, 97–114
11. Ehrenstein, M. *et al.* (1998) Targeted gene disruption reveals a role for natural secretory IgM in the maturation of the primary immune response. *Proc. Natl. Acad. Sci. U. S. A.* 95, 10089–10093
12. Boes, M. *et al.* (1998) Enhanced B-1 cell development, but impaired IgG antibody responses in mice deficient in secreted IgM. *J. Immunol.* 160, 4776–4787
13. Tsiantoulas, D. *et al.* (2017) Increased plasma IgE accelerate atherosclerosis in secreted IgM deficiency novelty and significance. *Circ. Res.* 120, 78–84
14. Tsiantoulas, D. *et al.* (2017) Secreted IgM deficiency leads to increased BCR signaling that results in abnormal splenic B cell development. *Sci. Rep.* 7, 1–9
15. Nguyen, T. *et al.* (2015) Natural IgM prevents autoimmunity by enforcing B cell central tolerance induction. *J. Immunol.* 194, 1489–1502
16. Pillai, S. and Cariappa, A. (2009) The follicular versus marginal zone B lymphocyte cell fate decision. *Nat. Rev. Immunol.* 9, 767–777
17. Griffin, D.O. *et al.* (2011) Human B1 cells in umbilical cord and adult peripheral blood express the novel phenotype $CD20^{+}CD27^{+}CD43^{+}CD70^{-}$. *J. Exp. Med.* 208, 67–80
18. Youinou, P. *et al.* (1999) CD5 expression in human B-cell populations. *Immunol. Today* 20, 312–316
19. Bemark, M. (2015) Translating transitions – how to decipher peripheral human B cell development. *J. Biomed. Res.* 29, 264–284
20. Appelgren, D. *et al.* (2018) Marginal-zone B-cells are main producers of IgM in humans, and are reduced in patients with autoimmune vasculitis. *Front. Immunol.* 9, 2242
21. Allman, D. and Pillai, S. (2008) Peripheral B cell subsets. *Curr. Opin. Immunol.* 20, 149–157
22. de Agüero, M.G. *et al.* (2016) The maternal microbiota drives early postnatal innate immune development. *Science* 351, 1296–1302
23. Pettengill, M.A. *et al.* (2016) Distinct TLR-mediated cytokine production and immunoglobulin secretion in human newborn naïve B cells. *Innate Immun.* 22, 433–443
24. Xia, L. and Gildersleeve, J.C. (2019) Anti-glycan IgM repertoires in newborn human cord blood. *PLoS One* 14, e0218575
25. Jennewein, M.F. *et al.* (2017) Transfer of maternal immunity and programming of the newborn immune system. *Semin. Immunopathol.* 39, 605–613

26. Hurley, W.L. and Theil, P.K. (2011) Perspectives on immunoglobulins in colostrum and milk. *Nutrients* 3, 442–474
27. Boraschi, D. *et al.* (2013) The gracefully aging immune system. *Sci. Transl. Med.* 5, 185ps8
28. Puga, I. *et al.* (2011) B cell-helper neutrophils stimulate the diversification and production of immunoglobulin in the marginal zone of the spleen. *Nat. Immunol.* 13, 170–180
29. Cerutti, A. *et al.* (2013) Marginal zone B cells: virtues of innate-like antibody-producing lymphocytes. *Nat. Rev. Immunol.* 13, 118–132
30. Clarke, T.B. *et al.* (2010) Recognition of peptidoglycan from the microbiota by Nod1 enhances systemic innate immunity. *Nat. Med.* 16, 228–231
31. Ochsenbein, A.F. and Zinkernagel, R.M. (2000) Natural antibodies and complement link innate and acquired immunity. *Immunol. Today* 21, 624–630
32. Meng, Q.-H. and White, H.N. (2017) CD21intCD23^{+} follicular B cells express antigen-specific secretory IgM mRNA as primary and memory responses. *Immunology* 115, 211–218
33. Pinto, D. *et al.* (2013 16) A functional BCR in human IgA and IgM plasma cells. *Blood* 121, 4110–4114
34. Nair, N. *et al.* (2016) High-dimensional immune profiling of total and rotavirus VP6-specific intestinal and circulating B cells by mass cytometry. *Mucosal Immunol.* 9, 68–82
35. Magri, G. *et al.* (2017) Human secretory IgM emerges from plasma cells clonally related to gut memory B cells and targets highly diverse commensals. *Immunity* 47, 118–134
36. Le Gallou, S. *et al.* (2018) A splenic IgM memory subset with antibacterial specificities is sustained from persistent mucosal responses. *J. Exp. Med.* 215, 2035–2053
37. Alugupalli, K.R. *et al.* (2004) B1b lymphocytes confer T cell-independent long-lasting immunity. *Immunity* 21, 379–390
38. Papillion, A.M. *et al.* (2017) Early derivation of IgM memory cells and bone marrow plasmablasts. *PLoS One* 12, e0178853
39. Lindner, C. *et al.* (2015) Diversification of memory B cells drives the continuous adaptation of secretory antibodies to gut microbiota. *Nat. Immunol.* 16, 880–888
40. Vuyyuru, R. *et al.* (2011) Characteristics of *Borrelia hermsii* infection in human hematopoietic stem cell-engrafted mice mirror those of human relapsing fever. *Proc. Natl. Acad. Sci. U. S. A.* 108, 20707–20712
41. Bueno, C. *et al.* (2016) Immunophenotypic analysis and quantification of B-1 and B-2 B cells during human fetal hematopoietic development. *Leukemia* 30, 1603–1606
42. Xu, Z. *et al.* (2013) Teleost skin, an ancient mucosal surface that elicits gut-like immune responses. *Proc. Natl. Acad. Sci. U. S. A.* 110, 13097–13102
43. Wang, H. and Shlomchik, M.J. (1998) Maternal Ig mediates neonatal tolerance in rheumatoid factor transgenic mice but tolerance breaks down in adult mice. *J. Immunol.* 160, 2263–2271
44. Polte, T. and Hansen, G. (2008) Maternal tolerance achieved during pregnancy is transferred to the offspring via breast milk and persistently protects the offspring from allergic asthma. *Clin. Exp. Allergy J. Br. Soc. Allergy Clin. Immunol.* 38, 1950–1958
45. Pineda-Martínez, S. *et al.* (2016) Immunoglobulin concentrations in plasma and saliva during the neonatal period. *Pediatr. Neonatol.* 57, 213–218
46. Demers-Mathieu, V. *et al.* (2018) Comparison of human milk immunoglobulin survival during gastric digestion between preterm and term infants. *Nutrients* 10, E631
47. Pels, E.J. (2017) Oral mucositis and saliva IgA, IgG and IgM concentration during anti-tumor treatment in children suffering from acute lymphoblastic leukemia. *Adv. Clin. Exp. Med.* 26, 1351–1358
48. Holodick, N.E. *et al.* (2016) Age-related decline in natural IgM function: diversification and selection of the B-1a cell pool with age. *J. Immunol.* 196, 4348–4357
49. Lee-Chang, C. *et al.* (2014) Accumulation of 4-1BBL^{+} B cells in the elderly induces the generation of granzyme-B^{+} CD8^{+} T cells with potential antitumor activity. *Blood* 124, 1450–1459
50. Lee-Chang, C. *et al.* (2016) Aging converts innate B1a cells into potent CD8^{+} T cell inducers. *J. Immunol.* 196, 3385–3397
51. Yazdani, R. *et al.* (2016) Selective IgA deficiency: epidemiology, pathogenesis, clinical phenotype, diagnosis, prognosis and management. *Scand. J. Immunol.* 85, 3–12
52. Fadlallah, J. *et al.* (2018) Microbial ecology perturbation in human IgA deficiency. *Sci. Transl. Med.* 10, eaan1217
53. Catanzaro, J.R. *et al.* (2019) IgA-deficient humans exhibit gut microbiota dysbiosis despite secretion of compensatory IgM. *Sci. Rep.* 9, 1–10
54. Louis, A.G. and Gupta, S. (2014) Primary selective IgM deficiency: an ignored immunodeficiency. *Clin. Rev. Allergy Immunol.* 46, 104–111
55. Louis, A.G. *et al.* (2016) Analysis of subsets of B cells, Breg, CD4Treg and CD8Treg cells in adult patients with primary selective IgM deficiency. *Am. J. Clin. Exp. Immunol.* 5, 21–32
56. Mensen, A. *et al.* (2015) Altered B-cell subsets and functional B-cell defects in selective IgM deficiency. *Clin. Immunol.* 161, 96–102
57. Gupta, S. *et al.* (2016) FcμR in human B cell subsets in primary selective IgM deficiency, and regulation of FcμR and production of natural IgM antibodies by IGIV. *Hum. Immunol.* 77, 1194–1201
58. Hodkinson, J.P. *et al.* (2017) Low IgA and IgM is associated with a higher prevalence of bronchiectasis in primary antibody deficiency. *J. Clin. Immunol.* 37, 329–331
59. Michaelsen, T. *et al.* (2016) Human secretory IgM antibodies activate human complement and offer protection at mucosal surface. *Scand. J. Immunol.* 85, 43–50
60. Weber, G.F. *et al.* (2014) Pleural innate response activator B cells protect against pneumonia via a GM-CSF-IgM axis. *J. Exp. Med.* 211, 1243–1256
61. del Barrio, L. *et al.* (2015) Production of anti-LPS IgM by B1a B cells depends on IL-1β and is protective against lung infection with *Francisella tularensis* LVS. *PLoS Pathog.* 11, e1004706
62. McKay, J.T. *et al.* (2017 15) PD-L2 regulates B-1 cell antibody production against phosphorylcholine through an IL-5-dependent mechanism. *J. Immunol.* 199, 2020–2029
63. Boehme, J.D. *et al.* (2017) Chronic lung inflammation primes humoral immunity and augments antipneumococcal resistance. *Sci. Rep.* 7, 1–13
64. Nguyen, T.T.T. *et al.* (2017) sIgM-FcμR interactions regulate early B cell activation and plasma cell development after influenza virus infection. *J. Immunol.* 199, 1635–1646
65. Jackson-Jones, L.H. and Bénézech, C. (2018) Control of innate-like B cell location for compartmentalised IgM production. *Curr. Opin. Immunol.* 50, 9–13
66. Zhivaki, D. *et al.* (2017) Respiratory syncytial virus infects regulatory B cells in human neonates via chemokine receptor CX3CR1 and promotes lung disease severity. *Immunity* 46, 301–314
67. Brandtzaeg, P. (1981) Transport models for secretory IgA and secretory IgM. *Clin. Exp. Immunol.* 44, 221–232
68. Rochereau, N. *et al.* (2013) Dectin-1 is essential for reverse transcytosis of glycosylated SIgA-antigen complexes by intestinal M cells. *PLoS Biol.* 11, e1001658
69. In, N. *et al.* (1999) Regulation of the formation and external transport of secretory immunoglobulins. *Crit. Rev. Immunol.* 19, 481–508
70. Shao, W. *et al.* (2016) Epithelial cells are a source of natural IgM that contribute to innate immune responses. *Int. J. Biochem. Cell Biol.* 73, 19–29
71. Haneberg, B. and Aarskog, D. (1975) Human faecal immunoglobulins in healthy infants and children, and in some with diseases affecting the intestinal tract or the immune system. *Clin. Exp. Immunol.* 22, 210–222
72. Plebani, A. *et al.* (1983) IgM and IgD concentrations in the serum and secretions of children with selective IgA deficiency. *Clin. Exp. Immunol.* 53, 689–696
73. Giuca, M.R. *et al.* (2014) Levels of salivary immunoglobulins and periodontal evaluation in smoking patients. *BMC Immunol.* 15, 5
74. Peebles, R.S. *et al.* (1995) IgA, IgG and IgM quantification in bronchoalveolar lavage fluids from allergic rhinitics, allergic asthmatics, and normal subjects by monoclonal antibody-based immunoenzymetric assays. *J. Immunol. Methods* 179, 77–86

75. El-Loly, M.M. *et al.* (2018) Antibodies of human milk within the first week of birth. *J. Food Dairy Technol.* 6, 10–18
76. Coyle, P.K. and Sibony, P.A. (1986) Tear immunoglobulins measured by ELISA. *Invest. Ophthalmol. Vis. Sci.* 27, 622–625
77. Gonzalez-Quintela, A. *et al.* (2008) Serum levels of immunoglobulins (IgG, IgA, IgM) in a general adult population and their relationship with alcohol consumption, smoking and common metabolic abnormalities. *Clin. Exp. Immunol.* 151, 42–50
78. Tamura, K. *et al.* (2015) Increased production of intestinal immunoglobulins in Syntenin-1-deficient mice. *Immunobiology* 220, 597–604
79. Deslauriers, N. *et al.* (1986) The oral immune system: dynamics of salivary immunoglobulin production in the inbred mouse. *Immunol. Investig.* 15, 339–349
80. Osebold, J.W. *et al.* (1979) Immunological alterations in the lungs of mice following ozone exposure: changes in immunoglobulin levels and antibody-containing cells. *Arch. Environ. Health* 34, 258–265
81. Phillips, T.E. *et al.* (2010) M cell-targeted ocular immunization: effect on immunoglobulins in tears, feces, and serum. *Investig. Opthalmol. Vis. Sci.* 51, 1533
82. Mink, J.G. and Benner, R. (1979) Serum and secretory immunoglobulin levels in preleukaemic AKR mice and three other mouse strains. *Adv. Exp. Med. Biol.* 114, 605–612
83. Enyindah-Asonye, G. *et al.* (2017) CD6 receptor regulates intestinal ischemia/reperfusion-induced injury by modulating natural IgM-producing B1a cell self-renewal. *J. Biol. Chem.* 292, 661–671
84. Inamine, T. *et al.* (2016) Genetic loss of immunoglobulin A does not influence development of alcoholic steatohepatitis in mice. *Alcohol. Clin. Exp. Res.* 40, 2604–2613
85. Smathers, R. *et al.* (2016) Soluble IgM links apoptosis to complement activation in early alcoholic liver disease in mice. *Mol. Immunol.* 72, 9–18
86. Longet, S. *et al.* (2014) Reconstituted human polyclonal plasma-derived secretory-like IgM and IgA maintain the barrier function of epithelial cells infected with an enteropathogen. *J. Biol. Chem.* 289, 21617–21626
87. Kelly, C. *et al.* (2017) Rainbow trout (*Oncorhynchus mykiss*) secretory component binds to commensal bacteria and pathogens. *Sci. Rep.* 7, 41753
88. Kubagawa, H. *et al.* (2009) Identity of the elusive IgM Fc receptor (FcμR) in humans. *J. Exp. Med.* 206, 2779–2793
89. Shen, X. *et al.* (2018) Possible correlation between gut microbiota and immunity among healthy middle-aged and elderly people in southwest China. *Gut Pathog.* 10, 4
90. Yadav, S.K. *et al.* (2017) Gut dysbiosis breaks immunological tolerance toward the central nervous system during young adulthood. *Proc. Natl. Acad. Sci. U. S. A.* 114, E9318–E9327
91. Ray, A. *et al.* (2015) Gut microbial dysbiosis due to *Helicobacter* drives an increase in marginal zone B cells in the absence of IL-10 signaling in macrophages. *J. Immunol.* 195, 3071–3085
92. Kirkland, D. *et al.* (2012) B cell-intrinsic MyD88 signaling prevents the lethal dissemination of commensal bacteria during colonic damage. *Immunity* 36, 228–238
93. Maglione, P.J. *et al.* (2014) IRAK-4 and MyD88 deficiencies impair IgM responses against T-independent bacterial antigens. *Blood* 124, 3561–3571
94. De Palma, G. *et al.* (2010) Intestinal dysbiosis and reduced immunoglobulin-coated bacteria associated with coeliac disease in children. *BMC Microbiol.* 10, 63
95. Chen, B. *et al.* (2018) Oral microbiota dysbiosis and its association with Henoch-Schönlein purpura in children. *Int. Immunopharmacol.* 65, 295–302
96. Larsen, J.M. (2017) The immune response to *Prevotella* bacteria in chronic inflammatory disease. *Immunology* 151, 363–374
97. Machiels, K. *et al.* (2014) A decrease of the butyrate-producing species *Roseburia hominis* and *Faecalibacterium prausnitzii* defines dysbiosis in patients with ulcerative colitis. *Gut* 63, 1275–1283
98. Quévrain, E. *et al.* (2016) Identification of an anti-inflammatory protein from *Faecalibacterium prausnitzii*, a commensal bacterium deficient in Crohn's disease. *Gut* 65, 415–425
99. Mirsepasi-Lauridsen, H.C. *et al.* (2018) Disease-specific enteric microbiome dysbiosis in inflammatory bowel disease. *Front. Med.* 5, 304
100. Pararasa, C. *et al.* (2019) Reduced CD27^{-}IgD^{-} B cells in blood and raised CD27–IgD– B cells in gut-associated lymphoid tissue in inflammatory bowel disease. *Front. Immunol.* 10, 361
101. Preisker, S. *et al.* (2019) Crohn's disease patients in remission display an enhanced intestinal IgM^{+} B cell count in concert with a strong activation of the intestinal complement system. *Cells* 8, 78
102. Hurst, M.M. *et al.* (1975) C1 fixation and classical complement pathway activation by a fragment of the Cmu4 domain of IgM. *J. Exp. Med.* 142, 1322–1326
103. Sørensen, V. *et al.* (2000) Structural requirements for incorporation of J chain into human IgM and IgA. *Int. Immunol.* 12, 19–27
104. Davis, A.C. *et al.* (1988) On the structure of polymeric IgM. *Eur. J. Immunol.* 18, 1001–1008
105. Wiersma, E.J. *et al.* (1997) Analysis of IgM structures involved in J chain incorporation. *J. Immunol.* 158, 1719–1726
106. Natvig, I.B. *et al.* (1997) Mechanism for enhanced external transfer of dimeric IgA over pentameric IgM: studies of diffusion, binding to the human polymeric Ig receptor, and epithelial transcytosis. *J. Immunol.* 159, 4330–4340
107. Crottet, P. and Corthésy, B. (1998) Secretory component delays the conversion of secretory IgA into antigen-binding competent F(ab')2: a possible implication for mucosal defense. *J. Immunol.* 161, 5445–5453
108. Arnold, J. *et al.* (2005) Human serum IgM glycosylation identification of glycoforms that can bind to mannan-binding lectin. *J. Biol. Chem.* 280, 29080–29087
109. Giannone, C. *et al.* (2017) Roles of N-glycans in the polymerization-dependent aggregation of mutant Ig-μ chains in the early secretory pathway. *Sci. Rep.* 7, 41815
110. Colucci, M. *et al.* (2015) Sialylation of N-linked glycans influences the immunomodulatory effects of IgM on T cells. *J. Immunol.* 194, 151–157
111. Torii, T. *et al.* (2017) Sialic acid level is significantly elevated in IgM enriched protein fraction in sera of cancer patients. *J. Immunoass. Immunochem.* 38, 127–139
112. Bosseboeuf, A. *et al.* (2017) Pro-inflammatory state in monoclonal gammopathy of undetermined significance and in multiple myeloma is characterized by low sialylation of pathogen-specific and other monoclonal immunoglobulins. *Front. Immunol.* 8, 1347
113. Maverakis, E. *et al.* (2015) Glycans in the immune system and the Altered Glycan Theory of Autoimmunity: a critical review. *J. Autoimmun.* 57, 1–13
114. Ouchida, R. *et al.* (2012) Critical role of the IgM Fc receptor in IgM homeostasis, B-cell survival, and humoral immune responses. *Proc. Natl. Acad. Sci. U. S. A.* 109, E2699–E2706
115. Vire, B. *et al.* (2011) TOSO, the Fcmicro receptor, is highly expressed on chronic lymphocytic leukemia B cells, internalizes upon IgM binding, shuttles to the lysosome, and is down-regulated in response to TLR activation. *J. Immunol.* 187, 4040–4050
116. Honjo, K. *et al.* (2012) Altered Ig levels and antibody responses in mice deficient for the Fc receptor for IgM (FcμR). *Proc Natl Acad Sci. U. S. A.* 109, 15882–15887
117. Choi, S.-C. *et al.* (2013) Mouse IgM Fc receptor, FCMR, promotes B cell development and modulates antigen-driven immune responses. *J. Immunol.* 190, 987–996
118. Shibuya, A. *et al.* (2000) Fc alpha/mu receptor mediates endocytosis of IgM-coated microbes. *Nat. Immunol.* 1, 441–446
119. Shibuya, A. and Honda, S. (2015) Immune regulation by Fcα/μ receptor (CD351) on marginal zone B cells and follicular dendritic cells. *Immunol. Rev.* 268, 288–295
120. Honda, S. *et al.* (2016) Marginal zone B cells exacerbate endotoxic shock via interleukin-6 secretion induced by Fcα/μR-coupled TLR4 signalling. *Nat. Commun.* 7, 11498
121. Derudder, E. *et al.* (2016) Canonical NF-κB signaling is uniquely required for the long-term persistence of functional mature B cells. *Proc. Natl. Acad. Sci. U. S. A.* 113, 5065–5070

122. Fonte, E. *et al.* (2017) Toll-like receptor 9 stimulation can induce IκBζ expression and IgM secretion in chronic lymphocytic leukemia cells. *Haematologica* 102, 1901–1912
123. Ghosh, A.K. *et al.* (2017) IL-15 stimulates NKG2D while promoting IgM expression of B-1a cells. *Cytokine* 95, 43–50
124. Zheng, K.H. *et al.* (2016) Increasing B1a lymphocytes through APRIL overexpression in apolipoprotein E-deficient mice stabilizes advanced atherosclerotic lesions by decreasing necrotic area and increasing smooth muscle cell content. *Atherosclerosis* 252, e177
125. Tran, N.L. *et al.* (2017) TACI-dependent APRIL signaling maintains autoreactive B cells in a mouse model of systemic lupus erythematosus. *Eur. J. Immunol.* 47, 713–723
126. Basu, M. *et al.* (2016) B cell activating factor is induced by toll-like receptor and NOD-like receptor-ligands and plays critical role in IgM synthesis in *Labeo rohita*. *Mol. Immunol.* 78, 9–26
127. Kanti Ghosh, A. *et al.* (2016) IL-15 temporally reorients IL-10 biased B-1a cells toward IL-12 expression. *Cell. Mol. Immunol.* 13, 229–239
128. Heine, G. *et al.* (2014) Autocrine IL-10 promotes human B-cell differentiation into IgM- or IgG-secreting plasmablasts. *Eur. J. Immunol.* 44, 1615–1621
129. Savage, H.P. *et al.* (2017) Blimp-1-dependent and -independent natural antibody production by B-1 and B-1-derived plasma cells. *J. Exp. Med.* 214, 2777–2794
130. Castro, C.D. *et al.* (2013) Noncoordinate expression of J-chain and Blimp-1 define nurse shark plasma cell populations during ontogeny. *Eur. J. Immunol.* 43, 3061–3075
131. Tellier, J. *et al.* (2016) Blimp-1 controls plasma cell function through regulation of immunoglobulin secretion and the unfolded protein response. *Nat. Immunol.* 17, 323–330
132. Bertolotti, M. *et al.* (2016) AQP8 transports NOX2-generated H2O2 across the plasma membrane to promote signaling in B cells. *J. Leukoc. Biol.* 100, 1071–1079
133. Nguyen, T.T.T. *et al.* (2017) The IgM receptor FcμR limits tonic BCR signaling by regulating expression of the IgM BCR. *Nat. Immunol.* 18, 321–333
134. Maddur, M.S. *et al.* (2019) Natural antibodies: from first-line defense against pathogens to perpetual immune homeostasis. *Clin. Rev. Allergy Immunol.* https://doi.org/10.1007/s12016-019-08746-9

Annexe 2 – Revue sur les MICI

Les maladies inflammatoires chroniques de l'intestin (MICI) : qui dit MICI dit dysbiose

Inflammatory bowel diseases (IBD): where IBD is, dysbiosis goes

Éva Michaud*, Rémi Gayet*, Stéphane Paul*, Xavier Roblin**

Les maladies inflammatoires chroniques de l'intestin (MICI) comprennent la maladie de Crohn (MC) et la rectocolite hémorragique (RCH). Les MICI touchent principalement les pays occidentaux, avec environ 1 million de cas aux États-Unis et 2,5 millions en Europe *(1)*. Cependant, de plus en plus de cas sont recensés dans les nouveaux pays industrialisés. Les MICI constituent ainsi un problème majeur avec des implications sanitaires, économiques, mais aussi sociétales en raison des conséquences délétères sur la qualité de vie des patients à long terme. L'intestin est colonisé par un ensemble de micro-organismes commensaux appelé microbiote. Une forte corrélation existe entre les MICI et le phénomène de dysbiose, qui consiste en un déséquilibre du microbiote. Le lien entre dysbiose et MICI a pu être démontré, mais l'influence du microbiote sur les MICI est difficile à étudier du fait du caractère ambivalent de ce dernier. Cette revue a pour but de souligner les principales avancées sur les liens entre MICI et dysbiose qui pourraient conduire à la mise en place de traitements innovants, plus spécifiques et plus efficaces.

Le microbiote : "MICI-ce que c'est ?"

Le microbiote est un réseau complexe d'interactions stables entre plusieurs populations microbiennes qui contribuent à l'homéostasie intestinale. Les bactéries dont il est constitué se répartissent entre 4 phyla majeurs. Une dysbiose se caractérise par l'expansion d'un ou de plusieurs nouveaux groupes de bactéries dans l'intestin, qui modifie le ratio de ces 4 grands phyla de bactéries présents dans l'intestin *(2)*.

Généralités sur le microbiote humain

Le microbiote est constitué à 0,1 % par des *Fungi*, en particulier du genre *Candida*, qui permettent la stimulation du système immunitaire intestinal. La présence d'un virome dans l'intestin a mis en évidence le rôle important des virus dans le microbiote, et notamment des bactériophages, mais qui restent cependant peu étudiés *(3)*. Toutefois, la majeure partie du microbiote est constituée de plus de 1 100 espèces bactériennes, dont les plus nombreuses sont des *Bacteroidetes* et des *Firmicutes*, suivies par des *Actinobacteria* et des *Proteobacteria*. Même si le microbiote varie d'un individu à l'autre, sa composition générale est relativement conservée dans la population. Cette stabilité est liée aux fonctions du microbiote dans l'homéostasie intestinale, à savoir des processus métaboliques aidant la nutrition, la fourniture de nutriments (vitamines), ainsi que la maturation du système immunitaire *(4)*. Le microbiote d'un individu se forme dès la naissance. Des méthodes de métagénétique fondées sur le séquençage de l'ARN ribosomal (ARNr) bactérien 16S ont permis d'étudier la composition du microbiote au cours de la vie. Il apparaît que le microbiote d'un enfant âgé de moins de 1 an est peu diversifié, et provient principalement du microbiote maternel. Sa composition évolue au fur et à mesure de l'intégration d'une alimentation plus complexe, ce qui contribue aux différences interindividuelles.

* *Laboratoire d'immunologie et d'immunomonitoring, CIC 1408, Inserm, GIMAP EA3064, CHU de Saint-Étienne.*

** *Département de gastro-entérologie, CHU de Saint-Étienne.*

Résumé

Le microbiote est composé de bactéries, virus et fungi essentiels à la digestion, à la mise en place du système immunitaire et à la protection contre les agents pathogènes tout au long de la vie d'un individu. Sa composition varie d'un individu à l'autre mais conserve une composition générale qui comprend les espèces *Bacteroidetes, Firmicutes, Actinobacteria* et *Proteobacteria*. Les maladies inflammatoires chroniques de l'intestin (MICI), qui comprennent la maladie de Crohn et la rectocolite hémorragique, sont étroitement liées à une dérégulation du microbiote, appelée dysbiose. Des facteurs comme l'héritage génétique et l'alimentation vont conduire à une modification de la composition du microbiote, à l'exemple de la réduction des populations bactériennes inductrices de tolérance comme *Faecalibacterium prausnitzii* et des espèces *Roseburia* ou *Lachnospiracaea*. La dysbiose influence aussi les traitements mis en place contre les MICI. Cette revue vise à résumer les facteurs inducteurs de dysbiose conduisant à une MICI ainsi que les stratégies mises en place pour traiter ces maladies.

Mots-clés

MICI
Microbiote
Dysbiose
Traitement
Diagnostic

Anomalies du microbiote au cours des MICI

◆ *Microbiote bactérien*

Il est difficile de déterminer si les modifications du microbiote observées chez les patients atteints de MICI sont des causes ou des conséquences de la maladie. Néanmoins, on a pu observer une plus faible diversité de populations bactériennes au sein du microbiote lors d'une MICI. Deux groupes ont ainsi été identifiés : les bactéries protectrices et les aggravantes *(2)*. Les bactéries protectrices ont tendance à induire une tolérance immunitaire, comme dans le cas de l'espèce bactérienne *Faecalibacterium prausnitzii,* très documentée. D'autres espèces sont retrouvées dans ce groupe, telles que les *Lachnospiraceae*, les *Roseburia*, les *Sutterella* ou les *Bifidobacterium*. Toutes ces bactéries sont très souvent moins représentées en cas de MICI. À l'inverse, on note une forte augmentation des bactéries aggravantes dans les MICI. Les plus étudiées sont l'espèce *Escherichia coli* adhérente et invasive (ECAI), retrouvée chez 30 à 40 % des patients atteints d'une MC, et l'espèce *Enterococcus faecalis*, également impliquée dans l'aggravation des MICI. La première induit une sécrétion de l'interféron γ, alors que la seconde détériore la barrière épithéliale. Même si leurs mécanismes restent moins connus, d'autres bactéries sont davantage associées aux MICI, comme les *Proteobacteria*, *Ruminococcus gnavus* ou encore les *Fusobacterium*.

◆ *Microbiote fongique*

Peu étudié, le rôle des *Fungi* dans les MICI a récemment été identifié. Un premier indice était la présence de formes sévères de RCH en cas de polymorphisme du gène Dectin-1 codant pour un récepteur reconnaissant des motifs pariétaux de *Fungi*. Les propriétés anti-inflammatoires du fluconazole, un antifongique utilisé comme traitement chez les patients atteints de MICI, sont également un élément important. Une étude récente a démontré que la diversité des *Fungi* était modifiée dans la RCH mais pas dans la MC, à l'exception de *Candida albicans,* dont l'augmentation a également été confirmée chez des patients atteints d'une MC. En particulier, une augmentation des *Basidiomycota* parallèle à une diminution des *Ascomycota (Saccharomyces cerevisiae)* suggère que le ratio de ces 2 groupes pourrait constituer un indice de dysbiose *(5)*. Par ailleurs, les modifications du mycobiote étaient associées à une dysbiose bactérienne. En particulier, une expansion de *Candida tropicalis* a été corrélée à celle de *E. coli* et de *Serratia marcescens* chez des patients atteints d'une MC *(2)*.

◆ *Microbiote viral*

La présence de bactériophages possédant un cycle lysogénique peut modifier la virulence de certaines bactéries, conduisant potentiellement à une MICI. Ainsi, une augmentation de la diversité du virome et une expansion des bactériophages de l'ordre *Caudovirales* ont été observées chez des patients atteints de MICI *(3)*. Par ailleurs, une revue de littérature sur le sujet a rapporté une étude sur modèle murin montrant que la mutation du gène ATG16L1 n'induisait des colites qu'en cas d'infection par le norovirus. La mutation de ce gène étant retrouvée chez des patients atteints d'une MC, les virus eucaryotes pourraient donc également être impliqués dans les MICI. Enfin, le cytomégalovirus (CMV) est détecté dans 4 à 16 % des cas au stade actif de la maladie, ce qui suggère un lien prononcé entre CMV et MICI. Bien que l'action des virus reste peu claire, il semble évident qu'ils ont un rôle à jouer dans l'apparition des MICI, et pourraient donc nécessiter un traitement antiviral particulier.

Intérêt diagnostique de l'analyse du microbiote dans les MICI

La RCH et la MC se différencient par la localisation de l'inflammation au niveau de l'intestin. On pourrait donc s'attendre à une différence dans le microbiote associé à ces maladies. Néanmoins, peu de données permettent, à l'heure actuelle, d'appuyer cette théorie. Une étude récente a cependant mis en évidence une plus forte dysbiose ainsi que des groupes de bactéries caractéristiques de la MC *(6)*. Ainsi, les groupes *Faecalibacterium, Peptostreptococcaceae, Anaerostipes, Methanobrevibacter, Christensenellaceae, Collinsella* et, surtout, *Fusobacterium* et *Escherichia* seraient de bons marqueurs diagnostiques de la MC. Notons que

Summary

The intestinal microbiota plays a major role in shaping mucosal immune responses, as well as protecting the epithelium against external threats. Its composition varies from an individual to another, but has a common general composition that comprises Bacteroidetes, Firmicutes, Actinobacteria and Proteobacteria. Dysbiosis is a key feature of inflammatory bowel diseases (IBD), which comprise ulcerative colitis and Crohn's disease. Recent advances in metagenomics have yielded substantial documentation on the nature of the IBD-associated microbiota and its alteration. Notably, reduced Faecalibacterium prausnitzii is well documented, as well as the reduction of the Roseburia, Lachnospiracaea, and the Bifidobacterium species. Moving from the point where dysbiosis is a mere observation, it can also be demonstrated that changes in dietary habits and lifestyle have a direct influence over the microbiota and the response to IBD treatments. In this review, we offer to briefly assess the causes of dysbiosis in IBD and its effect on current therapeutic strategies.

Keywords

IBD
Microbiota
Dysbiosis
Treatment
Diagnosis

les cholangites sclérosantes primitives (CSP) sont associées dans 80 % des cas à une MICI (CSP-MICI). Des études portant sur le contenu du microbiote des CSP-MICI ont cherché à savoir si des liens pouvaient être établis avec les MICI. L'une d'elles, assez représentative de la littérature sur le sujet, a montré que la dysbiose était différente dans les CSP-MICI et dans les RCH *(7)*. Une augmentation de la représentativité des genres *Rothia, Enterococcus, Clostridium* et *Veillonella* dans les CSP-MICI par rapport à des sujets sains a été décrite. Cette augmentation n'est en revanche pas observée dans la RCH. À l'inverse, la RCH est caractérisée par un amoindrissement du microbiote en espèces *Akkermansia* et *Roseburia* qui n'est pas observé dans les CSP-MICI.

Facteurs inducteurs de dysbiose au cours des MICI

Une dysbiose est induite par la combinaison de plusieurs facteurs, soit intrinsèques à l'individu, soit extrinsèques. De très nombreux mécanismes sont associés aux dysbioses ; nous ne retiendrons ici que ceux pouvant conduire à une MICI *(4)*.

Génétique

Des mutations telles que les polymorphismes d'un seul nucléotide ont été identifiées comme des marqueurs de taxon pour certaines bactéries. Par exemple, les gènes VDR, LCT, FUT2 et NOD2 ont été décrits comme associés à la composition du microbiote. L'environnement génétique peut donc exercer une influence sur la composition du microbiote et être ainsi à l'origine d'une dysbiose *(8)*. Une des premières preuves est le caractère héréditaire des MICI. Le risque d'être atteint de MC ou de RCH serait ainsi respectivement d'environ 5 et 2 % lorsqu'un membre de la famille au premier degré a présenté une de ces pathologies. Par ailleurs, les risques de MICI pour les descendants d'un individu ayant contracté une MICI peuvent aller jusqu'à environ 10 %. Des études d'association pangénomiques ont été réalisées afin de déterminer les polymorphismes liés aux MICI. Il en résulte que :

- de nombreux gènes de l'immunité, tels que MST1 (voie des macrophages) ou encore FUT (lymphocytes T helper 17), ont été décrits comme directement liés à un risque plus important de MICI ;
- les mécanismes liés aux mutations génétiques facilitant les dysbioses sont complexes et, pour certains, encore mal connus. Par exemple, le variant FUT agit indirectement sur l'immunité en entraînant une diminution du nombre de bactéries anti-inflammatoires et une augmentation de celui des bactéries impliquées dans les MICI par l'absence de groupements fucose dans la muqueuse intestinale *(8)* ;
- une grande partie des polymorphismes facilitant la MC sont différents de ceux retrouvés pour la RCH *(9)*. Par exemple, la mutation du gène NOD2 est le principal facteur lié à l'apparition de la MC, alors qu'il n'y a pas de gènes prépondérants pour la RCH ;
- enfin, notons que les mécanismes de modification épigénétique pourraient faire l'objet de plus amples recherches, puisque des liens avec les MICI ont été démontrés. Par exemple, la méthylation de l'ADN, les microARN et les modifications des histones semblent être impliqués dans le développement des MICI *(10)*.

Alimentation

Les similarités dans l'organisation générale des microbiotes ont permis la définition d'entérotypes. L'entérotype *Bacteroides* est associé à une alimentation riche en protéines et graisses animales, alors que l'entérotype *Prevotella* apparaît lié à un régime riche en carbohydrates. Certains aliments ont donc tendance à favoriser la présence de bactéries plus propices à déclencher des MICI *(10)*. Un régime alimentaire composé de fruits et légumes est ainsi associé à un risque plus faible de MICI qu'un régime à teneur élevée en graisses animales et en glucides. En outre, une forte corrélation entre le développement d'une RCH et l'absorption de graisses polyinsaturées a été mise en évidence. D'autres éléments ont été décrits comme exerçant une influence sur l'apparition des MICI, comme le fer, les vitamines A et B et certains additifs (des émulsifiants comme la carboxyméthylcellulose et le polysorbate 80 testés chez la souris) retrouvés dans le régime alimentaire occidental. Étant donné le rôle de l'alimentation sur le mycobiote *(11)* et les récentes découvertes concernant le rôle des *Fungi* dans les MICI, l'étude de l'influence de l'alimentation sur les MICI via les *Fungi* mériterait d'être approfondie.

Infections

Une dysbiose peut résulter d'une infection ayant modifié les populations du microbiote. Une infection chronique de l'intestin peut aussi induire une inflam-

mation chronique conduisant à une MICI. Ces hypothèses sont difficiles à mettre en évidence, puisque le microbiote ne peut pas être isolé comme une culture pure. En outre, très peu de preuves contre des agents infectieux directement impliqués dans l'apparition de MICI sont recensées, mais quelques pathogènes sont régulièrement associés aux MICI *(12)*. Des bactéries du genre *Mycobacterium* sont retrouvées très tôt chez certains patients atteints de MICI et peuvent servir de marqueurs de la maladie. D'autres bactéries du genre *Clostridium* sont présentes dans les stades actifs de la maladie, mais leur rôle reste à préciser. Par ailleurs, les entérobactéries sont plus fréquentes chez les patients atteints d'une MC *(13)*. Le cas le plus représentatif reste *E. coli*, puisque *E. coli* O157:H7 provoque les symptômes cliniques des MICI et qu'on retrouve souvent de forts taux d'anticorps dirigés contre *E. coli* chez les patients atteints de MICI, ce qui suggère un lien prononcé entre la bactérie et la maladie.

Utilisation des antibiotiques

L'utilisation d'antibiotiques détériore la flore intestinale. Bien que des études soulignent le rétablissement rapide d'une flore stable, il apparaît de plus en plus évident que le microbiote n'est pas restauré tel qu'il était à l'état initial *(14)*. Les antibiotiques à spectre large, comme la ciprofloxacine et la clindamycine, altéreraient la diversité des populations de *Bacteroides* après la fin du traitement, alors que l'amoxicilline diminuerait les populations de *Lactobacillus* ainsi que la sécrétion de peptides antimicrobiens. Ainsi, les traitements antibiotiques, même de courte durée, perturbent le microbiote sur le long terme et favoriseraient l'apparition de MICI, en particulier en cas de traitement chez les enfants de moins de 1 an.

Stratégies thérapeutiques

L'une des principales caractéristiques observées dans les MICI est la production croissante de TNF *(Tumor Necrosis Factor)* favorisant la réorganisation de la réponse immunitaire vers un profil inflammatoire au détriment de l'induction de lymphocytes T régulateurs. Le TNF est donc l'une des premières cibles thérapeutiques, au travers d'anticorps bloquants, l'infliximab et l'adalimumab faisant partie des plus utilisés. À cela s'ajoutent des stratégies visant l'inhibition de la migration des effecteurs vers le site inflammatoire. Parmi celles-ci, le védolizumab est un anticorps bloquant l'intégrine α4β7, impliquée dans le *homing* des cellules T et B vers de la muqueuse. Enfin, la résection chirurgicale de la zone lésée est l'un des derniers ressorts thérapeutiques.
Les réponses du microbiote en termes de diversité et de métabolisme sont de bons prédicteurs de l'efficacité de ces choix sur le long terme : la production de n-butyrate, associée à un métabolisme carboné dépendant des acides gras, favorise la tolérance immune et la production de mucine.

Dysbiose et efficacité thérapeutique

Plusieurs études ont recherché un lien entre dysbiose et succès thérapeutique des différentes stratégies. Le principal constat n'est pas un lien entre index de dysbiose et efficacité, mais une signature microbiologique commune aux non-répondeurs. Une première étude permet d'identifier la réduction du genre *Coprococcus* en association avec un profil non répondeur et pointe 3 genres bactériens reliés à la distinction entre répondeurs et non-répondeurs : *Coprococcus*, *Adlercreutzia* et *Dialister (15)*. La réponse microbienne aux anti-intégrines (védolizumab) présente un net enrichissement de la diversité bactérienne, avec une réémergence de l'espèce *Roseburia inulinivorans* et des *Burkholderiales (16)*. Ici encore, le genre *Dialister* et une espèce du genre *Bifidobacterium* sont associés au profil répondeur. À noter que la grande majorité des patients présentant une signature microbienne associée à la réponse aux anti-intégrines sont des patients atteints de MC. Des études similaires ont été menées sur les réponses aux thérapies anti-TNF. Chez les patients souffrant de MC, on trouve une élévation de la proportion des espèces *Bifidobacterium*, cette fois chez les non-répondeurs *(17)*. Ici, c'est la réémergence des lactobacilles qui suggère une atténuation de la dysbiose. Dans la RCH, la qualité de la réponse aux anti-TNF semble dépendre du taux de *F. prausnitzii* présents avant traitement *(18)*.
Plusieurs métabolites bactériens sont également nécessaires à l'efficacité thérapeutique. Une augmentation de la production d'acides gras à chaîne courte (dont le n-butyrate) et de l'activation des voies de synthèse des acides aminés branchés *(branched-chain amino acids* [BCAA]*)* est observée chez les patients atteints de MC ou de RCH répondeurs. Par ailleurs, la production de butyrate est associée à la rémission postchirurgicale. La chirurgie elle-même peut induire la dysbiose : la rechute peut être associée à un enrichissement de la flore en

Lachnospiraceae anaérobies. De plus, la différence de la flore au-dessus et au-dessous de l'anastomose est associée à la rechute postopératoire. À l'inverse, les groupes *Bacteroides*, *Dorea* et *Dialister* sont associés à la rémission, en particulier si la similarité entre ces 2 sites est élevée *(19)*.
Un profil favorable à la rémission est donc non seulement lié à l'abondance de certaines espèces bactériennes, mais aussi à leur capacité à sécréter différents métabolites, générant un terrain favorable à la thérapie choisie. Le constat général de ces différents travaux est la valeur prédictive de la composition précoce de la flore pour l'entrée en rémission et le suivi à long terme.

Traitements à l'essai

◆ *Thérapie nutritionnelle*

La dysbiose, qui caractérise les MICI, entraîne un changement métabolique : les souches jusqu'alors minoritaires y trouvent des conditions de croissance favorables via l'utilisation de la mucine comme source carbonée *(20)*. Un régime pauvre en fibres favorise la croissance de ces souches mucolytiques. Ces fibres, dont l'amidon, stimulent en effet la fermentation bactérienne de la flore. En réponse, celle-ci produit le n-butyrate qui entraîne la diminution des taux d'interleukines 6 et 12 ainsi que l'induction de lymphocytes T régulateurs *(21)*. Un régime de faible index glycémique favorise la réduction des taux sériques de TNFα et d'interleukine 6. Il y a également un lien direct entre l'alimentation et l'efficacité des thérapies anti-TNF *(20)*. À l'inverse, les déficiences en vitamine D, la consommation d'acides gras saturés et le surdosage en fer contribuent au développement de la colite *(21, 22)*. La maltodextrine (aspartame, sucralose), le gluten et la consommation de viande rouge, caractéristiques de l'alimentation occidentale, sont également des facteurs aggravants. Leurs effets peuvent être atténués par un fort apport en amidon ; ainsi, la consommation de légumineuses s'accompagne d'une réduction des symptômes *(22)*. Dans la pratique, il semble cependant que seule la nutrition entérale ait un effet (soit délétère, soit bénéfique). La technique ne semble cependant pas permettre une rediversification de la flore mais plutôt de ses métabolites. La dysbiose influence le succès de cette stratégie, d'autant que celle-ci tend souvent à réduire la diversité bactérienne en dépit de son efficacité. Suivant les études, on trouve une réduction de *F. prausnitzii* et des commensales *Bifidobacterium* et *Ruminococcus (23)*.

◆ *Probiotiques*

Les probiotiques sont des organismes non pathogènes vivants, dont l'objectif est la repopulation de la muqueuse. Ils ont des effets positifs sur l'équilibre de la flore commensale, le profil inflammatoire de la muqueuse et l'absorption des nutriments. Il n'y a pas encore de consensus au sujet de leur utilisation dans les MICI. Ils semblent présenter un intérêt dans le traitement de la RCH : une récente méta-analyse des différents travaux sur le sujet montre en effet une association significative entre la prise de probiotiques et la rémission *(24)*. Tant pour la RCH que la MC, les probiotiques favorisent la rémission des patients recevant des corticostéroïdes. Ils sont également associés à la rémission postchirurgicale dans la RCH, mais pas dans la MC *(24, 25)*. Plusieurs formulations existent pour les probiotiques : lactobacilles seuls ou combinés avec *Saccharomyces boulardii*, ou encore lactobacilles et bifidobactéries. Cette dernière association a un fort potentiel d'évolution vers la rémission dans la RCH ou dans les suites d'une chirurgie *(24, 25)*. Il semble qu'il faille une combinaison de ces formulations pour induire des effets significatifs dans la prise en charge d'une MC. Il manque, pour confirmer ce constat, des études de suivi à long terme. Les probiotiques peuvent avoir un effet bénéfique sur les MICI, mais l'hétérogénéité des essais conduits et des résultats obtenus nécessite une plus ample analyse. Il est par ailleurs nécessaire de catégoriser les effets obtenus selon les stratégies thérapeutiques choisies et dans des suivis à très long terme.

◆ *Traitement par les immunoglobulines*

Une des plus récentes avancées dans la recherche sur le traitement des MICI est l'administration orale d'immunoglobulines. Une étude pilote menée chez des enfants atteints de MC permet de comparer les effets de la nutrition entérale et l'administration d'immunoglobulines G par voie orale (OHIG). Si les effets des 2 traitements se révèlent positifs, l'OHIG permet non seulement la cicatrisation de la muqueuse, mais aussi, et surtout, la réduction de la perméabilité intestinale *(26)*. Les immunoglobulines A étant responsables de la sélection de la flore, il semble intéressant de choisir celles-ci pour traiter la dysbiose. L'équipe qui a travaillé sur le sujet avait précédemment utilisé cette stratégie pour le traitement de la MC avec un succès mitigé. En revanche, les immunoglobulines A sécrétoires ont été brevetées dans le traitement oral des infections à *Clostridium difficile*, des allergies et intolérances alimentaires et de la maladie cœliaque. Peu de travaux

s'intéressent à cette option pour le traitement des MICI ; or, elle offre une voie thérapeutique physiologique et peu invasive qui mérite une plus ample investigation *(27)*.

◆ ***Transplantation fécale***

Les très bons résultats du traitement des colites à *Clostridium difficile* offrent de nouvelles pistes thérapeutiques. Cependant, les transplantations de microbiote fécal (TMF) dans le contexte des MICI induisent des poussées aiguës de la maladie. Une amélioration des taux de rémission est possible chez les patients atteints de RCH transplantés. Des essais soulignent la nécessité de l'adéquation entre la flore du donneur et celle du patient *(28)*. Il y a en revanche peu d'éléments qui soutiennent l'intérêt d'une TMF chez les patients souffrant de MC. Elle semble plus intéressante dans le traitement de la forme pédiatrique de la maladie *(29)*.

Conclusion

L'association entre MICI et dysbiose est la résultante d'un ensemble de facteurs environnementaux, génétiques et culturels. L'articulation entre ces différents composants reste mal comprise, notamment en ce qui concerne le lien entre environnement (alcool, tabagisme), dysbiose et MICI. Toutefois, les nombreuses avancées en matière d'étude du microbiote et de tests génétiques ont permis d'isoler les comportements et les facteurs de risque. Ces éléments indiquent qu'il est possible de réguler les populations bactériennes de l'intestin en combinant les traitements immunosuppresseurs, les probiotiques et une hygiène de vie favorisant la croissance de souches tolérogènes. L'idée est de proposer un traitement permettant à l'organisme de retrouver naturellement son état optimal. Cette vue doit être contrebalancée par :

- les défauts génétiques, qui ne sont à ce jour pas compensables ;
- l'influence du microbiote initial sur l'efficacité thérapeutique ;
- l'importante variabilité des réponses aux nouvelles approches, qui impose des stratégies thérapeutiques individualisées.

La MC et la RCH sont aujourd'hui bien caractérisées sur le plan immunitaire ; les interactions entre le système muqueux et la flore commensale constituent maintenant l'enjeu principal de la recherche sur les MICI. Il est cependant certain, au vu du nombre croissant de cas de MICI, que la prise en charge de ces maladies doit inclure une réflexion sur l'hygiène de vie et l'alimentation liées à l'industrialisation. ■

Les deux premiers auteurs Éva Michaud et Rémi Gayet ont contribué à parts égales à la rédaction de cet article.

Les auteurs déclarent ne pas avoir de liens d'intérêts.

Références bibliographiques

1. *Kaplan GG. The global burden of IBD: from 2015 to 2025. Nat Rev Gastroenterol Hepatol 2015;12:720-7.*

2. *Sartor RB, Wu GD. Roles for intestinal bacteria, viruses, and fungi in pathogenesis of inflammatory bowel diseases and therapeutic approaches. Gastroenterology 2017;152:327-39.e4.*

3. *Norman JM, Handley SA, Baldridge MT et al. Disease-specific alterations in the enteric virome in inflammatory bowel disease. Cell 2015;160:447-60.*

4. *Weiss GA, Hennet T. Mechanisms and consequences of intestinal dysbiosis. Cell Mol Life Sci CMLS 2017;74:2959-77.*

5. *Sokol H, Leducq V, Aschard H et al. Fungal microbiota dysbiosis in IBD. Gut 2017;66:1039-48.*

6. *Pascal V, Pozuelo M, Borruel N et al. A microbial signature for Crohn's disease. Gut 2017;66:813-22.*

7. *Bajer L, Kverka M, Kostovcik M et al. Distinct gut microbiota profiles in patients with primary sclerosing cholangitis and ulcerative colitis. World J Gastroenterol 2017;23:4548-58.*

8. *Hall AB, Tolonen AC, Xavier RJ. Human genetic variation and the gut microbiome in disease. Nat Rev Genet 2017;18:690-9.*

9. *Zoetendal EG, de Vos WM. Effect of diet on the intestinal microbiota and its activity. Curr Opin Gastroenterol 2014;30:189-95.*

10. *Rapozo DCM, Bernardazzi C, de Souza HSP. Diet and microbiota in inflammatory bowel disease: The gut in disharmony. World J Gastroenterol 2017;23:2124-40.*

11. *Sam QH, Chang MW, Chai LY. The fungal mycobiome and its interaction with gut bacteria in the host. Int J Mol Sci 2017;18:pii:E330.*

12. *Mann EA, Saeed SA. Gastrointestinal infection as a trigger for inflammatory bowel disease. Curr Opin Gastroenterol 2012;28:24-9.*

13. *De Hertogh G, Geboes K. Crohn's disease and infections: A complex relationship. MedGenMed 2004;6:14.*

14. *Sommer F, Anderson JM, Bharti R, Raes J, Rosenstiel P. The resilience of the intestinal microbiota influences health and disease. Nat Rev Microbiol 2017;15:630-8.*

15. *Shaw KA, Bertha M, Hofmekler T et al. Dysbiosis, inflammation, and response to treatment: a longitudinal study of pediatric subjects with newly diagnosed inflammatory bowel disease. Genome Med 2016;8:75.*

16. *Ananthakrishnan AN, Luo C, Yajnik V et al. Gut microbiome function predicts response to anti-integrin biologic therapy in inflammatory bowel diseases. Cell Host Microbe 2017;21:603-10.e3.*

17. *Ding NS, Perdones-Montero A, Sarafian M et al. P787 The microbiota and it's role in anti-TNF therapy non-response. J Crohns Colitis 2017;11(suppl. 1):S482-3.*

18. *Magnusson MK, Strid H, Sapnara M et al. Anti-TNF therapy response in patients with ulcerative colitis is associated with colonic antimicrobial peptide expression and microbiota composition. J Crohns Colitis 2016;10:943-52.*

19. *Mondot S, Lepage P, Seksik P et al. Structural robustness of the gut mucosal microbiota is associated with Crohn's disease remission after surgery. Gut 2016;65:954-62.*

20. *Andersen V, Hansen AK, Heitmann BL. Potential impact of diet on treatment effect from anti-TNF drugs in inflammatory bowel disease. Nutrients 2017;9:286.*

21. *Sarbagili-Shabat C, Sigall-Boneh R, Levine A. Nutritional therapy in inflammatory bowel disease. Curr Opin Gastroenterol 2015;31:303-8.*

22. *Tasson L, Canova C, Vettorato MG, Savarino E, Zanotti R. Influence of diet on the course of inflammatory bowel disease. Dig Dis Sci 2017;62:2087-94.*

23. *MacLellan A, Connors J, Grant S et al. The impact of Exclusive Enteral Nutrition (EEN) on the gut microbiome in Crohn's disease: A review. Nutrients 2017;9:447.*

24. *Ganji-Arjenaki M, Rafieian-Kopaei M. Probiotics are a good choice in remission of inflammatory bowel diseases: A meta analysis and systematic review. J Cell Physiol 2018;233:2091-103.*

25. *Derwa Y, Gracie DJ, Hamlin PJ, Ford AC. Systematic review with meta-analysis: the efficacy of probiotics in inflammatory bowel disease. Aliment Pharmacol Ther 2017;46:389-400.*

26. *Sundqvist T, Stenhammar L, Tjellström B, Magnusson KE, Forslund T, Högberg L. Oral immunoglobulin treatment improved intestinal permeability in children with active Crohn's disease. Acta Paediatr 2017;106:647-53.*

27. *Simon MR. Treatment of celiac disease, C. difficile infection, food intolerance and food allergy with secretory IgA/IgM. http://www.google.com/patents/US20160319039*

28. *Allegretti J, Eysenbach LM, El-nachef N, Fischer M, Kelly C, Kassam Z. The current landscape and lessons from fecal microbiota transplantation for inflammatory bowel disease: past, present, and future. Inflamm Bowel Dis 2017;23:1710-7.*

29. *Bak SH, Choi HH, Lee J et al. Fecal microbiota transplantation for refractory Crohn's disease. Intest Res 2017;15:244-8.*

Travaux annexes

Participation aux études :

1. **YAP/TAZ are regulators of resident cells in response to inflammation**
   Caire R, Audoux E, Courbon G, Petit C, **Michaud E**, Thomas M, Vanden-Bossche A, Chafchafi M, Navarro L, Linossier MT, Peyroche S, Guignandon A, Vico L, Paul S, Marotte H

Communication orale :

1. « **Rôle des Immunoglobulines A sécrétoires dans la maladie de Crohn** »,
   Eva Michaud, *Journée Stéphanoise de cytométrie (CYTIMA), 15-16 Mai 2018, Andrézieu.*

Communications affichées

1. « **Alterations in IgA1- and IgA2-driven selection of the microbiota in Corhn's disease**», E**va Michaud**, Blandine Chanut, Fabienne Jospin, Katell Bathany, Nicolas Rochereau, Stéphane Paul. *Keystone Symposia « Microbiome : therapeutic implications », 8 Octobre 2019, Killarney (Irlande).*.

2. « **Nature, structure and functionality of intestinal secretory IgA in Inflammatory Bowel Diseases**», **Eva Michaud**, Blandine Chanut, Katell Bathany, Nicolas Rochereau, Stéphane Paul. *Journée Scientifique MSD Avenir, 27 Novembre 2018, Paris.*

3. « **Nature, structure and functionality of intestinal secretory IgA**», E**va Michaud**, Blandine Chanut, Fabienne Jospin, Katell Bathany, Jean-Marie Schmitter, Nicolas Rochereau, Stéphane Paul. *Centre International de Recherche en Infectiologie (CIRI), 4-6 Mai 2018, Voguë.*

4. « **Rôle des Immunoglobuline Sécrétoires dans la Maladie de Crohn**», **Eva Michaud**, Nicolas Rochereau, Stéphane Paul. *Journée de l'ED. SIS, 14 Juin 2018, Saint-Etienne. 3ème prix ex-aequo, meilleure présentation.*

YAP/TAZ are regulators of resident cells in response to inflammation

Caire R[1], Audoux E[2], Courbon G[1], Petit C[3], Michaud E[2], Thomas M[1], Vanden-Bossche A[1], Chafchafi M[1], Navarro L[3], Linossier MT[1], Peyroche S[1], Guignandon A[1], Vico L[1], Paul S[2,4], Marotte H[1,5]*

[1]INSERM U1059-SAINBIOSE, Université de Lyon, Saint-Etienne, France

[2]GIMAP EA3064, Université de Lyon, Saint-Etienne, France

[3]INSERM U1059-SAINBIOSE, Mines Saint-Etienne, Université de Lyon, Saint-Etienne, France

[4]CIC INSERM 1408, Université de Lyon, Saint-Etienne, France

[5]Department of Rheumatology, Hôpital Nord, University Hospital Saint-Etienne, Saint-Etienne, France

*Corresponding author: Hubert Marotte (Phone: +33-477-12-76-43, e-mail: hubert.marotte@chu-st-etienne.fr)

Conflict of interest:

The authors have declared that no conflict of interest exists

ABSTRACT

Rheumatoid arthritis (RA) is an inflammatory disease where fibroblast-like synoviocytes (FLS) are key players. Mechanisms of aggressive “tumour-like” phenotype in RA FLS are still unclear. Here we identified YAP/TAZ, two transcription cofactors activated in several cancers, as major arthritis actors. Stiff support of culture or pro-inflammatory cytokines activated YAP in RA FLS. Inhibiting YAP/TAZ transcriptional effect with verteporfin (VP) restored a common phenotype in RA FLS, blocking their ability to form a hyperplasic lining layer in an organoid model of synovial membrane. *In vivo*, VP treatment reduced the severity of arthritis by restoring synovial homeostasis and decreased systemic inflammation. Furthermore, we show that synovial stiffening occurred during arthritis related to YAP/TAZ activity. YAP/TAZ inhibition was also relevant in a mouse colitis model with reduction of disease severity by similar mechanisms than those described in arthritis. This work revealed an unprecedent YAP/TAZ involvement in arthritis relevant for future inflammatory disorders comprehension and treatment.

INTRODUCTION

Rheumatoid arthritis (RA) is a common immune disorder associated with strong joint inflammation and destruction *(1)*. Fibroblast-like synoviocytes (FLS) are the resident cells of the synovial tissue. In physiological conditions, FLS form with some macrophages a synovial lining layer constituted of 2 or 3 rows of cells *(2)*. During RA, there is hyperplasia of the synovial lining layer mainly through FLS hyperproliferation and apoptosis resistance mechanisms *(3*, *4)*, but also due to inflammatory cell infiltrate. Targeting FLS by different ways was already effective *in vivo* with a reduction of arthritis severity *(4*, *5)*. Indeed, FLS are key actors in initiating and maintaining immune cell recruitment contributing to joint destruction by the invasion of cartilage and bone, partly linked to the secretion of matrix metalloproteinases (MMPs) *(6)*. Furthermore, FLS have been called “imprinted aggressors” because of their tumour-like phenotype induced by chronic inflammation that persists even after the inflammation has stopped *(2)*. The mechanisms involved in this phenotype are still unclear and several alterations were reported: transcription factors as c-Jun modulation *(7)*, nuclear factor κB (NF-κB) pathway anomalies *(8);* apoptosis regulation with p53 anomalies or increased expression of antiapoptotic proteins such as B-cell lymphoma 2 (Bcl-2) family members *(8)* without effect on Bcl2-associated X protein (Bax, a pro-apoptotic molecule) *(9)*; or epigenetic alterations *(10)*. Due to these properties, FLS targeting is an important emerging research axis in RA. Their similarities with tumour cells highlight the opportunity to identify cancer-shared mechanisms.

Among cancer-targeted factors, yes-associated protein (YAP) and transcriptional co-activator with PDZ-binding motif (TAZ) are two cotranscription factors sharing important structural similarities. Upon specific *stimuli*, YAP/TAZ are activated, and they both translocate to the nucleus *(11)* to induce transcription by interacting with their

main transcription factor called transcriptional enhanced associate domains (TEAD) *(12*, *13)*. YAP/TAZ are partly regulated by the Hippo pathway, which leads to their phosphorylation and subsequent retention in the cytoplasm *(14)*. Initially, YAP/TAZ are linked with tissue size homeostasis by promoting overgrowth in case of hyperactivation *(15)*. YAP/TAZ were also reported as major mechanotransduction actors since they convert cell mechanical *stimuli* perception into transcriptional responses for cell behaviour adaptation, thus independently from the Hippo pathway *(11)*. YAP/TAZ also play an important role in several types of cancer and contribute to cancer cell phenotypes with apoptosis resistance, invasion abilities, and hyperproliferation *(16)*. Recently, inflammation was also reported to activate YAP/TAZ. Indeed, pro-inflammatory cytokines such as TNF and IL-6 have been reported to directly activate YAP in some cancers *(17*, *18)*. Since inflammation is a crucial process in inflammatory related diseases, like RA or inflammatory bowel diseases (IBD), pro-inflammatory cytokines may activate YAP in various cells, in particular the resident FLS in RA. Furthermore, inflammation is often linked with fibrosis development and tissue stiffening *(19)*. Consequently, inflammation or synovial stiffening could also act in RA through YAP/TAZ activation.

Recently, involvement of YAP was reported in RA with alterations of the Hippo pathway, responsible for YAP inhibition *(20)*. YAP inhibition with verteporfin (VP), a chemical inhibitor of the binding of YAP/TAZ to TEAD *(21)*, decreased RA FLS invasion, MMP13 expression, and inflammation improving arthritis in a mouse model *(20)*. However, no clear mechanism of this anti-inflammatory effect was reported *(20)*. In addition to involvement of YAP in resident cells, TAZ was a key regulator of the balance between IL-17 producing CD4+ T helper lymphocyte (Th17) and T regulatory lymphocyte (Tregs) through stimulating retinoic acid receptor-related orphan receptor-

γ (RORγT) transcription in favour of increasing Th17 differentiation *(22)*. Indeed, Th17 are the main source of IL-17, a pro-inflammatory cytokine and is strongly involved in RA pathogenesis *(23)*. In addition to a direct effect of YAP/TAZ inhibition on FLS, we hypothesized that a systemic YAP/TAZ inhibition could also decrease Th17 cells and inflammation.

In this paper, we demonstrated for the first time a strong YAP transcriptional activation during arthritis with involvement of inflammation for its activation in FLS, contributing to aggressive cell phenotype and, consequently synovial hyperplasia. Then we also demonstrated that the synovial membrane became stiffer during arthritis by using atomic force microscopy (AFM), and that YAP/TAZ inhibition reduced this stiffening. Finally, YAP/TAZ inhibition with VP decreased arthritis severity as well as colitis through similar mechanisms, suggesting YAP/TAZ as a promising target in inflammatory disorders.

RESULTS

YAP was active in RA FLS and its activation was enhanced by pro-inflammatory cytokines independently from mechanical cues

In human RA FLS, YAP was localized in the nucleus when cultivated on classic substrate (stiff, approximately 2 GPa) due to its sensitivity to stiff substrate *(11)*. Accordingly, we cultivated RA FLS on soft substrate (2 kPa), closer to physiological condition. On soft substrate, the percentage of cells with YAP nuclear localization was nevertheless around 30% (Fig. 1AB), suggesting autonomous activation in RA FLS, even in the absence of known activators for YAP. Then the effect of two keys pro-inflammatory cytokines involved in RA (TNF and IL-17) on YAP nuclear localization was assessed independently of stiff support activation. Accordingly, RA FLS on soft substrate were treated with TNF and IL-17 for 48 hours. TNF or IL-17 alone increased the percentage of cells with YAP nuclear localization with a synergistic effect when administered together (Fig. 1AB). These results were completed with a trend toward increased expression of a YAP target gene, cysteine-rich angiogenic protein 61 (CYR61), at the protein level with TNF and IL-17 treatment (Fig. 1CD); while this was not the case at the mRNA level at this time point (Fig. 1E). This YAP activation depended on YAP nuclear translocation rather than a YAP global increase since the total YAP protein level trended to decrease with TNF and IL-17 treatment (Fig. 1F). Of note, the YAP/TAZ ratio at the protein level was increased with TNF and IL-17 (Fig. 1G) due to the reduction of total TAZ amount (Supplementary Fig. 1A). VP treatment strongly decreased CYR61 expression at the protein (Fig. 1CD) and mRNA levels (Fig. 1E), highlighting the transcriptional blockage of YAP/TAZ even with TNF and IL-17 stimulation. A similar pattern was observed for connective tissue growth factor (CTGF) and hexokinase 2 (HK2), two other YAP target genes (Supplementary Fig. 1BC); while

no differences in expression of another YAP target gene, ankyrin repeat domain-containing protein 1 (Ankrd1), was observed (Supplementary Fig 1D). As expected, VP did not reduce YAP nuclear localization (Fig. 1B), since we observed that VP blocked YAP transcriptional activity. VP also trended to decrease YAP and TAZ total protein levels, with a significant reduction when co-administered with TNF and IL-17 (Fig. 1C, F; Supplementary Fig. 1A). Despite clear YAP nuclear labelling in our experiments, no nuclear TAZ labelling was observed (data not shown). Thus, YAP nuclear localization was induced by TNF and IL-17 *in vitro*, independently of mechanical cues. VP blocked YAP transcriptional activity even in the presence of TNF and IL-17 without changes in YAP nuclear localization.

YAP nuclear localization *in vitro* was increased by time spent in rigid environment

Mesenchymal stem cells can be mechanically primed, as the time spent on stiff substrate increased YAP nuclear localization, and maintained its nuclear localization even after a shift to soft substrate *(24)*. Since YAP nuclear localization was around 30% in FLS on soft substrate in the absence of mechanical or inflammation cues (Fig. 1AB), we hypothesized that this could reflect prior FLS mechanical priming. To investigate this purpose, we assessed the percentage of cells with YAP nuclear localization cultivated on stiff substrate (classic culture substrate 2 GPa) up to passage (P) 3, P4, or P5, followed by a switch to soft substrate for 72 hours after each of these passages (P4, P5 or P6, respectively; Supplementary Fig. 2A). YAP nuclear localization was higher at P5 than P4 (Supplementary Fig. 2BC). Furthermore, Ankrd1 expression was increased at P6 compared to P5 (Supplementary Fig. 2D). Hence time spent by RA FLS on stiff substrate enhanced YAP activity when assessed on a soft substrate, confirming the influence of mechanical priming on YAP activity in RA FLS.

To summarize, inflammation or mechanical *stimuli* were activators of different YAP target genes. CYR61 was not increased at P6 compared to P5 (Supplementary Fig. 2E), but was increased by inflammation on soft substrate (Fig. 1D). Contrariwise, Ankrd1 was not increased by inflammation on soft substrate (Supplementary Fig. 1D), but was increased at P6 compared to P5 (Supplementary Fig. 2D). However, inflammation and mechanical *stimuli* (stiff substrate) had a synergistic effect when applied together on CYR61 and Ankrd1 expressions (Supplementary Fig. 2DE).

YAP/TAZ inhibition blocked RA FLS aggressive phenotype

Since YAP was activated in RA FLS, we explored its involvement in the RA FLS aggressive phenotype. Subsequently, we treated RA FLS with VP or YAP siRNA for 48 hours with or without TNF and IL-17 and assessed apoptosis, invasion, and proliferation.

YAP/TAZ inhibition restored apoptosis

No cell mortality was observed with VP treatment for 48 hours at the dose used (10 µM) in our *in vitro* experiments assessed by lactate deshydrogenase (LDH) assay (data not shown), suggesting no toxic effect in our experiments. We then assessed apoptosis by detection of annexin V positive cells quantified by flow cytometry. As expected, annexin V was barely detected in RA FLS treated with vehicle or TNF and IL-17. However, addition of VP to TNF and IL-17 induced around 10% annexin V positive cells showing restoration of apoptosis (Fig. 2A-ab). At the mRNA level, Bcl2 was reduced by VP treatment (Fig. 2A-c) or YAP siRNA transfection (Supplementary Fig. 3E) with or without TNF and IL-17, while Bax expression was similar (data not shown). Furthermore, phospho(p)-NF-κB on serine 546 (active form) was almost undetected with VP treatment (Fig. 2A-de). With YAP siRNA transfection, a trend toward reduction of the p-NFκB/total NFκB ratio was observed, compared to siCTRL mainly in presence

of TNF and IL-17 (Supplementary Fig. 3AD). This reduction was in accordance to CYR61 expression decrease upon YAP siRNA with or without TNF and IL-17 (Supplementary Fig. 3AC). Altogether these data suggested that YAP drove RA FLS apoptosis resistance by maintaining Bcl2 expression and NF-κB activation.

YAP/TAZ inhibition reduced invasion of RA FLS and MMP-13

Since RA FLS already have a huge invasion ability, VP trended to decrease invasion ability of RA FLS in a transwell assay, even with pro-inflammatory (TNF and IL-17) *stimuli* (Fig. 2B-ab). MMP-13, which was described as an essential molecule for FLS invasion ability *(25)*, was trended to decrease at the protein level by VP treatment and was barely detectable when TNF and IL-17 were co-administered with VP (Fig. 2B-cd). These results showed the importance of YAP for MMP-13 synthesis during arthritis, probably contributing to RA FLS invasion ability.

YAP/TAZ inhibition decreased proliferation ability in RA FLS

Another key feature of RA FLS is their excessive proliferation. The number of Ki-67 (present only in proliferating cells) positive RA FLS was decreased after 48 hours of VP treatment in immunofluorescence (Fig. 2C-ab) or flow cytometry (data not shown) in the presence of TNF and IL-17. Furthermore, the inhibition of p-NF-κB by VP could also contribute to decrease RA FLS proliferation (Fig. 2A-de).

Altogether, YAP transcriptional effects could drive RA FLS to an aggressive phenotype by contributing to their three main features.

YAP/TAZ inhibition by VP prevented and reversed synovial hyperplasia in an organoid model of synovial lining layer

Since YAP drove FLS to an aggressive phenotype *in vitro*, we hypothesized that YAP inhibition could prevent and reverse synovial hyperplasia independently of a pro-inflammatory environment. To assess this hypothesis, an *in vitro* organoid model of

synovial lining layer was performed, inspired from a previous report *(26)*. This *in vitro* model recapitulated features of the synovial membrane *in vivo*. In this model, RA FLS formed a thicker lining layer than that constituted with osteoarthritis FLS after 21 days of culture (data not shown), confirming RA FLS ability of hyperplasia formation. Since RA FLS organoids were already hyperplasic without any stimuli, TNF and IL-17 treatment induced a heterogenous effect on hyperplasia formation with some areas showing a strong hyperplasia formation compared to vehicle alone (Fig. 3AB). VP treatment started from the beginning of organoid formation completely blocked this hyperplasia formation, even in presence of TNF and IL-17 (Fig. 3AB). In addition, VP treatment started at day 14 (time where synovial hyperplasia was already observed) inhibited also the hyperplasia formation suggesting its potential effect to reverse synovial hyperplasia like a curative approach (Fig. 3AB). To explore signaling pathways involved in the hyperplasia formation observed with RA FLS, we investigated c-Jun subcellular localization. Nuclear localization of c-Jun in FLS was higher at the "lining layer" site compared to the "stroma" site. This suggested different activations according to FLS localization inside the organoid. Additionally, VP treatment suppressed this difference suggesting a YAP/TAZ role on c-Jun activity (Fig. 3 CD).

YAP was active in the rat adjuvant-induced arthritis (AIA) model and VP prevented or decreased arthritis severity

YAP mRNA was increased in the ankle of a rat AIA model at days 6 and 8 after the induction, before the arthritis onset (Supplementary Fig. 4). This was followed by an increase in its target genes including Ankrd1, CYR61, CTGF, E2F1, and HK2 (Supplementary Fig. 4) at days 10 and 12, the time of arthritis onset (Fig. 4A). These results demonstrated a YAP transcriptional activation during arthritis in this model, reinforcing the assumption to target YAP in this model.

Then in order to assess involvement of YAP in arthritis onset and severity, we administered VP in AIA rats with two approaches: preventive and curative. In the preventive approach, intraperitoneal injection (IP) of VP at 20 mg/kg/day from days 6 to 16 (starting before arthritis onset) showed a delay in arthritis onset, with a lower arthritis severity (arthritic score and ankle circumference) compared to AIA vehicle rats (Fig. 4AB). The curative approach with IP 40 mg/kg/day of VP from days 12 to 16 (starting after arthritis onset) completely blocked arthritis progression and reduced arthritis severity (Fig. 4AB). After sacrifice (day 17), the reduction of arthritis severity was directly linked with a reduction of synovial hyperplasia observed in both VP groups (Fig. 4CD) confirming the direct effect on FLS previously observed *in vivo*. At the bone level, a decrease in bone volume per tissue volume (BV/TV) in AIA rats corresponding to bone erosion was observed at the distal tibia zone linked with FLS invasion (Fig. 4E). Strikingly, the preventive VP approach prevented this bone erosion in this area with a BV/TV close to the vehicle (non-arthritic) group; whereas the curative VP approach did not reduce the erosion. Thus, VP was able to prevent, but not to restore bone damage (Fig. 4EF). This bone protection in the preventive VP approach was associated with a lower expression of MMP2 compared to the AIA group (Fig. 4G). We also demonstrated a direct action of VP on CYR61 expression in both approaches compared to AIA vehicle rats (Fig. 4H), supporting a VP effect on YAP transcriptional activity. However, other genes affected by YAP were not modified by VP therapies in the joint at day 17 (data not shown), since they were not overexpressed at this time point in the rat AIA model (Supplementary Fig. 4).

VP decreased mRNA expression markers of lymphocyte Th17 in rat AIA model

Then we hypothesized that VP treatment, in addition to its effect on FLS, may also have anti-inflammatory properties by reducing Th17. RORγT labelling was highly

detected in the marginal zone of spleen from AIA rat compared to vehicle group. Both VP approaches strongly reduced this RORγT labelling (Supplementary Fig. 5A). IL17 mRNA level was reduced in the preventive VP group, while a trend in decrease was observed in the curative VP group (Supplementary Fig. 5B). At the ankle site, IL-17 mRNA was reduced only in the preventive VP group compared to AIA group (Supplementary Fig. 5C). Regarding other inflammatory actors, no differences in IL10 expression (Supplementary Fig. 5D) or Foxp3 (Treg marker) labelling (data not shown) were observed in the spleen, suggesting that VP had no effect on Tregs. In addition, TNF expression was lower in spleen of VP treated animals compared to AIA rats, with no change at the ankle (Supplementary Fig. 5EF). IL6 expression was unchanged with VP approaches at both ankle and spleen sites (Supplementary Fig. 5GH). In addition to the direct effect of VP on RA FLS, VP also had a direct anti-inflammatory effect mainly through Th17 inhibition in the rat AIA model.

Synovial tissue became stiffer during arthritis under YAP/TAZ control

Since YAP was activated in RA FLS on stiff substrate and that chronic inflammation was reported to be linked with stiffening processes *(19)*, the stiffness of the synovial membrane was assessed during arthritis in our rat AIA model. Accordingly, Young's modulus, also known as the sample stiffness, was measured using nanoindentation by AFM in the four groups of the rodent experiment (Fig. 5A-D). First, synovial stiffness was increased in AIA rats compared to the vehicle (non-arthritic) group, showing for the first time that synovial tissue became stiffer during arthritis (Fig. 5A, C and E). Furthermore, both preventive and curative VP approaches strongly reduced synovial membrane stiffness compared to AIA untreated rats, whose synovial stiffness was close to that of vehicle (non-arthritic) rats (Fig. 5 A-E). These results strongly suggested that YAP activation induced synovial stiffening in arthritis. Moreover, tenascin C (tenC)

and periostin, two molecules involved in stiffening processes *(19)*, were overexpressed before arthritis onset between days 6 and 12 for tenC and after arthritis onset for periostin. It is thus possible that stiffening of the synovial membrane had already begun when curative VP treatment started, highlighting a possible reverse effect on synovial stiffness. TenC (Fig. 5F) and periostin (not shown) were strongly labelled in the extracellular matrix (ECM) of the synovial sublining layer of AIA rats and almost absent in vehicle or VP groups. TenC and periostin mRNA levels decreased significantly in the preventive VP group and to a lower extent in the curative VP group compared to rat AIA group (Fig. 5G, H). *In vitro*, VP was also effective in blocking tenC and periostin expressions in RA FLS with or without TNF and IL-17 stimulation (Fig. 5I, J). Notably, at the cellular level, we observed the presence of actin stress fibers in FLS from AIA rats (Fig. 5F) and in RA FLS in organoids (Fig. 3C), which are representative of mechanical stiffening in cells *(27)*. Furthermore, these actin stress fibers were absent with VP treatment in both models (Fig. 3C and Fig. 5F). All together, we demonstrated that synovial tissue stiffening occurred during arthritis, potentially through tenC and periostin synthesis and cytoskeletal reorganization in FLS.

YAP/TAZ inhibition with VP in the dextran sulfate sodium induced colitis mice model also prevented the disease by the same mechanisms observed in arthritis

To extend our findings on YAP/TAZ regulation in arthritis to other inflammatory diseases, we focused on another inflammatory model where resident and immunity cells are involved. YAP/TAZ activation has already been described in IBD *(18)*, with a decreased severity by VP in a mouse colitis model *(28)*. In this context, we evaluated the effect of VP in another colitis model, the dextran sulfate sodium (DSS) induced colitis mouse model. The colitis severity was reduced mostly through a drastic decrease in diarrhea, a common symptom of intestinal inflammation (Fig. 6A).

Histologically, intestinal villi appeared less damaged in the VP group associated with a reduction in the Peyer's patches area compared to control (Fig. 6BC and E). As previously shown for FLS or synovial tissue, VP also trended to downregulate CYR61 expression at the gut level, confirming again YAP/TAZ transcriptional inhibition in this colitis model (Fig. 6D). Similarly to our results in the rat AIA model, an inhibition of TNF expression without changes in IL-6 expression was observed in the VP group compared to the control group (Fig. 6FG). However, no difference in IL-17 expression was observed in the gut (Fig. 6H). MMP2 expression was also reduced under VP treatment, while only a trend toward reduction for MMP13 was observed (Fig. 6IJ).

DISCUSSION

In this study, we clearly demonstrated that YAP/TAZ transcriptional activity was involved in inflammatory disorder pathogenesis, especially RA. In RA, YAP/TAZ transcriptional activity inhibition suppressed RA FLS aggressive phenotype with a decrease in synovial stiffness in the rat AIA model and Th17 inhibition. Some of these effects were also reproduced in colitis, another inflammatory disease. Accordingly, YAP/TAZ could be a key target in inflammatory related diseases.

Hippo pathway alterations were already described in RA, such as YAP inhibition in RA FLS reduced their invasion abilities by inhibiting MMP13 expression and VP treatment in an arthritic mouse model and improved the disease *(20)*. Here, we confirmed these previous data on YAP involvement in RA FLS invasion abilities and we provided deep evidence on YAP/TAZ involvement in RA pathophysiology. First of all, we demonstrated that YAP was active in RA FLS and in the ankle of AIA rats. Hence, YAP activation drove the aggressive phenotype of FLS by enhancing apoptosis resistance, invasion, and proliferation. However, specific mechanisms underlying these actions open the way for new investigations. Considering the action of VP and the timing of YAP inhibition (48 hours for siRNA or VP inhibition in RA FLS), we were looking at transcriptional effects, YAP acting mainly through TEAD interaction *(16)* (VP targeted) *(21)*. These effects may be directly connected with our data on CYR61, a YAP target gene. CYR61 has already been extensively considered during arthritis and is critical for the pathophysiology of RA, such as proliferation control *(29)*, invasion/migration abilities of FLS connected with bone erosion *(30, 31)*, and inflammatory responses *(32*, *33)*. Our data emphasized involvement of CYR61 in RA pathogenesis since we observed its strong decrease by YAP inhibition in RA FLS and in AIA rat ankles. As for apoptosis resistance ability, YAP inhibition drastically decreased the mRNA level of

Bcl2, deciphering partially a mechanism of apoptosis resistance driven by YAP. Furthermore, new evidence highlights YAP to act on transcriptional programs by concomitant action with other transcription factors *(34*, *35)*. Interestingly, YAP can indirectly interact with AP-1 via TEAD; AP-1 and YAP-TEAD interact and bind to the same gene binding zones and activate very specific transcription programs (migration/invasion, oncogenic growth). This could explain in our results the alteration of c-Jun nuclear localization repartition in organoids. Inhibiting YAP-TEAD interaction also blocks some of the AP-1 transcriptional activity *(34*, *35)*. In RA, AP-1 was already proposed as a therapeutic target *(7)*, emphasizing the relevance of YAP inhibition for AP-1 regulation in this context. In this perspective, we have hypothesized that the difference observed in terms of gene regulation (CYR61 or Ankrd1) by YAP upon mechanical or inflammatory stimuli may be due to different YAP-TEAD partners recruited; thus, regulating specific transcription programs. However, when these *stimuli* are applied together, a synergistic effect on both CYR61 and Ankrd1 expression was observed and which may indicate a broader transcriptional regulation. Furthermore, VP inhibition completely blunted the serine 546 active phosphorylated form of NF-κB, which is also involved in RA pathogenesis *(8)*. Thus, YAP may control several transcription factors involved in apoptosis and proliferation, although the intracellular pathways underlying these regulations are still to be determined.

YAP has been extensively reported to be an oncogene through its TEAD mediated transcriptional activity through interaction with its TEAD binding motif *(16)*. However, other YAP functions are related to other domains. In fact, YAP has been described has a tumour suppressor by promoting apoptosis through p73 interaction through its WW domain *(36)* and through its role in scaffolding β-catenin in the cytoplasm *(37)*, independently of the YAP/TEAD interaction, so not related to the VP effect. In this

context, a siRNA or a total YAP knockdown may be effective through positive inhibition of YAP-TEAD transcriptional effects but also negative by suppressing its effect through WW domain interactions. In accordance to this statement, we observed that YAP siRNA treatment on RA FLS enhanced the activity of a nonphospho (active) form of β-catenin, suggesting that this YAP cytoplasmic activity is also present in RA FLS (data not shown).

Thus, VP treatment appears as a good candidate for YAP/TAZ inhibition. However, some other VP properties could be involved in our results. VP is a photosensitizer originally used for choroidal neovascularization in age-related macular degeneration *(38)*. Under infrared wavelength exposure, VP releases a singlet of highly reactive oxygen that presents toxicity for cells. In order to avoid this effect, all our experiments were performed in relative darkness under blue light. However, even in absence of infrared light, VP has been shown to release low levels of oxidative compounds *(39)*. Nevertheless, with our experimental settings, and at least in RA FLS experiments, we did not detect cell toxicity by VP treatment using LDH assay. The crucial role of YAP in the cytoplasm, the low rate of silencing efficacy by YAP siRNA, and a possible compensation by TAZ when YAP is absent (that has been previously reported in other context *(18)*) may explain the lower efficiency of YAP siRNA strategy as compared to VP treatment. To strengthen our strategy, specific peptide inhibitors of YAP/TAZ-TEAD or chimeric YAP/TAZ construct protein interfering only with its TEAD mediated transcriptional activity may be used.

In a model of human cornea, chronic inflammation activated YAP which resulted in tissue stiffening *(19)*. We showed for the first time by nanoindentation using AFM an increase in synovial stiffening during arthritis in the rat AIA model. YAP/TAZ inhibition by VP blocks this stiffening as well as specific stiff ECM component expression and

actin stress fiber formation. Accordingly, tissue stiffening may occur through YAP/TAZ signalling. Such tissue stiffening in RA brings new exciting perspectives. FLS are described to be “passive responders” and “imprinted aggressors” *(2)*, emphasizing the ability of RA FLS to keep their aggressive phenotype even when inflammation has been stopped. An explanation for this behaviour has been searched in epigenetics and mutation of genes without finding complete explanations *(2)*. We showed here that RA FLS can be mechanically primed with long term passages on stiff substrate, programming YAP to remain nuclear even after switching to soft substrate. Furthermore, evidence of Hippo pathway methylome dysregulation was already reported in RA *(20)*. This may enhance YAP nuclear localization and explain how YAP may remain active on soft substrate in our context; thus methylome changes may be induced by mechanical priming. Long term YAP activation in RA FLS by pro-inflammatory cytokines and a remodelling of the ECM providing a stiff environment may give them autonomous properties by mechanical priming, keeping their pathogenic features even in the absence of YAP known activation *stimuli*. We thus speculate that mechanical priming constitutes a mechanism by which RA FLS became autonomous even after inflammation stoppage. This new mechanism offers a new area to investigate in the context of arthritis.

Another advantage of targeting YAP/TAZ in RA is for its immunomodulation effect. Indeed, in AIA rats we showed that VP also has anti-inflammatory properties by decreasing IL-17 expression likely through Th17 targeting in the spleen. This action may occur through TAZ inhibition in T cells as previously described *(22)*. T cells are also described to be activated by a stiff microenvironment *(40)*; thus, possibly suggesting that tissue stiffening decreases with VP treatment in arthritis and may also act to inhibit T cell activation. We also showed a TNF inhibition in spleen. This also

may be explained by Th17 inhibition because Th17 cells are able to produce TNF, although in a lesser extent than IL-17 *(41)*. Nevertheless, the absence of changes in IL-6 expression, of which Th17 cells are one of the sources *(41)*, suggested that TNF regulation by YAP/TAZ inhibition may come from other mechanisms. These mechanisms may come from macrophage regulation by YAP as already reported *(42)* or another unknown mechanism. Comparing this effect to the strong effect of VP on FLS, we hypothesize that the main VP effect is on FLS targeting.

Finally, YAP/TAZ have been shown to be active in other inflammatory diseases such as in IBD *(18*, *22*, *28*, *42*, *43)*, psoriasis *(44)*, scleroderma *(45)*, asthma *(46)*, and Sjogren's syndrome *(47)*. Focusing on a colitis context, YAP has been described to enhance aberrant enterocyte differentiation and proliferation driving hyperplasia in intestinal villi *(18)*. Moreover, TAZ inhibition through inhibition of Th17 differentiation decreased colitis severity *(22)*. In our study, YAP/TAZ inhibition with VP in a mouse colitis model (DSS treated mice) improved the symptoms by mechanisms similar to those for arthritis treatment, with inflammation modulation and decreased expression of markers involved in the inflammatory response by enterocytes. Fibrosis can occur in IBD *(48)*, and even if we do not provide evidence on possible tissue stiffening under YAP/TAZ control in this model, it may be a further line of investigation.

In summary, we propose that the presence of pro-inflammatory cytokines such as TNF and IL-17 in RA are responsible for YAP activation in FLS, thus participating in the pathophysiology of the disease. This activation drives a FLS aggressive phenotype and controls changes in the microenvironment. Consequences include altered mechanical properties of the tissue that become stiffer, creating a vicious circle in which YAP/TAZ activity is maintained even after inflammation stoppage. Such a mechanism probably exists in other inflammatory contexts with a key involvement of

resident cells. Our data give new insight into YAP/TAZ biology in the context of inflammation and suggest that YAP/TAZ play a central role in inflammatory pathologies and could be targeted with VP to improve these inflammatory diseases.

METHODS

Cell culture. RA FLS were obtained during surgery procedure as previously described *(49)*. All RA patients gave a written consent after oral information (IRB # 2014-A01688-39). Cells were cultivated in Dulbecco's modified Eagle's medium (DMEM, Sigma, St. Louis, MO, US) with 10% fetal bovine serum (FBS), 1% glutamine and 2% penicillin and streptomycin (PS) on classic support substrate until their use for experiments (2 GPa). For soft substrate culture (2 kPa), well plates (Cell guidance system, Cambridge, UK) or dishes (ExCellness, Lausanne, Switzerland) were used. Plates were coated with fibronectin (1:100, Sigma) for 2 hours at 37°C. TNF at 10 ng/ml and IL-17 at 50 ng/ml (R&D system, Minneapolis, MN, US) were used. Verteporfin (VP, Sigma) was used at 10 µM. For all VP experiments, cells were kept in relative darkness with blue light during manutention avoiding any aspecific activation of VP (due to its photosensitivity).

Western blot. Protein extraction was performed with Allprep RNA/protein kit (Qiagen Inc, Hilden, Germany). Proteins (5 µg) were denatured and separated for 2 hours at 90 Volts before being transferred onto PVDF membranes (Thermo Fisher Scientific). The membrane was blocked and incubated with primary antibody overnight at 4°C.Then membrane was incubated with a horseradish peroxidase-conjugated secondary antibody (1:5000; Thermo Fisher Scientific, 31460) for 1 hour at RT. Immunoreactive protein bands were visualized with Clarity™ Western ECL Substrate (BioRad, Hercules, CA, US). Blots were stripped using a mild antibody stripping solution (200 mM glycine, 3.5 mM SDS, 1% Tween 20) and reprobed. Western blot (WB) was performed using the following primary antibodies (1:1000): YAP/TAZ (8418, Cell Signaling Technology, Leiden, The Netherlands), CYR61 (14479, Cell Signaling Technology) MMP-13 (ab39012, Abcam, Cambridge, UK), NF-κB p65 (8242, Cell

Signaling Technology) and phospho NF-κB p65 ser536 (3031, Cell Signaling Technology).

Flow cytometry. FLS grown on soft dishes at 2 kPa (ExCellness) for 72 hours coated with fibronectin with various *stimuli* for 48 hours were collected by trypsination. RA FLS were incubated in 1X annexin V binding buffer with Annexin V-PE detection kit (ab14155, Abcam). Data were acquired using a FACSCanto II cytometer and analyzed with the BD FACS Diva software 6.1.3 (BD Nova Biosciences, UK).

Invasion assay. RA FLS invasion abilities were assessed using BioCoat™ Growth Factor reduced Matrigel Invasion Chamber (Corning, Corning, NY, US). FLS were seeded in the upper chamber at 50,000 cells per insert in DMEM containing 1% glutamine, 1% PS and 0.1% BSA. DMEM containing 20% FBS, 1% glutamine, 1% PS and 0.1% BSA was added to the wells. The invasion chambers were then incubated for 48 h with or without TNF, IL-17, and VP (which were added in the insert chamber and in the wells at the same concentrations). After incubation, noninvading cells were removed from the upper surface of the membrane, inserts were fixed in 4% PFA for 20 minutes at RT, and then stained with hematoxylin and eosin (H&E). Membranes of insert were imaged at x100 magnification and invading cells were counted. Results are represented by the mean of two inserts for each condition, and the mean of three images at x100 counting per insert.

siRNA transfection technique. RA FLS were cultivated on classic substrate coated with fibronectin, in classic medium antibiotic free for 24 hours and transfected at 80% confluency. RA FLS were transfected by adding YAP siRNA or control siRNA (Santa Cruz Biotechnology, Dallas, TX, US) at 7.5 µg/ml in siRNA transfection reagent (Santa Cruz Biotechnology; diluted 6/100 in transfection medium) for 6 hours at 37°C in a CO_2

incubator. Medium was replaced with or without TNF and IL-17 for 48 hours before extraction.

Organoids culture and processing. Synovial organoids assembly protocol was inspired by previous publication*(26)*. Briefly, cells from RA patients were used at passage (P6) and mixed with Matrigel (Corning) at 4.10^6 cells/ml of Matrigel, 22 µl droplets (representing approximatively 88,000 cells) were added to 96-well U-shaped very low attachment surface plates (Corning). Gelation was then allowed for 45 minutes at 37°C in a CO_2 incubator. Then specific medium was added: DMEM supplemented with 10% FBS, 1% glutamine, ITS solution, nonessential amino acids, 1% PS, and ascorbic acid. Organoids were maintained for 21 days in culture media. VP with or without TNF and IL-17 were used at the same concentration as for cell culture. At day 21, organoids were fixed with glyoxal/ethanol solution for 1 hour at RT (PFA fixation being deleterious). Organoids were then embedded in paraffin, cut at 6µm and stained with H&E. Other organoids were embedded in a gelatin-sucrose solution and frozen in an isopentane bath at -50°C for 2 minutes before storage at -80°C. 30µm thick cryosections were then used for immunofluorescence.

Animals

Adjuvant induced arthritis (AIA) rat. The arthritis (rat AIA n=21) was induced by 1.5mg of *Mycobacterium butyricum* (Difco Laboratories, Detroit, MI, US) injection in 6-weeks old Lewis female rats (Charles River Laboratories, L'arbresle, France) as previously described *(49)*. Control (non-AIA n=7) rats received only injection without *Mycobacterium butyricum*. In the preventive group, daily intraperitoneal (IP) injections of VP (Tocris biosciences, Bristol, UK) at 20 mg/kg/days started at day 6 (before arthritis onset); whereas in the curative VP treatment group, daily IP injections of VP at 40 mg/kg/days started at day 12 (after arthritis onset). For all groups, IP injections

started at day 6 (with or without VP) and were performed with 600 µL of vehicle containing 10% DMSO. All rats were followed as previously described *(49)*. Rats were killed at day 17, ankle and spleen were stored at -80°C for further analysis. At necropsy, the right ankle was frozen and stored for mRNA analysis. A synovial biopsy was performed on the left ankle, then the fragment of synovial membrane was fixed in 4% PFA for 20 minutes and stored in 10% ethanol solution at 4°C before atomic for microscopy (AFM) measurements. After synovial fragment collection, left ankles were fixed with 4% PFA solution for 48 hours at 4°C. Microcomputed tomography analysis was conducted prior to decalcification in 0.5 M EDTA. Spleens were sectioned into two pieces, one for mRNA analysis and the second was fixed in 4% PFA. Spleens and decalcified ankles were next cryoprotected, then embedded and frozen at -80°C. Sections were performed using Microm HM 560 cryostat (Thermo Fisher Scientific).

AIA rats for mRNA kinetics. For rat mRNA kinetics analysis, samples from our previous work were used *(49)*, where arthritis was induced by the same protocol and rats killed at different time points (at day 6, 8, 10, 12, 17, and 24) with five control animals for each time point.

Dextran sulfate sodium (DSS) induced colitis mice. Eight-weeks old female Balb/cByJ mice (Charles River Laboratories) were treated with an IP injection of VP at 40 mg/kg/day (100 µL, in 10% DMSO) or 10% DMSO one day prior to the beginning of DSS (MP Biomedicals) treatment. The latter was administered at 1.5% in drinking water, fresh solutions were prepared and changed every day for 11 days (n=14). Control mice received only drinking water and an injection of 10% DMSO (n=7). For all groups, daily IP injections were continued during DSS treatment until mice were sacrificed at day 11. Disease activity index (DAI) scoring comprised of several scales evaluating physiological and behavioral parameters including percentage of weight

loss, stool consistency, evidences of intestinal leakage with the presence of blood in stool, animal general aspect and animal pain behavior. Scoring and weighing were performed each day. After death, intestinal tracts of mice were dissected and cut into pieces with each containing a Peyer's patch. Two pieces were snap frozen for further mRNA analysis and two other pieces were placed in 4% PFA at 4°C for 48 hours, embedded and frozen in the same process than AIA rats ankles.

Immunofluorescence. This technique was done on frozen sections (organoids, spleen and ankle of rats, and mice gut) or on RA FLS fixed with 4% PFA at RT for 20 minutes. For RORγT (Biorbyt, San Francisco, CA, US) labelling on spleen and gut, citrate antigen retrieval was performed. Before labelling, sections or cells were rehydrated, permeabilized in 0.3% Triton X-100, blocked in 1% BSA, 5% goat serum and 0.1% Triton solution for 60 minutes at RT, and probed with the primary antibody diluted in the blocking solution overnight at 4°C. The following primary antibodies were used: YAP (63.7 sc-101199, Santa Cruz Biotechnology; 1:100), YAP (D8H1X, Cell Signaling Technology; 1:100), Ki67 (NB-110-89717, Novus Biologicals, Abingdon, UK; 1:100), c-Jun (9165, Cell Signaling Technology, 1:200), and tenascin C (ab215369, Abcam, 1:100). After washing, sections or cells were incubated with secondary antibodies, goat anti-rabbit rhodamine coupled antibody (31686, Thermo Fisher; 1:300) and/or goat anti-mouse 488 (A11034, Thermo Fisher) for 75 minutes at RT, all diluted at 1:400. Slides or cells were counterstained with DAPI alone (10 minutes at 37°C) or coupled with rhodamine (R415, Thermo Fisher; or ab176753, Abcam) for 1 hour at 37°C.Isotypic controls were always performed using rabbit IgG isotype control (31235, Thermo Fisher) and mouse IgG isotype control (31903, Thermo Fisher), diluted at the same concentration as the primary antibody.

Image acquisition. Images were acquired using a confocal laser microscope (LSM) 800 airyscan (Zeiss, Oberkochen, Germany) equipped with Zen software. This microscope was used in epifluorescence, classic confocal or airyscan confocal mode depending on the needs.

Image analysis and quantification

***Immunofluorescence images quantification*.** Ki-67 and YAP labelling on RA FLS were evaluated by automatically defining nuclear region of interest (ROI) area based on DAPI staining, ROI nuclear mask was then added on YAP and Ki67 images. Positive cells for YAP or Ki67 labeling in the nucleus were then counted and divided by the total number of nuclei (DAPI). This quantification was performed on large acquisition tiles at x100 magnification, representing approximately 50 to 200 cells per well. C-Jun labelling on frozen sections of organoid was quantified by measuring mean intensity in DAPI ROI in the synovial lining layer divided by the same measurement in the stroma.

Organoid synovial hyperplasia. This quantification was performed on H&E paraffin sections. Each organoid assessment was the result of two organoid slices. Images were binarized and a synovial lining layer area was automatically selected. Organoid perimeters were also measured. Hyperplasia criteria was the result of synovial lining layer area divided by synovial organoid perimeter.

Peyer's patches area. This quantification was performed on H&E frozen intestinal sections. Area of Peyer's patches was evaluated by manual ROI drawing based on histology. For each mouse, result was the mean of two distinct Peyer's patches (one from the beginning and one from the end of the intestinal tract).

Comparison between groups for image analysis and quantification were performed using the exact same settings from antibodies labelling to image processing.

RNA extraction and RT-qPCR. For animal tissues (spleen, gut and ankle) lysis was performed in TRI Reagent (Sigma). RNA was purified with RNeasy plus (Qiagen Inc.). For cell culture, RNA was extracted using Allprep RNA/protein kit (Qiagen Inc.). Quality and quantity of RNA were assessed by Experion RNA analysis (BioRad) and QuantIT RiboGreen RNA assay (Thermo Fisher Scientifc), respectively. Complementary DNA (cDNA) was synthesized using the iscript cDNA synthesis kit (Biorad). Quantitative RT polymerase chain reaction (PCR) was conducted on CFX96 RealTime System (BioRad) with LightCycler FastStart DNA Master plus SYBRgreen I (Roche Diagnostics, Basel, Switzerland). The results were normalized to the housekeeping gene expression hypoxanthine-guanine phosphoribosyltransferase (HPRT).

AFM measurement. AFM measurements were performed using standard force mode on a Veeco Multimode AFM equipped with Nanoscope IIIa controller and Picoforce extension. Briefly, we glued a 50-µm polystyrene microsphere (Alpha Nanotech, Morrisville, NC, US) on a 0.1 N/m rigidity cantilever (Bruker MLCT-Bio, E triangular) and this cantilever was used for all measurements. Rat synovial samples were dissected under binocular microscope from the same area. A nano-indentation was performed in force mode by recording two force curves on three independent areas twice for each sample. The acquired force curves were exported in ASCII format with nanoscope V614r1 software, and then the data were processed using a proper Matlab® code. The code includes the fitting of the contact area from the force curves with a Hertz contact model in order to extract Young's elastic modulus (rigidity in kPa) *(50)*.

Microcomputed tomography. Rat AIA ankles were scanned *ex vivo* with vivaCT40 (Scanco, Brüttisellen, Switzerland) at 55 kVp (peak kilovoltage) and reconstructed under a resolution of 12.5 µm. Quantification and 3-D imaging were performed after

reconstruction. Reconstruction was performed under 0.5/2/307 (Gauss sigma/Gauss support/lower threshold).

Statistical analysis. Data are represented as single values, with mean and standard deviation or median and interquartile range, accordingly to normality. Some parameters are expressed as percentage of the mean of control values. Two comparisons were done with Mann-Whitney test or unpaired Student t-test. Multiple comparisons were performed by ANOVA or Kruskal-Wallis test, post hoc comparisons were corrected with the false discovery rate method of Benjamini and Hochberg (q-values). Results were considered significantly different when $p<0.05$ or $q<0.05$. All statistical analyses were performed on GraphPad Prism 8.2.0 software.

Study approval. All animal studies were performed in accordance to the European Community legislation and approved by the Ethical Committee for Animal Experiments of Saint-Etienne University, agreement number: 2019032816186046 for rat AIA model and 2019032010448893 for DSS mice.

AUTHORS CONTRIBUTIONS. RC and HM designed the study. RC performed most of the experiments and contributed to all of them. EA performed WB techniques. GC contributed to AIA rat mRNA kinetics and RA cell harvesting. CP and LN contributed to AFM experiments. EM contributed to DSS mice experiments. MT contributed to RT-qPCR experiments. HM and A.V.-B contributed to rat AIA model handling. RC, EA, EM, CP and HM analyzed the results. MTL designed the mRNA primers. MC contributed to the organoid model experiments. SP gave technical support for cell culture experiments. RC, HM, AG, LV, GC and SP wrote the paper. All authors agreed to the final version of the paper.

ACKNOWLEDGMENT. We thank the members of the Sainbiose unit for feedback and support. We thank the hematology team and Carmen Aanei at the Saint-Etienne hospital for access to flow cytometer and technical advice. We thank Stephane Avril and Jerôme Molimard from the Ecole des Mines in Saint-Etienne for their support in the AFM experiment. We thank Myriam Normand from the Sainbiose unit for providing advice on statistical analysis. We thank Remi Philippot from Saint-Etienne hospital for access to human synovial samples. This work was supported by a Novartis DREAMER grant.

REFERENCES

1. McInnes IB, Schett G. The pathogenesis of rheumatoid arthritis. *N. Engl. J. Med.* 2011;365(23):2205–2219.
2. Bottini N, Firestein GS. Duality of fibroblast-like synoviocytes in RA: passive responders and imprinted aggressors. *Nat. Rev. Rheumatol.* 2013;9(1):24–33.
3. Imamura F et al. Monoclonal expansion of synoviocytes in rheumatoid arthritis. *Arthritis Rheum.* 1998;41(11):1979–1986.
4. Hong S-S et al. PUMA gene delivery to synoviocytes reduces inflammation and degeneration of arthritic joints. *Nat. Commun.* 2017;8(1):146.
5. Bonaventura P et al. Protective effect of low dose intra-articular cadmium on inflammation and joint destruction in arthritis [Internet]. *Sci. Rep.* 2017;7(1). doi:10.1038/s41598-017-02611-5
6. Ahmed S et al. Epigallocatechin-3-gallate inhibits IL-6 synthesis and suppresses transsignaling by enhancing soluble gp130 production. *Proc. Natl. Acad. Sci.* 2008;105(38):14692–14697.
7. Han Z et al. c-Jun N-terminal kinase is required for metalloproteinase expression and joint destruction in inflammatory arthritis. *J. Clin. Invest.* 2001;108(1):73–81.
8. Ahmed S et al. Down-regulation of myeloid cell leukemia 1 by epigallocatechin-3-gallate sensitizes rheumatoid arthritis synovial fibroblasts to tumor necrosis factor alpha-induced apoptosis. *Arthritis Rheum.* 2009;60(5):1282–1293.
9. Matsumoto S, Müller-Ladner U, Gay RE, Nishioka K, Gay S. Ultrastructural demonstration of apoptosis, Fas and Bcl-2 expression of rheumatoid synovial fibroblasts. *J. Rheumatol.* 1996;23(8):1345–1352.
10. Karouzakis E, Gay RE, Gay S, Neidhart M. Epigenetic control in rheumatoid arthritis synovial fibroblasts. *Nat. Rev. Rheumatol.* 2009;5(5):266–272.

11. Dupont S et al. Role of YAP/TAZ in mechanotransduction. *Nature* 2011;474(7350):179–183.
12. Vassilev A, Kaneko KJ, Shu H, Zhao Y, DePamphilis ML. TEAD/TEF transcription factors utilize the activation domain of YAP65, a Src/Yes-associated protein localized in the cytoplasm. *Genes Dev.* 2001;15(10):1229–1241.
13. Yagi R, Chen L-F, Shigesada K, Murakami Y, Ito Y. A WW domain-containing yes-associated protein (YAP) is a novel transcriptional co-activator. *EMBO J.* 1999;18(9):2551–2562.
14. Huang J, Wu S, Barrera J, Matthews K, Pan D. The Hippo signaling pathway coordinately regulates cell proliferation and apoptosis by inactivating Yorkie, the Drosophila Homolog of YAP. *Cell* 2005;122(3):421–434.
15. Dong J et al. Elucidation of a Universal Size-Control Mechanism in Drosophila and Mammals. *Cell* 2007;130(6):1120–1133.
16. Zanconato F, Cordenonsi M, Piccolo S. YAP/TAZ at the Roots of Cancer. *Cancer Cell* 2016;29(6):783–803.
17. Gao Y et al. TNFα-YAP/p65-HK2 axis mediates breast cancer cell migration. *Oncogenesis* 2017;6(9):e383.
18. Taniguchi K et al. A gp130–Src–YAP module links inflammation to epithelial regeneration. *Nature* 2015;519(7541):57–62.
19. Nowell CS et al. Chronic inflammation imposes aberrant cell fate in regenerating epithelia through mechanotransduction. *Nat. Cell Biol.* 2016;18(2):168–180.
20. Bottini A et al. PTPN14 phosphatase and YAP promote TGFβ signalling in rheumatoid synoviocytes. *Ann. Rheum. Dis.* 2019;78(5):600–609.

21. Liu-Chittenden Y et al. Genetic and pharmacological disruption of the TEAD–YAP complex suppresses the oncogenic activity of YAP. *Genes Dev.* 2012;26(12):1300–1305.
22. Geng J et al. The transcriptional coactivator TAZ regulates reciprocal differentiation of TH17 cells and Treg cells. *Nat. Immunol.* 2017;18(7):800–812.
23. Chabaud M et al. Human interleukin-17: A T cell-derived proinflammatory cytokine produced by the rheumatoid synovium. *Arthritis Rheum.* 1999;42(5):963–970.
24. Li CX et al. MicroRNA-21 preserves the fibrotic mechanical memory of mesenchymal stem cells. *Nat. Mater.* 2017;16(3):379–389.
25. Kumkumian GK et al. Platelet-derived growth factor and IL-1 interactions in rheumatoid arthritis. Regulation of synoviocyte proliferation, prostaglandin production, and collagenase transcription. *J. Immunol. Baltim. Md 1950* 1989;143(3):833–837.
26. Kiener HP, Lee DM, Agarwal SK, Brenner MB. Cadherin-11 Induces Rheumatoid Arthritis Fibroblast-Like Synoviocytes to Form Lining Layers in Vitro. *Am. J. Pathol.* 2006;168(5):1486–1499.
27. Tavares S et al. Actin stress fiber organization promotes cell stiffening and proliferation of pre-invasive breast cancer cells. *Nat. Commun.* 2017;8(1):1–18.
28. Yu M et al. MicroRNA-590-5p Inhibits Intestinal Inflammation by Targeting YAP. *J. Crohns Colitis* 2018;12(8):993–1004.
29. Zhang Q et al. A critical role of Cyr61 in interleukin-17–dependent proliferation of fibroblast-like synoviocytes in rheumatoid arthritis. *Arthritis Rheum.* 2009;60(12):3602–3612.

30. Huang T-L et al. DDR2-CYR61-MMP1 Signaling Pathway Promotes Bone Erosion in Rheumatoid Arthritis Through Regulating Migration and Invasion of Fibroblast-Like Synoviocytes: DDR2-CYR61-MMP1 LOOP PROMOTES BONE EROSION IN RA. *J. Bone Miner. Res.* 2017;32(2):407–418.
31. Ganesan R, Rasool M. Interleukin 17 regulates SHP-2 and IL-17RA/STAT-3 dependent Cyr61, IL-23 and GM-CSF expression and RANKL mediated osteoclastogenesis by fibroblast-like synoviocytes in rheumatoid arthritis. *Mol. Immunol.* 2017;91:134–144.
32. Lin J et al. Cyr61 Induces IL-6 Production by Fibroblast-like Synoviocytes Promoting Th17 Differentiation in Rheumatoid Arthritis. *J. Immunol.* 2012;188(11):5776–5784.
33. Lin J et al. A Novel p53/microRNA-22/Cyr61 Axis in Synovial Cells Regulates Inflammation in Rheumatoid Arthritis: Novel p53/miR-22/Cyr61 Axis in Synovial Cells. *Arthritis Rheumatol.* 2014;66(1):49–59.
34. Liu X et al. Tead and AP1 coordinate transcription and motility. *Cell Rep.* 2016;14(5):1169–1180.
35. Zanconato F et al. Genome-wide association between YAP/TAZ/TEAD and AP-1 at enhancers drives oncogenic growth. *Nat. Cell Biol.* 2015;17(9):1218–1227.
36. Strano S et al. Physical Interaction with Yes-associated Protein Enhances p73 Transcriptional Activity. *J. Biol. Chem.* 2001;276(18):15164–15173.
37. Azzolin L et al. YAP/TAZ Incorporation in the β-Catenin Destruction Complex Orchestrates the Wnt Response. *Cell* 2014;158(1):157–170.
38. Michels S, Schmidt-Erfurth U. Photodynamic therapy with verteporfin: a new treatment in ophthalmology. *Semin. Ophthalmol.* 2001;16(4):201–206.

39. Donohue E, Balgi AD, Komatsu M, Roberge M. Induction of Covalently Crosslinked p62 Oligomers with Reduced Binding to Polyubiquitinated Proteins by the Autophagy Inhibitor Verteporfin. *PLOS ONE* 2014;9(12):e114964.

40. Saitakis M et al. Different TCR-induced T lymphocyte responses are potentiated by stiffness with variable sensitivity. *eLife* 2017;6:e23190.

41. Langrish CL et al. IL-23 drives a pathogenic T cell population that induces autoimmune inflammation. *J. Exp. Med.* 2005;201(2):233–240.

42. Zhou X et al. YAP Aggravates Inflammatory Bowel Disease by Regulating M1/M2 Macrophage Polarization and Gut Microbial Homeostasis. *Cell Rep.* 2019;27(4):1176-1189.e5.

43. Kim H-B et al. Prostaglandin E2Activates YAP and a Positive-Signaling Loop to Promote Colon Regeneration After Colitis but Also Carcinogenesis in Mice. *Gastroenterology* 2017;152(3):616–630.

44. Jia J et al. Yes-associated protein promotes the abnormal proliferation of psoriatic keratinocytes via an amphiregulin dependent pathway. *Sci. Rep.* 2018;8(1):14513.

45. Toyama T et al. Therapeutic Targeting of TAZ and YAP by Dimethyl Fumarate in Systemic Sclerosis Fibrosis. *J. Invest. Dermatol.* 2018;138(1):78–88.

46. Xie H, Wu L, Deng Z, Huo Y, Cheng Y. Emerging roles of YAP/TAZ in lung physiology and diseases. *Life Sci.* 2018;214:176–183.

47. Enger TB et al. The Hippo signaling pathway is required for salivary gland development and its dysregulation is associated with Sjogren's-like disease. *Lab. Investig. J. Tech. Methods Pathol.* 2013;93(11):1203–1218.

48. Latella G, Di Gregorio J, Flati V, Rieder F, Lawrance IC. Mechanisms of initiation and progression of intestinal fibrosis in IBD. *Scand. J. Gastroenterol.* 2015;50(1):53–65.

49. Courbon G et al. Early sclerostin expression explains bone formation inhibition before arthritis onset in the rat adjuvant-induced arthritis model. *Sci. Rep.* 2018;8(1):3492.

50. Lin DC, Dimitriadis EK, Horkay F. Robust strategies for automated AFM force curve analysis--I. Non-adhesive indentation of soft, inhomogeneous materials. *J. Biomech. Eng.* 2007;129(3):430–440.

FIGURES

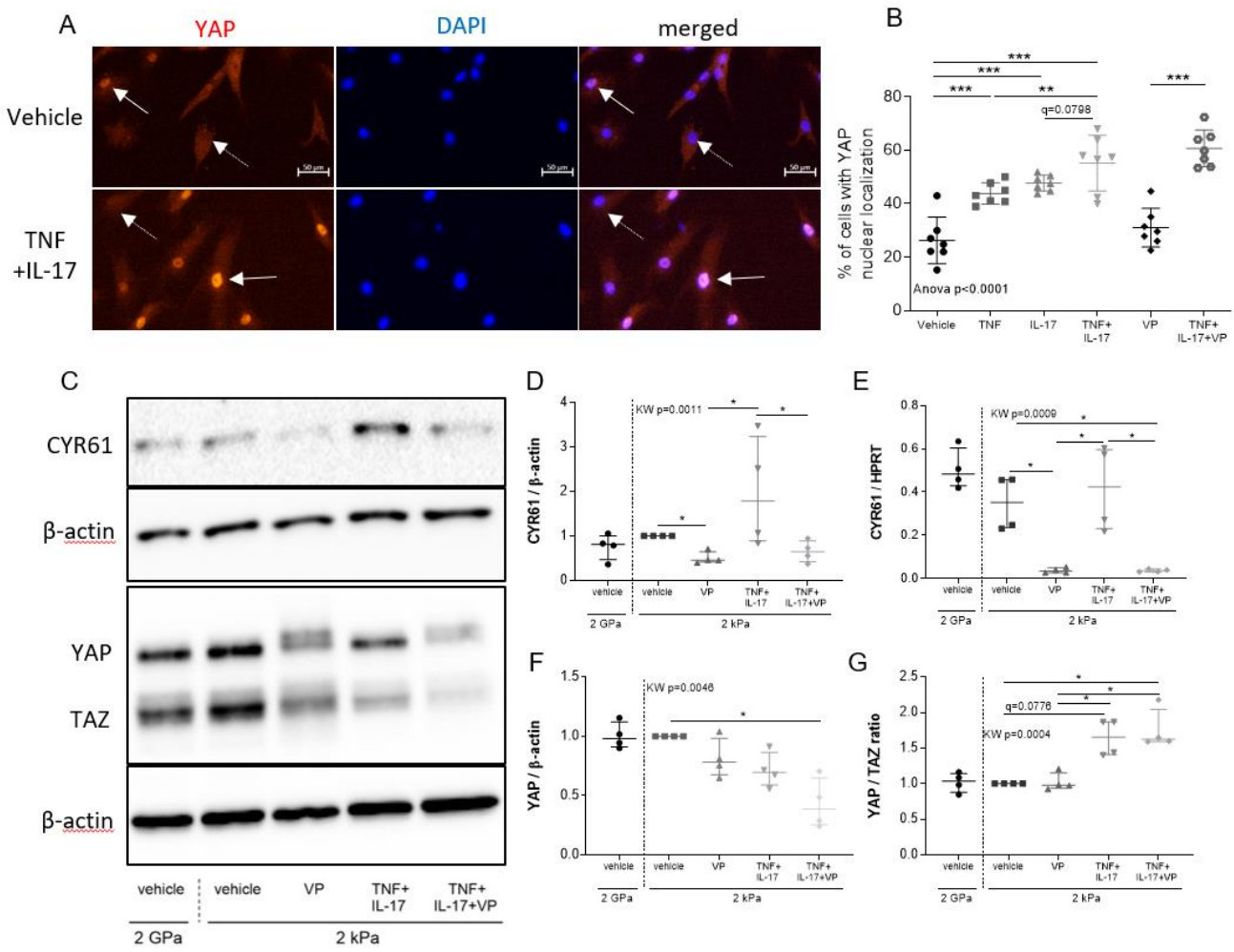

Figure 1. YAP was active in RA FLS and its activation was increased by pro-inflammatory cytokines independently from mechanical cues. FLS from RA patients were cultured on soft (2 kPa) or classic stiff (2 GPa) substrates as indicated and coated with fibronectin for 72 hours. FLS were treated with VP, TNF, IL-17 alone or in combination for 48 hours. The culture medium was identical for all groups containing DMSO (0.035%). A: Epifluorescence representative images of YAP (immunofluorescence technique, orange), DAPI (nucleus, blue), and merged images (luminosity and contrast were enhanced identically for each image for clarity purpose) of RA FLS were cultivated on soft (2 kPa) substrate for all conditions. Arrows: cells with

positive YAP nuclear localization; dotted arrows: cells with negative YAP nuclear localization. B: Corresponding quantification of the percentage of cells with YAP nuclear localization for FLS from one RA patient (n=7), experiments were repeated for FLS from three others RA patients showing the same pattern. RA FLS were cultivated on soft (2 kPa) substrate for all conditions. C: Representative WB results of CYR61, total YAP-TAZ, and β-actin. D-F: WB quantification results for FLS from four different RA patients. Because WBs were performed on different membranes, results shown were normalized to the 2 kPa group for each patient and to β-actin. G: qPCR quantification of CYR61 expression normalized to HPRT expression. ANOVA or Kruskal Wallis (KW) test with FDR corrected (q-value) for multiple comparisons post hoc tests were performed between soft conditions (2kPa): * $q<0.05$; ** $q<0.01$; *** $q<0.001$. Data are presented as individual values with mean ± SD (B) or median and interquartile range (D-G). Verteporfin (VP): 10 µM; TNF: 10 ng/ml; IL-17: 50 ng/ml.

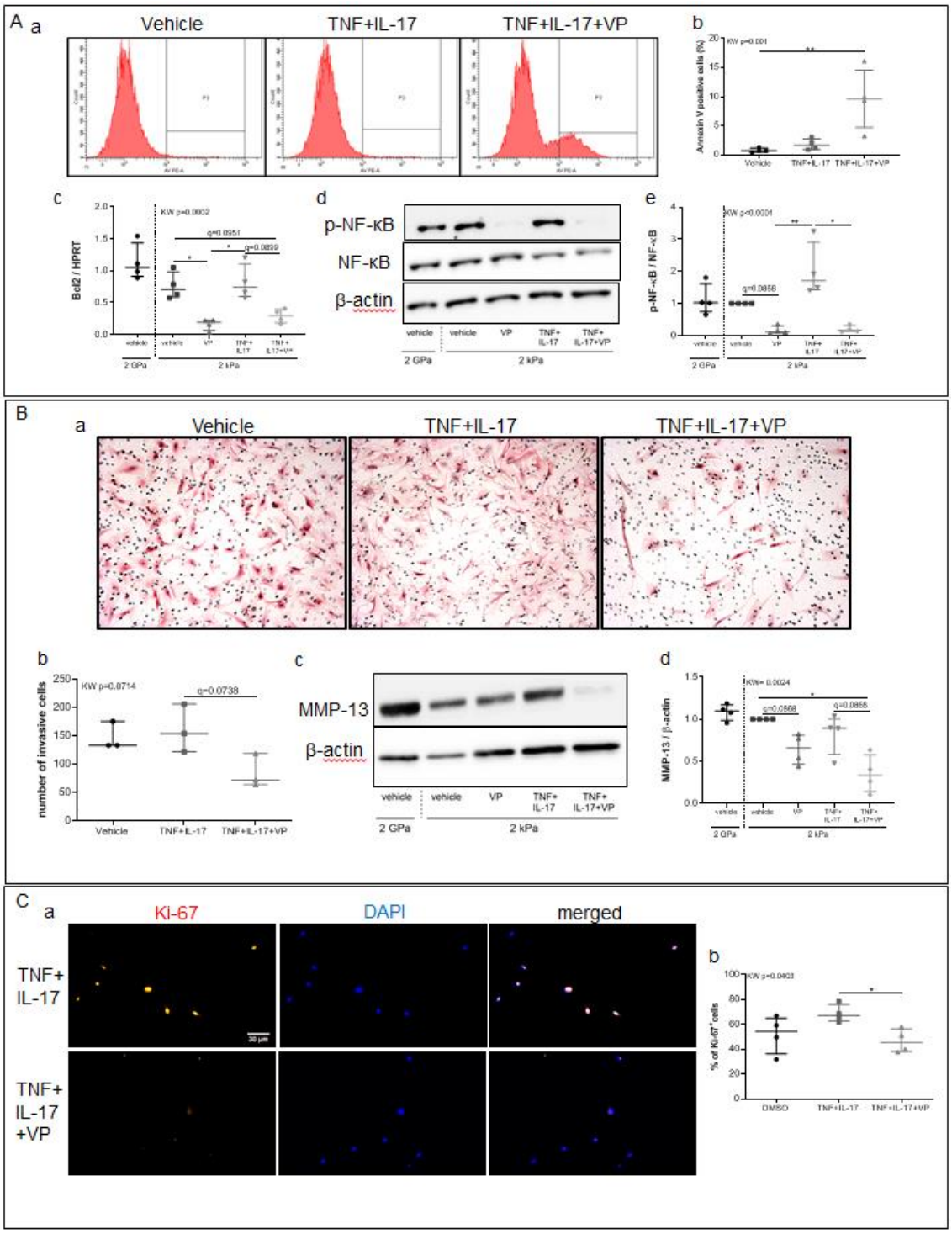

Figure 2. YAP inhibition blocked RA FLS aggressive phenotype. FLS from four RA patients were cultured on soft (2 kPa) or classic stiff (2 GPa) substrate coated with fibronectin for 72 hours. FLS were treated with VP, TNF, IL-17 for 48 hours. The culture medium was identical for all groups containing DMSO (0.035%). A-a: Flow cytometry representative histograms showing the number of annexin V negative (left) and

positive cells (P3 box right). A-b: Corresponding flow cytometry quantification for FLS from four RA patients of the percentage of positive annexin V cells. A-c: qPCR quantification of Bcl2 expression normalized by HPRT expression. A-d: Representative WB results of phospho(p)-NF-κB p65 (serine536: active form), total NF-κB p65 and β-actin. A-e: WB quantification, results for FLS from four different RA patients. Because WBs were performed on different membranes, results shown were normalized to the 2kPa group for each patient and to β-actin. B-a: Representative brightfield images of invasion transwell assay results of RA FLS stained with H&E at x10 magnification. B-b: Quantification of invasive cells number. Results represented the mean of 3 random fields at x10 for each insert, each condition was performed in duplicate for 3 RA patients. B-c: Representative WB results of MMP-13 and β-actin. B-d: WB quantification for MMP-13 (n=4). C-a: Representative epifluorescence images of Ki-67 (Immunofluorescence technique, orange) DAPI (blue) and merged. C-b: Immunofluorescence quantification representing the percentage of Ki-67 positive nucleus, results were expressed as the mean of 4 replicates for each FLS from 4 RA patients. Kruskal Wallis (KW) test with FDR corrected (q-value) for multiple comparisons post hoc tests: * $q<0.05$; ** $q<0.01$; *** $q<0.001$. Data are presented as individual values with median and interquartile range. Verteporfin (VP): 10 µM; TNF: 10 ng/ml; IL-17: 50 ng/ml.

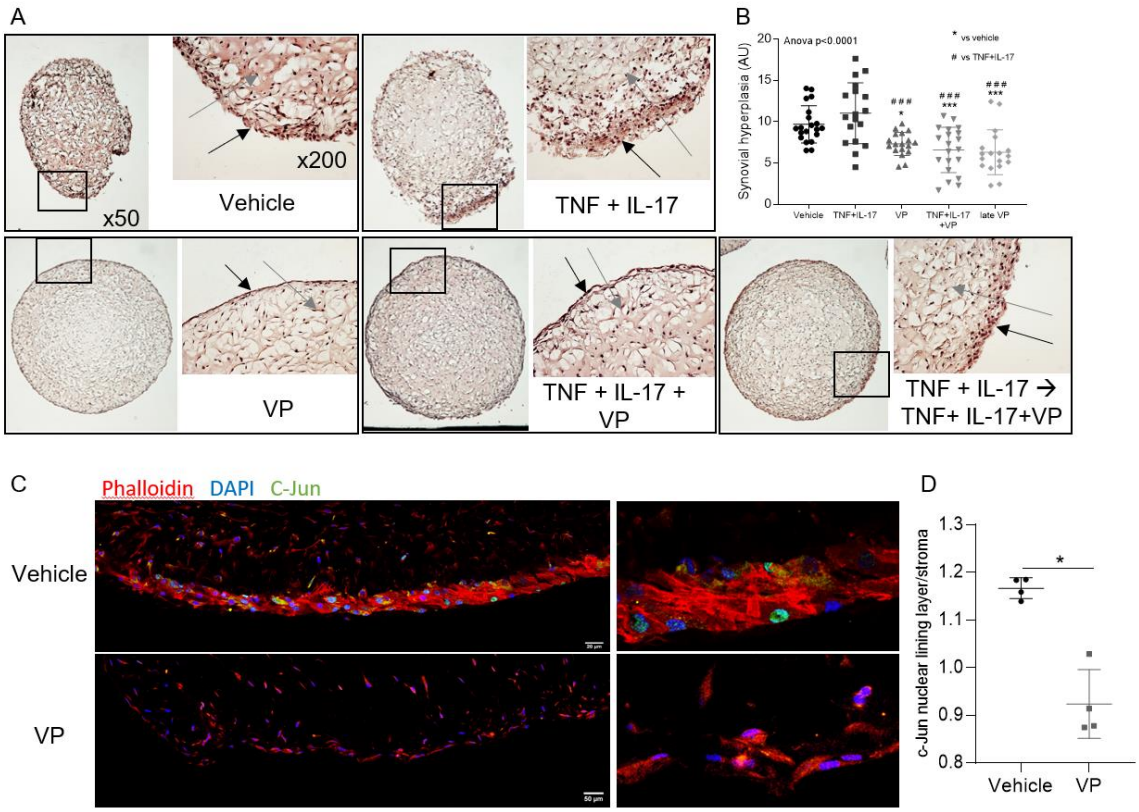

Figure 3. YAP inhibition by VP prevented and reversed synovial hyperplasia in an organoid model of synovial lining layer. A: Representative brightfield images at x50 and x200 magnification of 10-µm thick paraffin sections of synovial organoids with RA FLS from the same patient, H&E staining; black arrows: synovial lining layer, grey arrows: synovial stroma. B: Corresponding quantification of synovial hyperplasia in organoids coming from four RA patients (n=15-20 per group), measurements were performed by dividing the synovial lining layer area by organoid perimeter (AU=arbitrary units). ANOVA test with FDR post hoc test corrected (q-value) for multiple comparisons, * comparisons vs. vehicle group, # comparisons vs. TNF+IL-17 group. *q<0.05; **q<0.01; *** or # # # q<0.001 C: Representative airyscan confocal images for c-Jun (immunofluorescence technique, green), counterstained with phalloidin (actin, red) and DAPI (blue) showing tiles images at x63 (left) of 30-µm thick cryosections on RA organoids, and zoom on synovial lining layer (right), brightness

and contrast were enhanced identically for clarity purpose. D: Immunofluorescence quantification, representing the ratio of nuclear c-Jun for cells in lining layer and nuclear c-Jun for cells in the stroma, results represented four organoids coming from one RA patient FLS, Mann-Whitney test, *$p<0.05$. Data are presented as individual values with mean ± SD (B) or median and interquartile range (D). Verteporfin (VP): 10 µM; TNF: 10 ng/ml; IL-17: 50 ng/ml.

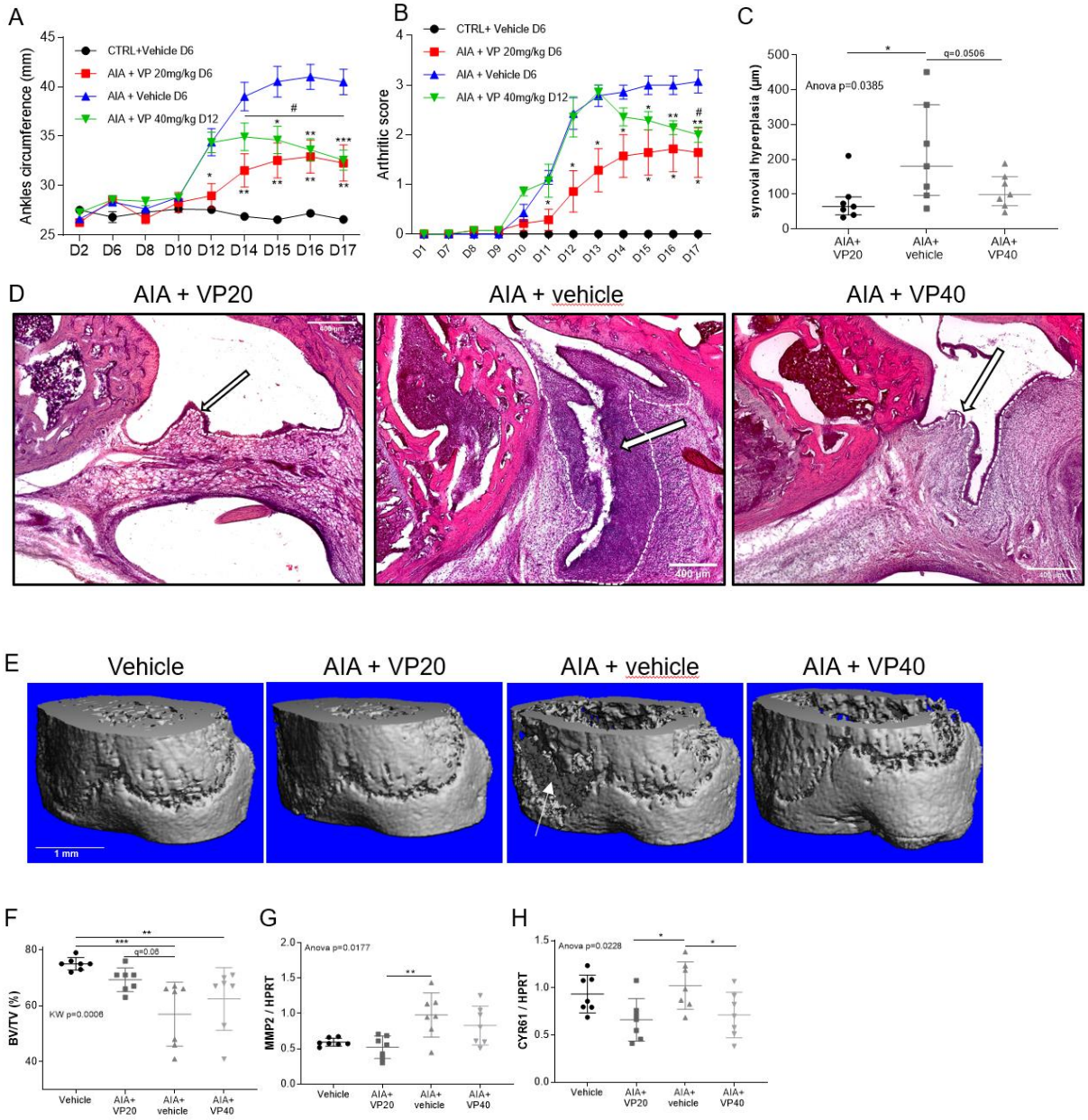

Figure 4. VP treatment prevented and decreased severity of arthritis in rat AIA model. Day 0 was defined by the day of AIA induction. All animals received IP injection each day from days 6 to 16. Control or arthritic (AIA) rats were injected with vehicle containing 10% DMSO, whereas treated AIA rats received 20 µg/kg/day of VP from day 6 (VP20) as a preventive approach or 40 µg/kg/day VP from day 12 (VP40) as a curative approach. A-B: Ankle circumference measurement and arthritic score; results were expressed as the mean of the two ankles for each measurement. Two-way ANOVA with FDR post hoc test corrected for multiple comparison (*), and paired t-test

between days 14 and 17 (#) for VP40 group. * or # q<0.05; **q<0.01; ***q<0.001. D: Representative brightfield tiles images at x10 magnification of 40-µm thick cryosections at the tibio-astragal anterior joint, H&E staining; the dotted lines represent the limit between synovial lining layer and synovial stroma. C: Corresponding quantification of H&E staining for hyperplasia in the lining layer (arrows) of the synovial membrane located at the anterior part of the tibio-astragal joint; results represented the area of synovial lining layer divided by synovial lining layer length. E: Representative 3-D reconstruction of micro-computed tomography scan for distal tibia epiphysis; of note, important bone erosion was present in the AIA group (arrow). F: Corresponding quantification of BV/TV (bone volume/tissue volume) for the tibial distal epiphysis in each group. G-H: qPCR quantification of MMP2 (G) and CYR61 (H) expression normalized to HPRT expression. Kruskal Wallis (KW) or ANOVA test with FDR post hoc test corrected (q-value) for multiple comparisons. *q<0.05; **q<0.01; ***q<0.001. Data are presented as individual values with mean ± SEM (A-B) or mean ± SD (C, F-H).

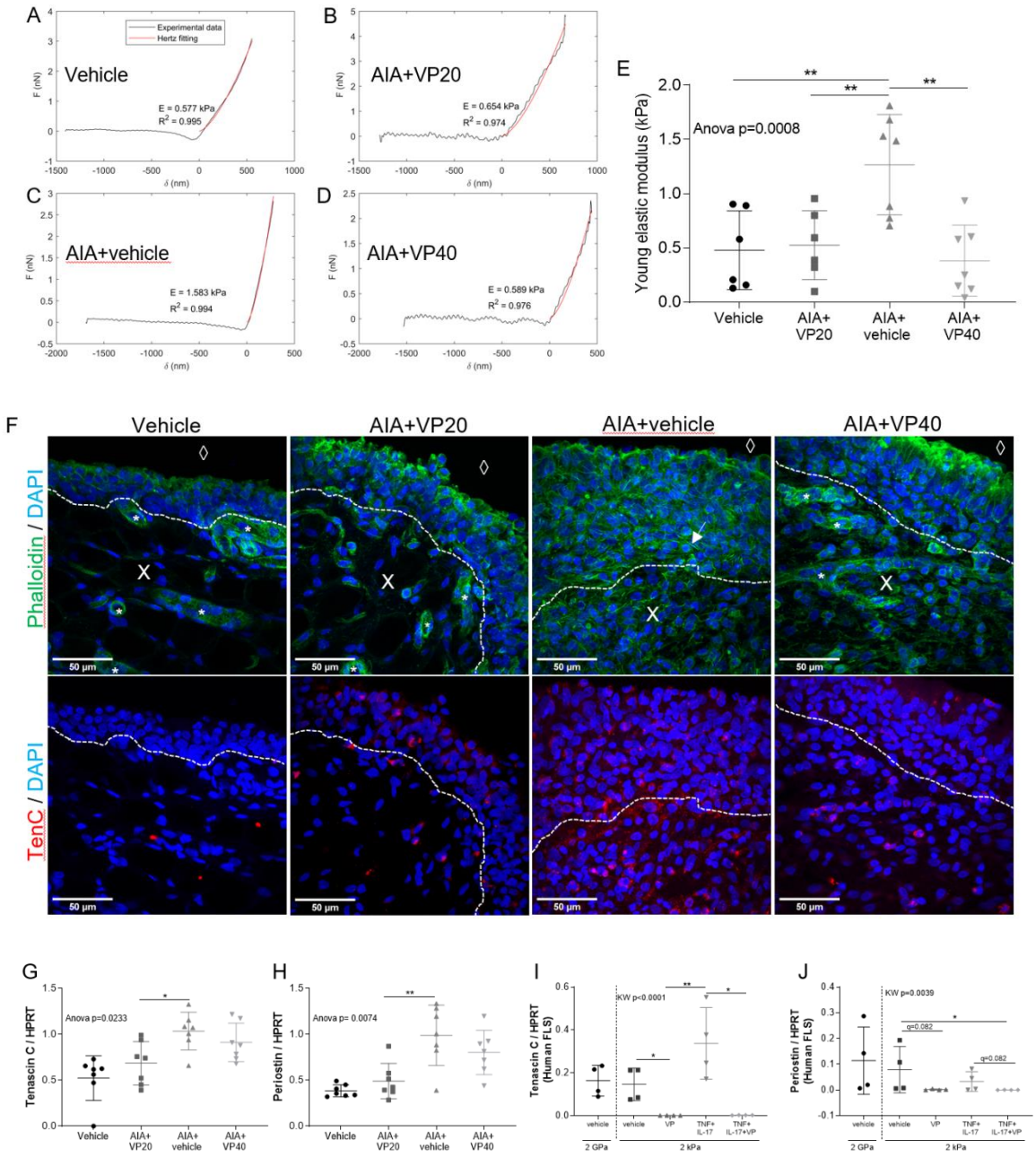

Figure 5. Synovial tissue became stiffer during arthritis under YAP/TAZ control. Samples used came from the animal protocols described in Figure 4. A-D: Representative punctual nanoindentation curves for rat synovial membrane using AFM. Note in the AIA group the more important slope corresponding, when fitted with Hertz model (red slope), to an increased Young's modulus (E). A: Vehicle B: VP20 C: AIA D: VP40. E: Corresponding quantification of Young's modulus (kPa). F: Representative airyscan confocal tiled images of tenascin C (tenC,

immunofluorescence technique, red) for each group, counterstained with DAPI (blue) and phalloidin (green); upper panel: phalloidin and DAPI, lower panel: tenC and DAPI; dotted lines represents the limit between synovial lining layer and synovial stroma; X: stromal compartment, diamond: synovial fluid compartment; star: blood vessels; arrow: actin stress fiber G-J: qPCR quantification of tenC and periostin in rat ankle (G-H) or in FLS from RA patient (I-J); for human FLS cell culture condition see Figure 2. Kruskal Wallis (KW) or ANOVA test with FDR post hoc test corrected (q-value) for multiple comparisons *q<0.05; **q<0.01; ***q<0.001. Data are presented as individual values with mean ± SD (E, G, H) or median and interquartile range (I, J).

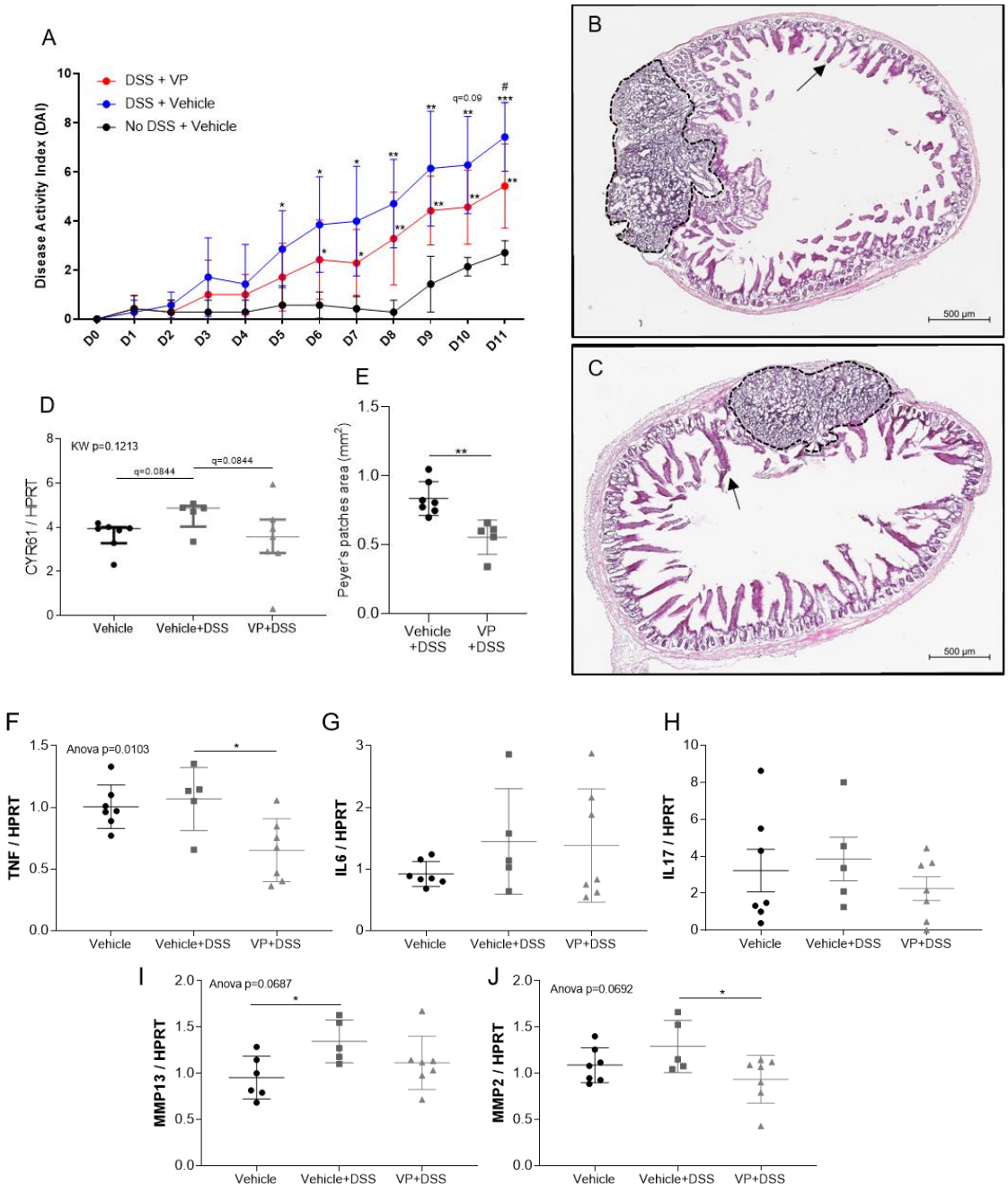

Figure 6. YAP/TAZ inhibition with VP in a dextran sulfate sodium (DSS) induced colitis mice model also prevented the disease by the same mechanisms observed in arthritis. All animals received IP injection each day from day -1 to day 10; control (vehicle) or DSS mice (1.5% DSS in water) were injected with vehicle containing 10% DMSO, treated DSS mice were injected with 40 mg/kg/day of VP. A: Disease activity index (DAI) represents the severity of the disease by evaluating percentage weight loss, general aspect of the mice like pain behavior and feces aspect; two-way ANOVA test

with FDR post hoc test corrected (q-value) for multiple comparison; # : DSS vs. vehicle and * : DSS vs VP. B-C: Representative brightfield tiled images at x200 magnification of 10-µm thick paraffin transverse sections of intestinal tract, H&E staining. B: DSS, C: DSS+VP; dotted line represents Peyer's patches limit; black arrows: intestinal villi. E: Corresponding quantification of Peyer's patches area in DSS and DSS+VP group; results represent the mean of 3 sections per Peyer's patches in duplicate for each mouse, Mann-Whitney test. D and F-J: qPCR quantification on intestinal tract; results are normalized to HPRT. Kruskal Wallis (KW) or ANOVA test with FDR post hoc test corrected (q-value) for multiple comparisons. # or *q<0.05; **q<0.01; ***q<0.001. Data are presented as individual values with median and interquartile range (D) or mean ± SD (E, F-K).

844

SUPPLEMENTARY FIGURES

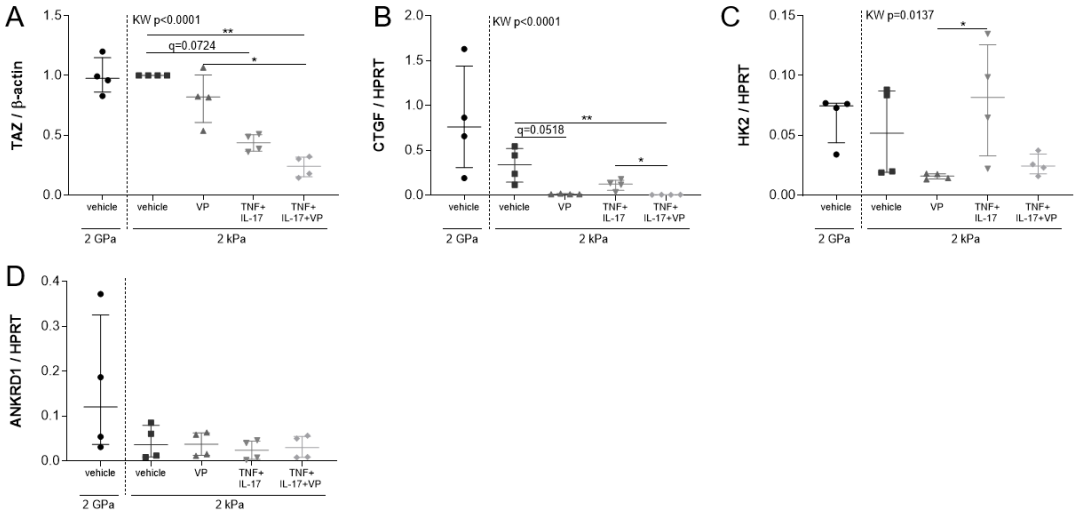

Supplementary Figure 1. Complementary data on YAP activation in RA FLS.

FLS from RA patients were cultivated on soft (2 kPa) or classic stiff (2 GPa) substrate coated with fibronectin for 72 hours. FLS were treated with VP, TNF, and IL-17 for 48 hours. The culture medium was identical for all groups containing DMSO (0.035%). A: WB quantification of TAZ protein, results for FLS from four RA patients. Because WB were performed on different membranes, results shown were normalized to the 2 kPa group for each patient and to β-actin. B-E: qPCR quantification, results were normalized to HPRT. Kruskal Wallis (KW) test with FDR corrected (q-value) for multiple comparison post hoc tests were performed between soft conditions (2 kPa): * q<0.05; ** q<0.01; *** q<0.001. Data are presented as individual values with median and interquartile range. Verteporfin (VP): 10 µM; TNF: 10 ng/ml; IL-17: 50 ng/ml.

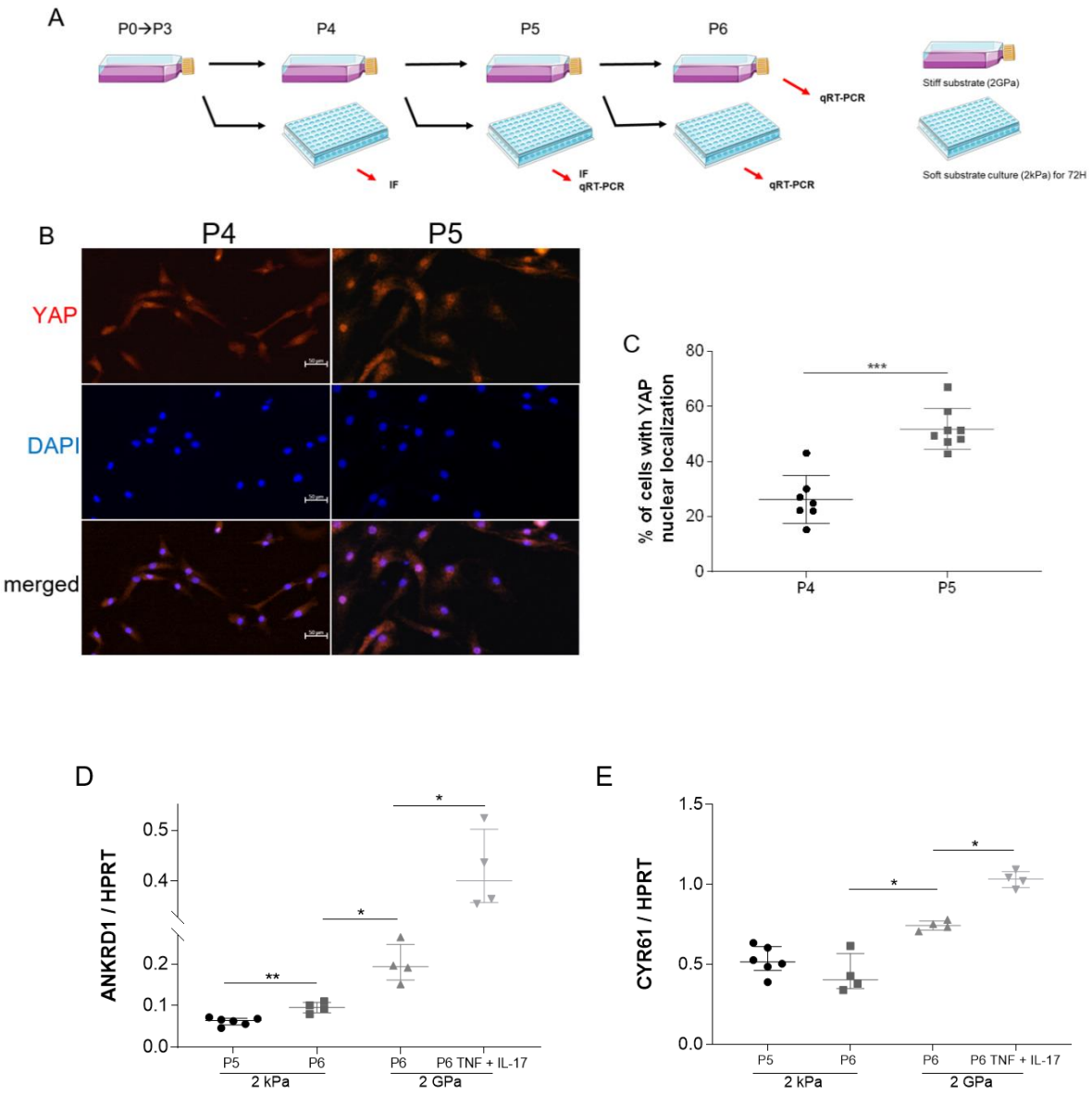

Supplementary Figure 2. YAP activation in RA FLS was increased by the time spent on stiff substrate

A: Schematic representation of RA FLS culture experiment. FLS were passed on soft support at passage (P) 4 or P5 or P6 following IF or RT-qPCR analysis; time spent by FLS on stiff support was increased at each passage (P6>P5>P4). B: Epifluorescence representative images of YAP (IF technique, red), on RA FLS at x10 magnification at P4 and P5 (luminosity and contrast were enhanced identically for each images for

clarity purpose); for all conditions, cells were cultured on soft (2 kPa) 96-well culture dishes coated with fibronectin. C: Corresponding quantification of the percentage of cells with YAP nuclear localization for FLS from one RA patient (n=7 P4, n=8 P5), experiment was repeated for one other RA patient showing the same pattern. D: qPCR quantification of ANKRD1 for FLS from one RA patient (n=6 P5 and n=4 P6) on soft (2 kPa) or stiff (2 GPa) support; results were normalized to HPRT. T-test and Mann-Whitney test * $p<0.05$; ** $p<0.01$; *** $p<0.001$. Data are presented as individual values with mean ± SD (C) or median and interquartile range (D,E). IF: Immunofluorescence.

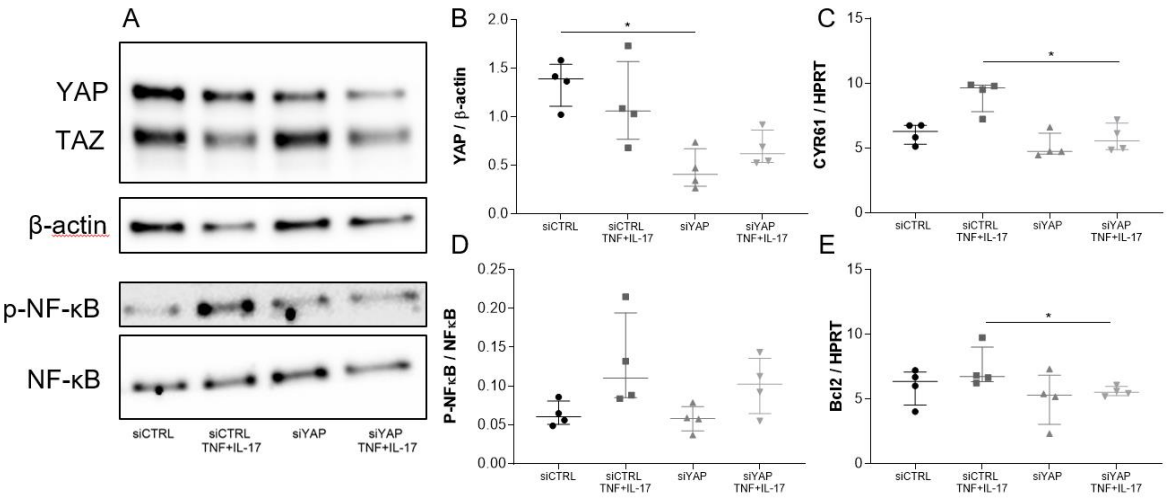

Supplementary Figure 3. YAP inhibition with siRNA on RA FLS.

FLS from RA patient were cultivated on stiff (2 GPa) substrate coated with fibronectin for 72 hours. Following YAP siRNA transfection, FLS were treated with TNF and IL-17 for 48 hours. The culture medium was identical for all groups containing DMSO (0.035%). A: Representative WB results of total YAP-TAZ, phospho-NF-κB p65 (serine536 = active form), total NF-κB p65, and β-actin. B: WB quantification results for YAP of four replicates for one arthritic patient, results were normalized to β-actin. C: qPCR quantification of CYR61; results were normalized to HPRT. D: WB quantification of phospho-NF-κB divided by total NF-κB, results of four replicate for FLS from one RA patient; results were normalized to β-actin expression. E: qPCR quantification of Bcl2; results were normalized to HPRT expression. Mann-Whitney tests: * $p<0.05$. Data are presented as individual values with median and interquartile range. TNF: 10 ng/ml; IL-17: 50 ng/ml.

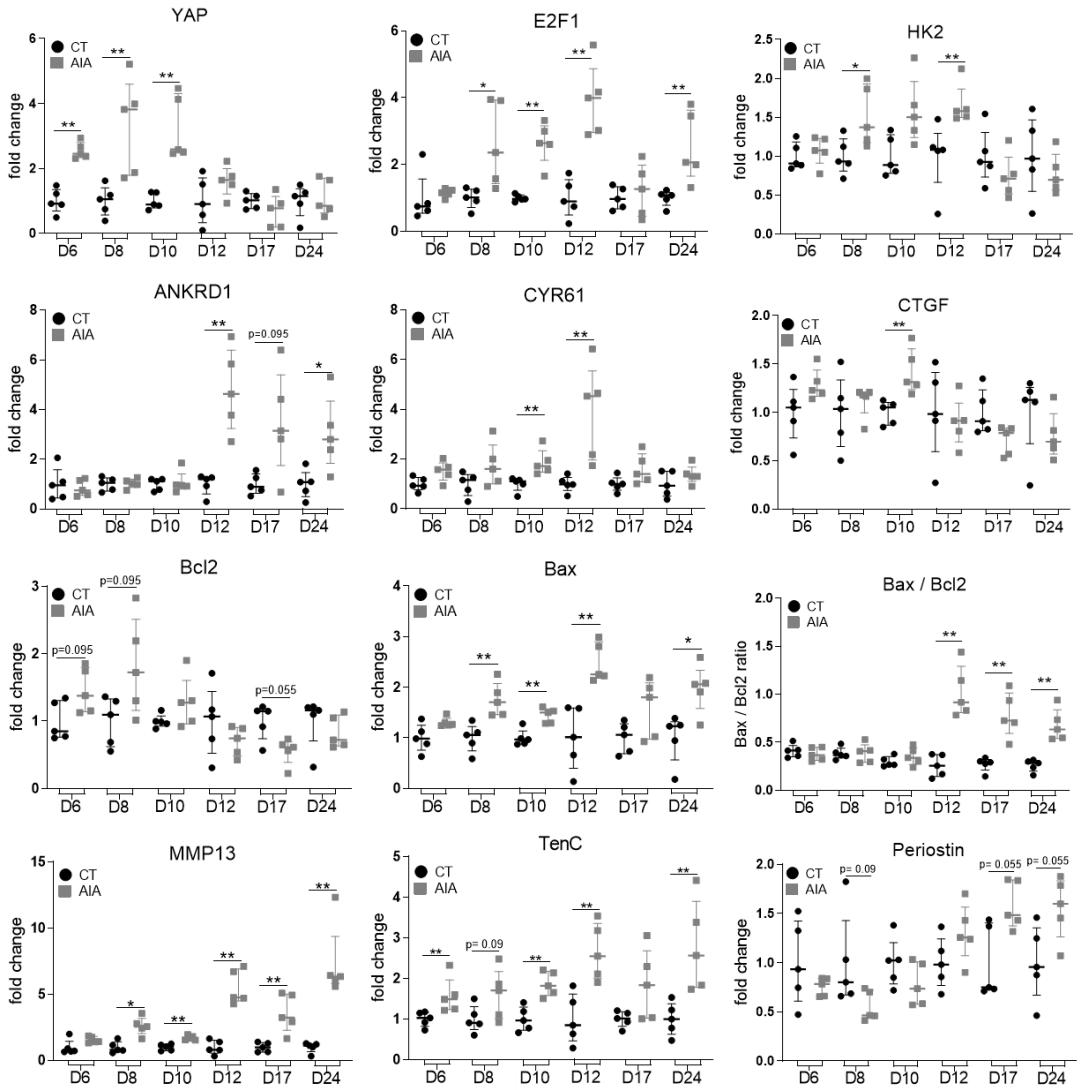

Supplementary Figure 4. Rat AIA mRNA kinetics.

RT-qPCR results of mRNA from ankle of AIA and control (CT) rats. Results were normalized to HPRT expression and expressed as fold change vs. CT at each day. Rats were killed at different times (n=5), arthritis onset was at day 10. Mann-Whitney test *p<0.05; **p<0.01; *** p<0.001. Data are presented as individual values with median and interquartile range.

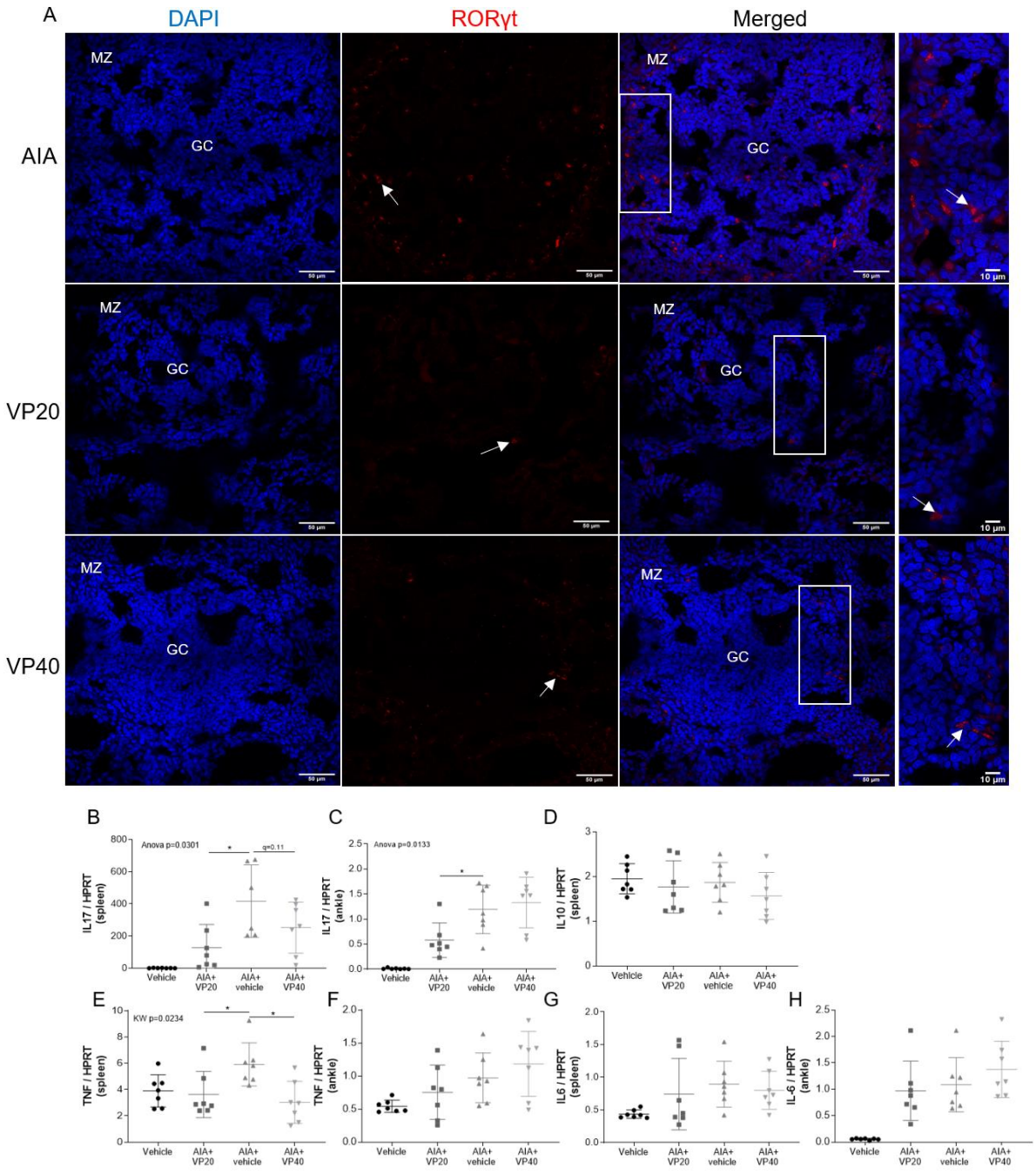

Supplementary Figure 5. VP decreased mRNA expression markers of lymphocyte Th17 in the rat AIA model.

All animals received IP injection each day from days 6 to 16, control (vehicle) or arthritic (AIA) rats were injected with vehicle containing 10% DMSO, treated AIA rats were injected with a preventive (VP20) 20 µg/kg/day VP dose from day 6 or a curative (VP40) 40 µg/kg/day VP dose from day 12. A: Representative airyscan confocal tiled images for RORγt (immunofluorescence technique, red), counterstained with DAPI

(blue), 10-µm thick cryosections of rat spleen, right image = corresponding cropped image of merged in the marginal zone. GC= germinal center; MZ= marginal zone; arrows: RORγt positive cells located in the marginal zone. B-H: qPCR quantification in spleen and ankle as indicated, results were normalized to HPRT. Kruskal Wallis (KW) or ANOVA test with FDR post hoc tests corrected (q-value) for multiple comparisons. *q<0.05; **q<0.01; ***q<0.001. Data are presented as individual values with mean ± SD.

RÉFÉRENCES BIBLIOGRAPHIQUES

1. Gyires, K. & Feher, A. Stress, Neuropeptides and Gastric Mucosa. *Curr. Pharm. Des.* **23**, 3928–3940 (2017).
2. Peterson, L. W. & Artis, D. Intestinal epithelial cells: regulators of barrier function and immune homeostasis. *Nat. Rev. Immunol.* **14**, 141–153 (2014).
3. Porter, E. M., Bevins, C. L., Ghosh, D. & Ganz, T. The multifaceted Paneth cell. *Cell. Mol. Life Sci. CMLS* **59**, 156–170 (2002).
4. Muñoz, M. *et al.* Interleukin-22 induces interleukin-18 expression from epithelial cells during intestinal infection. *Immunity* **42**, 321–331 (2015).
5. Brogden, K. A. Antimicrobial peptides: pore formers or metabolic inhibitors in bacteria? *Nat. Rev. Microbiol.* **3**, 238–250 (2005).
6. Bevins, C. L. Innate immune functions of α-defensins in the small intestine. *Dig. Dis. Basel Switz.* **31**, 299–304 (2013).
7. Wilson, C. L. *et al.* Regulation of intestinal alpha-defensin activation by the metalloproteinase matrilysin in innate host defense. *Science* **286**, 113–117 (1999).
8. Specian, R. D. & Oliver, M. G. Functional biology of intestinal goblet cells. *Am. J. Physiol.* **260**, C183-193 (1991).
9. Birchenough, G. M. H., Johansson, M. E., Gustafsson, J. K., Bergström, J. H. & Hansson, G. C. New developments in goblet cell mucus secretion and function. *Mucosal Immunol.* **8**, 712–719 (2015).
10. Nasri, I. *et al.* PAR2-dependent activation of GSK3β regulates the survival of colon stem/progenitor cells. *Am. J. Physiol. Gastrointest. Liver Physiol.* **311**, G221-236 (2016).
11. Parikh, K. *et al.* Colonic epithelial cell diversity in health and inflammatory bowel disease. *Nature* **567**, 49–55 (2019).
12. Okumura, R. & Takeda, K. Roles of intestinal epithelial cells in the maintenance of gut homeostasis. *Exp. Mol. Med.* **49**, e338 (2017).
13. Yamada, T. *et al.* Mucin O-glycans facilitate symbiosynthesis to maintain gut immune homeostasis. *EBioMedicine* **48**, 513–525 (2019).
14. Jung, C., Hugot, J.-P. & Barreau, F. Peyer's Patches: The Immune Sensors of the Intestine. *Int. J. Inflamm.* **2010**, 823710 (2010).
15. Cupedo, T., Coles, M. C. & Veiga-Fernandes, H. Structure and Development of Peyer's Patches in Humans and Mice. in *Developmental Biology of Peripheral Lymphoid Organs* (ed. Balogh, P.) 97–106 (Springer, 2011). doi:10.1007/978-3-642-14429-5_9.
16. Lorenz, R. G. & Newberry, R. D. Isolated lymphoid follicles can function as sites for induction of mucosal immune responses. *Ann. N. Y. Acad. Sci.* **1029**, 44–57 (2004).
17. Pabst, O. *et al.* Adaptation of solitary intestinal lymphoid tissue in response to microbiota and chemokine receptor CCR7 signaling. *J. Immunol. Baltim. Md 1950* **177**, 6824–6832 (2006).
18. Knoop, K. A. & Newberry, R. D. Isolated Lymphoid Follicles are Dynamic Reservoirs for the Induction of Intestinal IgA. *Front. Immunol.* **3**, (2012).
19. Motta, J.-P. *et al.* Active thrombin produced by the intestinal epithelium controls mucosal biofilms. *Nat. Commun.* **10**, 1–12 (2019).
20. Elewaut, D. *et al.* NF-kappa B is a central regulator of the intestinal epithelial cell innate immune response induced by infection with enteroinvasive bacteria. *J. Immunol. Baltim. Md 1950* **163**, 1457–1466 (1999).
21. Pappo, J. & Mahlman, R. T. Follicle epithelial M cells are a source of interleukin-1 in Peyer's patches. *Immunology* **78**, 505–507 (1993).
22. Yang, S. K., Eckmann, L., Panja, A. & Kagnoff, M. F. Differential and regulated expression of C-X-C, C-C, and C-chemokines by human colon epithelial cells. *Gastroenterology* **113**, 1214–1223 (1997).
23. Eckmann, L., Kagnoff, M. F. & Fierer, J. Epithelial cells secrete the chemokine interleukin-8 in response to bacterial entry. *Infect. Immun.* **61**, 4569–4574 (1993).
24. Reinecker, H. C. *et al.* Monocyte-chemoattractant protein 1 gene expression

in intestinal epithelial cells and inflammatory bowel disease mucosa. *Gastroenterology* **108**, 40–50 (1995).
25. Izadpanah, A., Dwinell, M. B., Eckmann, L., Varki, N. M. & Kagnoff, M. F. Regulated MIP-3alpha/CCL20 production by human intestinal epithelium: mechanism for modulating mucosal immunity. *Am. J. Physiol. Gastrointest. Liver Physiol.* **280**, G710-719 (2001).
26. Youakim, A. & Ahdieh, M. Interferon-gamma decreases barrier function in T84 cells by reducing ZO-1 levels and disrupting apical actin. *Am. J. Physiol.* **276**, G1279-1288 (1999).
27. Scheibe, K. *et al.* IL-36R signalling activates intestinal epithelial cells and fibroblasts and promotes mucosal healing in vivo. *Gut* **66**, 823–838 (2017).
28. Price, A. E. *et al.* Systemically dispersed innate IL-13–expressing cells in type 2 immunity. *Proc. Natl. Acad. Sci. U. S. A.* **107**, 11489–11494 (2010).
29. Moro, K. *et al.* Innate production of T(H)2 cytokines by adipose tissue-associated c-Kit(+)Sca-1(+) lymphoid cells. *Nature* **463**, 540–544 (2010).
30. Shimotoyodome, A., Meguro, S., Hase, T., Tokimitsu, I. & Sakata, T. Short chain fatty acids but not lactate or succinate stimulate mucus release in the rat colon. *Comp. Biochem. Physiol. A. Mol. Integr. Physiol.* **125**, 525–531 (2000).
31. Ciorba, M. A. *et al.* Lactobacillus probiotic protects intestinal epithelium from radiation injury in a TLR-2/cyclo-oxygenase-2-dependent manner. *Gut* **61**, 829–838 (2012).
32. Meng, D., Zhu, W., Ganguli, K., Shi, H. N. & Walker, W. A. Anti-inflammatory effects of Bifidobacterium longum subsp infantis secretions on fetal human enterocytes are mediated by TLR-4 receptors. *Am. J. Physiol.-Gastrointest. Liver Physiol.* **311**, G744–G753 (2016).
33. Abt, M. C. *et al.* TLR-7 activation enhances IL-22-mediated colonization resistance against vancomycin-resistant enterococcus. *Sci. Transl. Med.* **8**, 327ra25 (2016).
34. Vora, P. *et al.* Beta-defensin-2 expression is regulated by TLR signaling in intestinal epithelial cells. *J. Immunol. Baltim. Md 1950* **173**, 5398–5405 (2004).
35. Kirkland, D. *et al.* B Cell-Intrinsic MyD88 Signaling Prevents the Lethal Dissemination of Commensal Bacteria during Colonic Damage. *Immunity* **36**, 228–238 (2012).
36. Maglione, P. J. *et al.* IRAK-4 and MyD88 deficiencies impair IgM responses against T-independent bacterial antigens. *Blood* **124**, 3561–3571 (2014).
37. Hosseini, H. *et al.* Toll-Like Receptor (TLR)4 and MyD88 are Essential for Atheroprotection by Peritoneal B1a B Cells. *J. Am. Heart Assoc.* **5**, e002947 (2016).
38. Guo, S., Al-Sadi, R., Said, H. M. & Ma, T. Y. Lipopolysaccharide causes an increase in intestinal tight junction permeability in vitro and in vivo by inducing enterocyte membrane expression and localization of TLR-4 and CD14. *Am. J. Pathol.* **182**, 375–387 (2013).
39. Mueller, T., Terada, T., Rosenberg, I. M., Shibolet, O. & Podolsky, D. K. Th2 cytokines down-regulate TLR expression and function in human intestinal epithelial cells. *J. Immunol. Baltim. Md 1950* **176**, 5805–5814 (2006).
40. Inohara, N., Ogura, Y., Chen, F. F., Muto, A. & Nuñez, G. Human Nod1 confers responsiveness to bacterial lipopolysaccharides. *J. Biol. Chem.* **276**, 2551–2554 (2001).
41. Sorbara, M. T. *et al.* The protein ATG16L1 suppresses inflammatory cytokines induced by the intracellular sensors Nod1 and Nod2 in an autophagy-independent manner. *Immunity* **39**, 858–873 (2013).
42. Osorio, F. *et al.* DC activated via dectin-1 convert Treg into IL-17 producers. *Eur. J. Immunol.* **38**, 3274–3281 (2008).
43. Rochereau, N. *et al.* Dectin-1 Is Essential for Reverse Transcytosis of Glycosylated SIgA-Antigen Complexes by Intestinal M Cells. *Plos Biol* **11**, e1001658 (2013).
44. Drummond, R. A. *et al.* CD4 + T-cell survival in the GI tract requires dectin-1 during fungal infection. *Mucosal Immunol.* **9**, 492–502 (2016).
45. Taylor, P. R. *et al.* Dectin-1 is required for beta-glucan recognition and control of fungal infection. *Nat. Immunol.* **8**, 31–38 (2007).

46. Saijo, S. *et al.* Dectin-2 recognition of alpha-mannans and induction of Th17 cell differentiation is essential for host defense against Candida albicans. *Immunity* **32**, 681–691 (2010).
47. Robinson, M. J. *et al.* Dectin-2 is a Syk-coupled pattern recognition receptor crucial for Th17 responses to fungal infection. *J. Exp. Med.* **206**, 2037–2051 (2009).
48. Ritter, M. *et al.* Schistosoma mansoni triggers Dectin-2, which activates the Nlrp3 inflammasome and alters adaptive immune responses. *Proc. Natl. Acad. Sci. U. S. A.* **107**, 20459–20464 (2010).
49. Kaisar, M. M. M. *et al.* Dectin-1/2–induced autocrine PGE2 signaling licenses dendritic cells to prime Th2 responses. *PLOS Biol.* **16**, e2005504 (2018).
50. Eberl, G., Colonna, M., Di Santo, J. P. & McKenzie, A. N. J. Innate lymphoid cells. Innate lymphoid cells: a new paradigm in immunology. *Science* **348**, aaa6566 (2015).
51. Panda, S. K. & Colonna, M. Innate Lymphoid Cells in Mucosal Immunity. *Front. Immunol.* **10**, (2019).
52. van Wijk, F. & Cheroutre, H. Mucosal T cells in gut homeostasis and inflammation. *Expert Rev. Clin. Immunol.* **6**, 559–566 (2010).
53. Romagnani, S. T-cell subsets (Th1 versus Th2). *Ann. Allergy Asthma Immunol. Off. Publ. Am. Coll. Allergy Asthma Immunol.* **85**, 9–18; quiz 18, 21 (2000).
54. Geginat, J. *et al.* Reverse plasticity: TGF-β and IL-6 induce Th1-to-Th17-cell transdifferentiation in the gut. *Eur. J. Immunol.* **46**, 2306–2310 (2016).
55. Harrison, O. J. *et al.* Epithelial-derived IL-18 regulates Th17 cell differentiation and Foxp3 + Treg cell function in the intestine. *Mucosal Immunol.* **8**, 1226–1236 (2015).
56. Neurath, M. F. & Finotto, S. IL-9 signaling as key driver of chronic inflammation in mucosal immunity. *Cytokine Growth Factor Rev.* **29**, 93–99 (2016).
57. Chistiakov, D. A., Bobryshev, Y. V., Kozarov, E., Sobenin, I. A. & Orekhov, A. N. Intestinal mucosal tolerance and impact of gut microbiota to mucosal tolerance. *Front. Microbiol.* **5**, (2015).
58. Björkander, S. *et al.* FOXP3+ CD4 T-cell maturity and responses to microbial stimulation alter with age and associate with early life gut colonization. *J. Allergy Clin. Immunol.* **138**, (2016).
59. Mabbott, N. A., Donaldson, D. S., Ohno, H., Williams, I. R. & Mahajan, A. Microfold (M) cells: important immunosurveillance posts in the intestinal epithelium. *Mucosal Immunol.* **6**, 666–677 (2013).
60. Nair, V. R. *et al.* Microfold Cells Actively Translocate Mycobacterium tuberculosis to Initiate Infection. *Cell Rep.* **16**, 1253–1258 (2016).
61. Rios, D. *et al.* Antigen sampling by intestinal M cells is the principal pathway initiating mucosal IgA production to commensal enteric bacteria. *Mucosal Immunol.* **9**, 907–916 (2016).
62. Williams, I. R. & Owen, R. L. Chapter 13 - M Cells: Specialized Antigen Sampling Cells in the Follicle-Associated Epithelium. in *Mucosal Immunology (Fourth Edition)* (eds. Mestecky, J. et al.) 211–229 (Academic Press, 2015). doi:10.1016/B978-0-12-415847-4.00013-6.
63. Wolf, J. L. *et al.* Intestinal M cells: a pathway for entry of reovirus into the host. *Science* **212**, 471–472 (1981).
64. Shim, S., Park, H.-E., Soh, S. H., Im, Y. B. & Yoo, H. S. Induction of Th2 response through TLR2-mediated MyD88-dependent pathway in human microfold cells stimulated with chitosan nanoparticles loaded with Brucella abortus Mdh. *Microb. Pathog.* **142**, 104040 (2020).
65. Kim, S.-H. & Jang, Y.-S. Yersinia enterocolitica Exploits Signal Crosstalk between Complement 5a Receptor and Toll-like Receptor 1/2 and 4 to Avoid the Bacterial Clearance in M cells. *Immune Netw.* **17**, 228–236 (2017).
66. Gicheva, N., Macauley, M. S., Arlian, B. M., Paulson, J. C. & Kawasaki, N. Siglec-F is a novel intestinal M cell marker. *Biochem. Biophys. Res. Commun.* **479**, 1–4 (2016).
67. Kolesnikov, M. *et al.* Intravital visualization of interactions of murine Peyer's patch-resident dendritic cells with M cells. *Eur. J. Immunol.* **n/a**,.

68. Nakamura, Y. *et al.* Microfold cell-dependent antigen transport alleviates infectious colitis by inducing antigen-specific cellular immunity. *Mucosal Immunol.* (2020) doi:10.1038/s41385-020-0263-0.
69. Komban, R. J. *et al.* Activated Peyer′s patch B cells sample antigen directly from M cells in the subepithelial dome. *Nat. Commun.* **10**, 1–15 (2019).
70. Fabich, A. J. *et al.* Comparison of carbon nutrition for pathogenic and commensal Escherichia coli strains in the mouse intestine. *Infect. Immun.* **76**, 1143–1152 (2008).
71. Brestoff, J. R. & Artis, D. Commensal bacteria at the interface of host metabolism and the immune system. *Nat. Immunol.* **14**, 676–684 (2013).
72. Bugaut, M. Occurrence, absorption and metabolism of short chain fatty acids in the digestive tract of mammals. *Comp. Biochem. Physiol. B* **86**, 439–472 (1987).
73. Bergman, E. N. Energy contributions of volatile fatty acids from the gastrointestinal tract in various species. *Physiol. Rev.* **70**, 567–590 (1990).
74. Miquel, S. *et al.* Ecology and metabolism of the beneficial intestinal commensal bacterium Faecalibacterium prausnitzii. *Gut Microbes* **5**, 146–151 (2014).
75. Miquel, S. *et al.* Faecalibacterium prausnitzii and human intestinal health. *Curr. Opin. Microbiol.* **16**, 255–261 (2013).
76. Sokol, H. *et al.* Faecalibacterium prausnitzii is an anti-inflammatory commensal bacterium identified by gut microbiota analysis of Crohn disease patients. *Proc. Natl. Acad. Sci. U. S. A.* **105**, 16731–16736 (2008).
77. Chia, L. W. *et al.* Deciphering the trophic interaction between Akkermansia muciniphila and the butyrogenic gut commensal Anaerostipes caccae using a metatranscriptomic approach. *Antonie Van Leeuwenhoek* **111**, 859–873 (2018).
78. Hooper, L. V. *et al.* Molecular analysis of commensal host-microbial relationships in the intestine. *Science* **291**, 881–884 (2001).
79. Schneeberger, M. *et al.* Akkermansia muciniphila inversely correlates with the onset of inflammation, altered adipose tissue metabolism and metabolic disorders during obesity in mice. *Sci. Rep.* **5**, 1–14 (2015).
80. Inoue, D., Tsujimoto, G. & Kimura, I. Regulation of Energy Homeostasis by GPR41. *Front. Endocrinol.* **5**, (2014).
81. Kimura, I., Inoue, D., Hirano, K. & Tsujimoto, G. The SCFA Receptor GPR43 and Energy Metabolism. *Front. Endocrinol.* **5**, 85 (2014).
82. Serpa, J. *et al.* Butyrate-rich Colonic Microenvironment Is a Relevant Selection Factor for Metabolically Adapted Tumor Cells. *J. Biol. Chem.* **285**, 39211–39223 (2010).
83. Belzer, C. *et al.* Microbial Metabolic Networks at the Mucus Layer Lead to Diet-Independent Butyrate and Vitamin B12 Production by Intestinal Symbionts. *mBio* **8**, (2017).
84. Nepelska, M. *et al.* Commensal gut bacteria modulate phosphorylation-dependent PPARγ transcriptional activity in human intestinal epithelial cells. *Sci. Rep.* **7**, 1–13 (2017).
85. Yang, J.-Y. *et al.* Gut commensal Bacteroides acidifaciens prevents obesity and improves insulin sensitivity in mice. *Mucosal Immunol.* **10**, 104–116 (2017).
86. Tazi, A. *et al.* Disentangling Host-Microbiota Regulation of Lipid Secretion by Enterocytes: Insights from Commensals Lactobacillus paracasei and Escherichia coli. *mBio* **9**, (2018).
87. Jia, W., Xie, G. & Jia, W. Bile acid-microbiota crosstalk in gastrointestinal inflammation and carcinogenesis. *Nat. Rev. Gastroenterol. Hepatol.* **15**, 111–128 (2018).
88. Grosserichter-Wagener, C. *et al.* Differences in Systemic IgA Reactivity and Circulating Th Subsets in Healthy Volunteers With Specific Microbiota Enterotypes. *Front. Immunol.* **10**, (2019).
89. Mariat, D. *et al.* The Firmicutes/Bacteroidetes ratio of the human microbiota changes with age. *BMC Microbiol.* **9**, 123 (2009).
90. Obata, T. *et al.* Indigenous opportunistic bacteria inhabit mammalian gut-associated lymphoid tissues and share a mucosal antibody-mediated symbiosis. *Proc. Natl. Acad. Sci.* **107**, 7419–7424 (2010).
91. Ley, R. E., Turnbaugh, P. J., Klein, S. & Gordon, J. I. Microbial ecology: human

gut microbes associated with obesity. *Nature* **444**, 1022–1023 (2006).
92. Colliou, N. *et al.* Commensal *Propionibacterium* strain UF1 mitigates intestinal inflammation via Th17 cell regulation. *J. Clin. Invest.* **127**, 3970–3986 (2017).
93. Park, J.-S. *et al.* Lactobacillus acidophilus Improves Intestinal Inflammation in an Acute Colitis Mouse Model by Regulation of Th17 and Treg Cell Balance and Fibrosis Development. *J. Med. Food* **21**, 215–224 (2018).
94. Larsen, J. M. The immune response to Prevotella bacteria in chronic inflammatory disease. *Immunology* **151**, 363–374 (2017).
95. Cosseau, C. *et al.* The Commensal Streptococcus salivarius K12 Downregulates the Innate Immune Responses of Human Epithelial Cells and Promotes Host-Microbe Homeostasis. *Infect. Immun.* **76**, 4163–4175 (2008).
96. Asarat, M., Vasiljevic, T., Apostolopoulos, V. & Donkor, O. Short-Chain Fatty Acids Regulate Secretion of IL-8 from Human Intestinal Epithelial Cell Lines in vitro. *Immunol. Invest.* **44**, 678–693 (2015).
97. Martin-Gallausiaux, C. *et al.* Butyrate produced by gut commensal bacteria activates TGF-beta1 expression through the transcription factor SP1 in human intestinal epithelial cells. *Sci. Rep.* **8**, 1–13 (2018).
98. Engevik, M. A. *et al.* Bifidobacterium dentium Fortifies the Intestinal Mucus Layer via Autophagy and Calcium Signaling Pathways. *mBio* **10**, (2019).
99. Engevik, M. A., Luk, B. K., Visuthranukul, C. & Versalovic, J. Bifidobacterium dentium regulates intestinal mucus production and glycosylation. *FASEB J.* **31**, 954.5-954.5 (2017).
100. Gray, J. *et al.* Intestinal commensal bacteria mediate lung mucosal immunity and promote resistance of newborn mice to infection. *Sci. Transl. Med.* **9**, (2017).
101. Sassone-Corsi, M. & Raffatellu, M. No vacancy: how beneficial microbes cooperate with immunity to provide colonization resistance to pathogens. *J. Immunol. Baltim. Md 1950* **194**, 4081–4087 (2015).
102. Jacobson, A. *et al.* A Gut Commensal-Produced Metabolite Mediates Colonization Resistance to Salmonella Infection. *Cell Host Microbe* **24**, 296-307.e7 (2018).
103. Ramsey, M. M., Freire, M. O., Gabrilska, R. A., Rumbaugh, K. P. & Lemon, K. P. Staphylococcus aureus Shifts toward Commensalism in Response to Corynebacterium Species. *Front. Microbiol.* **7**, 1230 (2016).
104. Kamada, N. *et al.* Regulated virulence controls the ability of a pathogen to compete with the gut microbiota. *Science* **336**, 1325–1329 (2012).
105. Pickard, J. M. *et al.* Rapid fucosylation of intestinal epithelium sustains host-commensal symbiosis in sickness. *Nature* **514**, 638–641 (2014).
106. Leung, C.-H., Lam, W., Ma, D.-L., Gullen, E. A. & Cheng, Y.-C. Butyrate mediates nucleotide-binding and oligomerisation domain (NOD) 2-dependent mucosal immune responses against peptidoglycan. *Eur. J. Immunol.* **39**, 3529–3537 (2009).
107. Mestecky, J., Moro, I., Kerr, M. & Woof, J. Chapter 9. Mucosal Immunoglobulins. in *Mucosal Immunology, Two-Volume Set* 153–181 (2005). doi:10.1016/B978-012491543-5/50013-9.
108. Childers, N. K., Bruce, M. G. & McGhee, J. R. Molecular Mechanisms of Immunoglobulin a Defense. *Annu. Rev. Microbiol.* **43**, 503–536 (1989).
109. Brandtzaeg, P. Induction of secretory immunity and memory at mucosal surfaces. *Vaccine* **25**, 5467–5484 (2007).
110. Brandtzaeg, P. & Prydz, H. Direct evidence for an integrated function of J chain and secretory component in epithelial transport of immunoglobulins. *Nature* **311**, 71–73 (1984).
111. Xiong, E. *et al.* MZB1 promotes the secretion of J-chain-containing dimeric IgA and is critical for the suppression of gut inflammation. *Proc. Natl. Acad. Sci. U. S. A.* **116**, 13480–13489 (2019).
112. Phalipon, A. *et al.* Secretory Component: A New Role in Secretory IgA-Mediated Immune Exclusion In Vivo. *Immunity* **17**, 107–115 (2002).
113. Natvig, I. B., Johansen, F. E., Nordeng, T. W., Haraldsen, G. & Brandtzaeg, P. Mechanism for enhanced external transfer

of dimeric IgA over pentameric IgM: studies of diffusion, binding to the human polymeric Ig receptor, and epithelial transcytosis. *J. Immunol. Baltim. Md 1950* **159**, 4330–4340 (1997).
114. Crottet, P. & Corthésy, B. Secretory component delays the conversion of secretory IgA into antigen-binding competent F(ab')2: a possible implication for mucosal defense. *J. Immunol. Baltim. Md 1950* **161**, 5445–5453 (1998).
115. Michaelsen, T. *et al.* Human secretory IgM antibodies activate human complement and offer protection at mucosal surface. *Scand J Immunol* (2016) doi:10.1111/sji.12508.
116. Mattu, T. *et al.* The glycosylation and structure of human serum IgA1, Fab, and Fc regions and the role of N-glycosylation on Fcα receptor interactions. *J Biol Chem* **273**, 2260–72 (1998).
117. Tarelli, E., Smith, A. C., Hendry, B. M., Challacombe, S. J. & Pouria, S. Human serum IgA1 is substituted with up to six O-glycans as shown by matrix assisted laser desorption ionisation time-of-flight mass spectrometry. *Carbohydr. Res.* **339**, 2329–2335 (2004).
118. Royle, L. *et al.* Secretory IgA N- and O-glycans provide a link between the innate and adaptive immune systems. *J. Biol. Chem.* **278**, 20140–20153 (2003).
119. Arnold, J. *et al.* Human Serum IgM Glycosylation IDENTIFICATION OF GLYCOFORMS THAT CAN BIND TO MANNAN-BINDING LECTIN. *J Biol Chem* **280**, 29080–29087 (2005).
120. Woof, J. M. & Russell, M. W. Structure and function relationships in IgA. *Mucosal Immunol.* **4**, 590–597 (2011).
121. Stadtmueller, B. M. *et al.* The structure and dynamics of secretory component and its interactions with polymeric immunoglobulins. *Elife* **5**, (2016).
122. Oortwijn, B. D. *et al.* Differential glycosylation of polymeric and monomeric IgA: a possible role in glomerular inflammation in IgA nephropathy. *J. Am. Soc. Nephrol. JASN* **17**, 3529–3539 (2006).
123. Zauner, G. *et al.* Glycoproteomic analysis of antibodies. *Mol. Cell. Proteomics MCP* **12**, 856–865 (2013).
124. Bondt, A. *et al.* Longitudinal monitoring of immunoglobulin A glycosylation during pregnancy by simultaneous MALDI-FTICR-MS analysis of N- and O-glycopeptides. *Sci. Rep.* **6**, 27955 (2016).
125. Huang, J. *et al.* Site-Specific Glycosylation of Secretory Immunoglobulin A from Human Colostrum. *J Proteome Res* **14**, 1335–1349 (2015).
126. Ohyama, Y. *et al.* Analysis of O -glycoforms of the IgA1 hinge region by sequential deglycosylation. *Sci. Rep.* **10**, 1–11 (2020).
127. Novak, J., Julian, B. A., Mestecky, J. & Renfrow, M. B. Glycosylation of IgA1 and pathogenesis of IgA nephropathy. *Semin. Immunopathol.* **34**, 365–382 (2012).
128. Steffen, U. *et al.* IgA subclasses have different effector functions associated with distinct glycosylation profiles. *Nat. Commun.* **11**, 1–12 (2020).
129. Giannone, C., Fagioli, C., Valetti, C., Sitia, R. & Anelli, T. Roles of N-glycans in the polymerization-dependent aggregation of mutant Ig-μ chains in the early secretory pathway. *Sci. Rep.* **7**, 41815 (2017).
130. Bosseboeuf, A. *et al.* Pro-inflammatory State in Monoclonal Gammopathy of Undetermined Significance and in Multiple Myeloma Is Characterized by Low Sialylation of Pathogen-Specific and Other Monoclonal Immunoglobulins. *Front. Immunol.* **8**, 1347 (2017).
131. Bunker, J. J. & Bendelac, A. IgA Responses to Microbiota. *Immunity* **49**, 211–224 (2018).
132. Le Gallou, S. *et al.* A splenic IgM memory subset with antibacterial specificities is sustained from persistent mucosal responses. *J. Exp. Med.* **215**, 2035–2053 (2018).
133. Magri, G. *et al.* Human Secretory IgM Emerges from Plasma Cells Clonally Related to Gut Memory B Cells and Targets Highly Diverse Commensals. *Immunity* **47**, 118-134.e8 (2017).
134. Meyer-Bahlburg, A. B-1 cells as a source of IgA. *Ann. N. Y. Acad. Sci.* **1362**, 122–131 (2015).
135. Lycke, N. Y. & Bemark, M. The regulation of gut mucosal IgA B-cell responses: recent developments. *Mucosal Immunol.* **10**, 1361–1374 (2017).

136. Ordoñez, C. *et al.* Both B-1a and B-1b cells exposed to Mycobacterium tuberculosis lipids differentiate into IgM antibody-secreting cells. *Immunology* (2018) doi:10.1111/imm.12909.
137. Bunker, J. J. *et al.* Natural polyreactive IgA antibodies coat the intestinal microbiota. *Science* **358**, (2017).
138. Rothstein, T. L., Griffin, D. O., Holodick, N. E., Quach, T. D. & Kaku, H. Human B-1 cells take the stage. *Ann. N. Y. Acad. Sci.* **1285**, 97–114 (2013).
139. Griffin, D. O., Holodick, N. E. & Rothstein, T. L. Human B1 cells in umbilical cord and adult peripheral blood express the novel phenotype CD20+CD27+CD43+CD70−. *J. Exp. Med.* **208**, 67–80 (2011).
140. Roy, B. *et al.* An Intrinsic Propensity of Murine Peritoneal B1b Cells to Switch to IgA in Presence of TGF-β and Retinoic Acid. *PLOS ONE* **8**, e82121 (2013).
141. Robak, O. H. *et al.* Antibiotic treatment–induced secondary IgA deficiency enhances susceptibility to *Pseudomonas aeruginosa* pneumonia. *J. Clin. Invest.* **128**, 3535–3545 (2018).
142. Mishima, Y. *et al.* Microbiota maintain colonic homeostasis by activating TLR2/MyD88/PI3K signaling in IL-10-producing regulatory B cells. *J. Clin. Invest.* **130**, 3702–3716 (2019).
143. Xia, L. & Gildersleeve, J. C. Anti-glycan IgM repertoires in newborn human cord blood. *PLOS ONE* **14**, e0218575 (2019).
144. Proietti, M. *et al.* ATP released by intestinal bacteria limits the generation of protective IgA against enteropathogens. *Nat. Commun.* **10**, (2019).
145. Melo-Gonzalez, F. *et al.* Antigen-presenting ILC3 regulate T cell-dependent IgA responses to colonic mucosal bacteria. *J. Exp. Med.* **216**, 728–742 (2019).
146. Lindner, C. *et al.* Age, microbiota, and T cells shape diverse individual IgA repertoires in the intestineIntestinal IgA repertoire diversity. *J. Exp. Med.* **209**, 365–377 (2012).
147. Perruzza, L. *et al.* Enrichment of intestinal Lactobacillus by enhanced secretory IgA coating alters glucose homeostasis in P2rx7 −/− mice. *Sci. Rep.* **9**, 1–11 (2019).
148. Cao, A. T. *et al.* Interleukin (IL)-21 promotes intestinal IgA response to microbiota. *Mucosal Immunol.* **8**, 1072–1082 (2015).
149. Nagashima, K. *et al.* Identification of subepithelial mesenchymal cells that induce IgA and diversify gut microbiota. *Nat. Immunol.* **18**, 675–682 (2017).
150. Cho, H. *et al.* Defective IgA response to atypical intestinal commensals in IL-21 receptor deficiency reshapes immune cell homeostasis and mucosal immunity. *Mucosal Immunol.* **12**, 85–96 (2019).
151. Neumann, C. *et al.* c-Maf-dependent Treg cell control of intestinal TH17 cells and IgA establishes host-microbiota homeostasis. *Nat. Immunol.* **20**, 471–481 (2019).
152. Capron, M. *et al.* [Existence and function of a receptor for immunoglobulin A on human eosinophils]. *C. R. Acad. Sci. III* **307**, 397–402 (1988).
153. Honorio-França, A. C., Launay, P., Carneiro-Sampaio, M. M. & Monteiro, R. C. Colostral neutrophils express Fc alpha receptors (CD89) lacking gamma chain association and mediate noninflammatory properties of secretory IgA. *J. Leukoc. Biol.* **69**, 289–296 (2001).
154. Patry, C., Sibille, Y., Lehuen, A. & Monteiro, R. C. Identification of Fc alpha receptor (CD89) isoforms generated by alternative splicing that are differentially expressed between blood monocytes and alveolar macrophages. *J. Immunol. Baltim. Md 1950* **156**, 4442–4448 (1996).
155. Geissmann, F. *et al.* A subset of human dendritic cells expresses IgA Fc receptor (CD89), which mediates internalization and activation upon cross-linking by IgA complexes. *J. Immunol. Baltim. Md 1950* **166**, 346–352 (2001).
156. Hamre, R., Farstad, I. N., Brandtzaeg, P. & Morton, H. C. Expression and modulation of the human immunoglobulin A Fc receptor (CD89) and the FcR gamma chain on myeloid cells in blood and tissue. *Scand. J. Immunol.* **57**, 506–516 (2003).
157. Togo, S., Shimokawa, T., Fukuchi, Y. & Ra, C. Alternative splicing of myeloid IgA Fc receptor (FcαR, CD89) transcripts in inflammatory responses. *FEBS Lett.* **535**, 205–209 (2003).
158. Wang, R., Fu, Y., Zhao, Q., Pan, L. & Zhang, W. Human Fcalpha/muR and pIgR distribute differently in intestinal tissues.

Biochem. Biophys. Res. Commun. **381**, 148–152 (2009).
159. Shibuya, A. & Honda, S. Immune regulation by Fcα/μ receptor (CD351) on marginal zone B cells and follicular dendritic cells. *Immunol. Rev.* **268**, 288–295 (2015).
160. Honda, S. *et al.* Marginal zone B cells exacerbate endotoxic shock via interleukin-6 secretion induced by Fcα/μR-coupled TLR4 signalling. *Nat. Commun.* **7**, ncomms11498 (2016).
161. Marsee, D. K., Pinkus, G. S. & Yu, H. CD71 (Transferrin Receptor)An Effective Marker for Erythroid Precursors in Bone Marrow Biopsy Specimens. *Am. J. Clin. Pathol.* **134**, 429–435 (2010).
162. Moura, I. C. *et al.* Glycosylation and size of IgA1 are essential for interaction with mesangial transferrin receptor in IgA nephropathy. *J. Am. Soc. Nephrol. JASN* **15**, 622–634 (2004).
163. Matysiak-Budnik, T. *et al.* Secretory IgA mediates retrotranscytosis of intact gliadin peptides via the transferrin receptor in celiac disease. *J. Exp. Med.* **205**, 143–154 (2008).
164. Abed, J. *et al.* Abnormal apical-to-basal transport of dietary ovalbumin by secretory IgA stimulates a mucosal Th1 response. *Mucosal Immunol.* **7**, 315–324 (2014).
165. Jameson, B. *et al.* Expression of DC-SIGN by dendritic cells of intestinal and genital mucosae in humans and rhesus macaques. *J. Virol.* **76**, 1866–1875 (2002).
166. van den Berg, L. M., Gringhuis, S. I. & Geijtenbeek, T. B. H. An evolutionary perspective on C-type lectins in infection and immunity. *Ann. N. Y. Acad. Sci.* **1253**, 149–158 (2012).
167. Erbacher, A., Gieseke, F., Handgretinger, R. & Müller, I. Dendritic cells: functional aspects of glycosylation and lectins. *Hum. Immunol.* **70**, 308–312 (2009).
168. Sánchez-Navarro, M. & Rojo, J. Targeting DC-SIGN with carbohydrate multivalent systems. *Drug News Perspect.* **23**, 557–572 (2010).
169. Baumann, J., Park, C. G. & Mantis, N. J. Recognition of secretory IgA by DC-SIGN: implications for immune surveillance in the intestine. *Immunol. Lett.* **131**, 59–66 (2010).
170. Agarwal, S. *et al.* Human Fc Receptor-like 3 Inhibits Regulatory T Cell Function and Binds Secretory IgA. *Cell Rep.* **30**, 1292-1299.e3 (2020).
171. Armitage, C. W., O'Meara, C. P. & Beagley, K. W. Chlamydial infection enhances expression of the polymeric immunoglobulin receptor (pIgR) and transcytosis of IgA. *Am. J. Reprod. Immunol. N. Y. N 1989* **77**, (2017).
172. Reséndiz-Albor, A. A. *et al.* Regionalization of pIgR expression in the mucosa of mouse small intestine. *Immunol. Lett.* **128**, 59–67 (2010).
173. Honjo, K. *et al.* Altered Ig levels and antibody responses in mice deficient for the Fc receptor for IgM (FcμR). *Proc. Natl. Acad. Sci.* **109**, 15882–15887 (2012).
174. Ouchida, R. *et al.* Critical role of the IgM Fc receptor in IgM homeostasis, B-cell survival, and humoral immune responses. *Proc Natl Acad Sci* **109**, E2699–E2706 (2012).
175. Choi, S.-C. *et al.* Mouse IgM Fc receptor, FCMR, promotes B cell development and modulates antigen-driven immune responses. *J. Immunol. Baltim. Md 1950* **190**, 987–996 (2013).
176. Nguyen, T., Elsner, R. & Baumgarth, N. Natural IgM Prevents Autoimmunity by Enforcing B Cell Central Tolerance Induction. *J Immunol* **194**, 1489–1502 (2015).
177. Fujimoto, K. *et al.* Antigen-Specific Mucosal Immunity Regulates Development of Intestinal Bacteria-Mediated Diseases. *Gastroenterology* **157**, 1530-1543.e4 (2019).
178. Hansen, I. S., Hoepel, W., Zaat, S. A. J., Baeten, D. L. P. & den Dunnen, J. Serum IgA Immune Complexes Promote Proinflammatory Cytokine Production by Human Macrophages, Monocytes, and Kupffer Cells through FcαRI-TLR Cross-Talk. *J. Immunol. Baltim. Md 1950* **199**, 4124–4131 (2017).
179. Fransen, F. *et al.* BALB/c and C57BL/6 Mice Differ in Polyreactive IgA Abundance, which Impacts the Generation of Antigen-Specific IgA and Microbiota Diversity. *Immunity* **43**, 527–540 (2015).
180. Mikulic, J., Bioley, G. & Corthésy, B. SIgA-Shigella Immune Complexes

Interact with Dectin-1 and SIGNR3 to Differentially Regulate Mouse Peyer's Patch and Mesenteric Lymph Node Dendritic Cell's Responsiveness. *J. Mol. Biol.* **429**, 2387–2400 (2017).
181. Hashizume-Takizawa, T. *et al.* Distinct roles for Peyer's patch B cells for induction of antigen-specific IgA antibody responses in mice administered oral recombinant Salmonella. *Int. Immunol.* **31**, 531–541 (2019).
182. Okai, S. *et al.* High-affinity monoclonal IgA regulates gut microbiota and prevents colitis in mice. *Nat Microbiol* **1**, 16103 (2016).
183. Boullier, S. *et al.* Secretory IgA-mediated neutralization of Shigella flexneri prevents intestinal tissue destruction by down-regulating inflammatory circuits. *J. Immunol. Baltim. Md 1950* **183**, 5879–5885 (2009).
184. Fernandez, M. I. *et al.* Anti-inflammatory role for intracellular dimeric immunoglobulin a by neutralization of lipopolysaccharide in epithelial cells. *Immunity* **18**, 739–749 (2003).
185. Bioley, G. *et al.* Plasma-Derived Polyreactive Secretory-Like IgA and IgM Opsonizing Salmonella enterica Typhimurium Reduces Invasion and Gut Tissue Inflammation through Agglutination. *Front. Immunol.* **8**, 1043 (2017).
186. Murthy, A. K. *et al.* Mannose-containing oligosaccharides of non-specific human secretory immunoglobulin A mediate inhibition of Vibrio cholerae biofilm formation. *PloS One* **6**, e16847 (2011).
187. Corthésy, B. Role of secretory immunoglobulin A and secretory component in the protection of mucosal surfaces. *Future Microbiol.* **5**, 817–829 (2010).
188. Malik, A. *et al.* IL-33 regulates the IgA-microbiota axis to restrain IL-1α–dependent colitis and tumorigenesis. *J Clin Invest* (2016) doi:10.1172/JCI88625.
189. Koch, M. A. *et al.* Maternal IgG and IgA Antibodies Dampen Mucosal T Helper Cell Responses in Early Life. *Cell* **165**, 827–841 (2016).
190. Gopalakrishna, K. P. *et al.* Maternal IgA protects against the development of necrotizing enterocolitis in preterm infants. *Nat. Med.* **25**, 1110–1115 (2019).
191. Diana, J. *et al.* Secretory IgA Induces Tolerogenic Dendritic Cells through SIGNR1 Dampening Autoimmunity in Mice. *J. Immunol.* **191**, 2335–2343 (2013).
192. Mestecky, J. & Russell, M. W. Specific antibody activity, glycan heterogeneity and polyreactivity contribute to the protective activity of S-IgA at mucosal surfaces. *Immunol. Lett.* **124**, 57–62 (2009).
193. Wold, A. E. *et al.* Secretory immunoglobulin A carries oligosaccharide receptors for Escherichia coli type 1 fimbrial lectin. *Infect. Immun.* **58**, 3073–3077 (1990).
194. Kamada, N., Seo, S.-U., Chen, G. Y. & Núñez, G. Role of the gut microbiota in immunity and inflammatory disease. *Nat. Rev. Immunol.* **13**, 321–335 (2013).
195. Kurashima, Y. & Kiyono, H. Mucosal Ecological Network of Epithelium and Immune Cells for Gut Homeostasis and Tissue Healing. *Annu. Rev. Immunol.* **35**, 119–147 (2017).
196. Ruane, D. *et al.* Microbiota regulate the ability of lung dendritic cells to induce IgA class-switch recombination and generate protective gastrointestinal immune responses. *J. Exp. Med.* **213**, 53–73 (2016).
197. Mikulic, J., Longet, S., Favre, L., Benyacoub, J. & Corthesy, B. Secretory IgA in complex with Lactobacillus rhamnosus potentiates mucosal dendritic cell-mediated Treg cell differentiation via TLR regulatory proteins, RALDH2 and secretion of IL-10 and TGF-β. *Cell. Mol. Immunol.* **14**, 546–556 (2017).
198. Jia, L. *et al.* Tolerogenic dendritic cells induced the enrichment of CD4+Foxp3+ regulatory T cells via TGF-β in mesenteric lymph nodes of murine LPS-induced tolerance model. *Clin. Immunol. Orlando Fla* **197**, 118–129 (2018).
199. Hansen, I. S. *et al.* FcαRI co-stimulation converts human intestinal CD103+ dendritic cells into pro-inflammatory cells through glycolytic reprogramming. *Nat. Commun.* **9**, 863 (2018).
200. Shen, C., Detry, B., Lecocq, M. & Pilette, C. A novel IgA/Delta-like 4/Notch axis induces immunosuppressive activity in human dendritic cells. *Clin. Immunol.* **168**, 37–46 (2016).

201. Hoces, D., Arnoldini, M., Diard, M., Loverdo, C. & Slack, E. Growing, evolving and sticking in a flowing environment: understanding IgA interactions with bacteria in the gut. *Immunology* **159**, 52–62 (2020).
202. Bansept, F. *et al.* Enchained growth and cluster dislocation: A possible mechanism for microbiota homeostasis. *PLoS Comput. Biol.* **15**, (2019).
203. Moor, K. *et al.* High-avidity IgA protects the intestine by enchaining growing bacteria. *Nature* **544**, 498–502 (2017).
204. Okai, S. *et al.* Intestinal IgA as a modulator of the gut microbiota. *Gut Microbes* **8**, 486–492 (2017).
205. Briliūtė, J. *et al.* Complex N -glycan breakdown by gut Bacteroides involves an extensive enzymatic apparatus encoded by multiple co-regulated genetic loci. *Nat. Microbiol.* **4**, 1571–1581 (2019).
206. Joglekar, P. *et al.* Intestinal IgA Regulates Expression of a Fructan Polysaccharide Utilization Locus in Colonizing Gut Commensal Bacteroides thetaiotaomicron. *mBio* **10**, (2019).
207. Bergstrom, K. S. B. & Xia, L. Mucin-type O-glycans and their roles in intestinal homeostasis. *Glycobiology* **23**, 1026–1037 (2013).
208. Catanzaro, J. R. *et al.* IgA-deficient humans exhibit gut microbiota dysbiosis despite production of compensatory IgM (preprint available at www.biorxiv.org). (2018).
209. Fadlallah, J. *et al.* Microbial ecology perturbation in human IgA deficiency. *Sci. Transl. Med.* **10**, (2018).
210. Sterlin, D. *et al.* Immune/microbial interface perturbation in human IgA deficiency. *Gut Microbes* **10**, 429–433 (2019).
211. Fadlallah, J. *et al.* Synergistic convergence of microbiota-specific systemic IgG and secretory IgA. *J. Allergy Clin. Immunol.* **143**, 1575-1585.e4 (2019).
212. Donaldson, G. P. *et al.* Gut microbiota utilize immunoglobulin A for mucosal colonization. *Science* **360**, 795–800 (2018).
213. Schofield, W. B. & Palm, N. W. Gut Microbiota: IgA Protects the Pioneers. *Curr. Biol. CB* **28**, R1117–R1119 (2018).
214. den Besten, G. *et al.* The role of short-chain fatty acids in the interplay between diet, gut microbiota, and host energy metabolism. *J. Lipid Res.* **54**, 2325–2340 (2013).
215. Sun, J. *et al.* IgA-Targeted Lactobacillus jensenii Modulated Gut Barrier and Microbiota in High-Fat Diet-Fed Mice. *Front. Microbiol.* **10**, (2019).
216. Bunker, J. J. *et al.* B cell superantigens in the human intestinal microbiota. *Sci. Transl. Med.* **11**, (2019).
217. Uchimura, Y. *et al.* Antibodies Set Boundaries Limiting Microbial Metabolite Penetration and the Resultant Mammalian Host Response. *Immunity* **49**, 545-559.e5 (2018).
218. Kawashima, T. *et al.* The molecular mechanism for activating IgA production by Pediococcus acidilactici K15 and the clinical impact in a randomized trial. *Sci. Rep.* **8**, 5065 (2018).
219. Arai, S. *et al.* Orally administered heat-killed Lactobacillus paracasei MCC1849 enhances antigen-specific IgA secretion and induces follicular helper T cells in mice. *PloS One* **13**, e0199018 (2018).
220. Sterlin, D. *et al.* Human IgA binds a diverse array of commensal bacteria. *J. Exp. Med.* **217**, (2020).
221. Rollenske, T. *et al.* Cross-specificity of protective human antibodies against Klebsiella pneumoniae LPS O-antigen. *Nat. Immunol.* **19**, 617–624 (2018).
222. Bello-Gil, D. *et al.* The Formation of Glycan-Specific Natural Antibodies Repertoire in GalT-KO Mice Is Determined by Gut Microbiota. *Front. Immunol.* **10**, (2019).
223. Khan, A. A. *et al.* Polymorphic Immune Mechanisms Regulate Commensal Repertoire. *Cell Rep.* **29**, 541-550.e4 (2019).
224. Pettengill, M. A. *et al.* Distinct TLR-mediated cytokine production and immunoglobulin secretion in human newborn naïve B cells. *Innate Immun.* **22**, 433–443 (2016).
225. Janzon, A. *et al.* Interactions between the Gut Microbiome and Mucosal Immunoglobulins A, M, and G in the Developing Infant Gut. *mSystems* **4**, (2019).
226. Matsui, S. *et al.* Dysregulation of Intestinal Microbiota Elicited by Food

Allergy Induces IgA-Mediated Oral Dysbiosis. *Infect. Immun.* **88**, (2019).
227. Hara, S. *et al.* Dietary Antigens Induce Germinal Center Responses in Peyer's Patches and Antigen-Specific IgA Production. *Front. Immunol.* **10**, (2019).
228. Luck, H. *et al.* Gut-associated IgA+ immune cells regulate obesity-related insulin resistance. *Nat. Commun.* **10**, (2019).
229. Abreu, M. T. Toll-like receptor signalling in the intestinal epithelium: how bacterial recognition shapes intestinal function. *Nat. Rev. Immunol.* **10**, 131–144 (2010).
230. Bonner, A., Almogren, A., Furtado, P. B., Kerr, M. A. & Perkins, S. J. The Nonplanar Secretory IgA2 and Near Planar Secretory IgA1 Solution Structures Rationalize Their Different Mucosal Immune Responses. *J. Biol. Chem.* **284**, 5077–5087 (2009).
231. Ladjeva, I., Peterman, J. H. & Mestecky, J. IgA subclasses of human colostral antibodies specific for microbial and food antigens. *Clin. Exp. Immunol.* **78**, 85–90 (1989).
232. Corthésy, B. Multi-Faceted Functions of Secretory IgA at Mucosal Surfaces. *Front Immunol* **4**, (2013).
233. Ungaro, R., Mehandru, S., Allen, P. B., Peyrin-Biroulet, L. & Colombel, J.-F. Ulcerative colitis. *The Lancet* **389**, 1756–1770 (2017).
234. Feuerstein, J. D. & Cheifetz, A. S. Crohn Disease: Epidemiology, Diagnosis, and Management. *Mayo Clin. Proc.* **92**, 1088–1103 (2017).
235. Molodecky, N. A. *et al.* Increasing incidence and prevalence of the inflammatory bowel diseases with time, based on systematic review. *Gastroenterology* **142**, 46-54.e42; quiz e30 (2012).
236. Kaplan, G. G. The global burden of IBD: from 2015 to 2025. *Nat. Rev. Gastroenterol. Hepatol.* **12**, 720–727 (2015).
237. Brotherton, C. S., Martin, C. A., Long, M. D., Kappelman, M. D. & Sandler, R. S. Avoidance of Fiber Is Associated With Greater Risk of Crohn's Disease Flare in a 6-Month Period. *Clin. Gastroenterol. Hepatol. Off. Clin. Pract. J. Am. Gastroenterol. Assoc.* **14**, 1130–1136 (2016).
238. Silverberg, M. S. *et al.* A population- and family-based study of Canadian families reveals association of HLA DRB1*0103 with colonic involvement in inflammatory bowel disease. *Inflamm. Bowel Dis.* **9**, 1–9 (2003).
239. Cleynen, I. *et al.* Genetic factors conferring an increased susceptibility to develop Crohn's disease also influence disease phenotype: results from the IBDchip European Project. *Gut* **62**, 1556–1565 (2013).
240. Newman, B. *et al.* CARD15 and HLA DRB1 alleles influence susceptibility and disease localization in Crohn's disease. *Am. J. Gastroenterol.* **99**, 306–315 (2004).
241. Venkateswaran, S. *et al.* Enhanced Contribution of HLA in Pediatric Onset Ulcerative Colitis. *Inflamm. Bowel Dis.* **24**, 829–838 (2018).
242. Goyette, P. *et al.* High-density mapping of the MHC identifies a shared role for HLA-DRB1*01:03 in inflammatory bowel diseases and heterozygous advantage in ulcerative colitis. *Nat. Genet.* **47**, 172–179 (2015).
243. Economou, M., Trikalinos, T. A., Loizou, K. T., Tsianos, E. V. & Ioannidis, J. P. A. Differential effects of NOD2 variants on Crohn's disease risk and phenotype in diverse populations: a metaanalysis. *Am. J. Gastroenterol.* **99**, 2393–2404 (2004).
244. Cuthbert, A. P. *et al.* The contribution of NOD2 gene mutations to the risk and site of disease in inflammatory bowel disease. *Gastroenterology* **122**, 867–874 (2002).
245. Ogura, Y. *et al.* A frameshift mutation in NOD2 associated with susceptibility to Crohn's disease. *Nature* **411**, 603–606 (2001).
246. Philpott, D. J. & Viala, J. Towards an understanding of the role of NOD2/CARD15 in the pathogenesis of Crohn's disease. *Best Pract. Res. Clin. Gastroenterol.* **18**, 555–568 (2004).
247. Travassos, L. H. *et al.* Nod1 and Nod2 direct autophagy by recruiting ATG16L1 to the plasma membrane at the site of bacterial entry. *Nat. Immunol.* **11**, 55–62 (2010).
248. Franke, A. *et al.* Meta-Analysis Increases to 71 the Tally of Confirmed Crohn's Disease Susceptibility Loci. *Nat. Genet.* **42**, 1118–1125 (2010).

249. Hall, A. B., Tolonen, A. C. & Xavier, R. J. Human genetic variation and the gut microbiome in disease. *Nat. Rev. Genet.* **18**, 690–699 (2017).
250. Cheng, Y. *et al.* Association between TLR2 and TLR4 Gene Polymorphisms and the Susceptibility to Inflammatory Bowel Disease: A Meta-Analysis. *PLOS ONE* **10**, e0126803 (2015).
251. Boltin, D., Perets, T. T., Vilkin, A. & Niv, Y. Mucin function in inflammatory bowel disease: an update. *J. Clin. Gastroenterol.* **47**, 106–111 (2013).
252. Liso, M. *et al.* A Specific Mutation in Muc2 Determines Early Dysbiosis in Colitis-Prone Winnie Mice. *Inflamm. Bowel Dis.* doi:10.1093/ibd/izz279.
253. Genome-wide association study of ulcerative colitis identifies three new susceptibility loci, including the HNF4A region. *Nat. Genet.* **41**, 1330–1334 (2009).
254. Jostins, L. *et al.* Host-microbe interactions have shaped the genetic architecture of inflammatory bowel disease. *Nature* **491**, 119–124 (2012).
255. Cleynen, I. *et al.* Inherited determinants of Crohn's disease and ulcerative colitis phenotypes: a genetic association study. *The Lancet* **387**, 156–167 (2016).
256. Nimmo, E. R. *et al.* Genome-wide methylation profiling in Crohn's disease identifies altered epigenetic regulation of key host defense mechanisms including the Th17 pathway. *Inflamm. Bowel Dis.* **18**, 889–899 (2012).
257. Tsaprouni, L. G., Ito, K., Powell, J. J., Adcock, I. M. & Punchard, N. Differential patterns of histone acetylation in inflammatory bowel diseases. *J. Inflamm. Lond. Engl.* **8**, 1 (2011).
258. Ventham, N. T., Kennedy, N. A., Nimmo, E. R. & Satsangi, J. Beyond Gene Discovery in Inflammatory Bowel Disease: The Emerging Role of Epigenetics. *Gastroenterology* **145**, 293–308 (2013).
259. Shaw, S. Y., Blanchard, J. F. & Bernstein, C. N. Association between the use of antibiotics and new diagnoses of Crohn's disease and ulcerative colitis. *Am. J. Gastroenterol.* **106**, 2133–2142 (2011).
260. Lewis, J. D. *et al.* Inflammation, Antibiotics, and Diet as Environmental Stressors of the Gut Microbiome in Pediatric Crohn's Disease. *Cell Host Microbe* **18**, 489–500 (2015).
261. García Rodríguez, L. A., Ruigómez, A. & Panés, J. Acute gastroenteritis is followed by an increased risk of inflammatory bowel disease. *Gastroenterology* **130**, 1588–1594 (2006).
262. Gradel, K. O. *et al.* Increased short- and long-term risk of inflammatory bowel disease after salmonella or campylobacter gastroenteritis. *Gastroenterology* **137**, 495–501 (2009).
263. Mikhailov, T. A., Christensen, M. A. & Furner, S. E. A matched case-control study of breastfeeding and other factors in pediatric Crohn's disease. *Adv. Pediatr. Res.* **4**, 1–10 (2017).
264. Calkins, B. M. A meta-analysis of the role of smoking in inflammatory bowel disease. *Dig. Dis. Sci.* **34**, 1841–1854 (1989).
265. Sands, B. E. *et al.* Risk of early surgery for Crohn's disease: implications for early treatment strategies. *Am. J. Gastroenterol.* **98**, 2712–2718 (2003).
266. Benjamin, J. L. *et al.* Smokers with active Crohn's disease have a clinically relevant dysbiosis of the gastrointestinal microbiota. *Inflamm. Bowel Dis.* **18**, 1092–1100 (2012).
267. Xu, L. *et al.* Systematic review with meta-analysis: breastfeeding and the risk of Crohn's disease and ulcerative colitis. *Aliment. Pharmacol. Ther.* **46**, 780–789 (2017).
268. Klement, E., Cohen, R. V., Boxman, J., Joseph, A. & Reif, S. Breastfeeding and risk of inflammatory bowel disease: a systematic review with meta-analysis. *Am. J. Clin. Nutr.* **80**, 1342–1352 (2004).
269. Bager, P., Simonsen, J., Nielsen, N. M. & Frisch, M. Cesarean section and offspring's risk of inflammatory bowel disease: a national cohort study. *Inflamm. Bowel Dis.* **18**, 857–862 (2012).
270. Malmborg, P., Bahmanyar, S., Grahnquist, L., Hildebrand, H. & Montgomery, S. Cesarean section and the risk of pediatric Crohn's disease. *Inflamm. Bowel Dis.* **18**, 703–708 (2012).
271. Khalili, H. *et al.* Hormone therapy increases risk of ulcerative colitis but not Crohn's disease. *Gastroenterology* **143**, 1199–1206 (2012).

272. Cornish, J. A. *et al.* The risk of oral contraceptives in the etiology of inflammatory bowel disease: a meta-analysis. *Am. J. Gastroenterol.* **103**, 2394–2400 (2008).
273. Beaugerie, L. *et al.* Impact of cessation of smoking on the course of ulcerative colitis. *Am. J. Gastroenterol.* **96**, 2113–2116 (2001).
274. To, N., Ford, A. C. & Gracie, D. J. Systematic review with meta-analysis: the effect of tobacco smoking on the natural history of ulcerative colitis. *Aliment. Pharmacol. Ther.* **44**, 117–126 (2016).
275. Koloski, N. A., Bret, L. & Radford-Smith, G. Hygiene hypothesis in inflammatory bowel disease: A critical review of the literature. *World J. Gastroenterol. WJG* **14**, 165–173 (2008).
276. Beaugerie, L. *et al.* Differences in epidemiological features between ulcerative colitis and Crohn's disease: The early life-programmed versus late dysbiosis hypothesis. *Med. Hypotheses* **115**, 19–21 (2018).
277. Torres, J., Mehandru, S., Colombel, J.-F. & Peyrin-Biroulet, L. Crohn's disease. *The Lancet* **389**, 1741–1755 (2017).
278. Cheifetz, A. S. Management of active Crohn disease. *JAMA* **309**, 2150–2158 (2013).
279. Gomollón, F. *et al.* 3rd European Evidence-based Consensus on the Diagnosis and Management of Crohn's Disease 2016: Part 1: Diagnosis and Medical Management. *J. Crohns Colitis* **11**, 3–25 (2017).
280. Marteau, P. *et al.* Review article: gut flora and inflammatory bowel disease. *Aliment. Pharmacol. Ther.* **20 Suppl 4**, 18–23 (2004).
281. Limketkai, B. N. *et al.* Levels of Vitamin D Are Low After Crohn's Disease Is Established But Not Before. *Clin. Gastroenterol. Hepatol. Off. Clin. Pract. J. Am. Gastroenterol. Assoc.* (2019) doi:10.1016/j.cgh.2019.09.034.
282. Zeissig, S. *et al.* Changes in expression and distribution of claudin 2, 5 and 8 lead to discontinuous tight junctions and barrier dysfunction in active Crohn's disease. *Gut* **56**, 61–72 (2007).
283. Lerner, A. & Matthias, T. Changes in intestinal tight junction permeability associated with industrial food additives explain the rising incidence of autoimmune disease. *Autoimmun. Rev.* **14**, 479–489 (2015).
284. Pochard, C. *et al.* Defects in 15-HETE Production and Control of Epithelial Permeability by Human Enteric Glial Cells From Patients With Crohn's Disease. *Gastroenterology* **150**, 168–180 (2016).
285. Marini, M. *et al.* TNF-alpha neutralization ameliorates the severity of murine Crohn's-like ileitis by abrogation of intestinal epithelial cell apoptosis. *Proc. Natl. Acad. Sci. U. S. A.* **100**, 8366–8371 (2003).
286. Su, L. *et al.* TNFR2 activates MLCK-dependent tight junction dysregulation to cause apoptosis-mediated barrier loss and experimental colitis. *Gastroenterology* **145**, 407–415 (2013).
287. Nava, P. *et al.* Interferon-gamma regulates intestinal epithelial homeostasis through converging beta-catenin signaling pathways. *Immunity* **32**, 392–402 (2010).
288. Coskun, M. Intestinal Epithelium in Inflammatory Bowel Disease. *Front. Med.* **1**, (2014).
289. Vrakas, S. *et al.* Intestinal Bacteria Composition and Translocation of Bacteria in Inflammatory Bowel Disease. *PloS One* **12**, e0170034 (2017).
290. Souza, H. S. P. de & Fiocchi, C. Immunopathogenesis of IBD: current state of the art. *Nat. Rev. Gastroenterol. Hepatol.* **13**, 13–27 (2016).
291. Liu, T.-C. *et al.* Interaction between smoking and ATG16L1T300A triggers Paneth cell defects in Crohn's disease. *J. Clin. Invest.* **128**, 5110–5122 (2018).
292. Palmieri, O. *et al.* Functional Implications of MicroRNAs in Crohn's Disease Revealed by Integrating MicroRNA and Messenger RNA Expression Profiling. *Int. J. Mol. Sci.* **18**, (2017).
293. Lin, X.-T. *et al.* MicroRNA-143 Targets ATG2B to Inhibit Autophagy and Increase Inflammatory Responses in Crohn's Disease. *Inflamm. Bowel Dis.* **24**, 781–791 (2018).
294. Cadwell, K. *et al.* A key role for autophagy and the autophagy gene Atg16l1 in mouse and human intestinal Paneth cells. *Nature* **456**, 259–263 (2008).

295. Aschard, H. *et al.* Genetic effects on the commensal microbiota in inflammatory bowel disease patients. *PLOS Genet.* **15**, e1008018 (2019).
296. Courth, L. F. *et al.* Crohn's disease-derived monocytes fail to induce Paneth cell defensins. *Proc. Natl. Acad. Sci. U. S. A.* **112**, 14000–14005 (2015).
297. Kabeerdoss, J., Jayakanthan, P., Pugazhendhi, S. & Ramakrishna, B. S. Alterations of mucosal microbiota in the colon of patients with inflammatory bowel disease revealed by real time polymerase chain reaction amplification of 16S ribosomal ribonucleic acid. *Indian J. Med. Res.* **142**, 23–32 (2015).
298. Rojas-Feria, M. *et al.* Modulation of faecal metagenome in Crohn's disease: Role of microRNAs as biomarkers. *World J. Gastroenterol.* **24**, 5223–5233 (2018).
299. Seksik, P. [Gut microbiota and IBD]. *Gastroenterol. Clin. Biol.* **34 Suppl 1**, S44-51 (2010).
300. Nagalingam, N. A. & Lynch, S. V. Role of the microbiota in inflammatory bowel diseases. *Inflamm. Bowel Dis.* **18**, 968–984 (2012).
301. Gevers, D. *et al.* The treatment-naive microbiome in new-onset Crohn's disease. *Cell Host Microbe* **15**, 382–392 (2014).
302. Rengarajan, S. *et al.* Dynamic immunoglobulin responses to gut bacteria during inflammatory bowel disease. *Gut Microbes* 1–16 (2019) doi:10.1080/19490976.2019.1626683.
303. Quévrain, E. *et al.* Identification of an anti-inflammatory protein from Faecalibacterium prausnitzii, a commensal bacterium deficient in Crohn's disease. *Gut* **65**, 415–425 (2016).
304. Das, P., Ji, B., Kovatcheva-Datchary, P., Bäckhed, F. & Nielsen, J. In vitro co-cultures of human gut bacterial species as predicted from co-occurrence network analysis. *PLOS ONE* **13**, e0195161 (2018).
305. Takahashi, K. *et al.* Reduced Abundance of Butyrate-Producing Bacteria Species in the Fecal Microbial Community in Crohn's Disease. *Digestion* **93**, 59–65 (2016).
306. Yilmaz, B. *et al.* Microbial network disturbances in relapsing refractory Crohn's disease. *Nat. Med.* **25**, 323–336 (2019).
307. Liu, T.-C. *et al.* Paneth cell defects in Crohn's disease patients promote dysbiosis. *JCI Insight* **1**, e86907 (2016).
308. Çekin, A. H. A microbial signature for Crohn's disease. *Turk. J. Gastroenterol. Off. J. Turk. Soc. Gastroenterol.* **28**, 237–238 (2017).
309. Brandtzaeg, P., Carlsen, H. S. & Halstensen, T. S. The B-cell system in inflammatory bowel disease. *Adv. Exp. Med. Biol.* **579**, 149–167 (2006).
310. Calderón-Gómez, E. *et al.* Commensal-Specific CD4(+) Cells From Patients With Crohn's Disease Have a T-Helper 17 Inflammatory Profile. *Gastroenterology* **151**, 489-500.e3 (2016).
311. Lin, R. *et al.* Clinical significance of soluble immunoglobulins A and G and their coated bacteria in feces of patients with inflammatory bowel disease. *J. Transl. Med.* **16**, 359 (2018).
312. Viladomiu, M. *et al.* IgA-coated E. coli enriched in Crohn's disease spondyloarthritis promote TH17-dependent inflammation. *Sci Transl Med* **9**, eaaf9655 (2017).
313. Chen, B. *et al. Adherent Bacteria in the Terminal Ileum of Children Correlates with Increased Th17 Cell Activation and Luminal Secretory IgA.* https://papers.ssrn.com/abstract=3397178 (2019).
314. Preisker, S. *et al.* Crohn's Disease Patients in Remission Display an Enhanced Intestinal IgM^+ B Cell Count in Concert with a Strong Activation of the Intestinal Complement System. *Cells* **8**, (2019).
315. Gupta, S., Basu, S., Bal, V., Rath, S. & George, A. Gut IgA abundance in adult life is a major determinant of resistance to dextran sodium sulfate-colitis and can compensate for the effects of inadequate maternal IgA received by neonates. *Immunology* **158**, 19–34 (2019).
316. Armstrong, H. *et al.* Host immunoglobulin G selectively identifies pathobionts in pediatric inflammatory bowel diseases. *Microbiome* **7**, 1 (2019).
317. Hart, A. L. *et al.* Characteristics of intestinal dendritic cells in inflammatory bowel diseases. *Gastroenterology* **129**, 50–65 (2005).

318. Geremia, A. *et al.* IL-23-responsive innate lymphoid cells are increased in inflammatory bowel disease. *J. Exp. Med.* **208**, 1127–1133 (2011).
319. Bernink, J. H. *et al.* Human type 1 innate lymphoid cells accumulate in inflamed mucosal tissues. *Nat. Immunol.* **14**, 221–229 (2013).
320. Smith, A. M. *et al.* Disordered macrophage cytokine secretion underlies impaired acute inflammation and bacterial clearance in Crohn's disease. *J. Exp. Med.* **206**, 1883–1897 (2009).
321. Kamada, N. *et al.* Unique CD14 intestinal macrophages contribute to the pathogenesis of Crohn disease via IL-23/IFN-gamma axis. *J. Clin. Invest.* **118**, 2269–2280 (2008).
322. Xavier, R. J. & Podolsky, D. K. Unravelling the pathogenesis of inflammatory bowel disease. *Nature* **448**, 427–434 (2007).
323. Britton, G. J. *et al.* Microbiotas from Humans with Inflammatory Bowel Disease Alter the Balance of Gut Th17 and RORγt+ Regulatory T Cells and Exacerbate Colitis in Mice. *Immunity* **50**, 212-224.e4 (2019).
324. Saha, C. *et al.* Monomeric Immunoglobulin A from Plasma Inhibits Human Th17 Responses In Vitro Independent of FcαRI and DC-SIGN. *Front. Immunol.* **8**, 275 (2017).
325. Riaz, T., Sollid, L. M., Olsen, I. & de Souza, G. A. Quantitative Proteomics of Gut-Derived Th1 and Th1/Th17 Clones Reveal the Presence of CD28+ NKG2D-Th1 Cytotoxic CD4+ T cells. *Mol. Cell. Proteomics MCP* **15**, 1007–1016 (2016).
326. Wang, Z. *et al.* T-bet-Expressing B Cells Are Positively Associated with Crohn's Disease Activity and Support Th1 Inflammation. *DNA Cell Biol* **35**, 628–635 (2016).
327. Atarashi, K. *et al.* Ectopic colonization of oral bacteria in the intestine drives TH1 cell induction and inflammation. *Science* **358**, 359–365 (2017).
328. Friedrich, M., Pohin, M. & Powrie, F. Cytokine Networks in the Pathophysiology of Inflammatory Bowel Disease. *Immunity* **50**, 992–1006 (2019).
329. Glocker, E.-O. *et al.* Inflammatory Bowel Disease and Mutations Affecting the Interleukin-10 Receptor. *N. Engl. J. Med.* **361**, 2033–2045 (2009).
330. Spencer, S. D. *et al.* The Orphan Receptor CRF2-4 Is an Essential Subunit of the Interleukin 10 Receptor. *J. Exp. Med.* **187**, 571–578 (1998).
331. Reinisch, W., Reinink, A. R. & Higgins, P. D. R. Factors associated with poor outcomes in adults with newly diagnosed ulcerative colitis. *Clin. Gastroenterol. Hepatol. Off. Clin. Pract. J. Am. Gastroenterol. Assoc.* **13**, 635–642 (2015).
332. Annese, V. *et al.* European evidence based consensus for endoscopy in inflammatory bowel disease. *J. Crohns Colitis* **7**, 982–1018 (2013).
333. Dignass, A. *et al.* Second European evidence-based consensus on the diagnosis and management of ulcerative colitis part 1: definitions and diagnosis. *J. Crohns Colitis* **6**, 965–990 (2012).
334. Johansson, M. E. V. *et al.* Bacteria penetrate the normally impenetrable inner colon mucus layer in both murine colitis models and patients with ulcerative colitis. *Gut* **63**, 281–291 (2014).
335. Podolsky, D. K. & Isselbacher, K. J. Glycoprotein composition of colonic mucosa. Specific alterations in ulcerative colitis. *Gastroenterology* **87**, 991–998 (1984).
336. Mashimo, H., Wu, D. C., Podolsky, D. K. & Fishman, M. C. Impaired defense of intestinal mucosa in mice lacking intestinal trefoil factor. *Science* **274**, 262–265 (1996).
337. Heller, F. *et al.* Interleukin-13 is the key effector Th2 cytokine in ulcerative colitis that affects epithelial tight junctions, apoptosis, and cell restitution. *Gastroenterology* **129**, 550–564 (2005).
338. Schmitz*, H. *et al.* Altered tight junction structure contributes to the impaired epithelial barrier function in ulcerative colitis. *Gastroenterology* **116**, 301–309 (1999).
339. Dubuquoy, L. *et al.* Impaired expression of peroxisome proliferator-activated receptor gamma in ulcerative colitis. *Gastroenterology* **124**, 1265–1276 (2003).
340. Bajer, L. *et al.* Distinct gut microbiota profiles in patients with primary sclerosing cholangitis and ulcerative

colitis. *World J. Gastroenterol.* **23**, 4548–4558 (2017).
341. Mirsepasi-Lauridsen, H. C. *et al.* Disease-Specific Enteric Microbiome Dysbiosis in Inflammatory Bowel Disease. *Front. Med.* **5**, 304 (2018).
342. Machiels, K. *et al.* A decrease of the butyrate-producing species Roseburia hominis and Faecalibacterium prausnitzii defines dysbiosis in patients with ulcerative colitis. *Gut* **63**, 1275–1283 (2014).
343. Frank, D. N. *et al.* Molecular-phylogenetic characterization of microbial community imbalances in human inflammatory bowel diseases. *Proc. Natl. Acad. Sci. U. S. A.* **104**, 13780–13785 (2007).
344. Fuentes, S. *et al.* Microbial shifts and signatures of long-term remission in ulcerative colitis after faecal microbiota transplantation. *ISME J.* **11**, 1877–1889 (2017).
345. Ohkusa, T. & Koido, S. Intestinal microbiota and ulcerative colitis. *J. Infect. Chemother.* **21**, 761–768 (2015).
346. Kiernan, M. G. *et al.* The Human Mesenteric Lymph Node Microbiome Differentiates Between Crohn's Disease and Ulcerative Colitis. *J. Crohns Colitis* **13**, 58–66 (2019).
347. Ishikawa, D. *et al.* The Microbial Composition of Bacteroidetes Species in Ulcerative Colitis Is Effectively Improved by Combination Therapy With Fecal Microbiota Transplantation and Antibiotics. *Inflamm. Bowel Dis.* **24**, 2590–2598 (2018).
348. Yang, H. *et al.* Ulcerative Colitis-associated E. coli pathobionts potentiate colitis in susceptible hosts. *J. Immunol.* **202**, 192.3-192.3 (2019).
349. Sartor, R. B. & Wu, G. D. Roles for Intestinal Bacteria, Viruses, and Fungi in Pathogenesis of Inflammatory Bowel Diseases and Therapeutic Approaches. *Gastroenterology* **152**, 327-339.e4 (2017).
350. Sokol, H. *et al.* Fungal microbiota dysbiosis in IBD. *Gut* gutjnl-2015-310746 (2016) doi:10.1136/gutjnl-2015-310746.
351. Badr-el-Din, S., Trejdosiewicz, L. K., Heatley, R. V. & Losowsky, M. S. Local immunity in ulcerative colitis: evidence for defective secretory IgA production. *Gut* **29**, 1070–1075 (1988).
352. KAZEMI-SHIRAZI, L. *et al.* IgA autoreactivity: a feature common to inflammatory bowel and connective tissue diseases. *Clin. Exp. Immunol.* **128**, 102–109 (2002).
353. Ellerbroek, P. M. *et al.* Neutrophil cytoplasmic antibodies (p-ANCA) in ulcerative colitis. *J. Clin. Pathol.* **47**, 257–262 (1994).
354. Halstensen, T. S., Mollnes, T. E., Garred, P., Fausa, O. & Brandtzaeg, P. Epithelial Deposition of Immunoglobulin G1 and Activated Complement (C3b and Terminal Complement Complex) in Ulcerative Colitis. *Gastroenterology* **98**, 1264–1271 (1990).
355. Thoree, V. C. *et al.* Related IgA1 and IgG producing cells in blood and diseased mucosa in ulcerative colitis. *Gut* **51**, 44–50 (2002).
356. Uo, M. *et al.* Mucosal CXCR4+ IgG plasma cells contribute to the pathogenesis of human ulcerative colitis through FcγR-mediated CD14 macrophage activation. *Gut* **62**, 1734–1744 (2013).
357. Castro-Dopico, T. *et al.* Anti-commensal IgG Drives Intestinal Inflammation and Type 17 Immunity in Ulcerative Colitis. *Immunity* **50**, 1099-1114.e10 (2019).
358. Pearson, C. *et al.* ILC3 GM-CSF production and mobilisation orchestrate acute intestinal inflammation. *eLife* **5**, e10066 (2016).
359. Muthas, D. *et al.* Neutrophils in ulcerative colitis: a review of selected biomarkers and their potential therapeutic implications. *Scand. J. Gastroenterol.* **52**, 125–135 (2017).
360. Zhou, G. *et al.* CD177+ neutrophils as functionally activated neutrophils negatively regulate IBD. *Gut* **67**, 1052–1063 (2018).
361. Poholek, C. H., Dulson, S. J., Zajac, A. J. & Harrington, L. E. IL-21 Controls ILC3 Cytokine Production and Promotes a Protective Phenotype in a Mouse Model of Colitis. *ImmunoHorizons* **3**, 194–202 (2019).
362. Bhatt, B. *et al.* Gpr109a limits microbiota-induced IL-23 production to constrain ILC3-mediated colonic inflammation. *J.*

Immunol. Baltim. Md 1950 **200**, 2905–2914 (2018).
363. Huang, E. *et al.* NKT cells mediate the recruitment of neutrophils by stimulating epithelial chemokine secretion during colitis. *Biochem. Biophys. Res. Commun.* **474**, 252–258 (2016).
364. Bennike, T. B. *et al.* Neutrophil Extracellular Traps in Ulcerative Colitis: A Proteome Analysis of Intestinal Biopsies. *Inflamm. Bowel Dis.* **21**, 2052–2067 (2015).
365. Matsuno, H. *et al.* CD103+ Dendritic Cell Function Is Altered in the Colons of Patients with Ulcerative Colitis. *Inflamm. Bowel Dis.* **23**, 1524–1534 (2017).
366. Rosen, M. J. *et al.* Mucosal Expression of Type 2 and Type 17 Immune Response Genes Distinguishes Ulcerative Colitis From Colon-Only Crohn's Disease in Treatment-Naive Pediatric Patients. *Gastroenterology* **152**, 1345-1357.e7 (2017).
367. Li, J. *et al.* Profiles of Lamina Propria T Helper Cell Subsets Discriminate Between Ulcerative Colitis and Crohn's Disease. *Inflamm. Bowel Dis.* **22**, 1779–1792 (2016).
368. Fuss, I. J. *et al.* Disparate CD4+ lamina propria (LP) lymphokine secretion profiles in inflammatory bowel disease. Crohn's disease LP cells manifest increased secretion of IFN-gamma, whereas ulcerative colitis LP cells manifest increased secretion of IL-5. *J. Immunol. Baltim. Md 1950* **157**, 1261–1270 (1996).
369. Seidelin, J. B. *et al.* IL-33 promotes GATA-3 polarization of gut-derived T cells in experimental and ulcerative colitis. *J. Gastroenterol.* **50**, 180–190 (2015).
370. Inoue, S. *et al.* Characterization of cytokine expression in the rectal mucosa of ulcerative colitis: correlation with disease activity. *Am. J. Gastroenterol.* **94**, 2441–2446 (1999).
371. Feng, B.-S. *et al.* Bcl2L12 mediates effects of protease-activated receptor-2 on the pathogenesis of Th2-dominated responses of patients with ulcerative colitis. *Arch. Biochem. Biophys.* **657**, 8–14 (2018).
372. Zundler, S. *et al.* Blockade of αEβ7 integrin suppresses accumulation of CD8+ and Th9 lymphocytes from patients with IBD in the inflamed gut in vivo. *Gut* **66**, 1936–1948 (2017).
373. Intensified Th9 Response is Associated with the Immunopathogenesis of Active Ulcerative Colitis. doi:10.1080/08820139.2018.1486411.
374. Gerlach, K. *et al.* TH9 cells that express the transcription factor PU.1 drive T cell-mediated colitis via IL-9 receptor signaling in intestinal epithelial cells. *Nat. Immunol.* **15**, 676–686 (2014).
375. Wang, D. *et al.* TL1A modulates the severity of colitis by promoting Th9 differentiation and IL-9 secretion. *Life Sci.* **231**, 116536 (2019).
376. Russell, S. E. *et al.* IL-36α expression is elevated in ulcerative colitis and promotes colonic inflammation. *Mucosal Immunol.* **9**, 1193–1204 (2016).
377. Harusato, A. *et al.* IL-36γ signaling controls the induced regulatory T cell-Th9 cell balance via NFκB activation and STAT transcription factors. *Mucosal Immunol.* **10**, 1455–1467 (2017).
378. Townsend, C. M. *et al.* Antibiotics for induction and maintenance of remission in Crohn's disease. *Cochrane Database Syst. Rev.* **2**, CD012730 (2019).
379. Kirchgesner, J. *et al.* Therapeutic management of inflammatory bowel disease in real-life practice in the current era of anti-TNF agents: analysis of the French administrative health databases 2009-2014. *Aliment. Pharmacol. Ther.* **45**, 37–49 (2017).
380. Harbord, M. *et al.* Third European Evidence-based Consensus on Diagnosis and Management of Ulcerative Colitis. Part 2: Current Management. *J. Crohns Colitis* **11**, 769–784 (2017).
381. Mondot, S. *et al.* Structural robustness of the gut mucosal microbiota is associated with Crohn's disease remission after surgery. *Gut* **65**, 954–962 (2016).
382. Cosnes, J. *et al.* Factors affecting outcomes in Crohn's disease over 15 years. *Gut* **61**, 1140–1145 (2012).
383. Bak, S. H. *et al.* Fecal microbiota transplantation for refractory Crohn's disease. *Intest. Res.* **15**, 244–248 (2017).
384. Kunde, S. *et al.* Safety, tolerability, and clinical response after fecal transplantation in children and young

adults with ulcerative colitis. *J. Pediatr. Gastroenterol. Nutr.* **56**, 597–601 (2013).
385. Shi, Y. *et al.* Fecal Microbiota Transplantation for Ulcerative Colitis: A Systematic Review and Meta-Analysis. *PloS One* **11**, e0157259 (2016).
386. Costello, S. P. *et al.* Systematic review with meta-analysis: faecal microbiota transplantation for the induction of remission for active ulcerative colitis. *Aliment. Pharmacol. Ther.* **46**, 213–224 (2017).
387. Keshteli, A. H., Millan, B. & Madsen, K. L. Pretreatment with antibiotics may enhance the efficacy of fecal microbiota transplantation in ulcerative colitis: a meta-analysis. *Mucosal Immunol.* **10**, 565–566 (2017).
388. Adachi, T. *et al.* CD22 serves as a receptor for soluble IgM. *Eur J Immunol* **42**, 241–7 (2011).
389. Rochereau, N. *et al.* Delivery of antigen to nasal-associated lymphoid tissue microfold cells through secretory IgA targeting local dendritic cells confers protective immunity. *J. Allergy Clin. Immunol.* **137**, 214-222.e2 (2016).
390. Rochereau, N. *et al.* Secretory IgA as a vaccine carrier for delivery of HIV antigen to M cells. *Eur. J. Immunol.* **45**, 773–779 (2015).
391. Catanzaro, J. R. *et al.* IgA-deficient humans exhibit gut microbiota dysbiosis despite secretion of compensatory IgM. *Sci. Rep.* **9**, 1–10 (2019).
392. Bhaskaran, N. *et al.* Role of Short Chain Fatty Acids in Controlling Tregs and Immunopathology During Mucosal Infection. *Front. Microbiol.* **9**, 1995 (2018).
393. LeBlanc, J. G. *et al.* Beneficial effects on host energy metabolism of short-chain fatty acids and vitamins produced by commensal and probiotic bacteria. *Microb. Cell Factories* **16**, 79 (2017).
394. Benus, R. F. J. *et al.* Association between Faecalibacterium prausnitzii and dietary fibre in colonic fermentation in healthy human subjects. *Br. J. Nutr.* **104**, 693–700 (2010).
395. Bosca-Watts, M. M. *et al.* Pathogenesis of Crohn's disease: Bug or no bug. *World J. Gastrointest. Pathophysiol.* **6**, 1–12 (2015).
396. Magri, G. *et al.* Human Secretory IgM Emerges from Plasma Cells Clonally Related to Gut Memory B Cells and Targets Highly Diverse Commensals. *Immunity* **47**, 118-134.e8 (2017).
397. Chen, C.-M., Gong, Y., Zhang, M. & Chen, J.-J. Reciprocal cross-talk between Nod2 and TAK1 signaling pathways. *J. Biol. Chem.* **279**, 25876–25882 (2004).
398. Richardson, W. M. *et al.* Nucleotide-binding oligomerization domain-2 inhibits toll-like receptor-4 signaling in the intestinal epithelium. *Gastroenterology* **139**, 904–917, 917.e1–6 (2010).
399. Al Nabhani, Z. *et al.* Nod2 Deficiency Leads to a Specific and Transmissible Mucosa-associated Microbial Dysbiosis Which Is Independent of the Mucosal Barrier Defect. *J. Crohns Colitis* **10**, 1428–1436 (2016).
400. De Palma, G. *et al.* Intestinal dysbiosis and reduced immunoglobulin-coated bacteria associated with coeliac disease in children. *BMC Microbiol.* **10**, 63 (2010).
401. Joossens, M. *et al.* Dysbiosis of the faecal microbiota in patients with Crohn's disease and their unaffected relatives. *Gut* **60**, 631–637 (2011).
402. Leake, I. IBD: Microbial drivers of IBD identified by levels of IgA coating. *Nat Rev Gastroenterol Hepatol* **11**, 642 (2014).
403. Cobrin, G. & Abreu, M. Defects in mucosal immunity leading to Crohn's disease. *Immunol Rev* **206**, 277–95 (2005).
404. Danese, S., Vuitton, L. & Peyrin-Biroulet, L. Biologic agents for IBD: practical insights. *Nat. Rev. Gastroenterol. Hepatol.* **12**, 537–545 (2015).
405. Ananthakrishnan, A. N. *et al.* Gut Microbiome Function Predicts Response to Anti-integrin Biologic Therapy in Inflammatory Bowel Diseases. *Cell Host Microbe* **21**, 603-610.e3 (2017).
406. Ollech, J. E. *et al.* Efficacy and safety of induction therapy with calcineurin inhibitors followed by vedolizumab maintenance in 71 patients with severe steroid-refractory ulcerative colitis. *Aliment. Pharmacol. Ther.* **51**, 637–643 (2020).
407. Leonard, K. A. *et al.* Discovery of a Gut-Restricted JAK Inhibitor for the

Treatment of Inflammatory Bowel Disease. *J. Med. Chem.* **63**, 2915–2929 (2020).
408. Sun, Y., Shi, X., Zheng, X., Nie, S. & Xu, X. Inhibition of dextran sodium sulfate-induced colitis in mice by baker's yeast polysaccharides. *Carbohydr. Polym.* **207**, 371–381 (2019).
409. Kanwal, S. *et al.* Attenuation of DSS induced colitis by Dictyophora indusiata polysaccharide (DIP) via modulation of gut microbiota and inflammatory related signaling pathways. *J. Funct. Foods* **64**, 103641 (2020).
410. Liu, W. *et al.* The α-D-glucan from marine fungus Phoma herbarum YS4108 ameliorated mice colitis by repairing mucosal barrier and maintaining intestinal homeostasis. *Int. J. Biol. Macromol.* **149**, 1180–1188 (2020).
411. Muthuramalingam, K. *et al.* Dietary intervention using (1,3)/(1,6)-β-glucan, a fungus-derived soluble prebiotic ameliorates high-fat diet-induced metabolic distress and alters beneficially the gut microbiota in mice model. *Eur. J. Nutr.* (2019) doi:10.1007/s00394-019-02110-5.
412. Chen, J. *et al.* Dectin-1-activated dendritic cells: A potent Th9 cell inducer for tumor immunotherapy. *OncoImmunology* **5**, e1238558 (2016).
413. Wagener, M., Hoving, J. C., Ndlovu, H. & Marakalala, M. J. Dectin-1-Syk-CARD9 Signaling Pathway in TB Immunity. *Front. Immunol.* **9**, (2018).
414. Lee, M. J. *et al.* Phosphoinositide 3-Kinase δ Regulates Dectin-2 Signaling and the Generation of Th2 and Th17 Immunity. *J. Immunol.* **197**, 278–287 (2016).
415. Kalantari, P. *et al.* CD209a Synergizes with Dectin-2 and Mincle to Drive Severe Th17 Cell-Mediated Schistosome Egg-Induced Immunopathology. *Cell Rep.* **22**, 1288–1300 (2018).
416. Papista, C. *et al.* Gluten induces coeliac-like disease in sensitised mice involving IgA, CD71 and transglutaminase 2 interactions that are prevented by probiotics. *Lab. Invest.* **92**, 625–635 (2012).
417. Heinsbroek, S. E. M. *et al.* Orally delivered β-glucans aggravate dextran sulfate sodium (DSS)-induced intestinal inflammation. *Nutr. Res.* **35**, 1106–1112 (2015).
418. Kelly, E. K., Wang, L. & Ivashkiv, L. B. Calcium-Activated Pathways and Oxidative Burst Mediate Zymosan-Induced Signaling and IL-10 Production in Human Macrophages. *J. Immunol. Baltim. Md 1950* **184**, 5545–5552 (2010).
419. Bulman, S. E. *et al.* Pullulan: a new cytoadhesive for cell-mediated cartilage repair. *Stem Cell Res. Ther.* **6**, 34 (2015).
420. Chang, T.-H. *et al.* Dectin-2 is a primary receptor for NLRP3 inflammasome activation in dendritic cell response to Histoplasma capsulatum. *PLOS Pathog.* **13**, e1006485 (2017).
421. Yamada, K. *et al.* Inhibition of STAT3 Signaling Reduces IgA1 Autoantigen Production in IgA Nephropathy. *Kidney Int. Rep.* **2**, 1194–1207 (2017).
422. Colucci, M. *et al.* Sialylation of N-Linked Glycans Influences the Immunomodulatory Effects of IgM on T Cells. *J Immunol* **194**, 151–157 (2015).
423. Xue, J., Zhao, Q., Zhu, L. & Zhang, W. Deglycosylation of FcalphaR at N58 increases its binding to IgA. *Glycobiology* **20**, 905–915 (2010).
424. Ben Mkaddem, S., Benhamou, M. & Monteiro, R. C. Understanding Fc Receptor Involvement in Inflammatory Diseases: From Mechanisms to New Therapeutic Tools. *Front. Immunol.* **10**, 811 (2019).
425. Kulkarni, V. & Ruprecht, R. M. Mucosal IgA Responses: Damaged in Established HIV Infection—Yet, Effective Weapon against HIV Transmission. *Front. Immunol.* **8**, (2017).
426. Chen, B. *et al.* Oral microbiota dysbiosis and its association with Henoch-Schönlein Purpura in children. *Int. Immunopharmacol.* **65**, 295–302 (2018).
427. Angelis, M. *et al.* Microbiota and Metabolome Associated with Immunoglobulin A Nephropathy (IgAN). *Plos One* **9**, e99006 (2014).
428. Calderón-Gómez, E. *et al.* Commensal-Specific CD4(+) Cells From Patients With Crohn's Disease Have a T-Helper 17 Inflammatory Profile. *Gastroenterology* **151**, 489-500.e3 (2016).
429. Lamb, C. A. *et al.* αEβ7 Integrin Identifies Subsets of Pro-Inflammatory Colonic CD4+ T Lymphocytes in Ulcerative

Colitis. *J. Crohns Colitis* **11**, 610–620 (2017).
430. Lin, J.-R. *et al.* Interleukin-17 promotes the production of underglycosylated IgA1 in DAKIKI cells. *Ren. Fail.* **40**, 60–67 (2018).
431. Lu, G. *et al.* CCL20 secreted from IgA1-stimulated human mesangial cells recruits inflammatory Th17 cells in IgA nephropathy. *PLOS ONE* **12**, e0178352 (2017).
432. De Palma, G. *et al.* Intestinal dysbiosis and reduced immunoglobulin-coated bacteria associated with coeliac disease in children. *BMC Microbiol.* **10**, 63 (2010).
433. Ma, H.-Q., Yu, T.-T., Zhao, X.-J., Zhang, Y. & Zhang, H.-J. Fecal microbial dysbiosis in Chinese patients with inflammatory bowel disease. *World J. Gastroenterol.* **24**, 1464–1477 (2018).
434. Fenton, T. M. *et al.* Immune Profiling of Human Gut-Associated Lymphoid Tissue Identifies a Role for Isolated Lymphoid Follicles in Priming of Region-Specific Immunity. *Immunity* **52**, 557-570.e6 (2020).
435. Cheng, H.-Y., Ning, M.-X., Chen, D.-K. & Ma, W.-T. Interactions Between the Gut Microbiota and the Host Innate Immune Response Against Pathogens. *Front. Immunol.* **10**, (2019).
436. Juyal, G. *et al.* Genome-wide association scan in north Indians reveals three novel HLA-independent risk loci for ulcerative colitis. *Gut* **64**, 571–579 (2015).
437. Cleynen, I. *et al.* Inherited determinants of Crohn's disease and ulcerative colitis phenotypes: a genetic association study. *Lancet Lond. Engl.* **387**, 156–167 (2016).
438. Long, Y. *et al.* The Imbalance of Circulating Follicular Helper T Cells and Follicular Regulatory T Cells Is Associated With Disease Activity in Patients With Ulcerative Colitis. *Front. Immunol.* **11**, (2020).
439. de Vries, H. S. *et al.* Genetic association analysis of the functional c.714T>G polymorphism and mucosal expression of dectin-1 in inflammatory bowel disease. *PloS One* **4**, e7818 (2009).
440. Beaudoin, M. *et al.* Deep Resequencing of GWAS Loci Identifies Rare Variants in CARD9, IL23R and RNF186 That Are Associated with Ulcerative Colitis. *PLoS Genet.* **9**, (2013).
441. Zhernakova, A. *et al.* Genetic Analysis of Innate Immunity in Crohn's Disease and Ulcerative Colitis Identifies Two Susceptibility Loci Harboring CARD9 and IL18RAP. *Am. J. Hum. Genet.* **82**, 1202–1210 (2008).
442. Iliev, I. D. *et al.* Interactions between commensal fungi and the C-type lectin receptor Dectin-1 influence colitis. *Science* **336**, 1314–1317 (2012).
443. Qiu, X. *et al.* Alterations in the mucosa-associated fungal microbiota in patients with ulcerative colitis. *Oncotarget* **8**, 107577–107588 (2017).
444. Sam, Q. H., Chang, M. W. & Chai, L. Y. A. The Fungal Mycobiome and Its Interaction with Gut Bacteria in the Host. *Int. J. Mol. Sci.* **18**, (2017).
445. Weiss, G. A. & Hennet, T. Mechanisms and consequences of intestinal dysbiosis. *Cell. Mol. Life Sci. CMLS* **74**, 2959–2977 (2017).
446. Michaud, E., Mastrandrea, C., Rochereau, N. & Paul, S. Human Secretory IgM: An Elusive Player in Mucosal Immunity. *Trends Immunol.* **41**, 141–156 (2020).
447. Petrušić, V. *et al.* Hexameric immunoglobulin M in humans: desired or unwanted? *Med. Hypotheses* **77**, 959–961 (2011).
448. Moh, E., Lin, C.-H., Morten, T.-A. & Packer, N. Site-Specific N-Glycosylation of Recombinant Pentameric and Hexameric Human IgM. *J Am Soc Mass Spectr* **27**, 1143–1155 (2016).
449. Klemola, T., Savilahti, E. & Koskimies, S. Transient IgA and IgM deficiencies are frequent in children with ulcerative colitis. *Eur. J. Pediatr.* **147**, 184–187 (1988).
450. Patrone, F., Dallegri, F. & Sacchetti, C. IgA-related defective neutrophil chemotaxis in ulcerative colitis. *Boll. DellIstituto Sieroter. Milanese* **57**, 204–207 (1978).
451. Longet, S. *et al.* Reconstituted Human Polyclonal Plasma-derived Secretory-like IgM and IgA Maintain the Barrier Function of Epithelial Cells Infected with an Enteropathogen. *J Biol Chem* **289**, 21617–21626 (2014).
452. Hartstra, A. V., Bouter, K. E. C., Bäckhed, F. & Nieuwdorp, M. Insights Into the Role of the Microbiome in Obesity and Type 2

Diabetes. *Diabetes Care* **38**, 159–165 (2015).
453. Lebreton, C. *et al.* Interactions Among Secretory Immunoglobulin A, CD71, and Transglutaminase-2 Affect Permeability of Intestinal Epithelial Cells to Gliadin Peptides. *Gastroenterology* **143**, 698-707.e4 (2012).
454. Salas-Cuestas, F. *et al.* Higher Levels of Secretory IgA Are Associated with Low Disease Activity Index in Patients with Reactive Arthritis and Undifferentiated Spondyloarthritis. *Front. Immunol.* **8**, (2017).
455. Inamine, T. & Schnabl, B. Immunoglobulin A and liver diseases. *J. Gastroenterol.* **53**, 691–700 (2018).
456. Sterlin, D., Fadlallah, J., Slack, E. & Gorochov, G. The antibody/microbiota interface in health and disease. *Mucosal Immunol.* **13**, 3–11 (2020).
457. Allegretti, J. *et al.* The Current Landscape and Lessons from Fecal Microbiota Transplantation for Inflammatory Bowel Disease: Past, Present, and Future. *Inflamm. Bowel Dis.* **23**, 1710–1717 (2017).
458. Bakken, J. S. *et al.* Treating Clostridium difficile Infection With Fecal Microbiota Transplantation. *Clin. Gastroenterol. Hepatol.* **9**, 1044–1049 (2011).
459. Weingarden, A. R. & Vaughn, B. P. Intestinal microbiota, fecal microbiota transplantation, and inflammatory bowel disease. *Gut Microbes* **8**, 238–252 (2017).
460. Rochereau, N. *et al.* Secretory IgA as a vaccine carrier for delivery of HIV antigen to M cells. *Eur J Immunol* **45**, 773–9 (2015).